Geochemical evolution of Phanerozoic Lithospheric mantle beneath S.E. South Australia

by

Suckhwan Song
Master of Sciences (Yonsei University, South Korea, 1988)

Submitted in fulfilment of the requirement
for the degree of Doctor of Philosophy

Department of Geology and Geophysics
The University of Adelaide
South Australia

October, 1994

Table of Contents

Chapter 3. Petrogenesis of Quaternary Alkali Basalt, South Australia (SQAB): northern volcanic area and southern volcanic area

Chapter 4. Mineral chemistry and whole rock chemistry of the upper mantle xenoliths entrained by the SQAB

Chapter 5. Petrology and geochemistry of South Australian kimberlites and lamprophyres

List of Figures

page

Chapter 1

Chapter 2

Chapter 3

Chapter 4

Chapter 5

Chapter 6

Chapter 7

List of Tables

Chapter 5

Chapter 6

ABSTRACT

The Adelaide Fold Belt (and western Victoria) forms the limit of eastern Australian Phanerozoic geotectonic activity and records a long history of lithospheric evolution and growth which relate to several episodes of lithospheric rifting, thinning and magmatic underplating since Archaean-Early Proterozoic periods. The Precambrian craton-forming history is recorded in the Gawler Craton to the west of the AFB. In order to the study the geochemical evolution of the southern South Australian lithosphere from the Late Neoproterozoic, a number of igneous suites whose ages span the Phanerozoic were collected from the Adelaide Fold Belt and adjacent regions. These include Ordovician lamprophyres from Truro, Jurassic kimberlites from Port Augusta, Terowie, and Pine Creek, Quaternary alkaline basalt from Mt Gambier and adjacent areas of S.E. South Australia, and suites of mafic and ultramafic xenoliths transported by these magmas. Of these, selected whole-rock and mineral samples were analysed for major and trace elements and for Sr and Nd isotopic compositions.

The Quaternary alkaline basalt province in S.E. South Australia represents a small part of the Tertiary to Quaternary province found throughout eastern Australia. These basalts are predominantly *ne*-normative and most of them contain peridotite xenoliths. Two main geochemical and isotopic groups of basalts are recognised; i) a Southern group of younger hawaiites and ii)a Northern group of older olivine analcimites. The hawaiites are derived from two eruptive centres, Mt Gambier and Mt Schank.

The hawaiite suites show systematic variations of most major and incompatible trace elements, and of the REE with Mg#. The hawaiites have εNd of +2.26 - +3.23, $^{87}Sr/^{86}Sr$ of 0.7035 - 0.7041 and $TNd_{(DM)}$ of 0.43 - 0.6 Ga. The geochemical variations support the derivation of the Mt Schank hawaiites from the Mt Gambier hawaiites by fractional crystallisation of clinopyroxene (54.3 %), plagioclase (29.2 %) and olivine (16.5 %). The Mt Gambier hawaiites can be modelled by small degree of partial melting of highly enriched upper mantle peridotites (4 - 5 %), though temporal isotopic variation suggests derivation from mixed sources.

The olivine analcimites from the northern sub-province are characterised by high Mg# (61-71), Ni, Cr, low K_2O (mainly < 1 wt %), Rb and Sr. The analcimites have εNd of +0.92 - +2.58, $^{87}Sr/^{86}Sr$ of 0.7039 - 0.7049 and $TNd_{(DM)}$ of 0.4 - 0.52 Ga. High Mg# (>66) are shown in samples containing high Ni (>200 ppm) and Cr (>400 ppm) contents, suggesting that some of these rocks are probably primary basaltic liquids equilibrated with upper mantle peridotite. Systematic chemical changes are shown between magnesian and less

magnesian analcimites. This variation can be attributed to olivine dominant fractionation (98 %) with minor clinopyroxene. High Mg# in some samples may originate from olivine accumulation, which is supported by cumulate textures shown under the microscope. However, these rocks in general have significantly higher Ba, Ti, Zr, Nb, LREE concentrations than the Southern group of hawaiites in spite of their high Cr, Ni, Mg#. The analcimites also have slightly lower $TNd_{(DM)}$, εNd and higher $^{87}Sr/^{86}Sr$ relative to the Southern group of hawaiites.

The Quaternary alkaline basalts host xenoliths of spinel lherzolite and rarely minor dunite or pyroxenite. The spinel lherzolites are divided into two varieties according to their different microscopic textures and mineralogical composition, the coarse equant lherzolite (CEL) and the deformed sheared lherzolite (DSL). The CELs show homogeneous equigranular texture while the DSLs show a submylonitic texture. Clinopyroxenes of the CELs show higher Mg#, Cr_2O_3, Na_2O, TiO_2, lower CaO, and orthopyroxenes and spinels of the CELs show higher Mg#, Cr_2O_3, MnO, Cr/Cr+Al ratios than those of DSLs. The CELs show a higher Al_2O_3, Na_2O, P_2O_5, CaO, TiO_2, Sr, Zr, Y, Sc, V, Ba, and lower Mg#, SiO_2, Ni, Cr, relative to the DSLs. The concentrations of most elements are like those of unmetasomatised Victorian spinel lherzolites and are however distinctive from the much more incompatible element-rich Victorian metasomatised xenoliths.

The geochemical differences between the CELs and the DSLs may reflect higher modal proportions of pyroxene in the CELs. Calculated temperatures range from 930 °C to 1100 °C with slightly higher temperatures shown by the CELs. Oxygen fugacities estimated from the spinel lherzolites lie between QFM and WM, like those of Western Europe and eastern Australia sub-continental lherzolite samples, suggestive of similar redox states of the sub - continental lithospheric mantle in a large scale.

The Jurassic kimberlites from the central AFB and eastern edge of the Gawler Craton, occur as dykes, sills and stocks. They are dominantly *ne*- normative and show high Ni (~430), Cr (~1050), MgO (~15.5 wt %), low SiO_2 (~44 wt %), Al_2O_3 (~7.15 wt %), enrichment of LIL and LREE. They have εNd of +0.36 - -2.34, $^{87}Sr/^{86}Sr$ of 0.7088 - 0.7123 and $TNd_{(DM)}$ of 0.51 Ga - 0.73 Ga. Their chemical compositions are like those of ultramafic lamprophyres (Rock, 1991) and Group 2 kimberlites of South Africa (Smith *et al.*, 1985), but are distinctive from Western Australian lamproites in being less enriched in LILs (e.g. Rb, Ba).

The Ordovician lamprophyres from the AFB are characterised by their porphyritic texture and distinctive lineation. They have modest Ni (~241), Cr (~470), MgO (~7 wt %), high SiO_2 (~56.5 wt %), Al_2O_3 (~12 wt %), Nd (low Nb/Zr) and show distinctive enrichments in LREE and LIL. These chemical characteristics suggest that these fractionated lamprophyres are of shallow mantle origin or have experienced crustal assimilation as supported by the presence of quartz xenocrysts. The lamprophyres have εNd of -5.1 - -7.0, $^{87}Sr/^{86}Sr$ of 0.7155 - 0.7199 and $TNd_{(DM)}$ of 0.94 -1.17 Ga. However, the lamprophyres

are clearly distinguished from the Jurassic kimberlites by their low Nb, Ti, MgO, Mg#, high Rb, Th, K and Al_2O_3.

The Jurassic kimberlites host mafic eclogitic and granulitic xenoliths and less common quartzo-feldspathic rocks. The xenoliths show several types of internal contact relationships including those of granulitic to eclogitic and pyroxenitic to amphibolitic rocks, suggestive of interlaying of basaltic materials and many show remnants of the partial melting, preserving Px-Gt dominant part and Qt-Feld dominant parts. They also show transitional variations in microscopic texture including gabbroic to granulitic and granulitic to eclogitic, through replacement, exsolution and recrystallization.

Among the xenoliths from three South Australian localities, Port Augusta xenoliths are more granulitic while those of Calcutteroo and Pine Creek are more eclogitic. The P-T calculated for equilibrated mineral pairs range from 750 to 1050 °C using garnet-orthopyroxene geothermometry. The Port Augusta xenoliths show slightly low temperatures. The Calcutteroo xenoliths show a wide range of composition from *ne* -through *ol* -to *Q* - normative composition, which are similar to the field of typical Cainozoic Victorian and South Australian basalts. The eclogite-granulite xenoliths are characterised by high Mg# (mainly >64), Cr, Ni, low K_2O (mainly <0.3 wt %) and distinctive enrichment in Ba. They are also characterised by distinctive REE abundances, showing variation from strongly LREE depleted to enriched relative to the HREE and an wide range of isotopic composition, εNd of -8 - + 6, $^{87}Sr/^{86}Sr$ of 0.7063 - 0.7124 and $TNd_{(DM)}$ of 0.85 - 1.9 Ga.

High Cr (>250 ppm) and Ni (>130 ppm) contents occur in samples with high Mg# (>65). The low K_2O contents of the xenoliths which have high Mg# suggest that many of the xenoliths are basaltic cumulates with little interstitial melt or that they have lost K_2O during metasomatism. The unusual REE patterns of the Calcutteroo xenoliths with high La/Nd and low Nd/Sm relationships are not be expected from the andesite model of crustal growth.

The mafic dominant xenoliths show similar isotopic and have some geochemical affinities to Neoproterozic Adelaidean and Cambrian basalts, suggesting that the xenoliths reflect underplating near the Moho during rifting and basin formation at those times. The Jurassic kimberlites are also isotopically and geochemically similar to undersaturated, highly alkaline basalts from the lower Cambrian Heatherdale Shale in the southern AFB, suggesting that the kimberlites reflect a geochemical enrichment in CLM during the Late Proterozoic and Early Palaeozoic. However, all these rocks show significant differences in geochemical and isotopic composition when compared to Palaeo-Mesoproterozoic mafic rocks from the Gawler Craton, suggesting that lithospheric mantle beneath the Craton has experienced different histories of enrichment and depletion related to magmatic underplating much earlier in the Precambrian.

The South Australian Quaternary alkaline basalts are isotopically and geochemically very like the Victorian Newer Basalts showing an EM type OIB signature, while the Tasmanian Tertiary basalts having HIMU characteristics. The Continental Lithospheric

Mantle beneath the Quaternary alkaline basalt province was enriched by the metasomatism, which is directly observed in some lherzolite samples showing amphibole-apatite-phlogopite growth. A possible model of evolution for the South Australian lithosphere suggests that the South Australian alkaline basalts are a mixture (about 20 - 35 %) of OIB like asthenospheric plume-related melts with a kimberlitic component from the CLM. In the South Australian alkaline basalts, the Northern group of older olivine analcimites have a higher CLM (kimberlite) component relative to the Southern group of younger hawaiites, suggesting decreasing role of CLM enrichment with time.

NAME: Suckhwan Song COURSE: Ph D

I give consent to this copy of my thesis, when deposited in the University Library, being avaliable for loan and photocopying.

SIGNED: DATE: 19/10/94

Statement of Originality:

I hereby certify that this thesis does not incorporate, without acknowledgement, any material which has been previously submitted for a degree in any Universituy, and to the best of my knowledge and belief, it does not contain any written or published material by another person, except where due reference is made in the text.

Suckhwan Song
October, 1994

Acknowledgements

There are many people to say hearty thanks for last three years when this thesis have been written. Firstly I would like to thank my supervisor, John Foden, for his friendship, enthusiasm and help. Without his useful comments, criticisms and numerous ideas, this thesis would not be exist. He also supplied some of samples used in this thesis and unpublished data to me.

Special thanks are extend to staffs of the Department of the Geology and Geophysics who provided critical technical assistance. They include D. Bruce, J. Stanley, G. Trevelyan, W. Mussared, R. Barrett, J. Willoughby and P. McDuie. In particular, I would like to thanks to D. Bruce, G. Trevelyan and J. Stanley for their friendships and personal assistance. I would like to remember to my friends, Abidan, Sha, Hou Bau and Amil. They came from all overseas and did not forget smile whenever we met in this department. I have enjoyed discussions with Dr John Cooper and Dr Robin Oliver in the mineralogical and geochemical interpretations.

I am also extremely grateful to M.Sheard, .B.J. Morris, and M.G. Farrand from the South Australian Department of Mines and Energy. Malcom Sheard provided some samples for this thesis as well as helped a field trip of Mt Gambier area during the rainy day. B.J. Morris and M.G. Farrand also provided many information for the South Australian kimberlites and lamprophyres. Morris also provided his own samples. These assistances are considerably critical during the earlier stage of this thesis.

I also would like to say hearty thanks to Professor, Hayoung LEE, Hisoo Moon of the Yonsei University and Professor Haesoo Youn and Hyeungoo Lee of the Chungnam national University, Dr. Gunjoo Moon and Youngyou Kim of the Korea Institution of mines and minerals in Korea. They have provided encouragement for forgoing three years.

I wish to sincerely thank to my family in Korea, my respect parents, brother Suckwoo, sister in law, Jin, and their daughter, Jiyoun, and two sisters, Myungjoo, Myunghee and in Adelaide, my wife, Aesook, and two children, Seonjoo, and Junyoung. I can not thank them enough for their continuous support and encouragement through this thesis. In particular, I would like to hearty thanks to my wife, Aesook, who did not hesitate to support me many works, including typing and drifting despite she was busy to take care of two children as a mother.

Abbreviations

Am.....Amphibole
Apt.....Apatite
Bi.....Biotite
Cal.....Calcite
Chl.....Chlorite
Cpx.....Clinopyroxene
Gt.....Garnet
Il.....Ilmenite
K-Fd..... K-Feldspar
Ky.....Kyanite
Ol..... Olivine
Opx..... Orthopyroxene
Phlo..... Phlogopite
Pl..... .Plagioclase
Qt.....Quartz
Rt..... Rutile
Ser.....Sericite
Sp.....Spinel
Ver.....Vermiculate

Chapter 1. Introduction; A review of Australian lithosphere and asthenosphere

1.1. General introduction

This thesis examines the evidence for the long-term geochemical evolution of subcontinental lithospheric mantle beneath southeastern Australia, in particular in the transition zone where the Precambrian craton gives way eastwards to the Tasman Foldbelt where Phanerozoic re-working and growth have been effective. To this end, we presented new petrological data from Jurassic kimberlitic rocks in the Adelaide Fold Belt and from Pleistocene -Recent alkaline basalts from S.E. South Australia. This chapter provides a summary of the definition of the lithosphere and in particular, of the physical characteristics of the Australian lithosphere

The continental lithospheric mantle (CLM) is potentially one of the major terrestrial geochemical reservoirs. Unfortunately this region of the earth is inaccessible and our knowledge of its composition and age are only achieved by relatively indirect means. The geochemical signatures of continental flood basalts, of some continental alkaline basalts and of kimberlite and lamprophyre clan rocks, are all potentially partly derived from a component stored in the CLM. Likewise some of the enriched, asthenospheric mantle reservoirs sampled by ocean island magmas, comprising for instance the Dupal anomaly (Hart, 1984), have also been interpreted as originating as delaminated CLM (Gurnis and Davies, 1986).

It is important to know how and when the enrichment of the CLM occurred. If the lithosphere grows by thermal accretion of asthenospheric material at its base (Parsons and Sclater, 1977) then at first it must be geochemically indistinguishable from the asthenosphere from which it accretes and typically be of depleted MORB-source type peridotite. Alternatively, models which propose lithospheric growth by the basal underplating of melt-depleted mantle diapirs (Clarke and Ringwood, 1964; Ringwood, 1982) may even predict that the lithosphere is initially more depleted and refractory than the upper asthenosphere. However as suggested by McKenzie (1989), during periods of thermal retrogression or stasis, the lithosphere will become a trap for migrant fluids produced by very small amounts of melting of the asthenosphere. This same lithosphere will subsequently relinquish these enrichments as melts during prograde thermal events, extension and rifting, and may also contaminate mafic magmas in transit from the asthenosphere.

Basaltic melts that have traversed the CLM may well be contaminated to variable extent by the enriched components and the closest we may get to being able examine these

enrichments unalloyed, will be where their direct melts reach the surface as lamprophyre or kimberlite. A combination of studies of these magmas and of basaltic lavas known to have traversed a given CLM volume over a protracted period of geological time, may allow both the temporal monitoring of the geochemical evolution of that lithosphere, and will also permit the interpretation of the source component mixtures in the basalts themselves.

This above scenario predicts a petrologically heterogeneous lithosphere in which major elements and incompatible trace elements are essentially decoupled having been introduced by two very different processes. This hetrogeneity is borne out by the observations of the diverse rock types exhumed as xenoliths by continental alkali basalts. Such xenoliths whose calculated P-T equilibration conditions require they originated in the CLM, include garnet and spinel lherzolites, pyroxenites and eclogites (Jochum *et al.*, 1989; McDonough, 1990). The older the lithosphere, the more likely it is to be enriched and the residence time of these enrichments may then be judged by the extent of migration of their radiogenic isotope ratios from the asthenospheric reservoir. Dating of garnet included in diamonds from South Africa (Richardson *et al.*, 1984) for instance shows that some continents have ancient lithospheric keels.

An important aspect of the model of CLM enrichment by migration of very small melt volumes, is the extent to which this process leads to geochemical uncoupling of major elements from incompatible, lithophile, trace elements. This is an important consideration which needs to be incorporated into models of continental crustal growth and supposed complimentary mantle depletion. Where there is major decoupling of trace-and major elements, the radiogenic isotopic signals which are used to monitor the time-rate flux of mass are no longer usefully link the mantle residual reservoirs to the continental crustal reservoir in a simple way.

1.2. Lithosphere and asthenosphere, crust-mantle transition (Moho)

1.2.1. Lithosphere and asthenosphere

The lithosphere has been defined as a rigid outer shell of the Earth, decoupling from the underlying weak viscous or plastic asthenosphere where convection is the principal thermal mechanism. The lithosphere plays on important role in large-scale tectonic movements such as mountain building or surface load resulting in sedimentary basin formation (e.g. Muirhead and Drummond, 1991). It displays considerable thickness and structural variation between oceanic and continental lithosphere as well as among continents of variable ages.

The oceanic lithosphere is converted from the asthenosphere simply by cooling without any change of chemical composition (White, 1988) and its thickness is governed by the loss of heat from the convecting upper mantle (Parsons and McKenzie, 1978). However, thickness of the continental lithosphere is controlled by its age and its thermal structure is also

reliant on the current tectonic regions. Beneath Archaean cratons, the lithosphere is thicker than beneath the oceans or continental area undergone later Proterozoic or Phanerozoic orogenesis (Jordan, 1988; Richter, 1988), and is controlled by chemically differentiated regions rather than just by thermal structure (Jordan, 1981; White, 1988).

The thickness of the lithosphere depends on its defining thermal model (McKenzie, 1989). In the simple plate model in which the temperature of the lithosphere is function of depth and plates are thermally stabilised against mantle convection, the thickness of the lithosphere will be increased until conductive heat supply to the base of the lithosphere balances with heat lost through the lithosphere. In comparisons, in the half space model, thermal structure is a function of time and its lithospheric thickness will be increased until the plate is destroyed by subduction(McKenzie, 1989).

Simple thermal models divide the lithosphere into a mechanical boundary layer and a thermal boundary layer (Jordan, 1978, 1981; Parsons and McKenzie, 1978; McKenzie and Bickle, 1988). According to the models proposed by Parsons and McKenzie (1978) and McKenzie and Bickle (1988), the lithosphere is composed of a mechanical boundary layer and an a underlying thermal boundary layer. In the mechanical boundary layer, heat transfer is principally conduction and it is isotopically and geochemicaly anomalous whereas the underlying thermal boundary layer is not either totally rigid or plastic.

Jordan (1978, 1981) defined lithosphere, as three boundary layers, chemical, mechanical and thermal boundary layer. In these terms, mechanical boundary layer corresponds to a cold, strong elastic outer shell of Earth whereas thermal boundary layer is equivalent to the upper layer stabilised against convective disruption. The thickness of the thermal boundary layer increases with age because of decreasing heat flow and elevation at continent as well as ocean. However, thermal reactivation and subsequent conductive relaxation of the continental thermal boundary are common epeirogenic phenomena (Jordan, 1988). Thus the thermal boundary configuration of the older continents, including that beneath of ancient cratons, is similar to that of old ocean basin, because they could escape from any major thermal reactivation and collisional orogenesis.

The chemical boundary layer of Jordan (1978, 1981) is equivalent to upper lithosphere of lower density than typical mantle assemblages consistent with Ringwood's pyrolite (1966) and its composition is equivalent to the removal of about 20 mol % of olivine basalt from pyrolite. Its thickness is variable due to the variety of tectonic and magmatic processes. The reasons are multi stage formations by advective thickening of the lithosphere during major episodes of orogenic compression or by amalgamation of buoyancy mantle with its subjacent crustal columns in dispersed zones during the plate motions in thick cool basalt-depleted continental lithosphere for the thousands of million years. Thus, in active mobile belts and orogenic zones, the deep chemical boundary layer has never stabilised or destroyed by convective activity whereas, beneath continental craton nuclei, the chemical boundary layer was stabilised at an early date. This augmented chemical boundary layer in craton

areas controls thickness of the thermal boundary and the thicker layer behaviours as stable geochemical reservoirs. An eligible Sm-Nd model age of sub-calcic garnet in diamonds from Kaapvaal craton (Richardson *et al.*, 1984) suggest that basalt depleted chemical boundary layer extended below the minimum depth of diamond stability as long ago as 3200-3300 Ma. Seismic data also imply the existence of anomalous mantle to depths of 300-400 km beneath stable cratons (Jordan, 1988).

A mechanism for chemical compensation of continental thermal boundary layer can be explained by differences in normative density between less dense residual after extraction of basaltic constituents from the parental mantle mineralogy consisting of garnet lherzolite and the parental material (Green and Liebermann, 1976). This mechanism leads to the depletion of Fe relative to Mg in peridotite (Jordan, 1978). Generally, peridotite nodules derived from the shield areas are more depleted in major element composition than those derived from the oceanic upper mantle (Boyd and Mertzman, 1987; Nixon, 1987). The differences in normative density calculated from these compositions are enough to stabilise the superadiabatic thermal gradients inferred by geophysical methods (Jordan, 1988).

1.2.2. Lithosphere in different aspects

U.S. Geodynamic Committee (1983) defined the term "lithosphere" in different ways and the definitions were reviewed by Muirhead and Drummond (1991). They include four different definitions in terms of seismological, rheological, temperature, geochemical and petrological aspects as follows;

a) Seismological aspect; The base of the lithosphere is defined as the depth to a low velocity layer, resulting from a low shear modulus, probably caused by partial melting.

b) Rheological aspect; The lithosphere is a rigid outer part of the Earth able to support surface loads such as sedimentary basins and related to mountain building by bending and flexing by the underlying viscous and plastic asthenosphere.

c) Chemical and mineralogical aspect; The definition is based on the sampling of rocks from the deep lithosphere, as nodules in volcanics or kimberlitic magma and petrophysical evidences obtained from laboratory measurement.

d) Temperature aspect; The lower boundary of the lithosphere is defined to be an isotherm (surface of constant temperature) in which a typical temperature is approximately 1600 °K (~1300 °C).

According to the seismic definition, the lithospheric plate decouples from the underlying asthenospheric mantle at the depth of a low velocity layer (LVZ) which causes on drop in the shear modulus. The LVZ corresponds to a zone of incipient partial melting which exists beneath the deep lithosphere of many tectonically active continent (Anderson and Sammis, 1970; Law and Greenhouse, 1981; Lilley *et al.*, 1981; Belbo *et al.*, 1983). However, this definition is limited because existences of worldwide LVZ are not universal.

Green and Liebermann (1976) suggested three minor possible occurrences at the base of the low velocity layer, as: 1) the geotherm crosses the water saturated solidus, 2) the water content of the mantle decreases below about 150 km depth and, 3) water at depths below the low velocity zone is held in as yet undiscovered hydrous phases.

The second definition stresses effects of stress and tectonic processes on the lithosphere. According to this definition, lithospheric flexure is associated with the structure of many sedimentary basins because the rigidity of the lithosphere allows the plates to transmit elastic stresses during geological intervals and also allows them to bend when the lithosphere is subjected to a load (Jordan, 1978; McKenzie and Bickle, 1988). As a result of this flexure, the earth's surface has been depressed and the resulting depression filled with sediments.

However the entire lithosphere does not transmit the elastic stresses effectively because the upper half of the lithosphere is sufficiently rigid and the elastic stresses do not relax on time scales of 10^9 years (Turcotte and Schubert, 1982). The lithosphere thickness also varies because of its dependence on the type of rheology assumed for the lithosphere (elastic, viscose-elastic, etc). If the rheology is plastic, the lithosphere will responses up to a critical stress whereas, assuming a viscous rheology, the lithosphere may achieve relaxation of stress without deformation. If the lithosphere is effectively elastic, it can only support a limited amounts of loading. The rheological lithosphere is also dependent on temperature, even though the assumed geothermal gradient is uncertain (Muirhead and Drummond, 1991).

The isostasy model of Airy suggests that large mountant ranges such as Himalayas will be deep root. This suggest that a change in the buoyancy or elevation of lithosphere may lead to a displacement of asthenosphere. However, local definencies of mass at depth suggests that the lithosphere is sufficiently strong to redistribute loading on the Earth's surface. Displacement of asthenospheric mantle in the response to lithospheric loading may only occur over a finite length scale which is related to its effective viscosity.

The third definition of lithosphere has been discussed by many authors (e.g. Green and Liebermann, 1976; Green and Wallace, 1988). Green and Liebermann (1976) attempted to compare the pyrolite petrological model with the seismic model of the lithosphere in stable oceanic regions. They suggested that the low velocity zone in velocity profiles which is consistent with a region of incipient partial melting occurs at depths of 85-95 km, which extends to 165 km depths for a stable oceanic geotherm. The low velocity zone is overlain by a lithosphere of peridotite composition with a density increase at about 55 km depth due to the first appearance of garnet. Green and Liebermann (1976) also suggested that the geotherm intersects the pyrolite solidus at the depths of LVZ and that the existence of partial melting is dependent on the water content. Green and Wallace (1988) suggested that carbonatitic melts coexist with pargasite-bearing lherzolites at 21-31 kbar and 930-1080 °C on experiment of peridotite-CO_2-H_2O solidus for small water and carbonate contents (see Chapter 2). They suggest that the melt content is consistent with that of the LVZ.

The rhelogical definition of the lithosphere is supported by the sampling of rocks from the deep lithosphere (e.g. mafic to ultra basic xenoliths entrained by volcanic or kimberlitic rocks). In Australia, differences in the dominant xenoliths types are shown between Proterozoic Adelaide geosyncline and Phanerozoic eastern Australia. The xenoliths found within the Adelaide geosyncline are predominantly mafic whereas those of the eastern Australia are ultrabasic in composition. It may reflect differences of volumetrically dominant lithology within the lithospheric structure in different tectonic areas (see Chapter 6). However, wide-scale sampling representing all levels of the lithosphere is impossible although a large number of deep seated xenoliths allow an interpretation on the local scale of the lithospheric nature (Muirhead and Drummond, 1991).

The thermally defined lithosphere will be limited by the depth at which the rocks lose their rigidity and start to become plastic or viscous. Turcotte and Schubert (1982) suggested that the base of the lithosphere corresponds to the 1300 °C isotherm. The thermal lithosphere beneath the ocean basins has a thickness of about 100 km, whereas the thickness beneath the continents is about twice of that (White, 1988; Jordan, 1988). The temperature and depth nearly corresponds to the geotherm obtained by geothermometry for southeastern Australia by O'Reilly and Griffin (1985). It is difficult to state with any certainty the temperature at which lithosphere loses strength, because of uncertainties among the geotherms. The geothermal gradient estimates typically depend on two methods: use of equilibrated mineral suites, and extrapolation of surface temperatures and heat flux to depths. Generally, there are considerable differences between these two different geotherms as well as among the experimental geotherms .

1.2.3. Crust-mantle boundary (Moho) and its transitional variation

The crustal-mantle boundary was discovered as a seismic discontinuity from the interpretation of earthquake recordings (Mohorovicic, 1910). Integrated petrological, geochemical, petrophysical, and geophysical data suggest that the layers above the Moho discontinuity are characterised by lithological variation with depth and variation of thickness under different tectonic conditions (Furlong and Fountain, 1986; Fountain *et al.*, 1987; Griffin *et al.*, 1987).

The crust-mantle boundary can be defined by three methods as follows;

A) Seismological definition based on the identification of the separated boundary by S(Vs) and P(Vp) wave velocities,

B) Petrological definition based on xenolith studies. The phase changes are from mafic granulite to eclogitic rocks. The change from eclogitic rocks and peridotic is a compositional change.

C) Other geophysical methods including magnetic studies and electrical conductivity.

Early recognition of the Moho discontinuity depended on seismic observations. In the

seismic waves, the studies mainly depend on the observation of compressional velocity (P-wave) rather than shear wave velocity (S-wave) because recording of the P-wave is easier than S-wave and the former is clearly identified relative to the latter (Denham, 1991). The Moho depth in the seismic studies is usually defined as a velocity layer greater than 7.8 km/s (Vp) and 4.6 km/s (Vs) and ranges from 30 to 50 km in continental areas (Denham, 1991).

However, many studies have suggested that the crust-mantle boundary shows transitional velocity variation. Collins (1991) suggested that vertical profiles shown in the transitional zone is consist of fine bands of discontinuous reflection and the structure extend over a number of km depth. In the exposed high grade metamorphic zones (e.g. Ivrea-Verbano zones in Northern Italy), Hale and Thompson, (1982) also suggests a velocity transition. The tectonically exposed metamorphic section has a laminated structure with a total 6 km thickness, in which seismic transitions correspond to the meta-sedimentary/ meta-igneous layering.

Moho discontinuity defined by petrologic criteria rely on deep-seated xenolith studies. This approach is dependent on the dominant mafic xenoliths (e.g. eclogite, granulite) for the low crustal level and ultra-mafic xenoliths (e.g. spinel or garnet lherzolite) for the upper mantle level. The study possibly can be supported by the exposed high grade metamorphic belts believed to be slices of lower crust. The upward petrological variation is granulite to amphibolite facies rocks (see Fig. 1.7).

Finally, the Moho discontinuity may be defined as a conductivity anomaly layer of magnetic minerals (Wasilewski *et al.*, 1979; Law and Greenhouse, 1981; Belbo *et al.*, 1983). Wasilewski *et al.* (1979) and Wasilewski and Mayhew (1982) suggested that worldwide mantle xenoliths are volumetrically non-magnetic, so magnetisation of the xenoliths at mantle temperatures is negligible. However, granulite xenoliths are the primary source of information about the magnetisation of the lower crust, so the lower crust could be the most magnetic layer. Thus the crust/mantle boundary is defined as magnetic mineral discontinuity and the seismic Moho is also the magnetic boundary. They also suggested that the Curie isotherms depend on the type of the magnetic mineralogy and their depths vary with the regional geothermal gradients. For examples, the hot lithosphere in late Proterozoic to Phanerozoic tectonic area results in deeper Moho discontinuity whereas cool lithosphere in Archaean cratonic nuclei results in shallow Moho discontinuity.

However, Haggerty (1978) suggested that magnetite cannot be the magnetic mineral in large regions of the lower crust, because the curie temperature for impure natural magnetite in granulite is significantly lower than that for pure magnetite. Thus, Wasilewski's idea (1979, 1982) may be acceptable partly because of the diverse anomalous source of magnetisation in the crust. The anomalous sources of magnetisation include the temperature effect on rock magnetisation, and the kinds and quantity of magnetic minerals (see magnetic conductivity part). However, the existences of a high conductivity layer beneath many tectonically active areas (Law and Greenhouse, 1981) provides a possibility to interpret the

nature of the crust-mantle boundary with electro-magnetic characteristics.

1.3. Evolution of Australian lithosphere

The Present Australia is broadly divided into two segments along Tasman line, Precambrian terrain on the west and Phanerozoic terrain on the east (Veevers, 1984). The Precambrian terrain comprises large Archaean cratons distributed in Yilgarn and Pilbara Blocks of Western Australia and Gawler Block of South Australia, Proterozoic mobile belts encircling the craton and Proterozoic inliers occurring in western Australia and central northern portion of Australia. Geological history of the Australia has been summarised in large numbers of studies (Adams, 1981; Jones and Veevers, 1984; Veevers and Powell, 1984; McCulloch, 1987; Page, 1988; Wyborn *et al.*, 1988).

Archaean and Palaeo-Meso Proterozoic periods; Evolution models of Precambrian Australian lithosphere generally concentrate on Proterozoic time (McCulloch, 1987; Wyborn *et al.*, 1988), because most of the Archaean terrains were reworked during the Proterozoic and buried beneath basin cover (McCulloch, 1987). Models of tectonic evolution of Australian Proterozoic terrains dominantly involve intracontinental setting rather than processes related to sea floor spreading and subduction (e.g. Etheridge *et al.*, 1987). The reasons for this are 1) virtual absence of ophiolitic faces and oceanic faces, 2) the predominance of acid to bimodal igneous suites over intermediate ones of classical arc affinity, 3) the predominance of low pressure metamorphic facies, 4) the very narrow time range of particular events over the whole continent (Wyborn *et al.*, 1988).

Limited Sm-Nd data for the Archaean Pilbara and Yilgarn blocks suggest that Early Archaean material has predominantly derived from depleted mantle sources (McCulloch, 1987). Connection between Archaean and Proterozoic (2400 Ma-2500 Ma) is ambiguous because of the notable absence of igneous rocks of age ranging from 2400 Ma to 2000 Ma (McCulloch, 1987). McCulloch (1987) suggested that this period may reflect a quiescence of underplating resulting from a secular change in the upper mantle convection system.

Quiescence of crustal events in the earliest Proterozoic was broken with a major crust-forming episode between 1880 Ma and 1840 Ma (Page, 1988). These major crust-forming events initiated deformation, metamorphism and cratonization of the earliest Proterozoic basinal successions. Large volumes of felsic volcanism and granite emplacement covering large area of Australia were followed during the Palaeo- to Mesoproterozoic periods (Wyborn, 1988). The felsic magmas are compositionally uniform I-type.

These widespread igneous rocks were generated from mantle derived sources as a result of polygonal small-scale mantle convection, which lead to extensive underplating of Archaean crust (Wyborn, 1988) or intracrustal melting of pre-existing Early Archaean crust (Page, 1988). The partial melting at ~1850 Ma may reflect a worldwide thermal event

reflecting a major perturbation (McCulloch, 1987).

Neo Proterozoic periods; During the early Neoproterozoic periods (1300-900 Ma), the crustal forming events in Australia have restricted to narrow belts between or surrounding the major individual blocks. (Veevers, 1984). During the Adelaidean period, Australia have started to breakup by plate divergence on the east (Veevers and Powell, 1984).

The plate divergence results in three stages process of extension (Veevers and Powell, 1984). They are 1) 850-650 Ma - Precambrian craton underwent extension concentrated along rift valley complexes; 2) 650-575 Ma - localized dextral shear accompanied by extension and compression lead to marginal uplift; 3) 575 Ma - continental break-up and plate divergence, which lasted until 540 Ma ago. when plate motion on the east reversed to convergence.

At this time, older Adelaidean sediments in Tasmania were metamorphosed by the Frenchman Orogeny (Adams, 1981) and intruded by granite and dolerite about 734 Ma (McDougall and Leggo, 1965) and 720 Ma (Williams, 1976). In Epi-Adelaidean time (650-575 Ma), the main areas of Adelaidean deposition were uplifted and eroded causing a ubiquitous unconformity which is generally overlain by Early Cambrian deposits.

Palaeozoic periods; During the Cambro-Orodovician periods, tholeiitic volcanics, such as Truro volcanics and Bowers Group (N. Victoria land), were extruded on Precambrian platform deposits, and granitoids and metamorphic events by uplift of Delamerids followed at south eastern part of Australia (Veevers and Powell, 1984). The Ravenswood-Lolworth block and Anakie interior of NE Queensland also show abundant occurrences of granitic rocks of similar age. Ordovician-Carboniferous basaltic andesites or basaltic tuff and coeval granitioids are observed in southeastern part of Victoria and New South Wales. Acid to intermediate volcanic associated with I-type granitoids are also recorded in north-eastern Queensland.

Mesozoic and Cainozoic periods; Mesozoic igneous activities of Australia show a closer relationship with regional tectonism. They are mainly distributed within 300 km from continental margin and their distributions of Australia are concentrated on the Tasmanoids of New England Fold Belt, Lachlan Fold Belt and Tasmania (Jones and Veevers, 1984). Their ages range from 90 to 200 Ma. Their composition range from tholeiitic to rhyolitic or from gabbro to granite (Jones and Veevers, 1984), but are predominantly tholeiitic in composition

Cainozoic magmatisms are dominated by alkaline basalts which occur along the long narrow continental margin of the eastern Australia within Tasmanoids. The volcanic belt is one of the world's most extensive volcanic zones with limited ages and geochemical components (O'Reilly and Griffin, 1987). The origins of the volcanism were considered as association with a number of fixed hot spots (e.g. Sutherland, 1983).

Kimberlites, lamprophyres and/or lamproites are concentrated on the southeastern and northwestern parts of Australia, respectively. The kimberlites are dominantly Mesozoic to Cainozoic in age while lamproites have Proterozoic to Cainozoic ages (Rock 1991). The kimberlites and lamproites show distinctive enrichment characteristics and they are geochemically and isotopically distinguished from the alkaline basalts of eastern Australia and leucitites of New South Wales.

1.4. Lithosphere, asthenosphere and crust-mantle transition in Australia

1.4.1. Deep lithospheric structure in the Australian continent

The Australian continent shows two contrasting lithospheric structures separated by the Tasman line in geophysical aspects; Precambrian terrain on the west side and Phanerozoic terrain on the east side. They include seismic studies (Cleary *et al.*, 1972; Finlayson *et al.*, 1974; Finlayson, 1982; Muirhead and Drummond, 1991), and electro-magnetic sounding (Lilley *et al.*, 1981; Constable, 1991; Lilley, 1991).

A) Lithosphere-asthenosphere transition in the seismic aspect

Finlayson *et al.* (1974) recorded a velocity change between 8.18-8.23 km/s and 8.53 km/s at 165 km depth across the Tasman line in trans-Australian seismic refection data. Finlayson (1982) also suggested that the transition between the two regions occurs at depths greater than 200 km. He indicated that higher upper mantle velocities (8.1-8.6 km/s) occur at the shallower depths (about 165-175 km) in the Phanerozoic terrain than in the Precambrian craton.

Muirhead and Drummond (1991) provided a summary of the published seismic data of the Australian continent. Generally, seismic studies in the Australian continent showed that upper mantle structures under Precambrian shield regions of northern, central and southwestern Australian are different from those under the Phanerozoic provinces of eastern Australia. They also suggested that no LVZ is found within 200 km depth in the Australian shield whereas in eastern Australia, a LVZ occurs near 120 km depth.

B) Electrical conductivity, their application in the Australian continent

The nature of lithosphere and/or transition of lithosphere-asthenosphere can be estimated from electromagnetic properties. Many electromagnetic studies suggest that upper mantle beneath many tectonically active areas are characterised by a high conductivity layer (Law and Greenhouse, 1981; Lilley *et al.*, 1981; Belbo *et al.*, 1983). The conductors in this level may be contributed to the presence of partial melting (Shankland and Waff, 1977), the existence of water (Tozer, 1981), and of carbon (Duba and Shankland, 1982) in addition to the influences of temperature and pressure (Karato, 1990).

The main constituent minerals of the upper mantle are olivine and pyroxene (Duba *et*

al., 1973). Laboratory measurements of single or polycrystalline olivine and/or dunitic rock fragments investigated the properties of peridotic rock as a primary constituent of the upper mantle (Duba, 1972; Duba *et al.*, 1974; Shankland and Waff, 1977; Hirsch and Wang, 1986; Constable and Duba, 1990). The estimated electrical conductivity at high temperatures can provide important constraints to models of the thermal states and physical properties of the Earth's interior in combination with conductivity profiles with depth (Hirsch and Wang, 1986).

However, the results are highly variable. The reasons include the role of grain boundaries, including surface defects and impurities (Duba *et al.*, 1974; Kay and Kay, 1981; Keller, 1987), fo_2 dependence of the conductivity (Duba *et al.*, 1974; Hirsch and Wang, 1986; Constable and Duba, 1990), the difference of measured results between polycrystalline rocks and single crystals (Keller, 1987), and kinetic processes in silicate minerals caused by the dissolution of hydrogen (Giletti and Yund, 1984; Mackwell *et al.*, 1985; Karato *et al.*, 1986; Karato, 1990).

Despite these problems, upper mantle electrical conductivity could be considered in terms of earth dynamics, including mantle convection and other transport phenomena rather than upper mantle conductivity considered as representative of the upper mantle modelled on olivine assumed in a static earth (Tozer 1979; Finlayson, 1982). Tozer (1979) suggested that low temperature solution in lithospheric processes is regulated by viscosity rather than being controlled by thermal transport process and that conductivity of the upper mantle is changed by small scale chemical heterogeneities, or by fluid inclusions. Thus, on a local scale, there may be significant variation in the conductivity of composite mantle materials.

Shankland and Waff (1977) modelled the bulk conductivity of the upper mantle by an effective medium theory which allow identification of mantle regions of anomalously high electrical conductivity which are mainly associated with continental tectonic regions. Their results supported the existence of zones of partial melting (anomalous conductivity) under coninental rift zones, volcanic belts, high geothermal areas, and beneath the oceans.

More recent investigations of the conductivity anomalies of the deep lithospheric to upper asthenospheric level (Peyronneau and Poirier, 1989; Wood and Nell, 1991) have suggested that the dominant electrical conductor of the Earth's lower mantle, from a depth of 670 km down to the core-mantle boundary (2,990 km), reflected properties of perovskite (Mg, Fe) SiO_3 and magnesiowustite, (Mg, Fe) O.

The conductivity studies of the Australian lithosphere were summarised by Constable (1991). In general, their geographical distributions are mainly concentrated to a belt from north central Australia, south eastern margin of Australia, and southern parts of Western Australia. In these reviews, Constable (1991) indicated that the conductivity anomaly layer occurred at a depth of 90-200 km in the most of area. Probably it may represent the base of the lithosphere, and layers at many sedimentary basins (resistivity of 1-10 Ωm) reflecting high salinity of groundwater and pargasites in the sediment.

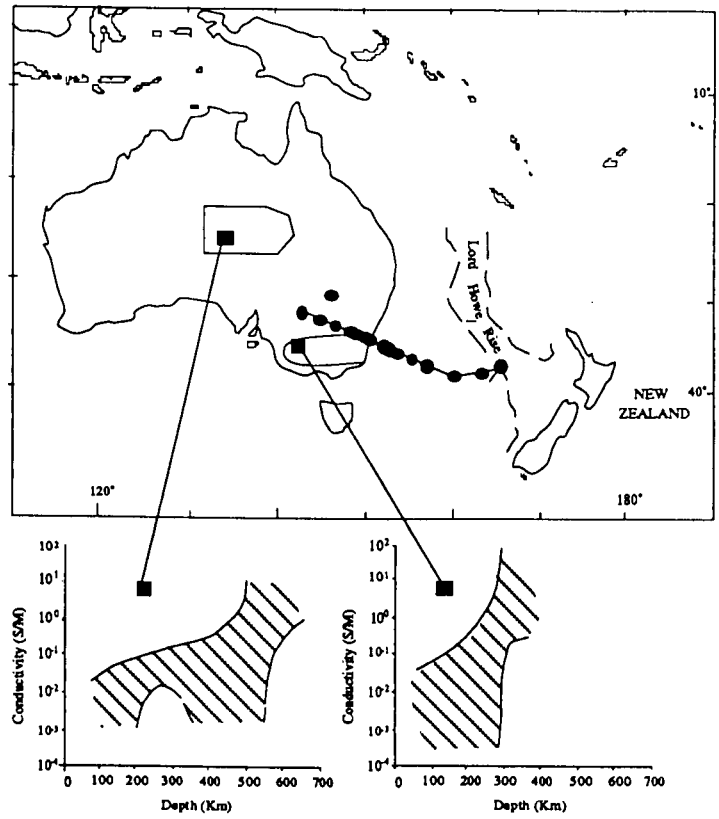

Fig. 1.1. Electrical conductivity models of central Australia and southeast Australia which show considerably different lithospheric structures (Lilley *et al.*, 1981).

Constable (1991) concluded that were clear distinctive structures are shown within the sub-basement lithosphere, except in some localities with a conductivity anomaly. No evidences were found for the electrical Moho.

Tammemagi and Lilley (1971) suggested that increase of the conductivity across the Lachlan Fold Belt from Moruya to Griffith in N.S.W. reflected a temperature difference at a depth of about 200 km. Constable, (1991) suggested that these results are consistent with the heat flow compilation of Cull (1982a) which showed a difference of up to 30 m w/m^2 across the Lachlan Fold Belt. Electrical studies of the Officer (Jupp *et al.*, 1979) and Cooper Basins (Moore *et al.*, 1977) also indicated the existence of anomaly at 200-250 km depth, and 90 km depth respectively, suggestive of the base of the lithosphere.

Clear interpretations of the lithospheric structures of the Australian continent have been provided by Lilley *et al.* (1981) and Lilly (1991). Lilley *et al.* (1981) indicated that major conductivity increases at about 200 km depth in the southeast Australia while the conductivity increase is not shown in central Australia until 500 km depth (Fig. 1.1). They interpreted that a conductivity anomalies at 200-300 km depth beneath SE Australia reflects a partial melting zone while absence of the zone beneath central Australia reflects a crystalline upper mantle.

Lilly (1991) provided a comparison of depth of the asthosphere between the Australian continent and the adjacent Tasman sea with an electrical conductivity estimate (Fig.

1.1). In this comparison, he indicated a steep asthenospheric downward trend from beneath the SE Australian ocean to beneath the Australian continent. He suggested that the results are consistent with a traditional continental geotherm and published laboratory measurements of the electrical conductivity for the recognised upper-mantle crystalline olivine materials. It was also suggested that this result is consistent with the seismic profile in southeastern Australia (Muirhead *et al.*, 1977), showing a zone of low seismic primary velocity in the depth range 155-190 km. Lilly (1991) interpreted that a higher conductivity in the depth range 200-300 km beneath southeastern Australia is effected by the presence of a partial melting zone of basalt.

These results of geomagnetic spatial gradient experiments in southeastern and central Australia provide significantly important constraints to characteristics of lithospheric structure between Precambrian and Phanaerozoic terrains. Thus these studies have been widely accepted by many scholars, who want to interpret to nature of Australian lithosphere (Finlayson 1982; Veevers, 1984; O'Reilly and Griffin, 1985).

1.4.2. Shallow lithospheric structure in the Australian continent

A) Crustal heterogeneity by heat flow evidences

Generation of surface heat flow relies on the decay of radioactive isotopes contained in crustal rocks, including K, U and Th as well as the flows of heat into lithosphere from the asthenosphere. The heat flow of shallow lithospheric structures are measured in boreholes at depths greater than 100 m.

Generally, the heat flow data show correlation with the age of the rocks. For examples, measurable values are about 41 mWm^{-2} in Archaean provinces, 51-54 mWm^{-2} in mid-Palaeozoic to the Proterozoic provinces and 72 mWm^{-2} in Mesozoic and younger rocks (Taylor and McLennan, 1985). As a result, the distributions of heat flow anomalies are concentrated on Phanerozoic tectonic belts, which are mainly related to mantle convection and/or mantle plumes as for eastern Australia (Cull, 1982b).

Surface heat flow data across Australia have been compiled by Cull and Denham (1979). These heat flow data show regional variation, suggestive of crustal heterogeneity (Fig. 1.2). In general, the measured heat flow data range from 30 to 120mWm^{-2}, but show a common range of values 30-60 mWm^{-2}. The results divide Australia into two areas along the Tasman line, the eastern Phanerozoic fold belt and the western Precambrian terrains. High heat flow anomalies ranging from 70 to 100 m Wm^{-2} are observed in regions of recent volcanism and of recent tectonism in northern Queensland and western Victoria whereas negative heat flow anomalies below 60 mWm^{-2} are observed at relatively stable Archaean and Proterozoic area of Western Australia. Distinctive high heat flow anomalies are also observed in the north of Spencer Gulf in South Australia, near Tennant Creek in Northern Territory and in eastern Tasmania, while distinctive lower heat flow anomalies are observed in the recharge margins of the Great Artesian Basin.

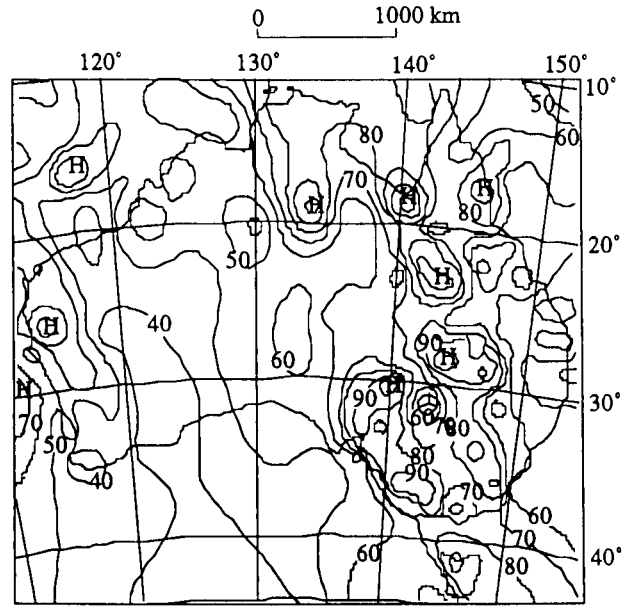

Fig. 1.2. Measured heat flow values in mW/m^{-2} contoured using 1° grid (Cull, 1982a).

O'Reilly and Griffin (1985) suggested that the high heat flow anomalies in eastern Australia were initiated by conductive heat transport associated with the crustal thinning associated with continental rifting and basaltic volcanism of eastern Australia. The hypothesis may support the coincidence in time of the basaltic activity in eastern Australia and the Tasman Sea opening together with basaltic provinces with the tectonic uplift of the eastern continental margin (Wellman, 1979; Jones *et al.*, 1983). The heat flow anomaly near Tennant Creek may be caused by the higher concentration of radioactive materials in the crust, and that near Great Artesian basin may result from the large scale vertical movement of heated water in sedimentary basins (Cull and Denham, 1979).

The heat flow data shows positive correlation with P-wave travel time residuals and negative correlation with upper mantle seismic velocity (Pn), suggesting that the mantle in lower heat flow regimes (lower NP velocity) is cool relative to high heat flow regimes (Mathur, 1974; Collins, 1978). However, correlation between heat flow and crustal thickness is not clear (Collins, 1991), suggesting that there are not linear relationships among the heat flow, crustal thickness and surface heat flow production at surface rocks of all over Australian continent.

B) Magnetic studies in the shallow lithospheric structures

Magnetic properties provide another tool with which to examine the nature of local or regional variations in the rock type and temperature at sub surface level. Rock magnetism depends on the kinds and quantity of magnetic minerals, (magnetite, haematite, limonite etc.). Magnetite strongly influences local magnetism because the main rock-forming silicate minerals are non- magnetic.

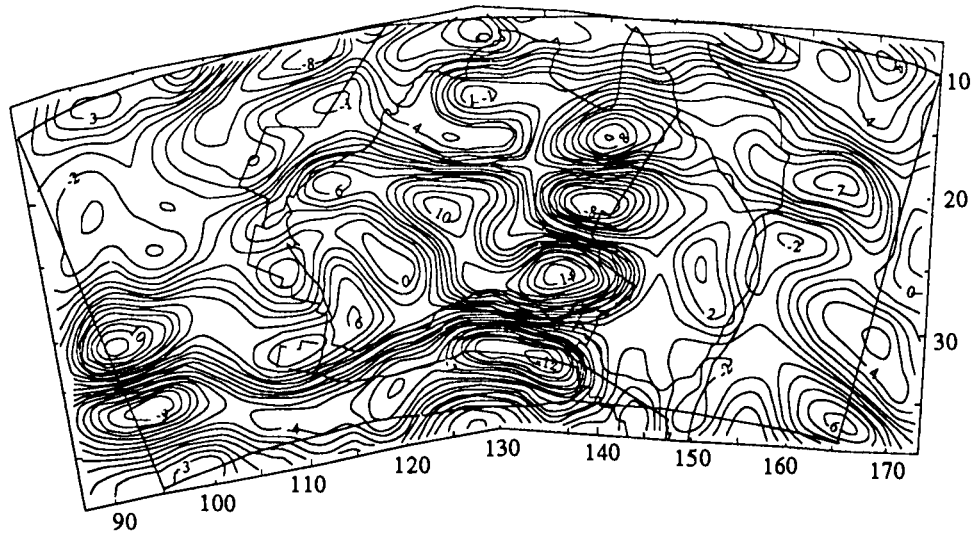

Fig. 1.3. Contours map of magnetization distribution based on Magsat data which show a separation of Australia along the Tasman line (Mayhew and Johnson, 1987).

Wellman *et al.* (1985) provided a review of the long-wavelength magnetic anomaly data with its comparison with a map of long-wavelength crustal properties determined from 400 km altitude using the MAGSAT satellite over Australia (Langel *et al.*, 1982). Mayhew and Johnson (1987) provided an equivalent layer magnetisation model for Australia and the adjacent oceanic area which was obtained by linear inversion of MAGSAT anomaly data (Fig. 1.3).

These two studies suggest that the magnetisation anomalies reflect certain major structural features of the Australian continent and a distinctive difference is seen at the east and west of Tasman line drawn by Powell (1984). In general, magnetisation anomalies show large amplitude in the Precambrian cratonic region while that in the Tasman zone is subdued, partly, suggestive of the different depths of the Curie isotherms in the Tasman zone. The magnetic high in central and western Australia is mainly associated with crustal block boundaries defined by elongated gravity anomaly trends (Wellman, 1978) whereas in eastern Australia, the anomaly correlates with areas of exposed basement (Wellman *et al.*, 1985).

The low magnetic anomalies in eastern Australia are mainly consistent with the major post-cratonisation sedimentary basins of Phanerozoic age, including Carpentaria Eromanga, and Murray Basins (Mayhew *et al.*, 1980) and those in Western Australia, but, generally correspond with the major post-cratonisation sedimentary basins of Proterozoic age (Wellman *et al.*, 1985).

The long-wavelength magnetic anomalies show clear correlation with the heat flow data of Cull and Conley (1983) and seismic refraction determination of crustal thickness (Wellman 1982; Finlayson *et al.*, 1984). The best examples of these are observed in south eastern Australia where high heat flow coincides with high magnetic anomalies and in the central part of western Australia where low heat flow coincides with low magnetic anomaly.

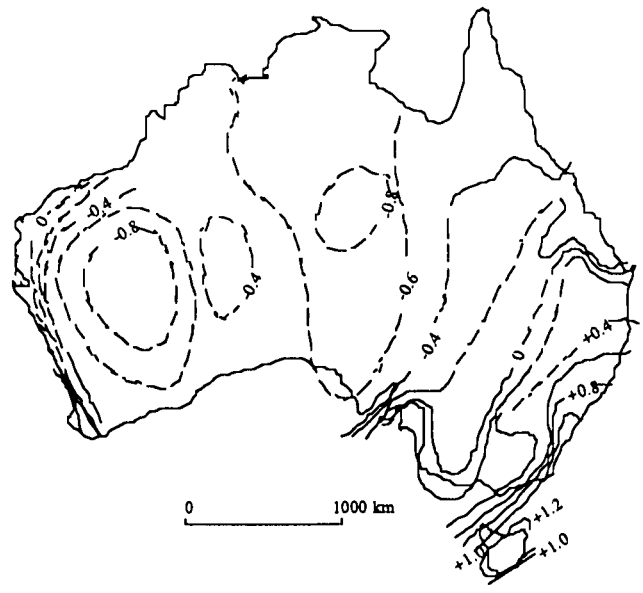

Fig. 1.4. Teleseismic travel time residuals of Australia reflecting the different lithospheric structures between Phanerozoic eastern Australia and western shield area divided by the Tasman line (Drummond *et al.*, 1989).

C) Teleseismic travel time studies

A study of the teleseismic travel time residuals also shows differences of structure in the upper mantle level within the Australian continent, possibly below 200 km depth (Drummond *et al.*, 1989). The teleseismic travel time residuals (Fig. 1.4) suggest that the deep lithospheric nature of the Australian continent is different along the Tasman line. The boundary between two regions corresponds approximately to the easternmost -0.4 s contour. Generally, the older Precambrian shield of central and western Australia has smaller residuals (negative) than those of Phanerozoic eastern Australia (positive). The maximum negative residuals in shield regions lie in the Yilgarn block in Western Australia and adjacent to the Arunta block in northern Australia while the largest positive residuals lie in the southeastern margin in eastern Australia and Tasmania.

The differences of the residuals are consistent with the presence of a lower velocity zone in the upper mantle in the Phanerozoic eastern Australia region and correlate with published geotherm gradients of Cull and Conley (1983) (Drummond *et al.* 1989). Drummond *et al.* (1989) indicates that the lowest residuals in the shield regions correspond to areas of low surface heat flow while the greatest residuals in Phanerozoic eastern Australia province correspond to high heat flow regions. They also suggested that these differences reflect the variations of seismic velocity with temperature.

D) Density variations and isostatic compensation in the Australian continent

Comparisons of elevation and free air anomaly of Anfiloff (1982), and of density

inferred from seismic refraction velocities and estimated mass in each depth profile of Dooley (1991) suggest that at least, some regions of the Australian continent are not in isostatic equilibrium. Anfiloff (1982) provides a comparison between elevation and gravity profiles along latitudes and latitudes across Australia (Fig. 1.5). To illustrate isostatic equilibrium, there must be a positive correlation between elevation and gravity profiles. However, no uniform relationships are found in overall topographic relief compared with bouguer gravity anomalies and free-air anomalies, with the exception of the highlands in eastern Australia.

In the elevation profiles of the eastern highlands, especially 136-152 °E longitudes (along latitudes 35 and 36 °S) and 10-44 °S latitude (along longitudes 144-147 °E), good positive relationships are seen among elevations, free-air anomalies and bouguer anomalies. The exposed Precambrian blocks and fold belts on the west of Tasman line show a more complicated correlation.

Dooley (1991) reviewed published seismic refection velocity profiles and attempted to show whether the Australian continent shows isostatic compensation. Dooley's results (1991) also showed that isostatic compensation is not complete at the base of the crust. He suggested that in eastern Australia, isostatic compensation probably occurs in the upper mantle level, at depths of about 110-130 km whereas in the shield area of Western Australia, isostatic compensation did not occur completely until 150 km depth.

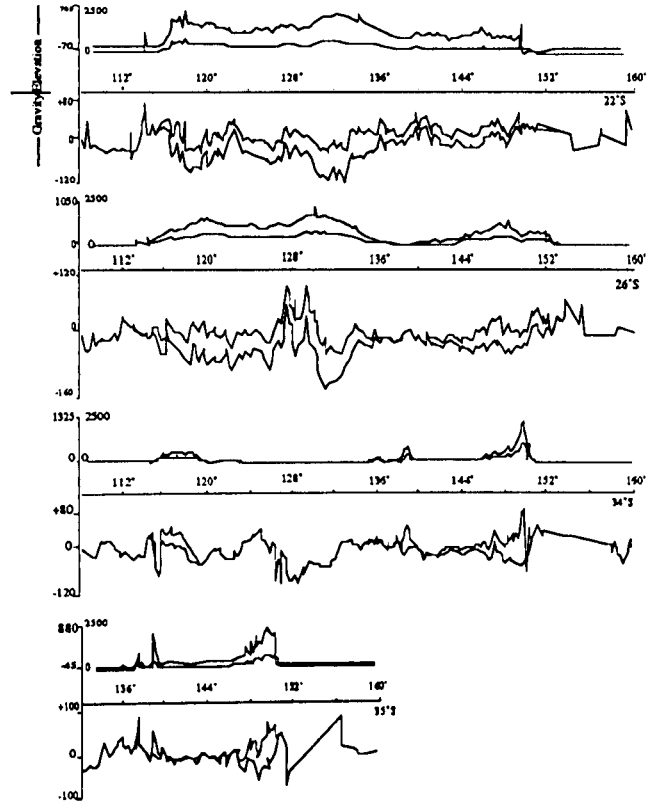

Fig. 1.5. Elevation (upper) and gravity (lower) profiles across Australia as latitudes 22 °S, 26 °S, 34 °S and 35 °S (modified from Anfiloff, 1982).

These compensation depths correspond to the evidence of S-wave velocity studies, showing the existence of a low velocity zone at about 110 km depth under eastern Australia and no clear evidence for the existence of a low-velocity layer in the shields area of Western Australia. Dooley (1991) suggested that the shield area has a dense crust underlain by lithospheric material with high velocities and that as a result, a relatively high-density upper mantle or high strength materials at depth is required to compensate the dense crust. He also suggested that estimated depths of compensation tend to increase with the age of the crust, consistent with a cooling and thickening lithosphere.

E) Moho in the Australian continent

The definition of the, "Moho" of the Australian continents is based on the following seismic, electromagnetic, petrologic and chemical properties.

1. Seismic Moho corresponds to a phase change from spinel lherzolite to garnet lherzolite whereas petrologic Moho is observed by a transition of the seismic velocity. Thus petrologic Moho is shallower than the seismic Moho (O'Reilly and Griffin, 1985; Griffin *et al.*, 1987).
2. In Precambrian or Palaeozoic areas including the Pilbara block, the petrologic Moho layer corresponds to a phase change of lower crustal mafic rocks to eclogite facies rocks (Griffin and O'Reilly, 1987b).
3. The petrologic Moho may be a zone of discrete bodies such as intrusions (Collins, 1991).

a) Seismic definition of the Moho

Published seismic profiles of Australia have been summarised by Collins (1988) and shear wave models and P-wave models are reviewed by Denham (1991) and Collins (1991), respectively. The results (Fig. 1.6) show that Moho depths in the Australian continent range from 25-56 km (mainly 34-50 km depths) in which the Pn velocity ranges from 7.81-8.47 km/s (mainly 8.0-8.25 km/s). In addition, shear wave velocities vary from 4.55-4.60 km/s in the uppermost mantle through 3.8-4.2 km/s in the lower crust to 3.4-3.6 km/s in the upper crust.

However, the Moho layer is largely divided into two groups in the Australian continent; a shallow but sharply defined Moho discontinuity beneath stable cratonic regions, and a deeper, thicker transitional Moho in tectonically active regions. The Pn velocities also separate the Australian continent along the Tasman line, with low Pn velocities in the shield regions of Western Australia and high Pn velocities within the Tasman Geosyncline (Collins, 1991). Each crustal block defined by the last major tectonic events (Wellman, 1978) show different transverses in velocity/depths curve, indicating the heterogeneity of the crustal block.

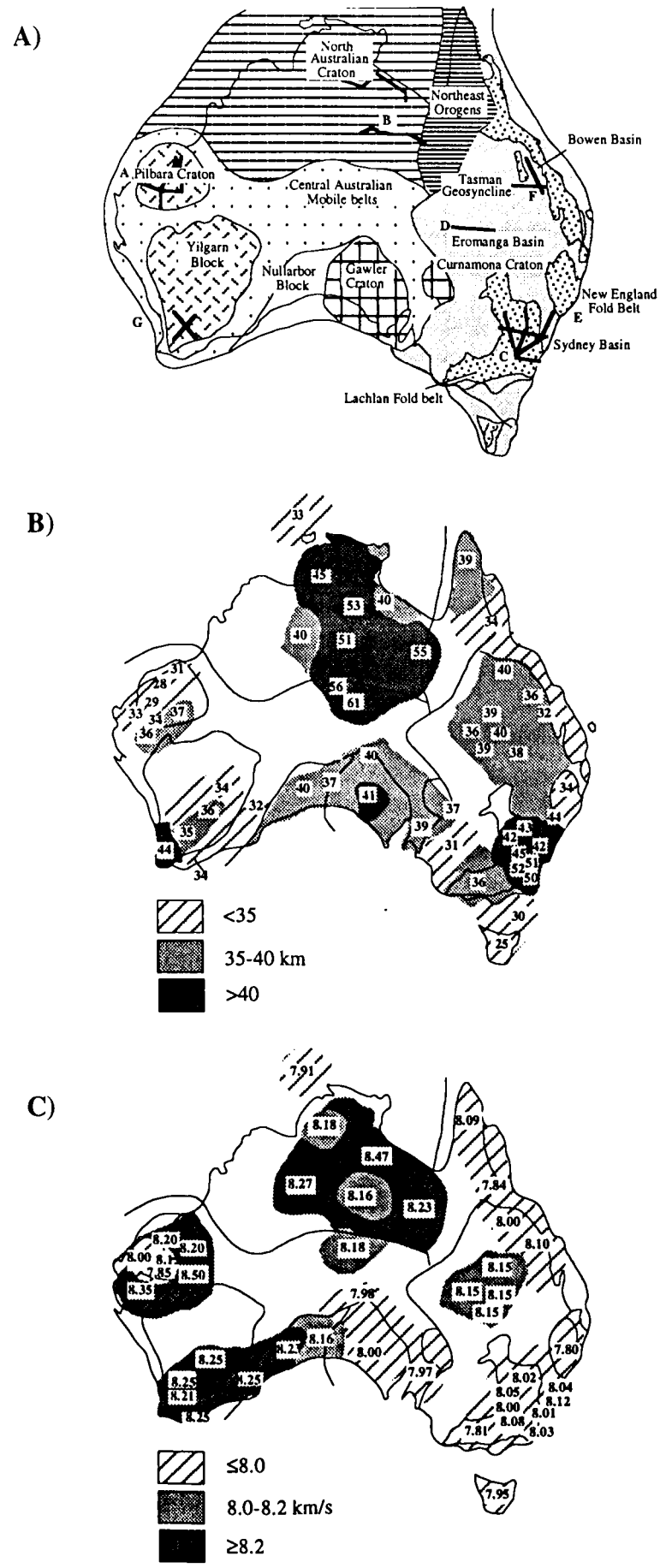

Fig. 1.6. A) Major geological province boundaries, B) Moho depths, C) Pn velocities by Collins (1991). B and C based on the summary of Collins (1988).

Collins (1991) also indicated that regions in which the Moho transition is most gradational coincide with areas of deeper Moho such as the Lachlan Fold Belt (42-52 km depths) and north Australian craton and central Australia (45-61 km depths). They are compared with the sharp and shallow Moho beneath the Archaean Pilbara Block (28-34 km depths) and Mesozoic Bowen Basin (32-34 km depths).

However, there is a clear negative correlation between Pn velocity and the heat flow of Cull and Denham (1979), except in the North Australian craton and the Eromanga Basin (Collins, 1991). The trend may be related to the higher geothermal gradients observed in eastern Australia (Dooley, 1971) due to temperature dependence of seismic velocities (Jackson, 1991). No clear correlations are also shown between Moho depth and heat flow as well as between Moho depth and Pn velocity (Collins, 1991). Collins (1991) interpreted that the north Australian craton near Tennant Creek may have a higher heat flow due to concentrations of radioactive isotopes in the crust, while the high heat flow of the Eromanga Basin resulted from the large-scale vertical movement of heated ground water at its southwestern margins. The Moho depth in Australia increases with age, like the European data of (Meissner *et al.*, 1987), with the exception of the Archaean Pilbara craton and Yilgarn Block. This corresponds to the trend observed in Australia which has been result of thickening of lower crust, probably by underplating (Drummond and Collins, 1986).

Reviews of the S-wave crustal models for the Australian continent suggest that depth of the Moho ranges from 38-40 km and no clear relationships are shown between age and depth (Denham, 1991). Generally, upper crustal velocities range from 3.4 to 3.6 km/s, lower crustal velocities range from 3.8 to 4.2 km/s, and uppermost mantle velocities range from 4.55 to 4.6 km/s. Models of surface wave paths across the Australian continent by Ellis and Denham (1985) showed that the upper crust in eastern Australia is thicker and has lower velocities relative to Western Australia.

Studies of the South Australian lithospheric structure suggest a Moho depth of 35 - 40 km and seismic velocities, P1 (crustal level) of 6.0 - 6.3, Pn of 7.97 - 8.21 (S1 of 3.55-3.58 and Sn of 4.56-4.75 km/s) (Bolt *et al.*, 1958; Thomas, 1969; White, 1969, 1971; Denham *et al.*, 1972; Stewart, 1972; Finalyson *et al.*, 1974; Shackleford and Sutton, 1981). More recent, Greenhalgh *et al.* (1989) have provided a tomographic velocity map of the South Australian area. They suggested that the crustal velocity lies in the range of 5.9-6.5 km/s and the Moho velocity is approximately 7.97±0.4 km/s under the Adelaide Geosyncline area. These results suggest that there are lateral variations in the crustal thickness and seismic velocity, Proterozoic sediment within the upper 20 km of the crust and variation of Moho depth on the order of 10 km within the Adelaide Geosyncline. They also suggested that there is a low crustal velocity and gravity anomaly in a N-S trending zone over the Spencer Gulf graben, at the western boundary of the Geosyncline. Greenhalgh *et al.* (1989) also indicated deep Moho and/or lower crustal velocities under most of Spencer and St Vincent Gulf, shallow Moho and/or high crustal velocities under Eyre Peninsula and a

shallow Moho and/or high crustal velocity along the meridional axis of the N-S trend in the Adelaide Geosyncline. They concluded that the high velocity together with the gravity trend in the northern end of the Flinders Ranges reflect the dense mafic core of a rift zone, while the lower velocity beneath the Stuart shelf and Adelaide Fold Belt suggests thin crust.

b) Petrological Moho

Studies of xenoliths from Cainozoic alkaline basalts in Phanerozoic eastern Australia suggest that the Moho layer shows a transitional variation in the range of 25-55 km depth (O'Reilly and Griffin, 1985; Griffin *et al.*, 1987). The xenolith studies suggest that the crust-mantle transition zone consist of mixture of mafic and ultramafic rocks, including spinel lherzolite, pyroxenite, websterite and/or garnet granulite with an increase in the relative abundance of the ultramafic rocks with depth. A phase transition from spinel lherzolite to garnet lherzolite occurs at a depth of about 55 km defined as the seismologic Moho (O'Reilly and Griffin, 1985). Xenolith studies of eastern-central Queensland suggest that the lower crust as defined by seismic reflection ranges from 20 to 36 km and the lithologically-defined Moho lies at least 6 km above the seismological-defined Moho (Griffin *et al.*, 1987). This interpretation for the deep lithosphere in eastern Australia may be supported by the wave velocity of the mantle xenoliths measured under controlled physical conditions (O'Reilly *et al.*, 1990).

The validity of a xenolith defined crust-mantle transition is questioned by some workers (McDonough *et al.*, 1991; Cull, 1991). McDonough *et al.* (1991) questioned whether garnet pyroxenites used to determine the geotherm of eastern Australia are fully equilibrated with spinel lherzolite. Cull (1991) indicated that Moho depth may not influence the geothermal gradients in similar petrological columns such as central-western Victoria (higher geothermal gradients and deep Moho) and northern Tasmania (high geothermal gradient and shallow Moho).

1.5. Mafic-ultramafic xenoliths as evidences for accretion of shallow lithospheric structures

1.5.1. Granulitic and eclogitic xenoliths, granulite and eclogite facies metamorphic rocks

It is generally accepted that the main constituents of the lower continental crust are as mafic dominant rocks including eclogite and granulite rocks. The xenoliths are hosted by world wide kimberlitic and intraplate basalts. Studies of the lower continental crust can be undertaken using exposed high grade metamorphic facies. They include Ivrea-Verbano and Stronaa-Ceneri zones, Fraser Range, Musgrave Range, Pikwitonei and Cross Lake subprovinces, Kasila Group, and Adirondark area (Fig. 1.7). The high grade metamorphic terrains are tectonically uplifted deep crust and they may be assumed as representatives of the

lower crustal components (Fountain and Salisbury, 1981).

The high grade metamorphic terrians provide a horizontal and vertical lithological change with depth which can not be obtained by the xenoliths. In general, the exposed cross-sections show a increasing metamorphic grade with depth from greenschist and amphibolite, to granulite facies, although lateral and vertical heterogeneities are present at a variety of scales (Fountain and Salisbury, 1981). Geophysical studies (Berckhemer, 1969; Salisbury and Fountain, 1976; Weaver and Tarney, 1980) indicate that the exposed metamorphic terrains are similar in geophysical nature to granulitic xenoliths entrained from deep seated magmas. Thus, studies of granulite facies metamorphic rocks from tectonically exposed high grade terrains can provide a useful comparison to the lower crustal rocks obtained from basaltic and kimberlitic host rocks.

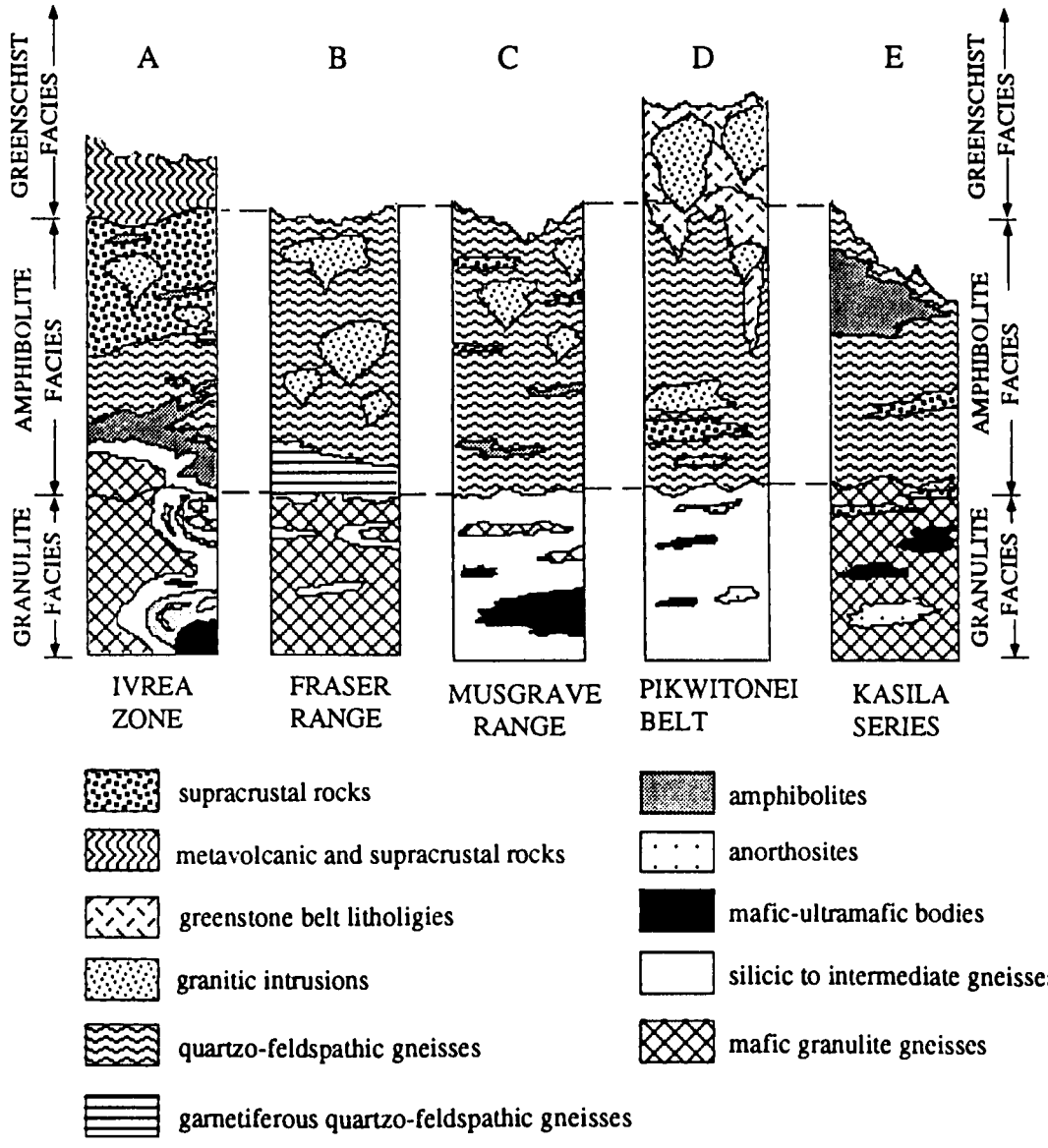

Fig. 1.7. Cross-sections of continental crust based on geological data for (a) Ivrea-Verbano and Strona-Ceneri Zones, (b) Fraser Range, (c) Musgrave Range, (d) Pikwitonei and Cross Lake subprovinces, and (e) Kasila group. (by Fountain and Salisbury, 1981)

Eclogitic xenoliths also can be compared with the eclogite facies metamorphic rocks which are defined in the order of the metamorphic grade by Eskola (1920). The metamorphic rocks contain the red-brown pyrope rich garnet and glass-green omphacitic pyroxenes. However, the eclogite facies metamorphic rocks are not common in the continental crust and do not occur as outcrops of regional scale. Their principal modes of occurrence are as follows (Hyndman, 1972; Miyashiro, 1973; Coleman *et al.*, 1965).

A) dominantly, as inclusions in alkali olivine basalt or kimberlite pipes, or layers in ultramafic rocks,

B) as layers, lenses, or bands in higher temperature metamorphic rocks including amphibolite and granulite terrains,

C) as lenses, bands, small massifs and layers up to 500 km in amphibolite facies rocks.

D) as randomly distributed pods in blueschist-greenschist-serpentinite terrians.

The first type of eclogite originates from lower crust-upper mantle level whereas the second two originate from the metamorphism of crustal material, commonly from recrystallised basaltic material. Last type would results from the conversions of oceanic crust and underlying lithosphere at deeper zones in subduction complexes.

1.5.2. Experimental results for the studies of the shallow lithospheric structure

A large number of laboratory studies suggest the appropriateness of the approach with the metamorphic facies rocks for the deep seated xenoliths (Birch, 1960, 1961; Manghnani *et al.*, 1974; Christensen and Fountain, 1975; Jackson and Arculus, 1984; O'Reilly and Griffin, 1985; Jackson *et al.*, 1990; O'Reilly *et al.*, 1990). Their results are summarised in the Table 1.1.

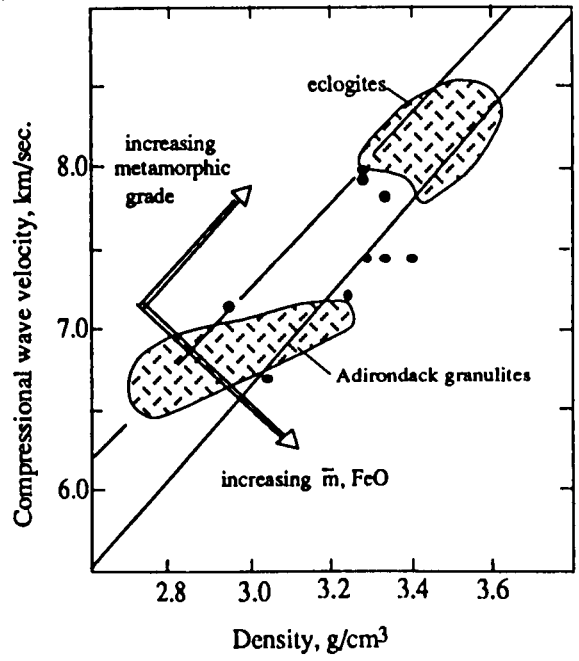

Fig. 1.8. Velocities of Calcutteroo xenoliths (Jackson and Arculus, 1984) plotted in between silicic granulites and mafic eclogites estimated by Manghnani *et al.* (1974).

in between silicic granulites and mafic eclogites estimated by Manghnani *et al.* (1974).

Table 1. 1. Summary of the estimated velocities for eclogitic and granulitic rocks.

Rock Type	4 Kbar		10 Kbar		Referance
	Vp	Vs	Vp	Vs	
Eclogite	7.73-8.38	4.2-4.78	7.73-8.53	4.23-4.86	Ma
	7.4-8.06	4.1-4.52			Ja
	7.52-7.98	7.97-8.07			Bi
	8.11-8.38	8.27-8.45			Ch
Granulite	6.43-7.23	3.45-4.13	6.5-7.4	3.5-4.2	Ma
	6.67-7.95	3.74-4.54			Ja
			6.86-7.04	3.53-3.7	O'R,a
Amphibolite	6.72-7.59		6.83-7.66		Bi
Dunite	7.5-8.1		7.6-8.3		Bi
Pyroxenite	7.6-8.1		7.8-8.2		Bi
			7.77-7.95	3.98-4.14	O'R,a
	7.66		7.93		O'R,b
			7.67-7.73		O'R,b
Hyd,Lherzolite			**7.56-7.94**	4.02-4.17	O'R,a
			7.68-7.74		O'R,b
Anhy,Lherzolite			**7.72-7.91**	4.11-4.27	O'R,a
Ol-rich-	7.8-8.1		*8.32-8.47*		O'R,b
Lherzolite			*7.86-7.92*		O'R,b
Ol-poor	7.5		8.11		O'R,b
Lherzolite			*7.78-7.84*		O'R,b
Gt Lherzolite			*7.98-8.04*		O'R,b

Data sources, Ma = Manghnani *et al.* (1974), Ja = Jackson and Arculus (1984), O'R, a = O'Reilly and Griffin (1985), O'R, b = O'Reilly *et al.* (1990), Bi = Birth (1960), Ch = Christensen (1975). (Bold = 300 1100 ℃, Italic = 7.5-21.8 Kbar, 800-1160 ℃, 25-70 km depth).

In general, lower crustal xenoliths at 1000 Mpa show Vp of 7.83-8.53 km/s and Vs of 4.23-4.86 km/s for eclogitic rocks and Vp of 6.5-7.4 km/s and Vs of 3.5-4.2 km/s for granulitic rocks. Their adjusted values to in situ lower crustal velocities (800 °C) following the idea of Jackson and Arculus (1984) are $7.43 < Vp < 8.13$ km/s and $3.93 < Vs < 4.56$ km/s for eclogitic rocks, and $6.1 < Vp < 7.0$ km/s and $3.2 < Vs < 3.9$ km/s for granulitic rocks. These ranges are consistent with those of lower crustal xenoliths from Calcutteroo (Fig. 1.8). The Vs of the South Australia (Jackson and Arculus, 1984) are plotted between the silicic granulite and eclogites measured by Manghnani *et al.* (1974). This consistency suggests that estimated seismic velocities of the granulitic and eclogitic metamorphic rocks may result in the velocities observed in the lower crust.

In contrast, velocities of mantle-derived xenoliths show Vp of 7.7-8.5 kms^{-1} and Vs of 3.9-4.3 kms^{-1} at 10 kbar. The wave velocities increase from pyroxenite, olivine-lherzolite, to garnet-lherzolite. Among the olivine lherzolites, hydrous lherzolite containing phlogopite has slightly lower compressional wave velocities. The compressional wave velocities of lherzolite, pyroxenite and mafic granulite are lower than expected for the lower crust and upper mantle level by seismic velocity. O'Reilly and Griffin (1985) and O'Reilly *et al.* (1990) interpreted these differences as effects of the magnesium contents in the lherzolite, the high hydrous mineral content of many xenoliths, the porosity of the rocks, and the P-T conditions. O'Reilly *et al.* (1990) also suggested from xenoliths geothermobarometry that

rock type at depths of about 30-60 km, in a temperature range of 850-1050 °C beneath eastern Australia.

1.5.3. Ideal shallow lithospheric structures in Australia based on the empirical estimates of deep seated xenoliths and seismic data

Two different models (Fig. 1.9) have been suggested for the shallow lithospheric structure of south eastern Australia (Ferguson *et al.*, 1979; Griffin *et al.*, 1984). A model by Griffin *et al.* (1984) proposes that mafic granulite is present in the 10-20 km depth, with transitional variation of mafic to ultra basic rocks in the range of 25-55 km and garnet lherzolites greater than about 55 km depths. An alternative model proposed by Ferguson *et al.* (1979) predict felsic and mafic granulites at the depths of 15 and 25 km respectively and a transition of mafic granulites to eclogitic or pyroxenites in the range of 25-50 km. Spinel lherzolite is thought to dominate below about 50 km until garnet lherzolite appears at a depth of 65 km.

An idealised cross-section of the Adelaide Geosyncline area (Fig. 1.9) shows Proterozoic strata to about 18 km depth, felsic granulites to 25 km and dominantly mafic granulites to 48 km depth with minor eclogites and pyroxenites (Ferguson *et al.*, 1979). Eclogites and pyroxenites occur from 48 to 60 km depth and spinel lherzolites occur to 65 km depth until garnet lherzolites appear.

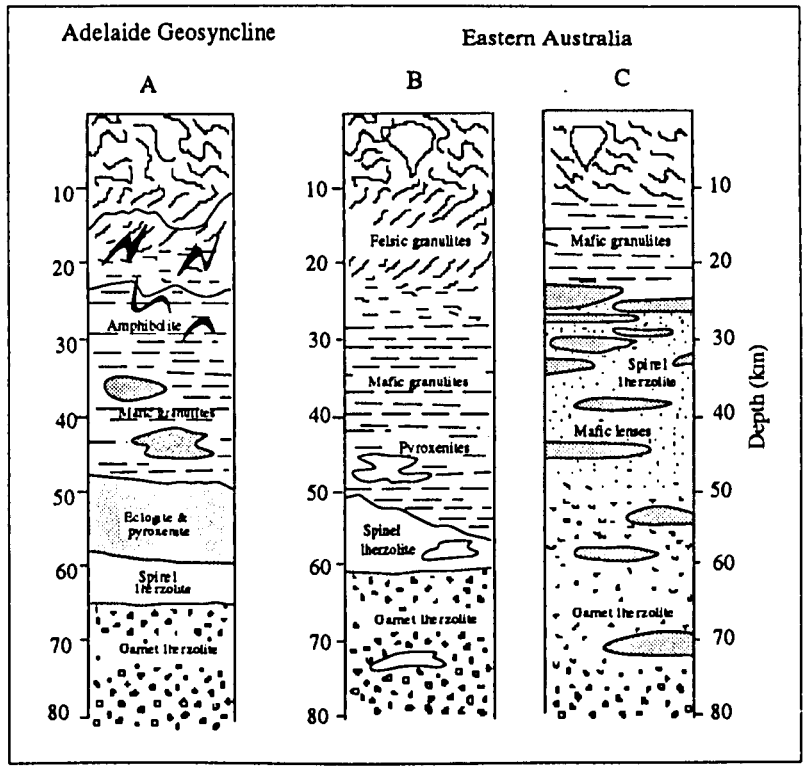

Fig. 1.9. Idealised shallow lithospheric structure of southeastern Australia and Adelaide Geosyncline (Ferguson *et al.*, 1979 for A, B; Griffin *et al.*, 1984 for C).

In the models of Ferguson *et al.* (1979), clear differences exist between eastern Australia and Adelaide Geosyncline area. Most obvious are the existences of the eclogite and pyroxenite layer, deep spinel lherzolite layer and thick Proterozoic strata in the Adelaide Geosyncline area. O'Reilly and Griffin (1985), with petrophysical evidences of O'Reilly and Griffin (1985) and O'Reilly *et al.* (1990), criticised a model of lithospheric structure provided by Ferguson *et al.* (1979) showing a very thick mafic granulite layer underlain by a very thin zone of spinel lherzolite.

However, neither of two contrasting models provide the shallow lithospheric structures beneath Palaeozoic Adelaide Geosyncline area. These models can not provide two obvious characteristics; a) the rare occurrences of garnet or spinel lherzolites among crustal xenoliths entrained from Mesozoic kimberlites which are derived from deep enriched lithosphere (see Chapter 5, 6); b) differences of lithospheric structure and of dominant xenolith type between Phanerozoic eastern Australia and Palaeozoic Adelaide Geosyncline system (see Chapter 6).

1.6. Conclusion

Several aspects of the lithosphere and asthenosphere have been reviewed here. The lithosphere is rigid outer shell of Earth and behaviours as an elastic layer which compensates mountain building or surface loading. The underlying asthenosphere is a viscous or plastic layer and support flexing or bending of the lithosphere. The lithosphere is heterogeneous and mechanism of heat transfer is dominantly by conduction whereas the asthenosphere is geochemically and isotopically homogeneous and convection is the principal thermal mechanism. The lithosphere shows differences between ocean and continent and a variable age structure.

The oceanic lithosphere is simply converted from asthenosphere by cooling without considerable change of chemical composition and its thickness is controlled by the loss of heat from convecting upper mantle. In contrast, the thickness of the continental lithosphere is governed by its ages and its thermal structures varies at different tectonic regions. Continental lithosphere is deeper beneath Archaean cratons than that beneath the oceanic or continental area undergone late Proterozoic or Phanerozoic orogeneies.

The lithosphere is defined in terms of seismological, rheological, termperature, geochemical and petrological aspects. The base of the seismic lithosphere is defined as the depth of the low velocity layer caused by partial melting and is consistent in temperature at about 1300 °C. The existence of the partial melting is supported by experimental evidence of small melt fractions under the mantle P-T conditions. Rheologically, the lithosphere is a layer in which stress of lithosphere can be compensated by flexure. However, lithosphere is sufficiently strong to redistribute stresses and tectonic processes by loading. Thus, isostasic compensation in mountain belts is not complete at small scales.

compensation in mountain belts is not complete at small scales.

Crust-mantle transitions are also complicate in different tectonic regions. The crust-mantle transition depths may be estimated by geophysical, petrological, petrophysical means. In general, a sharp shallow Moho layer characterise Precambrian or cratonised areas whereas a deep, transitional Moho characterise young or tectonically active areas.

Australian continent may be broadly divided into two areas along the Tasman line by magnetic, seismic properties and heat flow estimates; to the west the dominantly cratonic Precambrian area and to the east the dominantly Phanerozoic mobile Tasman Fold Belt. The Precambrian area is characterised by a thick cool lithosphere and a sharp crust-mantle transition while the Phanerozoic area is characterised by a shallow lithosphere, a deep transitional crust-mantle layer and high heat flow.

1.7. Thesis outline

This thesis is based on petrographical, mineralogical, geochemical and isotopic studies of the samples obtained at different localities showing a range of ages. All selected samples for these investigations are prepared and analysed in the Department of Geology and Geophysics at The University of Adelaide. The project is documented as follows;

Chapter 1 provides reviews of general geology of the Australian continent and South Australian area, of nature of the shallow structure (mantle-crust boundary) and the deep structure (lithosphere and asthenosphere), and their implications in the Australian continent.

Chapter 2 provides a review of possible lithospheric or asthenospheric source magmas, their diversities and the mantle processes related to their diversities in order to develop an understanding of the petrogenesis for South Australian Quaternary basalts, Jurassic kimberlites and Ordovcian lamprophyres.

Chapter 3 discusses the detailed petrogenesis of South Australian Quaternary alkaline basalts, a geochemical and isotopic comparison with Victorian Newer basalts, Tasman Tertiary basalts and other available data from Hawaii, Cameroon line, and Basin and Range.

Chapter 4 provides details of the petrogenesis of upper mantle xenoliths entrained by South Australian Quaternary alkaline basalts and their implications for the characteristics of the upper mantle, which are based on petrological, mineralogical, and geochemical evidences.

Chapter 5 discusses the petrogenesis of the kimberlites and lamprophyres, and depletion and enrichment of the lithospheric level beneath southeast South Australia, which are mainly based on isotopic and geochemical information.

Chapter 6 discusses petrology, mineralogy and geochemistry of the South Australian lower crustal xenoliths as an indicator of underplating by basaltic melts in the low crustal level. They are compared with the xenoliths from the different localities in terms of their geochemical and isotopic signatures and discusses their implications for lower crustal

evolution model developed from Archaean high grade terrains.

Chapter 7 presents general models for the evolution of the lithospheric-asthenospheric level in South Australia based on petrographical, geochemical and isotopic studies which were discussed on the foregoing chapters.

Chapter 2. The contrast between the Lithospheric mantle and the Asthenospheric mantle as potential magma sources

2.1. Introduction

In the preceding chapter, various definitions of the lithosphere and asthenosphere were discussed. Simple thermal models of Parsons and McKenzie (1978) and Jordan (1975) divided lithosphere into mechanical boundary layer and thermal boundary layer overlying well mixed layer by vigorous convection (Fig. 2.1). However, meanings of terms "mechanical and thermal boundary" in these two models are different.

The mechanical boundary of Parsons and McKenzie (1978) refers to a rigid outer shell of the Earth and the thermal boundary is intermediate layer between the upper mechanical and lower adiabatic interiors. The mechanical boundary of Jordan (1975) refers to the upper most lithosphere including the crust while thermal boundary layer refers to the lithosphere

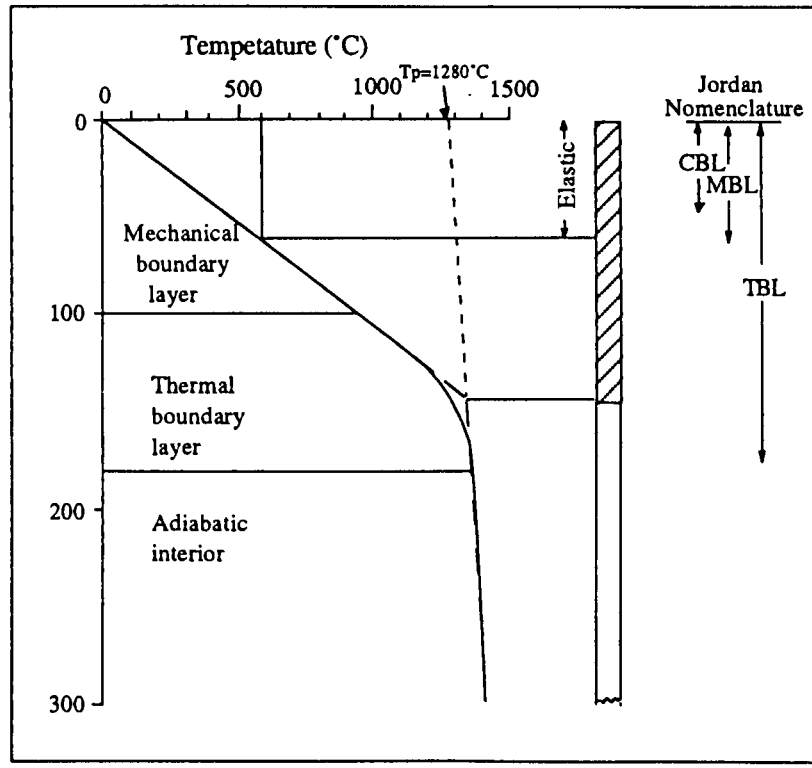

Fig. 2.1. Thermal structure of old ocean lithosphere over normal temperature asthenosphere (Tp = 1280 °C) (adopted from White, 1988). Left hand side of figure following Parsons and McKenzie (1978) and right hand side of figure following Jordan (1988). CBL = chemical boundary layer, MBL = mechanical boundary layer, TBL = thermal boundary layer.

underlying mantle convection and thus is consistent with a combined layer of mechanical and thermal boundary layer proposed by Parsons and McKenzie (1978).

Jordan (1981, 1988) also referred to the so called "chemical boundary layer" being the crust and that part of the subjacent mantle the density of which has been significantly reduced by extraction of a basaltic melt (White, 1988). CLM, particularly, beneath craton areas consists of lower density perodotite depleted in the basaltic constituents. The refractory nature helps the CLM as a stable geochemical reservoir. The thermal boundary layer is stabilised against convective distruption by a buoyant viscous chemical boundary layer. These models suggest that the lithosphere beneath the continent is of lower density than that of the oceanic lithosphere and has a variable age structure within individual continents as well as between different continents.

The important question then is to what extent does the CLM represent a significant global geochemical reservoir and if it is such, then how does this reservoir influence magmas which move to the crust ? This chapter analyses the possible distinctions between lithospheric and asthenospheric magmas by using the geochemical evidence available from worldwide data sources.

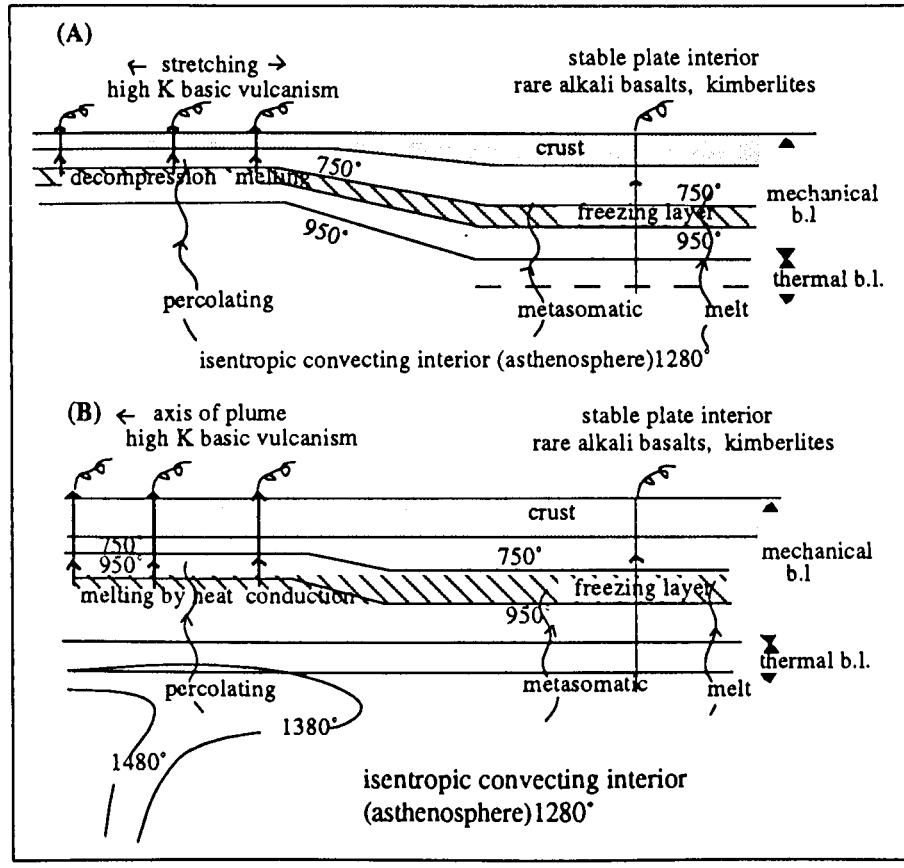

Fig. 2.2. Sketches showing production of the metasomatic layer (hatched) and its remelting by lithospheric stretching (A) or by plume impingement (B) (McKenzie, 1989).

2.2. Enrichment mechanism

There is a general agreement that metasomatism is an important enrichment process for the chemically heterogeneous CLM (Menzies *et al.*, 1983; McKenzie, 1989). Several models suggest that small melt fractions from the asthenosphere act as the agents of mantle metasomatism. Previous studies (e.g. Anderson, 1962; Ringwood, 1969) suggested that low shear wave velocity in the upper mantle is related to the existence of small melt fractions (1 % or less). The small melt fractions are enriched in water and carbonate, and are compositionally similar to kimberlite and potassium rich magmas. Experimental studies (e.g. Wallace and Green, 1988) have suggested that pargasite-bearing lherzolite and carbonate-rich melt occur as a very small melt fraction in equilibrium at a range of upper mantle temperature and pressure. However, the time scale and dimension of these enrichments are still ambiguous. In this section, several observations relating to physical processes in CLM enrichment are discussed.

McKenzie (1989) provided an evolutionary model for the lithosphere in which movement of small melt fractions derived from the underlying convecting mantle produce a metasomatic layer in the mechanical boundary layer. Its melting results in anomalous isotope ratios and K-rich enrichment in the CLM (Fig. 2.2). The remelting of the metasomatic layer occurs at low temperature when the steady state geotherm is distorted by adiabatic decompression during lithospheric stretching or by heat conduction from a mantle plume. The model provides evidence for the occurrences of rare alkali basalt and K-rich kimberlites generated from the asthenosphere in the interior of stable plates, and of relatively abundant K-rich basic volcanism in rift zone.

The depth at which the percolating melt freezes within the lithosphere depends on the thermal structure (McKenzie, 1967, 1989). In the half space model, the lithosphere thickens with time and all isotherms move steadily downwards until the plate is destroyed by subduction (Fig. 2.3).

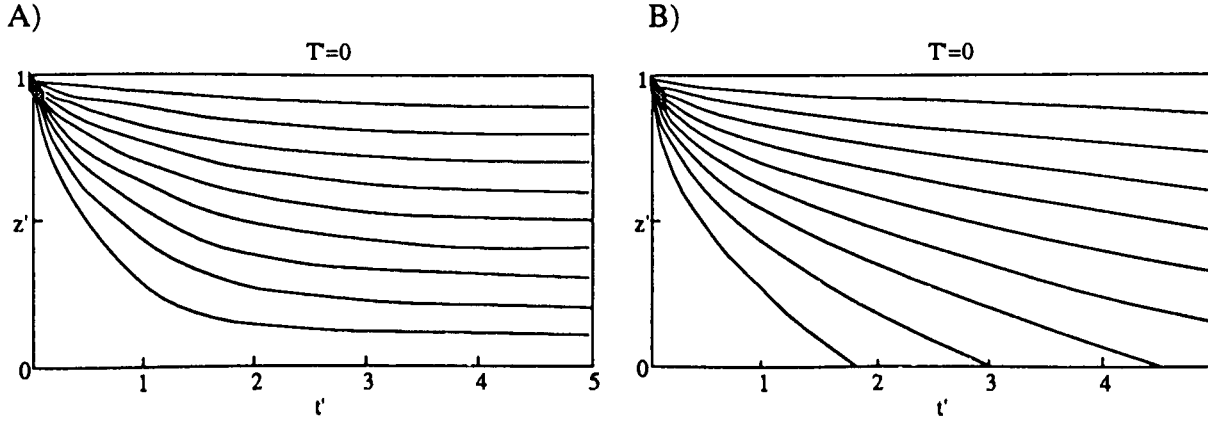

Fig. 2.3. Isotherms of the plate model (A) and the half space model (B) (McKenzie, 1967, 1989) in which T' is temperature at the base of plate, t' is dimentionless time, z' is height above the base of the plate.

Thus, the frozen melt could be distributed throughout the thickness of plate. In contrast, in the plate model, the temperature of the lithosphere is a function of depth and oceanic plate structure is thermally stabilised when the conductive heat supply to the base of the lithosphere balances heat lost through the lithosphere (Fig. 2.3). Thus the frozen melt is concentrated at a single level.

Menzies *et al.* (1987) suggested a different metasomatic process in the lithosphere. According to their model, asthenospheric melts transfer through lithospheric conduits, and this perturbation of the isotherms due to upwelling of the asthenosphere triggers production of lithospheric melts. The lithospheric melts mix with asthenospheric melts and form a melt segregation in the lithosphere, resulting in a series of differentiated mantle pegmatites (vein complexes) which contain a anomalous mineralogy and chemistry.

Other mechanisms also add complex lithospheric enrichment. These are processes of flow differentiation, plating of the crystal precipitates on to wall rock adjacent to conduits, and modification of the chemistry of the rising asthenospheric melt by the production of metasomatic aureoles and stoping of mantle wall rock. These processes result in anomalous enrichment in K, Ti, Fe, LREE and LIL in the lithospheric mantle and these trace elements are characteristically hosted by hydrous silicates and other accessory minerals.

Generally, it is agreed that the lithosphere of Archaean ages is deeper and cooler than the considerably younger oceanic (<0.2 Ga) or Phanerozoic continental lithosphere. These differences should be resulted in different degrees of enrichment within the two lithospheres (Jordan, 1981, 1988).

2.3. Complex records of metasomatic enrichment processes in the CLM

2.3.1. Petrography and mineralogy

High pressure inclusions in alkaline volcanic and kimberlitic rocks provide a unique sample of the lithosphere beneath both continental and oceanic crust (Menzies *et al.*, 1987). Even though the equilibration pressure and temperature, relationships with host rocks and spatial distributions with depths and areas remain ambiguous, it is generally agreed that the inclusions were derived from lithosphere by enriched lithosphere or underlying asthenosphere derived host rocks (e.g. Menzies *et al.*, 1987; McKenzie, 1989; McDonough, 1990). Xenolith studies suggest that the lithosphere is geochemically, isotopically and petrologically heterogeneous because of enrichment processes including metasomatism.

The metasomatic enrichment process can be further divided two modes; A) modal metasomatism which involves a change in modal mineralogy due to growth of newly introduced phases such as amphibole, apatite and phlogopite; B) cryptic metasomatism which is controlled mainly by the crystal chemistry of primary phases (e.g. clinopyroxene) without direct link to modal metasomatic processes (e.g. Menzies *et al.*, 1987; Griffin *et al.*, 1988; O'Reilly and Griffin, 1988; McKenzie, 1989). The metasomatism may be achieved by either

silica melt and hydrous fluid (Menzies *et al.*, 1987). The first type results in addition of Fe and Ti in CLM whereas second type results in addition of K-rich. The chemical characteristics of the first type are equivalent to basanites or alkali basalt whereas those of the second type are equivalent to micaceous kimberlite or lamproite.

The modal metasomatism involves growth of amphibole (kaersutite, pargasite, richterite), phlogopites (high Ti and low Ti varieties) with minor apatite, carbonate, rutile and magnetite-ilmenite in peridotites, pyroxenites and amphibolites. However, the cryptic metasomatism causes enrichment of LIL and LREE in peridotites without the introduction of hydrous phases. The mechanism is dominant in clinopyroxene and relies on fluid, CO_2 (e.g. Green and Wallace, 1988; O'Reily and Griffin, 1988). Xenolith studies suggest that clinopyroxenes from anhydrous lherzolites show a depleted isotopic composition (MORB) whereas those from hydrous (metasomatized) lherzolites have bulk Earth-like composition (OIB) (Menzies *et al.*, 1987; Stosch and Lugmair, 1986; Griffin B*et al.*, 1988).

Metasomatism in the subcontinental lithospheric mantle appear to show a vertical variation. Waters and Erlank (1988) suggested that degree of metasomatism exhibited by peridotites below Kimberley, South Africa increase with decreasing depths. They suggested that the degree of metasomatism shows a continuous trend from about 150 km depth and 1000 °C (rare phlogopite-bearing rocks) to 100 km depth and 780 °C (phlogopite-rich or some amphibole-bearing peridotites). Waters and Erlank (1988) also indicated negative correlation between P-T conditions and modal abundance of hydrous minerals or concentration of incompatible elements in both whole rocks and minerals.

In the asthenospheric or lithospheric derived igneous rocks, residuals of phlogopites may be influenced on the distinctive incompatible elements. Rogers *et al.* (1992) indicated that small melt fractions of the mantle under the conditions required for the generation of melilitite produced in equilibrium with a phlogopite-bearing restite. They suggested than the negative K anomalies and low buffered K_2O concentration in melilitites from South Africa reflect the effect of residual phlogopite during melting. This residual phlogopite accounts for low Rb/Sr, Ba/Sr and Th/U ratios in the melilitites.

2.3.2. Isotope and trace element evidences of mantle enrichment

Metasomatism influences the geochemical and isotopic variation of lithosphere as sampled by the mantle xenoliths from continent (McDonough and McCulloch, 1987) as well as some from oceanic regions (Nixon and Neal, 1987; Swanson *et al.*, 1987). Small melt fractions from the asthenosphere cause strong fractionation of Rb/Sr and Sm/Nd in the source regions and produce large isotopic anomalies via the decay of ^{87}Rb and ^{147}Sm (McKenzie, 1989).

There are two different opinions as to the role of metasomatic fluids represented by xenoliths of pyroxenites and metapyoxenites of the Al-augite suite whether they are in equilibrium with wall rocks (lherzolites). Menzies *et al.* (1987) suggested that metasomatic

fluids were in equilibrium with wall rock lherzolites and that possible changes in parent /daughter ratios are followed by ageing of the system to produce changes in isotopic ratios. However, Griffin *et al.* (1988) suggested that large changes in the Sr-Nd isotopic ratios in wall-rock lherzoites were produced at the time of metasomatism, thus changes in parent/daughter ratios are independent. As the evidence, they indicate that metasomatic fluids have very different $^{87}Sr/^{86}Sr$ and $^{143}Nd/^{144}Nd$ from wall-rock lherzolites. It was suggested that decoupling in fluid/rock partitioning during open metasomatic systems results in large changes in Rb/Sr and Sm/Nd ratios.

Several geochemical and isotopic studies of mantle enrichment have been carried out for xenoliths hosted by southeastern Australia alkaline basalts (McDonough and McCulloch, 1987; Griffin *et al.*, 1988; O'Reilly and Griffin, 1988; Stolz and Davies, 1988).

Stolz and Davies (1988) documents heterogeneous isotopic composition (Nd, Sr, Pb), extremely variable Nb/Th, Nb/U, and Ce/Pb ratios in a study of group I spinel lherzolite xenoliths from Lake Gnotuk and Bullenmerri. Another studies from the same locality (Griffin *et al.*, 1988; O'Reilly and Griffin, 1988) also indicate anomalous geochemical and isotopic compositions in Cr-diopsides lherzolites and Al-sugite pyroxenites. Both studies suggest that metasomatised xenoliths show significantly lower Rb/Sr (0.004-0.02) and higher U/Pb values than those of Bulk Earth, Ba/La, La/Nb ratios comparable with or lower than MORB and most OIB, and significantly lower than most subduction-related volcanics.

Variable degrees of enrichments due to different metasomatic minerals were also observed in xenoliths from same locality (Stolz and Davies, 1988; O'Reilly and Griffin, 1988). In general, mica-rich xenoliths show enrichment in K, Rb, Ba, Ta, Ti, Zr and low K/Rb and apatite-rich xenoliths show enrichment in Sr, U and Th, high ΣREE and LREE ((La/Yb)n = 40-100). Amphibole-rich xenoliths show strongly enrichment in Sr (thus low Rb/Sr), enrichment in LREE ((La/Yb)n = ~10-30), Zr, Nb, Ta, high K/Rb and show increase in Sr, Ba, Zr, Hf, Nb, Ta, Th, U, total REE and La/Yb with increase of modal amphibole in whole-rock.

The Victorian xenoliths have Sr-Nd isotopic composition ranging from MORB to enriched mantle ($\varepsilon Nd<0$, $\varepsilon Sr>0$) in the mantle array (Griffin *et al.*, 1988). In general, unmetasomatized samples have depleted isotopic composition (similar to MORB) and samples showing modal or cryptic metasomatism have OIB-like isotopic composition. Pb isotopic data of spinel lherzolites from the Victorian Newer Basalts (Stolz and Davies, 1988) range from values similar to Group II kimberlites to higher than their host basalts and associated volcanic rocks. Similar results for Pb isotopic data are shown at kaersutites from ultramafic nodules of the Basin and Range volcanic province, western USA (Ben Othman *et al.*, 1982) in which $^{207}Pb/^{204}Pb$-$^{206}Pb/^{204}Pb$ data of separated amphiboles spread along a regression line defined by MORB and Hawaiian basalts, suggestive of effect by metasomatic fluids.

A geochemical and isotopic study of hazburgite and lherzolite from southeastern Australia by McDonough and McCulloch (1987) yield several observatiions. There is 1) wide

variation in xenoliths from world-wide or a single locality, 2) differences between clinopyroxene separates and their host rocks in same xenoliths, 3) small differences between clinopyroxenes and whole rock in xenoliths showing cryptic metasomatism, 4) significant differences between coexisting phlogopite-clinopyroxene pairs in xenoliths which show modal metasomatism, 5) difference between coexisting clinopyroxene and orthopyroxene in an anhydrous lherzolite, 6) similar Sr/Nd ratios with PM, MORBs and intraplate alkaline basalt, 7) dependence on clinopyroxene rather than phlogopite of whole rock Sr-Nd isotopic composition in phlogopite bearing peridotites.

Mantle metasomatism shown in xenoliths may not Recent phenomenas at lithosphere beneath continent and ocean. Modal ages of the metasomatised xenoliths derived from kimberlites at Kimberley suggest that enrichment processes of CLM began in Neoproterozoic time (Menzies and Murthy, 1980; Erlank *et al.*, 1982). Xenolith studies of Phanerozoic eastern Australia (Griffin *et al.*, 1988) and of peridotitic and pyroxenitic xenoliths from Arizona (Menzies *et al.*, 1985) suggest that major metasomatism of xenoliths occurred 300-500 Ma and 300-900 Ma, respectively.

2.3.3. Phase relationships

Experimental results (Fig. 2.4) support the existence of a small melt fraction at a range of upper mantle P-T conditions as a precursor for mantle metasomatism (e.g. Green and Wallace, 1988; Wallace and Green, 1988). A study of the peridotite-CO_2-H_2O solidus for small water and carbonate contents suggests that sodic, dolomitic carbonatitic melts coexist with pargasite-bearing lherzolite at 21-31 kbar (930-1080 °C) and migrations of the carbonatitic melts redistributes certain elements effectively (e.g. LIL, LREE) in the lithosphere by mantle metasomatism (Green and Wallace, 1988). In the carbonatite melts, low water content causes stable persistence of residual pargasitic amphibole.

When the carbonatite melts infiltrate lherzolite at high pressure (21 kbar at 950-1050 °C), decarbonation reactions occur with the release of CO_2 vapour. The decarbonation results in a change from lherzolite or harzburgite of Cpx+Ol+Sp to wehrlite at P<21 kbar. In this case, the stability of amphibole and phlogopite relies on the both CO_2, H_2O and CO_2/H_2O ratios of the fluid released by decarbonation of the carbonate melt. The effects of the decarbonation raise the solidus temperature of the lherzolite to the dehydration solidus for pargasite lherzolite at high f_{CO_2} or, if pargasite breaks down owing to high f_{CO_2}, the solidus will be that for anhydrous peridotite or phlogopite peridotite at high f_{CO_2}, low f_{H_2O}.

Another experimental study by Thibault *et al.* (1992) also suggests that carbonate rich melt is produced from carbonated phlogopite-lherzolite and coexists with residual garnet lherzolite at 3.0 Ga, 1100 °C. Thibault *et al.* (1992) also suggest that carbonated phlogopite lherzolite is produced at the initial stage of continental rifting at the base of the lithosphere overlying hot asthenospheric mantle plume.

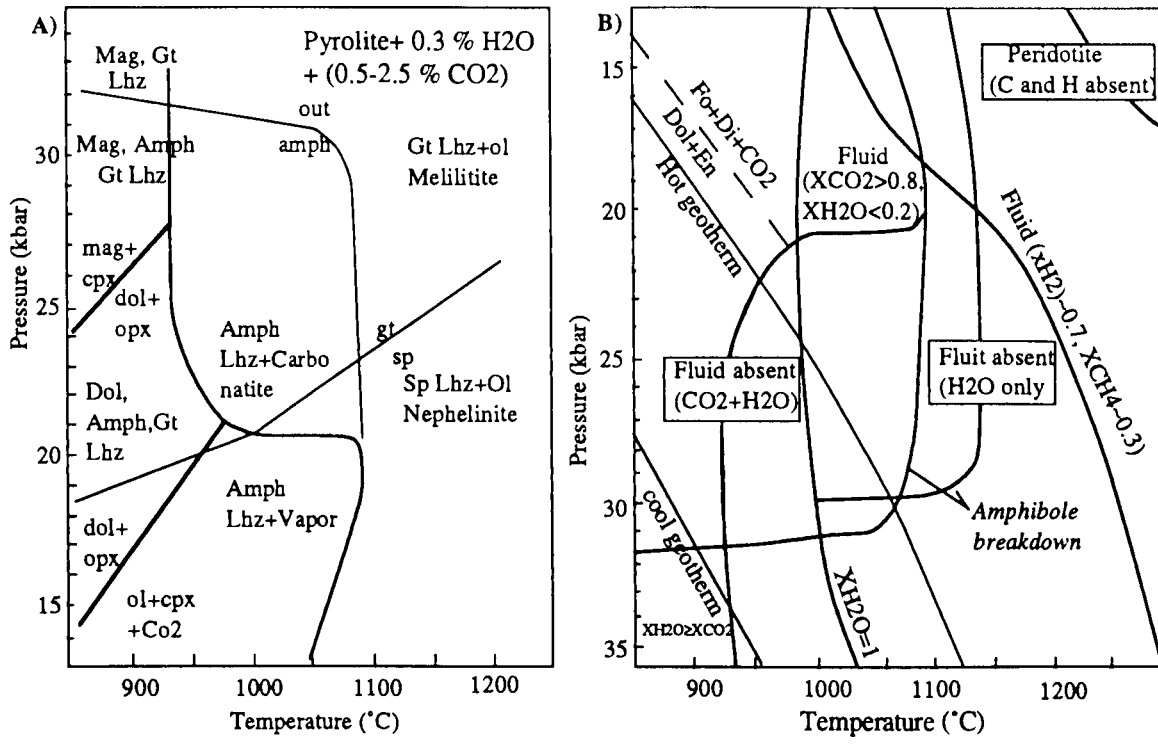

Fig. 2.4. A) Phase relationships of amphibole-rich Hawaiian Pyrolite (0.3 % H_2O) plus 5 % dolomite or 1.4 % magnesite. Carbonatite melt field is bounded by the carbonate solidus at 930 °C (heavy line) and amphibole breakdown and silicate melt field above 1080 °C (25 kbar). All runs were buffered with magnesite (fO_2 = EMOG). B) Solidi for peridotite-C-H-O, illustrating the contrasted effects of reduced fluids (H_2O-CH_4) and oxidised fluids (H_2O-CO_2) (Green and Wallace, 1988; Wallace and Green, 1988).

Green and Wallace (1988) cited the examples of the spinel lherzolite from Mt Leura, Victoria as an evidence for carbonate metasomatism. The carbonate metasomatism causes partial replacement of enstatite by magnesian diopside, an increase in Cpx/Opx ratios, a decrease in $MgAl_2O_4$ component in spinel and in $MgAl_2Si_2O_6$-solid solution in pyroxene. The metasomatism also produces an increase in Ca/Al and Na/Ca ratios, and an increase in LIL enrichments without considerable decrease in Mg# in the metasomatised lherzolite.

Experimental modelling of mantle metasomatism suggests that amphiboles are an effective reservoir for F and K and other incompatible elements (e.g. Sudo and Tatsumi, 1990). Subsolidus experiments (2.0-3.0 GPa, 850-950 °C) using H_2O rich solutions of K and Na carbonates demonstrate the transformation of olivine and pyroxene into phlogopite and pargasitic amphibole (e.g. McNeil and Edgar, 1987).

Large numbers of experimental studies have suggested that phlogopite is stable at super-solidus temperatures in the mantle (Fig. 2.5) (Rogers *et al.*, 1992). For example, Foley *et al.* (1986) demonstrated that fluorine-phlogopite is stable up to 1500 °C at 28 kb under F-rich conditions. Foley (1992) also reported coexisting Ol+Opx+Phl at the liquidus of olivine lamproites at 55 K bar and leucite lamproites at 17-20 K bar if a realistic amount of H_2O were present.

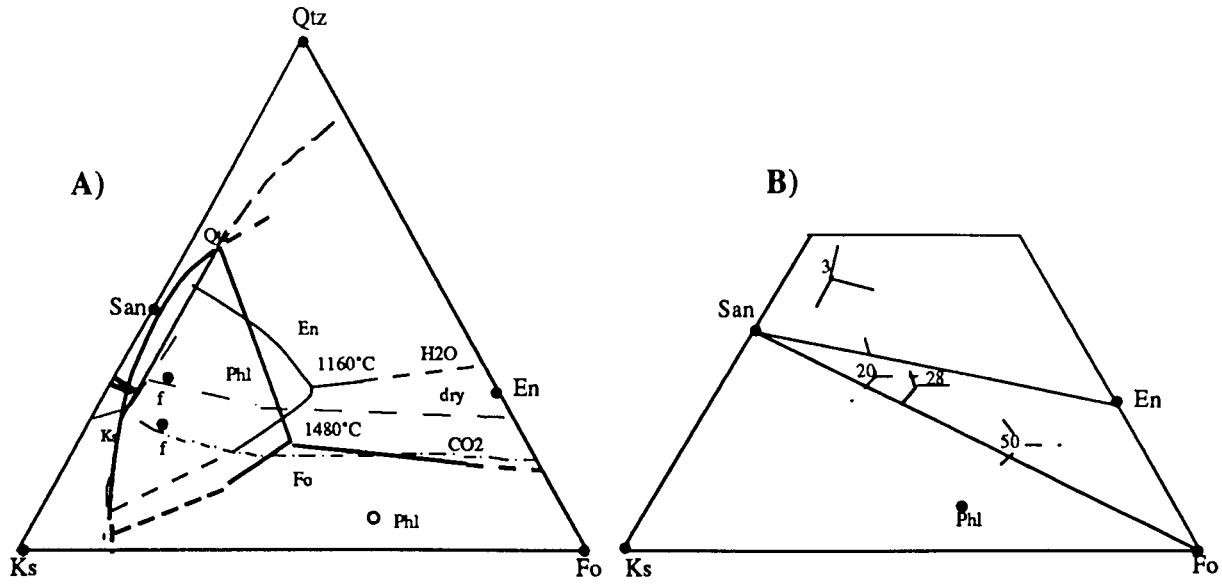

Fig. 2.5. A) Phase relations in the $KAlSiO_4$(Ks)-$MgSiO_4$(Fo)-SiO_2(Qtz) system without H_2O (dry)-thin dashed lines, H_2O saturated-thin full line, CO_2-saturated-dotted and dashed line and with 4 w% F-thick full line (Edgar and Vukadinovic, 1992), B) melt composition at different pressure. Triple junctions represent peritectic melting point Ol+Opx+Phl+Lq (Foley, 1992).

Experimental petrology (Fig. 2.6) supports the derivation of ultrapotassic magma by partial melting of a metasomatised mantle (phlogopite-harzburgite or wehrlitic) which has undergone episodic enrichment of characteristic incompatible and LIL elements (e.g. Edgar and Vukadinovic, 1992). The mantle metasomatism occurs at f_{O2} in the range of FMQ buffer and involves low density mantle fluids, mainly H_2O and CO_2, which are buffered by amphibole, phlogopite and carbonate.

Foley (1988) suggested that redox melting is a major process for generation of partial melts in upper mantle involving interaction of upwelling CH_4-rich fluids from a reduced deep asthenosphere with relatively oxidised lithosphere. In these redox melting models, oxidation of CH_4 produces H_2O and solid carbon, and increase in a_{H_2O} causes melting by depression of the mantle solidus temperature. Initial melt will be CO_2 rich, corresponding to kimberlitic, melilitic, or ultramafic lamproitic composition, depending on pressure and tectonic setting. The episodic reduced fluid introduction into oxidised lithosphere causes melting of the same mantle region and movement of the H_2O-rich fluid into the overlying layer produces hydrous phases by metasomatic reactions.

2.4. Magmatic sampling of enriched lithospheric mantle

Mantle plumes beneath the lithosphere may be up to 2000 km in diameter and can raise 100-200 °C in excess of normal (White and McKenzie, 1989). These mantle temperature increases result in the generation of huge quantities of melts due to decompression upwelling

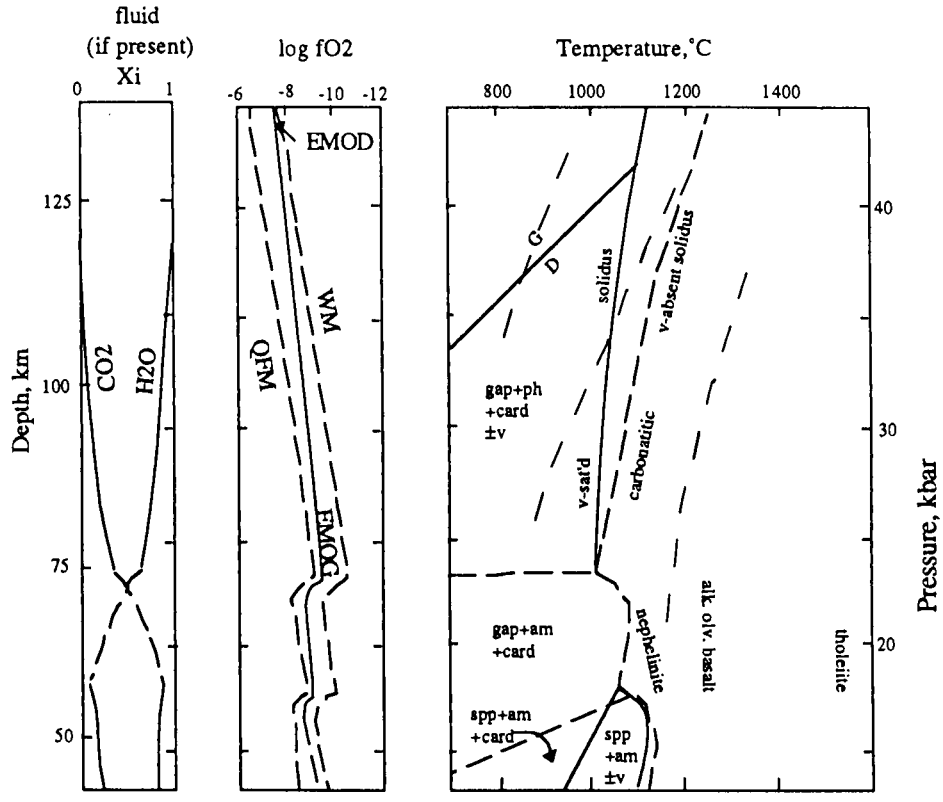

Fig. 2.6. Phase relations of a peridotite composition in the presence of small amounts of H_2O and CO_2 (Eggler, 1987) ph-phlogopite, carb-carbonite, v-H_2O-CO_2-vapour, am-amphibole, gap-garnet-olivine-orthopyroxene-diopside peredotite, spp-spinel-olivine-orthopyroxene diopside peridotite, thin dashed lines are geotherms for oceanic lithospheric ages of 30 Ma (right) and 180 Ma (middle), and for continental shield regions (left).

(White and McKenzie, 1989). The melt generated by decompression rises passively beneath the stretched and thinned lithosphere and is either extruded as basalt flows or intruded into or beneath the crust. The melt generate for varying amounts of stretching with a range of mantle temperature. Addition of large quantities of igneous rocks account for the increase of seismic velocity beneath crust. The time of volcanism depends on the time and rate of lithospheric thinning and time of melt to move upward from the zone of melting in the mantle to the surface.

The composition of melt is dependent on the variable degree of stretching in the lithosphere whereas the volume of melt generated by extension of the lithosphere is a function of pressure and temperature (Fig. 2.7). Fig. 2.7 is expressed in terms of ß, the ratio of the final to the initial surface area, in which melt generates for various values of ß when the interior potential temperature of the mantle (in hot rising jets) is 1480 °C.

Fig. 2.8 shows a model for the changes in crustal thickness resulting from stretching in which the volume of melt generated depends on the thickness of the mechanical boundary and on the potential temperature of the upper mantle. As an example, when the potential temperature is 1380 °C and mechanical boundary layer is 70 km thick, if ß is 5, about 10 km of melt occur whereas if ß is 2, about 4 km of melt occur.

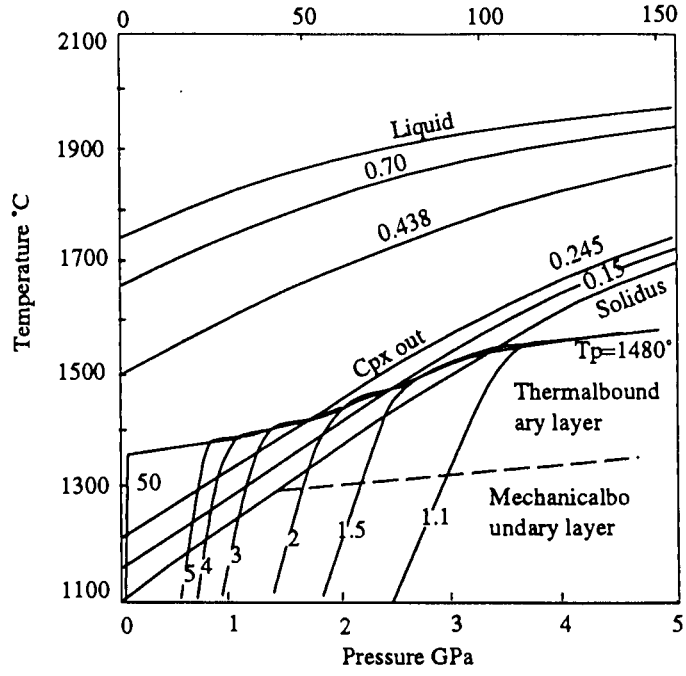

Fig. 2.7. Adiabatic upwelling due to stretching of a convective geotherm generated from a mechanical boundary thickness of 100 km with an interior potential temperature of 1480°C (McKenzie and Bickle, 1988).

However, no melt generation takes place during the extension of the continental lithosphere unless ß > 2 and Tp > 1380 °C. According to McKenzie and Bickle (1988), factors ß in the North Sea are less than 1.5 for the Jurassic-Cretaceous stretching events whereas that in the Basin and Range is as large as 2.

Thickness of Precambrian carbonised continental lithosphere is principally controlled by its age (Pollack and Chapman, 1977; Jordan, 1981) while lithospheric thickness beneath of oceanic crust is governed by the loss of heat from the vigorously convecting, adiabatic upper mantle (Parsons and McKenzie, 1978). Lithospheric thickness beneath Phanerozoic continental lithosphere seems to similar to that of old oceanic lithosphere and it behaves in a similar way thermally (McKenzie, 1978; Richter, 1988; White, 1988).

According to this model, a factor ß of 2 is typical value found in intracontinental sedimentary basins which have not subsequently developed into ocean basin. A factor ß of 5 is the point at which stretched continental crust breaks to fully igneous oceanic crust. A factor ß of 50 is a representative of the upwelling which occurs beneath oceanic spreading centres.

In Fig. 2.8, assuming the temperature of 1400 °C and factor of 2, thicker melt generates at a area showing a thin mechanical boundary. Thus cool, thick mechanical layer of Shield area suggest of thin melt thickness and thus, many of the melt generated by adiabatic decompression of asthenospheric mantle emplaces into the crust rather than erupted at the surface. Thus, thin mechanical boundary of the Phanerozoic continental lithosphere account for thick melt and eruption of a large volume by adiabatic decompression.

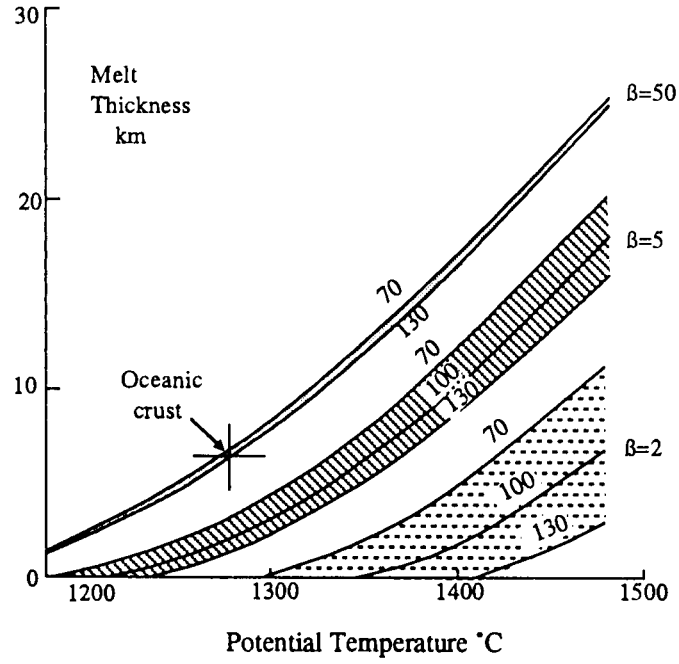

Fig. 2.8. Thickness of melt generated by adiabatic decompression of asthenospheric mantle over a range of potential temperatures. Curves are initial thickness of the MBL, ß is the factor of extension (White and McKenzie, 1989).

Fig. 2.9. illustrates the changing compositions of igneous rocks as stretching increases. According to White and McKenzie (1989), the composition of MORB showing 10 % MgO is generated by infinite stretching at normal potential temperature of 1280 °C. When the temperature increase from 1280 °C to 1480 °C, the percentage of MgO increases and that of Na_2O decrease. In this model, thinning of the lithosphere at ß = 2 and at 1480 °C, can generate alkali basalt and as the stretching is increased further, tholeiitic basalts are generated. Thus picrite containing high percent of MgO is indicative of abnormally high asthenospheric temperatures, and increases in percentages of Na_2O in the some of mantle plume related rocks are indicative of decreasing asthenospheric temperature.

The high MgO content of melt generated at asthenospheric temperature account for the systematic change in seismic velocity from 6.8 km/s for normal mantle temperature (1280 °C) to 7.2 km/s or higher. Many continental margin and flood basalts are related to the thermal anomaly created by a near mantle plume (White and McKenzie, 1989). Examples include Parana-Etendeka, Deccan Trap, Karoo-Antarctica and the Tertiary igneous province nearby east Greenland. All these areas show evidence of small scale tensional rifting before regional uplift resulting from the mantle plume itself and associated volumetrically larger basaltic volcanism. The evidence of the initial stages includes the thick lower crust, or seismic anomalies of 7.1-7.5 km/s in the lower crust due to intrusion of volumetrically small mafic rocks into the lower crust. With the increase of mantle decompress, increasing quantities of melt result in a continental break-up or large volumes of more felsic volcanism.

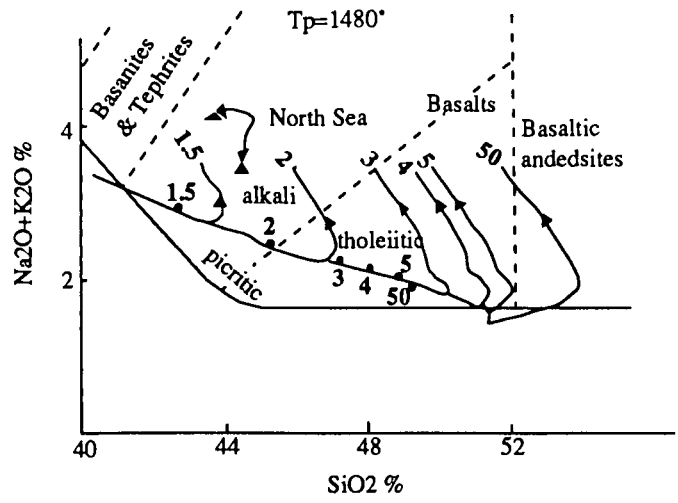

Fig. 2.9. Melt compositions generated by extension of the lithosphere assuming a mechanical boundary layer thickness of 100 km (McKenzic and Bickle, 1988), contoured for stretching factor ß.

In summary, the presence of a mantle plume beneath the lithosphere may lead to decompressive melting as it rises passively beneath the stretched and thinned lithosphere. The melt migrates upwards to extrude as basalt flows and intrude into or beneath the crust. The volume of melt predicted is a function of pressure and temperature and depends on the thickness of mechanical boundary. The composition of the igneous rocks formed by decompressive melting change as stretching increases.

2.5. Are continental lithospheric mantle components geochemically and isotopically recognisable in intra-continental magma suites ?

The recognition of asthenosphere- and lithosphere-derived magma within continent remains controversial, even though several rock types are considered to be representatives of lithospheric or asthenospheric mantle. They are geochemically and isotopically diverse and their petrogenesis are typically interpreted as a result of interaction between lithospheric and asthenospheric mantle. In general, majority of intraplate continental alkaline basalts show a OIBs like geochemical and isotopic characteristics and contain peridotitic and pyroxenitic xenoliths.

It is generally accepted that geochemical and isotopic characteristics of OIBs reflect mantle plume(asthenosphere) components because distribution of OIBs are away from continental lithosphere(subduction). Thus the nature of OIBs may be implicated to interpret for petrogenesis of the intraplate alkaline basalts as a asthenospheric fingerprints. The OIBs are geochemically and isotopically divided into four groups; HIMU, EMI, EMII, and DMM (Zindler and Hart, 1986). Their summary is as follows (Zindler and Hart, 1986; Sun and McDonough, 1989; Wilson, 1993).

- DMM is considered a depleted end member component which is isolated from hot spot volcanic activity. It is characterised by high $^{143}Nd/^{144}Nd$, low $^{87}Sr/^{86}Sr$ and $^{206}Pb/^{204}Pb$.

- HIMU type is characterised by high $^{206}Pb/^{204}Pb$, low $^{87}Sr/^{86}Sr$ and intermediate $^{143}Nd/^{144}Nd$ ratios. It show low Rb/Sr, low K/U and K/Nb ratios. This component is dominant in St Helena, Tubuaii and Mangaia.

- EM type is enriched mantle components which has a low $^{206}Pb/^{204}Pb$, $^{143}Nd/^{144}Nd$ and high $^{87}Sr/^{86}Sr$ ratios. This type is divided into two groups; EM I type and EM II type

A) EM I type is dominant in Kerguelen group (Gough, Tristan da Cunha) which show lower $^{87}Sr/^{86}Sr$ than samples within the mantle array and lower $^{143}Nd/^{144}Nd$ and $^{206}Pb/^{204}Pb$ than samples of HIMU types. The EMI types have higher Ba/Nb, Ba/Th, Rb/Nb, Ba/La ratios and lower Th/La than samples of EMII type (Weaver, 1991).

B) EMII type is dominant in Society Island type (Marquesas, Samoa, Sao Miguel) which show higher $^{87}Sr/^{86}Sr$ ratio than samples of the mantle array similar $^{143}Nd/^{144}Nd$ ratios with EMI type and higher $^{206}Pb/^{204}Pb$ ratios than samples of EMI type.

The EM-type OIB may be concentrated between the equator and 60 °S latitude (mainly centred at latitude 30 °S) in the southern hemisphere (Hart, 1984). The worldwide megascale isotopic anomalous region has been termed as Dupal anomaly region (Hart, 1984). Several studies suggest that the enrichment of OIBs in the southern hemisphere may be a shallow mantle characteristic caused by Pangeatic subduction of altered oceanic crust and sediment into the sub-Dupal mantle (Anderson, 1982; Zinder and Hart, 1986). Hart *et al.* (1986) suggest that the ultimate origin of the Dupal anomaly is the continental lithosphere. Studies of continental flood basalt also suggest that Dupal anomaly is shallow level phenomenon which evolved in the continental lithosphere, and is related to heating and remobilised in the lithospheric mantle before continental break-up between South Africa and South America (e.g. Hawkesworth *et al.*, 1986).

The EMI type source may spatially coexist with HIMU OIB(Hart *et al.*,1986). However, occurrence of isolated HIMU type OIB (e.g. South Island and Mary Byrd Land), numerous occurrences of EM type OIB (e.g. Azores, Oahu Island) and of EM-type continental alkaline basalts in the northern hemisphere can not support that (Sun and McDonough, 1989). EM2 type anomalies may not an young subduction-related phenomenon surrounding the Pangean continents (Sun and McDonough, 1989). Sun and McDonough (1989) cited absence of Dupal anomaly in the Pacific mid-ocean ridge of the southern hemisphere (Macdogall and Lugmair, 1986; White *et al.*, 1987) and existence of Archaean and Proterozoic Dupal-like anomalies in komatitites and granites of the southern continents as these evidence. Le Roex (1986) suggested that sources of Group I kimberlies are similar to Bouvet and Marion type hot spots while those of Group II kimberlies are similar to the Dupal

OIB.

A lithosphere delamination model may support the isotopic signature observed in the HIMU-or EM type rock in continent and ocean. Dudas *et al.* (1987) indicated that many EMI-type continental rocks (e.g. Smoky Butte) which fall well below the LoNd array may be caused by some delamination of continental lithosphere. However, the continental lithosphere lamination model may not explain these rare OIB samples showing strong subduction-zone related chemical and isotopic characteristics, which are anomaly found in continental mantle mafic and ultramafic volcanic rocks (Sun and McDonough, 1989). Sun and McDonough (1989) suggested that Archaean and Proterozoic rocks showing Dupal-like anomalies reflect long-term isolation of the enriched mantle within the lithosphere before delamination and recycling back into the convecting mantle.

In conclusion, an understanding of plume derived magma in the oceanic lithosphere can provide as a possible approach of interpretation of asthenosphere-derived magma found within continental lithosphere. Megascale isotopic anomalies of OIB in southern hemisphere may not characterise all OIB but appears to be an important feature.

2.6. Examination of time integrated magma geochemistry among intra-continental plumes

Four fields known as asthenosphere-derived volcanics have been reviewed for the possible approaches to geochemically distinguish lithospheric derived suites from asthenospheric derived rocks.

One such field is that of the Late Cenozoic basaltic lavas in the western United States. The volcanic fields include the Sierra Nevada, Basin and Range, and Colorado plateau. In these Cenozoic basaltic lavas, Basin and Range volcanic rocks (Fig. 2.10) have OIB-like geochemical and isotopic characteristics, which can be distinguished from the other volcanics by their high Nb/La (> 0.8), Nb/Y and Sr, Nd, Pb isotope ratios (e.g. Carlson, 1984; Fitton *et al.*, 1988; Bradshaw *et al.*, 1993). The Basin and Range lavas are volumetrically small, alkali basalt (*ne* -normative) erupted in later stages of the volcanic fields. They usually contain ultramafic inclusions and mantle xenolith materials. They show high Nb/Zr and Th/Zr, $^{208}Pb/^{204}Pb$ ratios that fall on or close to the fields for OIB and MORB. The other volcanics are tholeiitic (or calc-alkaline) and show distinctive depletion of Ta and Nb (low Nb/La = 0.3) and enrichment of Ba.

Experimental studies suggest that tholeiitic basalts are a product of low-pressure relatively high-degree melting, while silica undersaturated liquids are produced by low degree melting at higher pressures (e.g. Jaques and Green, 1980). Geochemical studies also suggest that Nb and/or Ta depletion relative to K and La are characteristics of subduction-related orogenic magma or arc magma (e.g. Gill, 1981; Kelemen *et al.*, 1993) and Nb depletion in CFBs are signature from shallow lithosphere (e.g. in Mesozoic CFBs studies).

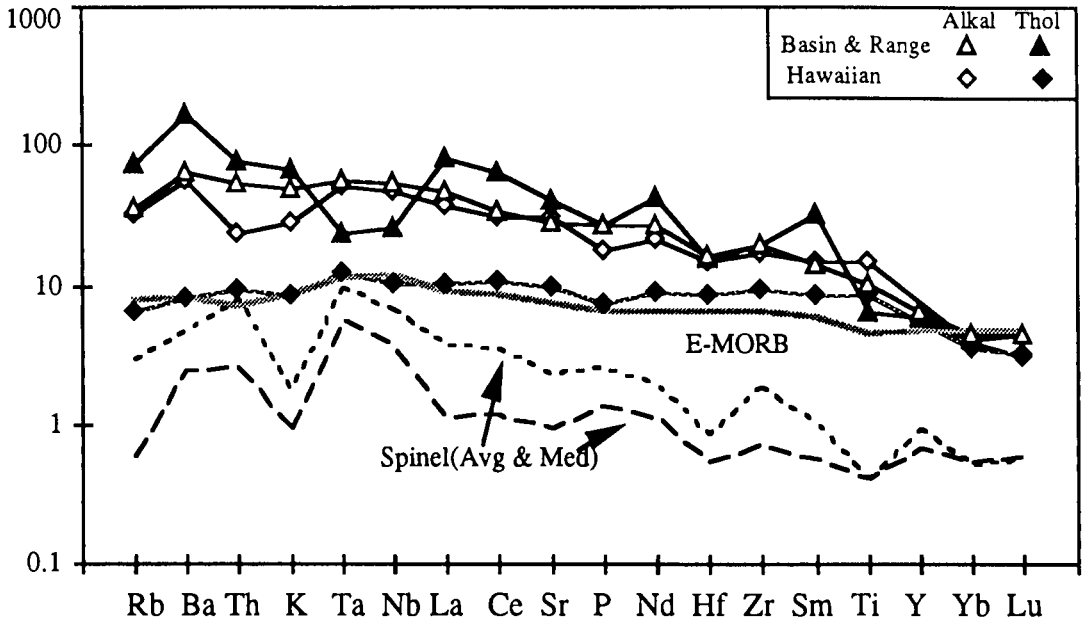

Fig. 2.10. PM normalised trace element abundance of Basin & Range basalt, Hawaiian basalt, E-MORB, Spinel lherzolite (Data sources, Chen and Frey, 1983; Sun and McDonough, 1989; Chen *et al.*, 1990; McDonough, 1990; Bradshaw *et al.*, 1993).

Thus, parental magma of the silica undersaturated rocks of Basin and Range province may be generated by smaller degree melting at deep level and high pressure whereas the other basalts may be generated from high degrees of partial melting at shallow levels.

A study of basaltic volcanism in the southern Basin and Range also reports increasing Nb/Y and Nb/La ratios with age (Bradshaw *et al.*, 1993). Bradshaw *et al.* (1993) suggested that most of the basalts in the Basin and Range were derived from the continental mantle lithosphere and the youngest were derived from the asthenospheric upper mantle. This volcanism was triggered by lithospheric extension rather than emplacement of mantle plumes as suggested by McKenzie and Bickle (1988).

Similar opinion was inferred in Tertiary volcanism of the Mogollon Datil volcanic field in southwestern New Mexico U.S.A. (Davis *et al.*, in press). The Tertiary volcanism show decrease of Ba/Nb, Zr/Nb and $^{86}Sr/^{87}Sr$ ratios and SiO_2 contents, and increase of TiO_2 contents with decreasing ages. Davis *et al.* (in press) interpreted these changes due to an overall shift from lithosphere-to asthenosphere derived magma with time. The triggering mechanism was lithospheric extension. It was also suggested that these chemical and isotopic change indicated transition in local stress region from quiescence-to ductile extension to brittle extension, with decreasing ages.

The Basin and Range alkali basalts are geochemically and isotopically similar to Cameroon line basalts which are considered as derived from the asthenosphere (Fitton, 1987; Fitton and Dunlop, 1985; Halliday *et al.*, 1988). The Cameroon line basalts often contain abundant peridotic xenoliths and clinopyroxene and anorthoclase megacrysts and granulite xenolith.

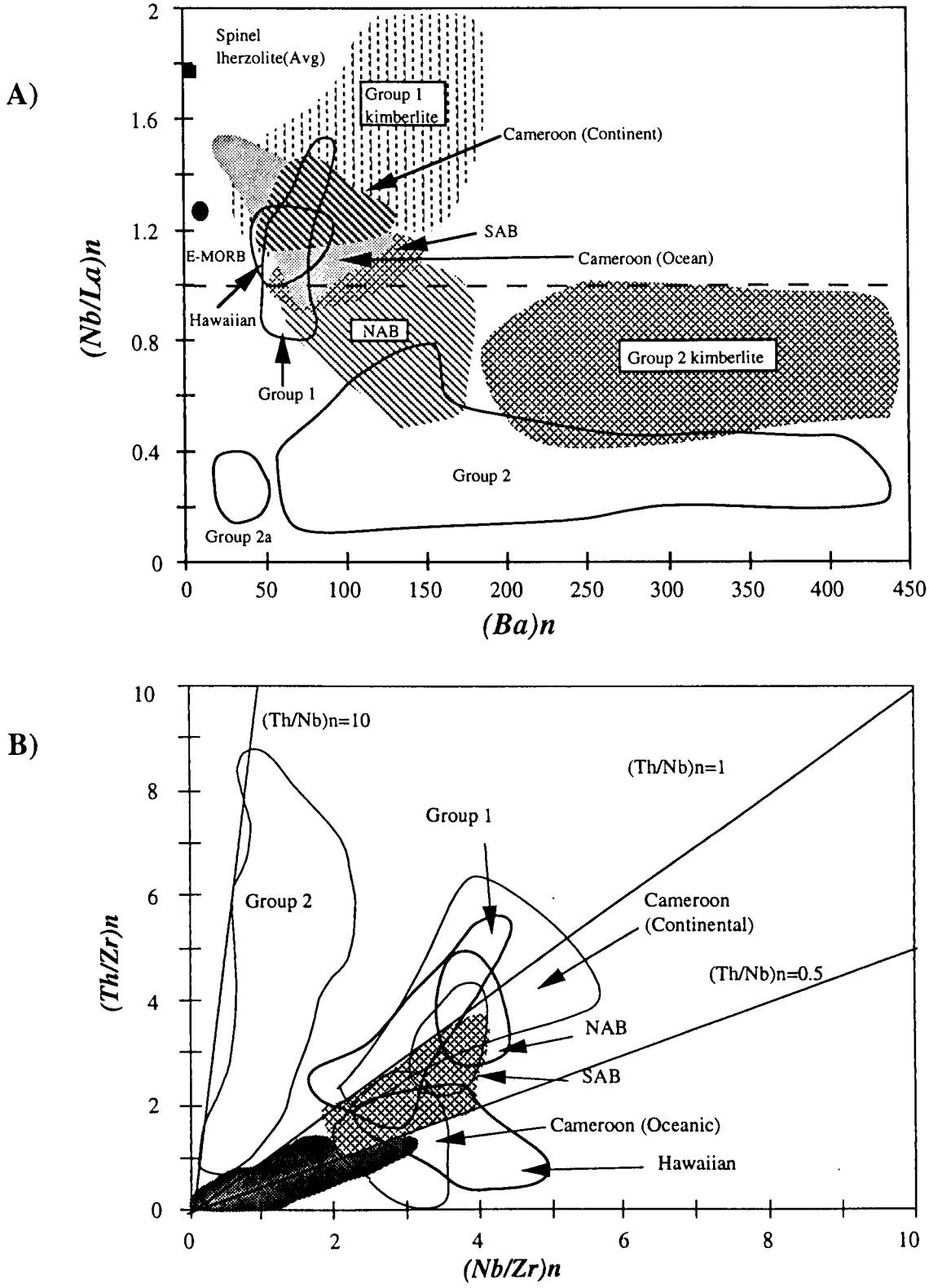

Fig. 2.11. Primitive mantle normalized A) Nb/La versus Ba and B) Th/Zr versus Nb/Zr (after Bradshaw *et al.*, 1993). Data sources (Basin and Range basalt (Group 1, 2, 2a) from Bradshaw *et al.* (1993), Kimberlites from Smith *et al.* (1985), Spinel lherzolite (avg) from McDonough (1990), Carmeroon mafic basalt from Fitton, (1987). Hawaiian alkaline basalt from Chen *et al.* (1990), South Australian basalt (SAB and NAB) from Ch 3, and E-MORB and normalized values from Sun and McDonough (1989).

The alkaline basalt comprises two istopically and geochemically similar basalts groups of oceanic and continental sector which are similar to OIBs but distinctive from MORBs (Fig. 2.11). Their isotopic composition ($^{87}Sr/^{86}Sr$ of 0.7029-0.7035, $^{143}Nd/^{144}Nd$ of 0.51287-0.51299, $^{206}Pb/^{87}Sr/^{86}Sr$ Pb of 19.0-20.6) is similar to those HIMU type Balleny plume basalts of Lanyon *et al.* (1993). Their distinctive incompatible element ratios (Zr/Nb of ~4.5), La/Nb of ~0.81) and Ba/La of ~9.8) are also similar to the Balleny plume basalts in southwest Pacific ocean as well as of HIMU type OIB (Weaver, 1991).

Another well known continental flood basalt province is Deccan trap, India. The Deccan Trap lavas show a decrease of crustal contamination up-sequence. Geochemical and isotopic features of upper two sections, the Ambbendli and Mahabaleshwar formations are interpreted as interaction between shallower level lithospheric mantle or asthenospheric material related to the Reunion hotspot and continental mantle lithosphere of the Indian plate (Cox and Hawkesworth, 1985; Lightfoot and Hawkesworth, 1988).

The upper two formations show a depletion in incompatible element (~ 0.15-0.35 * OIB) except LREE. Their dominant isotopic composition ($^{87}Sr/^{86}Sr$ of 0.7039-0.7043, $^{143}Nd/^{144}Nd$ of 0.51282-0.51288, $^{206}Pb/^{204}Pb$ of 17.9-18.4) is similar to those observed in evolved MORBs and incompatible element ratios (Zr/Nb of 10-13, La/Nb of 0.8-1.5, Ba/La of 4~7) are also similar to those observed in E-type MORB of Sun and McDonough (1989). The later sequences are isotopically distinctive from the early sequences by higher $^{87}Sr/^{86}Sr$ and lower $^{143}Nd/^{144}Nd$ ratios. These isotopic and geochemical changes can be explained by shifts from lithosphere- to asthenosphere-derived magma with time as lithospheric extension.

In summary, the majority of continental or oceanic rift-related volcanism show systematic changes, from volumetrically large tholeiitic (or more felsic) rocks to small alkaline (or more mafic) with ages. The later alkaline basalts are characterised by geochemical and isotopic composition similar to OIB while the earlier tholeiitic rocks are characterised by the distinctive depletion of Nb and Ta. These systematic geochemical or isotopic changes can be explained with shift from lithosphere to asthenosphere derived magmas with time in which magmatism was triggered by lithosphere extension.

2.7. Continental flood basalt

Studies of continental flood basalts (CFB) suggest that the CFB were generated by interaction between plume source-crust and plume source-CLM (continental lithospheric mantle). In general, earlier studies of the petrogenesis of CFBs were interaction of continental material. Thus these studies concentrated on the contamination of shallow lithospheric materials by continental material, different degrees of partial melting or fractionation processes at upper CLM or low crust. However, recent studies based mainly on Sr-Nd-Pb isotopes stress that some of CFBs were derived from interaction between CLM-asthenospheric magma, or from pure asthenosphere. For the understanding of the

petrogenesis of the CFBs, Gallagher and Hawkesworth (1992) indicated a several distinctive geochemical and isotopic characteristics of CFBs. They are A) uniform incompatible element abundance shown in low Ti basalts in large of the Gondwana CFB (Hergt *et al.*, 1991), B) relatively high SiO_2 contents, distinctive trace elements (e.g. high Nb/Ba), C) enriched Nd, Sr and Pb isotopic ratios shown at many of CFBs. In this section, two different models for the generation of CFBs proposed by White and McKenzie (1989) and McKenzie and Bickle (1988), and Gallagher and Hawkesworth (1992) are reviewed.

First model of White and McKenzie (1989) and McKenzie and Bickle (1988) is based on the anhydrous melting of peridotite and require an extension factors of over 2 and temperatures of over 1280 °C (see Fig. 2.2). According to this model, generation of the CFB is related to lithospheric stretching above anomalous mantle plumes where large amounts of basalts of MORB composition are generated by dry melting of the asthenosphere and mix with a small quantity of K-rich magma from the mechanical boundary layer. Additional melt generate through adiabatic decompression and the volume of melt depends on diverse thickness of the mechanical boundary.

Second model of Gallagher and Hawkesworth (1992) is based on the partial melting of peridotites in presence of small amounts of water (~0.4 %) within the mechanical boundary layer (MBL). In this model, the addition of water to peridotite lowers its solidus temperature and promotes the crystallisation of hydrous phases such as amphibole and phlogopite. Thus, melts produced from the hydrous peridotite are buffered by amphibole and the higher degree of dehydration melting of peridotites produce silica-saturated basaltic melts. This model requires a thick MBL to achieve the large proportions of dehydration melting, however, the extension factor is not important. In spite of minor extension factors (=1.2-1.3), increase of lithospheric extension allows asthemospheric melts within mechanical boundary of 100-200 km thick.

2.8. Summary and conclusion

Geochemical or isotopic evidence can provide a guide for distinguishing melts of lithospheric origin from those derived from the underlying asthenosphere, but with significant uncertainty. Distinction between lithospheric and asthenospheric magma is best illustrated with the comparison of basalts from continental rift zone with OIBs.

In general, mafic basalts from continental rift or extension zones, including the Basin and Range province or the Cameroon line, show a similar geochemical and isotopic characteristics with Hawaiian alkaline basalt even though components of mantle plume from Hawaiian volcanic fields may reflect those of younger plume (< 0.2 Ga). Their geochemical and isotopic characteristics are distinctive from the other continental basalts which are considered as derived from CLM or of mixing of CLM-plume components. Differences of the latter from plume-related rocks include distinctive depletion in Nb, Ta and less pronounced

depletion in Ti and less pronounced enrichment in Ba (thus low La/Nb, Ba/Ta and Nb/Y, high Zr/Nb and Ba/Nb), and a wide range of variation in Nd-Sr-Pb isotopic compositions.

The magmatisms observed in rift zones show geochemical and petrological changes with time, from volumetrically large tholeiitic (subalkaline) to volumetrically small, alkaline rocks. The characteristics suggest that generation of the igneous rocks is triggered by decompressional melting of hot asthenospheric mantle as it rises passively beneath the stretched and thinned lithosphere. Geophysical evidence also suggests intrusion of mafic magma in the low crust during initial stages of magmatism.

Several models have been presented to explain the enrichment mechanism of the lithosphere in terms of metasomatism. These may be grouped into two types, 1) generation of an enriched layer by small melt fractions derived from asthenosphere and their remelting by adiabatic decompression or heat conduction from the mantle (McKenzies and Bickle, 1988); 2) metasomatism by asthenospheric melts which transfer through lithospheric conduits and which are found as pyroxenitic rocks (Menzies *et al.*, 1987). Even though these two mechanism are significantly different, both account for anomalous isotopic compositions and enrichment of LILs and LREE within the lithosphere. The mechanisms of mantle metasomatism may be divided into two types, modal metasomatism and cryptic metasomatism. The specific nature of the metasomatism is reflected by the development of minerals which include pargasitic amphibole, phlogopite and apatite. However, many upper mantle peridotites show chemical and isotopic variation without changes of metasomatic mineralogy. This cryptic metasomatism is important in the interpretation of the enrichment of lithosphere.

In summary,

-lithosphere- and asthenosphere derived magma can be distinguished by integrated geochemical and isotopic evidences.

- geochemical and petrological changes over times at magmatism of rift zones can be explained in terms of the increasing decompression melting of hot asthenospheric mantle as it rises passively beneath the stretched and thinned lithosphere.

-metasomatism is an enrichment process of lithosphere which can be divided into two mechanism; modal metasomatism to produce a metasomatic mineralogy and cryptic metasomatism showing a chemical and isotopic enrichment in the CLM without adding of metasomatic mineralogy.

- the existence of a small melt fraction at a range of upper mantle P-T conditions as a precursor for mantle metasomatism can be supported by experimental results.

-a model of lithospheric evolution by movement of small melt fractions from asthenosphere provide considerable constraints to interpret petrogenesis of lithospheric or asthenospheric derived igneous rocks at Earth surface.

-a model of lithosphere, geochemically and isotopically anomalous lithosphere by

movement of small melt fractions from asthenosphere, provides a considerable constraint to interpret of petrogenesis of lithospheric or asthenospheric derived igneous rock found at Earth's surface.

Chapter 3. Petrogenesis of Quaternary Alkali Basalt, South Australia (SQAB): northern volcanic area and southern volcanic area

3.1. Introduction

An alkali basalt province occurs in the south-eastern corner of South Australia, near the towns of Millicient and Mt Gambier (Fig. 3.2, 3.3a). The province represents a small part of the south-western margin of the Tertiary to Quaternary basaltic province of eastern Australia. This widespread province of Mesozoic-Cainozoic age basalts occurs on the eastern side of the Tasman Fold Belts (Plumb, 1979) and extends from northern Queensland, across the highlands of New South Wales to Victoria extending westward to the South Australian volcanic province and southward to the Tasmanian basaltic province (Wellman and McDougall, 1974; Sutherland, 1981; Wass and Hollis, 1983; O'Reilly and Griffin, 1987).

The South Australian province includes 17 basaltic eruptive centres. These are grouped into two areas, the northern area near Millicient which contains 15 eruptive centres and the southern area which hosts the Mt Gambier and Mt Schank volcanoes (Sprigg, 1952; Sheard, 1990). The northern area volcanics are mainly distributed along three parallel lines, related to the Otway Basin Graben (Sprigg, 1952) and are overlain by the Pleistocene Bridgewater Formation. The southern area volcanics overlie the Bridgewater Formation and are therefore significantly younger than those in northern province.

These eruptive centres are mainly maars or scoria cone-type volcanoes and include composite domes, scoria domes, lava flow maars, agglomerate cones and tuff rings. The volcanic rocks have undersaturated alkaline basaltic composition (Fig. 3.1) and often host xenoliths entrained from the sub-continental lithospheric mantle (Walker, 1967; Sheard, 1983, see Table 3.1).

There is a general agreement that the southern area volcanics erupted during the Middle Holocene and the northern volcanics erupted during the Early Pleistocene, but were dormant or extinct by late Pleistocene (Sheard, 1990). In this study, the South Australian volcanics will be referred as South Australian Quaternary Alkaline Basalt (SQAB), distinguishing them as a distinctive sub-province of the Victorian Newer volcanic province and representing the south -western extension of that province. It is also observed that the Southern area younger volcanics (SAB) are *ne*-hawaiites and the Northern area older volcanics (NAB) are olivine analcimites as mentioned by Irving and Green (1976).

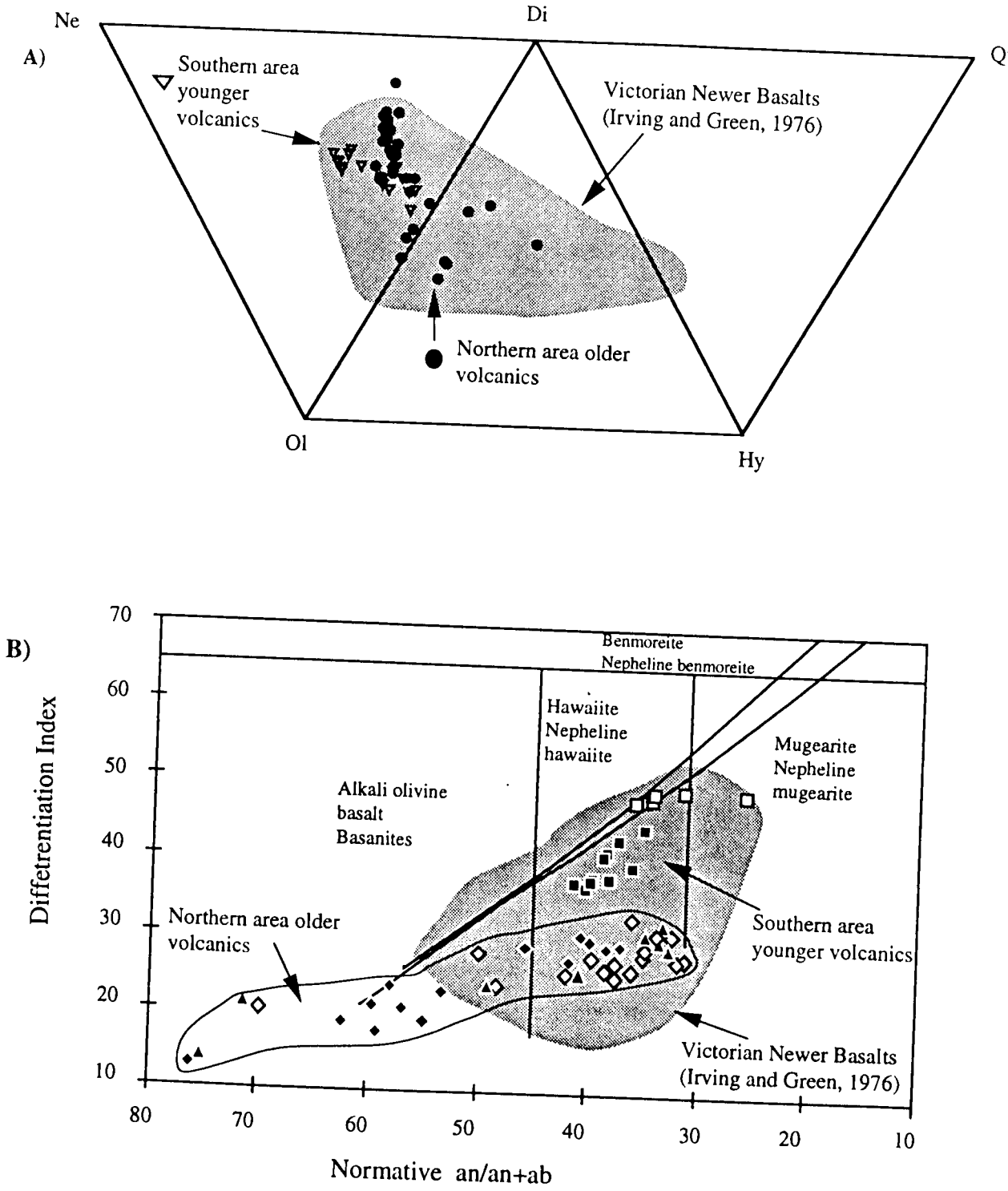

Fig. 3.1. A) C.I.P.W. normative compositions of the South Australian alkaline basalts and Victorian Newer basalts, B) Thornton -Tuttle differentiation Index (D.I.= normative qt+ab+or+ne+lc) against normative an/(an+ab) plot, and curve lines are Hebridean and Hawaiian trends (after Coombs and Wilkinson, 1969). Symbols, (▽) for hawaiites (●) for analcimites, (■) for Mt Gambier hawaiites,(□) for Mt Schank hawaiites, (◆) for NMF, (◇) for BSF, (▲) for MDF.

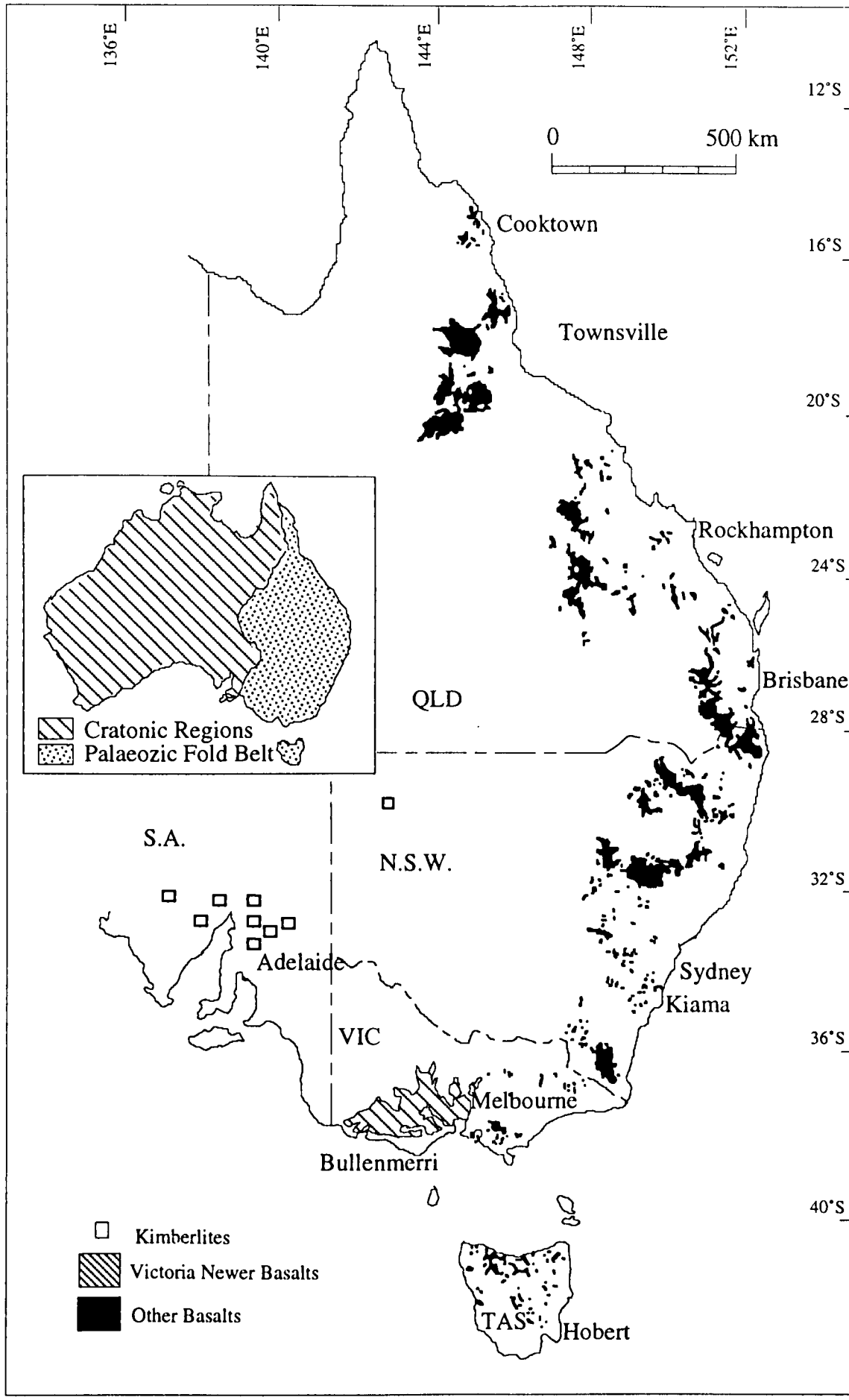

Fig. 3.2. Intraplate volcanic and kimberlite provinces of the eastern Australia (after O'Reilly and Griffin, 1987).

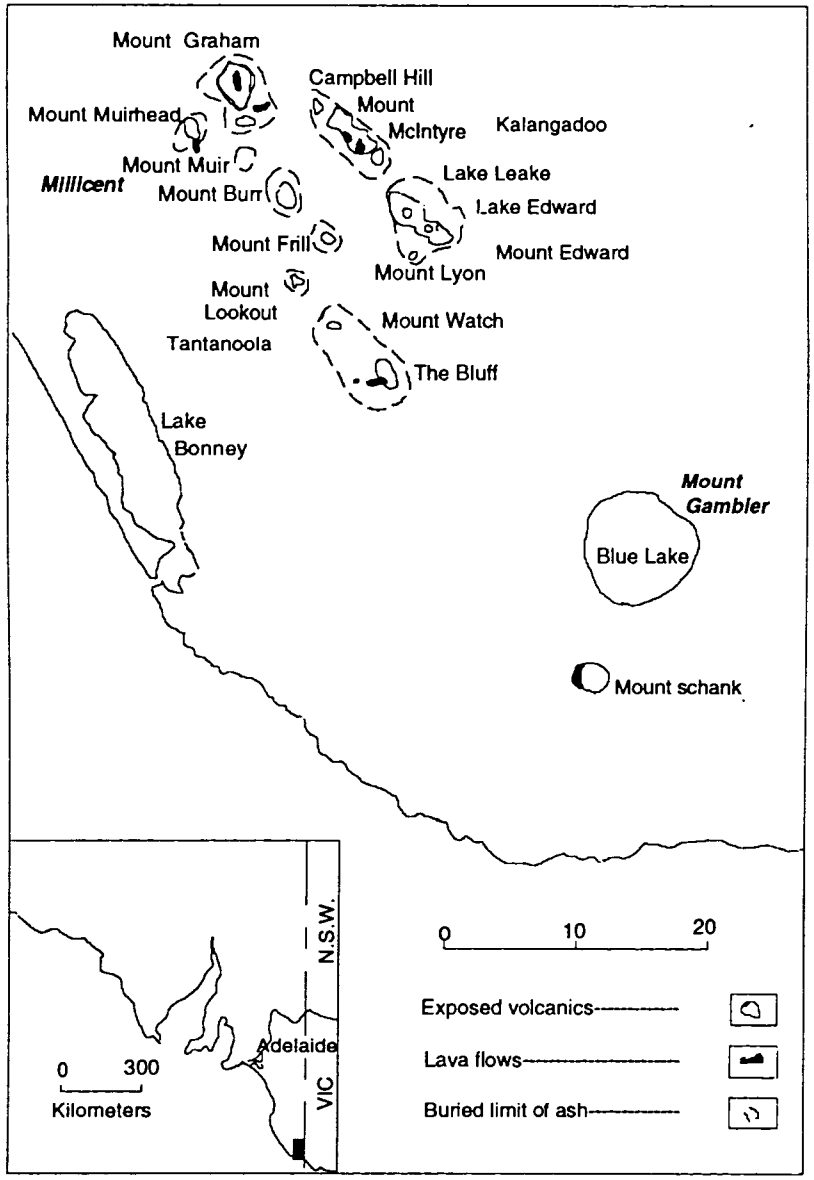

Fig. 3.3a. Geological map of the South Australian alkaline basaltic provinces. They are divided into two groups; the Southern younger volcanic and the Northern older volcanic province (Sheard, 1990).

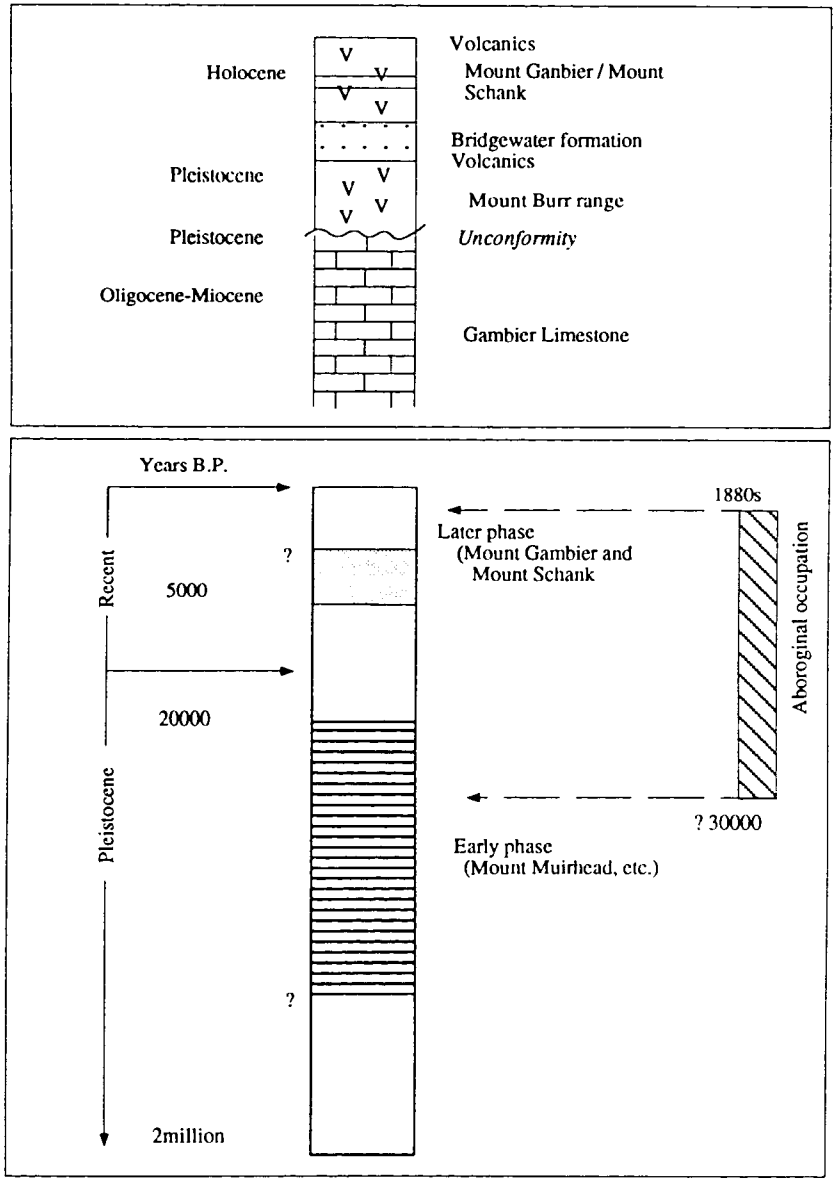

Fig. 3.3b. Stratigraphic sequence and postulated eruptive time of the South Australian alkaline basaltic provinces (Sheard, 1990).

3.2. Previous studies of South Australian alkaline basaltic provinces

Early studies (Fenner, 1921; Sprigg, 1952) considered the South Australian volcanic provinces as the western extension of the Victorian Newer Volcanic provinces of the Post-Miocene age (mainly Late Pliocene to Recent time), which are distinguished in Victoria from the Older Volcanics of the Palaeocene to Early Miocene age (Irving and Green, 1976).

Petrological and geological studies have been made by several authors (Stanley, 1909, 1910; Fenner, 1921; Fehlberg, 1968; Forbes, 1969; Joyce, 1975; Sheard, 1978, 1990). Stanley (1909, 1910) provided a whole rock chemical analysis of basalt from Blue Lake at Mt Gambier and additional chemical analyses of a lherzolite xenolith as well as a mineralogical data on olivine. Fehlberg (1968) reviewed the origin of lherzolite xenoliths of Mt Gambier and postulated the xenoliths as an initially accidental inclusion of peridotitic mantle material into ascending basaltic magma.

Fenner (1921) suggested the age of Mt Gambier volcanism as of late Tertiary Pliocene - Recent. This is deduced from the correlation with Victorian eruptions. He also provided a reconstructed model of a possible episode for the formation of Mt Gambier cone. Sprigg (1952) grouped the volcanics into two distinct areas; the earlier group being late Pliocene to Early Pleistocene as represented by the Mt Burr and Mt McIntyre volcanics; and late groups being Late Pleistocene represented by the Mt Gambier and Mt Shank volcanics. Forbes (1969) provided a review of Post-Precambrian volcanism in South Australia and suggested that the earlier volcanism defined by Sprigg (1952) was the Pre-Mid-Pleistocene or possibly Pliocene age.

Joyce (1975) reviewed Quaternary volcanism in Victoria and South Australia. He suggested dominance by the maar type volcanics of late Pliocene-Holocene in the southern edge of the these regions. It was also suggested that the Quaternary volcanism together with Older volcanics of the Palaeocene to Lower Miocene is related to uplift or local tectonic movements associated with separation of Australia from Antarctica. Sheard (1978) provided a well defined petrographical description of the Mt Gambier volcanics and a postulated episode of volcanic eruption related to the formation of the composite maars. It was also suggested two main periods of lavas followed by a highly gas charged magma eruption, resulting in the pyroclastic dominated stratigraphy and structurally controlled disposition of the craters. Sheard (1990) also provided a summarised geological guide of the South Australian alkaline volcanic provinces.

Geochemical and/or isotopic studies have been made by some authors (Cooper and Green, 1969; Irving and Green, 1976; McDonough *et al.*, 1985). However most of the studies are limited to very few localities in the South Australian provinces.

Irving and Green (1976) provided major element data from five localities, and described Mt Watch and Mt McIntyre volcanics as olivine analcimites, Mt Gambier volcanics as nepheline hawaiite, and Mt Shank and Mt Burr volcanics as K-rich nepheline hawaiite.

They also provided a fractionation model, suggesting that most of the basaltic magma types in the Newer volcanic provinces of Victoria and SE South Australia originated as progressively differentiated liquids from the primary melts of the dominantly basanitic composition which are derived by partial melting of the garnet-peridotite mantle.

McDonough *et al.* (1985) gave geochemical and isotopic results from four South Australian localities together with some from the Tertiary-Recent Tasmania and the Newer basaltic province of Victoria. They also provided a comparison of the Australian basalts with Hawaiian basalt. Based on the their studies of these rocks, they concluded that the sub-oceanic lithospheric mantle is different from the sub-continental lithospheric mantle and that isotopic difference among SE Australian alkaline basalts reflect a varying degree of exchange and mixing between the hotspot plume and lithospheric mantle melt components. Cooper and Green (1969) provided lead isotope analyses of Mt Gambier and Mt Schank volcanics and their xenoliths together with some from the Newer basaltic province. This data suggest that the Newer basalt are EM 1 type OIB-like whereas Tasmanian Tertiary basalt show HIMU type OIB-like characteristics (Lanyon *et al.*, 1993).

"Intraplate volcanism" (ed. by Johnson, 1989) summarised the geology, petrology, geochemistry and isotopic compositions of all eastern Australian basaltic provinces. In here, Cas (1989) suggested that maar type eruptive centres are widespread in the southern half of the New Volcanic province and Ewart (1989b) indicated that the eastern Australian region is dominated by mafic lavas.

3.3. Age of the South Australian alkaline basaltic provinces

The exact age range of the SQAB is still in question because of limited isotopic dating. The K-Ar data of the Victorian Newer Volcanics range from 4.5 to 0.57 Ma. (McDougall *et al.*, 1966; Rahman and McDougall, 1972; Wellman, 1974), carbon isotopic results on tuffs from Tower Hill (Gill, 1967) ranges from 5000 to 6000 years whereas isotopic data of all eastern Australia intraplate volcanics (Duncan and McDougall, 1989) range from 69.9 to 0.1 Ma (mainly 40 to 20 Ma).

Results from the SQAB have been provided by some authors (Gill, 1955; Dury and Langford-Smith, 1968; Polach *et al.*, 1978; Smith and Prescott, 1987). Their isotopic dating from charcoal under the tuff of Mt Gambier includes 1410±90 (Dury and Langford-Smith, 1968) and 4710±70 (Gill, 1955). Carbon isotopic dating of charcoal from Mt Gambier by Ferguson and Rafter (1957) also shows an age of less than about 4800 BP (Holocene age). Recent thermoluminescence dating of former beach sands overlain by the lava flow from Mt Schank (Smith and Prescott, 1987) gave an age of 4930±540 yr BP and a carbon isotopic age obtained from charcoal fragments in the Bridgewater Formation of Mt Schank give a maximum age of 18,100±350 years (Polach *et al.*, 1978).

In addition, palaeomagnetic measurements (Barbetti and Sheard, 1981) suggested that

the eruptive time of Mt Schank was either between 5000 to 1000 yr BP or older than 7000 yr BP. Pollen studies from a core sample from Lake Leake (Dodson, 1974) suggested that the sedimentation of Lake Leake began 20000 yeary ago. More clear relative timing of the SQAB can be provided by the stratigraphic relations (Fig. 3.3b). The northern volcanics are overlain by the Pleistocene Bridgewater formation and overlie Mt Gambier Limestone whereas the southern volcanics are underlain by the Bridgewater formation.

In summary, the exact eruption age of the South Australian alkali basaltic province has been so far inadequately recorded and may be as early as Tertiary or equivalent to the northern Victoria volcanics. The southern volcanic province is clearly much younger and probably less than 6000 yr BP.

3.4. General geology of South Australian Quaternary Alkaline basaltic provinces

General geology, volcanic type and petrography of the South Australian Quaternary alkaline basalt are summarised Table 3.1.

Table 3.1. General geology of the South Australian volcanic provinces (After Sheard, 1990).

Name of volcano	Type of volcano	Volcanic products	Xenoliths
Mt Gambier	Maars	Stratified tuff, agglomerate, scoria, lava	Lh, Px, Du
Mt Schank	Maar, cones	Lava, scoria and agglomerate	
Mt McIntyre	Composite	Lava, with minor scoria & ash (well bedded)	Px, Du
Lake Leake, Lake Edward	Tuff ring, Maar	Ash and agglomerate (well bedded)	Lh
Mt Edward	Maar	Bedded agglomerate, lapilli.	Lh
Mt Lyon	Ash cone	Bedded lapilli and agglomerate	Lh
Mt Muirhead	Maar, cone	Bedded agglomerate overlying lava flow	Lh, Du
Mt Watch	Scoria dome	Bedded scoria and lava bombs	Du, Lh
The Bluff	Composite	Lava, scoria, agglomerate	Du
Mt Graham	Composite	Lava, ash and agglomerate	
Burr lava flow	Lava flow	Lava Flow	
Mt Frill	Ash dome	Lapilli and agglomerate	
Mt Lookout	Ash cone	Agglomerate in soil below dune sands	
Boyce Hill	Ash cone	Lapilli and agglomerate	
Submarine flow (Beachport)	Flow	Lava? (no samples collected)	
Mt Muir	Ash cone	Ash, lapilli and agglomerate	
Campbell Hill	Ash dome	Ash and agglomerate	
Mt Burr	Composite	Lava, scoria and agglomerate	

Notice, Lh (lherzolite), Px (Pyroxenites) and Du (Dunites)

3.4.1. Southern area volcanics (SAB)

Mt Gambier volcanics; The Mt Gambier volcanics are evident now four main lakes and a cone shaped maar structure (Fig. 3.4). The Mt Gambier volcanic layer is underlain by the Upper Eocene to Miocene Gambier Limestone which is well exposed on the water level of Valley Lake and Blue Lake. The Gambier Limestone is overlain conformably by the Pleistocene dune sands at the New Pumping station of the Blue Lake and Nurses Landing of Valley Lake (Sheard, 1978).

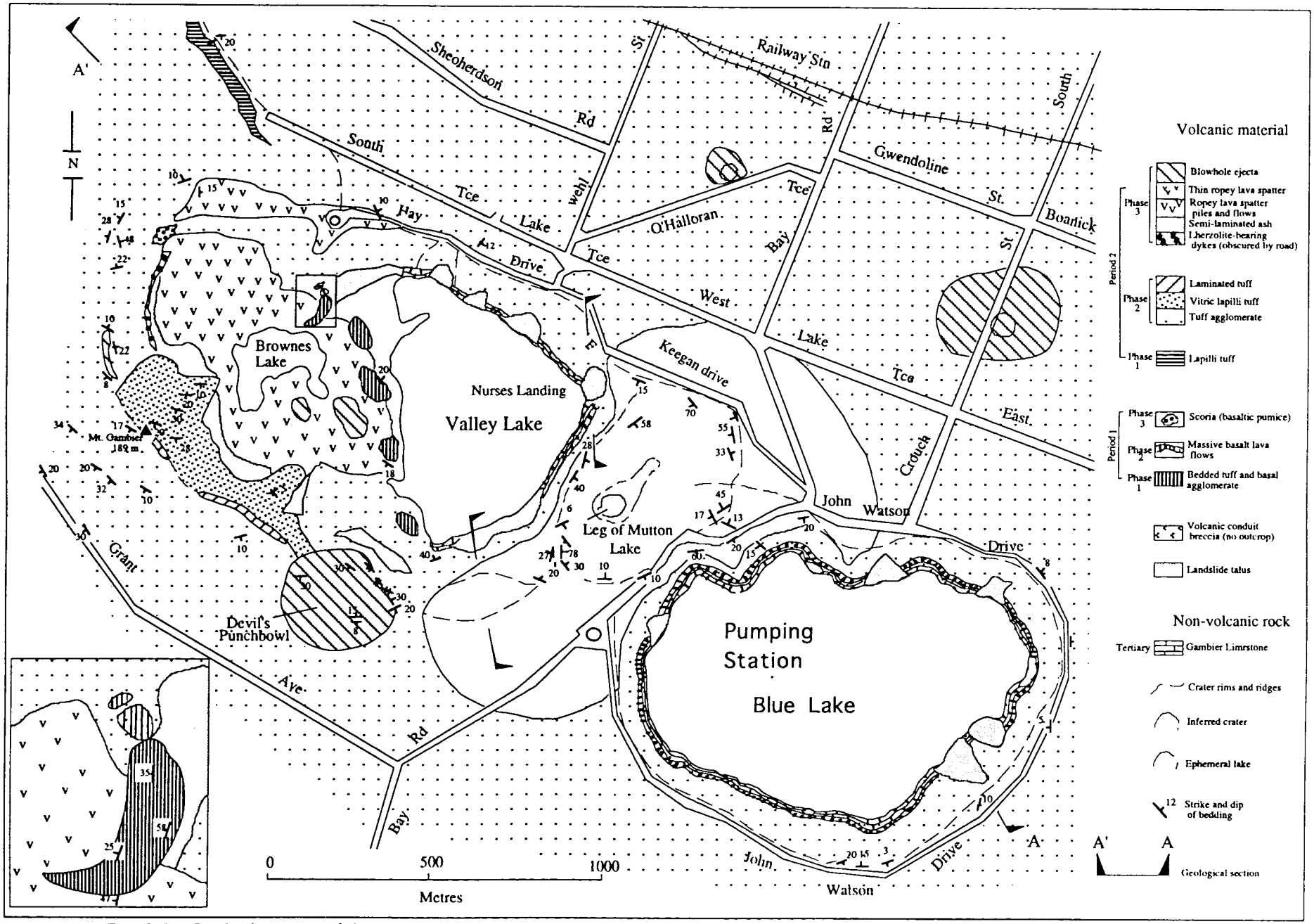

Fig. 3.4a. Geological map of the Mt Gambier volcanics (Sheard, 1990).

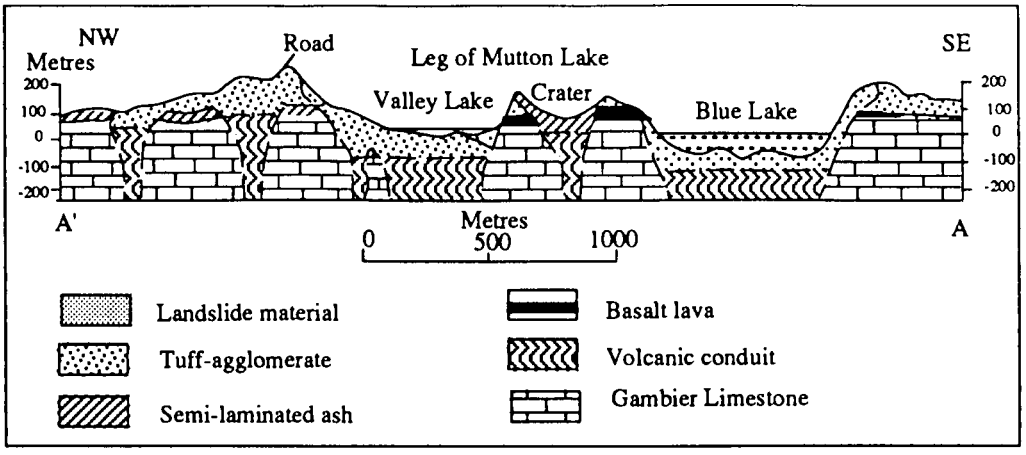

Fig. 3.4b. Cross section of the Mt Gambier crater (Sheard, 1986).

Well layered tuff is exposed adjacent to Centenary Tower which shows the alternating colours and the slightly outside dip from the inner vent. Tuff agglomerate layers adjacent to the Lookout near the camping site contain many fragments of basaltic components ranging from vitric and massive, to scorious basaltic rocks with many limestone fragments of variable size.

Lava flows showing darkish and reddish brown colours are well exposed at the edge of the road adjacent to Brownes Lake. Many fragments of peridotitic xenoliths with variable range of sizes occur in soils of vegetated Devil's Punchbowl and in the exposure of the all basaltic rocks on the road of Valley Lake and Brown Lake. An amphibole-bearing pyroxenitic xenolith of 2.5-4.5 cm wide is found at a core of scoriaous basaltic rock.

Carbon dating (Blackburn *et al.*, 1982), paleomagnetic results (Barbetti and Sheard, 1981) as well as field evidence, suggests that the composite maar structure resulted from at least two main eruptions within a short time.

Mt Schank volcanics; The Mt Schank volcanics are located 14 km to the south of Mt Gambier and show a similar eruption sequence to the Mt Gambier volcanics (Fig. 3.5a), but are distinguished by their smaller volume of eruption. They consist of two large adjacent craters, a small crater on the west side, and other scoracious or pumiceous lava flows extruded along the small fissures. The scoracious or pumiceous lava flows are well exposed on the NE side of the main crater and some of them form small hills or domes unlike the main crater of sharp cone structure.

Well layered tuff agglomerate outcrops at the top of the main crater. It show a darkish grey colour and most of the rock fragments in the tuff layer are finer than those of Mt Gambier. Miocene Gambier Limestone overlain by massive lava flows is well exposed in a small crater adjacent to the main craters. Four well exposed quarry sections (Fig. 3.5b) display a lava flow layer underlain by baked brick red quartz sands (site 3 and 1) and a breached lava beneath the lava-Bridgewater formation contact.

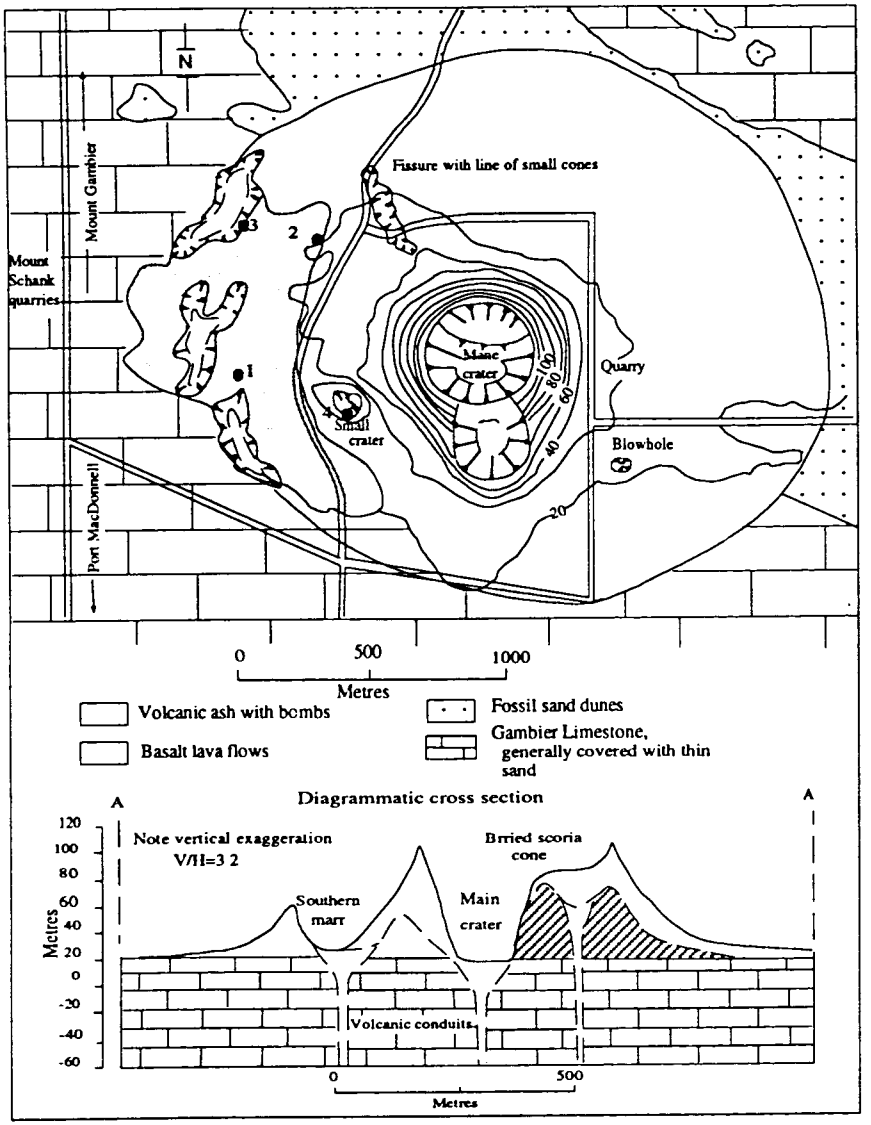

Fig. 3.5a. Geological map of the Mt Schank volcanics (Sheard, 1986).

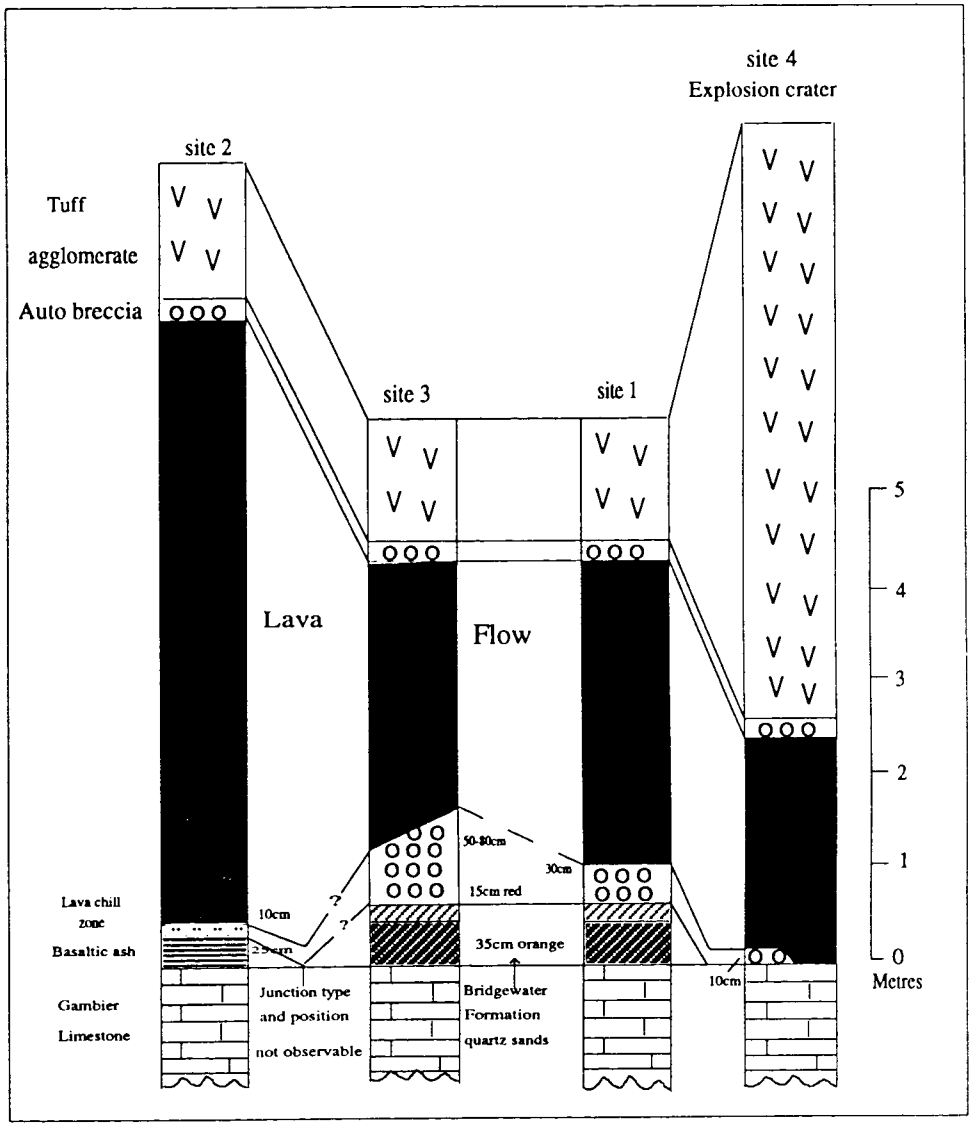

Fig. 3.5b. Stratigraphic sequence of the Mt Schank volcanics (Sheard, 1986). Site numbers shown in these Fig. are given in the Fig. 3.5a.

3.4.2. Northern area volcanics (NAB)

The NAB are considered to be controlled by fissures because of their distribution along three parallel NW-SE trending fault lines (Sprigg, 1952; Marker, 1975) (Fig. 3.6). Evidence from seismic profiling (Sheard, 1986) supports this notion. Most of the volcanics including The Bluff, Mt McIntyre and Mt Graham volcanics show multiple eruption events.

Volcanics distributed along the northernmost fault line (NMFV); The NMFV include Campbell Hill, Mt McIntyre, Boyce Hill, Mt Lynon, Lake Leake, Lake Edward and Mt Edward. In the Mt McIntyre volcanics, lava flows are well exposed in a cut quarry face. A small exposed cliff near the Lake Leake displays a fault face formed by the weight of overlying materials after deposition (Sheard, 1990). At this locality, well-layered agglomerates contain many basaltic bombs of 5-10 cm wide (mainly 1-2 cm) with country rock fragments. Cross-bedding caused by base surges was also reported in this exposure (Sheard, 1990).

In the Mt Edward volcanics, a disused quarry site near the fire Lookout tower exposes sandstone and limestone fragments in tuff-agglomerate like that of Lake Leake. Spinel bearing lherzolite xenoliths of 0.8-1.5 cm wide are also found in the tuff- agglomerate. The Mt Lyon volcanics are well vegetated and covered with soil. However, many weathered volcanic agglomerate of 20-30 cm wide are well exposed in the area. Upper mantle xenoliths were also reported from the tephra piles in these volcanics (Walker, 1967)

Volcanics distributed along the beach side fault line (BSFV); The BSFV include Mt Muirhead, Mt Lookout, Mt Watch and The Bluff. The Mt Muirhead volcanics are deeply eroded, and thus show a deeply developed soil profile on its lower slopes (Sheard, 1990). Thick volcanic exposures in a quarry display well layered tuff agglomerates containing 1-4 cm basaltic bombs and country rock fragments. The exposures show an alternation of light and dark dominant colour. A few spinel bearing lherzolites and dunitic xenoliths ranging from 0.4 to 1.2 cm wide are also found in the basaltic bombs. Many sedimentary structures on the lower western flanks were produced by coastal processes including the cross-bedded tuff structure with steep angles (Sheard, 1990). Sheard (1990) suggested that the Mt Muirhead form one of the oldest volcanos in northern volcanic group, based on field studies.

The Mt Watch volcanics form a subsidiary vent to The Bluff volcanic system (Sheard, 1990). Well layered bedding dips radially outward from the inner vent and overlying yellowish thick consolidated sand sequence of Pleistocene Bridgewater formation are exposed in the wall of the maar. The scoria piles show reddish colour because of oxidation by steam during the eruption (Sheard, 1990). Many ellipsoidal basalt bombs (20-50cm wide) are found in the layered scoria piles. The bombs show a slightly reddish skin at the contact with bedded scoria and the long side is parallel to the layering.

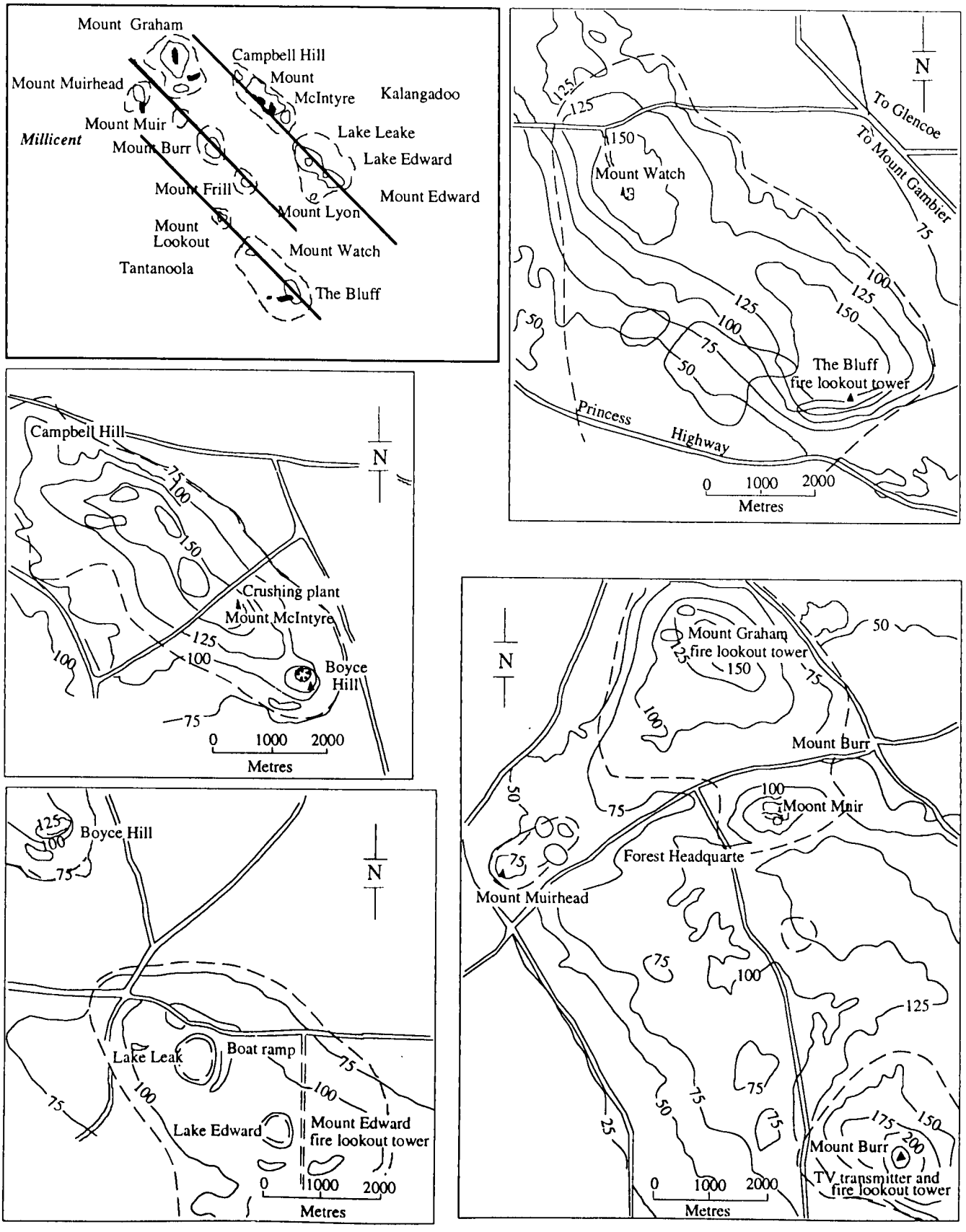

Fig. 3.6. Geological map of the Northern area older volcanics.
The volcanics are distributed along the three parallel fault lines (Sheard, 1986).

The Bluff volcanics may be younger than that adjacent Mt Watch volcanics although the boundary between two volcanics is covered with sandstone (Sheard, *pers. comm*, 1993). A few pyroxenitic and dunitic xenoliths (0.3 -0.9 cm wide) are also found in the massive basaltic rocks.

Volcanics distributed along the middle fault line (**MDFV**); The MDFV include Mt Graham, Mt Muir, Mt Burr and Mt Frill. Most of Mt Graham volcanics are well covered by sandstone of the Bridgewater formation. A quarry cutting shows a alternating sequence, more massive lava flow (top), stretched fine lava layer and auto-brecciated lava scoria (bottom), suggestive of the front part of a lava flow. Burr lava flow is exposed near the road along the Mt Burr. It is a reddish black color with many fragments basalts showing stream holes, suggestive of the top of the lava flow.

3.5. Petrogenesis of Southern area younger volcanics (SAB), Mt Gambier and Mt Schank hawaiites

3.5.1. Petrography and mineralogy

Twenty five samples have been selected for petrographic descriptions and these are summarised in Table 3.2. The SABs contain Ol±Cpx as phenocryst, Cpx±Pl±Opx as micro-phenocryst and Cpx+Pl+Ol+Sp ±K-Fd±Il as groundmass. They are characterised by the existence of groundmass plagioclases, a distinctive foliation and glomeroporphyritic textures. In the Mt Schank hawaiites, the plagioclase grains coexist with alkali-feldspar (sanidine-anorthoclase) groundmass. In general, the Mt Schank hawaiites are distinguished from those from Mt Gambier by their abundant clinopyroxene micro-phenocrysts, fine grained olivine phenocrysts and fluid inclusions in the vesicles with variable size. The Mt Gambier hawaiites are distinguished from those of Mt Schank by the existences of Ol+Px xenocrysts, inclusions of abundant secondary minerals (e.g. calcite and quartz) and country rock fragments (e.g. limestone).

Table 3.2. Petrography of the Southern area younger volcanics

Sample Name	963 GA-1 to 15	963 SC-1 to 10
Locality	Mt Gambier	Mt Schank
Name	Hawaiites	Hawaiites
Phenocrysts	Ol±Cpx (8-17 %)	Ol±Cpx (10-14 %)
Microphenocrysts	Cpx±Pl±Opx (5-15 %)	Cpx+Ol+Pl (8-15 %)
Groundmass	Cpx+Pl+Ol+Il+Sp (48-62 %)	Cpx+Pl+K-Fd+Ol+Il (42-58 %)
Second, Minerals	Qt, Cal	Qt
Texture	Massive, amigdaloidal to vesicular rock, fluidal, glomero-porphyritic, pseudo-trachytic texture, Pl-lath, groundmass, zonal Cpx	Pronounced foliation Pl-laths groundmass, coexisting alkali -Fd, fluidal glomero-porphyritic texture

Figures opposite;

Fig. 3.7a. Photomicrograph of eu- to sub-hedral olivine phenocrysts (o) and thin lath shaped plagioclase groundmass from the Mt Gambier hawaiite (Ga 10).

Fig. 3.7b. Photomicrograph of sub- to an-hedral olivine phenocrysts (o), lath shaped plagioclase groundmass in the Mt Schank hawaiite (Sh 1). The plagioclase groundmass coexists with alkali-fd (sanidine- anorthoclase).

Fig. 3.7c. Photomicrograph showing a different cooling history in the Mt Gambier hawaiite (MGa 1); One side(right) exhibits abundant olivine and clinopyroxene phenocrysts and plagioclase groundmass.

Fig. 3.7d. Photomicrograph showinga lineation by alignments of plagioclase groundmass and a glomeroporphyric texture by a aggregation of olivine microphenocrysts (o) in the Mt Schank hawaiite (Sh 6).

Fig. 3.7e. Photomicrograph of a olivine xenocryst (o) enveloped by lath shaped clinopyroxene micro-phenocrysts (cp) in the Mt Gambier hawaiite (Ga 5).

Fig. 3.7f. Photomicrograph of a clinopyroxene grain (cp) showing a zonal texture, olivine phenocrysts of variable grain sizes, and lath shaped plagioclase groundmass in the Mt Gambier hawaiite (MGa 28).

Fig. 3.7g. Photomicrograph showing a glomeroporphyritic texture by an aggregation of two coexisting pyroxenes (cp & op) from the Mt Gambier hawaiite (Ga. 9). In the Mt Gambier hawaiites, abundant pyroxene phenocryst-bearing rocks are olivine phenocryst-rich.

Fig. 3.7h. Photomicrograph of clinopyroxenes (cp) showing a hourglass zonal texture from the Mt Gambier hawaiite (MGa 20).

Width of a scale bar (left bottom) is 1 millimetre.

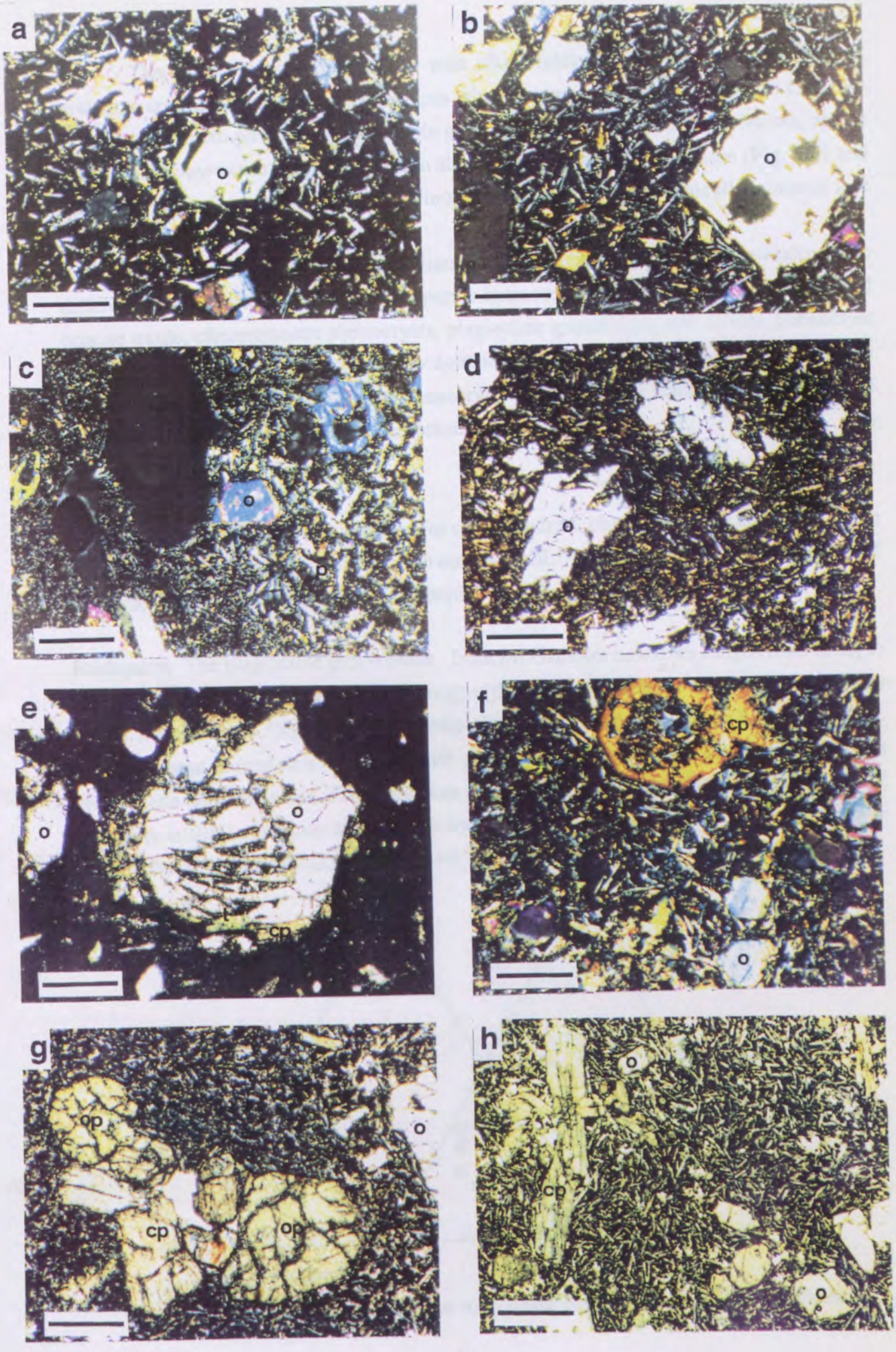
a
o
b
o
c
o
p
d
o
e
o
o
cp
f
cp
o
g
op
o
cp
op
h
o
cp
o

The plagioclases which coexist with alkali feldspar groundmass in Mt Schank hawaiites are mainly acicular or lath-shapes whereas many of those from the Mt Gambier hawaiites are micro-phenocrysts of variable grain sizes. In the Mt Gambier hawaiites, coarse euhedral clinopyroxene phenocrysts often show hourglass and zonal texture (Fig. 3.7) and samples containing more abundant clinopyroxene phenocrysts typically contain less abundant plagioclase groundmass.

Some of the Mt Gambier hawaiites contain microscopic textures revealing two different cooling history (Fig. 3.7). One part is characterised by abundant reddish coloured opaque oxide, clinopyroxene phenocrysts, plagioclase groundmass and olivine phenocryst whereas the other part is characterised by dominant blackish coloured opaque oxide, mainly glassy groundmass with a few olivine phenocryst. These different texture suggests different cooling a history during the repeated eruption.

3.5.2. Mineral chemistry

Selected samples were analysed for clinopyroxene, olivine, feldspar and Fe-Ti oxide compositions. The analyses were carried out by JEOL 733 microprobe at the University of Adelaide. Details of the analyses and calibration are shown in Appendix 1.

Feldspars; The plagioclase groundmass from Mt Gambier hawaiites ranges from An_{41} to An_{57} (andesine to labradorite, mainly An_{52-57}) whereas that from Mt Schank hawaiites ranges from An_{11} to An_{59} (andesine to oligoclase, mainly An_{47-59}) (Fig. 3.8, Table 3.3). Alkali feldspar groundmass coexisting with plagioclase groundmass in Mt Schank hawaiites are sanidine to anorthoclase. The continuous range of feldspar compositions in the Mt Schank hawaiites is similar to those of hawaiites and *ne* -hawaiites from eastern Australia, ranging from labradorite through calcic anorthoclase to sanidine in the groundmasses (Ewart, 1989a).

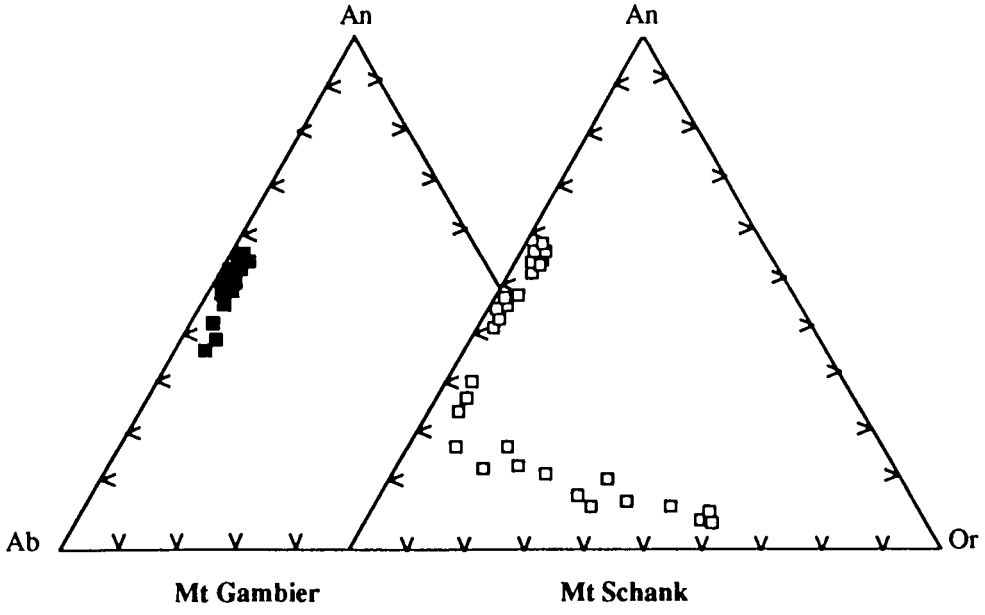

Fig. 3.8. Plagioclase and alkali feldspar compositions of the Southern area younger volcanics.

Table 3.3. Representative feldspar analyses of the Southern area younger volcanics.

Sample	963-Ga 7					963-Ga 10			963-Sh 2				
Locality	Mt Gambier					Mt Gambier			Mt Schank				
SiO2	55.02	53.50	53.97	54.92	54.22	54.19	53.62	54.97	53.56	60.91	61.36	58.47	60.02
TiO2	0.26	0.13	0.49	0.11	0.15	0.07	0.28	0.21	0.16	0.76	0.38	0.33	0.66
Al2O3	29.47	28.53	28.31	28.50	28.92	28.53	29.44	28.16	29.44	23.05	22.86	25.05	24.21
FeO	0.79	0.78	0.89	0.75	0.86	0.95	0.76	0.74	0.75	0.40	0.43	0.74	1.08
MnO	0.07	0.09	0.00	0.03	0.08	0.03	0.23	0.00	0.00	0.09	0.05	0.03	0.05
MgO	0.00	0.00	0.00	0.00	0.00	0.00	0.00	0.00	0.00	0.00	0.00	0.00	0.00
CaO	10.91	11.64	10.88	11.02	11.28	10.99	11.59	10.12	11.80	4.07	4.37	6.65	5.48
Na2O	4.72	4.73	4.71	5.02	4.63	4.77	4.76	4.99	4.53	6.72	8.37	6.77	7.63
K2O	0.33	0.32	0.41	0.37	0.28	0.26	0.35	0.46	0.42	2.67	1.45	0.61	0.88
Cr2O3	0.04	0.06	0.01	0.06	0.00	0.00	0.05	0.11	0.00	0.00	0.00	0.00	0.01
Total	100.60	99.78	99.69	100.79	100.40	99.79	101.10	99.75	100.67	98.68	99.27	98.65	100.02
An(Ca)	55.0	56.6	54.7	52.3	56.4	55.2	56.2	51.4	57.6	21.0	20.6	33.9	27.0
Ab(Na)	43.1	41.6	42.9	45.5	41.9	43.3	41.8	45.8	40.0	62.6	71.3	62.4	67.9
Or(K)	2.0	1.8	2.5	2.2	1.6	1.5	2.0	2.8	2.4	16.4	8.2	3.7	5.2

Sample	963-Sh 2			963-Sh 4									
Locality	Mt Schank			Mt Schank									
SiO2	61.48	60.02	60.91	63.59	63.81	64.15	63.53	63.88	56.76	57.21	55.74	56.17	54.11
TiO2	0.98	0.66	0.76	0.36	0.46	0.40	0.25	0.50	0.26	0.17	0.18	0.16	0.38
Al2O3	21.55	24.21	23.05	20.21	19.74	19.80	19.67	20.06	27.59	26.97	27.62	27.89	27.38
FeO	0.00	1.08	0.40	0.00	0.00	0.00	0.00	0.10	0.64	0.55	0.61	0.78	0.77
MnO	0.16	0.05	0.09	0.00	0.21	0.12	0.02	0.00	0.00	0.01	0.06	0.14	0.02
MgO	0.00	0.00	0.00	0.00	0.00	0.00	0.00	0.00	0.00	0.00	0.00	0.00	0.00
CaO	2.79	5.48	4.07	1.91	1.29	1.25	1.17	1.18	9.49	8.88	10.03	10.19	10.23
Na2O	5.38	7.63	6.72	5.48	4.11	4.15	4.15	4.26	5.66	5.97	5.82	5.67	5.71
K2O	6.20	0.88	2.67	7.45	9.86	9.52	9.52	10.21	0.26	0.39	0.14	0.29	0.41
Cr2O3	0.00	0.01	0.00	0.00	0.00	0.04	0.00	0.07	0.05	0.00	0.10	0.01	0.00
Total	98.53	100.02	98.68	99.00	99.47	99.43	98.31	100.25	100.71	100.15	100.29	101.30	99.01
An(Ca)	14.0	27.0	21.0	9.2	6.3	6.2	5.9	5.6	47.4	44.1	48.4	49.0	48.6
Ab(Na)	48.9	67.9	62.6	47.9	36.3	37.4	37.5	36.7	51.1	53.6	50.8	49.3	49.1
Or(K)	37.1	5.2	16.4	42.9	57.4	56.4	56.6	57.7	1.5	2.3	0.8	1.7	2.3

Clinopyroxenes; The clinopyroxenes show variable grain sizes ranging from groundmass to phenocrysts. The grains have diopsidic, salitic to augitic composition and Mg# (=100xMg/(Mg+Fe)) of 70-75. Their Mg# values increase with those of whole rocks composition (Fig. 3.9, Table 3.4). In general, clinopyroxenes of the Mt Gambier hawaiites are diopsidic to augitic and those from Mt Schank hawaiites are dominantly salitic composition. Their compositions are clearly distinguished from those of spinel lherzolite which have diopsidic and enstatic to bronzitic composition.

Clinopyroxene from the Mt Gambier hawaiites is distinguished from those of the Mt Schank hawaiites by more jadeitic component, low CaO and high Na_2O (Fig. 3.10). This may reflect differences of substitutions of Ca by Na in the W site of the general formula $(W)_{1-p}(X,Y)_{1+p}Z_2O_6$. Mt Gambier hawaiites show lower TiO_2 than Mt Schank hawaiites, but a wide variation of Cr_2O_3. This relationship may reflect a wide variation of Fe(3) in the Y site. The South Australian hawiites also show increase of Ti with Al(t) and decrease of Al_2O_3 with Mg# (or SiO_2), reflecting the increase of the solid solution in the Ca tschermak component, $CaAlAlSiO_6$, with silica undersaturation of the host basalts.

Many of the clinopyroxenes from the South Australian hawiites show insufficient occupations for the tetrahedral site (Si+Al) which enable to the stoichiometric 2 atom per formula unit in some of the hawaiites. This characteristic may reflect occupation of Ti in the tetrahedral site and an increase of the Fe(3) or Cr in the Y site. In the reviews of the eastern Australian volcanics, Ewart (1989a) observed an increase of Al (IV) and Ti with silica undersaturation of the host rocks and increase of Cr with Mg#. He also noticed insufficient of tetrahedral site (Si+Al = 2) in pyroxenes from leucitites.

Olivines; Olivine compositions from South Australian hawaiites are plotted in Fig. 3.9 and 3.11. In general, the olivines from Mt Gambier hawaiites are distinguished from the Mt Schank hawaiites by their high CaO, MnO and low Mg# (Table 3.5). No clear relationships are shown between coexisting olivine and clinopyroxene.

The Mg# of the host rocks could be expected to be correlated with those of olivine grains. Olivine composition from the South Australian hawaiites may not reflect Mg-Fe olivine-liquid partitioning (K_D). For example, Mt Gambier hawaiites which show a high Mg* (=Mg/Mg+Fe(t)+Mn+Ca) in whole rock compositions show a low Mg* in the olivine composition. These discrepancies of equilibrium between olivine and whole rock composition have also been reported in eastern Australian volcanics (Ewart, 1989a). In the olivine data from eastern Australia volcanics, olivine from the *ne* - normative rocks of the lava-field provinces show a equilibrium in Mg-Fe olivine-liquid partitioning (K_D) whereas those from the *ol* - and *q* -normative volcanics do not. Ewart (1989a) explained that olivines of higher Mg# (near Fo_{90}) and low CaO are xenocrystic or relic grains initially in equilibrium with their lherzolitic source in the region of magma segregation or disaggregated lherzolite

debris. Less magnesian olivine relative to the whole rock formed during early equilibrium crystallization, olivine accumulation, and supercooled crystallization.

In the South Australian hawaiites, the olivines of the Mt Gambier hawaiites showing high CaO and low Mg* can be explained by the increasing solubility of the Ca solid-solution in the olivine as a function of the silica activity (Stormer, 1973). Stormer, (1973) has reported an increase of Ca in olivine phenocrysts from nephelinites and basanites rather than those of the tholeiitic basalts, a decrease of Ca in olivine at constant pressure with cooling and an increase of Ca at the constant temperature as the magma rises. He also suggested increase of Fe with Ca reflect crystallisation at the stable pressure condition. However, Ca-content of the olivine may not unrelated to temperature of the crystallisation (Ferguson, 1978). In the South Australian hawaiites, olivine in the Mt Gambier hawaiites containing high CaO (wt %) with low Mg*. This relationship may reflect crystallization at a stable pressure, or an increase of Ca at constant temperature as the magma rises. Slightly high MnO are shown in low Mg* olivine from Mt Gambier. Ferguson (1978) suggested that the Mn content of the olivine is not related to Mg#, Ni and CaO.

Fe-Ti-Cr oxides; Oxide minerals are found as groundmass, scattered gains on the border of the ferrous minerals or scattered discrete grains. Ulvöspinels have been observed in two hawaiites whereas in the Mt Schank hawaiites, ulvöspinel and titanomagnetite coexist (Fig. 3.12, Table 3.6). Two coexisting Fe-Ti oxide pairs of the Mr Schank hawaiites are used to calculate quenching temperatures and oxygen fugacity of the South Australian basalt. At the T °C -fo2 method based on the coexisting Fe-Ti oxides (Buddington and Lindsley, 1964), the temperature are 890 °C and 925 °C respectively and lie along the QFM buffer. The results are consistent with those of mafic lavas from eastern Australia (Ewart *et al.*, 1980; Ewart, 1989a).

3.5.3. Whole rock geochemistry

A) Introduction

Sixteen selected samples were analysed for major and trace elements by the XRF in the University of the Adelaide. Four samples were analysed for REE composition with the Finnigan Mat 261 mass spectrometer in Department of Geology and Geophysics, University of Adelaide. Details of analytical methods and sample preparation are discussed in the Appendix 1. Analytical results are shown in the Table 3.7, 3.8 and 3.10.

B) Major element chemistry

The hawaiites show predominantly *ne*-normative composition, and range from hawaiites and nepheline hawaiites to mugearite and nepheline mugearite (Fig. 3.1). They show a typical basaltic or alkali basaltic composition (Fig. 3.13).

Table 3.4. Representative clinopyroxene analyses of the Southern area younger volcanics.

Sample	963-Ga 1						963-Ga 9			963-Ga 10						
Locality	Mt Gambier						Mt Gambier			Mt Gambier						
SiO2	49.35	47.84	48.91	50.28	49.24	48.58	48.38	48.97	50.28	50.40	50.58	50.13	49.15	49.07	49.59	48.94
TiO2	1.77	2.46	2.19	1.31	1.95	2.62	2.53	2.15	1.53	1.46	1.20	1.41	2.22	2.27	1.76	1.93
Al2O3	4.08	5.81	4.46	2.20	4.51	5.38	4.45	4.85	3.40	3.02	3.12	3.69	4.51	4.00	3.32	3.88
FeO	6.96	5.85	6.98	10.23	7.48	8.06	8.38	7.77	7.80	7.73	5.47	7.36	7.73	8.79	6.49	8.62
Fe2O3	1.34	1.80	0.86	0.89	1.05	0.40	1.16	0.03	1.02	0.06	1.09	0.49	0.98	0.54	3.63	2.03
MnO	0.07	0.32	0.33	0.31	0.26	0.36	0.35	0.12	0.38	0.20	0.17	0.39	0.35	0.46	0.42	0.31
MgO	14.67	13.98	14.27	12.81	14.23	13.63	13.20	14.47	15.03	14.90	15.85	14.31	13.98	13.45	13.20	12.46
CaO	21.02	22.09	21.59	21.45	21.14	21.28	21.58	20.72	20.67	20.89	21.56	21.68	21.66	21.35	21.53	21.84
Na2O	0.10	0.00	0.00	0.00	0.09	0.06	0.00	0.00	0.00	0.00	0.00	0.00	0.00	0.00	0.59	0.21
K2O	0.00	0.00	0.00	0.13	0.00	0.06	0.07	0.08	0.00	0.09	0.00	0.05	0.00	0.04	0.03	0.04
Cr2O3	0.09	0.36	0.30	0.00	0.22	0.31	0.12	0.27	0.30	0.38	0.53	0.18	0.01	0.01	0.00	0.19
Total	99.45	100.50	99.88	99.63	100.18	100.72	100.21	99.41	100.42	99.14	99.57	99.70	100.58	99.97	100.55	100.44
							Number of Ions on the Basis of 6 (0)									
Si	1.8504	1.7821	1.8286	1.9088	1.8368	1.8048	1.8199	1.8311	1.8695	1.8890	1.8809	1.8735	1.8294	1.8439	1.8655	1.8466
Ti	0.0498	0.0689	0.0617	0.0375	0.0547	0.0730	0.0716	0.0603	0.0429	0.1411	0.0335	0.0397	0.0622	0.0640	0.0499	0.0546
Al	0.1801	0.2551	0.1964	0.0982	0.1984	0.2356	0.1972	0.2137	0.1490	0.1332	0.1369	0.1625	0.1976	0.1770	0.1472	0.1724
Fe(2)	0.2175	0.1816	0.2178	0.3241	0.2328	0.2500	0.2628	0.2429	0.2421	0.2423	0.1698	0.2296	0.2401	0.2759	0.2024	0.2705
Fe(3)	0.0376	0.0503	0.0243	0.0255	0.0294	0.0111	0.0327	0.0008	0.0285	0.0016	0.0303	0.0139	0.0275	0.0151	0.1017	0.0574
Mn	0.0023	0.0100	0.0105	0.0100	0.0083	0.0114	0.0110	0.0039	0.0120	0.0064	0.0054	0.0123	0.0109	0.0147	0.0134	0.0099
Mg	0.8194	0.7757	0.7949	0.7245	0.7907	0.7541	0.7391	0.8060	0.8326	0.8319	0.8779	0.7969	0.7751	0.7525	0.7400	0.7000
Ca	0.8441	0.8812	0.8646	0.8722	0.8447	0.8469	0.8691	0.8296	0.8232	0.8386	0.8586	0.8678	0.8633	0.8591	0.8675	0.8826
Na	0.0072	0.0000	0.0000	0.0000	0.0063	0.0041	0.0000	0.0000	0.0000	0.0000	0.0000	0.0000	0.0000	0.0000	0.0408	0.0154
K	0.0000	0.0000	0.0000	0.0064	0.0000	0.0026	0.0032	0.0036	0.0000	0.0044	0.0002	0.0022	0.0000	0.0018	0.0012	0.0021
Cr	0.0027	0.0105	0.0087	0.0000	0.0066	0.0091	0.0034	0.0079	0.0087	0.0113	0.0155	0.0053	0.0021	0.0002	0.0000	0.0055
Wo	44.0	46.6	45.5	44.8	44.5	45.5	45.6	44.1	42.7	46.2	44.3	45.5	45.3	45.1	45.3	46.2
En	42.7	41.0	41.8	37.2	41.7	40.5	38.8	42.9	43.2	45.9	45.3	41.8	40.7	39.5	38.7	36.6
Fs	13.3	12.3	12.8	18.0	13.8	14.0	15.6	13.0	14.1	7.9	10.4	12.8	14.1	15.3	16.0	17.2
Mg/Mg+Fe(t)	76.2	76.9	76.6	67.4	75.1	74.3	71.4	76.8	75.4	85.3	81.4	76.6	74.3	72.1	70.7	68.0

Table 3.4 (continued)

Sample	963-Ga 2					963-Sh 1				963-Sh 2				
Locality	Mt Gambier					Mt Schank				Mt Schank				
SiO2	47.32	47.42	46.44	48.66	49.98	41.91	46.13	43.40	44.28	47.09	45.09	45.75	45.26	47.30
TiO2	2.33	2.27	2.74	1.81	1.50	5.79	3.00	4.75	4.20	2.68	3.63	2.91	3.36	2.42
Al2O3	4.84	3.96	5.71	2.50	2.99	8.63	5.30	8.01	6.66	4.20	6.58	5.36	6.02	3.92
FeO	7.03	5.33	6.28	3.64	5.05	5.58	5.36	5.22	5.27	5.91	4.64	2.82	3.88	3.67
Fe2O3	3.28	4.09	3.62	4.71	3.68	3.90	3.79	3.56	3.83	3.08	3.96	6.03	4.50	4.83
MnO	0.14	0.07	0.00	0.02	0.24	0.21	0.25	0.00	0.29	0.10	0.00	0.06	0.00	0.04
MgO	12.99	13.21	12.77	15.02	15.92	10.94	12.45	11.98	11.77	13.95	12.58	13.14	12.36	14.07
CaO	20.36	21.40	20.57	21.17	19.50	21.26	21.94	21.81	21.62	21.43	22.00	22.05	22.68	21.98
Na2O	0.59	0.59	0.58	0.45	0.54	0.59	0.44	0.33	0.61	0.04	0.40	0.57	0.51	0.35
K2O	0.02	0.02	0.00	0.05	0.01	0.04	0.00	0.04	0.02	0.08	0.02	0.03	0.00	0.04
P2O5	0.06	0.20	0.00	0.00	0.00	0.05	0.06	0.00	0.12	0.04	0.00	0.01	0.11	0.00
SO3	0.00	0.00	0.10	0.01	0.01	0.00	0.02	0.00	0.00	0.00	0.00	0.00	0.00	0.00
Cr2O3	0.53	0.47	0.51	0.88	0.65	0.24	0.37	0.53	0.25	0.18	0.37	0.34	0.50	0.46
NiO	0.00	0.00	0.05	0.00	0.04	0.00	0.00	0.00	0.10	0.00	0.00	0.00	0.00	0.00
Total	99.46	99.02	99.36	98.92	100.09	99.14	99.09	99.61	99.01	98.78	99.26	99.08	99.18	99.09
	Number of Ions on the Basis of 6 (0)													
Si	1.7993	1.8124	1.7687	1.8664	1.8668	1.6153	1.7659	1.6533	1.7020	1.7986	1.7176	1.7541	1.7248	1.7997
Ti	0.0665	0.0652	0.0784	0.0513	0.0422	0.1677	0.0863	0.1360	0.1213	0.0770	0.1040	0.0839	0.0964	0.0693
Al	0.2167	0.1785	0.2563	0.1108	0.1314	0.3921	0.2390	0.3595	0.3016	0.1890	0.2953	0.2423	0.2702	0.1759
Fe(2)	0.22	0.17	0.20	0.11	0.16	0.18	0.17	0.16	0.17	0.19	0.15	0.09	0.12	0.12
Fe(3)	0.09	0.12	0.10	0.13	0.10	0.11	0.11	0.10	0.11	0.09	0.11	0.17	0.13	0.14
Mn	0.0045	0.0022	0.0000	0.0007	0.0076	0.0067	0.0080	0.0000	0.0093	0.0032	0.0000	0.0020	0.0000	0.0012
Mg	0.7358	0.7522	0.7243	0.8406	0.8857	0.6285	0.7101	0.6795	0.6741	0.7937	0.7140	0.7504	0.7019	0.7976
Ca	0.8290	0.8757	0.8389	0.8522	0.7799	0.8779	0.8994	0.8900	0.8899	0.8765	0.8977	0.9054	0.9259	0.8958
Na	0.0435	0.0434	0.0425	0.0328	0.0391	0.0448	0.0325	0.0241	0.0457	0.0031	0.0292	0.0426	0.0376	0.0259
K	0.0008	0.0007	0.0000	0.0024	0.0004	0.0018	0.0000	0.0017	0.0007	0.0040	0.0010	0.0017	0.0000	0.0019
P	0.0019	0.0063	0.0000	0.0000	0.0000	0.0017	0.0018	0.0000	0.0040	0.0013	0.0000	0.0003	0.0037	0.0000
S	0.0000	0.0000	0.0029	0.0003	0.0003	0.0000	0.0007	0.0000	0.0000	0.0000	0.0000	0.0000	0.0000	0.0000
Cr	0.0158	0.0142	0.0154	0.0261	0.0191	0.0073	0.0109	0.0160	0.0076	0.0053	0.0111	0.0104	0.0152	0.0138
Ni	0.0000	0.0000	0.0014	0.0000	0.0013	0.0000	0.0000	0.0000	0.0030	0.0000	0.0000	0.0000	0.0000	0.0000
Wo	44.1	45.7	44.9	43.9	40.5	48.8	47.6	48.4	48.3	45.0	47.9	47.2	49.2	46.0
En	39.1	39.3	38.8	43.3	46.0	34.9	37.6	37.0	36.6	40.8	38.1	39.1	37.3	40.9
Fs	16.8	15.0	16.3	12.8	13.5	16.3	14.9	14.6	15.2	14.2	14.0	13.8	13.4	13.1
Mg/Mg+Fe(t)	69.9	72.3	70.5	77.3	77.2	68.2	71.7	71.7	70.7	74.1	73.2	73.9	73.5	75.8

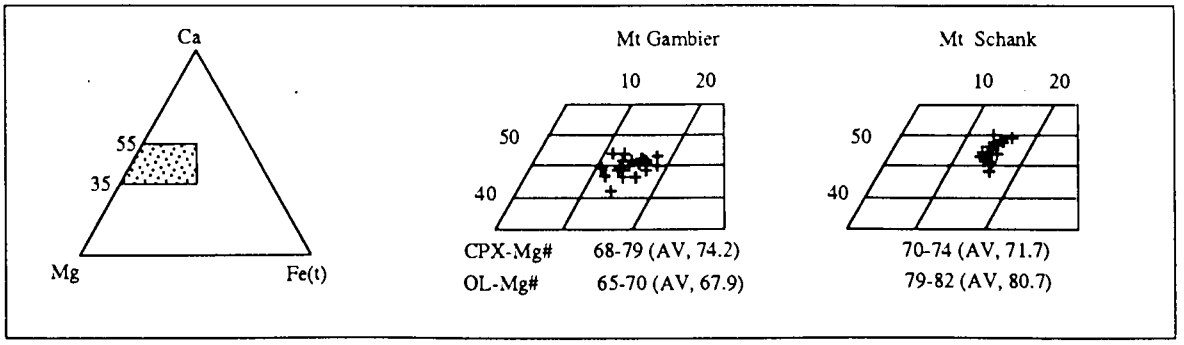

Fig. 3.9. Clinopyroxene and Olivine compositions of the Southern area younger volcanics.

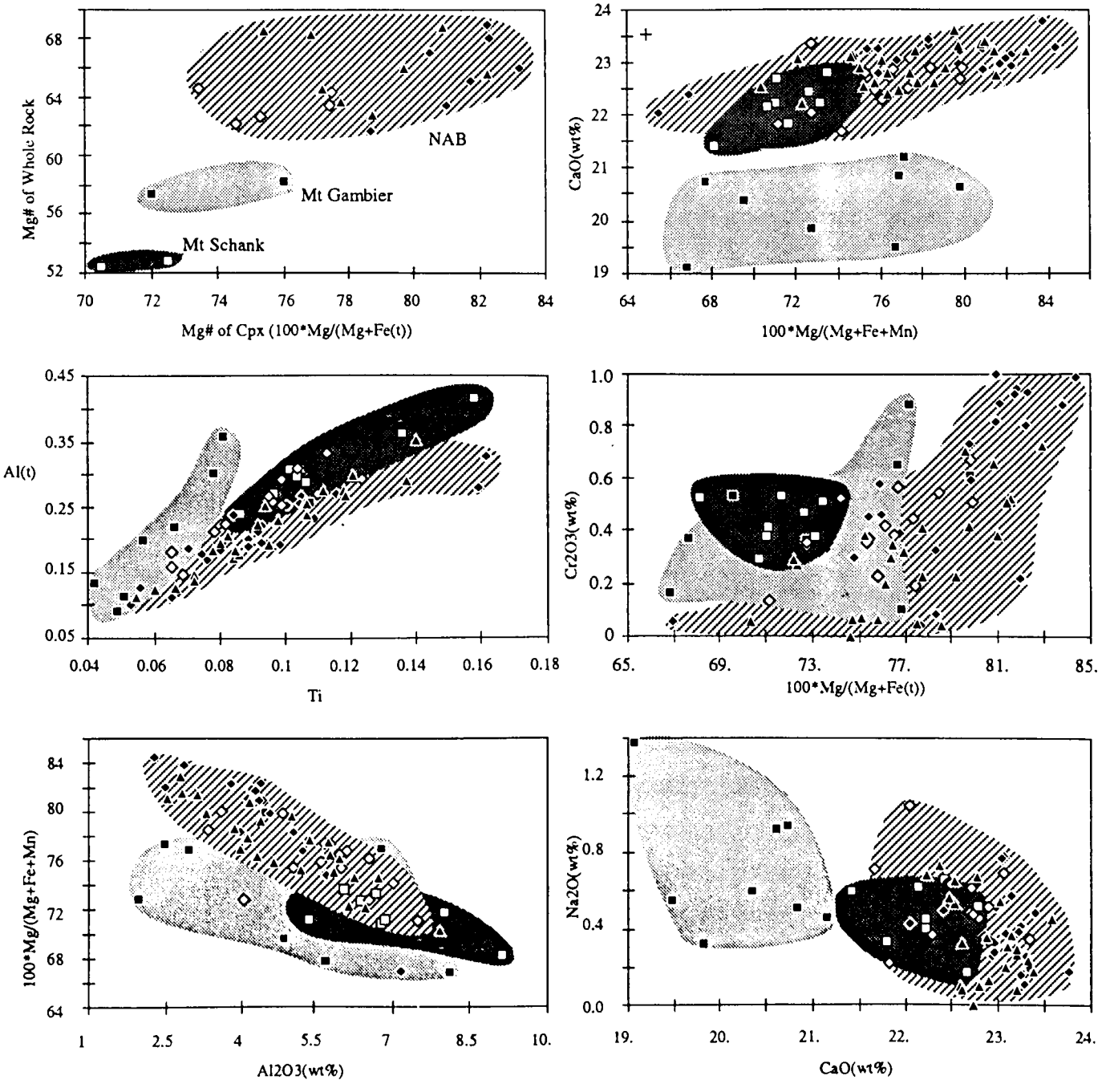

Fig. 3.10. Clinopyroxene compositions of the South Australian alkaline basalts. Symbols as for Fig. 3.1.

Table 3.5. Representative olivine analyses of the Southern area younger volcanics.

Sample	963-Ga 1			963-Ga 2							963-Ga 10			
Locality	Mt Gambier			Mt Gambier							Mt Gambier			
SiO2	35.86	36.72	36.69	35.99	36.75	36.29	36.34	36.62	36.19	36.52	33.94	34.25	33.60	34.71
TiO2	0.23	0.23	0.08	0.20	0.00	0.06	0.17	0.07	0.16	0.23	0.14	0.16	0.03	0.00
Al2O3	0.14	0.18	0.23	0.08	0.00	0.00	0.17	0.00	0.18	0.00	0.00	0.01	0.00	0.15
FeO	27.37	29.93	25.70	26.89	27.71	27.03	27.60	28.18	26.57	28.71	40.57	40.57	43.95	41.51
Fe2O3	3.41	0.28	1.50	2.61	0.75	2.87	1.85	0.59	2.96	1.45	1.79	1.79	1.50	0.40
MnO	0.75	0.53	0.47	0.52	0.41	0.39	0.28	0.39	0.50	0.54	0.66	0.63	0.86	0.64
MgO	32.05	31.61	34.54	33.66	33.66	33.69	33.30	33.67	33.04	32.85	22.33	21.12	19.81	22.63
CaO	0.55	0.49	0.44	0.57	0.52	0.47	0.46	0.47	0.52	0.53	0.88	0.83	0.74	0.65
Na2O	0.41	0.25	0.18	0.00	0.00	0.00	0.08	0.04	0.29	0.00	0.00	0.00	0.00	0.00
K2O	0.00	0.00	0.01	0.02	0.00	0.03	0.01	0.00	0.00	0.00	0.02	0.00	0.00	0.00
P2O5	0.13	0.12	0.19	0.17	0.00	0.00	0.00	0.13	0.00	0.00				
SO3	0.00	0.00	0.00	0.00	0.00	0.00	0.00	0.00	0.00	0.05				
Cr2O3	0.17	0.05	0.00	0.00	0.02	0.03	0.06	0.12	0.07	0.00	0.13	0.00	0.01	0.07
NiO	0.00	0.00	0.00	0.00	0.20	0.00	0.05	0.32	0.00	0.05				
Total	101.07	100.39	100.02	100.71	100.02	100.85	100.36	100.61	100.49	100.93	100.46	99.37	100.50	100.76
					Number of Ions on the Basis of 4 (0)									
Si	0.9717	0.9919	0.9824	0.9699	0.9901	0.9731	0.9795	0.9824	0.9779	0.9832	0.9818	0.9948	0.9871	0.9939
Ti	0.0047	0.0047	0.0015	0.0040	0.0000	0.0012	0.0034	0.0014	0.0033	0.0046	0.0029	0.0035	0.0007	0.0000
Al	0.0046	0.0057	0.0071	0.0024	0.0000	0.0000	0.0052	0.0000	0.0058	0.0000	0.0000	0.0003	0.0000	0.0050
Fe(2)	0.6146	0.6759	0.5730	0.6019	0.6221	0.6043	0.6195	0.6297	0.5960	0.6439	0.9764	0.9764	1.0749	0.9924
Fe(3)	0.0689	0.0056	0.0300	0.0525	0.0152	0.0578	0.0374	0.0119	0.0597	0.0293	0.0387	0.0387	0.0331	0.0087
Mn	0.0172	0.0122	0.0106	0.0120	0.0094	0.0089	0.0064	0.0090	0.0114	0.0124	0.0162	0.0156	0.0213	0.0155
Mg	1.2939	1.2721	1.3775	1.3513	1.3511	1.3455	1.3373	1.3455	1.3298	1.3175	0.9623	0.9138	0.8670	0.9650
Ca	0.0159	0.0141	0.0125	0.0164	0.0150	0.0134	0.0133	0.0136	0.0150	0.0154	0.0273	0.0259	0.0233	0.0199
Na	0.0215	0.0133	0.0092	0.0000	0.0000	0.0000	0.0041	0.0019	0.0153	0.0000	0.0000	0.0000	0.0000	0.0000
K	0.0000	0.0000	0.0005	0.0007	0.0000	0.0011	0.0002	0.0000	0.0000	0.0002	0.0008	0.0000	0.0000	0.0000
P	0.0030	0.0027	0.0044	0.0038	0.0000	0.0000	0.0000	0.0029	0.0000	0.0000				
S	0.0000	0.0000	0.0000	0.0001	0.0000	0.0001	0.0000	0.0000	0.0000	0.0009				
Cr	0.0037	0.0012	0.0000	0.0000	0.0004	0.0006	0.0012	0.0026	0.0016	0.0000	0.0029	0.0000	0.0002	0.0016
Ni	0.0000	0.0000	0.0000	0.0000	0.0044	0.0000	0.0011	0.0070	0.0000	0.0010				
Mg/Mg+Fe(t)	65.2	65.1	69.5	67.2	67.9	67.0	67.0	67.6	66.8	66.1	48.5	46.6	43.8	49.1

Sample	Sh1							Sh 2						
Locality	Mt Schank							Mt Schank						
SiO2	38.27	37.28	38.18	38.49	38.68	38.14	38.15	38.48	38.39	38.13	37.62	38.00	38.22	37.98
TiO2	0.13	0.09	0.11	0.11	0.01	0.11	0.00	0.00	0.21	0.18	0.30	0.04	0.00	0.00
Al2O3	0.14	0.00	0.09	0.18	0.36	0.00	0.00	0.00	0.08	0.12	0.00	0.10	0.00	0.08
FeO	18.12	14.80	15.77	17.00	17.56	17.96	16.70	16.85	16.14	16.85	23.02	19.21	16.00	18.61
Fe2O3	0.99	3.24	1.82	1.64	1.02	1.13	1.78	1.80	1.76	1.56	1.11	1.37	2.57	1.27
MnO	0.38	0.34	0.16	0.27	0.21	0.21	0.35	0.36	0.36	0.57	0.36	0.20	0.39	0.33
MgO	41.84	43.27	43.29	42.52	42.40	41.79	42.75	43.12	42.75	41.84	37.82	40.23	42.55	41.09
CaO	0.18	0.23	0.23	0.13	0.00	0.18	0.27	0.27	0.29	0.21	0.32	0.24	0.25	0.23
Na2O	0.00	0.00	0.00	0.00	0.00	0.00	0.00	0.00	0.00	0.00	0.00	0.00	0.00	0.00
K2O	0.02	0.00	0.00	0.00	0.01	0.00	0.00	0.00	0.00	0.00	0.00	0.06	0.09	0.04
P2O5	0.00	0.09	0.00	0.00	0.05	0.00	0.00	0.00	0.00	0.00	0.00	0.00	0.00	0.00
SO3	0.00	0.00	0.00	0.00	0.00	0.00	0.00	0.00	0.00	0.00	0.00	0.00	0.00	0.00
Cr2O3	0.14	0.00	0.04	0.05	0.00	0.17	0.14	0.15	0.14	0.03	0.06	0.05	0.12	0.17
NiO	0.37	0.52	0.35	0.04	0.00	0.31	0.52	0.53	0.00	0.00	0.07	0.00	0.12	0.39
Total	100.60	99.85	100.05	100.43	100.30	100.00	100.67	101.54	100.11	99.50	100.68	99.49	100.31	100.20
					Number of Ions on the Basis of 4 (0)									
Si	0.9801	0.9869	0.9762	0.9823	0.9874	0.9819	0.9809	0.9753	0.9796	0.9811	0.9833	0.9869	0.9798	0.9807
Ti	0.0025	0.0017	0.0022	0.0021	0.0002	0.0021	0.0013	0.0000	0.0040	0.0035	0.0059	0.0007	0.0000	0.0000
Al	0.0043	0.0000	0.0028	0.0054	0.0000	0.0000	0.0032	0.0000	0.0024	0.0037	0.0000	0.0031	0.0000	0.0025
Fe(2)	0.3860	0.3155	0.3348	0.3612	0.3733	0.3845	0.3541	0.3541	0.3434	0.3620	0.5020	0.4165	0.3406	0.3994
Fe(3)	0.0190	0.0622	0.0348	0.0314	0.0195	0.0218	0.0340	0.0340	0.0337	0.0302	0.0218	0.0268	0.0492	0.0246
Mn	0.0083	0.0072	0.0035	0.0058	0.0078	0.0045	0.0042	0.0077	0.0077	0.0125	0.0080	0.0044	0.0085	0.0072
Mg	1.5960	1.6193	1.6489	1.6166	1.6123	1.6025	1.6280	1.6280	1.6252	1.6038	1.4724	1.5563	1.6251	1.5808
Ca	0.0051	0.0062	0.0064	0.0035	0.0058	0.0049	0.0035	0.0073	0.0078	0.0058	0.0089	0.0065	0.0069	0.0064
Na	0.0000	0.0000	0.0000	0.0000	0.0000	0.0000	0.0000	0.0000	0.0000	0.0000	0.0000	0.0000	0.0000	0.0000
K	0.0008	0.0000	0.0000	0.0000	0.0000	0.0000	0.0008	0.0000	0.0000	0.0000	0.0000	0.0018	0.0031	0.0014
P	0.0000	0.0019	0.0000	0.0001	0.0002	0.0000	0.0020	0.0000	0.0000	0.0000	0.0000	0.0000	0.0000	0.0000
S	0.0000	0.0000	0.0000	0.0000	0.0000	0.0000	0.0000	0.0000	0.0000	0.0000	0.0000	0.0000	0.0000	0.0000
Cr	0.0028	0.0000	0.0008	0.0010	0.0007	0.0035	0.0015	0.0029	0.0028	0.0006	0.0012	0.0009	0.0024	0.0035
Ni	0.0076	0.0104	0.0072	0.0008	0.0000	0.0065	0.0064	0.0108	0.0000	0.0000	0.0014	0.0000	0.0024	0.0082
Mg/Mg+Fe(t)	79.7	81.3	81.6	80.4	80.4	79.7	81.0	80.6	81.1	80.3	73.7	77.8	80.5	78.8

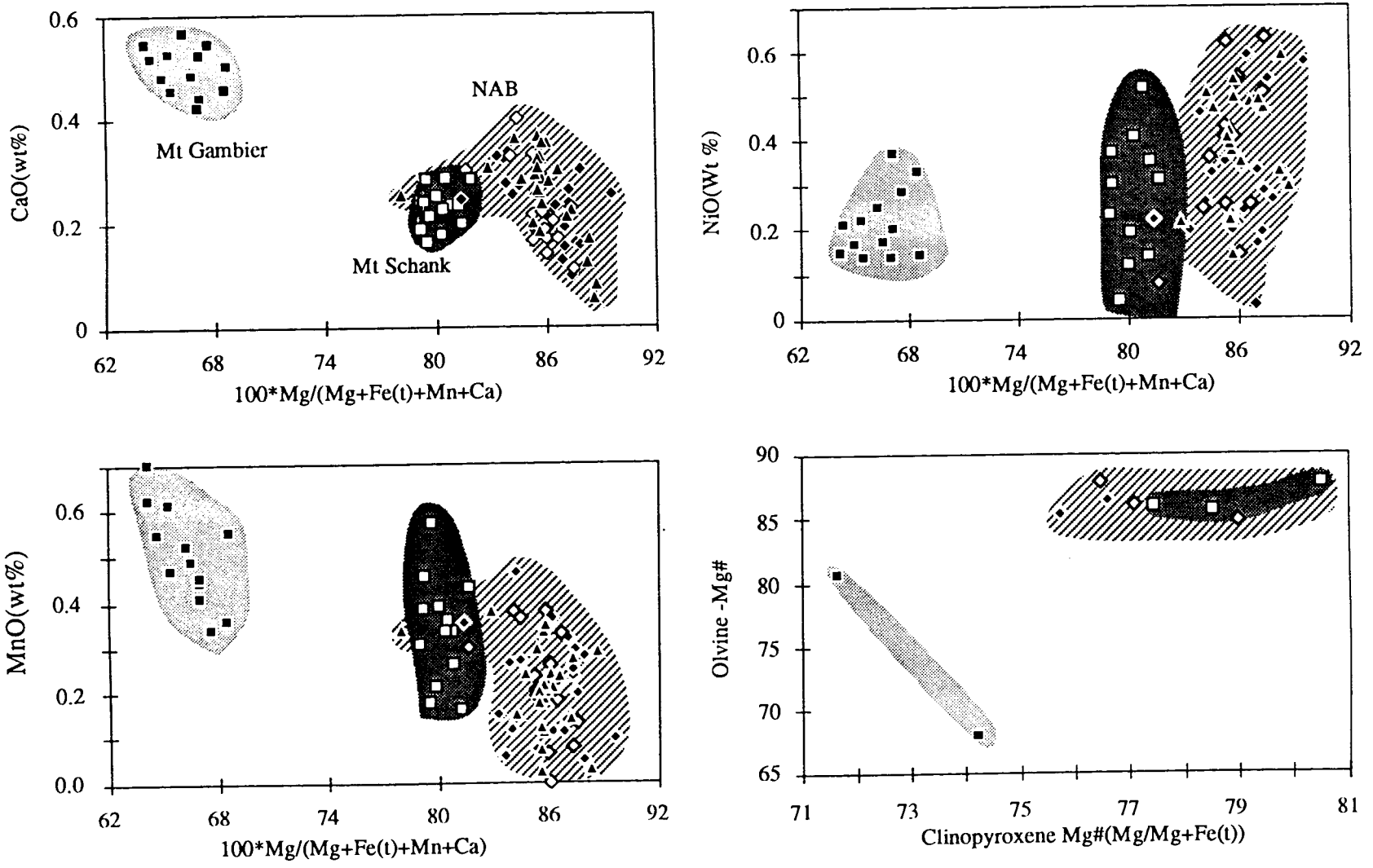

Fig. 3.11. Olivine compositions of the South Australian alkaline basalts. Symbols as for Fig. 3.1.

Table 3.6. Representative opaque oxide analyses of the Southern area younger volcanics.

Sample	963-GA 2	963-GA10				963-Sh 1	963-SH 2			963-SH 4	963-SH 4			
Locality	Mt Gambier	Mt Gambier				Mt Schank	Mt Schank			Mt Schank	Mt Schank			
SiO2	0.04	0.06	0.18	0.94	1.71	1.04	0.81	0.71	0.65	0.12	0.39	0.07	0.08	0.09
TiO2	25.03	25.48	26.15	26.05	26.33	26.22	23.09	22.54	22.01	27.26	50.34	50.58	50.51	51.01
Al2O3	2.58	2.10	2.08	1.43	1.82	1.55	2.77	2.26	2.30	0.84	0.24	0.28	0.02	0.05
FeO	46.29	46.14	50.16	50.65	51.03	49.52	47.03	45.00	47.17	50.33	39.35	39.61	39.33	40.02
Fe2O3	17.70	18.36	17.10	15.49	13.50	16.89	19.42	23.15	18.85	17.15	4.25	4.46	4.24	3.36
MnO	0.65	0.31	0.83	0.64	0.60	0.86	0.67	0.63	0.65	0.73	0.67	0.64	0.50	0.49
MgO	3.85	3.53	2.49	2.75	3.27	3.30	3.22	2.77	2.80	1.56	2.99	2.84	3.00	2.85
CaO	0.37	0.44	0.16	0.44	0.79	0.57	0.54	0.42	1.30	0.35	0.22	0.19	0.26	0.30
Na2O	0.26	0.39	0.19	0.09	0.00	0.22	0.00	0.48	0.12	0.58	0.00	0.00	0.00	0.00
K2O	0.00	0.07	0.01	0.04	0.20	0.02	0.00	0.11	0.10	0.07	0.03	0.00	0.00	0.00
P2O5	0.00	0.00	0.05	0.00	0.00	0.04	0.00	0.00	0.83	0.07	0.00	0.00	0.00	0.00
SO3	0.00	0.00	0.01	0.00	0.00	0.03	0.00	0.00	0.00	0.00	0.00	0.00	0.00	0.00
Cr2O3	0.87	0.20	0.06	0.14	0.20	0.01	0.00	0.15	0.00	0.21	0.14	0.00	0.00	0.00
NiO	0.17	0.00	0.00	0.11	0.12	0.00	0.00	0.00	0.47	0.00	0.00	0.00	0.00	0.00
Total	97.81	97.07	99.46	98.76	99.58	100.26	97.55	98.21	97.26	99.26	98.62	98.67	97.93	98.17
	Number of Ions on the Basis of 32 (0)										Number of Ions on the Basis of 6 (0)			
Si	0.0127	0.0173	0.0559	0.2910	0.5178	0.3161	0.2554	0.2270	0.2082	0.0380	0.0196	0.0034	0.0040	0.0048
Ti	5.8796	6.0598	6.0999	6.0822	5.9897	6.0086	5.4939	5.4149	5.2670	6.4290	1.9175	1.9313	1.9411	1.9466
Al	0.9517	0.7838	0.7610	0.5241	0.6506	0.5581	1.0341	0.8492	0.8645	0.3100	0.0144	0.0168	0.0010	0.0032
Fe(2)	11.4126	11.4773	12.2820	12.4617	12.3364	11.9112	11.6072	11.0447	11.6581	12.5077	1.6444	1.6583	1.6581	1.6840
Fe(3)	3.9269	4.1107	3.7674	3.4282	2.9379	3.6547	4.3124	5.1137	4.1919	3.8348	0.1600	0.1682	0.1607	1.1273
Mn	0.1726	0.0821	0.2168	0.1691	0.1544	0.2215	0.1800	0.1692	0.1763	0.1941	0.0288	0.0277	0.0216	0.0212
Mg	1.7926	1.6610	1.1506	1.2707	1.4728	1.5001	1.5182	1.3167	1.3288	0.7291	0.2253	0.2152	0.2284	0.2158
Ca	0.1221	0.1486	0.0530	0.1448	0.2571	0.1848	0.1821	0.1422	0.4436	0.1167	0.0120	0.0103	0.0145	0.0160
Na	0.1587	0.2361	0.1161	0.0541	0.0022	0.1289	0.0000	0.2998	0.0722	0.3539	0.0000	0.0000	0.0000	0.0000
K	0.0000	0.0293	0.0056	0.0169	0.0758	0.0066	0.0000	0.0445	0.0393	0.0282	0.0022	0.0000	0.0000	0.0000
P	0.0000	0.0000	0.0126	0.0000	0.0000	0.0094	0.0000	0.0000	0.2233	0.0172	0.0000	0.0000	0.0000	0.0000
S	0.0000	0.0000	0.0027	0.0000	0.0000	0.0067	0.0000	0.0000	0.0000	0.0000	0.0000	0.0000	0.0000	0.0000
Cr	0.2157	0.0507	0.0135	0.0340	0.0483	0.0026	0.0000	0.0373	0.0000	0.0514	0.0054	0.0000	0.0000	0.0000
Ni	0.0430	0.0000	0.0000	0.0268	0.0293	0.0000	0.0000	0.0000	0.1213	0.0000	0.0000	0.0000	0.0000	0.0000

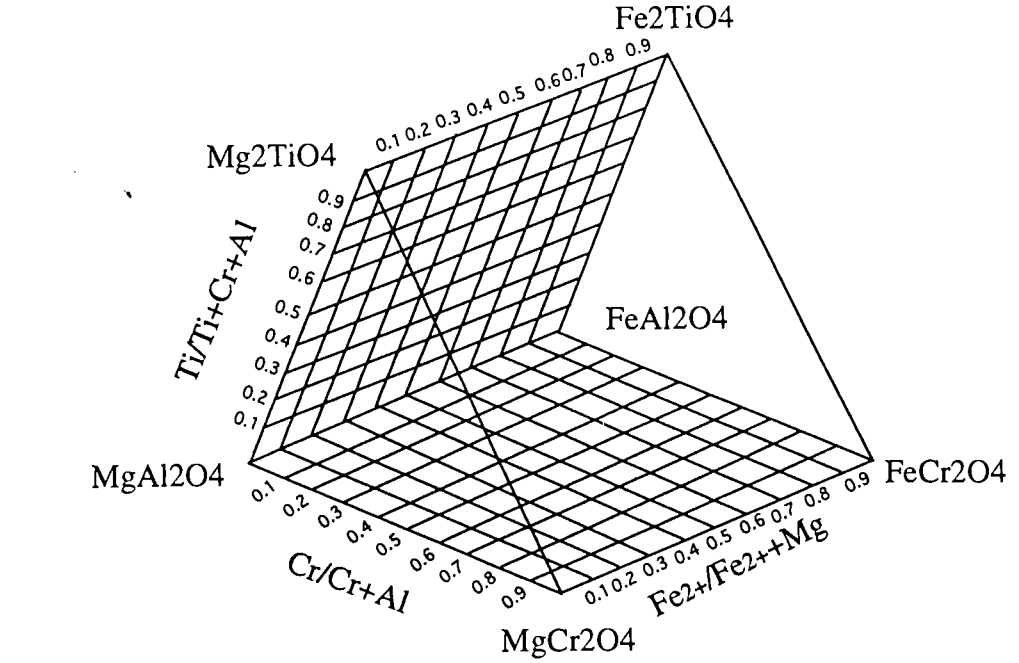

A) Southern area younger volcanics

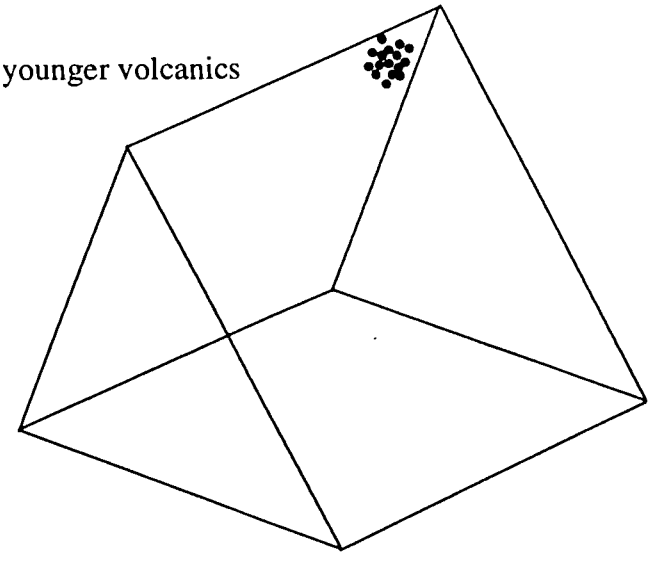

B) Northern area older volcanics

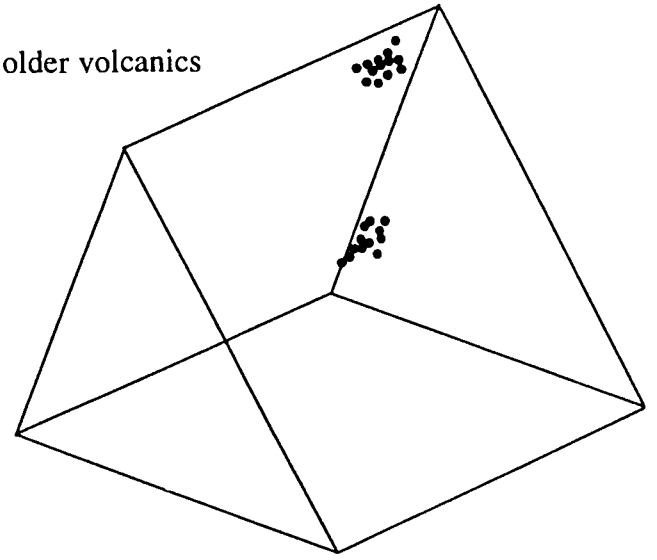

Fig. 3.12. Spinel compositions from the South Australian alkline basalts plotted in the multicomponent spinel prism.

The hawaiites show "Within Plate Basalts"-like characteristics in diagrams which attempt to discriminate the basalts from different tectonomagmatic environments and have OIB-like characteristics in the incompatible element ratios (Fig. 3.14). In the hawaiites, samples from the Mt Schank are plotted in the mugearites range and show more fractionated magma like characteristics. The hawaiites show Mg# of 52-60 (<54 for the Mt Schank hawaiites, 55-60 for the Mt Gambier hawaiites).

In the major elements versus Mg# plots (Fig. 3.15), K_2O, Al_2O_3, TiO_2 P_2O_5, and Na_2O contents decrease while CaO and SiO_2 contents increase with Mg#. The geochemical variations support the derivation of the Mt Schank hawaiites from the Mt Gambier hawaiites by fractional crystallisation of clinopyroxene (54.3 %), plagioclase (29.2 %) and olivine (16.5 %). In the Mt Gambier hawaiites, relationship between high magnesian rocks and less magnesian rocks can be explained with olivine dominant fractional crystallisation (Table 3.9, Fig. 3.19). However, large differences in K_2O and TiO_2 between Mt Gambier hawaiites and Mt Schank hawaiites may reflect added different degrees of partial melting or parent varieties

In the projection of olivine-plagioclase-clinopyroxene (Walker *et al.*, 1979), the hawaiites are plotted in the olivine + liquid volume, suggesting that they have undergone olivine crystallisation (Fig. 3.19). In the hawaiites, dispersion trends of the data towards plagioclase may reflect that their parental magma experienced olivine as well as clinopyroxene fractionation. The trend expanding toward the spinel- plagioclase cotectic (but more toward the clinopyroxene side) may reflect influences of the fractionation of spinel as well as plagioclase.

Previous studies (Ringwood, 1966; Nicholls, 1967; Grove *et al.*, 1973) suggest chemical composition of undepleted upper mantle (peridotite assemblages) have Mg# (=100 * Mg/Mg+Fe_2) of 87 to 90 and their equilibrium basaltic liquids show Mg# of 66 to 75 (K_D^{OL-LIQ} =0.33). It was also suggested that Mg# below 66 imply some history of crystal fractionation. Thus, low Mg# of the South Australian hawaiites can be attributed to have undergone some crystal fractionation.

C) Trace elements and REE chemistry

Other important genetic features of the South Australian hawaiites are illustrated by variation of trace elements relative to Mg# and PM normative plots (Fig. 3.16, 3.17). In the trace elements - Mg# relationships, the hawaiites show increasing Ni, Sc, Co and Cr, and decreasing La, Ce, Nd, Ba, Th, Zr, Zn, Ga, Rb, Sr and Y with Mg#. In the primitive mantle normalised incompatible element abundances, the hawaiites show parallel abundance patterns. These trace element patterns are similar to those of Victorian Newer Basalts and Tasmanian Tertiary basalts (Irving and Green, 1976; Frey *et al.*, 1978; McDonough *et al.*, 1985), Cameroon line basalts (Fitton, 1987) and Basin and Range basalts (Fitton *et al*, 1988).

Table 3.7. Major element analyses of the Southern area younger volcanics.

Sample	963-Ga 1	963-Ga 2	963-Ga 3	963-Ga 4	963-Ga 5	963-Ga 6	963-Ga 7	963-Ga 8	963-Ga 9	963-Ga 10	963-Sh 1	963-Sh 2	963-Sh 3	963-Sh 4	963-Sh 5	963-Sh 6
Locality	Mt Gambier										Mt Schank					
SiO2	48.55	48.27	47.25	49.28	47.20	48.47	48.56	49.63	47.41	47.83	47.30	46.82	47.28	47.23	47.14	47.29
Al2O3	14.14	13.84	13.55	13.47	13.55	13.44	13.37	13.50	13.16	13.07	14.41	14.36	14.48	14.46	14.48	14.36
Fe2O3(t)	12.16	12.34	12.00	12.25	11.94	12.38	12.46	12.41	12.16	12.51	12.38	12.25	12.39	12.37	12.29	12.26
MnO	0.16	0.16	0.17	0.16	0.17	0.16	0.16	0.16	0.16	0.16	0.16	0.16	0.16	0.16	0.16	0.16
MgO	7.78	8.37	8.51	9.07	8.37	8.42	8.80	8.19	8.55	8.91	6.89	6.92	6.99	6.96	6.89	7.01
CaO	8.53	8.58	8.38	8.88	8.48	9.37	9.33	9.05	9.47	9.30	7.43	7.44	7.40	7.42	7.42	7.39
Na2O	3.99	4.02	4.79	3.59	4.35	3.75	3.57	3.79	3.85	3.86	4.60	4.56	4.78	4.74	4.76	4.98
K2O	1.86	1.91	2.53	1.46	2.32	1.62	1.49	1.54	1.66	1.67	3.04	2.98	3.01	3.01	3.00	3.06
TiO2	2.43	2.38	2.43	2.18	2.47	2.36	2.30	2.28	2.33	2.32	3.06	3.07	3.10	3.03	3.09	3.05
P2O5	0.62	0.60	0.86	0.47	0.87	0.57	0.54	0.50	0.56	0.55	1.06	1.05	1.07	1.05	1.06	1.06
SO3	0.01	0.02	0.01	0.00	0.00	0.00	0.01	0.03	0.20	0.01	0.17	0.09	0.02	0.06	0.03	0.03
LOI	-0.46	-0.57	-0.45	-0.69	-0.50	-0.61	-0.58	-0.60	0.44	-0.53	0.38	0.09	-0.66	-0.60	-0.66	-0.52
Total	99.75	99.94	100.03	100.11	99.72	99.94	100.02	100.49	99.94	99.68	100.89	99.78	100.03	99.92	99.65	100.14
C.I.P.W. norm (calculated with Fe2O3/FeO=0.2).																
Ap	1.46	1.41	2.02	1.10	2.06	1.34	1.27	1.17	1.33	1.30	2.49	2.48	2.51	2.47	2.49	2.48
Il	4.67	4.56	4.66	4.16	4.77	4.52	4.40	4.35	4.51	4.46	5.87	5.93	5.93	5.81	5.93	5.84
Mt	2.67	2.71	2.63	2.68	2.49	2.72	2.73	2.71	2.70	2.75	2.72	2.71	2.71	2.71	2.70	2.69
Or	11.09	11.36	15.04	8.65	13.90	9.63	8.85	9.11	9.98	9.96	18.09	17.87	17.87	17.91	17.88	18.17
Ab	24.74	22.42	15.04	26.69	18.04	23.13	24.22	27.11	20.32	20.54	18.72	18.30	18.72	18.03	18.07	17.17
An	15.33	14.20	8.07	16.39	10.74	15.14	16.17	15.34	14.33	13.56	10.08	10.22	6.51	9.46	9.41	7.88
Di	18.99	20.12	22.85	20.10	21.27	22.71	21.83	21.47	24.20	23.92	16.39	16.55	19.06	16.90	16.92	17.96
Hy	0.00	0.00	0.00	0.00	0.00	0.00	0.00	0.00	0.00	0.00	0.00	0.00	0.00	0.00	0.00	0.00
Ol	15.99	16.84	15.75	18.18	16.19	16.06	17.19	16.08	15.87	16.78	14.69	14.71	13.83	14.66	14.40	14.21
Ne	5.03	6.37	13.93	2.05	10.44	4.76	3.32	2.64	6.57	6.72	10.78	11.14	11.84	12.00	12.16	13.58
Ac	0.00	0.00	0.00	0.00	0.00	0.00	0.00	0.00	0.00	0.00	0.00	0.00	0.00	0.00	0.00	0.00
C	0.00	0.00	0.00	0.00	0.00	0.00	0.00	0.00	0.00	0.00	0.00	0.00	0.00	0.00	0.00	0.00
Q	0.00	0.00	0.00	0.00	0.00	0.00	0.00	0.00	0.00	0.00	0.00	0.00	0.00	0.00	0.00	0.00
Total	99.97	99.99	99.99	100.00	99.90	100.01	99.98	99.98	99.81	99.99	99.83	99.91	98.98	99.95	99.96	99.98
AN#	38.26	38.78	34.92	38.05	37.32	39.56	40.03	36.14	41.36	39.77	35.00	35.83	25.80	34.41	34.24	31.46
DI	40.86	40.15	44.01	37.39	42.38	37.52	36.39	38.86	36.87	37.22	47.59	47.31	48.43	47.94	48.11	48.92
SI	31.66	32.95	31.96	36.07	32.46	33.78	35.10	33.18	0.66	34.67	26.84	27.16	26.96	26.93	26.80	26.88
LI	-9.21	-10.05	-9.41	-11.09	-9.54	-11.15	-11.66	-10.32	0.00	-11.85	-6.65	-6.80	-6.77	-6.76	-6.66	-6.61

Notice. **AN#= AN/(AN+AB)*100, S.I. (Solidification Index by Kuno), D.I. (Differentiation, Index by Thornton and Tuttle,1960) & L.I. (Larsen Index by Larsen, 1938).**

Table 3.8. Trace element analyses of the Southern area younger volcanics.

Sample	963-Ga 1	963-Ga 2	963-Ga 3	963-Ga 4	963-Ga 5	963-Ga 6	963-Ga 7	963-Ga 8	963-Ga 9	963-Ga 10	963-Sh 1	963-Sh 2	963-Sh 3	963-Sh 4	963-Sh 5	963-Sh 6
Locality	Mt Gambier										Mt Schank					
Y	27.9	25.9	30.5	22.8	30.6	25.7	24.1	24.7	25.2	24.3	30.2	30.3	30.8	29.9	33.3	30.9
Sr	739	731	1073	604	1086	674.5	649	565	675.2	683	1135	1145	1169	1153	1144.7	1160
Rb	43.3	44.2	58.5	33.6	56.6	37.9	33.4	35.7	36.6	36.7	69	70.3	71.5	71.1	69.2	71.7
Nb	58.7	56.7	89.9	41.3	90	48.6	45.9	41.5	48.3	47.8	88	87.8	84.9	88.4	91.6	85.6
Zr	260	255	358	189	357	198.2	190	186	195.3	197	386	388	387	390	388.8	388
Th	6	6.3	8	3.6	8.6	5.3	4.3	4.5	6.1	4.4	7.4	7.1	8.8	9.6	9.5	9
Pb	3.9	3.9	5.9	4.3	4.4	4.7	4.7	2.3	10	3.4	7.4	5.1	5.8	4.7	5.4	3
U	0.7	0.9	2	1.1	2.5	1.4	1	1.7	3	2.4	0.7	1.6	0.5	3	1.5	1.6
Ga	21.6	20.3	24.1	20.6	23.6	22.3	21.6	20	22.7	21.5	24	24.3	27.4	24	26.3	24.1
Zn	127	127	125	114	132	114.6	117	124	109.9	111	144	142	120	136	145.5	128
Cu	49.4	48.8	41.5	42.2	41	35.1	50.8	56.2	55.3	47	41	37	47	36	36	43
Ni	148	169	161	191	166	168.7	183	171	168.7	167	116	111	96	113	110.3	112
Ba	575	574	872	455	775	515	508	416	515.0	558	923	947	966	947	943	949
Sc	20.3	19.7	17.3	22	18.2	21.3	20.1	21	19.6	20	16	15.2	14	14.9	15.6	14.2
Cr	215	215	258	288	279	263	257	280	264.0	250	122	114	106	114	107	125
V	187	181	163	178	174	194.4	180	185	179.5	177	189	185	164	180	156.8	174
Co	68.6	56.4	43.9	49.8	47	49.9	53.9	53.7	47.4	48.9	51.8	44.7	37.4	44.6	43.7	41.8
Ce	90	92	127	71	125	86	76	63	77	83	135	131	137	140	148	136
Nd	38	37	53	29	56	34	32	29	35	32	62	61	64	61	66	62
La	55	56	73	41	74	47	48	40	46	46	76	77	78	78	83	79

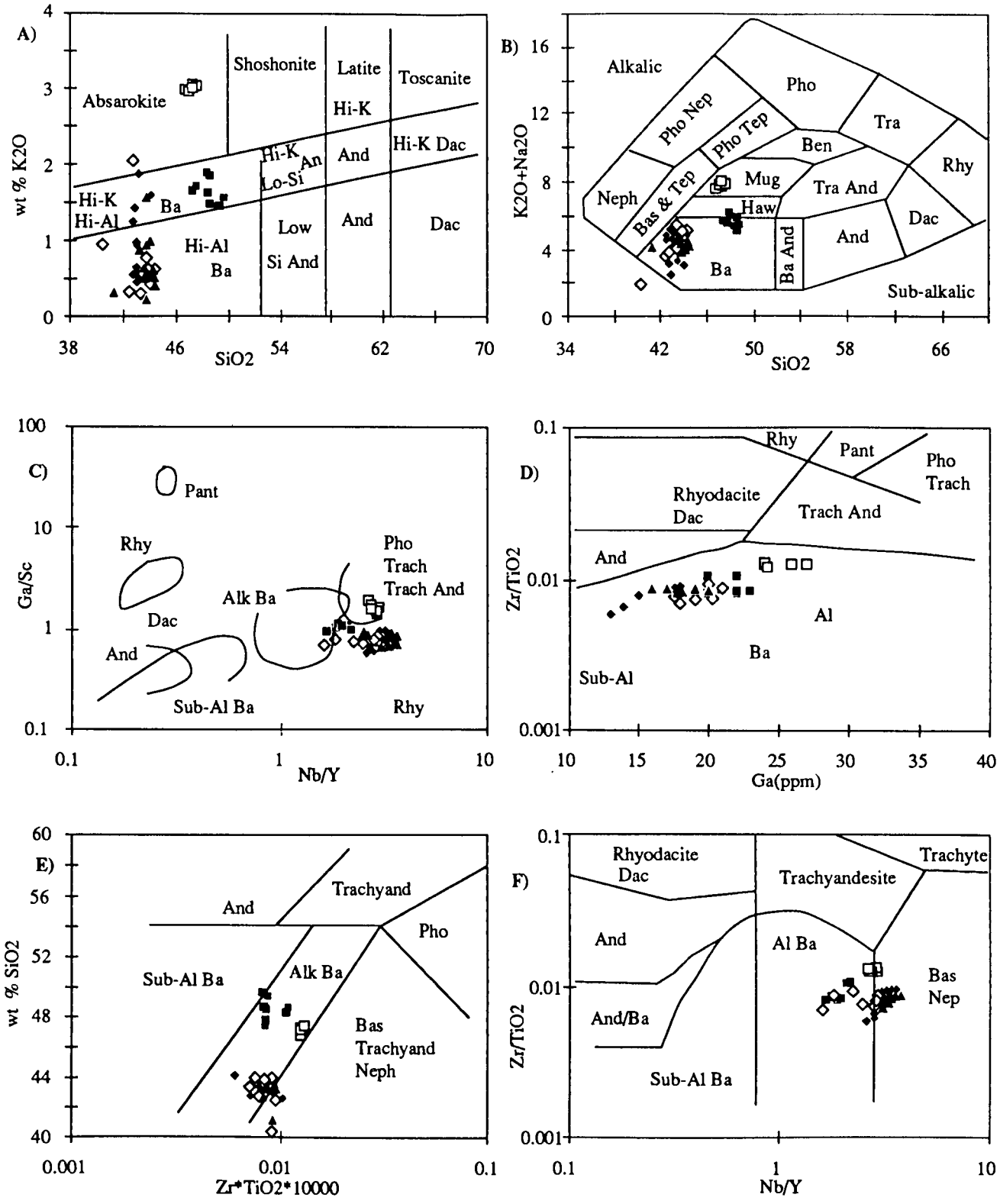

Fig. 3.13a. Classification of the South Australian alkaline basalts. A) K2O-SiO2 plot (MacKenzie & Chappell, 1972), B) Na2O+K2O-SiO2 plot (Cox *et al.*, 1979), C) Ga/Sc-Nb/Y plot, D) Zr/TiO2-Ga plot, E & F) SiO2- Zr/TiO2 *10000 and Zr/TiO2-Nb/Y (all from Winchester & Floyd, 1977). Notice; Symbols as for Fig. 3.1. (Al = Alkaline; And = Andesite; Ba = Basalt; Bas = Absanite; Ben = Benmoreites; Dac = Dacite; Haw = Hawaiites; Mug = Mugearites; Neph = Nephelinites; Pant = Pantellerite; Pho = Phonolites; Rhy = Rhyolites; Tep = Tephrites; Tra = Trachtes.

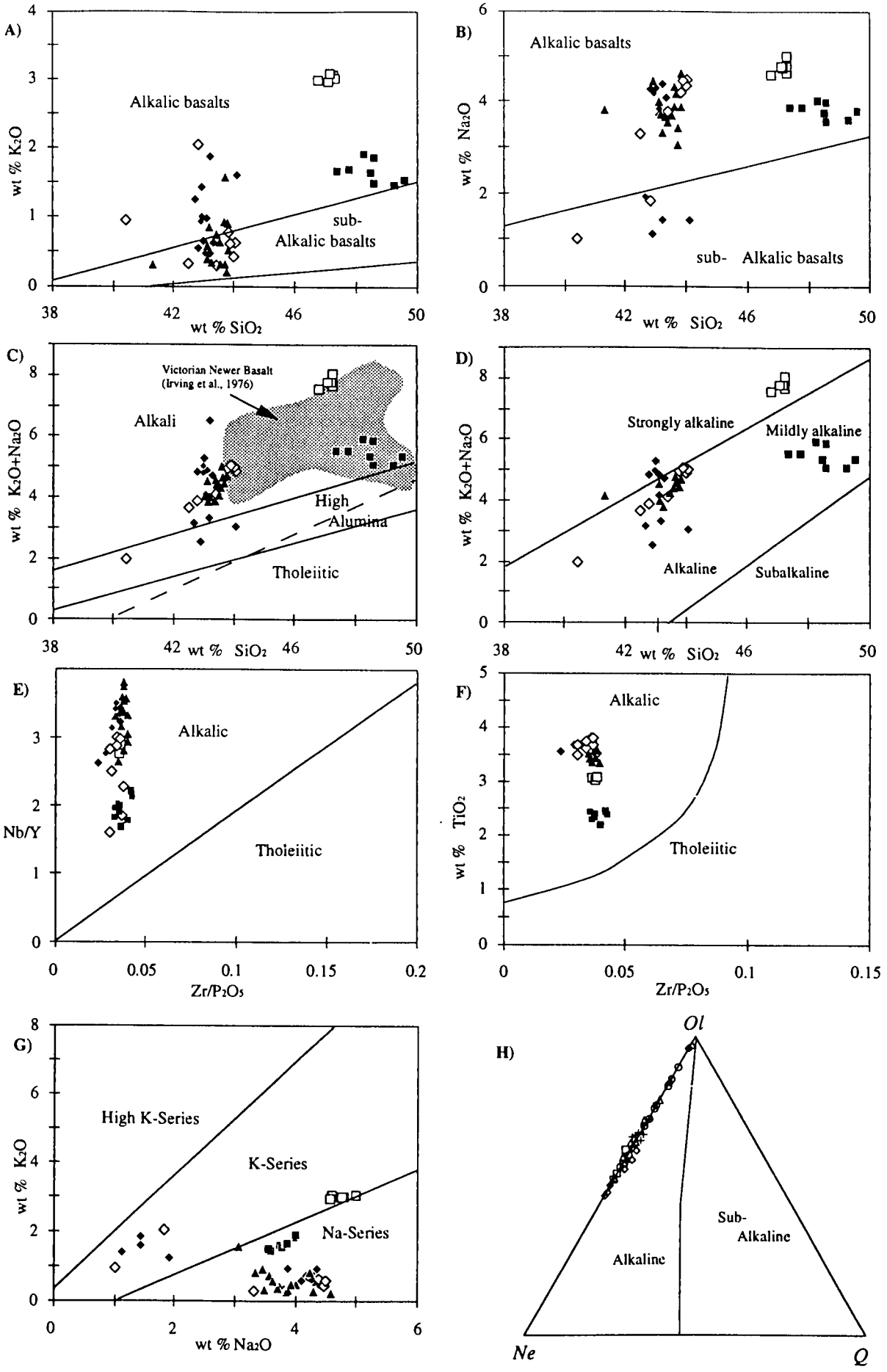

Fig. 3.13b. Chemical discriminations of the South Australian alkaline basalts. A) K2O-SiO2, B) Na2O-SiO2 plot (Middlemost, 1975), C) K2O+Na2O-SiO2 (Kuno, 1966), D) Na2O+K2O-SiO2 (alkaline/subalkaline dividing line from Irvine & Baragar (1971), strong alkaline/mildly alkaline dividing line from Saggerson & Williams (1964), E) Nb/Y-Zr/P2O5, F) TiO2- Zr/P2O5 plot (Winchester & Floyd, 1976), G) K2O-Na2O plot (Middlemost, 1975), H) Normative Ol-Ne -Qt plot (Irvine & Baragar, 1971). Notice; Symbols of Fig. A-G as for Fig. 3.1 and, for Fig. H. (o) for Mt Gambier hwaiites, (□) for Mt Schank hwaiites (◇) for NMF, (△) for BSF, and (+) for MDF.

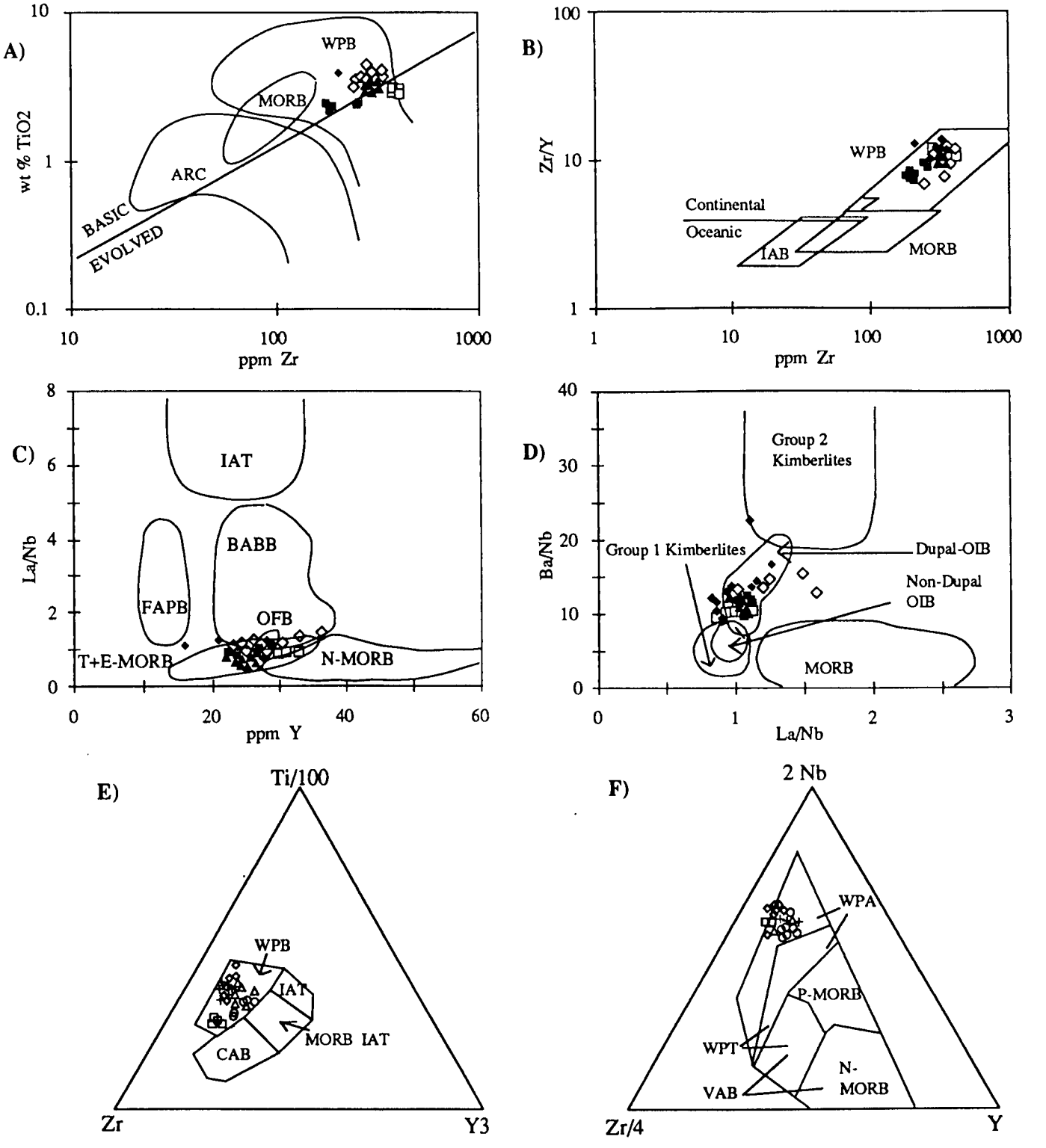

Fig. 3.14. Tectonomagmatic discriminations of the South Australian alkaline basalts. A) TiO2-Zr plot (Pearce, 1982), B) Zr/Y-Zr plot (Pearce & Norry, 1979), C) La/Nb-Y plot (Floyd *et al.*, 1986), D) Ba/Nb-La/Nb (Le Roex, 1986). E) Ti/100-Zr-Y3 (Pearce & Cann, 1973), F) 2Nb-Zr/4-Y (Meschede, 1986). Symbols of A-D as for Fig. 3.1. BABB = Back Arc Basin Basalt; FAPB = Forearc Plateau Basalt; IAB = Island Arc Basalt; IAT = Island Arc Tholeiite; MORB = Mid-Ocean Ridge Basalt; OIB = Ocean Island Basalt; N-MORB = Normal MORB; OFB = Ocean Floor Basalts; T+E-MORB = Transitional and Enriched MORB; VAB = Volcanic Arc Basalt; WPB = Within-Plate Basalts. Symbols for E-F (○) for Mt Gambier hwaiites, (□) for Mt Schank hwaiites (◇) for NMF, (△) for BSF, (+) for MDF (CAB = Calcalkaline; CONT = Continental Basalt; IAT = Island Arc Tholeiite; MORB = Mid-Ocean; Ridge Basalt; OI = Ocean Island Basalt; OIA = Ocanic Island Alkalic; OIT = Oceanic Island Tholeiite; N-MORB = Normal MORB; P-MORB = Plume-MORB; VAB = Volcanic Arc Basalt; WPA = Within-Plate Alkalic; WPB = Within-Plate Basalts; WPT = Within-Plate Tholeiite; SCI = Spreading Centre Island Basalt).

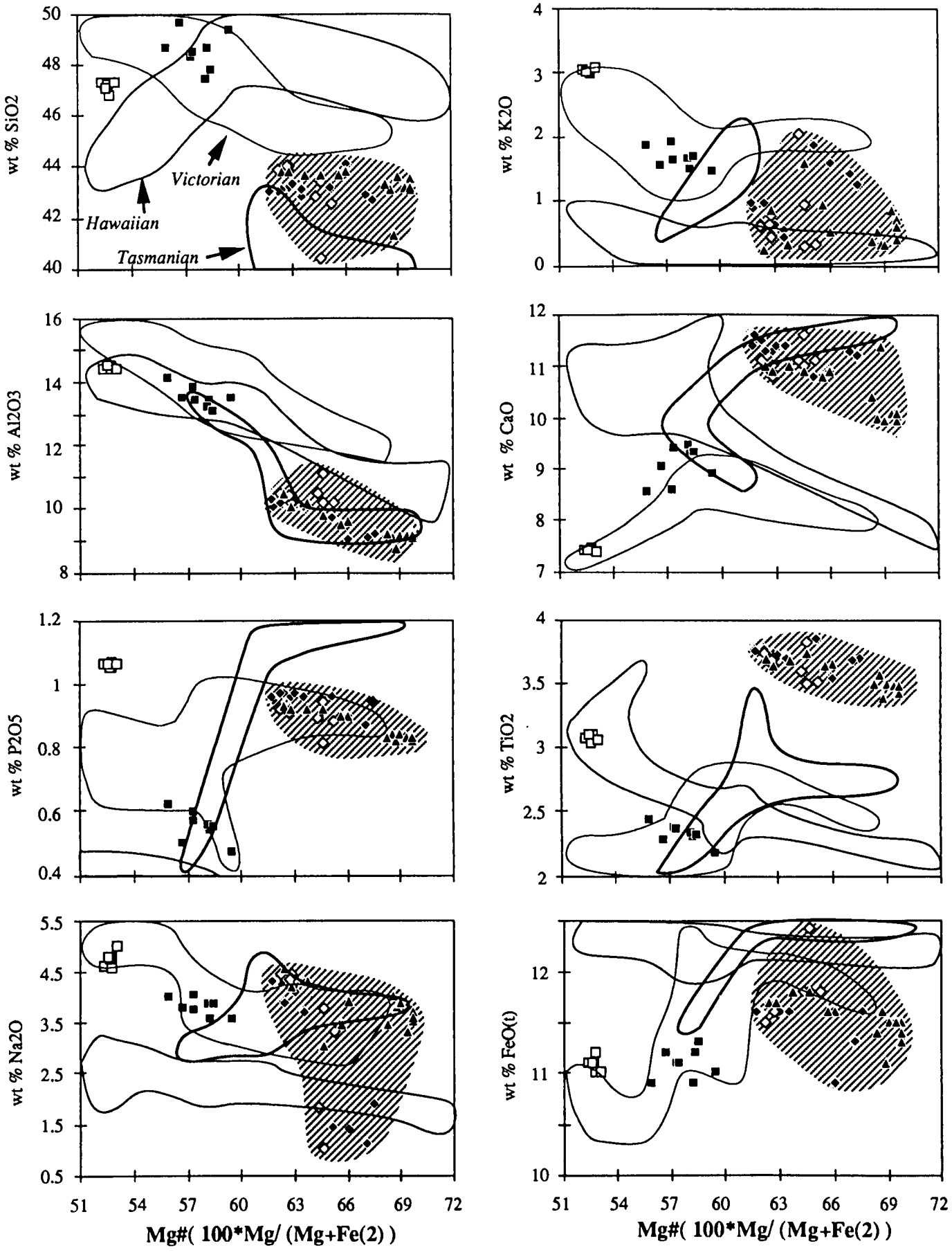

Fig. 3.15. Plots of major elements versus Mg# for the South Australian alkaline basalts and their comparisons with available data. Symbols as for Fig. 3.1. See text for data sources.

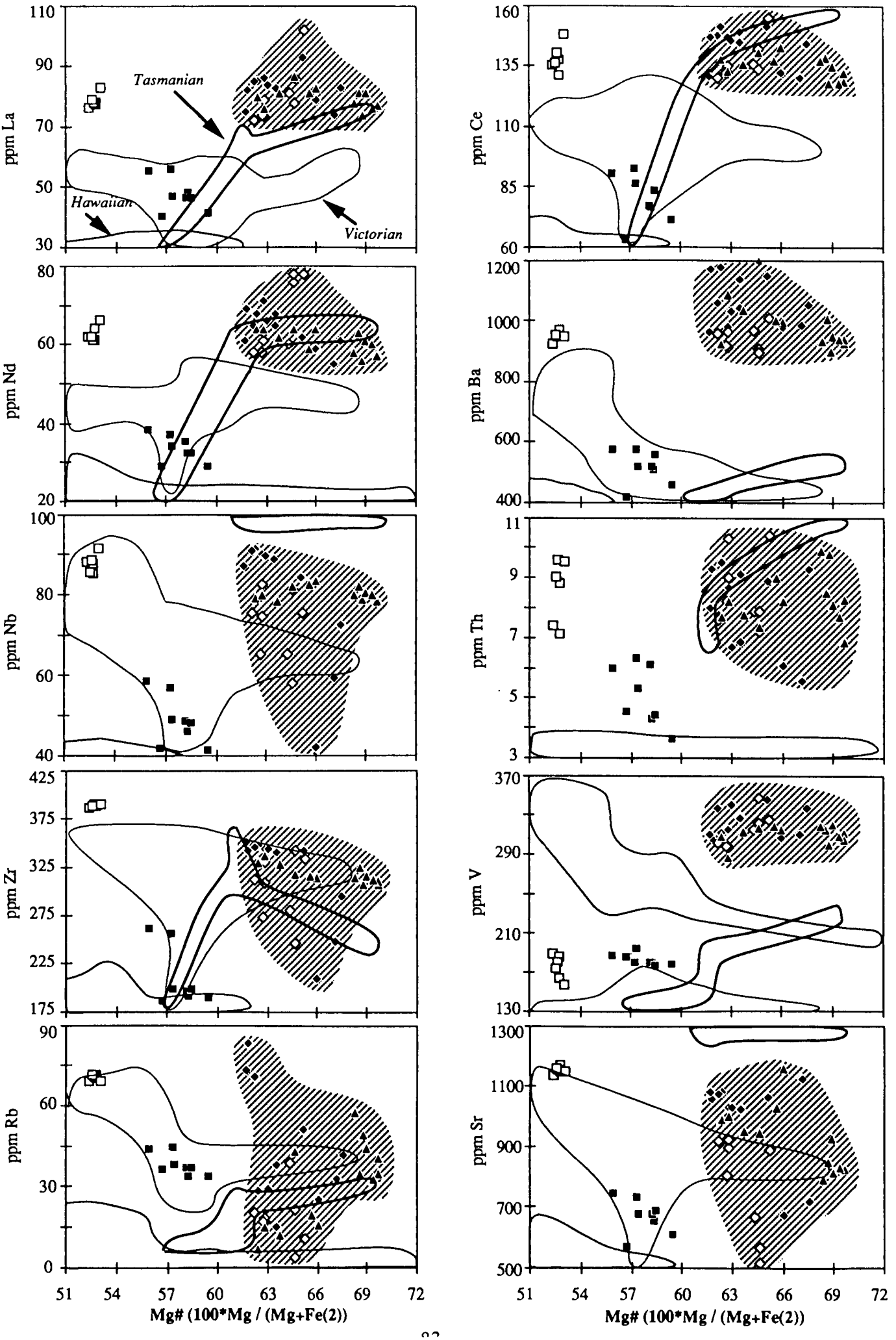
ppm La
ppm Ce
ppm Nd
ppm Ba
ppm Nb
ppm Th
ppm Zr
ppm V
ppm Rb
ppm Sr
Tasmanian
Hawaiian
Victorian
Mg# (100*Mg / (Mg+Fe(2))
Mg# (100*Mg / (Mg+Fe(2))

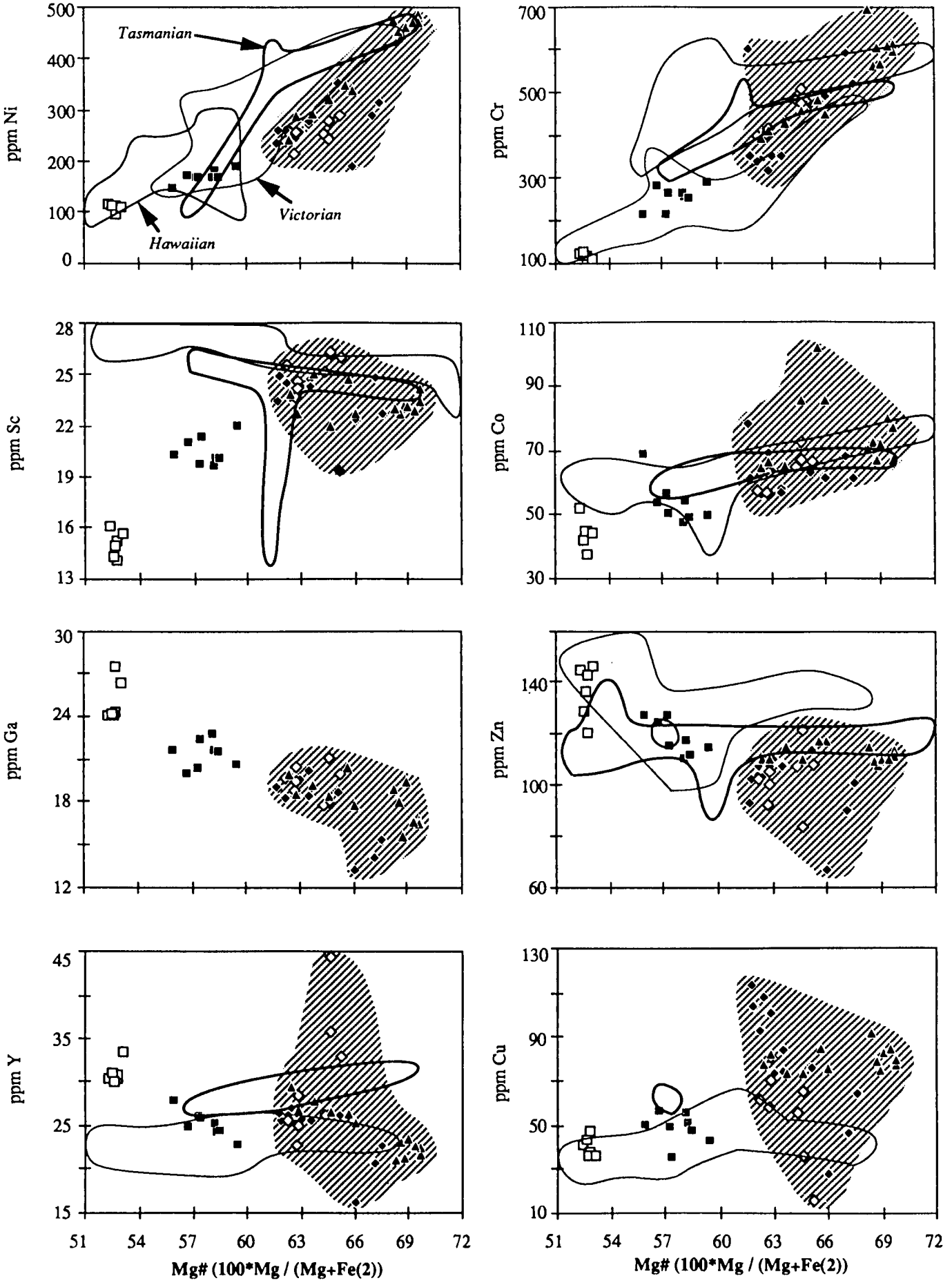

Fig. 3.16. Plots of trace elements versus Mg# for the South Australian alkaline basalts and their comparisons with available data. Symbols as for Fig. 3.1. See text for available data sources.

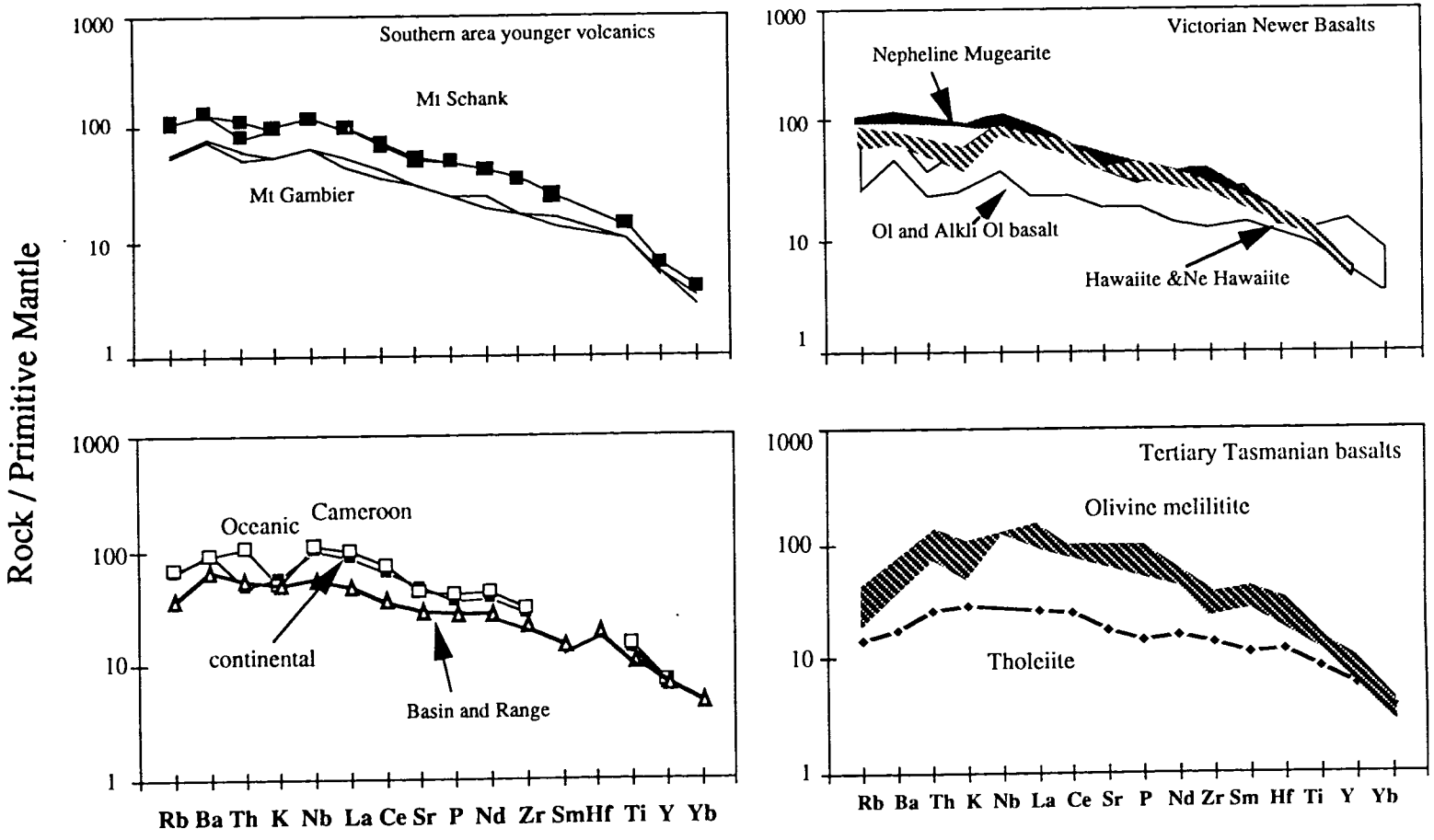

Fig. 3.17. Trace element abundances of the Southern area younger volcanics and their comparisons with those of Victorian Newer Basalts (Data sources; Victorian Newer Basalts from McDonough *et al.*, 1985), Tasmanian Tertiary basalts (Fery *et al.*, 1978), Cameroon line basalts (Fitton, 1987), and Basin and Range basalts (Fitton *et al.*, 1988). Normalized values from Sun and McDonough, (1989).

In the South Australian hawaiites, samples from Mt Schank volcanics show a similarity to mugeorite whereas Mt Gambier hawaiites show a similarity olvine or alkali olivine basalts of the Victorian Newer basalts.

These geochemical variations support the derivation of the Mt Schank hawaiites from the Mt Gambier hawaiites by fractional crystallisation of clinopyroxene (54.3 %), plagioclase (29.2 %) and olivine (16.5 %) (Table 3.9). A systematic changes of incompatible element contents between magnesian and less magneaisn rocks in the Mt Gambier hawaiites also may be attributed to olivine and plagioclase dominant fractional crystallisation (Table 3.9). However, large differences of Sr contents between two hawaiite samples suggest that these characteristics are source inherited or reflect different degrees of partial melting.

Partial melting in the upper mantle is also an important process in the interpretation of the Mt Gamber hawaiites which contain Cr-diopside lherzolites. In the incompatible element abundances, the Mt Gambier hawaiites can be modelled by small degree of partial melting of highly enriched upper mantle peridotites (4-5 %), though temporal isotopic variation suggests derivation from mixed sources (Fig. 3.19).

PM normalised REE abundances are shown in Fig. 3.18. The patterns are characterised by pronounced LREE enrichments and parallel patterns between Mt Gambier and Mt Schank hawaiites. Mt Schank hawaiites show enrichment in most REEs relative to Mt Gambier hawaiites implying different degree of fractionation or primary source-inherited differences. In the studies of eastern Australia basalts, increase of LREE enrichment relative to HREE is observed in mafic rocks such as leucitite, melilitite, nephelinite and basanite (Ewart and Chappell, 1989).

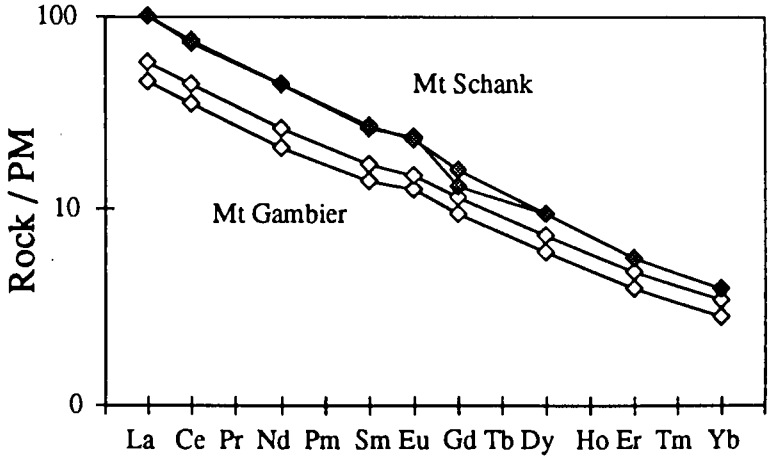

Fig. 3.18. Primitive Mantle normalised REE abundances of the Southern area younger volcanics (PM from Sun and McDonough, 1989).

Table 3.9. A least squares calculation and associated trace element model.

Major element

Sample	CPX	OL	PL	Parent (Ga 1)	Ga 4(obs)	Calc	Diff	Vector	wt. per cent
SiO2	48.87	36.74	54.92	48.6	49.15	49.3	-0.1479	CPX	0.0059
Al2O3	4.21	0.15	28.52	14.1	13.67	13.5	0.1698	OL	0.041
Fe2O3	8.68	27.07	0.75	12.2	12.41	12.3	0.1112	PL	0.034
MnO	0.14	0.36	0.03	0.2	0.2	0.2	0.0005	Ga 1	0.802
MgO	14.93	34.2	0	7.8	9.16	9.1	0.0647		
CaO	20.59	0.45	11.02	8.5	9.11	8.9	0.2128		
Na2O	0.61	0.44	5.02	4	3.75	3.6	0.1549		
K2O	0	0.08	0.37	1.9	1.69	1.5	0.1924		
TiO2	2.1	0.11	0.11	2.4	2.25	2.2	0.0501		
P2O5	0	0	0	0.6	0.53	0.5	0.0294		
Sum of squares of residuals							0.17694		

Sample	CPX	OL	PL	Parent(Sh.av)	Ga.av(obs)	Calc	Diff	Vector	wt. per cent
SiO2	47.63	39.71	54.97	47.2	48.09	48.2	-0.1113	CPX	0.158
Al2O3	5.71	0	28.16	14.4	13.66	13.5	0.1589	OL	0.048
Fe2O3	14.38	19.26	0.74	12.3	12.12	12.3	-0.1841	PL	0.085
MnO	0.34	0.21	0	0.2	0.21	0.2	0.0078	Sh.av	0.719
MgO	10.57	42.41	0	6.9	8.69	8.5	0.1857		
CaO	18.29	0.18	10.12	7.4	9.09	8.9	0.1903		
Na2O	0.68	0	4.99	4.7	3.91	4	-0.0877		
K2O	0.14	0	0.46	3	2.22	1.8	0.4183		
TiO2	3.33	0.11	0.21	3.1	2.78	2.3	0.4797		
P2O5	0	0	0	1.1	0.79	0.6	0.1909		
Sum of squares of residuals							0.5915		

Trace element

Sample	CPX	OL	PL	Parent (Ga 4)	Ga 1(obs)	Calc	Parent (Ga.av)	Sh.av(obs)	Calc
La	0.01	0.15	0.08	41.00	55.00	50.57	60.80	78.67	81.66
Ce	0.01	0.15	0.08	71.00	90.00	87.56	103.40	138.00	138.88
Y	0.01	0.7	0.01	22.80	27.90	28.05	27.84	31.27	34.13
Zr	0.01	0.24	0.01	189.00	260.00	234.27	285.40	387.67	379.76
Ba	0.01	0.01	0.1-0.6	455.00	575.00	566.08	670.80	937.67	921.93
Rb	0.01	0.01	0.01	33.60	43.30	41.80	47.86	69.50	66.35
Sr	0.01	0.12	2.0-2.3	604.00	739.00	623.79	862.40	1141.67	969.09
Nb	0.01	0.09	0.01	41.30	58.70	51.32	68.62	89.13	93.78
Ga	0.03	0.3	0.9-1.2	20.60	21.60	22.79	22.22	24.87	26.84
Nd	0.01	0.3	0.08	29.00	38.00	35.68	43.20	63.00	56.49

Table 3.10. REE analyses for selected samples of the South Australian alkaline basalts.

Sample	963-Ga 6	963-Ga 10	963-Sh 4	963-Sh 2	963-MC 1	963-MC 2	963-MC 4	963-LL 2	963-LL 3	963-ED 1	963-ED 3
Lithology	Hawaiite		Hawaiite		Analcimite			Analcimite		Analcimite	
Locality	Mt Gambier		Mt Schank		Mt McIntyre			Lake Leake		Mt Edward	
La	31.15	38.43	68.43	67.33	73.44	74.86	70.48	62.49	59.79	57.82	53.89
Ce	61.53	76.50	126.91	131.46	142.58	148.60	142.41	126.38	116.66	117.21	101.34
Nd	28.15	34.75	58.56	59.08	61.70	63.59	64.55	54.87	50.71	53.75	45.99
Sm	6.10	7.50	11.64	11.73	11.72	10.63	11.87	10.53	9.81	10.32	8.80
Eu	2.10	2.53	3.96	3.87	3.60	3.90	3.61	3.10	3.07	3.15	2.73
Gd	5.63	6.76	7.83	9.59	8.61	8.39	8.86	8.17	9.29	7.62	5.44
Dy	4.39	5.36	6.93	6.86	6.02	6.17	6.06	5.01	5.24	5.43	4.81
Er	1.87	2.28	2.70	2.71	2.38	2.69	2.40	2.84	2.07	2.09	1.94
Yb	1.37	1.71	1.94	1.96	1.71	1.98	1.76	1.57	1.43	1.44	1.39

Sample	963-GR 2	963-GR 4	963-BU 2	963-BU 4	963-MU 1	963-MU 2	963-WA 1	963-WA 2	963-WA 5	963-BL 1	963-BL 2
Lithology	Analcimite		Analcimite		Analcimite		Analcimite			Analcimite	
Lithology	Mt Graham		Burr		Mt Muirhead		Mt Watch			The Bluff	
La	85.95	65.61	67.01	77.55	65.86	66.67	79.29	65.90	60.51	65.74	54.15
Ce	129.51	121.48	125.59	133.95	130.04	125.60	162.96	131.10	122.06	132.88	105.63
Nd	68.48	60.13	60.35	61.47	57.35	57.88	75.14	60.46	52.61	59.72	46.88
Sm	13.05	11.00	11.59	12.16	11.43	11.15	14.36	11.46	9.72	11.07	8.78
Eu	4.04	3.47	3.59	3.68	3.57	3.50	4.42	3.54	2.92	3.43	2.67
Gd	9.96	9.30	9.55	9.81	11.09	8.26	10.54	9.30	8.28	9.57	9.80
Dy	7.84	6.07	6.53	7.13	6.31	6.07	7.57	6.12	4.99	5.79	4.56
Er	3.77	2.46	2.64	3.10	2.59	2.47	3.14	2.39	1.96	2.30	1.81
Yb	2.62	1.78	1.88	2.15	2.89	1.79	2.38	1.70	1.38	1.60	1.27

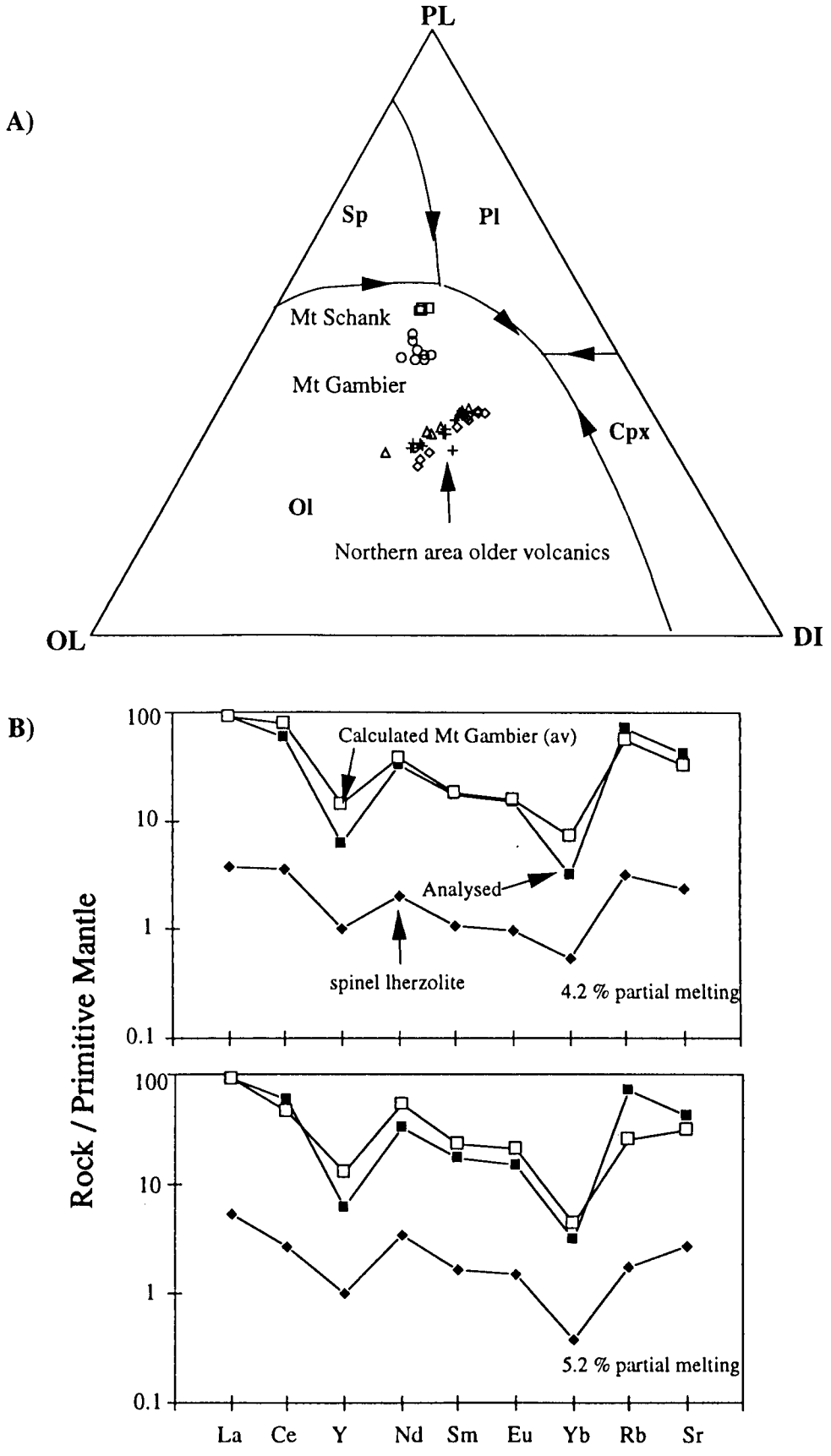

Fig. 3.19a. A) Ternary projection of Ol-Pl-Cpx for the South Australian alkaline basalts (Walker *et al.*, 1979). B) PM normalized trace element abundances, upper-spinel lherzolite (av) from McDonough (1990), lower-metasomatized spinel lherzolite (av) from O'Reilly and Griffin (1988).

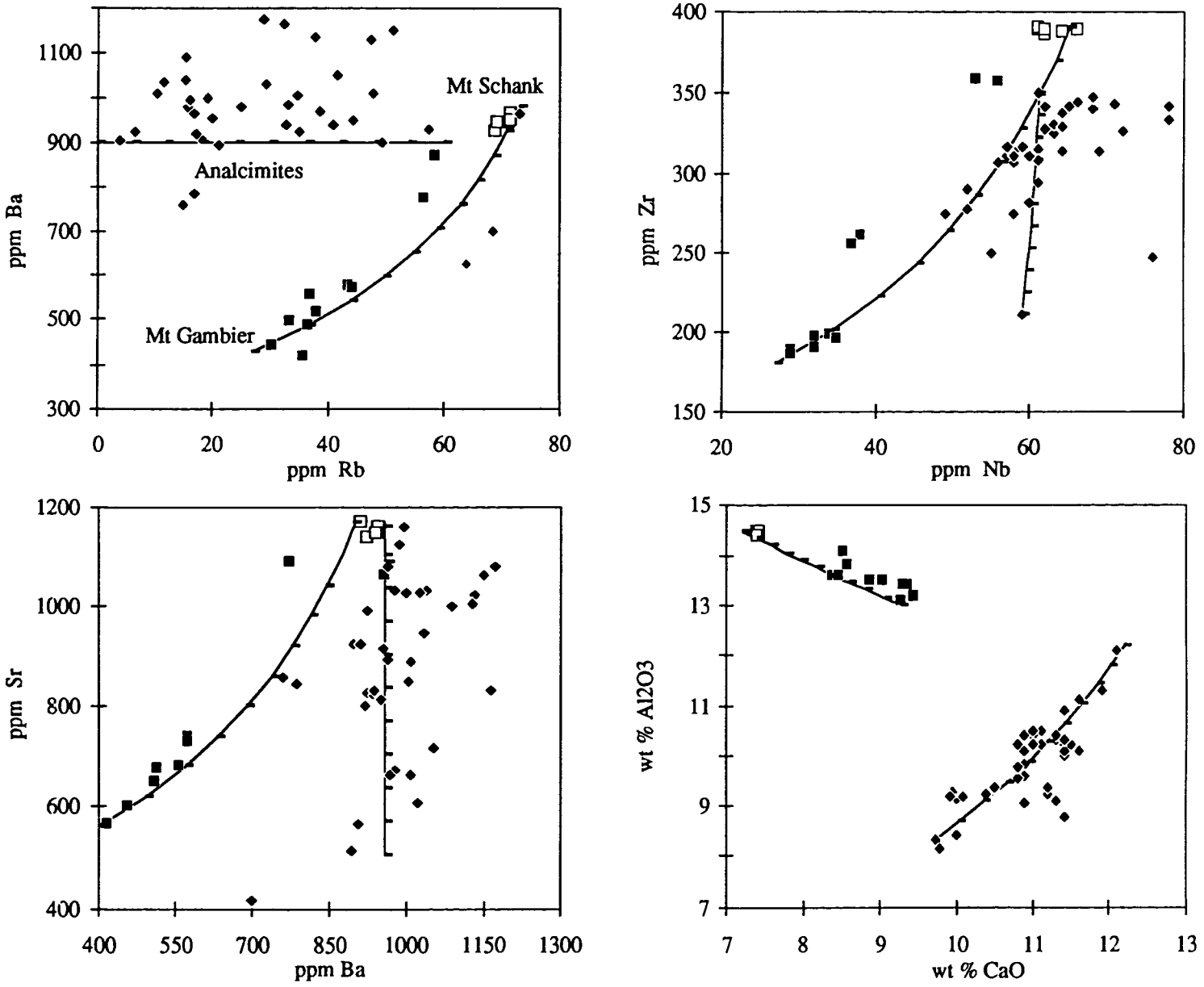

Fig. 3.19b. Possible mixing models between the Mt Gambier and Mt Schank, and two analcimite end members.

3.5.4. Isotope geochemistry

A) Introduction

All samples considered for whole rock chemistry were analysed for the Sr-Nd isotopic compositions. The analyses were completed with the Finnigan Mat 261 mass spectrometer in the Department of Geology and Geophysics, University of Adelaide. Details of analytical methods and sample preparation are shown in Appendix 1.

The hawaiites have εNd +2.26 - +3.23 and $^{87}Sr/^{86}Sr$ of 0.7035 - 0.7041, TNd_{DM} of 0.43 - 0.6 Ga (Fig. 3.20, Table 3.11). They also have Sm/Nd ratios of 0.18 - 0.22 and Rb/Sr ratios of 0.042 - 0.065. Generally, Mt Schank hawaiites contain higher $^{87}Sr/^{86}Sr$ (0.7040 - 0.7042) and Rb/Sr (> 0.058), lower Sm/Nd (< 0.195), high εNd(i) (7.6 - 8.4) relative to the Mt Gambier hawaiites.

3.6. Petrogenesis of Northern area volcanics (NAB), NMFV, BSFV & MDFV

3.6.1. Petrography and mineralogy

Forty five samples have been selected for petrographic descriptions which are summary are shown in Table 3.12.

Volcanics distributed along the northernmost fault line (NMFV, Fig. 3.6); The NMFV are characterised by cumulate texture, iddingsite rimmed olivine phenocrysts and the existences of analcites groundmass. They contain Ol±Cpx as phenocryst, Cpx±Ol as micro-phenocryst, and An±Cpx±Ol±Il±Pl as groundmass. Most of the NMFV show aggregation of micro-phenocryst or groundmass clinopyroxene to form a cumulate texture (Fig. 3.21). The clinopyroxene grains show elongated prismatic or lath- shapes and randomly oriented. Of the NMFVs, Mt McIntyre analcimites show more abundant analcite groundmass and aggregated clinopyroxene micro-phenocrysts than the others whereas Lake Leake and Mt Edward analcimites are characterised by abundant olivine and pyroxene xenocrysts originating from the fragments of mantle xenoliths.

In the Mt McIntyre analcimites, clinopyroxene phenocrysts show distinctive zonal or hourglass texture and most of the olivine and clinopyroxene phenocrysts are well enclosed by thin lamellae-shaped clinopyroxene groundmass. Some of fine grained olivine phenocrysts are completely altered to reddish-brown coloured grains. In the Lake Leake and Mt Edward analcimites, the xenocrysts are scattered in all sections and fill in vesicles within the basalts. In these analcimites, a few olivine and clinopyroxene xenocrysts show partially melted rims with the host basalt. The Lake Leake analcimites also contain abundant ray or ring shaped secondary calcites which are filled in vesicles of the basalts.

Table 3.11. Isotope analyses of the Southern area younger volcanics.

Sample	Locality	Lithology	Rb	Sr	87Rb/86Sr	87Sr/Sr86		87Sr/Sr86(T)	Nd	Sm	147Sm/144Nd	143Nd/144 Nd		143Nd/144Nd(T)	eps Nd (0)	eps Nd chT	T mod:dep
963-Ga 1	Mt Gambier	Hawaiites	42.3	786.2	0.155727	0.704153	± 50	0.703066	40.56	8.45	0.126015	0.512801	± 23	0.512396	3.18	7.48	0.498
963-Ga 2			44.2	725.1	0.176568	0.704002	± 28	0.702769	35.84	7.18	0.121248	0.512783	± 14	0.512394	2.83	7.43	0.502
963-Ga 3			58.5	1082.2	0.156567	0.703984	± 30	0.702891	50.01	9.16	0.110848	0.512802	± 38	0.512447	3.21	8.46	0.428
963-Ga 4			31.5	666.6	0.136948	0.704042	± 32	0.703086	29.63	6.40	0.130679	0.512765	± 31	0.512345	2.47	6.47	0.584
963-Ga 5			52.5	1230.5	0.123661	0.703955	± 44	0.703092	52.88	10.32	0.118060	0.512756	± 31	0.512377	2.30	7.09	0.526
963-Ga 6			34.8	674.5	0.149594	0.703986	± 49	0.702942	35.33	7.32	0.125259	0.512778	± 30	0.512376	2.73	7.07	0.530
963-Ga 7			32.2	649.0	0.143869	0.703766	± 28	0.702761	32.06	6.79	0.128147	0.512800	± 28	0.512389	3.17	7.33	0.510
963-Ga 8			35.7	570.9	0.181108	0.704111	± 35	0.702847	31.94	6.96	0.131869	0.512712	± 21	0.512289	1.45	5.38	0.680
963-Ga 9			36.6	675.2	0.157003	0.703566	± 22	0.702470	31.85	7.04	0.133776	0.512766	± 30	0.512336	2.49	6.30	0.602
963-Ga 10			36.7	682.8	0.155680	0.703964	± 39	0.702877	31.27	6.88	0.133125	0.512766	± 19	0.512339	2.50	6.35	0.597
963-Sh 1	Mt Schank	Hawaiites	69.5	1118.0	0.179974	0.704026	± 28	0.702770	59.69	11.05	0.111946	0.512804	± 23	0.512445	3.24	8.42	0.430
963-Sh 2			70.4	1129.3	0.180459	0.704084	± 25	0.702824	58.14	11.17	0.116235	0.512813	± 14	0.512440	3.42	8.33	0.434
963-Sh 3			71.6	1105.0	0.187578	0.704153	± 44	0.702843	57.93	10.91	0.113955	0.512767	± 38	0.512401	2.52	7.58	0.490
963-Sh 4			71.1	1141.9	0.180368	0.704012	± 35	0.702753	59.71	11.11	0.112552	0.512794	± 31	0.512433	3.05	8.19	0.446
963-Sh 5			71.7	1129.8	0.183811	0.704082	± 38	0.702799	60.65	11.02	0.109914	0.512763	± 31	0.512411	2.45	7.76	0.477
963-Sh 6			69.2	1195.8	0.167611	0.704133	± 24	0.702962	59.33	11.50	0.117288	0.512805	± 30	0.512428	3.25	8.10	0.451

Errors quoted are calculated as 2 standard error of the mean,

The value T is an initial age on recrystallization of a rock,

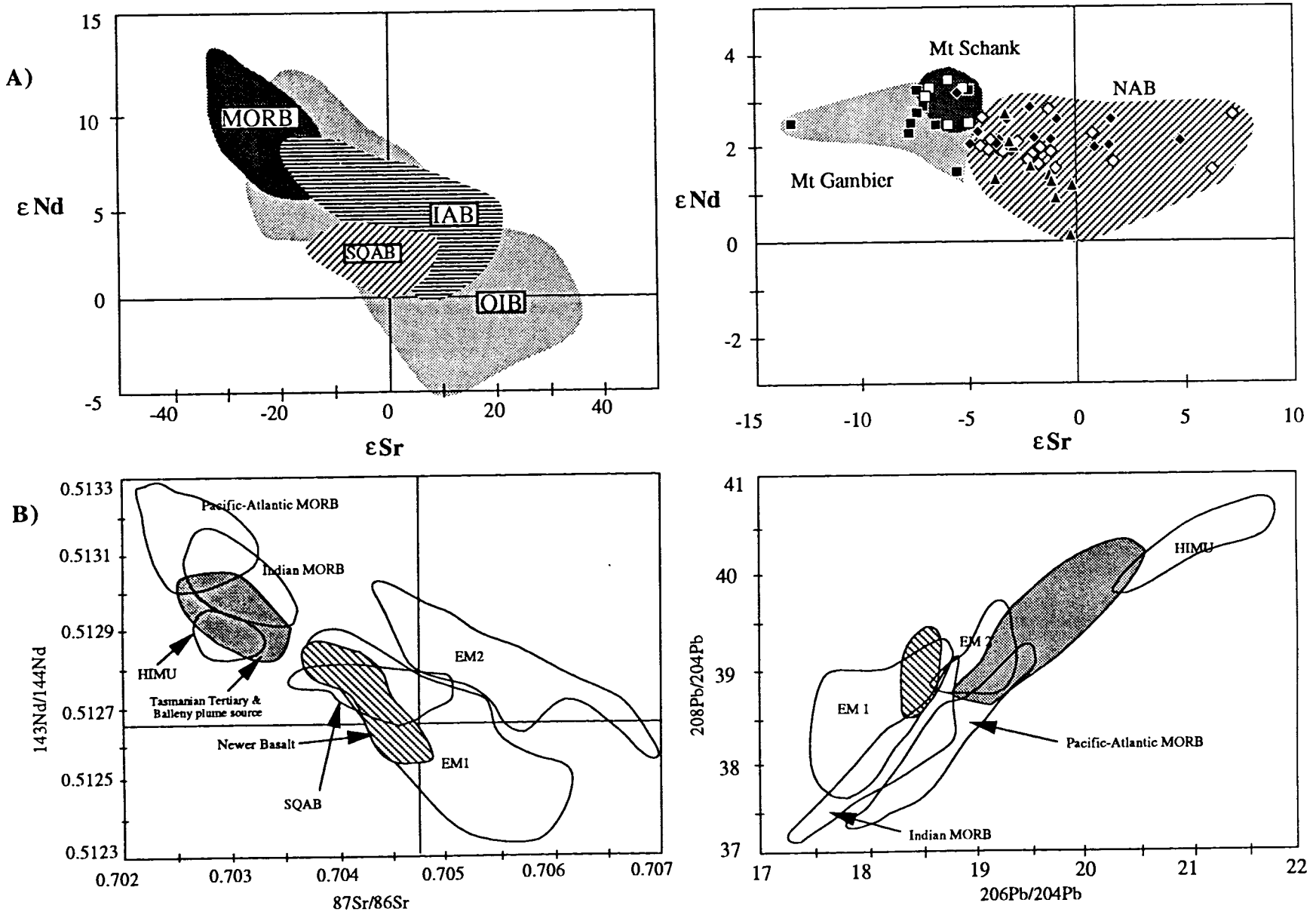

Fig. 3.20. A) Plots of Sr -Nd isotopic compositions for the South Australian alkaline basalts. B) Plots of Sr -Nd-Pb isotopic compositions of basalts from Cainozoic south eastern Australia (modified from Lanyon *et al.*, 1993).

Table 3.12. Petrography of the Northern area older volcanics.

Sample	Locality	Phenocryst	Microphenocrysts	Groundmass	Second, Min.	Texture
963-MC 1 to 8	Mt McIntyre	Ol+Cpx (10-18 %)).	Cpx±Ol (5-13 %)	An+Cpx+Ol+Il±Pl (52-64 %)	Cal	cumulate texture, An coexisting with Pl, glomeroporphyritic texture, foliation, thick iddingsite rimmed Ol pheno.
963-LL 1 to 5	Lake Leake	Ol±Cpx (9-14 %)	Cpx±Ol (5-8 %)	An+Cpx+Il+Ol (45-65 %)	Cal	distinctive iddingsite rimmed Ol pheno, Cal in vesicles, Ol or Cpx xenocr.
963-ED 1 to 4	Mt Edward	Ol (16-18 %)	Cpx±Ol (5-7 %)	Cpx+An+Ol+Il (58-67 %)	Cal, Qt	Ol or Cpx xenocr, relatively fine grained pheno.
963-MU 1 to 7	Mt Muirhead	Ol±Cpx (8-18 %)	Cpx±Ol (7-13 %	Cpx+An+Ol+Il+Pl (48-65 %)	Cal	glomeroporphyritic texture, cumulate texture, distinctive alteration rim of Ol.
963-WA 1 to 7	Mt Watch	Ol±Cpx (10-25 %)	Ol±Cpx (5-10 %)	Cpx+An+Ol+Il+Pl (20-60 %)	Cal	fludial texture, glomeroporphyritic texture, An coexising with Pl, Px. and Ol xenocr.
963-BL 1 to 4	The Bluff	OL±Cpx (13-24 %)	Cpx(6-12 %)	Cpx+An+Ol+Il+Pl (50-65 %)	Cal	abundant Cpx pheno, distinctive iddingsite rimmed Ol,, glomeroporphyritic texture.
963-GR 1 to 6	Mt Graham	Ol±Cpx(9-20 %)	Cpx±Ol (3-6 %)	Cpx+An+Ol+Il+Pl (40-67 %)		distinctive iddingsite rimmed Ol pheno, An coexisting Pl, distinctive foliation.
963-BU 1 to 4	Burr	Ol±Cpx(17-20 %)	Ol+Cpx (6-11 %)	Cpx+An+Ol+Il+Pl (40-52%)		aggregation of the Cpx micro pheno, abundant Cpx pheno.

* Pheno (Phenocryst), xenocr (Xenocryst)

Some of the vesicles are filled with quartz from country rocks, possibly from sandstones of the Bridgewater formation. In these Lake Leake volcanics, a few spine-shaped micas showing pale red pleochroic colour also occur as groundmass. The Mt Edward analcimites contain abundant vesicles which show slightly elongated spherulitic shapes in the direction of the pronounced lineation. Most of them contain gas bubbles trapped when the rock was solidified.

Volcanics distributed along the beach side fault line (BSFV, Fig. 3.6); The BSFV are characterised by cumulate textures by aggregated clinopyroxene microphenocryst and groundmass, existences of Ol+Px xenocrysts and of fragments of pyroxenitic, dunitic and/or spinel lherzolite xenoliths. They contain Ol±Cpx as phenocryst, Cpx±Ol as microphenocryst, and Cpx±An±Ol±Il±Pl as groundmass. In general, the BSFV contain abundant fluid inclusions and calcite in their vesicles, and xenocrysts showing reaction boundary with the host basalt.

The Mt Watch analcimites show variable microscopic textures and mineralogies relative to other analcimites. They range from scorious, vesicular to massive rocks and contain more abundant olivine, pyroxene xenocrysts relative to the other two volcanics. In the Mt Muirhead analcimites, olivine phenocrysts show well developed reddish-brown alteration rims relative to those of any other localities. Some of olivine xenocrysts are enveloped by the spine shaped pyroxene groundmass. Albite to oligoclase plagioclases coexisting with analcite occur as dusky, glassy, or spine-shaped groundmass. Clinopyroxene phenocrysts of the Mt Muirhead and The Bluff analcimites often show zonal and hourglass textures.

Volcanics distributed along the middle fault line (MDFV, Fig. 3.6); Mt Graham analcimites and Burr lava flow include in this group. They display glomeroporphyritic texture by a aggregation of olivine phenocryst and clinopyroxene microphenocryst. In general, the Mt Graham analcimites are characterised by the abundant dusky analcite groundmass coexisting with plagioclase groundmass while Burr lava flow is characterised by cumulate texture by aggregation of simple twinned elongate clinopyroxene microphenocryst, and existences of abundant clinopyroxene phenocrysts. In the Mt Graham analcimites, groundmass is principally glassy or cryptocrystalline whereas in the Burr lava flow, they are relatively coarse grained. Some samples from Mt Graham show relatively coarse grained clinopyroxene phenocrysts and a few Burr lava flow contain discrete coarse-grained orthopyroxenes.

Figures opposite;

Fig. 3.21a. Photograph of a fresh surface of a typical Northern area olivine analcimite from Mt McIntyre (MC 7). Yellow brown grains are olivines.

Fig. 3.21b. Photomicrograph of iddingsite rimmed olivine phenocrysts (o) and thin lath shaped clinopyroxene groundmass in the Mt McIntyre analcimite (MC 7). Groundmass includes dusky analcite. The grain often coexists with plagioclase (albite).

Fig. 3.21c. Photomicrograph showing a cumulate texture by an aggregation of clinopyroxene micro-phenocrysts (cp) and olivine phenocrysts (o) in the Mt Muirhead analcimite (MU 1)

Fig. 3.21d. Photomicrograph showing a cumulate texture by an aggregation of lath shaped clinopyroxene and olivine microphenocrysts in a vesicle in the Mt McIntyre analcimite (MC 2)

Fig. 3.21e. Photomicrograph of a zonal textured clinopyroxene (cp) and iddingsite rimmed olivine phenocrysts (o) in the Mt Graham analcimite (GR 3).

Fig.3.21f. Photomicrograph of a olivine xenocryst (o) enveloped by clinopyroxene groundmass from the Lake Leake analcimite (LL 2). The xenocryst is clearly distinguished from the iddingsite rimmed olivine phenocrysts (o, upper left).

Fig. 3.21g. Photomicrograph of a glomeroporphyritc texture by an aggregation of thin prismatic shaped clinopyroxenes (cp) and diamond shaped olivine phenocrysts (o) from the Burr lava flow (BU 1).

Fig. 3.21h. Photomicrograph showing zonal textured clinopyroxenes (cp) and iddingsite rimmed olivine phenocrysts (o) from the Mt McIntyre analcimite (MC 8). Groundmass include simple twined clinopyroxene, greyish coloured analcites and plagioclases.

Width of a scale bar (left bottom) is 1 millimetre.

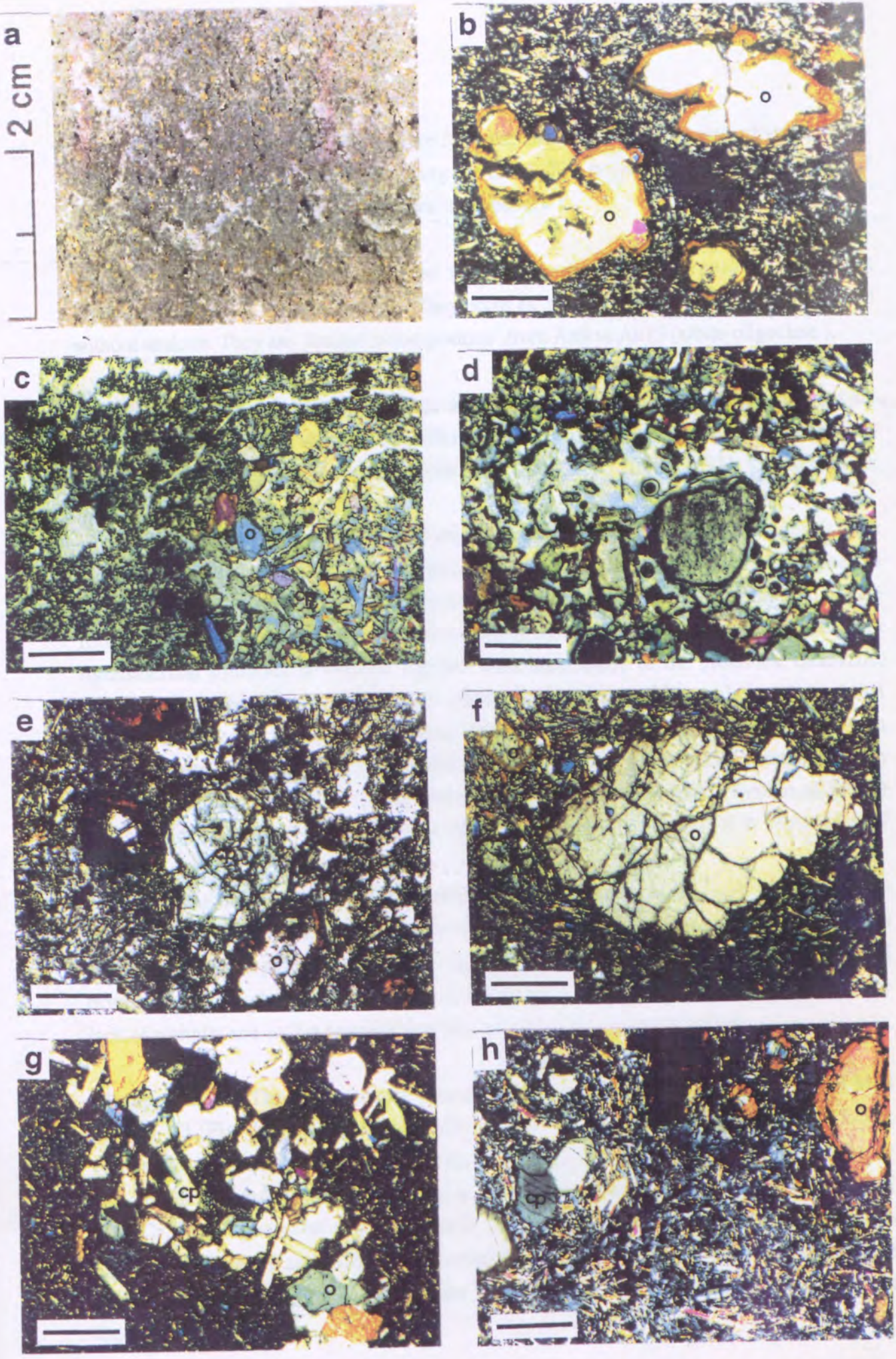
a
2 cm
b
o
o
c
o
o
d
e
o
f
o
o
g
cp
o
h
o
cp

3.6.2. Mineral Chemistry

Selected samples were analysed for feldspar, analcite, clinopyroxene, olivine and Fe-Ti oxide. Analyses were carried out using the JEOL 733 microprobe at the University of Adelaide. Details of the analysis are given in Appendix 1.

Feldspars; Plagioclase groundmasses are found in the most of olivine analcimites (e.g. Mt Watch, Mt Muirhead, and Mt Graham). They occur as acicular shaped groundmass with and without analcite. They are limited in composition from An9 to An15 (albite-oligoclase).

Analcites; Analcites are observed only in the groundmass. The representative analyses are shown in Table 3.13. Occurrences of analcite phenocryst and groundmass are reported from eastern Australian volcanic provinces (Wilkinson, 1963, 1977; Irving, 1971; Cundari, 1973; Birch, 1979) .

However, their petrogeneses and origins are still ambiguous. They may result from ion-exchanged leucite phenocrysts (Wilkinson, 1977) or replacement of the nepheline (Birch, 1979). Deer *et al.* (1966) suggested that the analcite is a primary mineral of late formation in intermediate and basic igneous rocks (magmatic origin) and is crystallized from hydrothermal solutions in vesicles together with association of the prehnites, chabazite, thomsonite and zeolites at a later stage (hydrothermal origin). They also explained that primary analcites in volcanic rocks occur dominantly as groundmass in association with pseudoleucites whereas in amigdaroidal basalts, analcites often occur in vesicles with association of the minerals mentioned above for the hydrothermal origin. Deer *et al.* (1966) also suggested their origin as an alteration of leucite and replacement by K in Na and Ca of feldspar.

In the South Australian olivine analcimites, the grains occur as a groundmass. They are not related to the filling in the vesicle and do not coexist with leucite. Many of analcites coexist with albite plagioclase. Thus it is very difficult to say whether the grains are of primary origin or whether they are from pseudomorphs after feldspar or feldspathoides. The lack of prehnite and zeolite suggests that they are not of hydrothermal origin.

Clinopyroxenes; The clinopyroxene grains show diopsidic to salitic composition and Mg# of 74 - 83 (Fig. 3.14, 3.22). High Cr_2O_3 is observed in the Mt Edward and Lake Leake volcanics which show high Mg#. Increase of Cr with increasing Mg# in the olivine analcimites may reflect a decrease of the substitutions of Fe(3) in the Y site in the rocks of high Cr, in the pyroxene general formula $(W)_{1-p}(X,Y)_{1+p}Z_2O_6$. However, insufficient (Si+Al) to fill the T site to the stoichiometric 2 atom per formula unit in many olivine analcimites may indicate occupation of the Ti in the T site and increase of the Fe(3) or Cr in the Y site.

Table 3.13. Representative analcite analyses of the Northern area older volcanics.

Sample	963-GR 5			963-MU 2		963-MU 3			
Locality	Mt Graham			Mt Mulrhead		Mt Mulrhead			
SiO2	52.64	52.06	53.89	55.25	56.91	52.17	52.46	51.24	51.39
TiO2	0.12	0.13	0.45	0.22	0.27	0.10	0.15	0.01	0.14
Al2O3	28.16	2.04	27.86	25.60	26.31	28.49	28.35	28.02	28.17
FeO#	0.62	0.56	0.78	0.60	0.70	0.20	0.21	0.33	0.45
MnO	0.05	0.05	0.12	0.02	0.00	0.03	0.11	0.00	0.11
MgO	0.00	0.00	0.19	0.12	0.00	0.00	0.00	0.00	0.00
CaO	0.33	0.21	0.52	0.65	0.28	0.20	0.23	0.15	0.29
Na2O	12.92	11.99	10.35	11.77	11.09	13.41	11.80	12.24	13.46
K2O	0.78	1.01	0.85	0.62	0.25	1.19	1.03	1.10	1.36
P2O5	0.00	0.00	0.00	0.00	0.00	0.06	0.20	0.11	0.00
SO3	0.00	0.01	0.00	0.00	0.00	0.00	0.12	0.02	0.00
Cr2O3	0.09	0.04	0.00	0.00	0.08	0.08	0.07	0.16	0.10
NiO	0.00	0.00	0.00	0.00	0.00	0.00	0.00	0.06	0.00
Total	95.70	95.11	95.01	94.84	95.88	95.92	94.72	93.43	95.46
	Number of Ions on the Basis of 7 (0)								
Si	2.1769	2.1599	2.2210	2.2849	2.3080	2.1584	2.1778	2.1669	2.1465
Ti	0.0036	0.0042	0.0138	0.0067	0.0083	0.0030	0.0046	0.0004	0.0045
Al	1.3723	1.4198	1.3529	1.2475	1.2571	1.3887	1.3867	1.3961	1.3867
Fe	0.0215	0.0195	0.0270	0.0208	0.0238	0.0070	0.0071	0.0115	0.0156
Mn	0.0017	0.0017	0.0043	0.0007	0.0000	0.0009	0.0039	0.0000	0.0038
Mg	0.0000	0.0000	0.0116	0.0077	0.0000	0.0000	0.0000	0.0000	0.0000
Ca	0.0146	0.0094	0.0229	0.0288	0.0123	0.0087	0.0103	0.0066	0.0131
Na	1.0353	0.9637	0.8261	0.9430	0.8711	1.0750	0.9494	1.0029	1.0889
K	0.0409	0.0534	0.0445	0.0324	0.0127	0.0627	0.0548	0.0593	0.0726
P	0.0000	0.0000	0.0000	0.0000	0.0000	0.0019	0.0068	0.0038	0.0000
S	0.0000	0.0039	0.0000	0.0000	0.0000	0.0000	0.0037	0.0007	0.0000
Cr	0.0031	0.0013	0.0000	0.0000	0.0026	0.0025	0.0024	0.0054	0.0031
Ni	0.0000	0.0000	0.0000	0.0000	0.0000	0.0000	0.0000	0.0021	0.0000
sum	4.6699	4.6368	4.5240	4.5724	4.4958	4.7089	4.6075	4.6559	4.7347

Table 3.14. Representative clinopyroxene analyses of the Northern area older volcanics.

Sample	963-MC 4		963-LL 1	963-LL 2	963-LL 4	963-ED 3	963-GR 4	963-GR 6	963-BU 1	963-BU 2	963-BU 3	963-MU 3		963-MU 3		963-BL 2			963-WA 2/1
Locality	Mt McIntyre		Lake Leake			Mt Edward	Mt Graham		Burr			Mt Mulrhead				The Bluff			Mt Watch
SiO2	47.60	46.36	46.91	43.01	47.04	47.76	45.95	48.34	47.39	45.14	48.54	47.95	48.54	47.50	46.70	44.08	48.01	48.45	47.45
TiO2	3.30	3.52	2.81	5.51	3.13	3.15	3.68	2.29	2.79	3.99	2.33	2.96	2.35	2.82	3.79	4.77	2.54	2.54	3.00
Al2O3	5.03	5.61	4.12	6.09	4.54	4.26	6.99	4.04	4.82	7.46	3.60	3.85	2.82	4.35	5.76	6.45	3.29	3.13	4.12
FeO	5.27	3.86	2.46	6.81	2.71	3.21	5.22	3.85	2.45	7.48	2.69	5.21	4.45	4.35	5.98	4.51	3.12	3.38	4.08
Fe2O3	1.43	3.65	3.87	4.06	4.09	2.61	2.81	4.95	4.39	1.17	4.37	1.83	1.75	2.49	1.24	4.17	3.82	2.87	3.39
MnO	0.15	0.00	0.07	0.09	0.00	0.23	0.00	0.14	0.07	0.00	0.00	0.07	0.06	0.03	0.12	0.12	0.00	0.12	0.22
MgO	13.30	12.68	14.43	11.22	14.14	14.55	12.51	12.62	14.38	11.80	14.80	14.28	15.05	14.12	13.16	12.19	14.52	14.96	14.45
CaO	23.30	22.78	23.33	22.05	22.95	22.95	21.67	22.04	22.69	21.83	22.90	22.59	22.74	22.90	22.79	23.07	23.33	23.20	22.62
Na2O	0.26	0.63	0.20	0.43	0.33	0.28	0.71	1.04	0.49	0.22	0.34	0.10	0.00	0.13	0.10	0.20	0.24	0.08	0.08
K2O	0.03	0.00	0.00	0.02	0.10	0.02	0.00	0.09	0.00	0.17	0.04	0.07	0.00	0.00	0.00	0.00	0.02	0.00	0.00
P2O5	0.02	0.00	0.00	0.19	0.00	0.00	0.02	0.00	0.01	0.22	0.00	0.00	0.17	0.09	0.00	0.00	0.20	0.00	0.00
SO3	0.05	0.00	0.00	0.16	0.00	0.00	0.06	0.20	0.09	0.00	0.08	0.00	0.14	0.09	0.00	0.00	0.04	0.00	0.23
Cr2O3	0.32	0.46	0.88	0.30	0.73	0.92	0.52	0.35	0.67	0.14	0.51	0.05	0.52	0.22	0.34	0.29	0.42	0.51	0.41
NiO	0.20	0.00	0.25	0.24	0.06	0.12	0.16	0.00	0.19	0.02	0.00	0.20	0.00	0.00	0.00	0.00	0.00	0.04	0.00
Total	100.13	99.55	98.95	99.78	99.42	99.79	100.02	99.46	99.98	99.89	99.75	99.15	98.70	98.84	99.87	99.43	99.17	98.99	99.71
						Number of Ions on the Basis of 6 (0)													
Si	1.7755	1.7567	1.7786	1.6545	1.7740	1.7872	1.7261	1.8282	1.7745	1.7144	1.8183	1.8090	1.8348	1.7945	1.7531	1.6831	1.8118	1.8262	1.7829
Ti	0.0925	0.1003	0.0800	0.1592	0.0889	0.0887	0.1039	0.0651	0.0784	0.1130	0.0656	0.0840	0.0666	0.0801	0.1069	0.1371	0.0720	0.0719	0.0847
Al	0.2213	0.2507	0.1841	0.2762	0.2016	0.1879	0.3095	0.1799	0.2125	0.3314	0.1589	0.1710	0.1258	0.1935	0.2547	0.2903	0.1464	0.1390	0.1826
Fe(2)	0.1643	0.1213	0.0772	0.2169	0.0845	0.0998	0.1628	0.1205	0.0759	0.2361	0.0834	0.1637	0.1403	0.1367	0.1872	0.1424	0.0977	0.1059	0.1275
Fe(3)	0.0401	0.1032	0.1090	0.1164	0.1150	0.0729	0.0789	0.1396	0.1224	0.0331	0.1220	0.0518	0.0496	0.0706	0.0350	0.1185	0.1076	0.0809	0.0995
Mn	0.0048	0.0000	0.0022	0.0030	0.0000	0.0071	0.0000	0.0044	0.0023	0.0000	0.0001	0.0024	0.0019	0.0011	0.0041	0.0038	0.0000	0.0038	0.0071
Mg	0.7560	0.7155	0.8150	0.6429	0.7945	0.8109	0.7000	0.7110	0.8018	0.6624	0.8256	0.8023	0.8475	0.7946	0.7358	0.6933	0.8159	0.8399	0.8087
Ca	0.9307	0.9245	0.9470	0.9084	0.9270	0.9197	0.8718	0.8928	0.9098	0.8808	0.9188	0.9128	0.9205	0.9265	0.9162	0.9432	0.9427	0.9366	0.9104
Na	0.0188	0.0461	0.0145	0.0317	0.0239	0.0201	0.0517	0.0765	0.0352	0.0158	0.0245	0.0072	0.0000	0.0098	0.0075	0.0146	0.0175	0.0062	0.0061
K	0.0015	0.0000	0.0000	0.0008	0.0048	0.0009	0.0000	0.0041	0.0000	0.0083	0.0018	0.0035	0.0000	0.0000	0.0001	0.0000	0.0011	0.0000	0.0000
P	0.0007	0.0000	0.0000	0.0062	0.0000	0.0000	0.0006	0.0000	0.0004	0.0069	0.0001	0.0000	0.0053	0.0030	0.0000	0.0000	0.0066	0.0000	0.0000
S	0.0013	0.0000	0.0000	0.0048	0.0000	0.0000	0.0018	0.0057	0.0024	0.0000	0.0021	0.0014	0.0040	0.0027	0.0000	0.0000	0.0010	0.0000	0.0065
Cr	0.0095	0.0137	0.0264	0.0092	0.0219	0.0272	0.0154	0.0105	0.0199	0.0041	0.0150	0.0060	0.0155	0.0067	0.0102	0.0088	0.0124	0.0152	0.0122
Ni	0.0059	0.0000	0.0076	0.0076	0.0019	0.0035	0.0049	0.0000	0.0058	0.0008	0.0000	0.0052	0.0000	0.0000	0.0000	0.0000	0.0000	0.0012	0.0000
Wo	49.2	49.5	48.6	48.1	48.2	48.3	48.0	47.8	47.6	48.6	47.1	47.3	47.0	48.0	48.9	49.6	48.0	47.7	46.9
En	40.0	38.3	41.8	34.1	41.3	42.6	38.6	38.1	41.9	36.6	42.3	41.5	43.3	41.2	39.2	36.5	41.5	42.8	41.6
Fs	10.8	12.1	9.6	17.8	10.5	9.1	13.4	14.1	10.5	14.8	10.6	11.2	9.7	10.8	11.9	13.9	10.5	9.6	11.5
Mg/Mg+Fe(t)	78.7	76.0	81.2	65.6	79.8	82.3	74.2	73.1	80.0	71.1	79.9	78.8	81.7	79.3	76.8	72.5	79.8	81.7	78.3

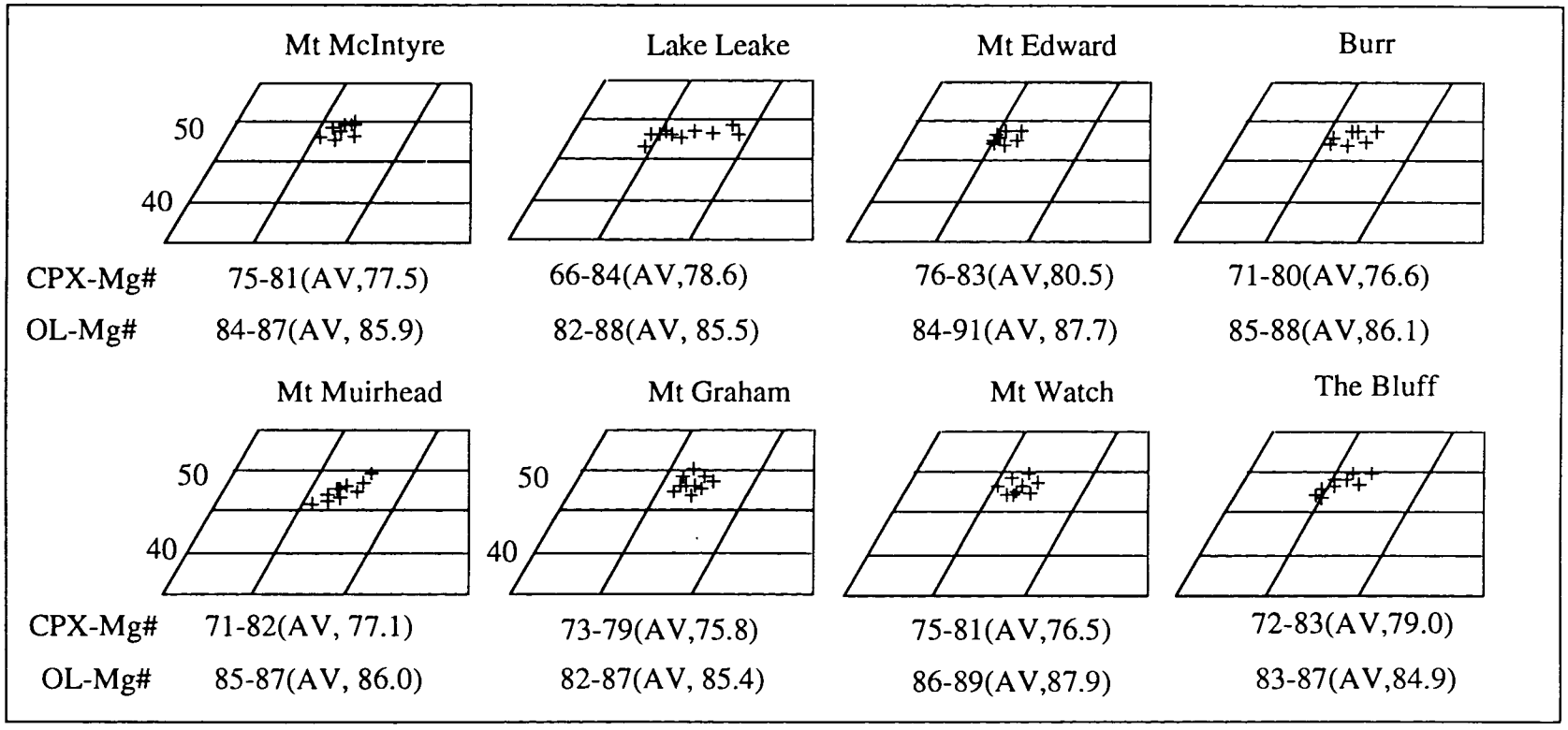

Fig. 3.22. Clinopyroxene and Olivine compositions of the Northern area older volcanics.

In addition, decrease of Na with Ca may reflect a relative increase of substitution of Ca rather than Na in the W site. No clear correlation are found in the coexisting clinopyroxene and olivine, suggestive of disequilibrium condition.

Olivines; The olivine phenocrysts range from Fo_{84} to Fo_{88} and show a decrease of MnO and CaO with Mg# (Fig. 3.22, Table 3.15). They also show a variable Ni contents. Ni contents in mafic basalts is a sensitive indicator of olivine-pyroxene fractionation. However, variable Ni with Mg# in olivines of the South Australian analcimites may reflect complexities of the Ni partitioning between the olivine and the silicate melts as mentioned by Hart and Davis (1978).

Hart and Davis (1978) suggested that large variations in the degree of partial melting or in the Ni contents of the mantle sources, and strong dependent of the D_{Ni} on pressure or some melt composition variable may cause anomalous Ni-Mg# trends in olivine. They stressed the strongly dependent on the composition of the melt rather than the temperature. However, Leeman and Lindstrom (1978) stressed the strong dependence on the temperature in olivine rather than the melt composition. Thus, it is not clear why the South Australian analcimites show a wide variation of Ni content.

In the reviews of the eastern Australian volcanics, Ewart (1989a) indicated an increase of Ca in olivine from tholeiitic, through hawaiites to strongly silica undersaturated rocks, and lower CaO with high Mg content in the more alkaline lava, such as alkali basalt, basanites and leucitities. He also suggested that Ca enrichment with Fe content does not indicate pressure as well as SiO_2 activity.

In the South Australian analcimites, olivine show a decrease of MnO and CaO with Mg#. The CaO-Mg# relationships can be explained by the increase of Fe content with Ca contents as result of crystallisation at the stable pressure condition (Stormer, 1973). The cause of the observed negative correlation of MnO with Mg# is not clear.

Fe-Ti-Cr oxides; The olivine analcimites contain ulvöspinel with minor Cr-spinels (Lake Leake). They are summarised in Fig. 3.12 and Table 3.16.

3.6.3. Whole rock geochemistry

A) Introduction

Forty five samples were analysed for the major and trace elements by XRF at the University of the Adelaide. Selected samples were analysed for REE by same methods as described in section Chater 3.5.3. Details of analytical methods and sample preparation are shown in Appendix 1. Representative analyses for major and trace elements arc presented in the Tables 3.17, 3.18, 3.20 and their complete list is shown in Appendix 2.

Table 3.15. Representative olivine analyses of the Northern area older volcanics

Sample	963-MC 4	963-MC 8	963-LL 1	963-LL 2	963-LL 4	963-ED 4	963-GR 4	963-GR 5	963-GR 6	963-BU 1	963-BU 2	963-BU 3	963-MU 1	963-MU 3	963-WA 2,1	963-WA 3	963-BL 1	963-BL 2	963-BL 3
Locality	lt McIntyre			Lake Leake		Mt Edward		Mt Graham		Burr			Mt Muirhead		Mt Watch		The Bluff		
SiO2	39.56	39.64	39.18	39.73	38.63	39.93	39.81	39.45	38.48	39.10	39.54	39.92	40.00	39.79	39.98	39.62	39.14	39.28	39.30
TiO2	0.00	0.07	0.10	0.04	0.16	0.00	0.00	0.15	0.37	0.00	0.00	0.01	0.05	0.05	0.08	0.20	0.04	0.05	0.00
Al2O3	0.22	0.06	0.00	0.00	0.00	0.00	0.00	0.00	0.00	0.18	0.00	0.06	0.29	0.02	0.00	0.21	0.00	0.00	0.00
FeO	12.97	13.66	12.87	11.52	13.67	11.22	12.08	13.50	13.24	12.54	11.72	13.31	13.35	12.83	11.68	12.26	12.77	13.28	13.12
Fe2O3	0.00	1.56	0.52	0.26	1.21	0.01	0.65	0.27	0.78	1.08	0.14	0.08	0.00	0.56	0.00	0.00	0.58	0.00	0.35
MnO	0.1:	0.27	0.20	0.30	0.12	0.28	0.18	0.24	0.36	0.20	0.13	0.00	0.29	0.18	0.27	0.24	0.22	0.02	0.20
MgO	46.19	45.39	45.84	46.94	44.62	47.38	46.49	45.77	44.87	45.72	47.25	46.01	45.77	46.38	46.98	46.44	45.80	45.62	45.73
CaO	0.18	0.27	0.27	0.10	0.33	0.16	0.20	0.17	0.40	0.33	0.11	0.14	0.41	0.24	0.23	0.30	0.18	0.36	0.29
Na2O	0.00	0.09	0.00	0.00	0.12	0.00	0.00	0.00	0.00	0.00	0.00	0.00	0.00	0.00	0.00	0.00	0.00	0.00	0.00
K2O	0.00	0.00	0.00	0.10	0.03	0.03	0.03	0.09	0.00	0.05	0.05	0.02	0.04	0.03	0.00	0.00	0.04	0.01	0.05
P2O5	0.06	0.00	0.10	0.00	0.02	0.00	0.00	0.00	0.00	0.00	0.00	0.00	0.00	0.00	0.00	0.00	0.00	0.00	0.00
SO3	0.15	0.00	0.16	0.18	0.21	0.00	0.13	0.00	0.16	0.14	0.04	0.04	0.00	0.08	0.14	0.13	0.00	0.00	0.18
Cr2O3	0.00	0.07	0.00	0.00	0.00	0.12	0.04	0.02	0.11	0.00	0.00	0.08	0.00	0.00	0.13	0.12	0.03	0.07	0.19
NiO	0.34	0.00	0.23	0.29	0.46	0.27	0.00	0.41	0.36	0.26	0.63	0.00	0.00	0.22	0.47	0.49	0.38	0.42	0.41
Total	99.79	101.08	99.47	99.45	99.57	99.41	99.63	100.05	99.12	99.60	99.64	99.66	100.20	100.38	99.95	100.00	99.19	99.12	99.81

Number of Ions on the Basis of 4 (0)

Si	0.9879	0.9887	0.9848	0.9911	0.9794	0.9944	0.9940	0.9888	0.9772	0.9837	0.9870	0.9978	0.9960	0.9904	0.9924	0.9864	0.9882	0.9911	0.9862
Al	0.0065	0.0018	0.0000	0.0000	0.0000	0.0000	0.0000	0.0000	0.0000	0.0052	0.0000	0.0018	0.0085	0.0005	0.0000	0.0061	0.0000	0.0000	0.0000
Ti	0.0000	0.0014	0.0018	0.0007	0.0030	0.0000	0.0000	0.0027	0.0070	0.0000	0.0000	0.0003	0.0009	0.0009	0.0015	0.0037	0.0008	0.0009	0.0000
Fe(2)	0.2708	0.2836	0.2703	0.2402	0.2888	0.2331	0.2522	0.2820	0.2804	0.2631	0.2437	0.2782	0.2778	0.2665	0.2423	0.2551	0.2685	0.2801	0.2748
Fe(3)	0.0000	0.0292	0.0098	0.0050	0.0231	0.0003	0.0123	0.0050	0.0149	0.0204	0.0027	0.0014	0.0000	0.0105	0.0000	0.0000	0.0110	0.0000	0.0066
Mn	0.0023	0.0056	0.0042	0.0062	0.0026	0.0059	0.0039	0.0050	0.0078	0.0043	0.0027	0.0000	0.0062	0.0039	0.0057	0.0050	0.0046	0.0005	0.0043
Mg	1.7180	1.6863	1.7161	1.7446	1.6852	1.7578	1.7291	1.7091	1.6976	1.7135	1.7569	1.7131	1.6977	1.7197	1.7371	1.7222	1.7225	1.7148	1.7091
Ca	0.0049	0.0073	0.0072	0.0026	0.0090	0.0042	0.0055	0.0044	0.0108	0.0090	0.0029	0.0037	0.0109	0.0063	0.0060	0.0081	0.0049	0.0098	0.0079
Na	0.0000	0.0042	0.0000	0.0000	0.0059	0.0000	0.0000	0.0000	0.0000	0.0000	0.0000	0.0000	0.0000	0.0000	0.0000	0.0000	0.0000	0.0000	0.0000
K	0.0000	0.0000	0.0000	0.0032	0.0011	0.0011	0.0009	0.0029	0.0000	0.0015	0.0017	0.0006	0.0014	0.0010	0.0000	0.0000	0.0014	0.0004	0.0016
P	0.0013	0.0000	0.0022	0.0000	0.0004	0.0000	0.0000	0.0000	0.0000	0.0000	0.0000	0.0000	0.0000	0.0000	0.0000	0.0000	0.0000	0.0000	0.0000
S	0.0028	0.0000	0.0030	0.0034	0.0039	0.0000	0.0025	0.0000	0.0030	0.0027	0.0009	0.0008	0.0000	0.0015	0.0026	0.0023	0.0000	0.0000	0.0034
Cr	0.0000	0.0013	0.0000	0.0000	0.0000	0.0024	0.0009	0.0005	0.0022	0.0000	0.0000	0.0016	0.0000	0.0000	0.0025	0.0025	0.0006	0.0014	0.0037
Ni	0.0069	0.0000	0.0047	0.0057	0.0094	0.0053	0.0000	0.0082	0.0074	0.0052	0.0126	0.0000	0.0000	0.0043	0.0094	0.0097	0.0077	0.0085	0.0082
Mg/Mg+Fe(t)	86.4	84.3	86.0	87.7	84.3	88.3	86.7	85.6	85.2	85.8	87.7	86.2	85.9	86.1	87.8	87.1	86.0	86.0	85.8

Table 3.16. Representative opaque oxide analyses of the Northern area older volcanics.

Sample	963-GR 5		963-LL 4		963-LL 2		963-GR 4	963-GR 6	963-BU 2	963-BU 3	963-MU 3		963-WA 7		963-MC 5	963-BL 3
Locality	Mt Graham		Lake Leake		Lake Leake		Mt Graham		Burr		Mt Muirhead		Mt Watch		Mt McIntyre	The Bluff
SiO2	0.09	0.11	0.61	0.36	0.61	0.36	0.64	0.07	0.15	0.06	0.18	0.33	0.33	0.25	0.15	0.00
TiO2	5.88	6.26	5.74	5.52	5.74	5.52	23.85	27.23	24.36	24.51	26.74	27.20	26.24	26.00	25.01	25.56
Al2O3	9.48	8.95	9.07	9.11	9.07	9.11	4.09	0.60	3.46	3.12	2.91	3.16	0.49	0.78	0.12	2.12
FeO	23.55	24.52	21.72	21.07	21.72	21.07	44.91	51.05	48.82	48.21	50.64	56.15	52.11	50.61	50.49	46.04
Fe2O3	20.10	19.76	18.71	19.74	18.71	19.74	17.54	15.01	16.77	17.50	15.32	8.48	15.54	18.21	18.93	18.76
MnO	0.47	0.49	0.65	0.63	0.65	0.63	0.87	0.83	0.94	1.01	0.76	0.97	0.99	0.89	0.94	0.79
MgO	9.40	9.29	10.67	10.81	10.67	10.81	4.28	2.82	2.44	2.40	3.23		1.99	2.26	1.80	3.96
CaO	0.00	0.05	0.26	0.05	0.26	0.05	0.81	0.39	0.25	0.30	0.00	0.05	0.25	0.22	0.25	0.19
Na2O	0.11	0.00	0.00	0.09	0.00	0.09	0.16	0.06	0.00	0.19	0.07	0.00	0.00	0.09	0.00	0.37
K2O	0.00	0.00	0.00	0.09	0.00	0.09	0.00	0.00	0.00	0.00	0.00	0.00	0.00	0.00	0.00	0.00
P2O5	0.00	0.02	0.10	0.11	0.10	0.11	0.02	0.06	0.00	0.00	0.00	0.28	0.31	0.00	0.11	0.03
SO3	0.03	0.07	0.01	0.20	0.01	0.20	0.06	0.07	0.12	0.00	0.00	0.00	0.00	0.00	0.00	0.06
Cr2O3	31.04	30.03	29.80	30.65	29.80	30.65	0.18	0.06	0.02	0.03	0.21	0.00	0.13	0.12	0.22	0.10
NiO	0.08	0.22	0.24	0.33	0.24	0.33	0.00	0.43	0.10	0.24	0.00	0.16	0.17	0.06	0.18	0.08
Total	100.21	99.77	97.58	98.73	97.58	98.73	97.41	98.66	97.42	97.56	100.06	96.76	98.54	99.47	98.21	98.05
							Number of Ions on the Basis of 32 (0)									
Si	0.0243	0.0324	0.1774	0.1027	0.1774	0.1027	0.1973	0.0222	0.0464	0.0177	0.0546	0.0974	0.1050	0.0788	0.0499	0.0011
Ti	1.2628	1.3555	1.2489	1.1886	1.2489	1.1886	5.5365	6.4111	5.7720	5.8321	6.1066	6.1347	6.2351	6.1566	6.0798	6.0099
Al	3.1926	3.0382	3.0936	3.0758	3.0936	3.0758	1.4895	0.2225	1.2737	1.1630	1.0428	1.1153	0.1808	0.2881	0.0450	0.7814
Fe(2)	6.0420	6.3072	5.6220	5.4319	5.6220	5.4319	10.9368	12.6657	12.1359	11.9834	12.2126	14.2784	13.0299	12.4963	12.7356	11.3181
Fe(3)	4.6406	4.5740	4.3565	4.5799	4.3565	4.5799	3.8445	3.3505	3.7512	3.9136	3.3238	1.9395	3.4973	4.0468	4.2971	4.1494
Mn	0.1130	0.1197	0.1600	0.1526	0.1600	0.1526	0.2279	0.2211	0.2495	0.2711	0.1953	0.2473	0.2638	0.2364	0.2560	0.2080
Mg	4.0018	3.9872	4.5974	4.6125	4.5974	4.6125	1.9678	1.3157	1.1463	1.1302	1.4627	1.3926	0.9356	1.0589	0.8669	1.8463
Ca	0.0000	0.0140	0.0797	0.0139	0.0797	0.0139	0.2681	0.1293	0.0844	0.1027	0.0000	0.0147	0.0830	0.0751	0.0876	0.0642
Na	0.0582	0.0000	0.0000	0.0503	0.0000	0.0503	0.0939	0.0376	0.0002	0.1147	0.0394	0.0000	0.0000	0.0537	0.0000	0.2262
K	0.0000	0.0000	0.0000	0.0333	0.0000	0.0333	0.0000	0.0000	0.0000	0.0000	0.0000	0.0000	0.0000	0.0000	0.0000	0.0000
P	0.0000	0.0050	0.0247	0.0266	0.0247	0.0266	0.0060	0.0152	0.0000	0.0000	0.0000	0.0705	0.0836	0.0000	0.0308	0.0084
S	0.0067	0.0141	0.0022	0.0432	0.0022	0.0432	0.0140	0.0154	0.0281	0.0000	0.0000	0.0000	0.0000	0.0000	0.0007	0.0139
Cr	7.0077	6.8359	6.8144	6.9398	6.8144	6.9398	0.0426	0.0144	0.0042	0.0078	0.0494	0.0000	0.0324	0.0287	0.0562	0.0248
Ni	0.0172	0.0518	0.0548	0.0754	0.0548	0.0754	0.0000	0.1071	0.0255	0.0601	0.0000	0.0390	0.0422	0.0150	0.0462	0.0211

B) Major element geochemistry

The analcimites are dominantly *ne* - normative alkali basalts and range from alkali olivine basalt-basanites to hawaiites-nepheline hawaiites (Fig. 3.1). They show predominantly "Within Plate Basalts" like characteristics (Fig. 3.13, 3.14). In the NAB, Lake Leake and Burr olivine analcimites show more sub alkaline like characteristics due to low K_2O and low Na_2O. They also show high K-and Al-basaltic composition in the K_2O-SiO_2 relationships and are plotted in K-series in K_2O-Na_2O relationships. Mg# of the analcimites range from 62 to 70. High Mg# are shown at the Mt Watch analcimites and low Mg# are shown at Mt Muirhead and Mt McIntyre analcimites (Fig. 3.23). Analcimites from Lake Leake, Mt Watch and Mt Edward (Mg# of the about 67.5-71) can be considered to be primary mantle liquid derived from a refractory upper mantle peridotite as mentioned by Irving and Green (1976) and Frey *et al.* (1978).

In the major elements versus Mg# relationships, most of the elements show a scattered patterns. P_2O_5, Al_2O_3 and TiO_2 only show negative correlations with Mg#. The Mt Watch analcimites are distinguished from the others by the low P_2O_5, Al_2O_3, CaO and TiO_2 whereas Lake Leake analcimites are distinguished from the others by the high K_2O and low Na_2O.

In the olivine analcimites, relationship between high magnesian rocks (e.g. Mt Watch) and less magnesian rocks (e.g. Mt McIntyre) can be explained with olivine dominant fractional crystallisation (Table 3.9, Fig. 3.19). In the projection of olivine-plagioclase-clinopyroxene (Fig. 3.19), the analcimites show a dispersion trend toward the clinopyroxene-plagioclase cotetectic, which are compared to those of the hawaiites. However, distinctive depletion but wide ranges of variation in K content among the analcimites (0.45-2.0 wt %) suggest that generation of the analcimites cannot be explained by simple fractional crystallisation.

C) Trace element and REE geochemistry

Most of the samples display scattered patterns in the trace elements versus Mg# relationships. However, pronounced correlation are observed for at Co, Cr and Ni, whereas less pronounced correlations are shown for Rb, and Ba and V with Mg#. Abnormally high Ni (> 400 ppm) and Cr (> 550 ppm) contents are recorded from the Mt Watch analcimites showing high Mg# (68-70). The Cr- and Ni-Mg# relationships suggest that the analcimites are derived by the olivine-clinopyroxene fractionation. This characteristic is similar to those of mafic basalts from eastern Australia, including melilititie, nephelinite and basanite (Ewart 1989b). McDonough *et al.* (1985) considered Victorian and South Australian basalts with 298 to 496 ppm Ni and 310 to 540 ppm Cr with high Mg# as primary magma derived from partial melting of a peridotitic mantle with no subsequent chemical modification, such as crustal fractionation or contamination during their ascent through the crust. However, some

of the analcimites may be generated as cumulates which are evidenced from cumulate textures under the microscope and low K_2O in spite of high Mg# (Fig. 3.7).

In the four possible mixing models (Fig. 3.19b), mixing trends of the olivine analcimites are separated from the South Australian hawaiites, suggesting that the analcimites have experienced a fractionation of considerably different mineralogy relative to the hawaiites. Relationships between less and high magnesian analcimites suggests that the analcimites are related to olivine dominant fractionation (Table 3.19). This is compared to relationships between Mt Schank and Mt Gambier hawaiites which show a clinopyroxene and plagioclase dominant fractionation trend.

Primitive Mantle normalised trace element abundances are shown in Fig. 3.25. The analcimites are characterised by a pronounced depletion in K and less pronounced depletion in Sr and Rb. The Mt Muirhead and Mt Graham analcimites show a more pronounced depletion of K, and samples from the Burr and Mt Edward show a more pronounced depletion of Sr (Fig. 3.26). McDonough *et al.* (1985) interpreted that more moderate Sr depletions compared to the large depletion of K and Rb reflected either that Sr behaved more compatibly during partial melting, or that the source region for these basalts is heterogeneous and relatively more depleted of Sr compared to the LREE. The depletion of K and Rb in the Mt Watch and Mt McIntyre analcimites is though to have occurred relatively recently because of the very low Rb/Sr ratios and high $^{87}Sr/^{86}Sr$ ratios (0.7043) compared with the other Victorian and South Australian Newer Basalts.

Primitive Mantle normalised REE abundances are shown in Fig. 3.27). The patterns are characterised by a distinctive LREE enrichment (Fig. 3.27). In the olivine analcimites, samples from Burr, Mt Graham, Mt McIntyre and Mt Watch show more pronounced LREE enrichment patterns.

3.6.4. Sr and Nd isotopic composition

All samples considered for whole rock chemistry were analysed for Sr-Nd isotopic composition by same methods as mentioned in section, 3.5.4. Their results are shown in Table 3.20. The olivine analcimites have εNd of +0.92 - +2.59 and $^{87}Sr/^{86}Sr$ of 0.7039 - 0.7049 and $TNd_{(DM)}$ of 0.40 ~ 0.52 Ga. Their Sm/Nd ratios range from 0.13 to 0.19 and Rb/Sr ratios range from 0.015 to 0.016. However, there are slight distinctions among the analcimites. Low Sm/Nd ratios are shown in the Mt McIntyre analcimites and high ratios are observed in Mt Edward analcimites. Low Rb/Sr ratios are evidenced in the Mt Graham and Mt Muirhead analcimites and high ratios are shown in the Lake Leake and Mt Watch analcimites. Low εNd values are seen in the Burr lava flow and Mt Watch analcimites and high values are observed in the Mt McIntyre and The Bluff analcimites. Low $TNd_{(DM)}$ is seen in the Mt McIntyre analcimites and high $TNd_{(DM)}$ is observed in the Mt Graham and Burr analcimites.

Table 3.17. Representative major element analyses of the Northern area older volcanics.

Sample	963-MC 1	963-MC 3	963-MC 4	963-LL 1	963-LL 2	963-ED 2	963-MU 2	963-MU 3	963-WA 1	963-WA 4	963-WA 5	963-BL 1	963-BL 3	963-GR 3	963-GR 4	963-GR 5	963-BU 1	963-BU 4
Locality	Mt McIntyre			Lake Leake		Mt Edward	Mt Muirhead		Mt Watch			The Bluff		Mt Graham			Burr	
SiO2	43.24	43.29	43.14	43.15	42.68	43.62	43.70	43.81	43.11	43.46	43.56	43.73	43.65	43.81	44.03	43.97	42.79	40.41
Al2O3	10.27	10.18	10.10	9.75	9.24	8.34	10.18	10.11	9.14	9.28	9.19	9.80	9.54	10.21	10.39	10.36	10.53	11.11
Fe2O3(t)	12.89	12.87	12.90	13.08	12.94	12.03	13.10	13.04	12.74	12.54	12.83	13.07	12.90	12.89	12.94	12.84	13.08	14.09
MnO	0.17	0.17	0.16	0.17	0.16	0.15	0.17	0.17	0.16	0.16	0.17	0.17	0.17	0.17	0.17	0.17	0.17	0.17
MgO	11.00	11.06	11.35	12.30	13.55	16.94	11.60	11.11	14.78	14.53	14.40	12.04	12.43	10.99	11.02	10.88	11.88	13.00
CaO	11.33	11.43	11.37	10.75	11.22	9.75	11.04	10.85	10.05	9.95	9.94	10.92	10.79	10.84	10.97	10.93	11.07	11.57
Na2O	4.38	4.09	3.71	1.44	1.92	1.29	4.30	4.22	3.71	3.55	3.88	3.06	3.45	4.20	4.45	4.37	1.83	1.01
K2O	0.49	0.63	0.45	1.87	1.25	1.29	0.32	0.87	0.41	0.74	0.34	1.59	0.95	0.77	0.44	0.64	2.04	0.96
TiO2	3.74	3.73	3.70	3.86	3.70	3.33	3.68	3.65	3.48	3.43	3.51	3.74	3.65	3.64	3.70	3.68	3.60	3.82
P2O5	0.96	0.97	0.96	0.96	0.94	1.06	0.92	0.92	0.83	0.82	0.84	0.92	0.90	0.91	0.91	0.91	0.89	0.94
SO3	0.01	0.01	0.01	0.06	0.01	0.03	0.01	0.01	0.05	0.04	0.02	0.01	0.00	0.00	0.00	0.00	0.01	0.01
LOI %	1.34	1.51	1.76	2.59	2.80	2.36	1.15	0.85	1.28	1.24	1.25	0.94	1.12	0.86	0.86	0.84	1.45	2.52
Total	99.83	99.63	99.61	99.96	100.40	99.45	100.19	99.61	99.74	99.74	99.93	99.95	99.57	99.30	99.78	99.59	99.34	99.62
C.I.P.W. norm (calculated with Fe2O3/FeO = 0.2)																		
Ap	2.3	2.33	2.31	2.33	2.27	2.56	2.19	2.2	1.99	1.96	2.01	2.19	2.16	2.18	2.17	2.17	2.15	2.29
Il	7.32	7.30	7.29	7.64	7.31	6.55	7.16	7.12	6.81	6.71	6.85	7.28	7.15	7.12	7.20	7.18	7.09	7.59
Mt	2.89	2.88	2.91	2.96	2.92	2.71	2.92	2.91	2.85	2.81	2.87	2.91	2.89	2.89	2.88	2.87	2.95	3.21
Or	2.97	3.83	2.75	11.48	7.66	7.88	1.94	5.27	2.49	4.49	2.06	9.60	5.77	4.68	2.65	3.88	12.46	5.92
Ab	12.12	11.94	13.85	11.09	9.09	11.18	14.43	12.21	13.02	12.44	14.95	8.58	12.13	13.29	14.85	13.91	6.03	7.66
An	7.13	7.79	9.92	15.31	13.40	13.66	7.72	6.23	7.36	7.47	6.86	8.52	7.95	6.92	7.22	6.93	15.00	23.97
Di	35.59	35.44	33.77	27.01	30.50	23.28	33.91	34.45	30.66	30.20	30.52	32.72	32.97	34.05	34.11	34.26	28.79	23.76
Hy	0.00	0.00	0.00	0.00	0.00	5.51	0.00	0.00	0.00	0.00	0.00	0.00	0.00	0.00	0.00	0.00	0.00	0.00
Ol	15.63	15.81	17.13	21.36	23.29	26.64	17.42	16.39	24.43	23.98	23.77	18.54	19.30	16.27	16.12	15.81	20.14	24.93
Ne	14.04	12.78	10.07	0.74	4.18	0.00	12.31	13.19	10.33	9.90	10.10	9.67	9.69	12.59	12.80	12.99	5.39	0.67
Ac	0.00	0.00	0.00	0.00	0.00	0.00	0.00	0.00	0.00	0.00	0.00	0.00	0.00	0.00	0.00	0.00	0.00	0.00
C	0.00	0.00	0.00	0.00	0.00	0.00	0.00	0.00	0.00	0.00	0.00	0.00	0.00	0.00	0.00	0.00	0.00	0.00
Q	0.00	0.00	0.00	0.00	0.00	0.00	0.00	0.00	0.00	0.00	0.00	0.00	0.00	0.00	0.00	0.00	0.00	0.00
Total	99.99	100.10	100.00	99.92	100.62	99.97	100.00	99.97	99.94	99.96	99.99	100.01	100.01	99.99	100.00	100.00	100.00	100.00
AN#	37.04	39.48	41.73	57.99	59.58	54.99	34.85	33.79	36.11	37.52	31.45	49.82	39.59	34.24	32.71	33.25	71.33	75.78
DI	29.13	28.55	26.67	23.31	20.93	19.06	28.68	30.67	25.84	26.83	27.11	27.85	27.59	30.56	30.30	30.78	23.88	14.25
SI	40.05	40.42	41.86	44.92	47.77	55.83	41.42	39.77	48.68	48.27	47.74	42.32	43.71	39.88	40.00	39.65	43.17	47.02
LI	-19.03	-19.01	-19.50	-18.57	-20.94	-21.68	-19.54	-18.22	-21.51	-20.54	-21.02	-18.55	-19.33	-18.06	-18.52	-18.07	-18.42	-22.82

Notice. AN#= AN/(AN+AB)*100, S.I. (Solidification Index by Kuno), D.I. (Differentiation, Index by Thornton & Tuttle,1960) & L.I. (Larsen Index by Larsen, 1938).

Table 3.18. Representative trace element analyses of the Northern area older volcanics.

Sample	963-MC 1	963-MC 3	963-MC 4	963-LL 1	963-LL 2	963-ED 2	963-MU 2	963-MU 3	963-WA 1	963-WA 4	963-WA 5	963-BL 1	963-BL 3	963-GR 3	963-GR 4	963-GR 5	963-BU 1	963-BU 4
Locality	Mt McIntyre			Lake Leake		Mt Edward	Mt Muirhead		Mt Watch			The Bluff		Mt Graham			Burr	
Y	26.2	25.8	25.6	26.2	22.8	17.0	27.9	26.8	21.6	21	22.5	26.7	26.4	24.9	28.4	22.8	26.3	44.4
Sr	1028.5	1027.6	1019.9	1060.5	719.4	464.9	948.4	998.7	827.6	824.9	816.3	946.2	1027.6	893.3	922.6	802.3	665.8	515.3
Rb	15.8	29.3	37.6	51.1	41.5	22.0	11.6	15.2	34.8	40.7	44.2	43.2	19.2	16.8	18.0	17.2	38.6	21.2
Nb	90.0	89.6	88.7	84.3	72.3	51.0	78.4	80.2	78.6	78.5	80.5	82.3	82.5	74.6	82.7	65.3	65.4	81.2
Zr	342.6	343.6	340.3	341.4	293.6	202.1	326.5	336.7	306.8	309.8	314.8	317.1	315.5	307.7	330.3	273.8	280.7	340.9
Th	8.7	6.7	9.1	8.9	9.3	6.9	7.8	8.2	6.9	8.3	8.1	7.4	9.0	10.3	9.0	8.2	7.9	7.9
Pb	5.1	3.7	1.4	5.5	5.3	4.2	5.4	5.4	3.6	4.4	5.5	3.3	7.3	5.2	2.1	4.7	5.4	8.5
U	0.6	n.d.	n.d.	n.d.	0.1	0.6	0.6	1.0	n.d.	1.4	2.5	n.d.	n.d.	1.0	2.1	n.d.	1.1	1.0
Ga	18.6	19.6	18.4	18.7	15.4	15.7	19.2	18.6	16.8	16.5	19.5	18.4	20.4	19.4	20.5	18.8	17.8	21.1
Zn	107	110	107	113	101	86	115	110	113	111	110	110	117	100	105	92	107	121
Cu	101	73	84	76	64	30	73	82	77	80	83	73	85	81	70	58	55	65
Ni	244	256	279	350	311	483	292	289	484	470	459	319	347	254	256	213	254	276
Ba	979	1027	1134	1149	1051	852	1035	1088	926	940	951	1200	1001	963	911	919	968	895
Sc	24.3	24.3	24.3	19.3	22.7	23.9	25	22.7	23.4	24.2	23.1	21.9	24.7	24.6	24.2	23.6	25.1	26.3
Cr	320	353	354	470	521	761	427	411	615	598	568	456	484	415	403	405	483	476
V	314.8	341.3	326.8	345.9	337.1	305.7	313.1	287.1	312.2	305.9	320.7	317	317.5	297.1	298.7	298.1	316	347.4
Co	69.5	63.5	56.8	63.1	61.5	79	65.4	66.4	77.3	67.1	72.2	85.7	102.2	63	56.2	57.1	64.8	67
Ce	147	146	149	151	144	114	136	133	129	132	135	141	137	132	135	132	136	161
Nd	71	66	68	62	61	51	62	64	58	57	61	64	59	61	63	58	60	78
La	86	84	83	93	83	69	81	76	77	77	81	87	81	73	79	74	81	115

n.d. indicates element not alalysed

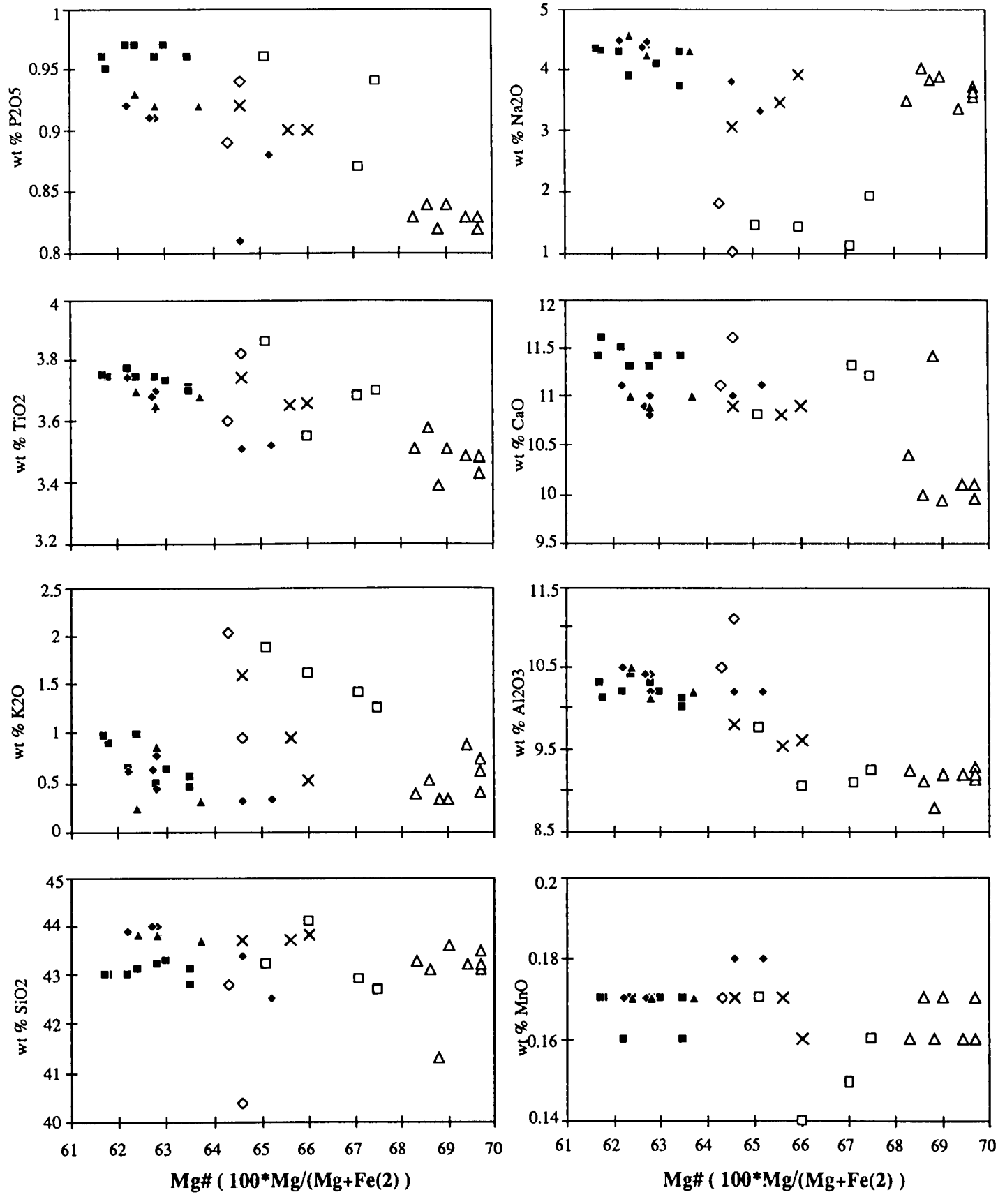

Fig. 3.23. Major elements versus Mg# plots for the Northern area older volcanics. Symbols, (■) for Mt McIntyre, (□) for Lake Leake, (◆) for Mt Graham, (◇) for Burr, (▲) for Mt Muirhead, (△) for Mt Watch, (✕) for The Bluff.

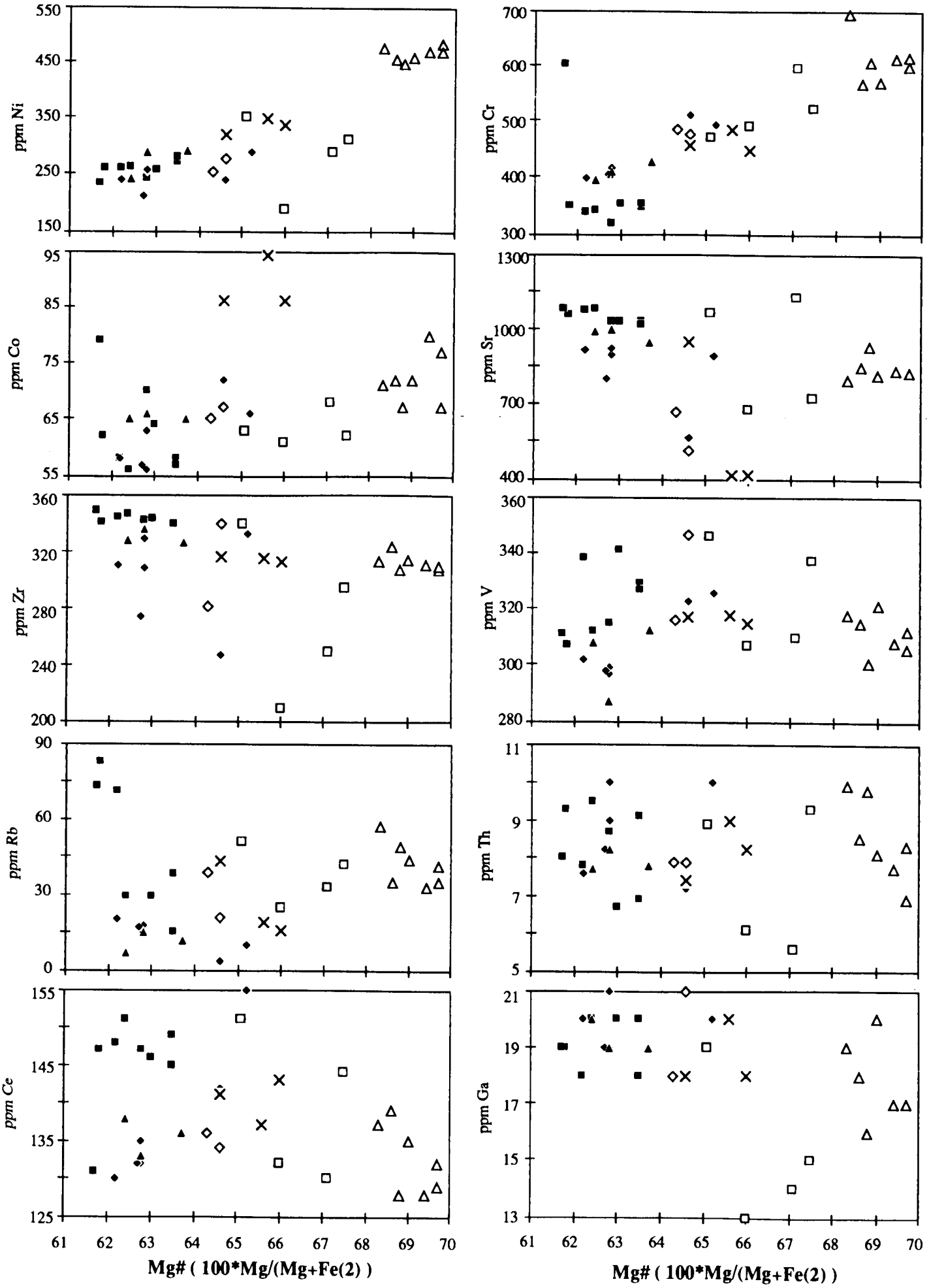
ppm Ni
550
450
350
250
150
ppm Cr
700
600
500
400
300
ppm Co
95
85
75
65
55
ppm Sr
1300
1000
700
400
ppm Zr
360
320
280
240
200
ppm V
360
340
320
300
280
ppm Rb
90
60
30
0
ppm Th
11
9
7
5
ppm Ce
155
145
135
125
ppm Ga
21
19
17
15
13
61
62
63
64
65
66
67
68
69
70
Mg# (100*Mg/(Mg+Fe(2))
Mg# (100*Mg/(Mg+Fe(2))

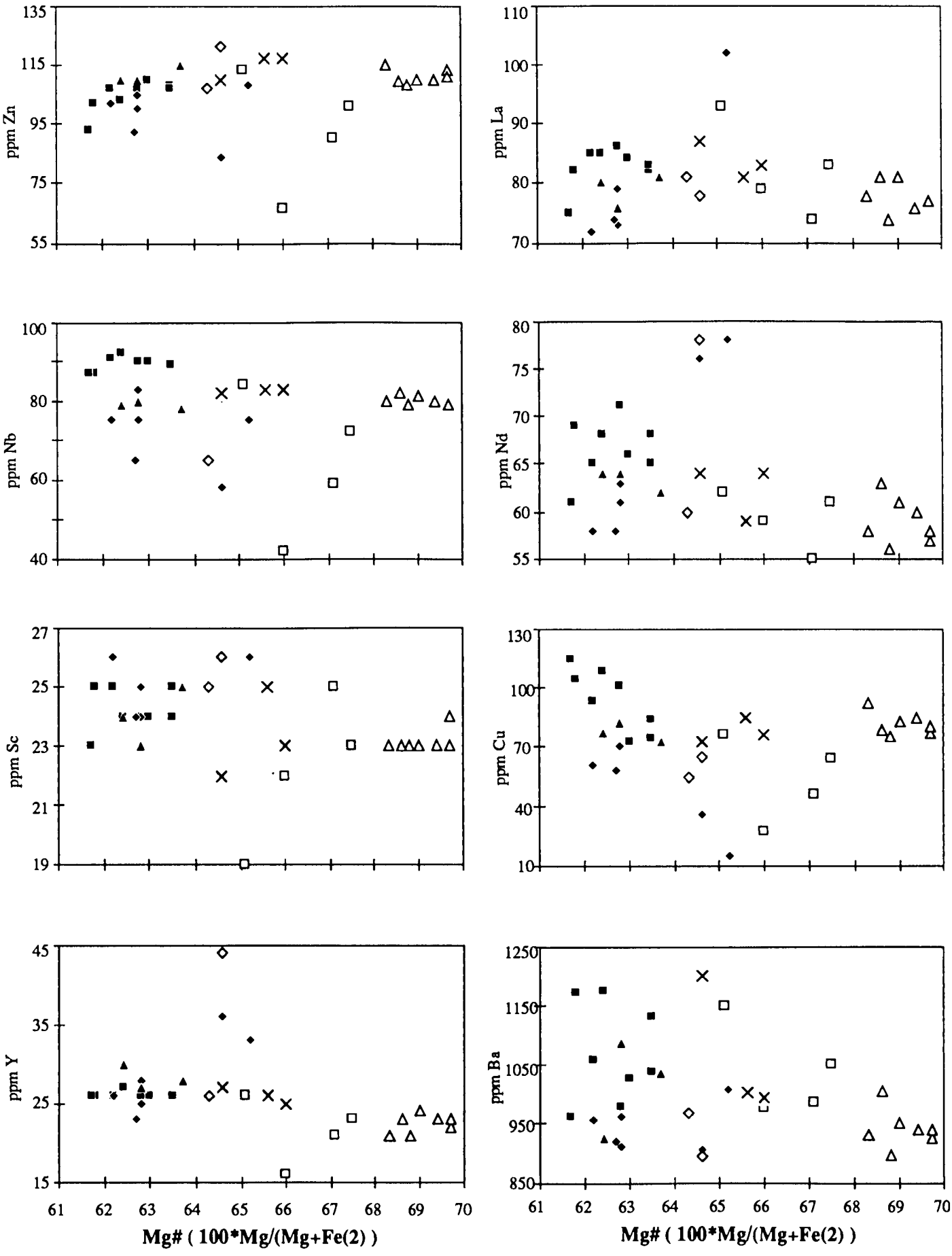

Fig. 3.24. Trace elements versus Mg# ratios plot for the Northern area older volcanics. Symbols as for Fig. 3.23.

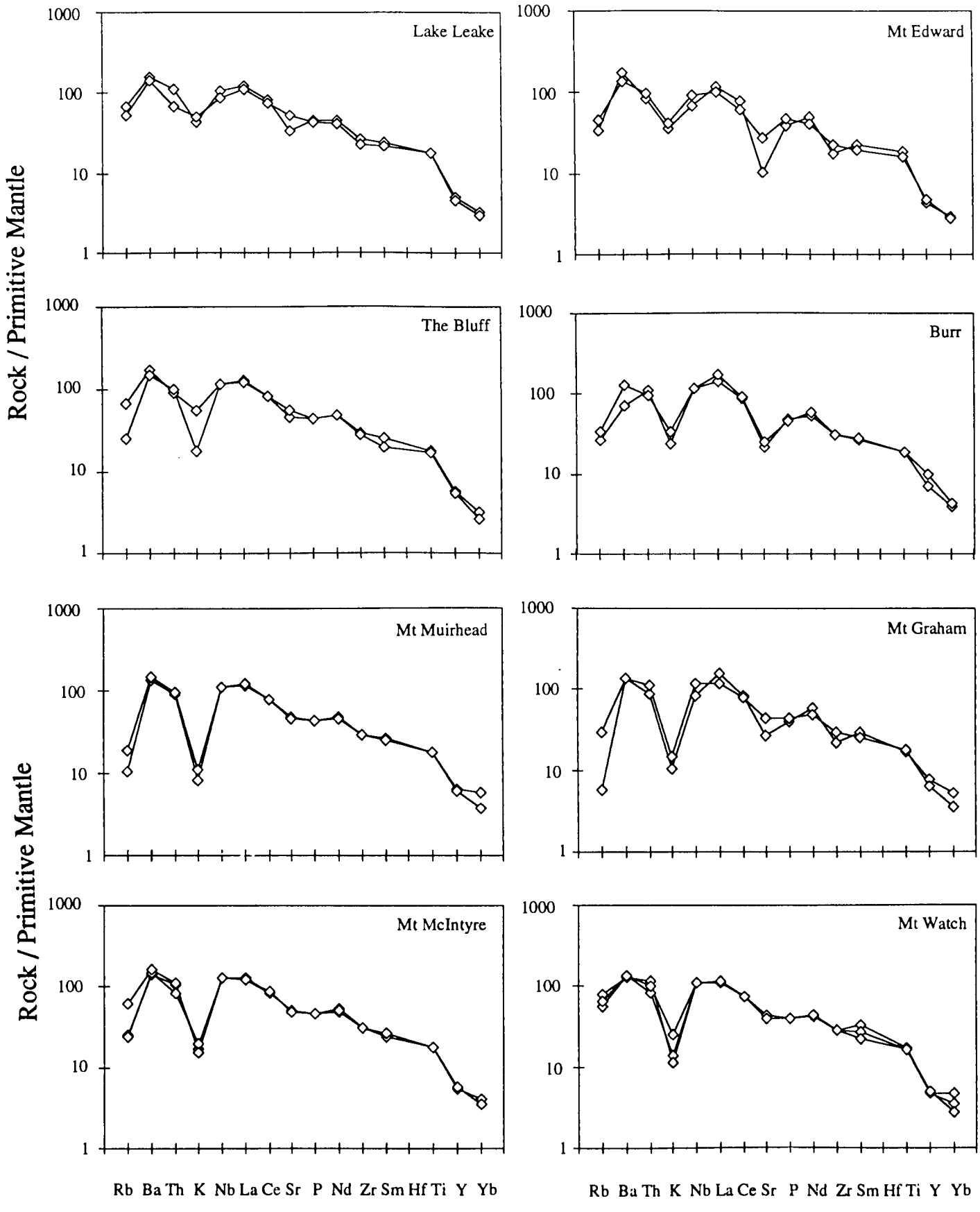

Fig. 3.25. Primitive Mantle normalized trace element abundances of the Northern area older volcanics (PM from Sun and McDonough, 1989).

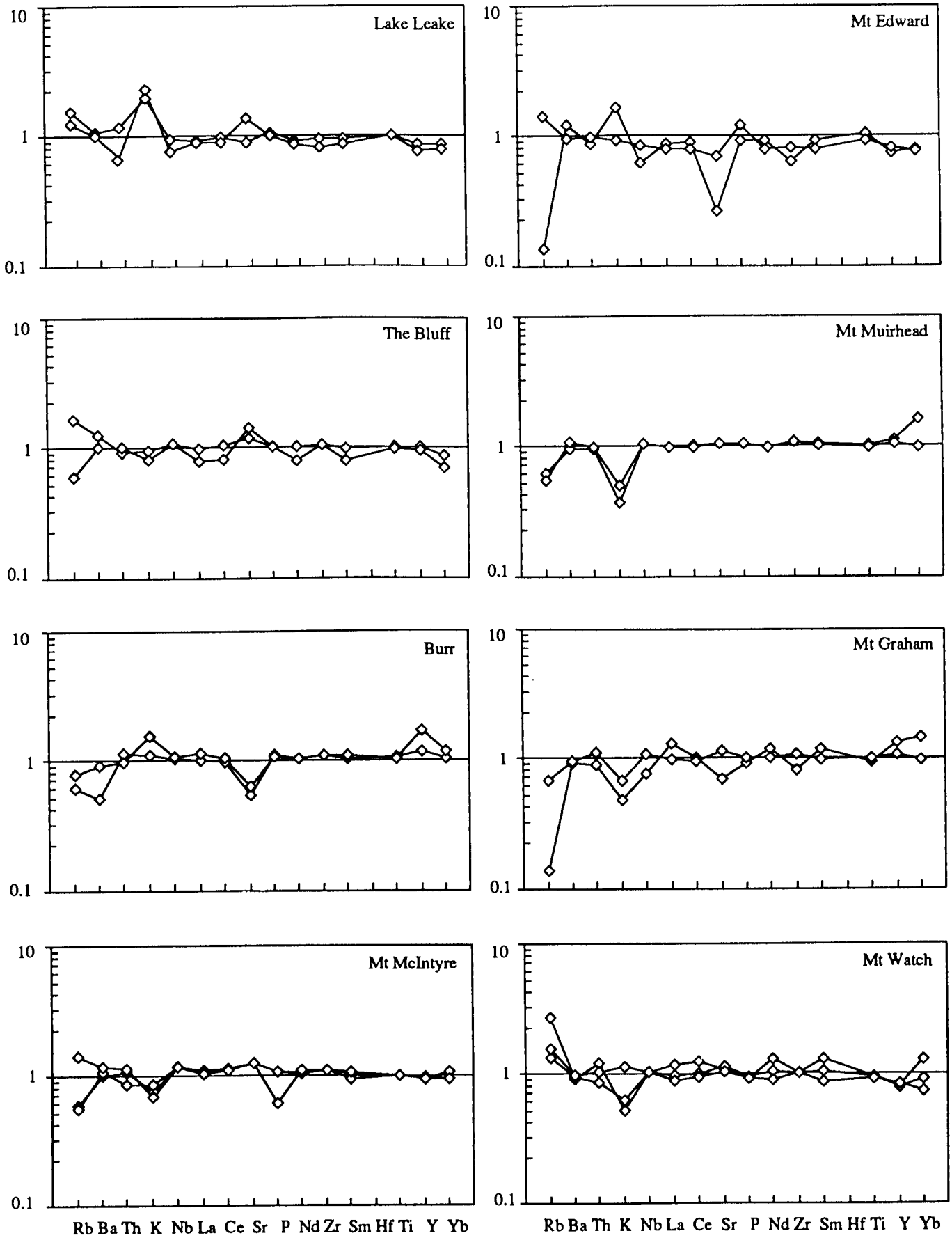

Fig. 3.26. Average analcimite normalized trace element abundances of the Northern area older volcanics. A vertical axis is a logarithmic scale.

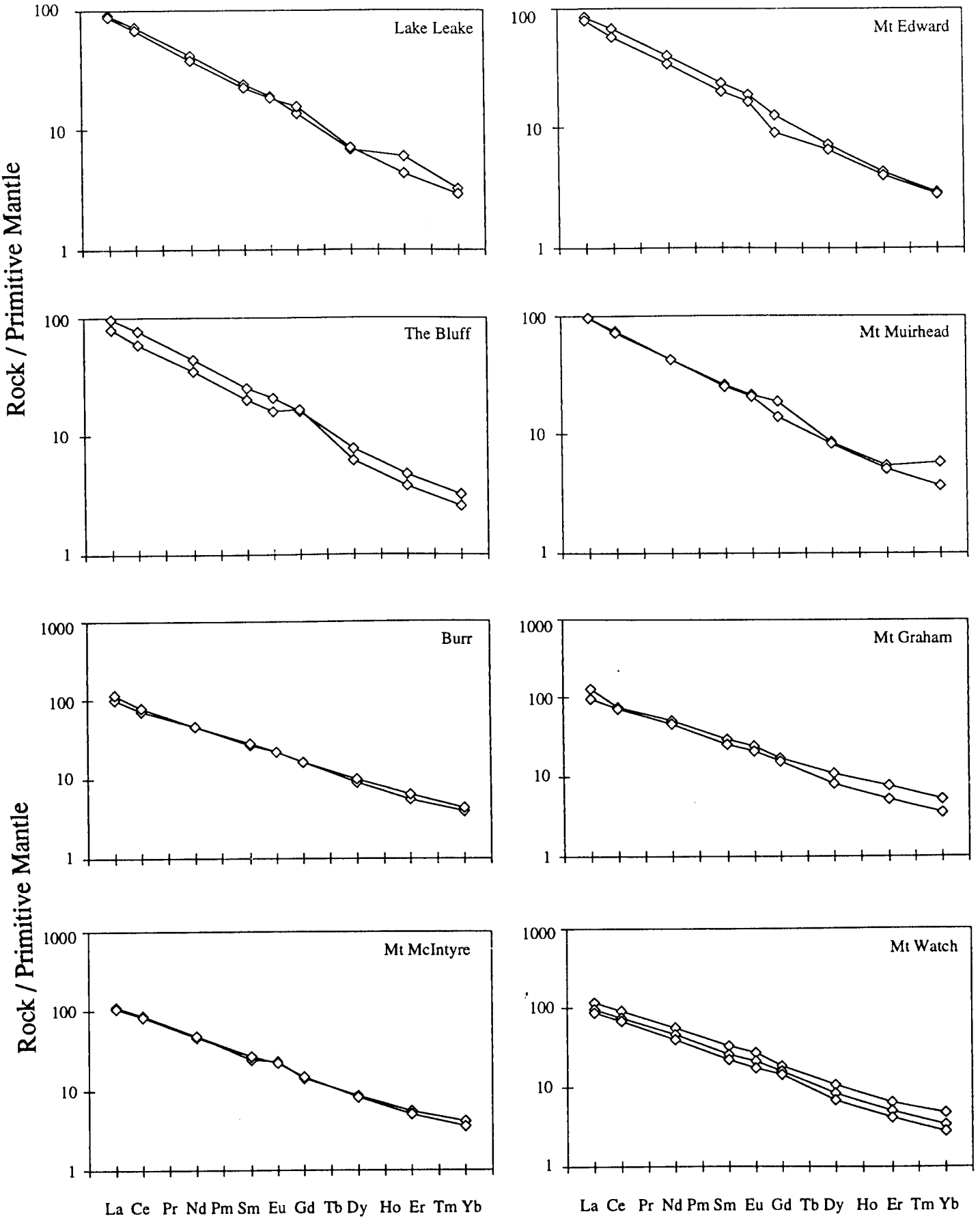

Fig. 3.27. Primitive Mantle normalized REE abundances of the Northern area older volcanics (PM from Sun and McDonough, 1989).

Table. 3.19. A least squares calculation and associated trace element model.

Major element

Sample	CPX	OL	Parent(MC 1)	WA 1(obs)	Calc	Diff	Vector	wt. per cent
SiO2	46.36	39.79	43.24	43.11	42.98	-0.131	CPX	0.007
Al2O3	5.61	0.02	10.27	9.14	9.16	0.0184	OL	0.108
Fe2O3	7.15	13.33	12.89	12.74	12.93	0.1861	MC 1	0.888
MnO	0	0.18	0.17	0.16	0.17	0.0103		
MgO	12.68	46.38	11	14.78	14.84	0.058		
CaO	22.78	0.24	11.33	10.05	10.24	0.1865		
Na2O	0.63	0	4.38	3.71	3.89	0.1834		
K2O	0	0.03	0.49	0.41	0.44	0.0283		
TiO2	3.52	0.05	3.74	3.48	3.35	-0.1305		
P2O5	0	0	0.96	0.83	0.85	-0.0042		
Sum of squares of residuals						0.14185		

Trace element

Sample	CPX	OL	PL	Parent(WA 1)	MC 1(obs)	Calc
La	0.01	0.15	0.08	77.00	86.00	86.52
Ce	0.01	0.15	0.08	129.00	147.00	144.95
Y	0.01	0.7	0.01	21.60	26.20	24.18
Zr	0.01	0.24	0.01	306.80	342.60	344.52
Ba	0.01	0.01	0.1-0.6	926.00	979.00	1041.55
Rb	0.01	0.01	0.01	34.80	15.80	39.14
Sr	0.01	0.12	2.0-2.3	823.00	1028.50	924.98
Nb	0.01	0.09	0.01	78.60	90.00	88.36
Ga	0.03	0.3	0.9-1.2	16.80	18.60	18.82
Nd	0.01	0.3	0.08	58.00	71.00	65.10

Table 3.20. Isotopic analyses of the Northern area older volcanics.

Sample	Locality	Lithology	Rb	Sr	87Rb/86Sr	87Sr/Sr86		87Sr/Sr86(T)	Nd	Sm	147Sm/144Nd	143Nd/144 Nd		143Nd/144Nd(T)	eps Nd (0)	eps Nd chT	T mod:dep
963-MC 1	Mt McIntyre	Analcimites	15.8	1028.5	0.044495	0.704179 ±	49	0.703868	71.32	11.31	0.095947	0.512756 ±	23	0.512448	2.31	8.49	0.433
963-MC 3			29.3	1027.6	0.082585	0.704249 ±	42	0.703672	64.93	10.84	0.101001	0.512749 ±	18	0.512425	2.16	8.03	0.461
963-MC 4			37.6	1019.9	0.106780	0.704272 ±	22	0.703527	65.49	10.90	0.100674	0.512770 ±	27	0.512447	2.57	8.46	0.433
963-LL 1	Lake Leake	Analcimites	51.1	1060.5	0.139563	0.704348 ±	47	0.703374	62.86	11.29	0.108656	0.512784 ±	31	0.512435	2.85	8.24	0.444
963-LL 2			41.6	719.4	0.167488	0.704366 ±	23	0.703197	58.80	10.67	0.109786	0.512750 ±	43	0.512398	2.19	7.51	0.495
963-ED 2	Mt Edward	Analcimites	27.8	464.9	0.172890	0.704607 ±	25	0.703400	47.28	8.69	0.111245	0.512741 ±	12	0.512384	2.01	7.24	0.514
963-MU 2	Mt Muirhead	Analcimites	14.8	856.8	0.050031	0.704192 ±	32	0.703843	59.61	10.91	0.110689	0.512772 ±	36	0.512417	2.61	7.87	0.469
963-MU 3			20.2	757.1	0.077278	0.704264 ±	29	0.703725	58.57	10.63	0.109745	0.512735 ±	33	0.512382	1.88	7.20	0.516
963-WA 1	Mt Watch	Analcimites	34.8	868.8	0.116011	0.704188 ±	21	0.703378	50.09	9.37	0.113196	0.512742 ±	11	0.512378	2.02	7.13	0.522
963-WA 4			57.4	1795.5	0.092596	0.704651 ±	31	0.705865	55.82	9.77	0.105926	0.512720 ±	29	0.512380	1.60	7.16	0.518
963-WA 5			40.7	838.4	0.140609	0.704416 ±	50	0.703434	55.09	9.69	0.106369	0.512734 ±	17	0.512393	1.87	7.40	0.502
963-BL 1	The Bluff	Analcimites	43.2	950.4	0.131653	0.704310 ±	29	0.703391	59.37	10.88	0.110894	0.512746 ±	27	0.512391	2.12	7.36	0.505
963-BL 3			19.2	1027.6	0.054117	0.704555 ±	48	0.704177	55.30	10.50	0.114841	0.512754 ±	33	0.512385	2.26	7.26	0.513
963-GR 3	Mt Graham	Analcimites	16.8	893.3	0.054472	0.704295 ±	13	0.703914	57.87	10.53	0.110112	0.512742 ±	8	0.512389	2.03	7.32	0.507
963-GR 4			18.0	922.6	0.056509	0.704266 ±	24	0.703872	60.13	11.00	0.110693	0.512778 ±	23	0.512423	2.73	7.99	0.461
963-GR 5			17.2	802.3	0.062094	0.704279 ±	24	0.703846	58.72	11.78	0.121323	0.512747 ±	37	0.512358	2.13	6.72	0.556
963-BU 4	Burr	Analcimites	21.2	515.3	0.119161	0.704487 ±	36	0.703655	66.09	11.82	0.108201	0.512700 ±	22	0.512352	1.20	6.62	0.556

Errors quoted are calculated as 2 standard error of the mean.

The value T is an initial age on recrystallization of a rock.

3.7. Discussion

Traditionally, the SQAB have been considered as a small part of the Victorian Newer basalts as a result of their geographical distribution. Only a few studies (Irving and Green, 1976; McDonough *et al.*, 1985) have recognised considerable difference between South Australian hawaiites and olivine analcimites. McDonough *et al.* (1985) attempted to compare the incompatible element abundances and isotopic compositions of the Victorian and South Australian Newer Basalt with Tertiary Tasmanian basalts. With limited geochemical evidence, Irving and Green (1976) and Frey *et al.* (1978) explained the petrogenesis of the SQAB with a simple systematic fractional model and a different degree of partial melting at different depths.

However, integrated petrography, geochemistry and isotopic signatures suggest that all SQAB are not geochemically and isotopically Victorian Newer Basalt like and a simplified model can not explain the petrogenesis of the SQAB. The SQAB are also clearly distinguished from the Tertiary basalt in the isotopic and geochemical signatures. These aspects are fully considered in this section.

3.7.1. SQAB, olivine analcimites and hawaiites

In the SQAB, two main geochemical and petrographic groups of basalts are recognised; Southern area younger and Northern area older olivine analcimites. The hawaiites are also divided into two area, Mt Gambier and Mt Schank.

The hawaiites are characterised by the existence of plagioclase groundmass (±k-fd), modest Ni, Cr, Sc, Mg#, and enrichments of LREE and LILs. The hawaiites have εNd of +2.26 - +3.23, $^{87}Sr/^{86}Sr$ of 0.7035 - 0.7041 and $TNd_{(DM)}$ of 0.43 - 0.6 Ga. The analcimites are characterised by the existence of groundmass analcite, iddingsite rimmed olivine phenocrysts an cumulate textures. They show high Mg# (60-70), Ni (>200 ppm), Cr (>300 ppm) and low K_2O (mainly < 1.5 wt %). They have εNd of +0.92 - +2.58, $^{87}Sr/^{86}Sr$ of 0.7039 - 0.7049 and $TNd_{(DM)}$ of 0.4 - 0.52 Ga. However, these rocks in general have significantly higher Ba, Ti, Zr, Nb, LREE concentrations than the Southern group of hawaiites in spite of their high Cr, Ni, Mg#. The analcimites also have slightly lower $TNd_{(DM)}$, εNd and higher $^{87}Sr/^{86}Sr$ relative to the Southern group of hawaiites.

Relationships among the trace element ratios and abundances for the SQAB are shown in Fig. 2.28. Three main groups of the SQAB are recognized; southern group of younger Mt Gambier and Mt Schank hawaiites, northern group of olivine analcimites. In general, the olivine analcimites are well distinguished from the hawaiites by high Ce/Y, Ti/Y, K/Y ratios, and Sc-Cr contents and Mt Gambier hawaiites are distinguished from other samples by low Zr/Y and high La/Ba ratios. Mt Schank hawaiites are distinguished from other samples by low Ti/Zr ratios and low Sc-Cr contents.

Nd and Sr isotopic compositions of the SQAB and their comparisons with Victorian

Newer Basalts are shown in Fig. 3.29. In this Fig. 3.29, southern subgroup of hawaiites show a lower $^{87}Sr/^{86}Sr$ and higher εNd relative to northern subgroup of analcimites. The Nd-Sr isotopic characteristics of the hawaiites are similar to Victorian Newer Basalts (McDonough *et al.*, 1985).

$^{87}Sr/^{86}Sr$ ratios versus major element relationships are shown in Fig. 3.30. No systematic relationships are found between the olivine analcimites and the hawaiites, as well as Mt Gambier and Mt Schank hawaiites. The olivine analcimites show higher CaO, TiO_2, Mg#, lower SiO_2, Al_2O_3, K_2O relative to the hawaiites. Samples from the Mt Schank show lower SiO_2, CaO, Mg#, higher Al_2O_3, Na_2O, TiO_2, P_2O_5, K_2O relative to those from the Mt Gambier .

Relationships between $^{87}Sr/^{86}Sr$ - or $^{143}Nd/^{144}Nd$ ratios versus trace element ratios are shown in Fig. 3.31. Three main geochemical and isotopic groups of the SQAB are also recognised. The olivine analcimites show higher Ti/Zr, Nb/Zr, Ce/Y, Ti/Y, low La/Ba, K/Y ratios relative to the hawaiites. Samples from the Mt Schank volcanics show higher Zr/Y, Ce/Y, Nb/Y, K/Y, Ti/Y, lower La/Ba, Ti/Zr ratios relative to those from the Mt Gambier volcanics.

Relationships among Sm, Nd, Rb, Sr, K and Ba relationships for the SQAB are shown in Fig. 3.32. No regular variation are seen between hawaiites and analcimites as well as between two hawaiites in the Sm/Nd-Nd and Rb/Sr-Sr relationships. The hawaiites show higher Rb/Sr and Sm/Nd ratios than the olivine analcimites. In the SQAB, the Mt Gambier hawaiites show higher Sm/Nd ratios, low Nd contents and the Mt Schank hawaiites show higher Rb and Sr contents relative to other volcanics. In the olivine analcimites, high Rb and Sr contents are obtained in samples from the Mt McIntyre.

Possibly, Sm/Nd-Nd and Rb/Sr-Sr relationships between Mt Gambier and Mt Schank hawaiites can be explained a conventional fractionation model. However, similar Rb/Sr ratios in spite of the significantly different Rb and Sr contents in both hawaiites, can be attributed to source inherited. In the Rb-K/Rb and Rb-Ba plots, the analcimites show wider ranges of Rb, K/Rb, higher Ba relative to the hawaiites. The hawaiites show a similar, but limited K/Rb ratios (~360) despite there are large difference in Rb contents.

3.7.2. Geochemical and isotopic comparisons of the SQAB with available data

Previous studies of Victorian Newer Basalts (McDonough *et al.*, 1985), Tasmanian Tertiary basalts (Irving and Green, 1976; McDonough *et al.*, 1985), eastern Australian Cainozoic basalts (Ewart and Chappell, 1989) Cameroon line basalts (Fitton and Dunlop, 1985; Fitton, 1987), and Basin and Range basalts (Bradshaw *et al.*, 1993) are reviewed to compare with the SQAB.

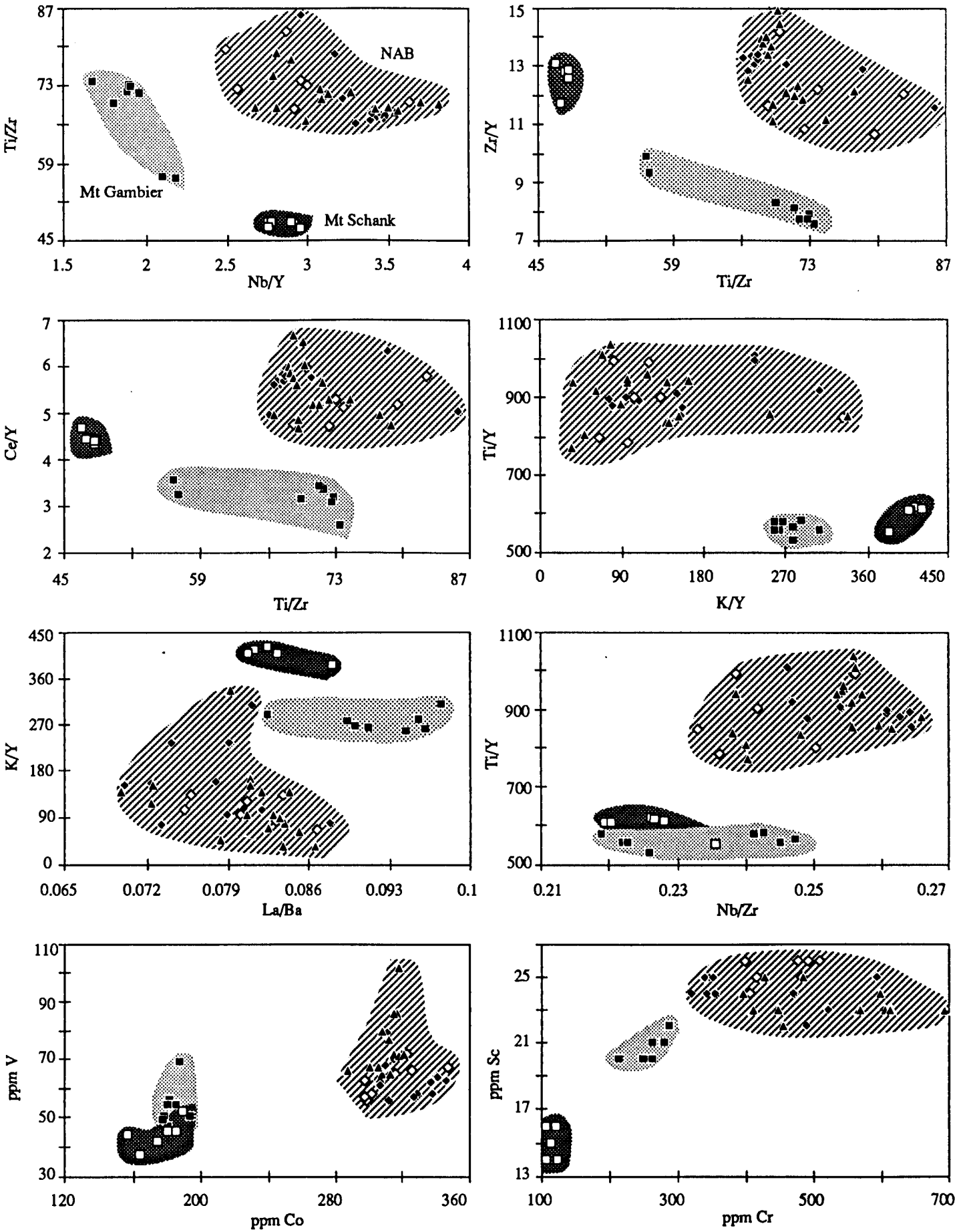

Fig. 3.28. Incompatible element ratios and compatible element contents of the South Australian alkaline basalts.

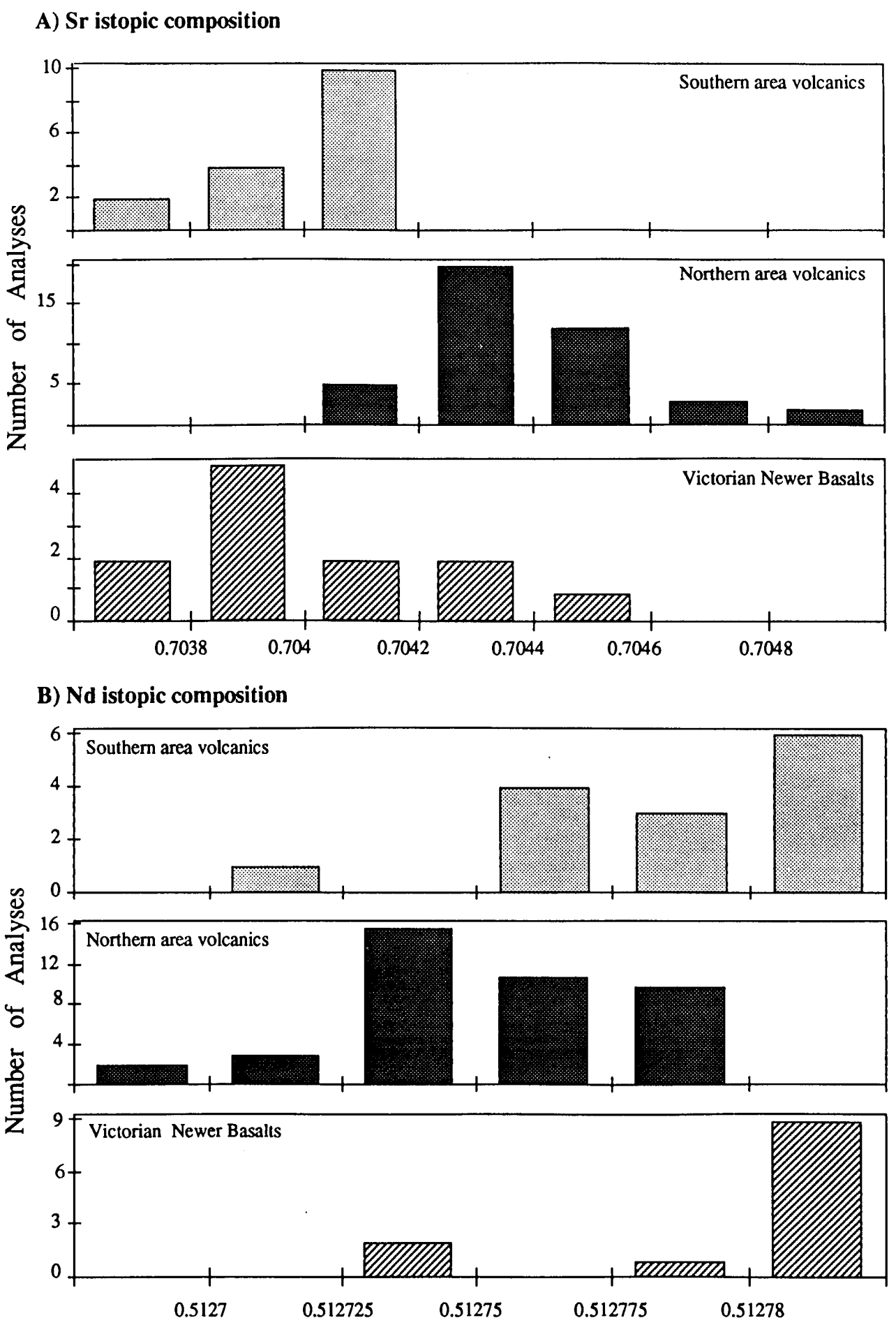

Fig. 3.29. Histograms of Nd-Sr isotopic compositions for the South Australian alkaline basalts and their comparsions with Victorian Newer Basalts (Data of the Victorian Newer Basalts from McDonough *et al.*, 1985)

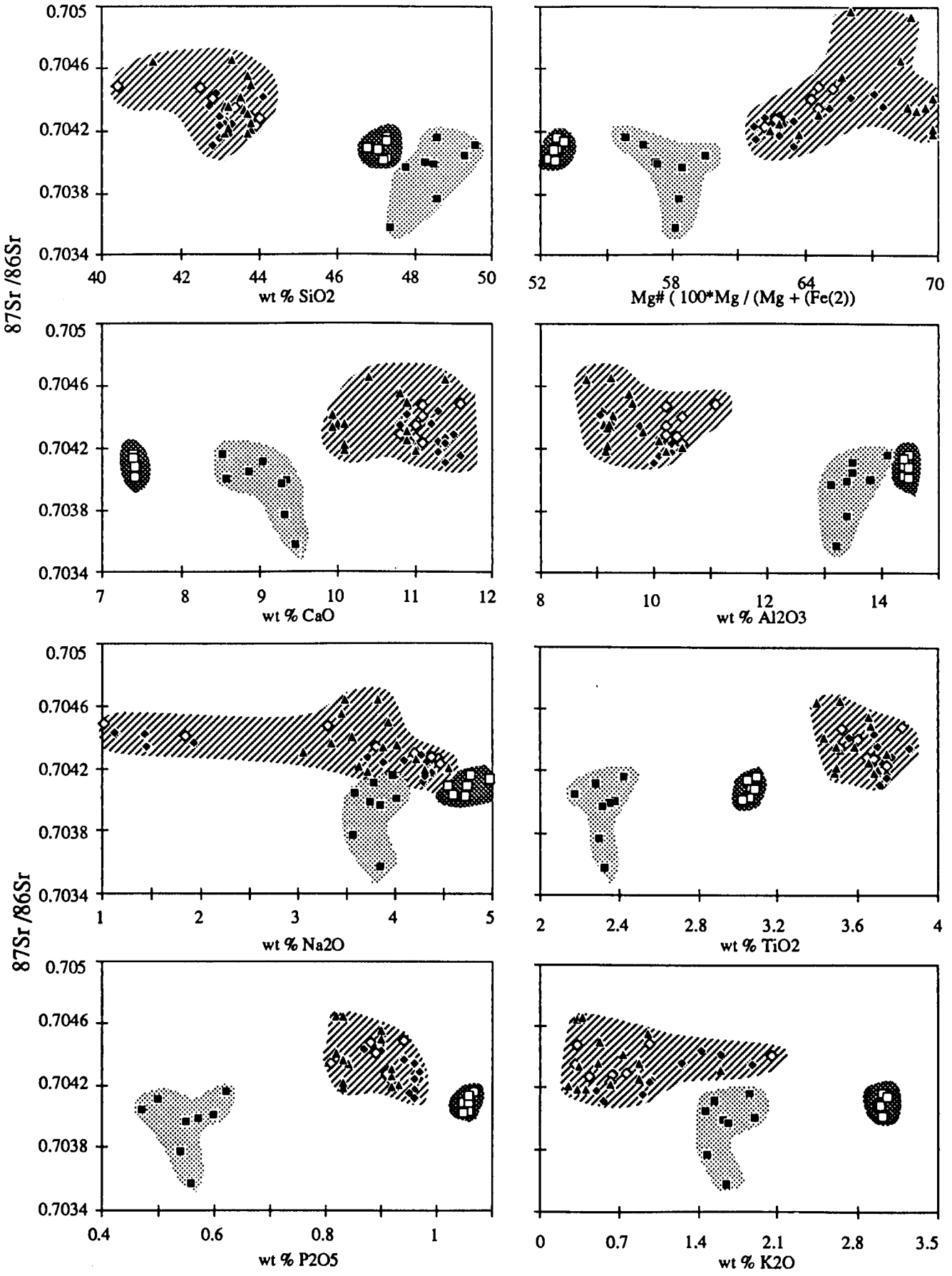

Fig. 3.30. 87Sr /86 Sr(0) ratios versus major elements for the South Australian alkaline basalts.

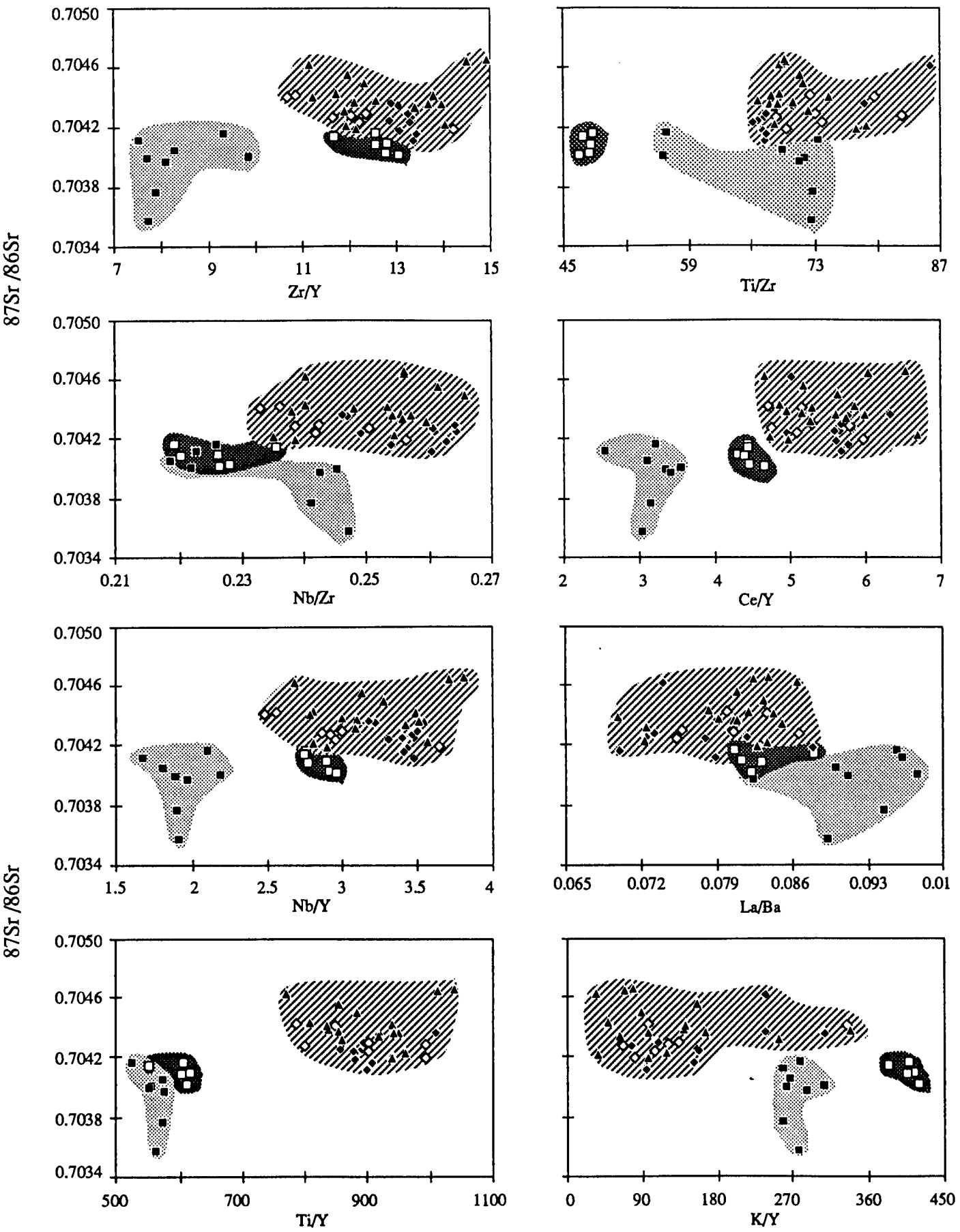

Fig. 3.31a. 87Sr /86Sr ratios versus incompatible element ratios for the South Australian alkaline basalts.

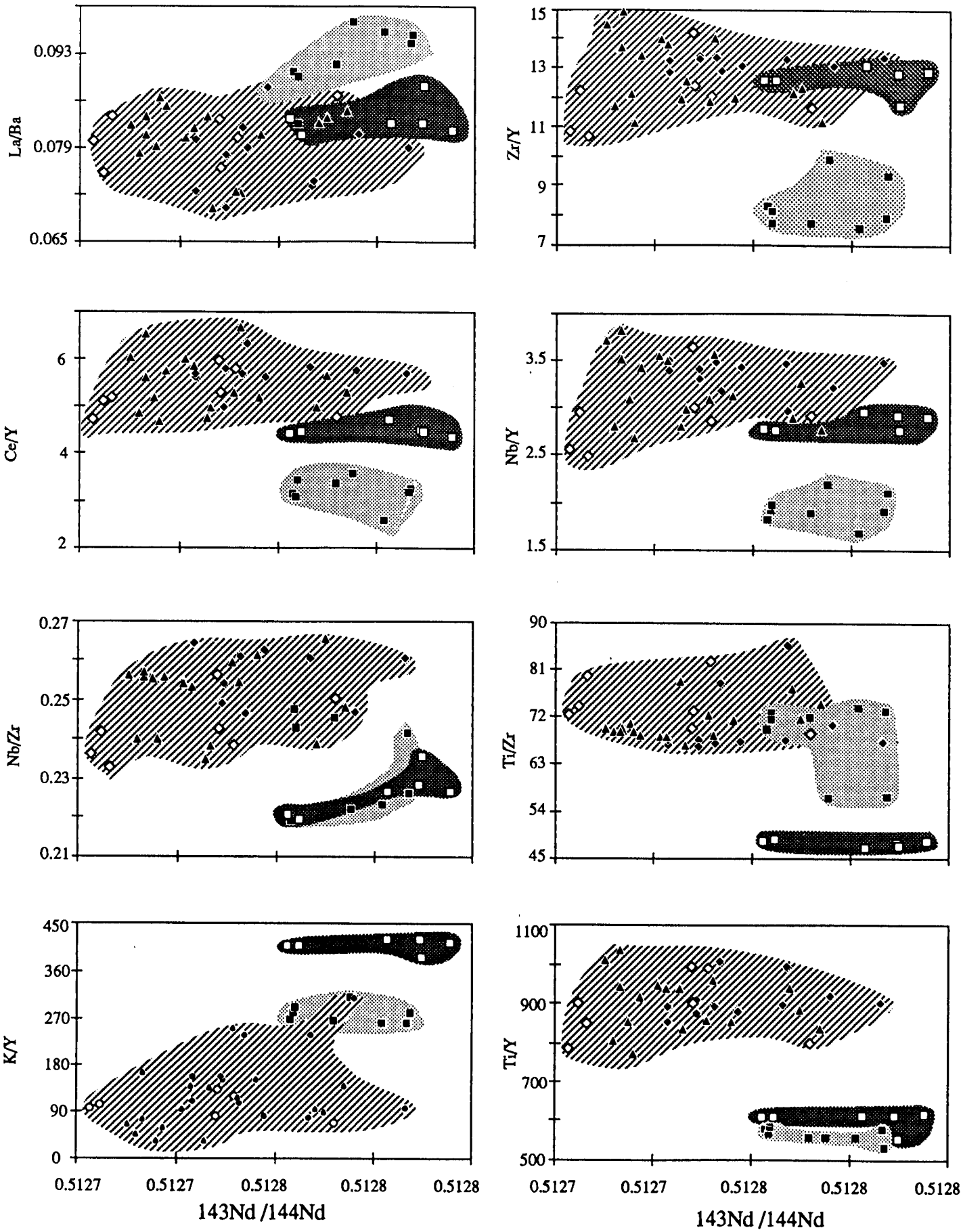

Fig. 3.31b. 143Nd /144Nd ratios versus incompatible element ratios for the South Australian alkaline basalts.

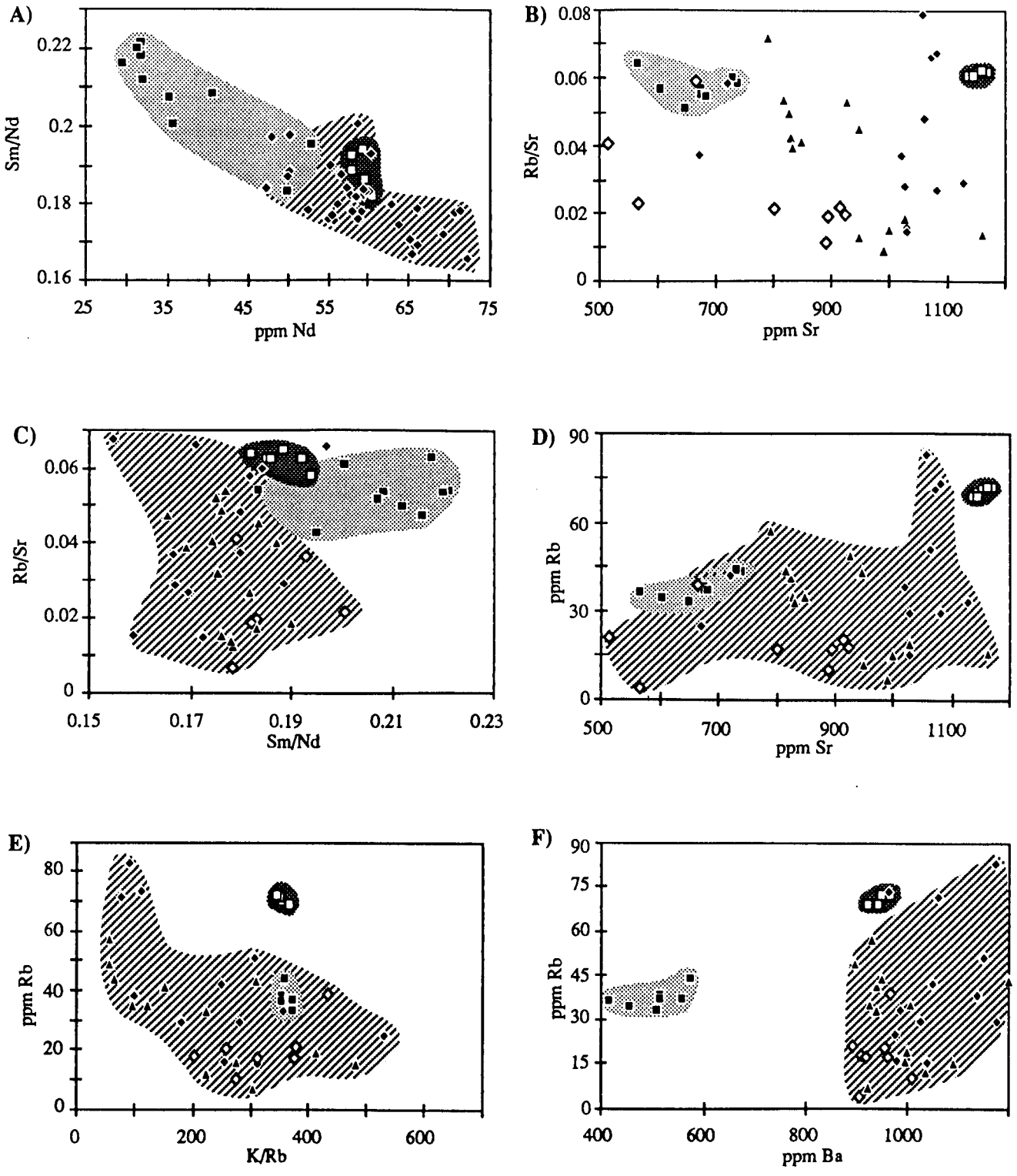

Fig. 3.32. Relationships among Rb, Sr, Nd, Sm, K and Ba for the South Australian alkaline basalts.

Table 3.21. Selected trace element ratios and abundances of the South Australian alkaline basalts.

Locality	Mt Gambier			Mt Schank			Mt McIntyre			Lake Leake			Mt Edward			Mt Muirhead			Mt Watch		
Lithology	Hawaiite			Hawaiite			Analcimite			Analcimite			Analcimite			Analcimite			Analcimite		
			Av			Av			Av			Av			Av			Av			Av
K/Rb	340.0 -	378.0	360.0	347.1 -	367.1	355.4	77.6 -	303.8	132.4	218.8 -	529.2	301.1	486.8 -	351.1	410.9	94.4 -	475.2	305.1	55.0 -	222.7	107.5
Rb/Sr	0.051 -	0.063	0.056	0.060 -	0.062	0.061	0.015 -	0.079	0.042	0.029 -	0.165	0.055	0.047 -	0.049	0.048	0.007 -	0.072	0.022	0.032 -	0.054	0.042
La/Yb	26.9 -	34.3	34.2	39.7 -	39.8	40.3	42.0 -	50.3	46.3	51.7 -	52.9	52.3	49.6 -	55.6	52.6	27.7 -	45.3	31.3	32.4 -	55.8	43.1
La	40.0 -	73.0	52.6	76.0 -	83.0	78.5	75.0 -	86.0	82.8	66.0 -	93.0	79.0	69.0 -	80.0	75.5	63.0 -	81.0	73.1	74.0 -	84.0	78.5
Rb/Zr	0.159 -	0.192	0.175	0.179 -	0.185	0.182	0.045 -	0.244	0.128	0.120 -	0.236	0.158	0.109 -	0.112	0.111	0.020 -	0.151	0.063	0.105 -	0.183	0.130
Rb/Ba	0.066 -	0.086	0.072	0.074 -	0.076	0.075	0.015 -	0.076	0.041	0.026 -	0.098	0.045	0.026 -	0.030	0.028	0.007 -	0.047	0.021	0.028 -	0.062	0.042
Ce/Pb	16.2 -	28.4	18.7	18.2 -	45.3	26.3	21.3 -	39.5	29.0	25.7 -	31.7	28.1	27.1 -	36.6	21.2	22.6 -	28.1	25.6	23.6 -	45.7	29.2
Nb/U	16.1 -	83.6	34.1	29.5 -	169.8	59.1	65.4 -	150.0	88.4				57.8 -	85.0	67.4	80.2 -	158.0	123.0	32.2 -	112.3	58.6
Zr/Y	7.5 -	11.7	9.1	11.7 -	13.0	12.6	12.9 -	13.4	13.2	12.1 -	14.7	13.1	9.9 -	11.9	11.7	11.2 -	12.6	12.0	13.4 -	14.9	14.0
Ti/Zr	4.1 -	73.5	59.0	46.6 -	48.0	47.4	64.2 -	65.5	65.1	67.8 -	101.3	78.8	82.6 -	117.1	99.5	64.9 -	74.6	69.5	66.2 -	67.9	66.8
Zr/Nb	3.9 -	4.5	4.2	4.2 -	4.6	4.4	3.8 -	4.0	3.9	4.0 -	5.0	4.3	3.9 -	4.2	4.0	3.9 -	4.3	4.1	3.9 -	3.9	3.9
Ba/Sr	0.714 -	0.817	0.770	0.813 -	0.827	0.822	0.891 -	1.112	1.018	0.876 -	1.684	1.218	1.638 -	5.400	2.957	0.798 -	1.521	1.025	0.520 -	1.392	1.007
Ba/La	10.2 -	11.2	11.0	11.4 -	12.4	12.0	11.4 -	14.3	12.9	10.6 -	13.3	12.3	12.4 -	14.5	13.5	9.2 -	14.3	12.1	11.7 -	13.8	12.3
Ba/Nb	8.6 -	11.7	10.1	10.3 -	11.4	10.8	10.9 -	13.5	12.0	11.0 -	23.2	15.1	14.7 -	24.5	18.6	9.4 -	13.6	12.1	11.4 -	14.6	12.1
Ba/Th	84.4 -	126.4	100.9	98.7 -	133.4	110.4	112.5 -	153.3	129.5	77.7 -	176.1	125.0	118.0 -	165.9	135.8	83.6 -	134.7	112.1	91.6 -	122.1	115.7
P2O5/Ce	65.2 -	79.4	69.0	71.6 -	80.2	76.8	64.2 -	73.3	66.2	64.5 -	68.2	65.6	58.3 -	93.0	75.6	65.9 -	79.1	69.9	64.3 -	64.1	61.7
Sr/Nd	19.3 -	21.3	19.9	17.4 -	18.9	18.4	14.5 -	17.7	15.8	8.0 -	20.5	13.8	3.2 -	10.5	7.6	11.6 -	17.5	15.3	13.4 -	30.7	16.0
Th/U	1.8 -	7.0	3.4	4.4 -	17.6	5.8	5.3 -	14.5	10.8				7.2 -	11.5	8.7	8.2 -	15.4	12.2	3.2 -	14.0	8.6
Ti/V	72.9 -	89.3	78.2	97.0 -	116.4	105.1	65.5 -	72.3	69.4	65.8 -	72.9	69.0	65.2 -	70.8	67.9	69.5 -	80.8	74.1	65.5 -	72.9	67.7
Ni(ppm)	148.0 -	183.0	169.4	96.0 -	116.0	109.7	234.0 -	279.0	258.1	189.0 -	372.0	302.2	483.0 -	795.0	608.0	198.0 -	342.0	261.3	447.0 -	483.0	467.8
Cr(ppm)	215.0 -	288.0	256.9	106.0 -	125.0	114.7	320.0 -	354.0	343.7	470.0 -	629.0	540.6	739.0 -	761.0	747.3	333.0 -	514.0	420.4	317.0 -	694.0	571.8

Table 3.21.(continued)

Locality	The Bluff			Mt Graham			Burr				Kangaroo Island		
Lithology	Analcimite			Analcimite			Analcimite				Qt tholeiites		
			Av			Av			Av			Av
K/Rb	168.8 -	410.8	266.6	202.9 -	695.5	299.9	347.2 -	438.7	399.4	227.7 -	265.8	246.0
Rb/Sr	0.014 -	0.047	0.030	0.007 -	0.022	0.017	0.015 -	0.058	0.043	0.242 -	0.256	0.249
La/Yb	54.4 -	65.4	60.3	40.5 -	44.4	42.4	50.0 -	53.5	51.7			
La	81.0 -	95.0	86.5	72.0 -	106.0	84.3	81.0 -	115.0	100.3	11.0 -	12.0	11.5
Rb/Zr	0.051 -	0.145	0.099	0.015 -	0.064	0.048	0.049 -	0.137	0.065	0.313 -	0.359	0.335
Rb/Ba	0.016 -	0.042	0.029	0.004 -	0.021	0.015	0.009 -	0.040	0.029	0.131 -	0.103	0.115
Ce/Pb	18.8 -	42.7	27.5	21.5 -	64.3	27.4	18.9 -	40.5	26.3	5.0 -	6.0	5.5
Nb/U				39.4 -	580.0	236.2	59.5 -	81.2	72.9	4.4 -	2.5	3.3
Zr/Y	11.2 -	12.3	11.8	6.9 -	12.4	11.0	6.6 -	10.8	8.6	4.5 -	4.6	4.5
Ti/Zr	69.2 -	72.4	70.6	63.3 -	85.2	72.4	67.1 -	96.0	75.9	43.9 -	44.5	44.2
Zr/Nb	3.8 -	4.0	3.9	4.0 -	4.4	4.2	4.2 -	4.4	4.3	22.2 -	26.1	23.9
Ba/Sr	0.858 -	1.268	1.045	0.987 -	1.604	1.136	1.099 -	1.738	1.475	1.843 -	2.470	2.159
Ba/La	11.9 -	13.8	12.5	8.5 -	13.3	11.2	3.3 -	12.0	6.8	19.3 -	24.1	21.8
Ba/Nb	12.0 -	14.6	13.1	11.0 -	15.6	13.1	6.2 -	14.8	9.6	53.0 -	90.3	69.6
Ba/Th	111.2 -	162.2	134.7	93.5 -	125.8	107.5	54.7 -	122.5	90.2	92.2 -	64.2	73.7
P2O5/Ce	62.9 -	65.7	64.7	56.8 -	70.8	64.6	58.4 -	65.5	62.0	38.5 -	38.5	38.5
Sr/Nd	13.9 -	18.1	16.0	7.4 -	15.8	12.7	2.7 -	11.1	6.5	10.5 -	9.8	10.1
Th/U				4.3 -	25.3	13.3	6.6 -	9.1	7.7	2.6 -	3.5	3.1
Ti/V	70.7 -	69.6	70.7	64.7 -	74.2	70.8	63.2 -	68.3	65.9	16.1 -	14.2	15.1
Ni(ppm)	137.0 -	347.0	284.8	213.0 -	287.0	248.3	254.0 -	283.0	267.3	75.0 -	73.0	74.0
Cr(ppm)	301.0 -	484.0	422.3	399.0 -	508.0	436.8	465.0 -	503.0	481.8	179.0 -	147.0	163.0

Table 3.22. Selected trace element ratios and abundances from the different major magma sources (after Ewart and Chappell, 1989).

Lithology	Melilitite	Basanite	Alkali-Basalt	Ne. Hawaiite	Hawaiite	Hawaiite#	Analcimite#	N-MORB	E-MORB	OIB
K/Rb	380 - 455	374 - 579	493 - 644	58 - 390	408 - 442	357.7	277.9	1071.4	416.7	387.1
Rb/Sr	0.018 - 0.025	0.029 - 0.049	0.026	0.036 - 0.052	0.033 - 0.044	0.058	0.038	0.008	0.033	0.047
La/Yb	18.2 - 42.7	22.7 - 30.3	8.9 - 10.9	31 - 41.9	13 - 23.6	37.2	47.5	0.820	2.658	17.130
La	41 - 90	32 - 52	19 - 20	44 - 45	23 - 30	65.6	82.5	2.5	6.3	37
Rb/Zr	0.052 - 0.12	0.13 - 0.14	0.09 - 0.13	0.14 - 0.61	0.16 - 0.12	0.178	0.100	0.008	0.069	0.111
Rb/Ba	0.052 - 0.077	0.053 - 0.078	0.068 - 0.07	0.081 - 0.16	0.064 - 0.069	0.073	0.031	0.089	0.088	0.089
Ce/Pb	87 - 210	82	23 - 38	41 - 53	25	22.5	26.8	25	25	25
Nb/U	37 - 45	33 - 39	48 - 57	52 - 55	40	46.6	107.8	49.6	46.1	47.1
Zr/Y	7.8 - 12.5	8.9 - 11.7	4.7 - 6.9	10 - 13	5.6 - 601	10.8	11.9	2.6	3.3	9.7
Ti/Zr	41 - 67	59 - 69	51 - 63	43 - 69	47 - 84	53.2	74.8	102.7	82.2	61.4
Zr/Nb	2.3 - 4	3.2 - 4.5	3.7 - 4.5	2.7 - 4.9	3.6 -	4.3	4.1	31.8	8.8	5.8
Ba/Sr	0.32 - 0.43	0.49 - 0.91	0.36 - 0.69	0.64 - 0.68	0.47 - 0.65	0.796	1.360	0.090	0.368	0.530
Ba/La	4.8 - 10.2	8.8 - 10.1	12.1 - 13	10.4 - 18.9	9.4 - 15.2	11.5	11.7	2.5	9.0	9.5
Ba/Nb	3 - 5.4	7.4 - 7.6	5.7 - 6.9	8.1 - 9.9	7.2 -	10.5	13.2	2.7	6.9	7.3
Ba/Th	33 - 49	48 - 81	71 - 88	64 - 133	61 - 121	105.7	118.8	52.5	95.0	87.5
P2O5/Ce	84 - 90	87 - 100	94 - 120	84 - 118	69 - 104	72.9	66.3	155.8	94.7	77.3
Sr/Nd	16 - 23	17 - 25	33 - 37	17 - 32	16 - 24	19.2	12.9	9.6	17.2	17.1
Th/U	4.2 - 4.4	3.6 - 4	3.9 - 5.8	4.5 - 7.3	2.6 - 5.2	4.6	10.2	2.6	3.3	3.9
Ti/V	67 - 97	85 - 94	53 - 61	69 - 76	42 - 76	91.7	69.4			
Ni(ppm)	236 - 458	308 - 447	299 - 356	409 - 445	346 -	139.5	337.2			
Cr(ppm)	419 - 510	310 - 391	440 - 478	479 - 537	388 - 543	185.8	495.6			

Data sources; Hawaiite# and Analcimite# from South Australia alkaline basalts, N-MORB, E-MORB and OIB from Sun and McDonough (1989).

Figure opposite:

Fig. 3.33. Comparisons of the South Australian basalts with Victorian Newer Basalts, Tamanian Tertiary basalts, Cameroon line basalts and Basin and Range basalts (Data from Frey *et al.* (1978), McDonough *et al.* (1985), Fitton (1987), Fitton *et al.* (1988)).

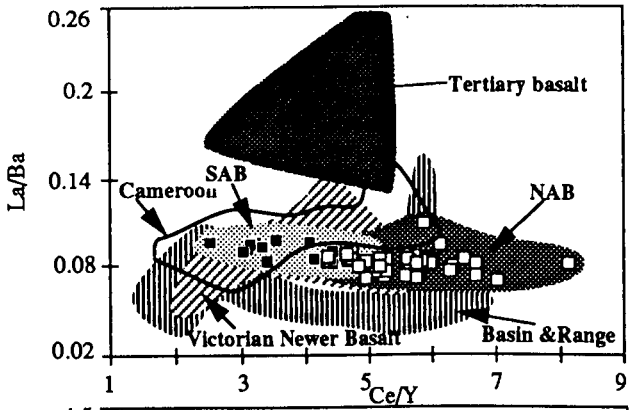
Tertiary basalt
SAB
Cameroon
NAB
Victorian Newer Basalt
Basin &Range
La/Ba
Ce/Y

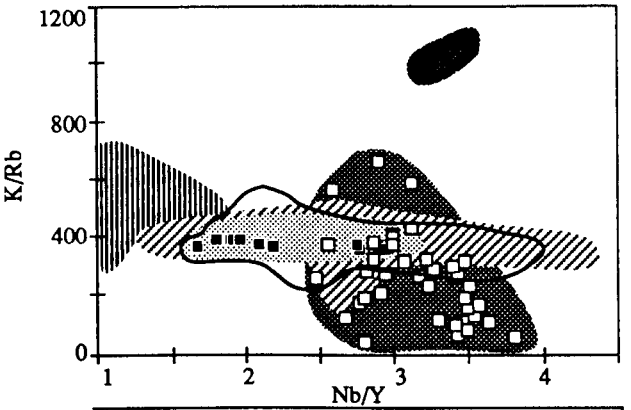
K/Rb
Nb/Y

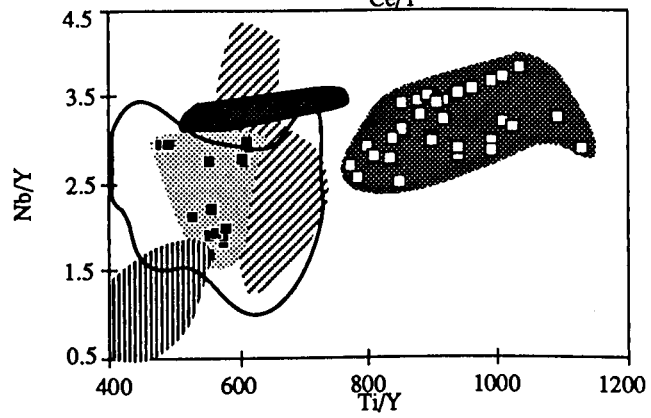
Nb/Y
Ti/Y

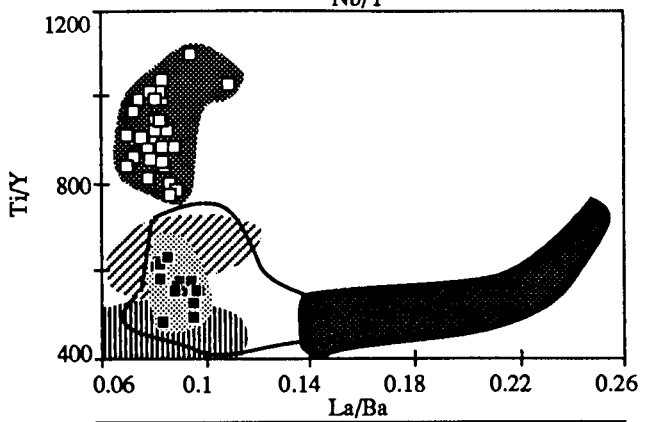
Ti/Y
La/Ba

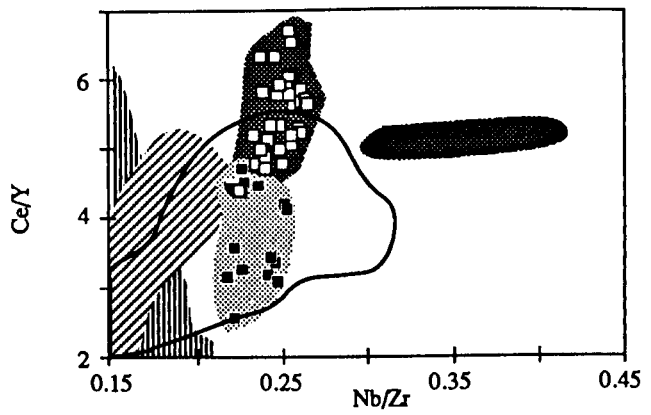
Ce/Y
Nb/Zr

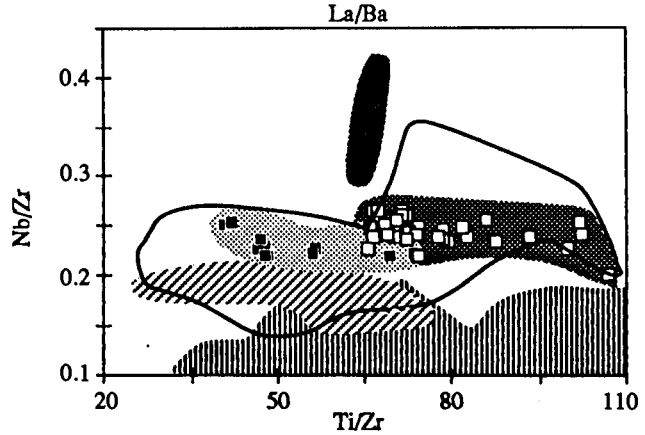
Nb/Zr
Ti/Zr

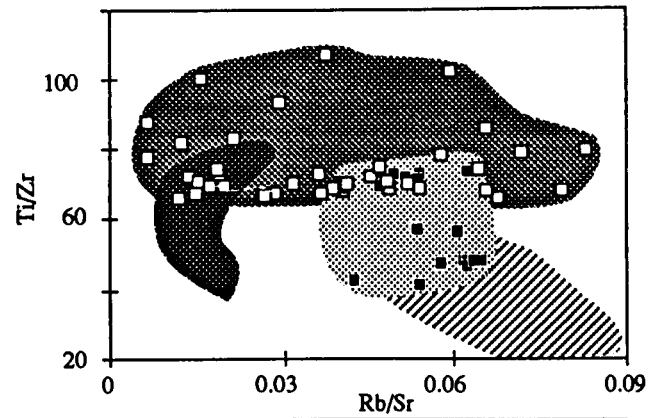
Ti/Zr
Rb/Sr

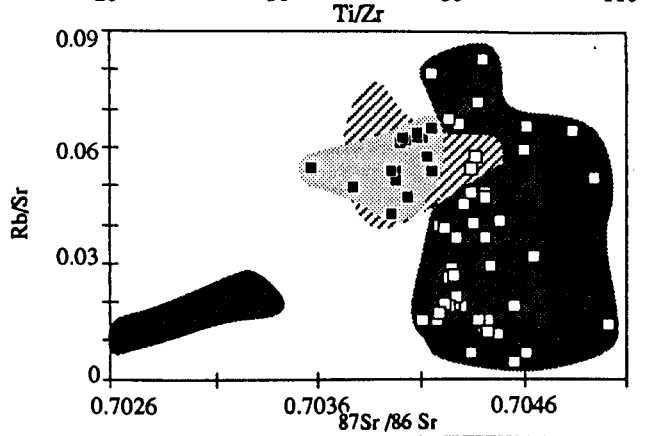
Rb/Sr
87Sr /86 Sr

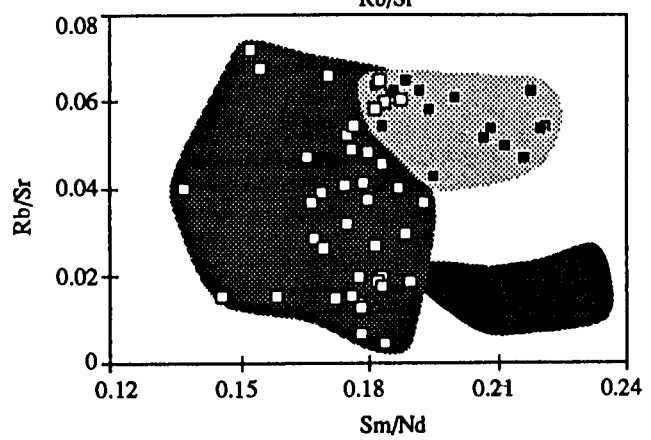
Rb/Sr
Sm/Nd

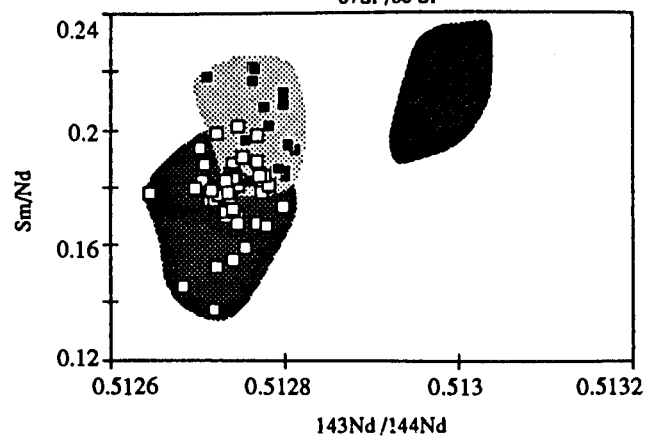
Sm/Nd
143Nd /144Nd

Summary of trace element abundances and ratios from eastern Australian Cainozoic basalts and their comparison with the SQAB are shown in the Table 3.22. In the SQAB, the hawaiites are similar to those of nepheline hawaiites of the eastern Australia volcanics while the olivine analcimites show a similarity with basanites, or melilitites of the eastern Australia volcanics. Geochemical and isotopic comparisons of the SQAB with available data are shown in Fig. 3.33. In general, the South Australian hawaiites are similar to Victorian Newer Basalts, but are clearly distinguished from the Tertiary Tasmanian basalts in terms of geochemical and isotopic characteristics. The Tertiary Tasmanian basalts show higher La/Ba, K/Rb, Nb/Zr, and Sm/Nd ratios relative to the South Australian hawaiites. In the SQAB, analcimites are distinguished from the Tertiary Tasmanian basalts as well as the Victorian Newer Basalts by high Ce/Y, Ti/Y, Ti/Zr and low Sm/Nd ratios. These characteristics may reflect a differences of the source magma as shown in the Fig. 3.20. In the Sr-Nd-Pb isotopic plots, the SQAB and Victorian Newer Basalts show EM type OIB-like signatures whereas the Tertiary Tasmanian basalts have HIMU type-OIB like characteristics. In addition, the Cameroon line basalts, and the Basin and Range basalts are generally overlapped in the ranges of SQAB and Victorian Newer Basalts in the incompatible element ratios.

3.8. Conclusion

1) Two main geochemical and petrographical groups of basalts have been recognised; Southern area younger hawaiites and Northern area older olivine analcimites. The hawaiites are also fall into two groups, Mt Gambier and Mt Schank.

2) The hawaiites are geochemically and isotopically Victorian Newer Basalt-or EM type OIB-like, but are clearly distinguished from the Tasmanian Tertiary basalts showing HIMU type OIB signatures.

3) The analcimites are distinguished from the hawaiites by higher Ba, Ti, Zr, Nb, LREE concentrations in spite of their high Cr, Ni, Mg#. The analcimites can be considered as primary basaltic liquids equilibrated with a refractory upper mantle peridotite or be originated from cumulates.

4) Major and incompatible element characteristics observed in the SQAB can be attributed to crystal fractionation as well as a low degree of partial melting of the upper mantle peridotites.

Chapter 4. Mineral chemistry and whole rock chemistry of the upper mantle xenoliths entrained by SQAB

4.1. Introduction

Xenoliths entrained by volcanic events or kimberlitic rocks provide a window of petrographic and geochemical nature in the lithosphere. Abundant mantle derived xenoliths are found in the Mesozoic to Cainozoic kimberlitic and Cainozoic basaltic rocks along the Phanerozoic eastern Australia (Irving, 1974; Ellis, 1976; Wass and Irving, 1976; Edward *et al.*, 1979; Wass and Hollis, 1983; Griffin *et al.*, 1984; O'Reilly and Griffin, 1987; O'Reilly, 1989b). The xenoliths are dominantly Cr-diopside spinel lherzolites with minor mafic, ultramafic, eclogitic and granulitic rocks (O'Reilly, 1989a) even though there are problems of sampling collection including sampling bias or alteration, (Jackson, 1968; Bloomer and Nixon, 1973).

In South Australia, they are found mainly at the Cainozoic basaltic provinces in the south eastern margin of South Australia (Stanley, 1910; Fehlberg, 1968; Sheard, 1978) with minor Mesozoic kimberlitic pipes in the Adelaide Geosyncline (Ferguson *et al.*, 1979). More abundant ultrabasic and basic xenoliths are found at large maar type volcanos including Mt Gambier and Mt Watch. They are dominantly spinel lherzolites with minor dunites and pyroxenites. The spinel lherzolites have dominantly olivine normative composition and are largely divided into two varieties according to the different microscopic textures; coarse equant varieties (CEL) and deformed sheared varieties (DSL). The Group 2 peridotites and garnet bearing pyroxenites which occur abundantly in Victorian basaltic provinces appear to be absent from South Australian.

This study is mainly concerned with the spinel lherzolites (Group 1 lherzolite of Frey and Prinz, 1978) entrained by the South Australian basalts. They are characterised in terms of petrography, mineral chemistry and whole rock chemistry.

4.2. Previous studies

Limited petrographic descriptions and/or mineral analyses have been carried out by Stanley (1910), Fehlberg (1968) and Sheard (1978) whereas geochemical and/or isotopic studies have been provided by Frey and Green (1974) and McDonough and McCulloch (1987). Stanley (1910) provided a chemical analyses of olivine grain and whole rock of Mt Gambier lherzolite. Frey and Green (1974) provided a major element, trace element, REE

and mineral chemistry of lherzolites samples from Mt Gambier with those of the Victorian basalts. They suggested that the lherzolites are not cognate with host magma but are accidental xenoliths. It has been suggested that REE abundances of the Mt Gambier lherzolites are similar to the chondrite composition (Frey and Green, 1974).

McDonough and McCulloch (1987) provided Sr-Rb and Nd-Sm isotope data on seven whole rocks and one clinopyroxene sample of peridotitic xenoliths from Mt Gambier volcanics with those from Victorian Newer Basalts. These studies indicate several points as follows; 1) most of xenoliths plot in the oceanic mantle array of Sr and Nd isotopic planes, 2) extremely large isotopic variations occur in individual basaltic provinces (for examples εNd of -7.5 - +10.6 in mantle xenoliths from Mt Leura), 3) clear distinction in the isotopic composition of peridotites is shown in samples of different microscopic structure, 4) Sr/Nd ratios are constant between minerals and their host rocks, and are similar to MORB or PM. McDonough and McCulloch (1987) concluded that the wide ranges of the isotope compositions observed in the peridotites are attributed to long-term, small scale heterogeneities related to lithospheric mantle growth involving the underplating of the refractory peridotite diapirs.

4.3. Petrography and Mineralogy

Fifteen samples were selected for petrographic descriptions. They range from several mm to cm in size. Large xenoliths (about 30-40 cm diameter) are only found in Mt Gambier volcanics. These are dominantly Cr-diopside or Group 1 type lherzolite (Frey and Prinz, 1978) and dunites with minor pyroxenites (Fig. 4.1).

The Group 1 spinel lherzolites are composed of Ol (65-78 %) +Opx (15-23 %) +Cpx (3-11 %)+Sp (0.5-3 %). More abundant clinopyroxene and orthopyroxene are shown in the CEL. The spinel lherzolites are largely divided into granular (CEL 1, 2, 3, 4, ED 4) and sheared varieties (DSL 1, 2, 3, WA IV- 2, 3, 4) by different microstructures. The CELs are characterised by relatively homogeneous equigranular textures whereas the DSL are characterised by submylonitic textures (Fig. 4.1). The DSLs show pronounced foliation and recrystallisation of olivine grains to fine grains at their margin. In the South Australian basaltic provinces, granular varieties are more common .

With abundant olivine, the dunitic xenoliths (WA-I, BL 3) contain clinopyroxene, orthopyroxene and opaque oxide. The olivine grains are recrystallised to fine granular grains in their rims and show weak alteration at their rims or along the fractures. An amphibole-bearing pyroxenite (GA 13) is also found in Mt Gambier volcanics. It is 3-4 cm wide and is hosted by a vesicular basalt. It contain orthopyroxene, clinopyroxene and amphibole with minor opaque oxide grains. The amphibole grains are mainly diamond shape with distinctive cleavages and most of the orthopyroxene and clinopyroxene grains are marginally recrystallised to fine granular grains.

Figures opposite;

Fig. 4.1a. Photograph of a typical coarse equant spinel lherzolite from the Mt Gambier volcanics (upper) and its photomicrograph (lower) which shows olivine (o) and orthopyroxenes (op).

Fig. 4.1b. Photograph of a typical deformed sheared spinel lherzolite from the Mt Gambier volcanics (upper) and its photomicrograph (lower) which shows a spinel (s), orthopyroxenes (op) and olivines (o).

Fig. 4.1c. Photograph of a typical amphibole bearing pyroxenite from the Mt Gambier volcanics (upper) and its photomicrograph (lower) which shows amphiboles (am) and clinopyroxenes (cp). Most of the clinopyroxenes are marginally recrystallised to fine granular aggregates.

Width of a scale bar (left bottom) is 1 millimetre.

a

b

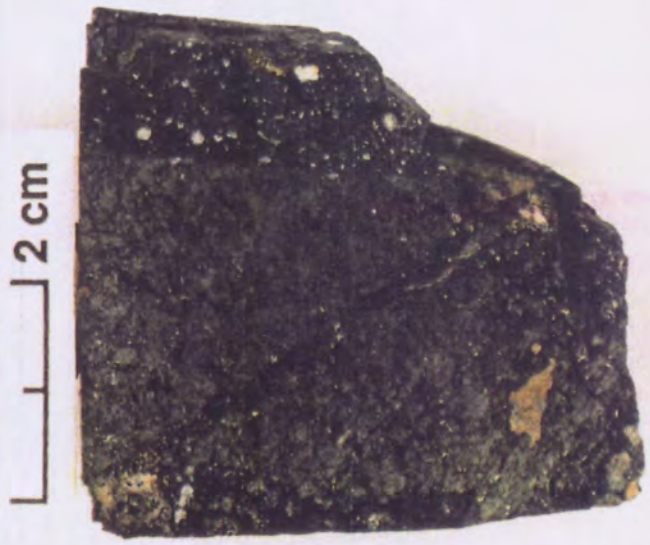

c

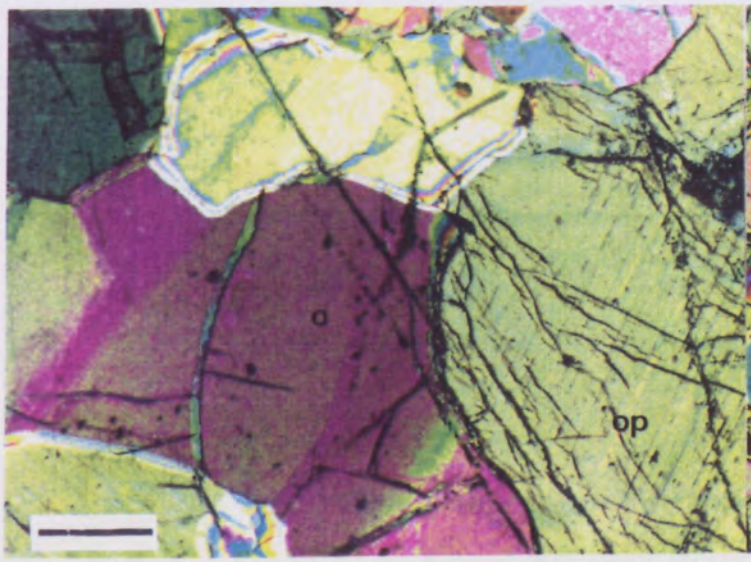

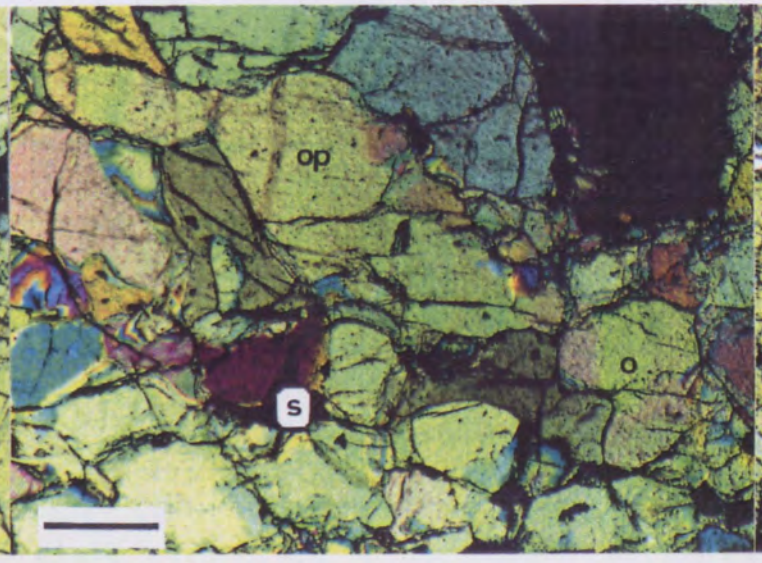

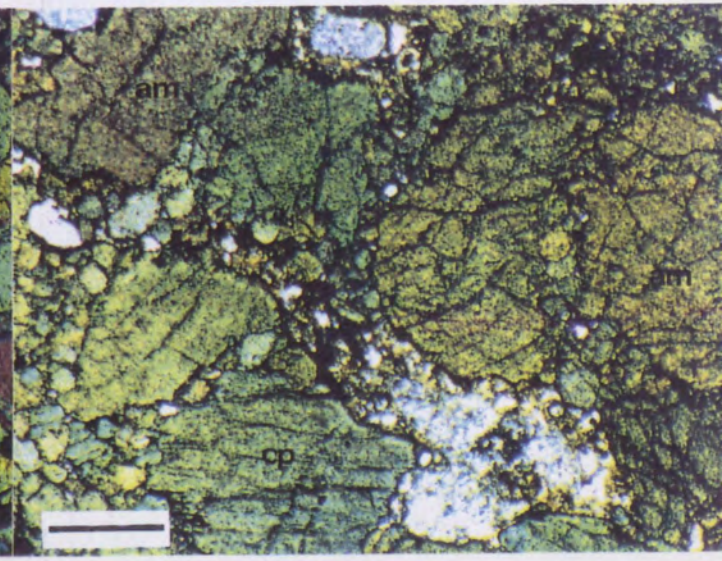

Figures opposite;

Fig. 4.1d. Photograph of coarse equant spinel lherzolites from the Mt Gambier volcanics. Notice that the xenoliths are mainly subangular or round shapes.

Fig. 4.1e. Photograph of flaser or submylonitic spinel lherzolites from the Mt Gambier volcanics.

Fig. 4.1f. Photograph of typical spinel lherzolites or dunites from the Mt Watch volcanics.

Fig. 4.1g. Photograph of typical spinel lherzolites from the Mt Edward volcanics. Notice that most of the xenoliths of the Northern area older volcanics are smaller than those of the Mt Gambier volcanics.

Fig. 4.1h. Photomicrograph of a typical dunitic xenolith from the Mt Watch volcanics showing a pronounced lineation by a alignment of olivine grains (o).

Fig. 4.1i. Photomicrograph of a spinel lherzolite from the Mt Edward volcanics showing recrystallised clinopyroxenes (cp), orthopyroxene (op) and olivine (o).

Width of a scale bar (left bottom) is 1 millimetre.

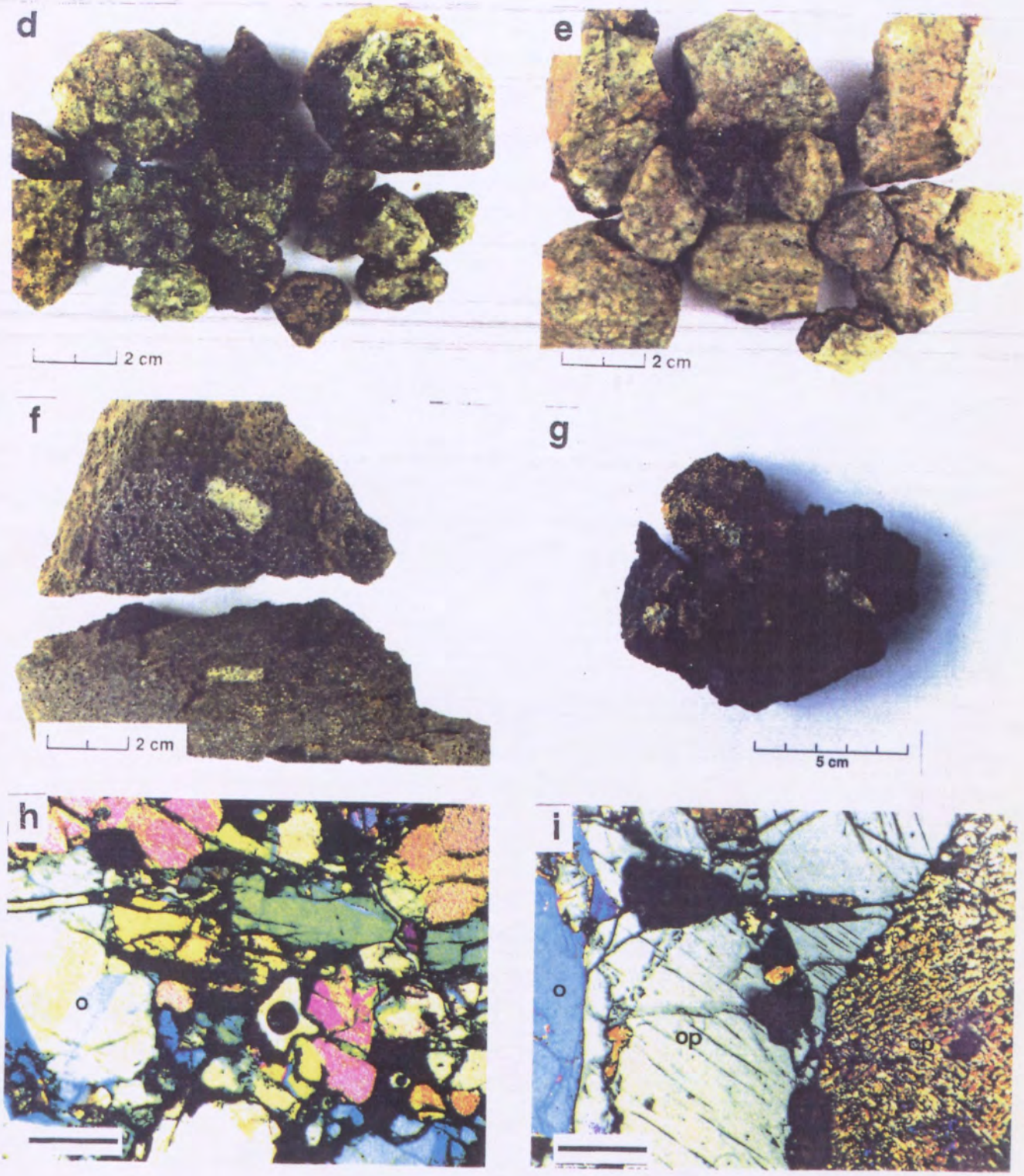

Width of a scale bar (left bottom) is 1 millimetre.

4.4. Mineral chemistry

Eight selected spinel lherzolite samples were analysed for olivine, pyroxene and spinel using the JEOL 733 microprobe at the University of the Adelaide. Details of analytical methods are shown in Appendix 1. Representative analyses are shown in Tables 4.1, 2, 3, and 4.

The clinopyroxenes are diopside and have Mg# ranging from 91 to 95. There are clear distinctions of mineral compositions between clinopyroxenes from CELs and DSLs. Clinopyroxenes from the CELs are more magnesian (92.5 - 94.7) and display high Cr_2O_3, Na_2O, TiO_2, low CaO and Al_2O_3 relative to those of DSLs (Fig. 4.2b). The high Cr_2O_3 with high Mg# in the clinopyroxenes suggest that they are more refractory than those of DSLs. In the common clinopyroxene structure, $X_{1-p}Y_{1+p}Z_2O_6$ low CaO in clinopyroxene of CELs may reflect high Na_2O in the X site while low MnO, Cr_2O_3 and TiO_2 in the clinopyroxene from DSLs may reflect high Fe in the Y site. Wide variations of Al(VI) in the clinopyroxenes of DSLs may reflect complicate replacements of Al(IV), or Si in the Z site.

The orthopyroxenes show enstatitic-bronzitic composition (Fig. 4.2, 4.3) and have Mg# of 89.5 - 92.5. Orthopyroxene compositions are also distinct in the two kinds of lherzolites. In general, orthopyroxenes from CELs show higher Mg#, Cr_2O_3, and slightly higher MnO and TiO_2 relative to those of DSLs whereas orthopyroxenes of DSLs have wider ranges of the variation in the Al_2O_3 and SiO_2 contents. In the Al(VI) -Al(IV) relationships, increase of Al(4) with Al(6) may reflect systematic substitution of the Al_2O_3 in the pyroxene structure. Decrease of SiO_2 with Al_2O_3 may reflect replacement of Al by Si in Z site although these replacements are negligible in normal orthopyroxene. In addition, the observed increase of Al_2O_3 with Ca may reflect that of Ca in X site with increase of Al into YZ site.

The olivines have Mg# of 89.5-94 (Fig. 4.4). No clear relationships are shown between olivine compositions of the two lherzolite varieties. Scattered patterns are shown in Mg# - CaO and Mg# -Cr_2O_3 relationships. The scattered CaO contents with Mg# may reflect Ca solid solution in the olivine grains as a function of the silica activity in the liquidous temperature and pressure (Stormer, 1973) or dependence of the silica activity on the controlling pressures (Ferguson, 1978). The scattered pattern of Cr_2O_3 with Mg# may reflect liquid-melt disequilibrium, even though increase in Cr_2O_3 with Mg# is predictable in the olivine grains.

The spinels show Mg# of 71-78 (71-76 of DSLs and 72-78 of CELs) (Fig. 4.5). They exhibit a negative correlation between Cr and Al which may reflect systematic replacement of Cr by Al. In a plot of Cr/Cr+Al ratios vs Mg# , spinels of the DSL are distinguished from those of CELs by low Cr/Cr+Al ratios and Mg#. This relationship suggests that substitution of Fe(2) into Mg ion site and Cr into the Al site in spinel of DSLs is more efficient than those in CELs.

Table 4.1a. Representative clinopyroxene analyses of the coarse equant lherzolites.

Sample	CEL 1			CEL 2			CEL 3.1		CEL 3.2			
SiO2	52.94	53.27	53.03	52.40	52.86	53.25	52.28	53.14	52.85	52.83	53.28	52.91
TiO2	0.34	0.39	0.26	0.47	0.33	0.40	0.53	0.46	0.54	0.42	0.28	0.41
Al2O3	5.56	5.60	5.39	5.37	4.77	4.85	4.94	4.60	4.44	4.32	4.58	4.81
FeO	1.86	1.87	1.99	1.83	2.11	1.83	1.72	2.03	1.70	1.62	1.73	1.73
Fe2O3	0.00	0.00	0.00	0.00	0.00	0.00	0.00	0.00	0.00	0.00	0.00	0.00
MnO	0.14	0.21	0.21	0.22	0.22	0.06	0.53	0.17	0.16	0.42	0.18	0.24
MgO	15.52	15.58	15.79	15.41	15.82	16.19	15.80	16.27	16.09	16.18	16.04	15.69
CaO	21.44	21.07	20.86	21.72	21.87	21.47	21.26	21.37	21.82	21.82	21.72	21.29
Na2O	1.13	1.23	1.07	1.06	0.94	1.07	0.85	0.90	0.93	0.98	0.85	0.79
K2O	0.00	0.00	0.03	0.07	0.01	0.00	0.00	0.00	0.00	0.04	0.06	0.00
Cr2O3	1.68	1.59	1.19	1.05	1.07	1.15	1.54	0.75	1.22	1.02	0.88	1.36
Total	100.60	100.81	99.81	99.59	99.99	100.25	99.43	99.69	99.74	99.64	99.59	99.21
				Number of Ions on the Basis of 6 (O)								
Si	1.9013	1.9069	1.9152	1.9028	1.9133	1.9161	1.9021	1.9229	1.9149	1.9178	1.9290	1.9226
Al(4)	0.0987	0.0932	0.0848	0.0972	0.0867	0.0839	0.0974	0.0772	0.0851	0.0822	0.0710	0.0774
Al(6)	0.1368	0.1429	0.1446	0.1326	0.1166	0.1217	0.1138	0.1189	0.1045	0.1025	0.1244	0.1284
Ti	0.0091	0.0105	0.0070	0.0127	0.0090	0.0107	0.0144	0.0125	0.0146	0.0114	0.0076	0.0113
Fe(2)	0.0560	0.0560	0.0600	0.0555	0.0639	0.0550	0.0522	0.0614	0.0516	0.0491	0.0523	0.0526
Fe(3)	0.0000	0.0000	0.0000	0.0000	0.0000	0.0000	0.0000	0.0000	0.0000	0.0000	0.0000	0.0000
Mn	0.0042	0.0065	0.0065	0.0068	0.0066	0.0017	0.0162	0.0052	0.0049	0.0130	0.0055	0.0072
Mg	0.8304	0.8307	0.8495	0.8335	0.8530	0.8676	0.8565	0.8768	0.8685	0.8751	0.8649	0.8493
Cr	0.0477	0.0450	0.0340	0.0301	0.0307	0.0327	0.0442	0.0215	0.0349	0.0292	0.0251	0.0389
Ca	0.8247	0.8078	0.8067	0.8446	0.8479	0.8274	0.8283	0.8280	0.8466	0.8482	0.8421	0.8285
Na	0.0785	0.0852	0.0746	0.0748	0.0657	0.0747	0.0599	0.0633	0.0653	0.0689	0.0599	0.0555
K	0.0000	0.0000	0.0013	0.0032	0.0002	0.0000	0.0000	0.0002	0.0000	0.0018	0.0029	0.0000
Wo	48.2	47.7	47.0	48.7	48.0	47.3	47.7	46.9	47.9	47.9	47.9	47.9
En	48.5	49.0	49.5	48.1	48.3	49.6	49.3	49.6	49.2	49.4	49.2	49.1
Fs	3.3	3.3	3.5	3.2	3.6	3.1	3.0	3.5	2.9	2.8	3.0	3.0
Mg/Mg+Fe(t)	93.7	93.7	93.4	93.8	93.0	94.0	94.3	93.5	94.4	94.7	94.3	94.2

Table 4.1b. Representative clinopyroxene analyses of the deformed sheared lherzolites.

Sample	DSL 1.1			DSL 3.3			DSL 3.4		DSL 4			DSL 4.3
SiO2	52.98	53.01	52.84	51.83	52.18	52.11	52.39	52.78	52.95	52.49	52.94	52.60
TiO2	0.13	0.41	0.18	0.34	0.25	0.17	0.00	0.19	0.30	0.26	0.03	0.09
Al2O3	4.58	4.40	5.80	5.40	5.36	5.29	4.61	4.50	4.49	4.62	4.98	4.55
FeO	1.86	1.85	2.27	1.91	2.11	2.47	1.96	2.16	2.38	1.96	2.19	2.28
Fe2O3	0.00	0.00	0.00	0.00	0.28	0.00	0.00	0.00	0.00	0.00	0.00	0.00
MnO	0.10	0.22	0.21	0.28	0.10	0.29	0.41	0.21	0.39	0.36	0.16	0.00
MgO	15.51	15.83	15.19	15.73	15.60	15.73	16.22	16.31	15.98	16.38	16.09	15.86
CaO	22.11	22.34	21.72	21.97	22.48	21.91	22.00	22.70	22.43	22.81	22.41	22.36
Na2O	0.79	0.97	0.79	0.73	0.81	0.35	0.63	0.56	0.29	0.82	0.34	0.75
K2O	0.00	0.03	0.00	0.07	0.01	0.00	0.00	0.05	0.00	0.00	0.03	0.01
Cr2O3	1.08	0.63	1.27	1.44	1.00	0.76	0.73	0.64	0.57	0.77	1.04	0.98
Total	99.12	99.68	100.27	99.70	100.17	99.08	98.95	100.09	99.78	100.47	100.21	99.48
				Number of Ions on the Basis of 6 (O)								
Si	1.9301	1.9235	1.9049	1.8852	1.8912	1.9034	1.9114	1.9112	1.9210	1.8970	1.9107	1.9155
Al(4)	0.0699	0.0765	0.0951	0.1149	0.1089	0.0966	0.0886	0.0889	0.0790	0.1030	0.0893	0.0845
Al(6)	0.1267	0.1115	0.1512	0.1168	0.1199	0.1312	0.1183	0.1030	0.1128	0.0939	0.1226	0.1109
Ti	0.0036	0.0111	0.0048	0.0092	0.0068	0.0046	0.0000	0.0053	0.0082	0.0063	0.0008	0.0025
Fe(2)	0.0566	0.0561	0.0684	0.0579	0.0638	0.0755	0.0596	0.0653	0.0722	0.0589	0.0661	0.0695
Fe(3)	0.0000	0.0000	0.0000	0.0000	0.0078	0.0000	0.0000	0.0000	0.0000	0.0000	0.0000	
Mn	0.0031	0.0066	0.0064	0.0086	0.0031	0.0090	0.0125	0.0064	0.0120	0.0109	0.0048	0.0000
Mg	0.8414	0.8559	0.8159	0.8523	0.8424	0.8555	0.8814	0.8795	0.8633	0.8820	0.8652	0.8606
Cr	0.0309	0.0180	0.0362	0.0413	0.0285	0.0220	0.0210	0.0184	0.0163	0.0221	0.0296	0.0282
Ca	0.8625	0.8682	0.8387	0.8557	0.8727	0.8570	0.8597	0.8801	0.8715	0.8830	0.8666	0.8722
Na	0.0555	0.0685	0.0553	0.0516	0.0568	0.0249	0.0442	0.0390	0.0206	0.0573	0.0236	0.0527
K		0.0014		0.0034	0.0002	0.0000	0.0000	0.0023	0.0002	0.0000	0.0015	0.0003
Wo	49.0	48.8	48.7	48.5	49.1	47.9	47.7	48.2	48.2	48.4	48.2	48.4
En	47.8	48.1	47.4	48.3	47.4	47.8	48.9	48.2	47.8	48.4	48.1	47.7
Fs	3.2	3.1	4.0	3.3	3.6	4.2	3.3	3.6	4.0	3.2	3.7	3.9
Mg/Mg+Fe(t)	93.7	93.9	92.3	93.6	92.2	91.9	93.7	93.1	92.3	93.7	92.9	92.5

Table 4.2a. Representative orthopyroxene analyses of the coarse equant lherzolites.

Sample	CEL 1			CEL 2			CEL 3.1	CEL 3.2			CEL 3.3	
SiO2	56.79	56.85	56.80	56.66	56.97	56.01	56.73	56.84	56.78	56.70	56.30	56.35
TiO2	0.18	0.19	0.12	0.01	0.00	0.15	0.13	0.30	0.00	0.05	0.04	0.00
Al2O3	2.93	2.76	2.87	2.48	2.82	3.17	2.93	2.79	2.94	3.12	3.42	3.41
FeO	5.67	5.28	5.56	4.90	5.45	5.27	5.12	5.37	4.99	5.14	5.20	5.07
Fe2O3	0.00	0.14	0.00	0.82	0.34	0.00	0.00	0.00	0.00	0.00	0.00	0.00
MnO	0.00	0.04	0.06	0.23	0.16	0.24	0.11	0.00	0.11	0.06	0.10	0.14
MgO	34.43	34.80	34.44	34.80	34.72	34.02	34.49	34.65	34.28	34.51	33.90	34.29
CaO	0.53	0.59	0.56	0.47	0.47	0.47	0.57	0.54	0.63	0.59	0.59	0.59
Na2O	0.00	0.00	0.00	0.00	0.00	0.00	0.00	0.00	0.00	0.00	0.00	0.00
K2O	0.00	0.01	0.02	0.00	0.00	0.03	0.00	0.00	0.03	0.00	0.02	0.00
Cr2O3	0.44	0.32	0.47	0.47	0.61	0.39	0.27	0.54	0.53	0.34	0.66	0.48
Total	100.97	100.98	100.91	100.84	101.53	99.76	100.34	101.03	100.29	100.50	100.22	100.34
				Number of Ions on the Basis of 6 (O)								
Si	1.9344	1.9353	1.9360	1.9369	1.9333	1.9299	1.9396	1.9336	1.9424	1.9356	1.9298	1.9280
Al(4)	0.0656	0.0647	0.0640	0.0631	0.0667	0.0701	0.0604	0.0664	0.0577	0.0644	0.0702	0.0720
Al(6)	0.0519	0.0460	0.0515	0.0369	0.0459	0.0587	0.0575	0.0454	0.0606	0.0612	0.0677	0.0656
Ti	0.0046	0.0048	0.0031	0.0004	0.0000	0.0039		0.0078	0.0000	0.0012	0.0011	0.0000
Fe(2)	0.1613	0.1503	0.1584	0.1397	0.1547	0.1517	0.1464	0.1526	0.1428	0.1465	0.1490	0.1449
Fe(3)	0.0000	0.0037	0.0000	0.0211	0.0088	0.0000	0.0000	0.0000	0.0000	0.0000	0.0000	0.0000
Mn	0.0000	0.0013	0.0018	0.0066	0.0045	0.0071	0.0031	0.0000	0.0031	0.0016	0.0028	0.0041
Mg	1.7471	1.7645	1.7486	1.7718	1.7550	1.7462	1.7562	1.7557	1.7465	1.7548	1.7308	1.7474
Cr	0.0119	0.0086	0.0126	0.0127	0.0162	0.0107	0.0072	0.0146	0.0144	0.0091	0.0179	0.0130
Ca	0.0194	0.0213	0.0204	0.0172	0.0172	0.0175	0.0210	0.0195	0.0231	0.0215	0.0216	0.0217
Na	0.0000	0.0000	0.0000	0.0000	0.0000	0.0000	0.0000	0.0000	0.0000	0.0000	0.0000	0.0000
K	0.0000	0.0004	0.0009	0.0000	0.0000	0.0013	0.0000	0.0000	0.0014	0.0000	0.0008	0.0000
Wo	1.0	1.1	1.1	0.9	0.9	0.9	1.1	1.0	1.2	1.1	1.1	1.1
En	90.6	91.1	90.7	91.9	91.1	91.2	91.3	91.1	91.3	91.3	91.0	91.3
Fs	8.4	7.8	8.2	7.2	8.0	7.9	7.6	7.9	7.5	7.6	7.8	7.6
Mg/Mg+Fe(t)	91.5	92.0	91.7	91.7	91.5	92.0	92.3	92.0	92.4	92.3	92.1	92.3

Table 4.2b. Representative orthopyroxene analyses of the deformed sheared lherzolites.

Sample	DSL 1.1			DSL 1	DSL 3.3		DSL 3		DSL 4.2			
SiO2	56.61	56.98	56.36	56.42	55.81	55.46	55.81	56.14	55.48	55.18	56.23	56.27
TiO2	0.16	0.18	0.04	0.09	0.00	0.00	0.00	0.11	0.09	0.00	0.05	0.03
Al2O3	2.66	2.06	2.76	2.95	3.82	3.61	3.62	3.45	3.60	4.43	2.91	3.30
FeO	5.18	4.93	5.47	4.46	6.34	5.24	5.16	6.08	5.31	5.71	4.87	6.28
Fe2O3	0.52	1.01	0.44	1.93	0.00	1.33	1.33	0.18	0.91		1.22	0.08
MnO	0.28	0.18	0.00	0.00	0.25	0.04	0.12	0.17	0.17	0.17	0.16	0.04
MgO	34.55	35.18	34.35	34.96	33.23	33.86	33.96	33.83	33.64	31.25	34.53	33.81
CaO	0.59	0.36	0.56	0.59	0.71	0.49	0.60	0.51	0.65	0.68	0.54	0.55
Na2O	0.00	0.00	0.00	0.00	0.00	0.00	0.00	0.00	0.00	0.00	0.00	0.00
K2O	0.00	0.00	0.00	0.00	0.00	0.01	0.05	0.00	0.04	0.00	0.00	0.00
Cr2O3	0.33	0.13	0.43	0.35	0.40	0.38	0.28	0.39	0.40	0.56	0.30	0.29
Total	100.88	101.02	100.41	101.75	100.55	100.43	100.93	100.87	100.28	97.97	100.81	100.64
				Number of Ions on the Basis of 6 (O)								
Si	1.9341	1.9441	1.9341	1.9181	1.9177	1.9108	1.9133	1.9214	1.9129	1.9118	1.9270	1.9286
Al(4)	0.0659	0.0559	0.0659	0.0819	0.0823	0.0892	0.0867	0.0786	0.0871	0.0882	0.0730	0.0714
Al(6)	0.0412	0.0268	0.0458	0.0363	0.0725	0.0572	0.0596	0.0607	0.0591	0.0924	0.0443	0.0519
Ti	0.0041	0.0047	0.0011	0.0023	0.0000	0.0000	0.0000	0.0027	0.0022	0.0000	0.0014	0.0008
Fe(2)	0.1478	0.1404	0.1567	0.1262	0.1821	0.1505	0.1474	0.1739	0.1527	0.1655	0.1391	0.1799
Fe(3)	0.0133	0.0258	0.0112	0.0491	0.0001	0.0345	0.0343	0.0047	0.0234		0.0314	0.0020
Mn	0.0082	0.0053	0.0000	0.0000	0.0071	0.0011	0.0034	0.0050	0.0050	0.0049	0.0045	0.0010
Mg	1.7585	1.7878	1.7559	1.7703	1.7007	1.7380	1.7341	1.7246	1.7278	1.6127	1.7626	1.7265
Cr	0.0089	0.0036	0.0116	0.0094	0.0109	0.0105	0.0076	0.0106	0.0110	0.0152	0.0082	0.0079
Ca	0.0217	0.0133	0.0207	0.0216	0.0259	0.0181	0.0219	0.0188	0.0239	0.0994	0.0199	0.0201
Na	0.0000	0.0000	0.0000	0.0000	0.0000	0.0000	0.0000	0.0000	0.0000	0.0000	0.0000	0.0000
K	0.0000	0.0000	0.0000	0.0000	0.0000	0.0004	0.0021	0.0000	0.0019	0.0000	0.0000	0.0000
Wo	1.1	0.7	1.1	1.1	1.4	1.0	1.2	1.0	1.3	5.3	1.0	1.0
En	91.2	92.1	90.8	92.3	89.1	91.2	91.1	89.9	90.7	85.9	91.7	89.6
Fs	7.7	7.2	8.1	6.6	9.5	7.9	7.7	9.1	8.0	8.8	7.2	9.3
Mg/Mg+Fe(t)	91.6	91.5	91.3	91.0	90.3	90.4	90.5	90.6	90.7	90.7	91.2	90.5

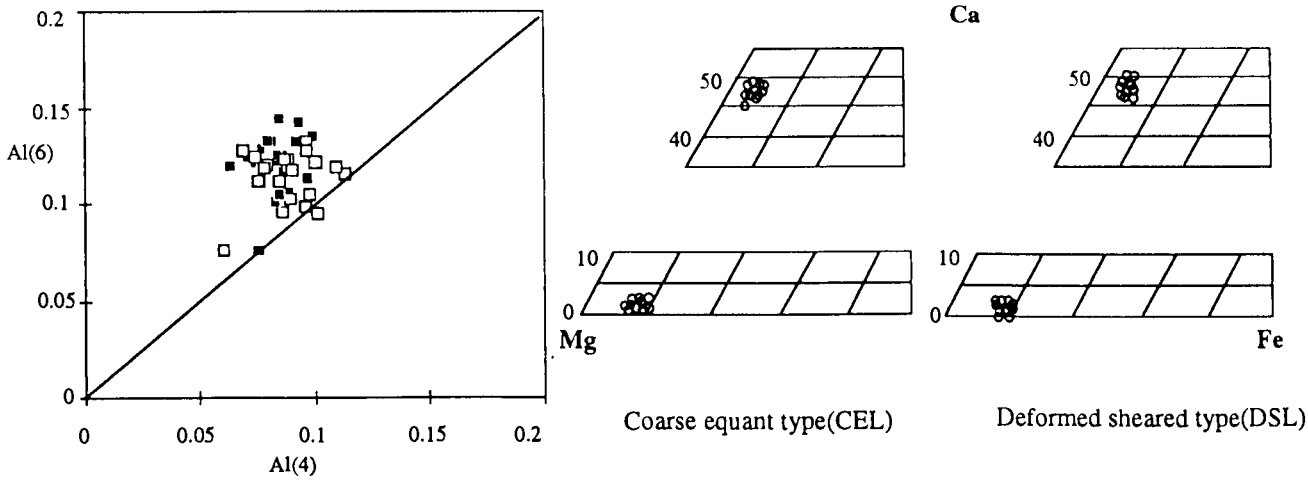

Fig. 4.2a. Pyroxene compositions for the Mt Gambier spinel lherzolites. Symbols; filled squares - CEL, open squares -DSL.

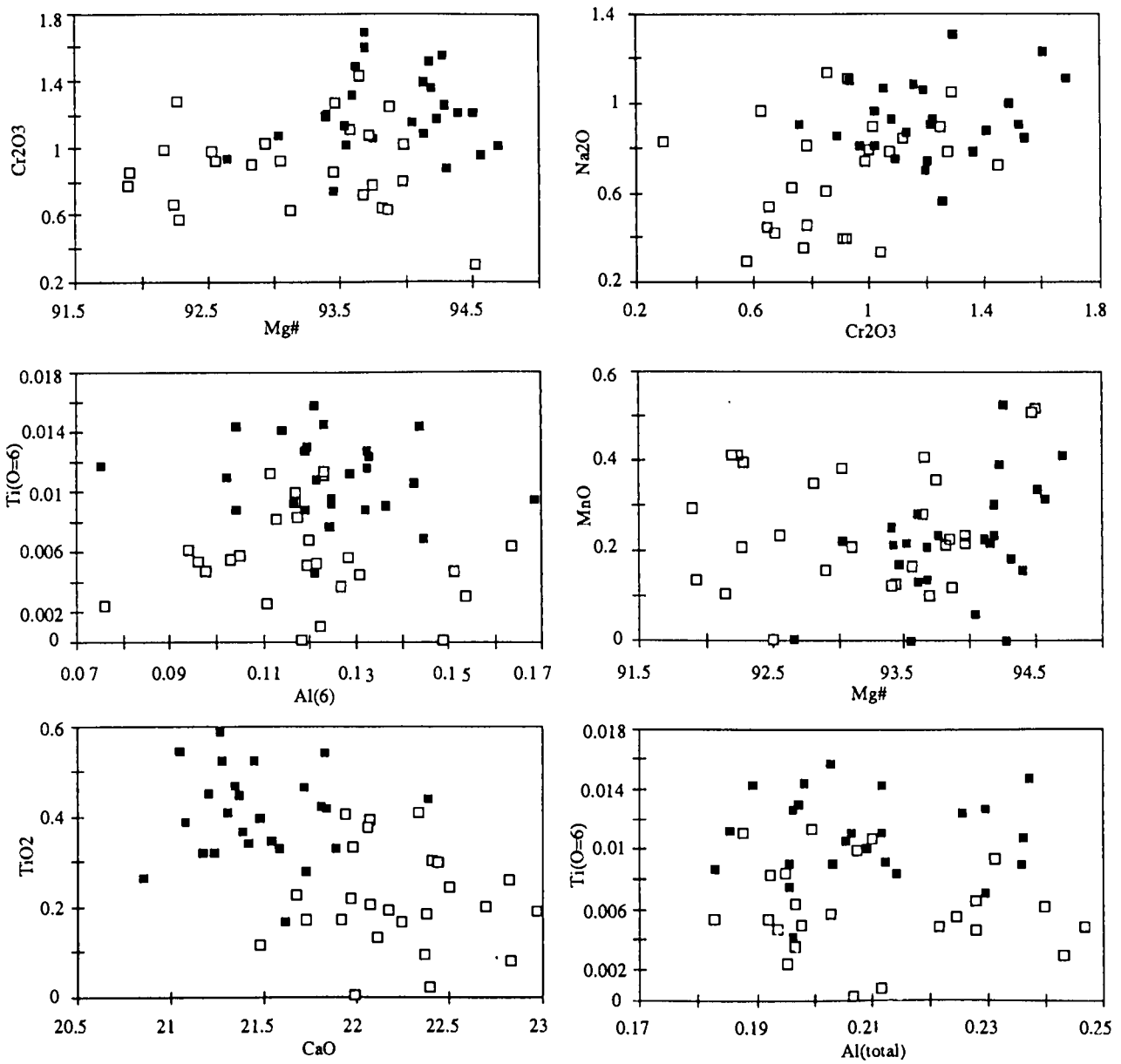

Fig. 4.2b. Clinopyroxene compositions for the Mt Gambier spinel lherzolites.

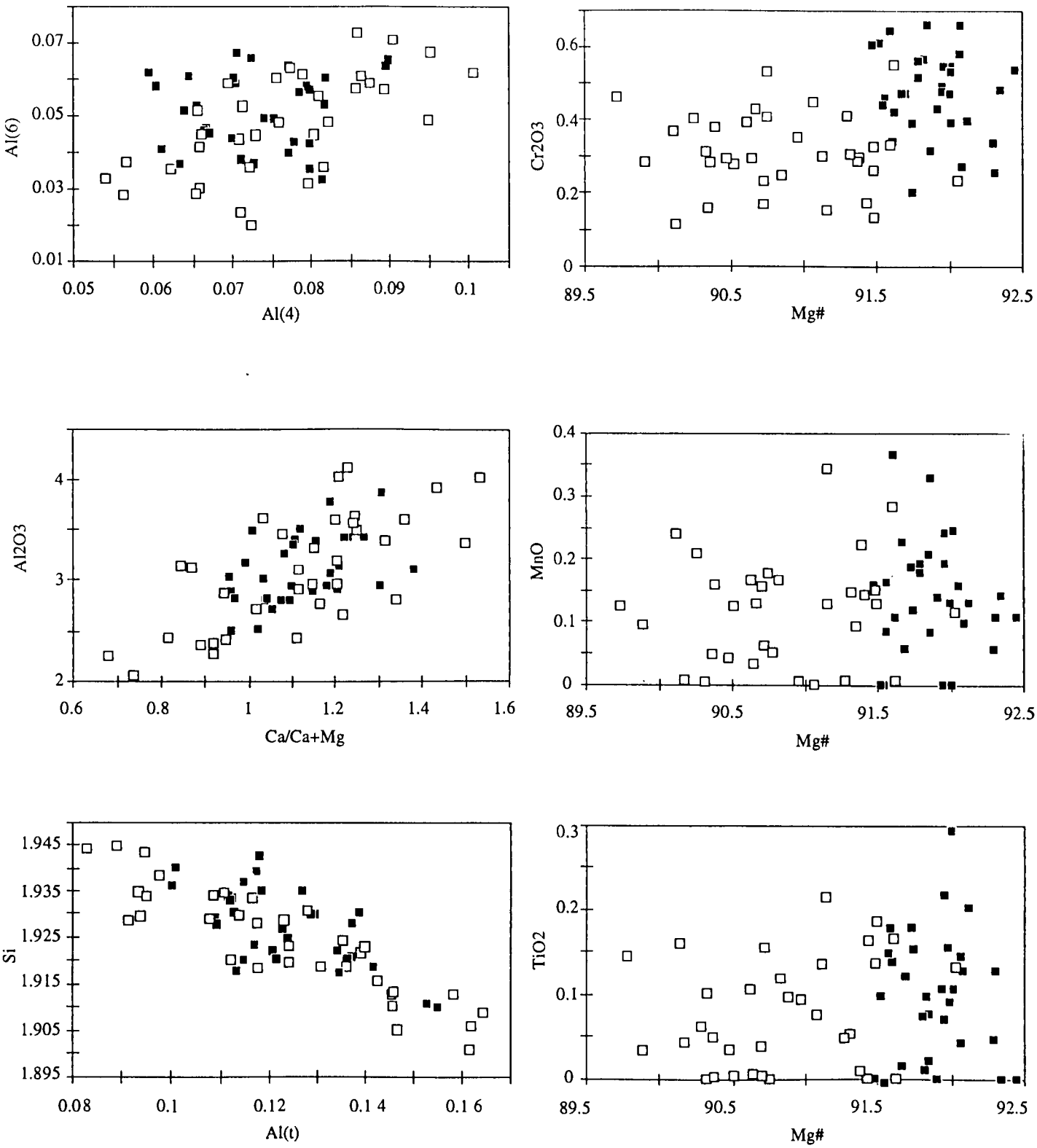

Fig. 4.3. Orthopyroxene compositions of the Mt Gambier spinel lherzolites. Symbols as for Fig. 4.2a.

Table 4.3a. Representative olivine analyses of the coarse equant lherzolites.

Sample	CEL 1				CEL 3.1		CEL 3.2				CEL 3.3	
SiO2	41.34	41.07	41.14	41.19	41.59	41.09	41.43	40.90	41.07	41.04	40.95	41.30
TiO2	0.10	0.00	0.00	0.00	0.00	0.09	0.00	0.09	0.00	0.00	0.26	0.09
Al2O3	0.29	0.43	0.65	0.39	0.41	0.21	0.41	0.28	0.43	0.42	0.21	0.54
FeO	8.70	8.60	8.78	8.54	8.50	8.43	8.41	8.28	8.36	8.35	8.47	8.51
Fe2O3	0.00	0.25	0.00	0.00	0.00	0.00	0.00	0.00	0.00	0.00	0.00	0.00
MnO	0.19	0.20	0.22	0.10	0.12	0.06	0.31	0.19	0.17	0.14	0.06	0.10
MgO	50.02	50.38	49.85	50.05	50.23	50.35	50.04	49.97	50.16	50.35	50.10	50.19
CaO	0.09	0.00	0.00	0.15	0.05	0.01	0.07	0.06	0.10	0.09	0.15	0.10
Na2O	0.00	0.00	0.00	0.00	0.00	0.00	0.00	0.00	0.00	0.00	0.00	0.00
K2O	0.00	0.00	0.02	0.05	0.00	0.00	0.00	0.00	0.00	0.00	0.00	0.04
Cr2O3	0.00	0.00	0.06	0.23	0.00	0.00	0.00	0.07	0.00	0.14	0.25	0.04
Total	100.73	100.94	100.71	100.67	100.90	100.22	100.66	99.84	100.29	100.53	100.43	100.90
					Number of Ions on the Basis of 4 (O)							
Si	1.0000	0.9927	0.9956	0.9968	1.0022	0.9974	1.0015	0.9969	0.9965	0.9938	0.9935	0.9963
Al	0.0082	0.0122	0.0184	0.0110	0.0116	0.0059	0.0116	0.0081	0.0123	0.0119	0.0060	0.0153
Ti	0.0017	0.0000	0.0000	0.0001	0.0000	0.0016	0.0000	0.0017	0.0000	0.0000	0.0048	0.0016
Fe(2)	0.1760	0.1736	0.1776	0.1727	0.1713	0.1711	0.1699	0.1687	0.1695	0.1690	0.1718	0.1715
Fe(3)	0.0000	0.0046	0.0000	0.0000	0.0000	0.0000	0.0000	0.0000	0.0000	0.0000	0.0000	0.0000
Mn	0.0040	0.0041	0.0045	0.0020	0.0025	0.0012	0.0063	0.0038	0.0036	0.0028	0.0011	0.0020
Mg	1.8021	1.8138	1.7972	1.8042	1.8030	1.8208	1.8016	1.8146	1.8129	1.8163	1.8106	1.8033
Ca	0.0022	0.0001	0.0000	0.0038	0.0013	0.0002	0.0019	0.0015	0.0026	0.0024	0.0038	0.0025
Na	0.0000	0.0000	0.0000	0.0000	0.0000	0.0000	0.0000	0.0000	0.0000	0.0000	0.0000	0.0000
K	0.0000	0.0001	0.0005	0.0014	0.0000	0.0000	0.0000	0.0000	0.0000	0.0001	0.0000	0.0014
Cr	0.0000	0.0000	0.0011	0.0044	0.0000	0.0000	0.0000	0.0013	0.0000	0.0027	0.0047	0.0008
Mg/Mg+Fe(t)	91.1	91.1	91.0	91.3	91.3	91.4	91.4	91.5	91.4	91.5	91.3	91.3

Table 4.3b. Representative olivine analyses of the deformed sheared lherzolites .

	DSL 1		DSL 1.1	DSL 3.3			DSL 4.2				DSL 4.3	DSL 4.4
SiO2	41.53	41.21	41.37	41.32	41.47	41.29	41.09	41.34	41.31	40.74	41.16	41.08
TiO2	0.07	0.10	0.10	0.00	0.00	0.06	0.00	0.00	0.06	0.00	0.06	0.01
Al2O3	0.43	0.31	0.24	0.49	0.31	0.35	0.21	0.53	0.29	0.21	0.29	0.30
FeO	8.07	8.99	8.58	9.37	9.35	9.45	9.72	9.05	8.99	9.34	9.27	9.91
Fe2O3	0.00	0.00	0.00	0.00	0.00	0.00	0.00	0.00	0.00	0.00	0.00	0.00
MnO	0.00	0.27	0.11	0.13	0.13	0.17	0.24	0.13	0.16	0.13	0.21	0.09
MgO	50.63	50.20	50.60	49.93	49.88	49.54	49.53	49.63	49.78	49.31	49.82	49.56
CaO	0.24	0.08	0.08	0.04	0.07	0.07	0.13	0.18	0.00	0.00	0.14	0.10
Na2O	0.00	0.00	0.00	0.00	0.00	0.00	0.00	0.00	0.00	0.00	0.00	0.00
K2O	0.02	0.00	0.05	0.00	0.00	0.00	0.00	0.00	0.00	0.00	0.00	0.00
Cr2O3	0.00	0.01	0.03	0.00	0.02	0.15	0.06	0.15	0.00	0.18	0.00	0.06
Total	100.98	101.17	101.16	101.28	101.22	101.07	100.98	101.00	100.59	99.90	100.97	101.11
					Number of Ions on the Basis of 4 (O)							
												0.00
Si	0.9985	0.9947	0.9961	0.9964	1.0004	0.9987	0.9969	0.9986	1.0001	0.9972	0.9965	0.9955
Al	0.0122	0.0088	0.0069	0.0139	0.0087	0.0100	0.0060	0.0149	0.0083	0.0061	0.0084	0.0085
Ti	0.0013	0.0019	0.0019	0.0000	0.0000	0.0011	0.0000	0.0000	0.0011	0.0000	0.0012	0.0002
Fe(2)	0.1621	0.1814	0.1726	0.1889	0.1885	0.1910	0.1972	0.1828	0.1822	0.1911	0.1876	0.2007
Fe(3)	0.0000	0.0000	0.0000	0.0000	0.0000	0.0000	0.0000	0.0000	0.0000	0.0000	0.0000	0.0001
Mn	0.0000	0.0055	0.0022	0.0027	0.0027	0.0035	0.0050	0.0027	0.0033	0.0026	0.0044	0.0019
Mg	1.8136	1.8047	1.8151	1.7936	1.7926	1.7848	1.7899	1.7859	1.7973	1.7977	1.7965	1.7890
Ca	0.0061	0.0020	0.0020	0.0011	0.0018	0.0019	0.0033	0.0046	0.0000	0.0000	0.0036	0.0027
Na	0.0000	0.0000	0.0000	0.0000	0.0000	0.0000	0.0000	0.0000	0.0000	0.0000	0.0000	0.0000
K	0.0005	0.0000	0.0017	0.0000	0.0000	0.0000	0.0000	0.0000	0.0000	0.0000	0.0001	0.0000
Cr	0.0000	0.0002	0.0006	0.0000	0.0004	0.0028	0.0012	0.0029	0.0000	0.0034		0.0011
Mg/Mg+Fe(t)	91.79	90.87	91.31	90.47	90.48	90.33	90.07	90.71	90.79	90.39	90.54	89.91

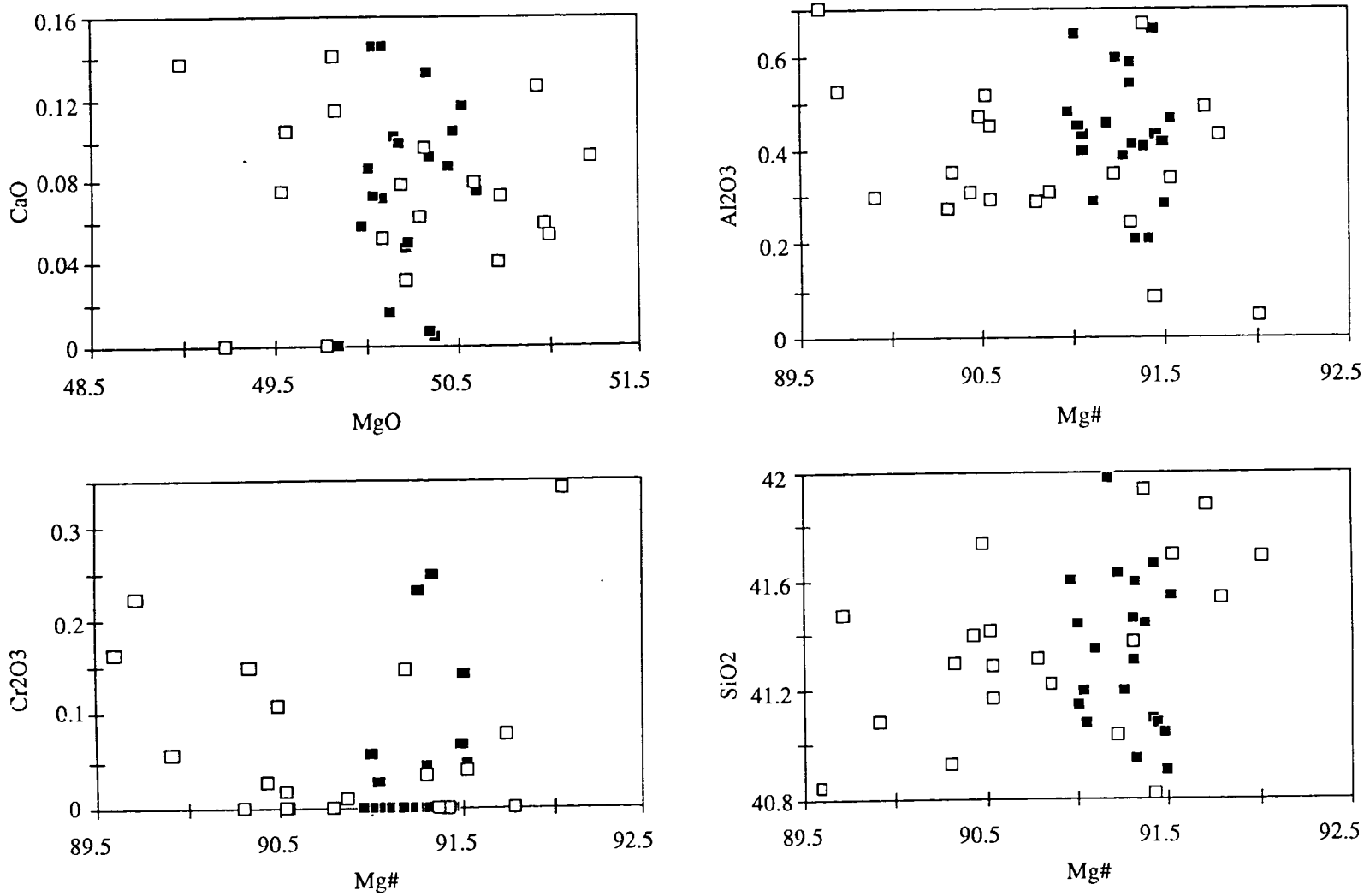

Fig. 4.4. Olivine compositions of the Mt Gambier spinel lherzolites. Symbols as for Fig. 4.2a.

Table 4.4a. Representative spinel analyses of the coarse equant lherzolites.

Sample	CEL 1			CEL 3.1		CEL 3.3			CEL 2			
SiO2	0.26	0.18	0.00	0.21	0.18	0.29	0.24	0.07	0.06	0.00	0.25	0.07
TiO2	0.11	0.11	0.14	0.07	0.25	0.11	0.29	0.16	0.00	0.07	0.00	0.00
Al2O3	47.63	49.06	43.70	43.40	44.02	47.56	47.14	47.23	47.10	46.93	48.37	48.91
FeO	10.30	9.57	11.66	10.99	11.02	8.88	9.79	9.72	12.62	11.82	11.75	11.97
Fe2O3	0.18	1.19	0.50	0.60	0.00	0.31	0.19	0.05	0.15	0.93	0.24	0.13
MnO	0.00	0.28	0.04	0.14	0.11	0.19	0.20	0.24	0.32	0.17	0.26	0.06
MgO	19.66	20.14	18.01	18.41	17.85	20.50	19.68	19.44	17.97	17.80	18.43	18.68
CaO	0.00	0.02	0.00	0.00	0.02	0.00	0.00	0.00	0.00	0.00	0.00	0.00
Na2O	0.00	0.00	0.00	0.00	0.00	0.00	0.00	0.00	0.00	0.11	0.06	0.00
K2O	0.00	0.00	0.01	0.06	0.00	0.00	0.00	0.00	0.00	0.03	0.00	0.00
Cr2O3	23.02	21.24	26.58	26.91	27.01	23.42	22.58	22.96	22.76	22.63	20.40	20.07
NiO									0.29	0.05	0.27	0.40
Total	101.16	101.79	100.62	100.79	100.48	101.26	100.10	99.89	101.27	100.54	100.04	100.28
				Number of Ions on the Basis of 32 (O)								
Si	0.0562	0.0379	0.0000	0.0450	0.0398	0.0623	0.0523	0.0523	0.0120	0.0000	0.0540	0.0154
Al	11.9586	12.2057	11.2915	11.1827	11.2922	11.8818	11.9451	11.9451	11.9998	12.0123	12.2950	12.3738
Ti	0.0167	0.0174	0.0226	0.0119	0.0412	0.0179	0.0463	0.0080	0.0000	0.0118	0.0000	0.0000
Fe(3)	0.0289	0.1888	0.0817	0.0981	0.0000	0.0489	0.0300	0.0263	0.0239	0.1507	0.0391	0.0218
Cr	3.8757	3.5436	4.6055	4.6491	4.6355	3.9229	3.8369	3.9120	3.8381	3.8839	3.4771	3.4044
Mg	6.2398	6.3344	5.8815	5.9955	5.7751	6.4751	6.3033	6.2436	5.7881	5.7581	5.9222	5.9734
Fe(2)	1.8331	1.6824	2.1338	2.0056	2.1449	1.5717	1.7591	1.7519	2.2709	2.1400	2.1156	2.1468
Mn	0.0000	0.0502	0.0077	0.0266	0.0209	0.0344	0.0362	0.0446	0.0594	0.0317	0.0482	0.0106
Ca	0.0000	0.0034	0.0000	0.0000	0.0056	0.0009	0.0000	0.0000	0.0000	0.0000	0.0000	0.0002
Na	0.0000	0.0000	0.0000	0.0000	0.0000	0.0000	0.0000	0.0000	0.0000	0.0465	0.0252	0.0000
K	0.0000	0.0000	0.0019	0.0176	0.0000	0.0000	0.0000	0.0000	0.0000	0.0079	0.0000	0.0000
Ni									0.0505	0.0092	0.0470	0.0686

Table 4.4b. Representative spinel analyses of the deformed sheared lherzolites.

	DSL 1			DSL 1.1			DSL 3.4					
SiO2	0.13	0.27	0.30	0.34	0.00	0.13	0.31	0.24	0.16	0.24	0.25	0.18
TiO2	0.00	0.20	0.00	0.00	0.26	0.23	0.24	0.00	0.03	0.10	0.00	0.25
Al2O3	48.39	47.74	48.80	46.36	46.48	46.53	53.47	54.64	55.43	56.91	56.96	58.56
FeO	11.86	11.92	12.06	12.49	12.37	12.18	12.00	12.55	12.10	12.15	11.98	11.21
Fe2O3	0.43	0.00	0.00	0.00	0.57	0.00	0.00	0.09	0.00	0.00	0.05	0.00
MnO	0.32	0.38	0.19	0.15	0.12	0.06	0.17	0.23	0.08	0.25	0.29	0.13
MgO	18.14	18.12	18.06	17.52	18.08	17.96	18.15	18.71	19.11	19.02	19.02	19.68
CaO	0.00	0.00	0.00	0.05	0.00	0.00	0.04	0.11	0.09	0.00	0.00	0.00
Na2O	0.00	0.00	0.00	0.00	0.00	0.00	0.00	0.00	0.00	0.00	0.00	0.00
K2O	0.00	0.00	0.00	0.00	0.00	0.01	0.00	0.00	0.00	0.00	0.00	0.00
Cr2O3	20.97	21.30	20.60	23.12	23.83	22.93	15.43	15.14	14.56	12.97	11.47	11.55
Total	100.23	99.93	100.00	100.03	101.71	100.04	99.81	101.72	101.56	101.63	100.02	101.57
				Number of Ions on the Basis of 32 (O)								
Si	0.0278	0.0585	0.0653	0.0750	0.0000	0.0292	0.0652	0.0505	0.0332	0.0487	0.0527	0.0366
Al	12.3151	12.1798	12.3980	11.9128	11.7944	11.9323	13.3497	13.3993	13.5414	13.8188	13.9999	14.0881
Ti	0.0000	0.0326	0.0000	0.0000	0.0417	0.0380	0.0385	0.0000	0.0043	0.0156	0.0000	0.0382
Fe(3)	0.0699	0.0000	0.0000	0.0000	0.0925	0.0000	0.0000	0.0145	0.0003	0.0000	0.0083	0.0000
Cr	3.5786	3.6433	3.5100	3.9832	4.0546	3.9434	2.5835	2.4902	2.3854	2.1112	1.8905	1.8633
Mg	5.8358	5.8437	5.8004	5.6899	5.8013	5.8238	5.7292	5.8000	5.9023	5.8394	5.9098	5.9864
Fe(2)	2.1377	2.1702	2.1730	2.2770	2.2234	2.2168	2.1252	2.1838	2.0977	2.0933	2.0889	1.9136
Mn	0.0577	0.0693	0.0340	0.0278	0.0222	0.0102	0.0302	0.0408	0.0138	0.0439	0.0518	0.0232
Ca	0.0000	0.0000	0.0000	0.0111	0.0000	0.0000	0.0083	0.0244	0.0209	0.0000	0.0000	0.0000
Na	0.0000	0.0000	0.0000	0.0000	0.0000	0.0000	0.0000	0.0000	0.0000	0.0000	0.0000	0.0000
K	0.0000	0.0000	0.0000	0.0000	0.0000	0.0024	0.0000	0.0000	0.0000	0.0000	0.0000	0.0000
Ni												

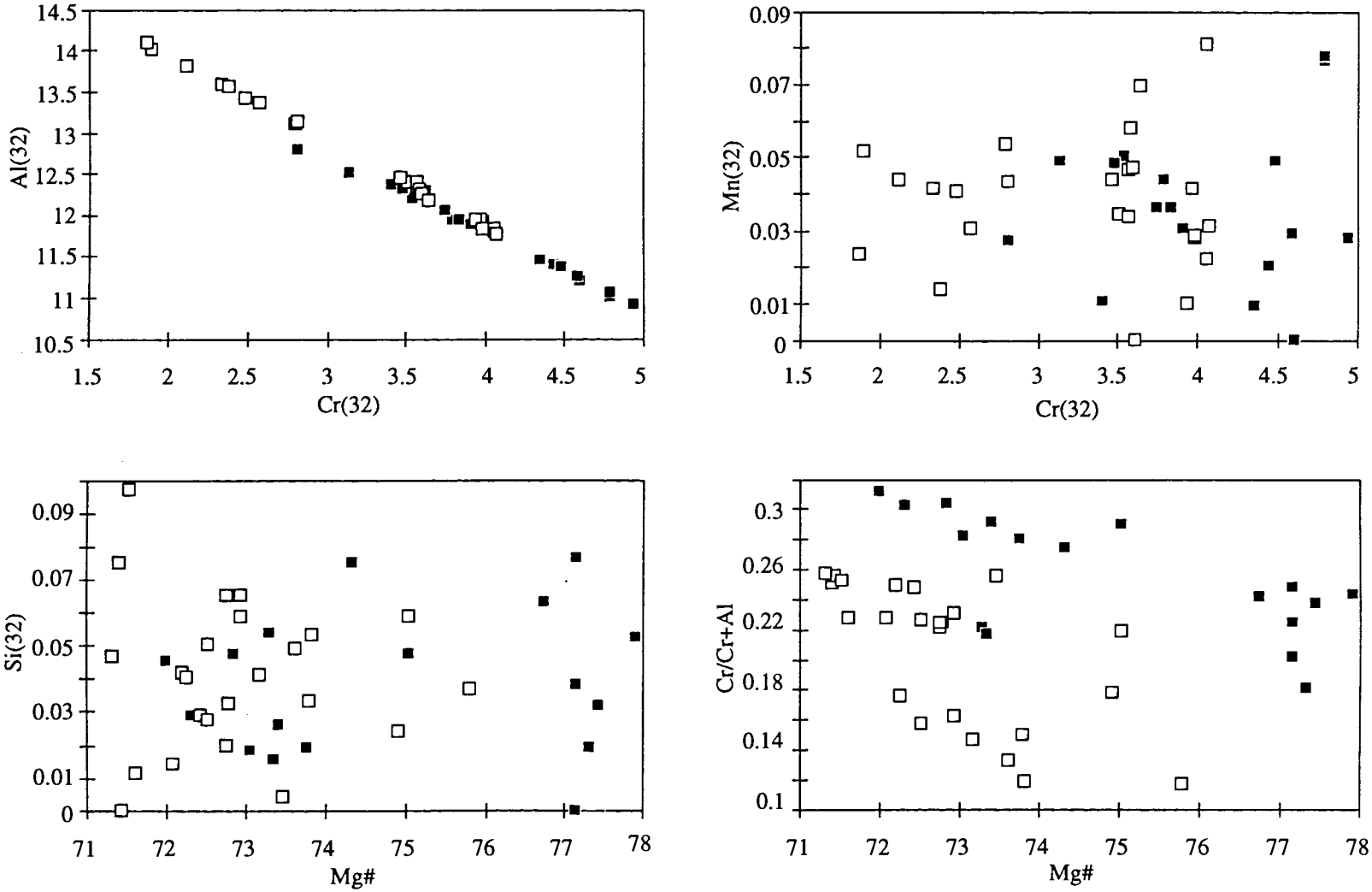

Fig. 4.5. Spinel compositions of the Mt Gambier spinel lherzolites. Symbols as for Fig.4.2a.

4.5. Whole Rock chemistry

4.5.1. Introduction

Twenty-three selected samples of the Mt Gambier spinel lherzolites were analysed for major and trace element compositions by XRF in the University of the Adelaide. Details of analytical methods and sample preparation are shown in the Appendix 1. Results are shown in the Table 4.5 and 4.6.

4.5.2. Major element composition

The spinel lherzolites show predominantly *ol* - normative composition (Fig. 4.6). They contain SiO_2 (43-46 wt %), Al_2O_3 (0.8-3.5 wt %), CaO (0.6-2.4 wt %), Na_2O (0.17-0.36 wt %), K_2O (<0.02 wt %), and restricted range of Mg#, 90-92.7 (90-91.6 for CELs, 90.9-92.7 for DSLs).

In the Mg#-major element relationships, Al_2O_3, CaO, K_2O, Na_2O and TiO_2 decrease and SiO_2 increase with Mg# (Fig. 4.7). Similar major element variations were reported from xenolith studies of Victoria (e.g. Nickel and Green, 1984; Griffin *et al.*, 1988) and of French (Downes, 1987). Nickel and Green (1984) and Griffin *et al.* (1988) indicated that the xenoliths entrained from the Victorian basalts show increase of Al_2O_3, CaO, weak correlations of Na_2O, BaO, Sr, Zr, with MgO and low concentrations of K_2O, P_2O_5, Rb, Y and Nb. In the study of the French spinel lherzolites, Downes (1987) indicated that the xenoliths show good correlations in the MgO-CaO, Al_2O_3, SiO_2, and TiO_2 relationships.

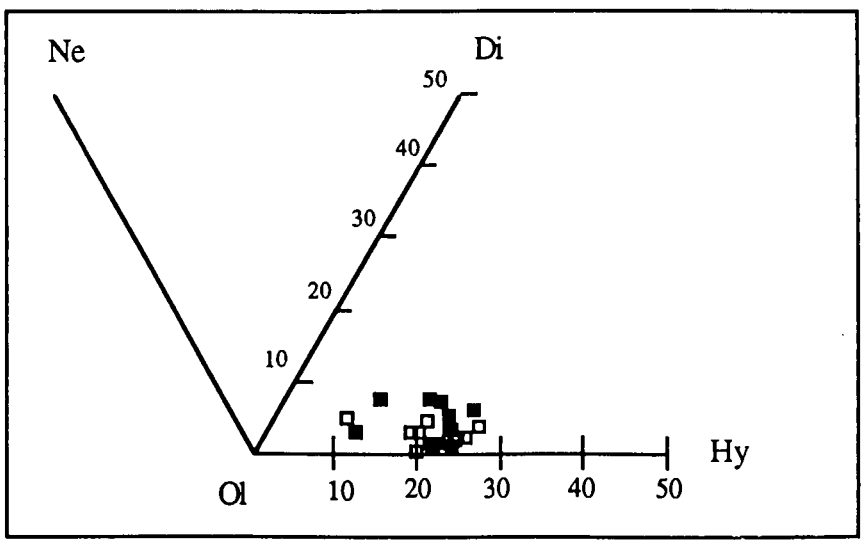

Fig. 4.6. C.I.P.W. normative compositions of the Mt Gambier spinel lherzolites. Symbols as for Fig. 4.2a.

Table 4.5. Major element analyses of the Mt Gambier spinel lherzolites.

A)	Coarse equant type										
Sample	UCEL 1	UCEL 2	UCEL 3	UCEL 4	UCEL 5	UCEL 6	UCEL 7	UCEL 8	UCEL 9	UCEL 10	UCEL 11
SiO2	43.24	44.86	45.27	44.74	45.00	44.84	45.80	43.92	45.05	45.04	44.96
Al2O3	1.07	1.26	3.48	1.30	2.12	1.39	2.07	2.06	2.00	1.78	3.40
Fe2O3#	9.38	8.20	8.54	8.27	8.28	8.24	8.57	8.73	8.07	8.79	8.34
MnO	0.12	0.12	0.13	0.12	0.12	0.12	0.13	0.12	0.12	0.13	0.13
MgO	45.68	44.83	39.40	44.94	42.52	44.69	41.73	42.51	42.41	43.86	39.41
CaO	1.04	0.66	3.03	0.69	1.62	0.80	2.25	2.46	1.97	1.00	2.97
Na2O	0.24	0.27	0.55	0.25	0.32	0.25	0.28	0.36	0.30	0.23	0.46
K2O	0.03	0.05	0.04	0.03	0.02	0.02	0.03	0.02	0.00	0.01	0.03
TiO2	0.06	0.04	0.12	0.05	0.08	0.04	0.07	0.11	0.08	0.07	0.15
P2O5	0.01	0.00	0.02	0.01	0.01	0.01	0.02	0.01	0.00	0.01	0.02
SO3	0.00	0.00	0.00	0.00	0.00	0.00	0.00	0.00	0.00	0.00	0.00
LOI	-0.62	-0.46	-0.49	-0.53	-0.52	-0.51	-0.47	-0.48	-0.36	-0.70	-0.38
Total	100.24	99.83	100.08	99.85	99.58	99.89	100.49	99.82	99.65	100.23	99.49
	C.I.P.W. norm (calculated with Fe2O3/FeO = 0.2)										
Ap	0.02	0	0.05	0.02	0.02	0.02	0.05	0.02	0	0.02	0.05
Il	0.11	0.08	0.23	0.1	0.15	0.08	0.13	0.21	0.15	0.13	0.29
Mt	2.05	1.8	1.87	1.81	1.82	1.8	1.87	1.91	1.77	1.92	1.83
Or	0.18	0.3	0.24	0.18	0.12	0.12	0.18	0.12	0	0.06	0.18
Ab	2.03	2.29	4.67	2.12	2.72	2.12	2.37	3.06	2.55	1.95	3.92
An	1.76	2.09	6.92	2.35	4.32	2.62	4.3	3.97	4.14	3.79	7.19
Di	2.64	0.95	6.32	0.81	2.92	1.02	5.3	6.49	4.51	0.87	5.96
Hy	10.7	20.6	15.51	20.3	20.39	20.72	21.94	10.96	19.76	21.93	16.95
Ol	80.52	71.9	64.21	72.31	67.53	71.49	63.87	73.25	67.12	69.33	63.62
Ne	0	0	0	0	0	0	0	0	0	0	0
Ac	0	0	0	0	0	0	0	0	0	0	0
C	0	0	0	0	0	0	0	0	0	0	0
Q	0	0	0	0	0	0	0	0	0	0	0
Total	100.01	100.01	100.02	100.00	99.99	99.99	100.01	99.99	100.00	100.00	99.99
AN#	46.44	47.72	59.71	52.57	61.36	55.27	64.47	56.47	61.88	66.03	64.72
DI	2.21	2.59	4.91	2.30	2.84	2.24	2.55	3.18	2.55	2.01	4.10
SI	83.99	85.34	82.64	85.34	84.52	85.33	83.88	83.77	84.87	84.33	83.14
LI	-40.72	-37.87	-34.98	-38.13	-36.57	-37.94	-36.39	-38.17	-36.62	-37.75	-34.87

B)	Deformed sheared type											
Sample	DUSL 1	DUSL 2	DUSL 3	DUSL 4	DUSL 5	DUSL 6	DUSL 7	DUSL 8	DUSL 9	DUSL 10	DUSL 11	DUSL 12
SiO2	46.25	45.08	44.64	44.74	43.43	45.07	44.35	44.64	43.30	45.52	44.46	45.22
Al2O3	1.78	1.77	1.52	1.99	1.07	0.84	1.08	0.96	1.30	1.25	1.14	1.40
Fe2O3#	8.15	7.75	8.20	8.27	9.02	8.16	7.56	8.30	8.92	7.13	8.79	8.22
MnO	0.12	0.12	0.12	0.12	0.13	0.12	0.11	0.12	0.13	0.11	0.13	0.12
MgO	44.24	42.38	44.26	43.26	45.67	45.30	46.57	45.49	45.08	45.21	44.70	43.99
CaO	1.41	1.56	1.15	1.89	0.87	0.68	0.38	0.63	1.55	0.93	1.06	1.01
Na2O	0.34	0.23	0.39	0.25	0.37	0.17	0.19	0.23	0.29	0.23	0.24	0.23
K2O	0.01	0.02	0.01	0.00	0.01	0.00	0.01	0.00	0.05	0.01	0.01	0.01
TiO2	0.02	0.02	0.04	0.01	0.02	0.02	0.05	0.03	0.10	0.06	0.03	0.05
P2O5	0.01	0.00	0.01	0.00	0.01	0.00	0.01	0.01	0.01	0.01	0.01	0.01
SO3	0.00	0.00	0.00	-0.01	0.00	0.00	0.00	0.00	0.00	0.00	-0.01	0.01
LOI	-0.49	-0.45	-0.48	-0.49	-0.51	-0.46	-0.45	-0.55	-0.53	-0.36	-0.53	-0.42
Total	101.82	98.47	99.84	100.06	100.08	99.89	99.82	99.87	100.19	100.09	100.02	99.84
	C.I.P.W. norm (calculated with Fe2O3/FeO = 0.2)											
Ap	0.02	0	0.02	0	0.02	0	0.02	0.02	0.02	0.02	0.02	0.02
Il	0.04	0.04	0.08	0.02	0.04	0.04	0.1	0.06	0.19	0.11	0.06	0.1
Mt	1.75	1.72	1.8	1.81	1.97	1.79	1.65	1.82	1.95	1.56	1.92	1.8
Or	0.06	0.12	0.06	0	0.06	0	0.06	0	0.3	0.06	0.06	0.06
Ab	2.83	1.98	3.32	2.12	3.14	1.45	1.62	1.95	2.45	1.95	2.04	1.92
An	3.25	3.81	2.38	4.32	1.23	1.54	1.83	1.59	2.1	2.35	2.01	2.79
Di	2.82	3.21	2.59	4.01	2.39	1.46	0	1.17	4.36	1.74	2.52	1.72
Hy	21.07	23.96	16.72	17.53	10.47	22.84	18.82	19.9	8.75	22.65	17.96	23.28
Ol	68.16	65.16	73.04	70.2	80.68	70.9	75.81	73.49	79.88	69.57	73.41	68.3
Ne	0	0	0	0	0	0	0	0	0	0	0	0
Ac	0	0	0	0	0	0	0	0	0	0	0	0
C	0	0	0	0	0	0	0.09	0	0	0	0	0
Q	0	0	0	0	0	0	0	0	0	0	0	0
Total	100.00	100.00	100.01	100.01	100.00	100.02	100.00	100.00	100.00	100.01	100.00	99.99
AN#	53.45	65.80	41.75	67.08	28.15	51.51	53.04	44.92	46.15	54.65	49.63	59.24
DI	2.89	2.10	3.38	2.12	3.20	1.45	1.68	1.95	2.75	2.01	2.10	1.98
SI	85.20	85.44	85.05	84.90	84.31	85.78	86.93	85.53	84.35	87.17	84.56	85.21
LI	-37.56	-35.87	-37.90	-37.68	-40.17	-38.30	-38.96	-38.71	-40.17	-37.37	-38.84	-37.31

all iron as Fe2O3

AN#= AN/(AN+AB)*100, S.I .(Solidification Index, Kuno), D.I. (Differentiation Index, Thornton and Tuttle,1960) & L.I. (Larsen Index, Larsen, 1938).

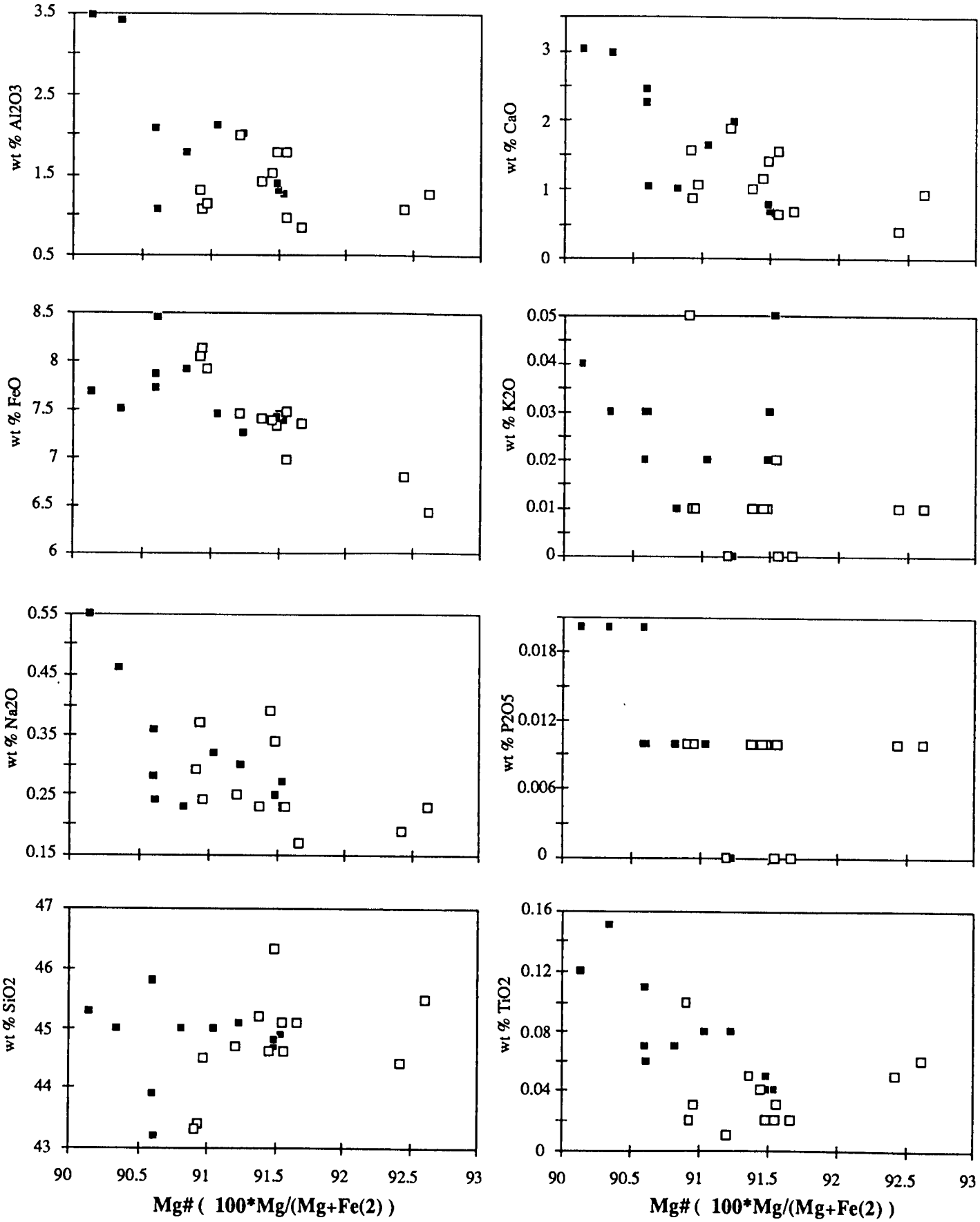

Fig. 4.7a. Mg# versus major element plots of the Mt Gambier spinel lherzolites. Symblos as for Fig. 4.2a.

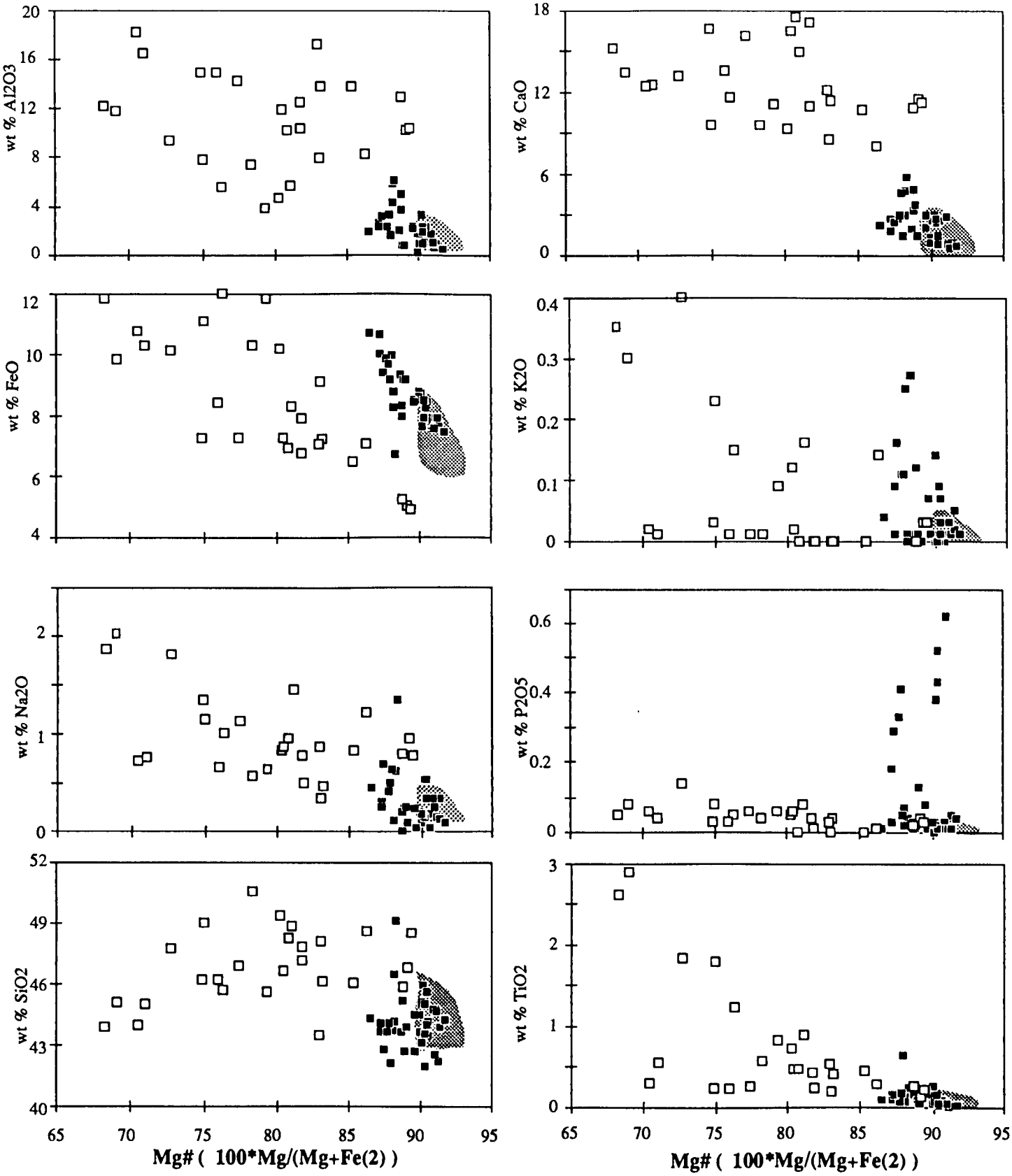

Fig. 4.7b. Mg# -major element plots of the Victorian pyroxenites and lherzolites, their comparisons with the Mt Gambier lherzolites. Symbols; open squares for Victorian pyroxenites, filled squares for Victorian lherzolites, shades area for range of Mt Gambier lhezolites (Data sources; Griffin *et al.*, 1988; O'Reilly and Griffin,1988).

Systematic changes of major elements contents with Mg# between CELs and DSLs can be explained with a simple phase diagram of the anhydrous system fosterite-diopside-enstatite (Yoder, 1976) because in the potential mantle rocks, peridotic mineralogy, Ol+Opx+Cpx+Sp, is common. The high Al_2O_3, CaO, Na_2O and TiO_2 of the Mt Gambier CELs probably reflect the high modal proportion of pyroxenes observed under the microscope. A similar conclusion resulted from studies of Victorian xenoliths (e.g. Frey and Green, 1974; Stolz and Davies, 1988). Stolz and Davies (1988) suggest that clinopyroxene-rich xenoliths show higher Al_2O_3, and CaO contents. Some of the Mt Gambier spinel lherzolites show slightly wide ranges of CaO and Al2O3 contents. These variations may reflect diversities of their primary mineral assemblages.

In addition, there are large differences in the major element compositions of the Mt Gambier spinel lherzolites and samples showing a mantle metasomatism of Victorian (Griffin *et al.*, 1988; O'Reilly and Griffin, 1988) and of French upper mantle xenoliths (Downes, 1987). Generally, the Mt Gambier spinel lherzolites exhibit higher Mg#, lower K_2O, Al_2O_3, CaO contents than the metasomatised xenoliths (Fig. 4.7).

4.5.3. Trace elements and REE

The Mt Gambier spinel lherzolites exhibit high Ni (1950-2600 ppm), Cr (2400-3600 ppm), Co (110-135 ppm). Generally, total contents of the most LIL and REE are low, below the detection limit of XRF (Appendix 1). These characterictics, depletions in the most of LIL and LREE, are compared to the metasomatised lherzolites and pyroxenites showing a enrichment in most of incompatible elements from the eastern Australia. In the Mt Gambier lherzolites, the CELs show enrichments in the most of elements (P, Sc, Ta, Rb, Sr, Nb, Mo, Au, Cd, Sb, Ba, Hf, W, Tl, U) relative to the DSLs. In the Mg# -trace element relationships, Sr, Zn, Sc, V and Co decrease and Cr and Ni increase with Mg#.

In the Mt Gambier lherzolites, increasing Cr and decreasing Al with increasing Mg# may be due to the relative abundances of clinopyroxene and spinel (Carswell *et al.* 1984). High Cr and low Al with Mg# in the DSLs are consistent with high modal proportions of clinopyroxenes whereas increasing Ni and Cr with Mg# may be explained in terms of increasing pyroxene/olivine ratios (O'Reilly and Griffin, 1988). In the Mt Gambier lherzolites, the olivine-rich DSLs exhibit higher Mg#, Ni and Cr contents relative to the CELs. Pb, U and Th contents of the Mt Gambier lherzolites are low, suggesting that these element contents of the Mt Gambier lherzolites can not be explained by the influence of apatite as mentioned in Victorian lherzolites (Griffin *et al.*, 1988).

Table 4.6. Trace element ananyses of the Mt Gambier spinel herzolites.

A) **Coarse equant type**

Sample	UCEL 1	UCEL 2	UCEL 3	UCEL 4	UCEL 5	UCEL 6	UCEL 7	UCEL 8	UCEL 9	UCEL 10	UCEL 11
Ni	2540	2159	2010	2110	2388	2027	1980	2219	2068	2197	2086
Sc	5.5	5	11.7	4.4	8.1	5.8	10.2	9.4	8.8	7.1	13.5
Cr	1902	2591	3385	3078	2748	3405	2757	2722	3129	2548	2701
V	37.7	34.9	71	36.6	51.6	37.6	61.4	54.8	53.4	45.4	73.9
Co	136	127	118	135	134	130	115	139	132	128	116
Sr	6.6	4.3	27	3.7	16.3	6.4	15.9	9.4	6.3	6.1	23.7
Zn	47.9	39.5	52.2	40.4	43	47.7	39.7	38.7	43.4	39.6	55
Zr	4.9	4.7	9	5	7.4	5.3	8	6.4	5.3	5.7	12.8
Rb	n.d.	n.d.	n.d.	n.d.	n.d.	n.d.	1.7	n.d.	n.d.	n.d.	n.d.
Ba	4	n.d.	12	n.d.	9	n.d.	15	4	n.d.	4	11
Th	n.d.	n.d.	n.d.	n.d.	n.d.	n.d.	n.d.	n.d.	n.d.	n.d.	n.d.
Nb	n.d.	n.d.	n.d.	n.d.	n.d.	n.d.	n.d.	n.d.	n.d.	n.d.	1.5
La	5	5	6	n.d.	6	5	6	5	5	5	n.d.
Ce	n.d.	n.d.	n.d.	n.d.	n.d.	n.d.	n.d.	n.d.	n.d.	n.d.	3
Nd	n.d.	n.d.	n.d.	n.d.	n.d.	n.d.	n.d.	n.d.	n.d.	n.d.	n.d.
Y	n.d.	n.d.	4.5	n.d.	n.d.	n.d.	n.d.	2.5	2	n.d.	2.8
Pb	n.d.	n.d.	n.d.	n.d.	n.d.	3.3	n.d.	4.2	n.d.	n.d.	n.d.
U	n.d.	n.d.	n.d.	n.d.	n.d.	n.d.	n.d.	n.d.	n.d.	n.d.	n.d.
Ga	n.d.	n.d.	n.d.	n.d.	n.d.	n.d.	n.d.	n.d.	n.d.	n.d.	3
Cu	n.d.	n.d.	9.1	4.3	4.9	6	n.d.	7.8	n.d.	6.9	18

B) **Deformed sheared type**

Sample	DUSL 1	DUSL 2	DUSL 3	DUSL 4	DUSL 5	DUSL 6	DUSL 7	DUSL 8	DUSL 9	DUSL 10	DUSL 11	DUSL 12
Ni	2081	2264	2251	2295	2442	2474	2410	2238	2403	2299	2309	1752
Sc	7.1	7.2	6.1	7.5	5.8	6.1	3.1	4.2	5.4	4.4	7.2	5.9
Cr	3484	3337	3220	3132	3058	2731	3087	2951	2912	2704	2984	2511
V	47.2	46.6	40.5	48.1	37.4	34.1	25.7	27.9	39.3	34.4	43	41.5
Co	129	126	130	131	131	125	117	123	127	110	122	115
Sr	8.5	2.2	6.6	1.7	3.9	6.9	2.3	3.5	6.5	5.5	5.9	5.8
Zn	44.4	41.9	44.3	46.5	44.6	40.2	43.5	37.6	48.3	38.5	46.4	36
Zr	4.8	4.8	4.8	3.8	4.2	3	6.1	4.2	7.4	12.6	4.4	4.7
Rb	n.d.	n.d.	n.d.	n.d.	n.d.	n.d.	n.d.	n.d.	2.5	n.d.	n.d.	n.d.
Ba	4	4	3	3	n.d.	n.d.	3	n.d.	19	n.d.	n.d.	7
Th	n.d.	n.d.	n.d.	n.d.	n.d.	n.d.	n.d.	n.d.	n.d.	n.d.	n.d.	n.d.
Nb	n.d.	n.d.	n.d.	n.d.	n.d.	n.d.	n.d.	n.d.	n.d.	n.d.	n.d.	n.d.
La	6	4	4	6	6	5	5	4	4	5	4	n.a.
Ce	n.d.	n.d.	n.d.	n.d.	n.d.	n.d.	n.d.	n.d.	n.d.	n.d.	n.d.	n.d.
Nd	n.d.	n.d.	n.d.	n.d.	n.d.	n.d.	n.d.	n.d.	n.d.	n.d.	n.d.	n.d.
Y	n.d.	n.d.	n.d.	n.d.	n.d.	n.d.	n.d.	n.d.	n.d.	n.d.	n.d.	n.d.
Pb	n.d.	n.d.	n.d.	n.d.	n.d.	n.d.	n.d.	n.d.	n.d.	n.d.	n.d.	n.d.
U	n.d.	n.d.	n.d.	n.d.	n.d.	n.d.	n.d.	n.d.	n.d.	n.d.	n.d.	n.d.
Ga	n.d.	n.d.	n.d.	n.d.	n.d.	n.d.	n.d.	n.d.	n.d.	n.d.	n.d.	n.d.
Cu	9.3	6.5	7.3	5.4	n.d.	n.d.	3.8	1.7	5.9	6.4	4	n.d.

n.d. indicates an element not detected.

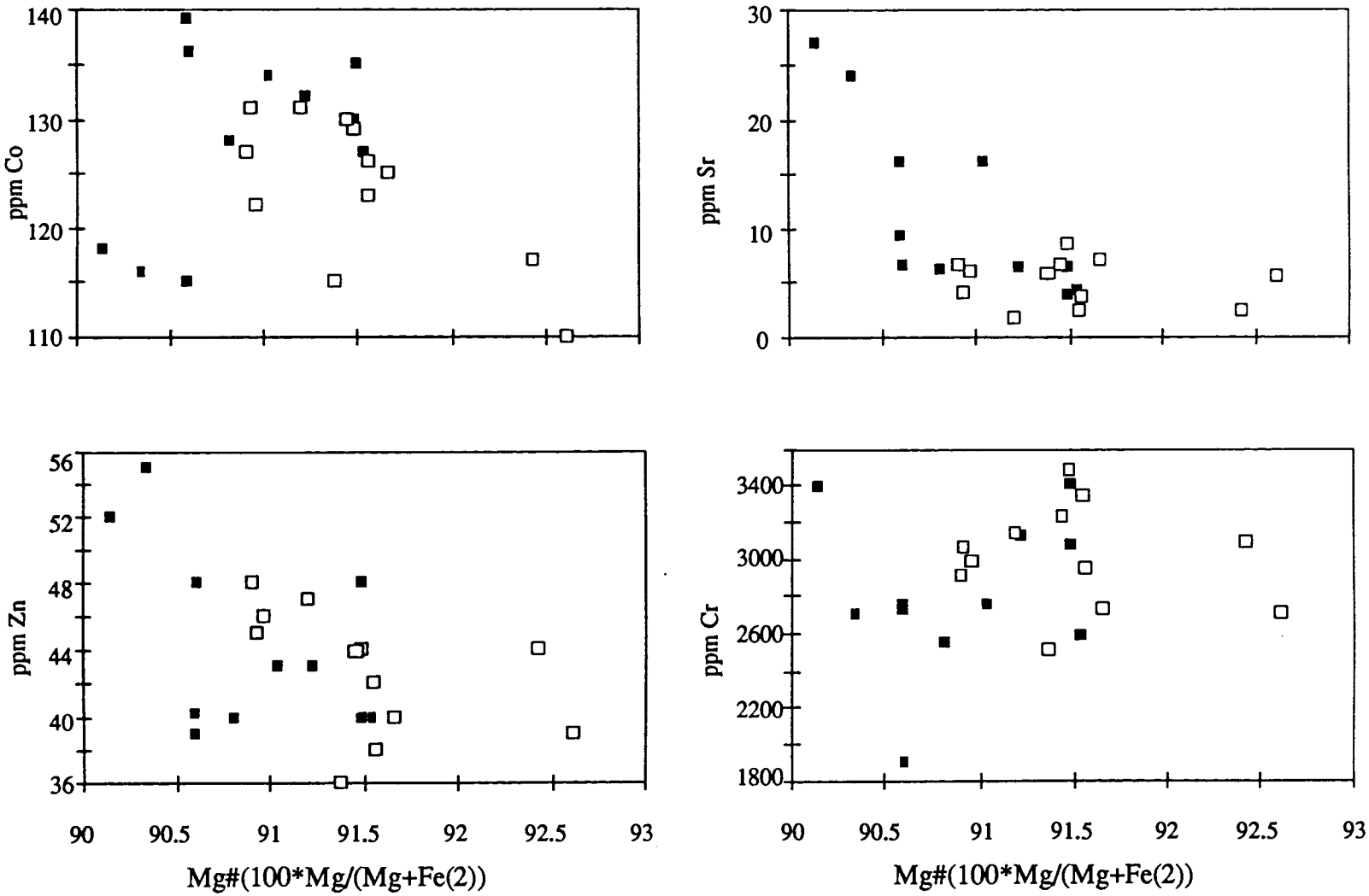
140
130
120
110
ppm Co
30
20
10
0
ppm Sr
56
52
48
44
40
36
ppm Zn
3400
3000
2600
2200
1800
ppm Cr
90
90.5
91
91.5
92
92.5
93
Mg#(100*Mg/(Mg+Fe(2))
Mg#(100*Mg/(Mg+Fe(2))

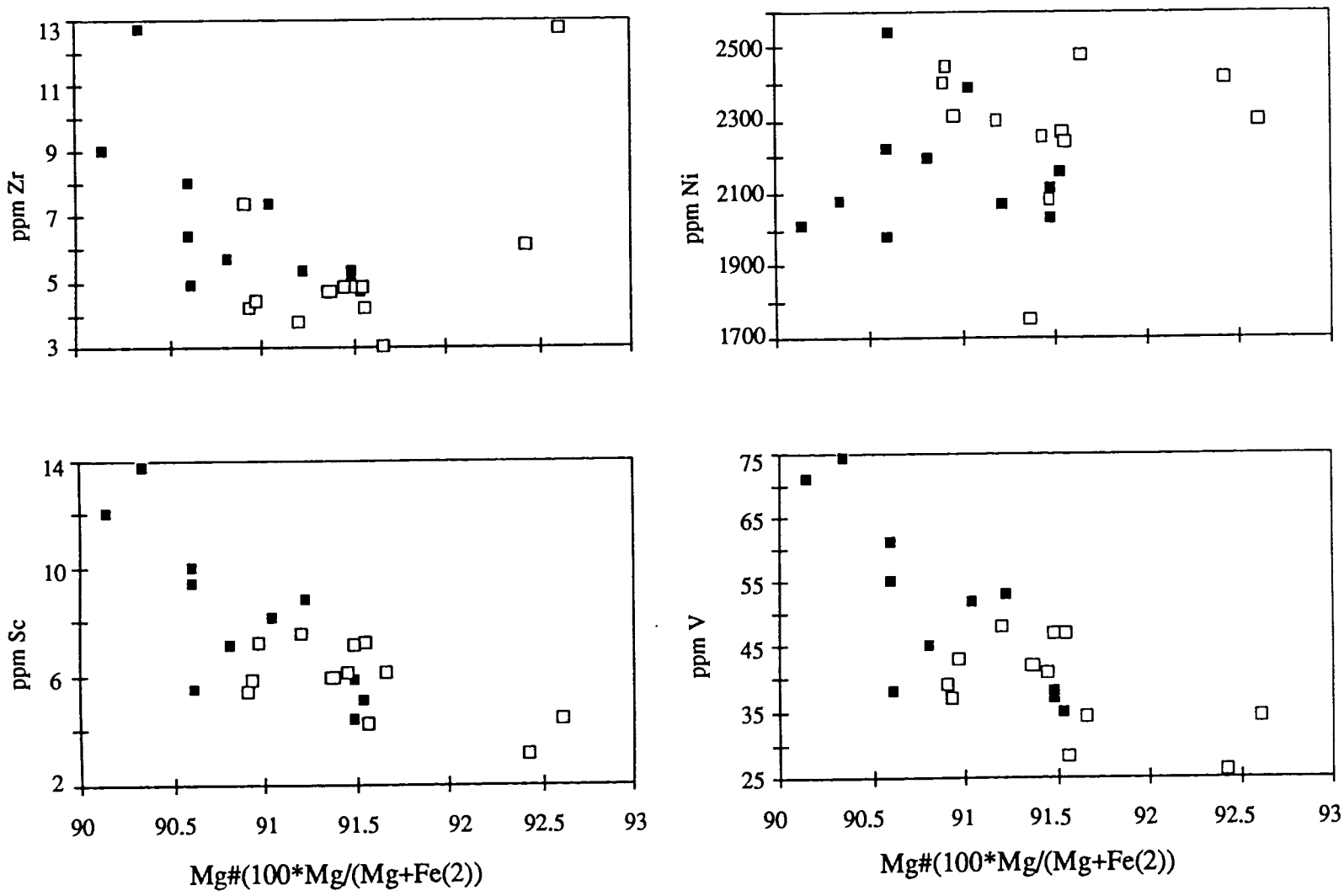

Fig. 4.8a. Mg# versus trace element plots of the Mt Gambier spinel lherzolites. Symbols as for Fig. 4.2a.

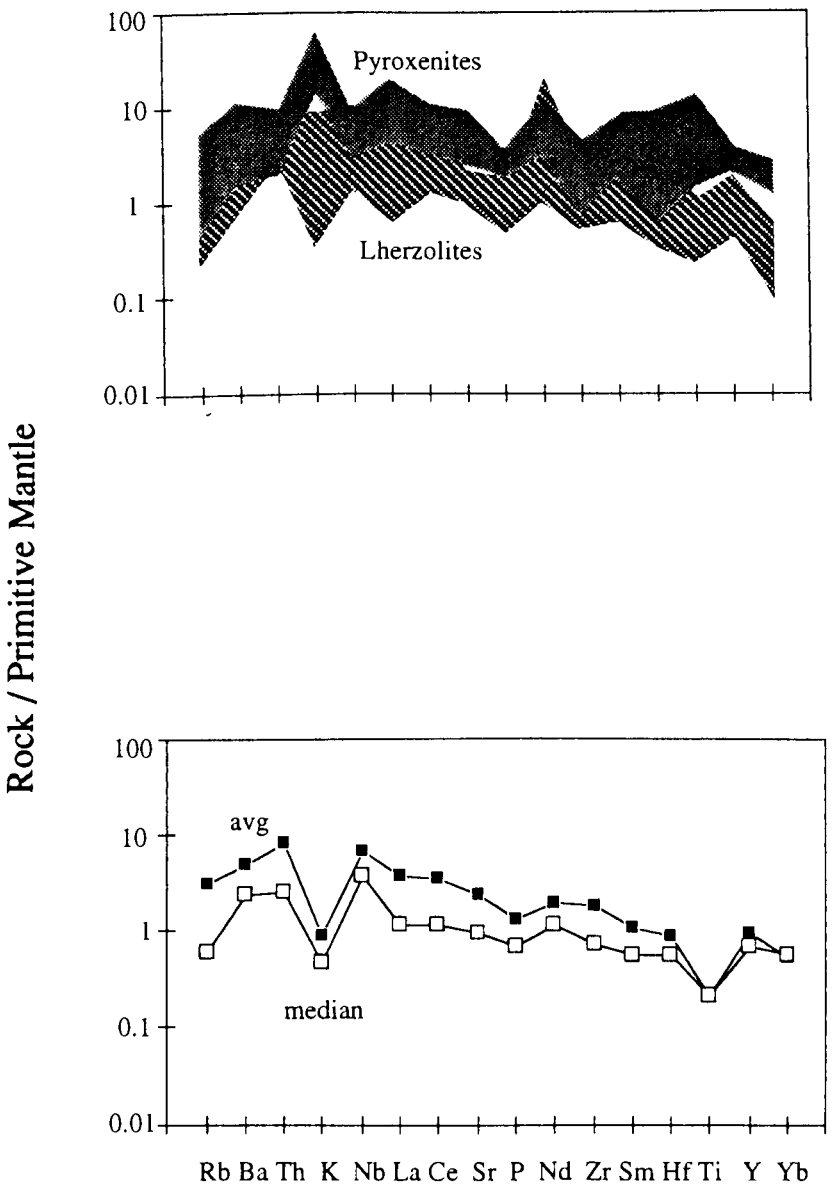

Fig. 4.8b. Trace element abundances of the Mt Gambier spinel lherzolites and the Victorian upper mantle xenoliths, and worldwide spinel lherzolite (Griffin *et al.*, 1988; O'Reilly and Griffin, 1988; McDonough, 1990).

In the Mr Gambier spinel lherzolites, CELs show higher Sc, V and lower Mg# relative to DSLs. These geochemical characteristics may reflect high modal proportions of clinopyroxene even though variations of the modal mineralogy are limited. In studies of lherzolites from western Victoria and South Australia, Frey and Green (1974) suggested that clinopyroxene-rich xenoliths contain high Ca, Na, Al, Sc, V, Cr, HREE and low Fo olivine, lower Mg# and Ni while refractory Mg-rich clinopyroxene-poor xenoliths contain high P, K, Ti, LREE, Th and U. In studies of ultramafic xenoliths from Kurile-Kamchatka and western Alaska, Swanson *et al.* (1987) also indicated the decrease of Mg# in the olivine and clinopyroxene with increasing modal proportions of clinopyroxene.

Available REE data (Frey and Green, 1974; Griffin *et al.*, 1988; O'Reilly and Griffin, 1988) are summarized in the Table 4.8. The REE abundances show that lherzolite can be easily distinguished from pyroxenites by depletion in the most of REE (Fig. 4.9).

Table 4.7. REE abundances of mantle derived xenoliths and their host basalts.

	Mt Gambier		Victoria			
	Lherzolites	Clinopyroxene	lherzolites	Pyroxenites	Host basalt	
La	0.271-1.083	1.07	0.4-28.4	2.9-16.5	31.154 ~	38.425
Ce	0.583-2.469	3	2.3-55.4	9.4-42.3	61.532 ~	76.504
Pr	0.082-0.303	0.68				
Nd	0.369-1.355	4.1	1.3-23.6	4.28-32	28.151 ~	34.750
Pm						
Sm	0.085-0.339	1.43	0.25-3.86	4.2-32	6.095 ~	7.496
Eu	0.028-0.122	0.62	0.15-1.0	0.21-1.7	2.096 ~	2.531
Gd	0.092-0.429	2.4			5.634 ~	6.755
Tb	0.016-0.083	0.42	0.033-0.427	0.18-0.69		
Dy	0.056-0.517				4.394 ~	5.361
Ho	0.021-0.113	0.62	0.07-0.271	0.26-0.61		
Er	0.058-0.337	1.75			1.867 ~	2.281
Tm	0.029	0.25				
Yb	0.049-0.335	1.43	0.05-0.66	0.49-1.33	1.373 ~	1.707
Lu	0.007-0.049	0.26				

Table 4.6. Representative geochemical ananyses of the Mt Gambier spinel herzolites (by ICP-MS, ppb).

	Coarse equant type		Deformed sheared type	
	UCEL 1	UCEL 4	DUSL 8	DUSL 10
Li	1447	1534	1141	1310
Be	45	89	60	45
P	36848	70088	26815	31049
Sc	11797	16506	11538	12061
Ti	319363	684817	278953	213216
V	36217	64712	29874	33461
Cr	1715355	2455889	2212123	2143895
Co	110299	90270	89396	91250
Ni	2325103	1877158	1938799	1885499
Cu	3247	12150	3485	4171
Zn	46154	46905	34473	36200
Ga	1032	2677	1078	1268
Rb	449	729	66	214
Sr	6058	23687	5445	5642
Y	595	3406	615	973
Zr	2464	11267	10583	3810
Nb	583	1154	114	69
Mo	406	425	87	104
Ag	4.4	4	2.9	3.8
Cd	16.3	12.2	5.7	5.2
Sn	931	92	297	17
Sb	5	7.9	1.5	3.1
Cs	8.3	28.6	3	8.5
Ba	3532	5724	69.5	1484
La	358	1083	254	478
Ce	687	2469	683	1009
Pr	82	303	115	124
Nd	369	1355	602	539
Sm	86	339	162	133
Eu	28	122	52	41
Tb	16	83	25	25
Gd	92	429	175	145
Dy	103	517	124	151
Ho	21	113	23	32
Er	63	337	58	95
Yb	78	335	49	103
Lu	14	49	7.2	17
Hf	55	257	248	88
Ta	596	253	116	121
W	150481	94844	54034	58053
Tl	3.5	16	1.6	3.2
Pb	119	160	126	127
Th	63	127	23	66
U	18	29	5.7	5.4

Notice that the coarse equant type lherzolites show enrichments in the most of elements(P, Sc, V, Ta, Zn, Rb, Sr, Nb, Mo,Au, Cd,Sb,Ba, Hf, W, Tl, U).

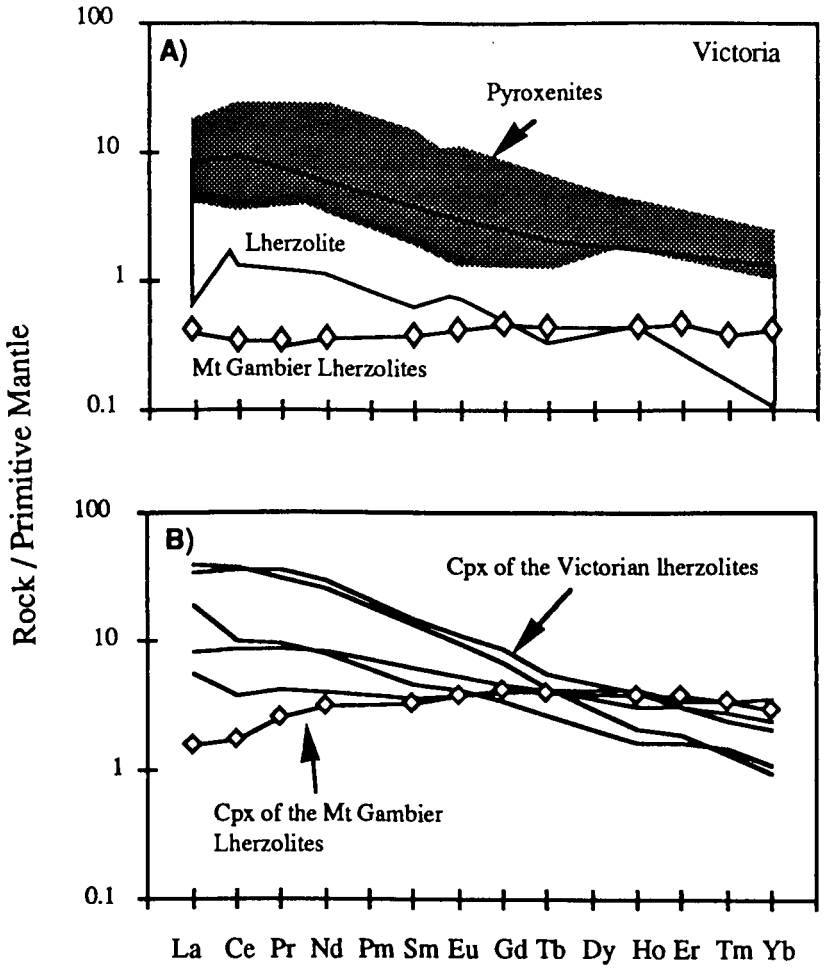

Fig. 4.9. REE abundances of A) the Victorian lherzolites (O'Reilly and Griffin, 1988), Pyroxenites (Griffin *et al.*, 1988), the Mt Gambier lherzolites (Frey and Green, 1974), B) Clinopyroxenes (Frey and Green, 1974).

4.6. Isotopic composition

Available isotope data from Victoria and South Australian (McDonough and McCulloch, 1987; Griffin *et al.*, 1988; Stolz and Davies, 1988) are summarised in the Table 4.9 and plotted in the Fig. 4.10. The lherzolites from the Mt Gambier show eNd of -4.5 - 9.2 for the whole rocks and eNd of -10 for a clinopyroxene grain from spinel lherzolites. Peridotites from Victoria have eNd of -6.5 - 10.5. The Sr-Nd isotopic compositions mainly lie in the ranges of OIB and MORB. However, no clear isotopic differences have been observed in the xenoliths with a different microscopic texture (McDonough and McCulloch, 1987) and no clear distinction has been observed between the $TNd_{(DM)}$ of lherzolites and pyroxenites (Griffin *et al.*, 1988). Pb isotopic data from the Victorian xenoliths show a wide range of variation from Group 2 kimberlites to host rocks or associated alkali basalts in $^{206}Pb/^{204}$ Pb ratios (Stolz and Davies, 1988). These isotopic characteristics suggest that many ultra basic xenoliths have been influenced by the mantle metasomatism.

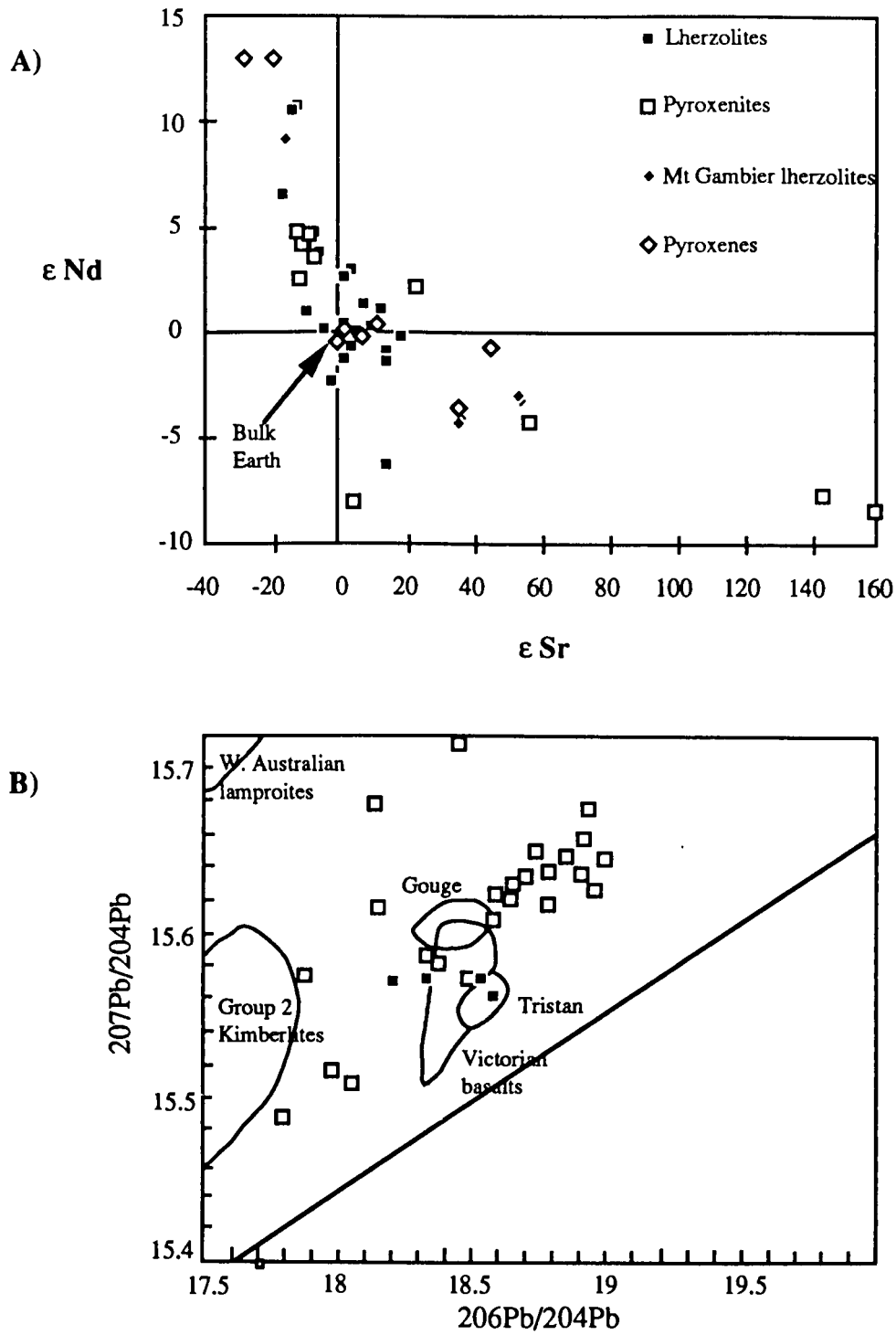

Fig. 4.10. **A)** Sr and Nd isotopic compositions of the mantle derived xenoliths from Victoria and South Australia (Data sources; McDonough and McCulloch, 1987; Griffin *et al.*, 1988), **B)** Plot of 207Pb/204Pb vs 206Pb/204Pb ratios for host Victorian Newer Basalts and associated xenoliths (from Stolz and Davies, 1988). Symbols; open squares for xenoliths, filled squares for host basalts.

Table 4.8. Isotopic compositions of mantle derived xenoliths (data sources; see text).

	Victoria										
	Mt Gambier			CPX	Lherzolites			Pyroxenites			
	Range			Average	Range			Average	Range		Average
Nd ppm	0.30	-	0.44	0.37	5.81	0.42	- 7.55	2.26	1.18	- 32.30	16.35
Sm ppm	0.07	-	0.15	0.10	1.36	0.09	- 1.58	0.48	0.56	- 6.49	3.89
143Nd/144 Nd	0.5124	-	0.5131	0.5127	0.5126	0.5126	- 0.5132	0.5127	0.5122	- 0.5129	0.5126
Sm/Nd	0.23	-	0.34	0.27	0.23	0.14	- 0.41	0.24	0.18	- 0.47	0.28
T mod:dep	0.04	-	1.16	0.99	0.98	0.40	- 1.78	0.68	0.65	- 1.74	1.06
eps Nd (0)	-4.29	-	9.36	0.64	-0.78	-6.32	- 10.71	1.48	-8.11	- 4.74	-0.73
143/144(T)	0.5120	-	0.5125	0.5122	0.5121	0.5120	- 0.5125	0.5122	0.5118	- 0.5122	0.5121
eps Nd chT	-1.07	-	9.08	2.78	0.51	0.002	- 8.66	4.45	-3.92	- 5.84	0.95
Sr87/86	0.7033	-	0.7083	0.7063	0.7078	0.7036	- 0.7058	0.7046	0.7037	- 0.7158	0.7069
Sr ppm	2.81	-	7.88	4.65	61.20	5.05	- 152.00	39.11	71.70	- 175.10	134.14
Rb ppm	0.07	-	0.39	0.22	0.35	0.08	- 36.32	5.09	0.12	- 4.12	1.62
Rb/Sr	0.0086	-	0.1140	0.0654	0.0057	0.0048	- 0.4099	0.0628	0.0015	- 0.0228	0.0100
Rb87/Sr86	0.0261	-	0.3375	0.1894	0.0164	0.0138	- 1.1872	0.1819	0.0042	- 0.0569	0.0289
eps Sr(0)	-15.89	-	54.50	25.27	46.13	-16.37	- 18.74	1.68	-11.82	- 159.77	34.09

4.7. Geothermobarometry of the Mt Gambier lherzolites

Temperatures of upper mantle xenoliths from Mt Gambier have been calculated using clinopyroxene-orthopyroxene pairs (Wood and Banno, 1973; Wells, 1977; Lindsley, 1983) and orthopyroxene-olivine-spinel pairs (Witt-Eickschen and Seck, 1991). The results are shown in Table 4.10 and plotted in the Wo-En-Fs diagram of Lindsley (1983) (Fig. 4.11). The calculated temperatures range from 932 to 1105 °C from two-Px pairs and 829 to 896 from orthopyroxene-olivine-spinel pairs. These results are similar to those of ultramafic xenolith for eastern Australia (Griffin *et al.*, 1984) and French spinel lherzolites (Downes, 1987).

Table 4.9. Calculated geothermometry for the Mt Gambier spinel lherzolites.

Sample name	Rock name	assemblages	Wells (1977)	W/B(1973)	W/S (1988)
CEL 1	Lherzolite	Ol, Opx, Cpx, Sp	939	1053	889
CEL 2	Lherzolite	Ol, Opx, Cpx, Sp	970	1076	896
CEL 3	Lherzolite	Ol, Opx, Cpx, Sp	1004	1105	
CEL 4	Lherzolite	Ol, Opx, Cpx, Sp	980	1088	859
DSL 1	Lherzolite	Ol, Opx, Cpx, Sp	952	1074	857
DSL 2	Lherzolite	Ol, Opx, Cpx, Sp	932	1042	851
DSL 3	Lherzolite	Ol, Opx, Cpx, Sp	947	1052	829

W/B for Wood and Banno, (1973) and W/S for Witt-Eickschen and Seck, (1991).

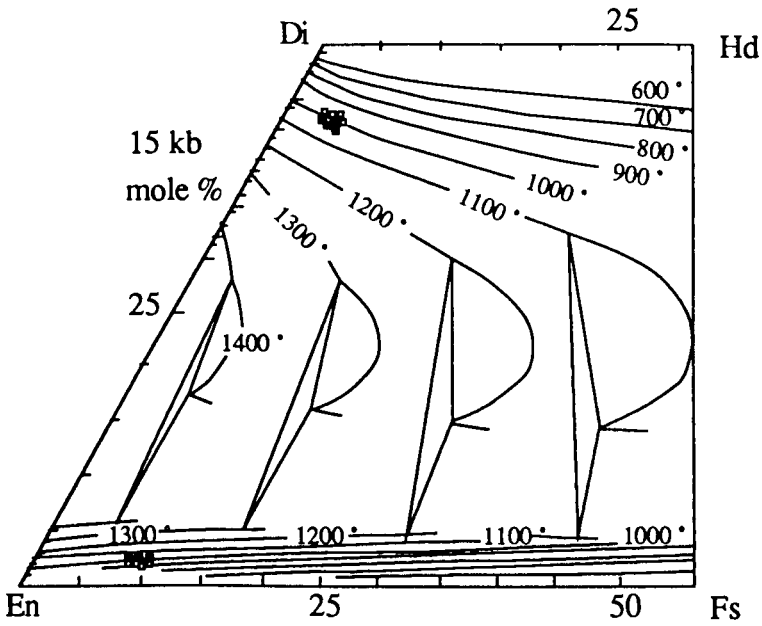

Fig. 4.11. Projection of pyroxene from the Mt Gambier spinel lherzolite onto the pyroxene quadrilateral of Lindsley, 1983. Symbols; Open square for DSL, filled square for CEL.

Differences of temperature have been observed between two varieties of lherzolites. Temperatures of DSLs range from 932 to 952 whereas those of CELs range from 939 to 1094 °C in Well's temperature. In the Wo-En-Fs diagram (at 15 kbar), temperature of DSLs range from 950 to 1030 °C whereas those of the CELs range from 1000 to 1060 °C. These results are opposite to those of the South African garnet-bearing lherzolites (Nixon and Boyd, 1973; Boyd and Nixon, 1975) in which coarse grained lherzolites yield lower temperatures relative to deformed or mylonized xenoliths. It is possible that the DSLs of the Mt Gambier lherzolites were derived than from shallower depth than South African suites, in which CEL and DSL type peridotites are intermingled horizontally.

4.8. Redox state of the Upper Mantle

Information about the oxygen fugacity of the lithospheric mantle is very important key to understand origin and evolution of the Earth such as volatile induced partial melting in the mantle and mantle metasomatism by such fluids (e.g. CO_2, H_2O) (O'Neill and Wall, 1987). The oxygen fugacities of the Mt Gambier spinel lherzolites are calculated from the olivine, orthopyroxene and spinel mineral assemblages (O'Neill and Wall, 1987) by the combination of oxygen geobarometer (O'Neill and Wall, 1987). They are plotted in Fig. 4.12. The results suggest that the redox state of the lithospheric mantle beneath Mt Gambier regions lies between quartz-fayalite-magnetite (QFM) and wustite-magnetite (WM) oxygen buffer (Fig. 4.12).

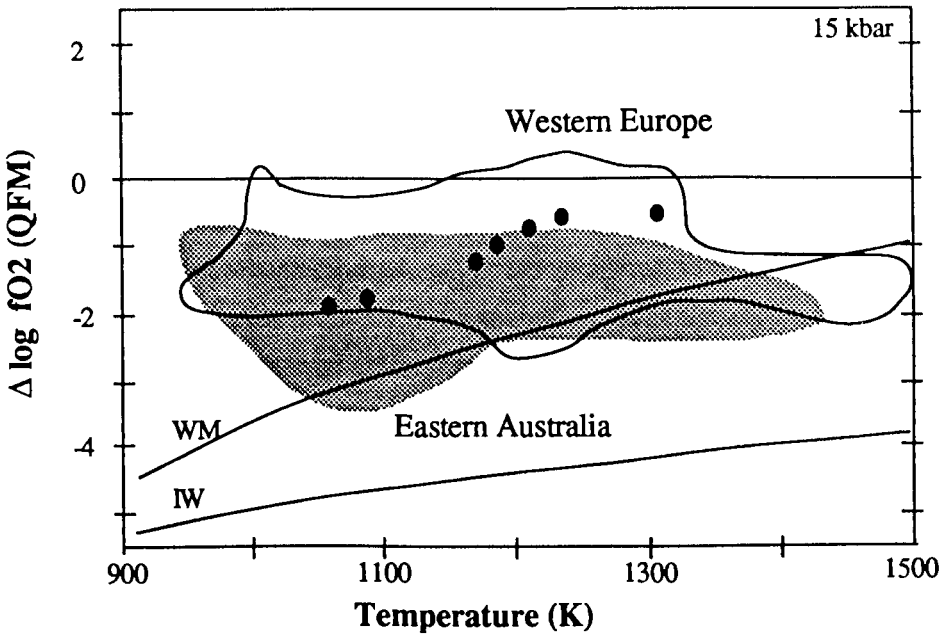

Fig. 4.12. Oxygen fugacities of the Mt Gambier spinel lherzolites, calculated with olivine - orthopyroxene-spinel oxygen geobarometer (O'Neill and Wall, 1987), relative to the QFM buffer.

No results are found below the IW and above QFM oxygen buffers. This is a similar result to that found for western Europe, eastern Australia (O'Neill and Wall, 1987), South Africa (Daniels and Gurney, 1991) and Western Australia (Jaques *et al.*, 1990).

O'Neill and Wall (1987) suggested that large regions of the lithospheric upper mantle are broadly homogeneous in oxygen fugacity. They also suggested that there are not significant differences in the f_{O_2} among the majority of the xenoliths considered as lithosphere derivatives (Hamlyn and Bonatti, 1980) or primitive MORB glasses (Christie *et al.*, 1986). Daniels and Gurney (1991) also showed that f_{O_2} determined from lherzolites in Dokolwayo kimberlites, Swaziland are laterally homogeneous in the range QFM-IW.

However, redox states of the upper mantle are more variable if metasomtized spinel lherzolites and harzburgites containing variable degree of LREE and LIL enrichment are considered (Ballhaus *et al.*, 1991). Ballhaus *et al.* (1991) suggested that more metasomatised upper mantle xenoliths are plotted to trend toward QFM and in the extremely metasomatized samples show a oxidation above QFM. As a result, the oxidised states of South Australian lithosphere may be homogeneous on a large scale.

4.9. Discussion and conclusion

Xenoliths from South Australian Quaternary alkaline basalts are dominantly Group 1 type lherzolite. Two groups of spinel lherzolites are recognised from the Mt Gambier volcanics; coarse equant types (CEL) and deformed sheared types (DSL). These groups may be distinguished petrographically, mineralogically and geochemically.

In general, the CELs have higher Al_2O_3, Na_2O, P_2O_5, CaO, TiO_2, Sr, Zr,, Sc, V, and lower SiO_2, Ni, Cr, Mg# relative to those of the DSLs. These chemical characteristics of the CELs may reflect higher modal proportions of clinopyroxene. Total CaO, TiO_2, P_2O_5,K_2O and LREE contents are low relative to Victorian metasomatised lherzolites and pyroxenites, but are similar to Victorian unmetasomatised lherzolites, suggesting that their geochemical characteristics can not be explained by mantle metasomatism. Mineralogically, clinopyroxenes of the CELs can be distinguished from those of the DSLs by high Cr_2O_3, Na_2O, TiO_2, Mg#, low CaO, and orthpyroxene and spinel of the CELs are distinctive from those of DSLs by high Cr_2O_3, MnO, Mg# and by high Mg#, Cr/Cr+Al ratios, respectively. Calculated temperature range from 930 to 1100 °C being slightly higher in CELs. Calculated oxygen fugacities plot in the range between QFM and WM and the ranges overlap those of Western Europe and eastern Australia, suggestive of similar redox states of the lithospheric mantle in a large scale.

Chapter 5. Petrology and Geochemistry of South Australian kimberlites and lamprophyres.

5.1. Introduction

An understanding of the petrogenesis and spatial distribution of kimberlites, lamprophyres and lamproites provides important constraints on the origin and evolution of their potential lithospheric mantle sources (Mitchell, 1989; Bergman, 1987). This chapter provides new data on a series of broadly lamprophyric to kimberlitic intrusions of Ordovician and Jurassic age in the southern Adelaide Fold Belt. This part of the study was undertaken for a number of reasons:

i) Kimberlites may represent unalloyed melt of metasomatic enrichments in the lithospheric mantle, and may therefore allowing closer estimation of the composition of these enrichments, also permitting the use of radiogenic isotopes as a means of estimation of the age of this enrichment.

ii) These rocks have possible sources in the lithospheric mantle of this geophysically significant and interesting zone of transition between eastern Australia and the Precambrian craton further west and may thus reflect possible geochemical features of this transition.

iii) As there are good indications that the Tertiary and Cainozoic alkali basalt provinces in S.E. South Australia incorporate a component of enriched lithospheric mantle, these Mesozoic and Palaeozoic alkaline rocks potentially provide an important definition of the timing of the establishment of this enrichment.

iv) Xenoliths transported by the kimberlites may provide information about lower crust or upper mantle.

These rock types occur as dykes, sills, stocks and as vents associated with minor lava, tuff and pyroclastic rocks (Rock, 1991). Traditionally, interest in them has been promoted by economic considerations, mainly the occurrence of diamonds, although minor occurrences of gold, silver and vermiculite are also occasionally important. Despite these interests, the origins and petrogenesis of these rocks have been the subject of extended debate, partly fuelled by poor preservation and their commonly weathered nature (Ferguson *et al.*, 1979; Scott Smith *et al.*, 1984; Rock, 1991). The nomenclature of rocks of this group is very variable and obscure, partly reflecting textural and mineralogical diversity. Aspects of this terminology are summarised in Tables 5.1 and 5.2.

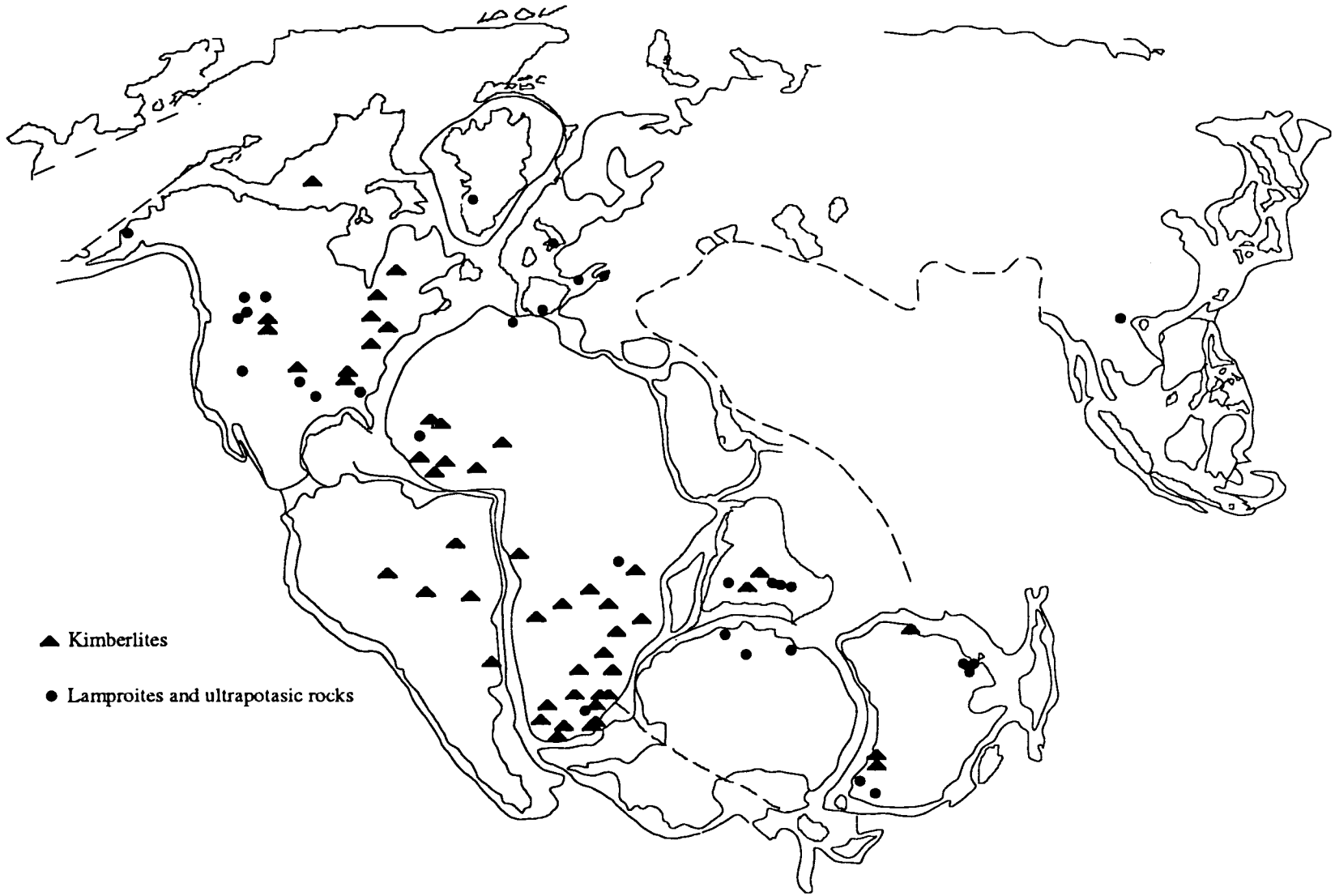

Fig. 5.1. Worldwide distribution of lamproites, ultrapotassic rocks and kimberlites showing a reconstruction of the Gondwana or 180-200Ma ago.

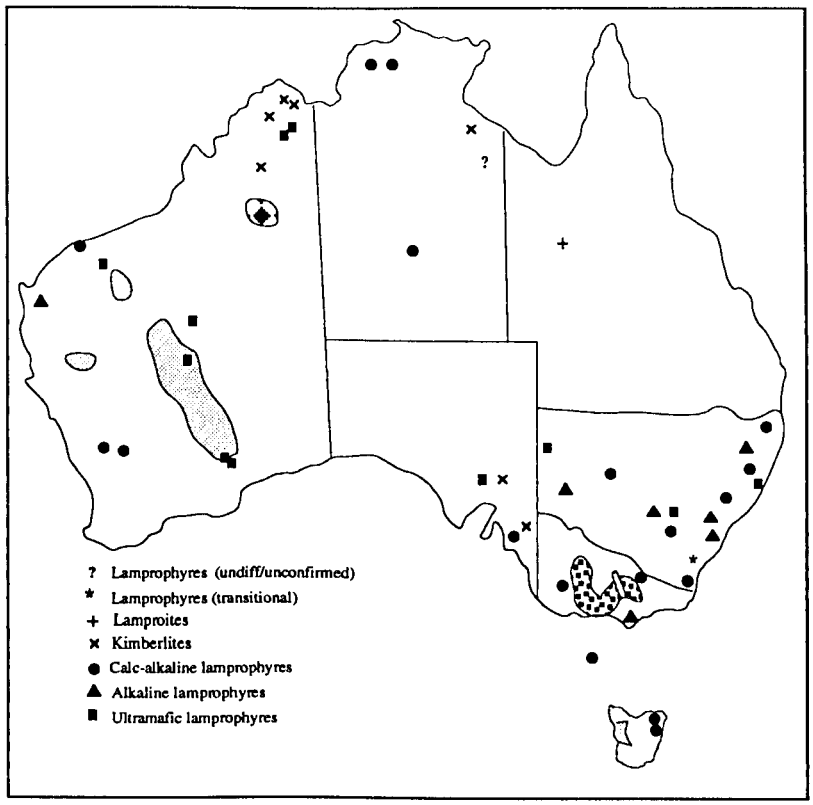

Fig. 5.2a. Distribution of the lamprophyres, lamproites and kimberlites in Australia (Rock, 1991).

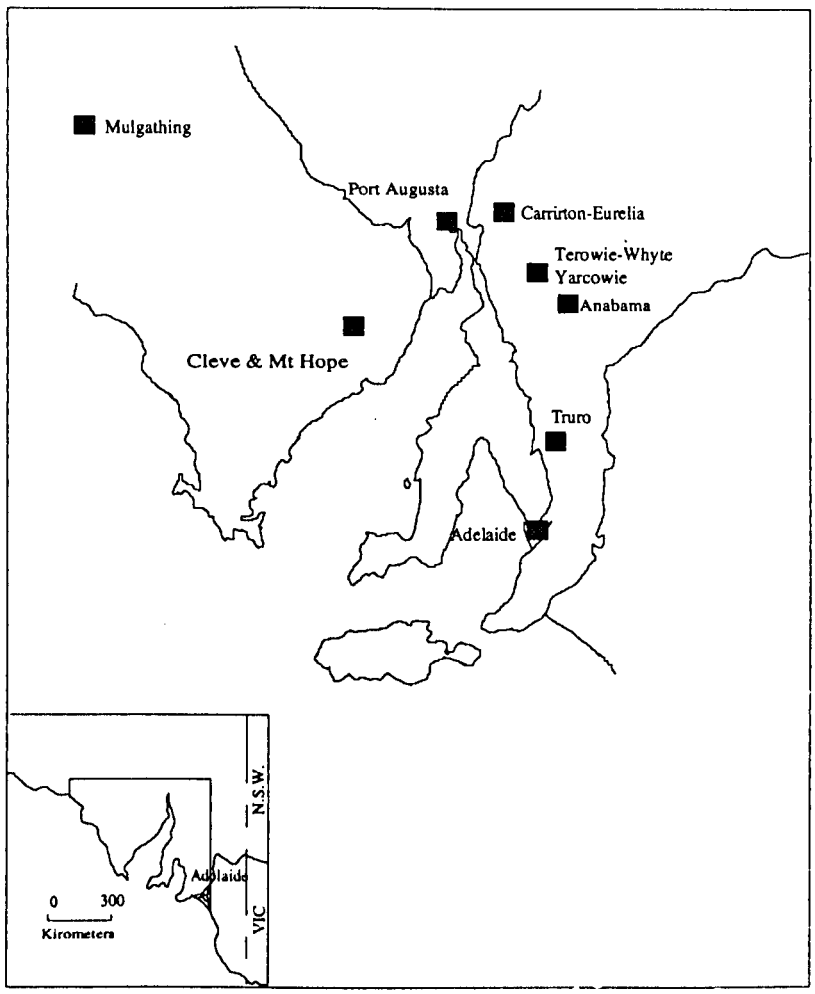

Fig. 5.2b. Distribution of known South Australian kimberlites and lamprophyres.

In South Australia, there are several kimberlite and lamprophyre occurrences in the Adelaide Geosyncline and Eyre Peninsula (Fig. 5.1, 5.3, Table 5.3). Their distribution is generally related to tectonic (structural) controls (Stracke *et al*, 1979; Müller *et al.*, 1993; Wyatt *et al.*, 1993) and their ages include Ordovician and Jurassic (Stracke *et al.*, 1979; Müller *et al.*, 1993).

In this thesis, the terminology and definitions used for the South Australian kimberlites and ultra-potassic rocks are those proposed by Rock (1991) (see Table 5.1, Fig. 5.2), in accord with which rocks from Pine Creek, Calcutteroo, Port Augusta and Eyre Peninsula are kimberlites and those from Truro are lamprophyres.

Table 5.1. Classification of the South African kimberlites (modified from Smith *et al.*, 1985).

	Group I	Group II
Mineralogy	Phlogopite-poor, perovskite-rich, zircon and ilmenite-present	Phlogopite-rich, perovskite poor, zircon, ilmenite
Xenolith 1) high P-T sheared lherzolite 2) high P-T subcalcic, Cr poor megacryst	Present in some present	believed absent believed absent
Geochemistry	enrichment in TiO2, Nb	enrichment in SiO2,K2O, Pb, Rb, Ba and LREE
Isotopes 87Sr/86Sr 143Nd/147Nd 206Pb/204Pb	 0.703-0.705 0.51268-0.51276 18.3-20	 0.7075-0.710 0.51206-0.51277 17.2-17.7
Emplacement (Ma)	80-100, 114, 150, 240	114-127, 145, 200
Presumed source magma	asthenospheric sources similar to OIB type	ancient enriched subcontinental lithospheric source (time-averaged LREE enrichment and elevared Rb/Sr and Pb/U ratios
Division	Group I A and Group I B GIB-low SiO2, LREE/HREE, high Fe, CaO, Nb, Zr, Y, shallow sources than GIB	

Table 5.2. Classification of lamprophyric rocks (Rock, 1991). Rock names of italic characteristics were classified into lamproites by Mitchell and Bergman (1991).

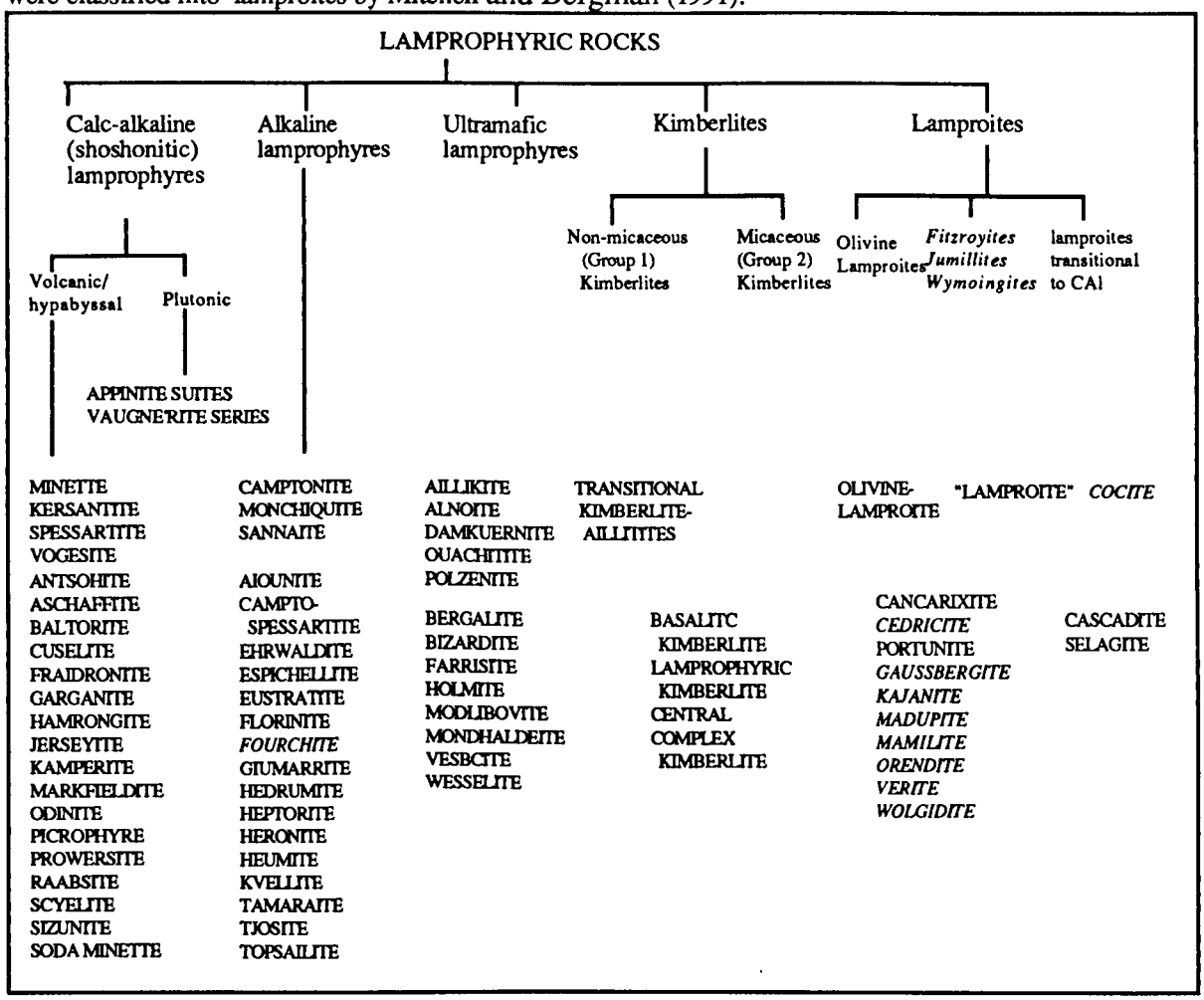

5.2. Nomenclature and classification of kimberlites, lamprophyres, and lamproites

The terminology "lamprophyre" (Greek Lampros porphyros) was defined by Gümbel (1874). The name means glistening porphyry (purple rocks) which reflect the presence of large lustrous biotite phenocrysts found in the type-rocks of Fichtelgebirge, Germany (Rock, 1991). The rocks were first recognised in Germany and Switzerland.

Lamproite is a term coined by Niggli (1923) and was redefined as K-and Mg-rich extrusive lamprophyre by Tröger (1935). The term "kimberlite" was introduced to describe a porphyritic peridotite which is the source rock of diamonds found at Kimberley, South Africa by Lewis (1887, 1888). The South African kimberlites are subdivided into two distinctive types (Fig.5.1); i) basaltic and ii) micaceous according to the petrological differences recognised by Wagner (1914) and into Group I and Group II kimberlites, based on isotopic signatures (Smith, 1983). Group I kimberlites were also divided into two groups; Group IA and Group I, on the basis of geochemical differences (Smith *et al.*, 1985).

Recently, Mitchell and Bergman (1991) and Rock (1991) provided comprehensive

reviews of worldwide kimberlite, lamprophyre and lamproite occurrences. Different definitions and classifications are shown by these two authors (Table 5.2).

Mitchell and Bergman (1991) grouped many sub-divisions of the potassic rocks into the lamproites and divided the potassic rocks into 8 types. On the other hand, Rock (1991) assigned rocks of the traditional associations; kimberlite, lamprophyre, and lamproite, into a lamprophyric branch in which he sub-divided into 5 types. In his classification, many rocks defined as lamproites by the Mitchell and Bergman (1991) are included in the 3 types of the lamprophyres and lamproites.

These two different classifications contain several logical problems. In the classification of the Mitchell and Bergman (1991), lamproitic rocks include wide varieties of potassic rocks with a wide range of mineralogy and geochemical composition. In his division, many ambiguous terms, including shoshonite association, potassium-rich intrusive rocks or leucitites and leucite basalts are included. On the other hand, in the Rock's classification, lamprophyres are divided using some ambiguous terms, including calc-alkaline, alkaline and ultramafic lamprophyre, even though many show overlapping chemical characteristics. Rock's classification is more systematic and comprehensive than that of the Mitchell and Bergman (1991).

5.3. Previous studies

The worldwide distribution of the kimberlite, lamprophyre and lamproite seem to be linked to extensional plate boundaries associated with continental rifting (Sharp, 1974; Helmstaedt *et al.*, 1979; Crough *et al.*, 1980). Recently, Rock (1991) and Mitchell and Bergman (1991) have examined the global distribution, petrography, mineralogy and geochemistry of kimberlitic, lamprophyritic and lamproitic rocks, suggesting that although these rocks have temporal and spatial relationship to tectonic activity they are generally not located directly on plate boundaries (Fig. 5.1). Rock (1991) indicated that more alkaline and mafic lamprophyres are related to divergent (rifting and triple junction) and passive (transform fault) tectonic regimes while kimberlites and lamproites occur in stable intraplate settings (ancient or recently stabilised cratons).

Rock (1991) also observed that the rocks range from Late Archaean or Proterozoic to Recent time (but mainly < 250 Ma) in age, and that the total volumetric abundance of the lamproites and kimbrerlites is very small. It was also suggested that there seemed to be anomalous abundance of kimberlites in the Upper Jurassic-Cretaceous, while lamproites have two major intrusive peaks, Tertiary (< 30 Ma) and Proterozoic (1200 Ma). In this review, he showed that the lamprophyres from the Yilgarn craton, Kaapvaal craton, South Africa, Canadian Shield, Ontario/ Quebeck mainly range from Proterozoic to Mesozoic in age while those from the Kimberley craton, W. Australia are Proterozoic. In addition, unlike the world wide situation, lamprophyres of the Tasman Fold Belt system in the Eastern

Australia were mainly emplaced during the Late Palaeozoic to Early Cainozoic. Rock (1991) suggested that these rocks are usually comagmatic with other igneous rocks. Distributions of kimberlites fairly coincident with the world-wide distribution of Continental Flood Basalts and many of them are concentrated in the Proterozoic or Archaean Cratons.

In Australia, these rocks are concentrated in south eastern Australia and in Western Australia (Fig. 5.2). An extensive province of lamproitic and kimberlitic rocks occurs in the Kimberley block, WA (McCulloch *et al.*, 1983; Jaques *et al.*, 1984; Fraser *et al.*, 1985), while kimberlitic and lamprophyric rocks are distributed in the Yilgarn blocks, Gawler Craton, Adelaide Geosyncline, Lachlan Fold Belt and in Tasmania (Stracke *et al.*, 1979; Scott Smith *et al.*, 1984; Jaques *et al.*, 1985; Hinde *et al.*, 1988; Wilkinson, 1988).

There have been several studies of South Australian kimberlites and lamprophyres (Scott Smith *et al.*, 1984; Morris, 1988; Wyatt *et al.*, 1993). A general summary of kimberlites in South Australian are shown in Table 5.3. Morris(1988) showed larger pipes of Pine Creek (a T-shaped body 350 x 400m) and Mitopitta (192 x 165 m), and predominant micaceous kimberlites (like South African Group 2 kimberlite ?). Limited field studies report a carbonatite occurrence coexisting with carbonated kimberlitic intrusives at Walloway (Ferguson and Sheraton, 1979) and an occurrence of diamonds from kimberlite dykes (Scott Smith *et al.*, 1984).

Recently, Wyatt *et al.* (1993) reported a discovery of eleven new Jurassic kimberlites on the Gawler Craton on Eyre Peninsula (three in the Cleve and eight in the Mt Hope areas) of South Australia. They suggested that the kimberlites are phlogopite-monticellite Group 1 kimberlite and all appear to be non- diamondiferous dykes or small pipes. The kimberlites appeared to be associated with the evolution of the Polda Trough, a Phanerozoic intracratonic half graben on Eyre Peninsula(Wyatt *et al*, 1993).

Geochemical and mineralogical studies have been reported for kimberlites from Port Augusta, Walloway and Terowie (Ferguson and Sheraton, 1979), from Eurelia (Ferguson *et al.*, 1979) and from Orroroo (Scott Smith *et al.*, 1984). Ferguson and Sheraton (1979) suggested that the Walloway kimberlites have normal South African kimberlite-like characteristics and they were originated from small degrees of fusion phlogopite-bearing garnet lherzolite at depths in excess of 125 km (~40kb).

Ferguson *et al.*, (1979) also suggested the chemistry of the kimberlitic rocks from Eurelia are similar to evolved kimberlitic rocks and associated alkaline ultra mafic rocks from southern Africa. Scott Smith *et al.* (1984) indicated that the Orroroo kimberlites are petrographically and geochemically similar to garnet bearing South African Group 1 kimberlites. Nelson *et al.* (1988) provided whole rock chemical and isotopic data on a carbonatite from Walloway and a micaceous kimberlite from Terowie. In this study, they observed close spatial and temporal relationships in kimberlitic and carbonatitic rocks from the Walloway/ Terowie regions, as well as a genetic relationship between the two suites in respect of the isotopic signatures.

Stracke *et al.* (1979) reported on Rb-Sr dating of kimberlitic rocks and their mineral separates from Walloway and Terowie together with some from White Cliffs and Jugiong in New South Wales. They suggested that SE Australian kimberlitic rocks postdate the Proterozoic and some of them may be as young as Tertiary from field evidence. Their isotopic data shows that the South Australian kimberlitic rocks are of Jurassic age (164 to 174 Ma) whereas New South Wales kimberlitic rocks are of Permian age (~260 Ma).

Studies of two lamprophyritic rocks from Truro and Anabama in the South Australia have been done by Müller *et al.* (1993) and McDonald (1992). Müller *et al.* (1993) provided whole rock and mineral chemistry, and age dating for the Truro lamprophyres. They grouped the lamprophyres into two types according to petrography and K-Ar age; i) phlogopite-phyric lamprophyres of 458±2 Ma age and ii) apatite-phlogopite-phyric lamprophyres of 480±3 Ma age. They also suggested that most of the samples have an ultra potassic composition and have a significantly high HFSE concentration (e.g. Zr, Nb, Hf). McDonald (1992) reported whole rock chemistry of a lamprophyritic dyke from 35 km South of Olary. The petrography and chemical composition are similar to those described by Müller *et al.* (1993).

5.4. Emplacement ages of South Australian kimberlites and lamprophyres

Studies of the intrusive ages of kimberlites and lamprophyres have been undertaken by several authors (Stracke *et al.*, 1979; Wyatt *et al.*, 1991; Black *et al.*, 1993; Müller *et al.*, 1993; Wyatt *et al.*, 1993). Intrusive ages of these rocks in South Australia are largely grouped into two distinctive times (Table 5.3); 170-180 Ma and 450-480 Ma. Their sites of emplacement are related to regional or local tectonic or structural settings. Those intrusions which range from 170 to 180 Ma may reflect regional tectonic activity associated with the earliest stages of separation of the Australian continent from Antarctica. This activity is approximately the same age as that of the Tasmanian dolerites (Hergt *et al.*, 1991) and of their extension into SA on Kangaroo Island (McDougall and Wellman, 1976).

This activity appears to be mantle plume-related and a viable model for kimberlite magmatism may place this towards the thermal margin of the plumes where only relatively low T melts are generated from metasomatised lithosphere. In New South Wales and Victoria, Late Triassic to Late Jurassic alkaline igneous activity overlaps the tholeiitic basaltic activity in Tasmania and South Australia (McDougall and Wellman, 1976). The alkaline magmatism is thought to be related to the initiation of rifting in this part of Gondwanaland (McDougall and Wellman, 1976; Jaques *et al.*, 1985). The lamprophyric dykes at Truro range from 450 to 480 Ma and may reflect the latest stages of the Delamerian orogeny. Interestingly these also occur at the same site where highly alkaline, undersaturated basaltic magmatism occured in the Early Cambrian in the Heatherdale Shale (Turner and Foden, 1990).

Table 5.3. Summary of the South Australian kimberlitic and lamprophyritic rocks.

Area		Location	Shape and type	Country Rock	Age
Port Augusta	137°45'E/32°30'S	3 km north of Corraberra Homestead	a remnant sill	Unfolded sedimants overlain by large Proterozoic quartzite formation forming mesa cappings	
		2 km south of El Alamein	a 1-2 m thick sill, 2 km long		
		8 km southeast of El Alamein	a 1-2 m thick sill, 1 km long		
Carrieton-Eurelia	138°30'E/32°30'S	Mainly distributed between adjacent to Eurelia and Carrieton (NW to SE direction)	13 dykes ranging from a few mms to 30 m thick and several hundred metres long	Siltstone of the Proterozoic	173±4 Ma (K-Ar)
			1 carbonatite dyke in drill hole CDO-10 (150 m depth)	Umberatane Group	172Ma (Rb-Sr)
			in 5 dykes of up to 100 m long and 1 m wide		170±2 Ma
Terowie-Whyte Yarcowie	139°0E/33°15'S	Nackara-27 km NE of Terowie	5 small and short dykes with NNE-SSW strike	Proterozoic marine sediment	164 Ma (Rb-Sr)
		Calcutteroo-20 km E of Terowie	pipes and dykes (two pipes; 66x44 m (T-shape) 33x27.5)		174 Ma (K-Ar)
		Pine Creek-7-8 km SE of Calcuttroo	a T-shaped large pipe (350x400 m (6.35 ha)		188 Ma (Rb-Sr)
		Mittopitta-10 km E of whyte and Yarcowie	several pipes and dykes		
		Mungibbie-5 km SW of Mittopitta	several small dykes of 0.6 m wide		
		Ulooloo-20 km S of Terowie	two-dykes of 0.8 m wide and 0.6 m wide		
Mulgathing	134°00'E/30°30'S	Aristarchus Rise-19 km N-NE of Wynbring	a dyke of 30 m wide		
		Blackfellow and Skuse Hill-25 km north of Wynbring	a dyke exposed in augar holes and a dyke of 25 m long in a percussion hole		
		Lake Barry 56 km NW of Tarcoola	a plug 600 m accross		
Northern Flinders Ranges		30 km NE of Arkaroola	a kimberlitic plug		
Anabama		35 km S of Olary	an ultrapotassic dyke		
Truro		8 km eastward and 13 km NE side of Truro	several dykes of 0.1 to 1.5 m thickness		458±2 Ma (type I) & 480±3 (type II) (K-Ar)
Eyre Peninsula		160 km SW of Port Augusta	similar to Group I kimberlite		180±3 Ma
		Gawler craton in the Eyre peninsula	3 Cleve and 8 Mt Hope area, dyke and pipes		Jurassic

Compiled sources, Stracke et al. (1979); Black et al. (1993); Wyatt et al. (1991,1993); Western Queen (S.A.) Pty. (envelope 4543) (1981); Müller et al. (1993); McDonald (1992); Ferguson & Sheraton (1979); Morris (1988, 1990).

5.5. General geology of South Australian kimberlites and lamprophyres

The distributions of South Australian kimberlites and lamprophyres (Fig. 5.2) are both concentrated in the Proterozoic Adelaide Geosyncline and the Gawler Craton.

5.5.1. Port Augusta area

The localities of three kimberlites in the Port Augusta area are shown in Fig. 5.3. Two sills ~1.2 m thick occur in the El Alamein Army Camp and another has been reported on a hill, 3km north of Corraberra Homestead (Stracke, 1974). The Port Augusta kimberlites intrude into the Proterozoic Tent Hill formation consisting of quartzite, sandstone, siltstone and shale.

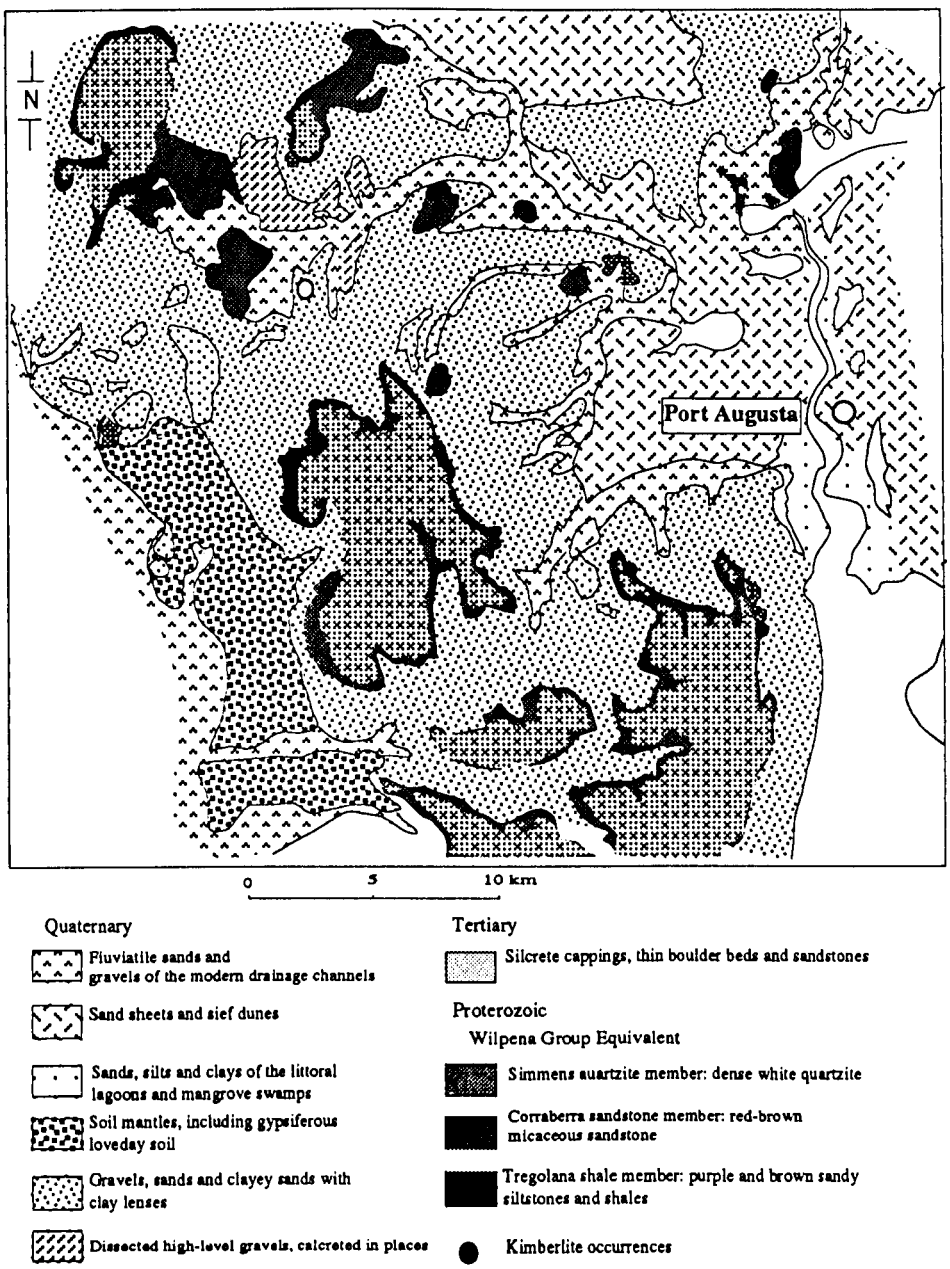

Fig. 5.3. Generalised geology of the Port Augusta area showing distribution of kimberlites.

In general, the sills are altered and they display a greyish or greenish colour. One sill, 8 km south-east of El Alamein camp, is well exposed along a small road built by a mining company. Strongly serpentinized host kimberlites and abundant lower crustal xenoliths and xenocrysts (or megacryst ?) are found in the exposed surfaces. Some of the kimberlite fragments contain relatively coarse grained micas (0.5-1.5 cm wide). Another small dyke is exposed at the top of a small hill, 6 km south-west of El Alamein Camp. This contains no xenocrysts.

5.5.2. Carrieton-Eurelia area

Fourteen kimberlite dykes with a few carbonatite dykes (Fig. 5.4) were reported in this area by Scott Smith *et al.* (1984). The dykes intrude siltstones of the Proterozoic Umberatana Group and are distributed along the NW-SE direction. However, most of these areas are covered with soil or have been revegetated after exploitation by mining companies. A few areas and newly built drill site in some paddocks expose weathered kimberlites with white greyish and faint greenish colour.

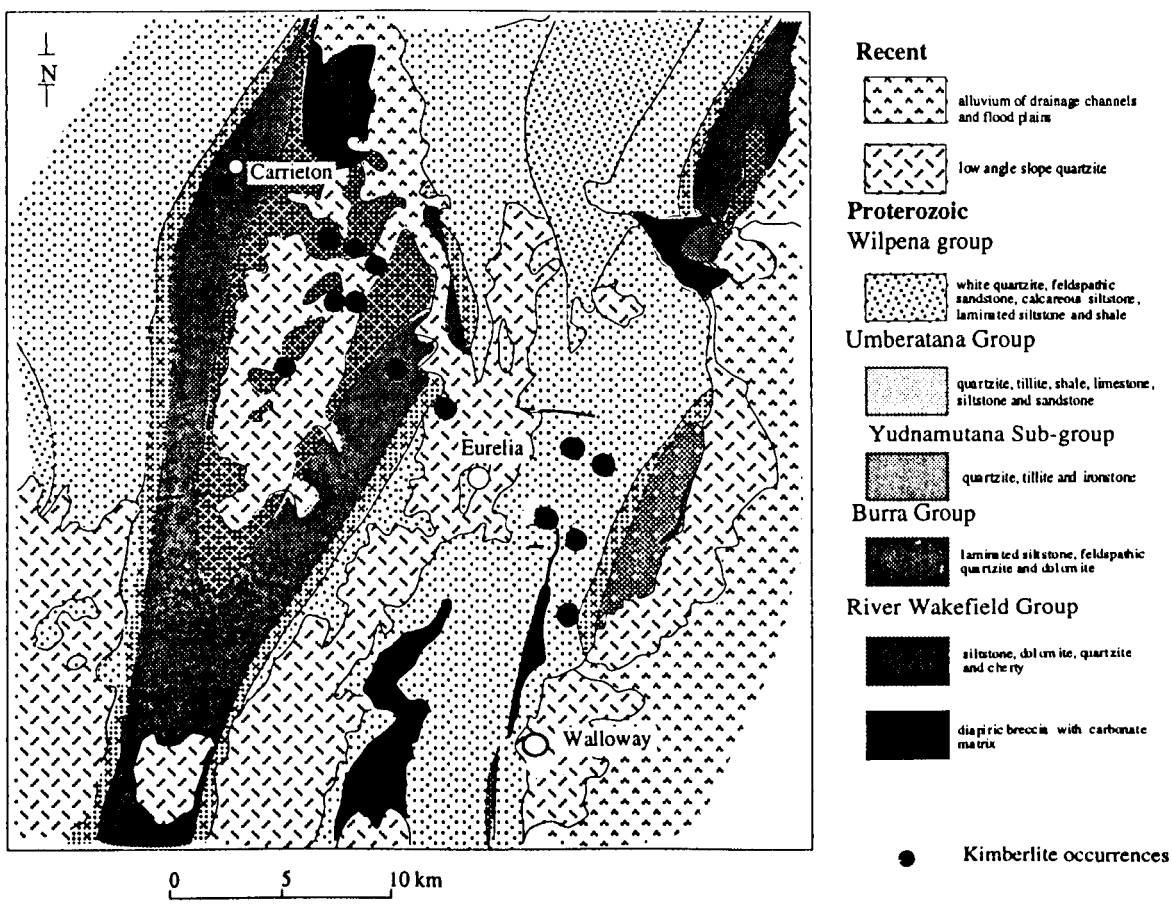

Fig. 5.4. Generalised geology of the Carrieton-Eurelia area showing distribution of kimberlites.

5.5.3. Terowie-Whyte, Yarcowie area

The largest and most abundant kimberlite pipes and dykes of South Australia are found in this area. Detailed geological descriptions by Hough and Morris (1989) and Western Queen (S.A.) Pty. Ltd. (1981) are shown in Fig. 5.5. Terowie occurs at the hinge zone of the Nackara Arc adjacent to the eastern margin of the exposed Proterozoic Adelaide Geosyncline (Western Queen (S.A.) Pty. Ltd., 1981). The area is consistent with the major regional structural trends of Adelaidean sediments, with faults, folds, and lineaments with N-S to NE orientation (Hough and Morris, 1989). Proterozoic Burra Group sediments consisting of quartzite, shale, dolomite, and sandstone lie in the core of the anticline and underlie unconformably those of the Umberatana Group consisting of sandstone, siltstone, quartzite and tillite (Western Queen (S.A.) Pty. Ltd., 1981).

The kimberlite pipes and dykes intrude the Proterozoic sediments near the hinge zone of regional anticline to the parallel fold axes, usually sub vertically and preferentially NW or NE strike intrusives (Western Queen (S.A.) Pty. Ltd., 1981). Their localities cluster in the "elbow" position of the Flinders Range as well as the central part of the crustal block in the Adelaide Geosyncline and, locally, they occur near Ordovician granitic plutons (Western Queen (S.A.) Pty. Ltd., 1981; Hough and Morris, 1989). Their distributions are also coincident with the eastern margin of the N-S earthquake zone as well as with low gravity and magnetic anomalies.

In the Calcutteroo area, a kimberlite dyke is exposed in the middle levels of two small hills and another is exposed in a small cliff (creek), located 100 m SE of the former sites. In the two small hills, abundant kimberlite fragments and their xenoliths are well exposed. They display a faint greenish colour in the weathered rocks and a blackish brown colour in the fresh rocks. In general, the kimberlite fragments are 4-8 cm across (some up to 30-50 cm) and contain country-rock fragments. The kimberlites are mica-rich (Fig. 5.7) and contain phlogopite xenocrysts (megacrysts?) ranging from 0.5 to 1.2 cm wide (some 1.5 to 2.5 cm wide). Abundant mafic dominant xenoliths and megacryst (or xenocryst) entrained by the host kimberlites are shown in the exposed soils of the hill (see Chapter 6). The other kimberlite exposed in a small cliff (creek) also contains abundant and very large high pressure xenoliths ~ 8-15 cm wide with variable forms. Some clinopyroxene and amphibole megacrysts (1.2-1.5 cm) are also found in the exposed surfaces.

Pine Creek kimberlites are located on a sheep farm 25 km east of Terowie, about 7-8 km SE of the Calcutteroo locality. The Pine Creek kimberlite was originally found by grid load sampling and shallow excavation (Western Queen (S.A.) Pty. Ltd., 1981). Detailed mapping suggested that the rock is a T shaped body of 0.35 km long and 4 km wide. In general, the exposed kimberlite rocks have an olive green colour and are intruded by many sieve-like carbonate veinlets of 0.2 to 1.5 cm wide. Many kimberlite fragments also contain coarse grained phlogopite of 0.7 to 3.5 cm size.

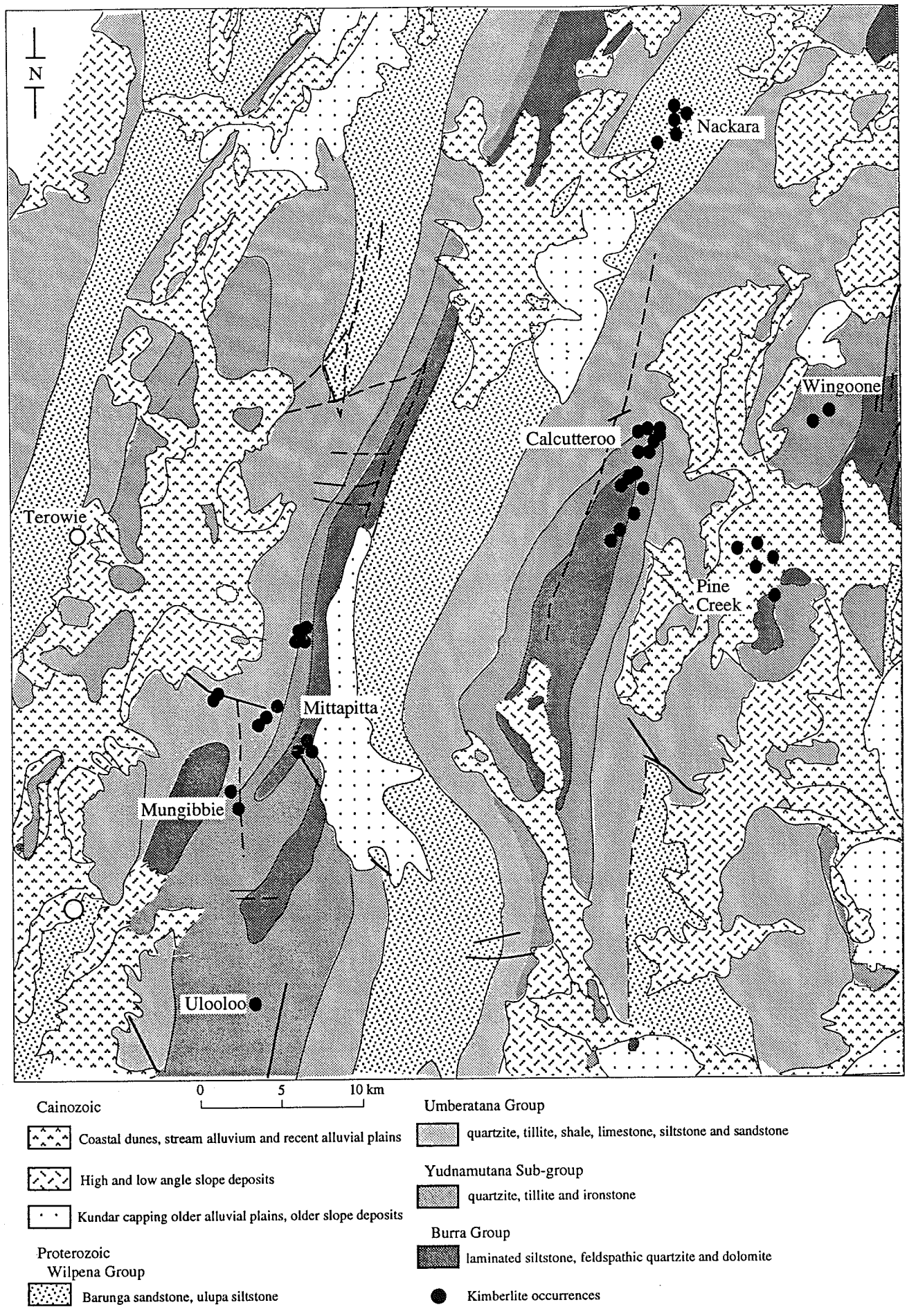

Fig. 5.5. Generalised geology of the Terowie-Whyte, Yarcowie area showing distribution of kimberlites.

Mitopitta kimberlites were naturally exposed in a small creek in fairly hilly country (Western Queen (S.A.) Pty. Ltd., 1981). A kimberlite pipe exposed by the bulldozing has been shown to have a highly brecciated texture with abundant heteroxenoliths of country rocks. The Mitopitta kimberlites were reported to be basaltic kimberlite (Group I kimberlites), because of the absence of mica phenocrysts (Western Queen (S.A.) Pty. Ltd., 1981).

5.5.4. Truro lamprophyres

Truro is located on 80 km NE of Adelaide. An Ordovician lamprophyre swarm occurs in the Karinya syncline in the northern part of the Cambrian Kanmantoo trough. They are adjacent to the eastern margin of N-NW lineament of the Adelaide Geosyncline, between Truro and Frankton (Müller *et al.*, 1993). Their geological description has been done by Morris (1990) and Müller *et al.* (1993) and they are shown in Fig. 5.6. The dykes have a thickness ranging from 0.1 to 1.5 m and intrude along joint planes of the country rocks, but dominantly in the NE strike direction (Müller *et al.*, 1993). In a large quarry located 6 km east of Truro adjacent to the Sturt highway, two large dykes of 6 to 8 m long and 0.1 to 0.6 m wide intrude into the metashales and metasiltstones in the direction of N30E and SE60.

5.6. Petrography and mineral chemistry of the South Australian kimberlites and lamprophyres

The freshest kimberlite and lamprophyre samples were selected for petrological descriptions. However, most of the kimberlites are strongly altered relative to the lamprophyres so that their petrographical description are limited. A general summary is shown in the Table 5.4.

Table 5.4. A summary of petrography and microscopic texture for the South Australian kimberlites and lamprophyres.

Rock type	Locality	Petrography	Texture & Comment
Kimberlite	Port Augusta	Phlo, Ol, Ver, Ser, Chl, Cal, Opaque Oxide	Abundant Ol pseudomorphs
Kimberlite	Calcutteroo	Phlo, Ol, Ver, Ser, Chl, Apt, Cpx, Cal, OPx, Opaque Oxide	Porphyritic texture, lineation, more mica rich
Kimberlite	Pine Creek	Phlo, Ol, Ver, Ser, Chl, Opaque Oxide	Distinctive lineation, porphyritic texture, abundant Calcite veins
Lamprophyre	Truro	Phlo, Apt, K-fd, Pl, Qt, Am, Cal, Il, Sul, Opaque Oxide	Distinctive porphyritic texture, lineation

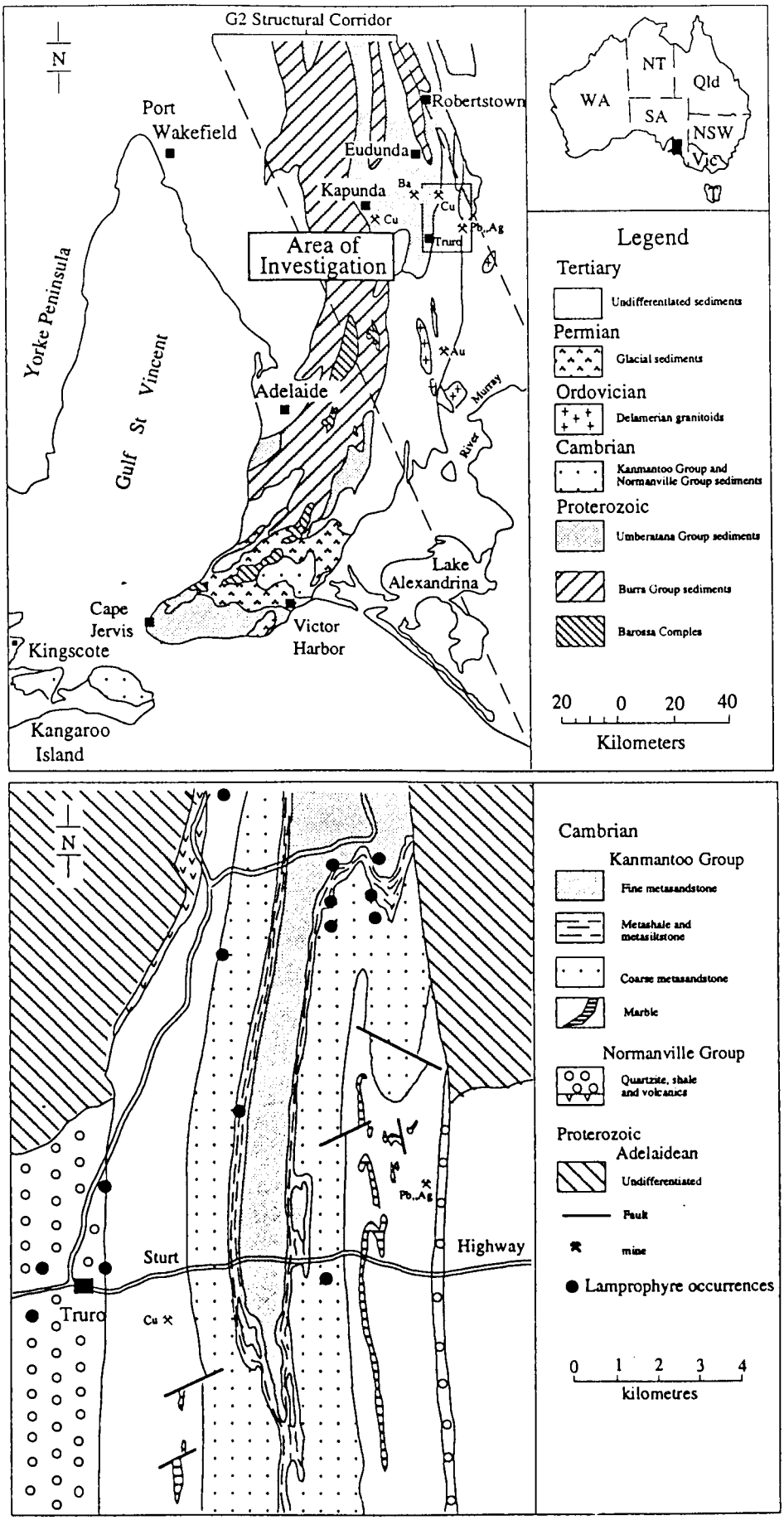

Fig. 5.6. Generalised geology of the Truro area showing distribution of lamprophyres (Müller *et al.*, 1993).

5.6.1. Port Augusta kimberlites

Port Augusta kimberlites are highly altered or serpentinized. The kimberlites show pale greenish (greyish) colour in the hand specimens (Fig. 5.7). In a few thin sections of the least altered samples, phlogopite and abundant pseudomorphsed olivine phenocrysts are recognisable together with minor reddish black opaque grains (Fig. 5.7). The Port Augusta kimberlites are distinguishable from those of Calcutteroo by their abundant pseudomorphosed olivine phenocrysts relative to phlogopite. The altered phlogopites (vermiculite) show a grain size ranging from 0.05 mm to 4 mm, and their pronounced cleavage and pleochroic colours are distinctive.

In general, the phenocryst phlogopites show green pleochroic rims or cleavage and red brown cores. Relatively coarse grained phlogopite phenocrysts show curved or kinked cleavage. Groundmass phlogopites occur as interstial grains among olivine pseudomorphs. They show fibrous textures. The olivine phenocrysts show equi-to sub-granular grain shape and some appear as polygonal quartz grains or serpentine. Secondary opaque oxides grains are found along the cleavage and in the rim of phlogopites. The opaque oxide grains show mainly reddish - black colour. Thin calcite veinlets also intrude into the olivine grains, but are not common in this area compared to their abundance in the Pine Creek kimberlites.

5.6.2. Calcutteroo kimberlites

Calcutteroo kimberlites contain rounded or angular shaped country rock fragments from the Proterozoic sedimentary rocks (Fig. 5.7). The kimberlites are characterised by abundant mica grains relative to the serpentinized or altered olivine pseudomorphs (?) and a pronounced flow texture. Other grains include phlogopites, two-pyroxenes, apatites and opaque oxides as a groundmass.

In general, phlogopite phenocrysts occur as porphyritic 0.1 to 0.4 cm grains. Many of them show zonation and faint red brown in core and darkish brown in their rim, suggestive of different chemical compositions (Fig. 5.7). The grains contain abundant scattered spotted blackish opaque grains and apatite as inclusion or in their rim. In general, the grains are lath shape and the rims of the grains are slightly altered at the long axis of the grains. Some of them show distinctive cleavages and curveratured grain shapes (kinking band). A few medium grained phlogopites having a round boundary show a yellow brown pleochroic colour. Olivine occurs as pseudomorphs of round grain shape. As the olivine grains are significantly altered to serpentine, it is difficult to find a remnant of the original grains. Many of them show a fibrous texture within the grain boundary with blackish fluid inclusions.

Groundmass phlogopites show mainly thin lath-prismatic shapes with minor spine-like shapes. Generally lath-or prismatic-shaped phlogopite grains envelop the serpentinized (or pseudomorphosed) olivine grains and porphyritic phlogopites (Fig. 5.7). Apatite occurs

mainly as a groundmass and minor inclusion in the phlogopite phenocrysts. Augitic-salitic and enstatitic pyroxenes also occur as a groundmass, dominantly as glassy or cryptocrystalline grains. Opaque oxides mainly occur as scattered spotted grains, as inclusions and in the rim of the ferrous grains as a result of the alteration. Amphibole also occurs as a groundmass.

5.6.3. Pine Creek kimberlites

These are carbonate-mica bearing kimberlites showing a light greenish grey colour (Fig. 5.7). Abundant porphyritic phlogopites ranging from 0.2 to 1.5 cm (mainly, 0.2 cm to 0.7 cm wide) are well exposed within altered kimberlites with a distinctive direction. Generally, the porphyritic phlogopite phenocrysts and megacrysts (?) are not altered whereas groundmass grains are mainly altered, probably, suggestive of different generation.

The kimberlites contain abundant altered pholgopites and pseudomorphs of olivine (?) as phenocrysts with relatively abundant calcite and accessory opaque oxide grains. In general, the phenocryst phlogopites are altered to chlorite (?), or vermiculite along their cleavages and in their rims, partly or completely. However, distinctive cleavage and pleochroic colours suggest that the original grains were phlogopites. Despite the alterations, the grains are arranged in a direction of the less pronounced lineation.

The phlogopite phenocrysts also show kinking banded (curveratured) grain shapes and display blue pleochroic colour by alteration. Pseudomorphed olivines (?) show a mainly euhedral granular grain shape and the grains are generally replaced by polygonal quartz grains. However, their modal proportions against phlogopite are low relative to those from Port Augusta.

Groundmass phlogopites are show a lath-shaped grain boundary. Abundant scattered blackish coloured opaque grains show remnants of ferrous minerals. Some of them show prismatic grain shape by the alteration of all grains, which were probably phlogopites. However, opaque oxides are mainly scattered in the rims or cleavages of altered grains. Most of the host kimberlites are intruded by thin calcite veinlets. Calcite grains also occur by alteration of the previous constitutional minerals in the kimberlites.

5.6.4. Truro lamprophyres

Truro lamprophyres are characterised by a distinctive lineation with the alignment of phlogopites, and porphyritic textures (Fig. 5.7). These rocks contain phlogopite as phenocrysts and phlogopite, apatite, K-feldspar, plagioclase, quartz, amphibole, calcite, ilmenite, sulphide and opaque oxide as groundmass. The phenocryst phlogpoites show dominantly prismatic shapes with minor diamond shapes. They usually show a corroded grain boundary to their long axes suggestive of the reaction during crystallisation (Müller *et al.*, 1993). Usually, the phenocrysts show a zonal texture, but are common in the diamond shaped grains. The grains also contain many fine grained inclusions. Apatite also shows a

variable grain size and is relatively abundant.

The lamprophyres are also largely divided into two types; porphyritic phlogopite phenocryst dominant types and apatite-phlogopite dominant type. The first types are characterised by an abundant felsic groundmass, and minor accessory apatites, whereas the second types are characterised by less distinctive porphyritic phlogopite phenocryst, and relatively coarse grained apatites.

The first type (LPTU 3, 4) contains abundant voids which are enveloped by many thin lamellae shaped phlogopite groundmass. Felsic groundmass grains are dominantly K-feldspar (orthoclase) showing radiated cluster shapes. Minor groundmass includes thin lamellae shaped albite-twinned plagioclase, thin prismatic shaped apatite, with scattered opaque oxide. In general, phlogopite phenocrysts of this group shows corroded borders, and groundmass phlogopites are coarser than those of the second group. Many glassy or cryptocrystalline grains also occur as their inclusions.

The second type (LPTU 1, 2) is characterised by abundant long prismatic or rectangular shaped apatites and thin lamellae shaped phlogopite phenocrysts. In this group, phlogopite phenocrysts show dominantly lath or prismatic shaped grains and generally groundmass occur as cryptocrystalline or glassy grains. A few broken diamond shaped phlogopite phenocrysts only show a distinctive zonal texture, faint brown pleochroic colour in their core and red brown pleochroic colour in their rim.

Sample, LPTU 2 shows an aggregation, a felsic groundmass dominant part and a phlogopite groundmass dominant part with a complicated flow texture. It may suggest that the aggregation of the distinctive mineralogy occurred before the lamprophyre dykes separated from parental magma by partial melting of the parental magma.

As a groundmass, the feldspars mainly occur as white greyish coloured dusty grains. Thus, it is difficult to distinguish the two grains under the microscope. The plagioclases are albite and K-feldspars are sanidine. Quartz also occurs as a groundmass. A few amphibole grains showing edenitic composition occur as a groundmass in the sample LPTU 2.

Calcite also occurs as a groundmass. However, it is not clear whether the grains are originated from parent magma or from alteration of the different minerals. As other accessory minerals, iron sulphide and ilmenite occur as a scattered grains or dusty within the groundmass. Probably, the grains are from alteration of ferrous minerals, but a few ilmenite may be originated from host magma (?). Groundmass phlogopites are thin lamellae shaped or spine-like grains. The grains show a faint brown pleochroic colour. Other scattered opaque oxides are mainly found within and adjacent to the ferrous grains.

Figures opposite;

Fig. 5.7a. Photograph of serpentinized Port Augusta kimberlites.

Fig. 5.7b. Photograph of a phlogopite in serpentinized Port Augusta kimberlites.

Fig. 5.7c. Photograph of fresh Calcutteroo kimberlites containing fragments of the Proterozoic Burra Group sediments.

Fig. 5.7d. Photograph of a Pine Creek kimberlite which are mainly intruded by carbonate veinlets of 0.2 to 1.5 cm wide.

Fig. 5.7e. Photograph of a Pine Creek kimberlite containing coarse grained phlogopites of 0.7-3.5 cm size.

Fig. 5.7f. Photograph of of a Truro lamprophyre.

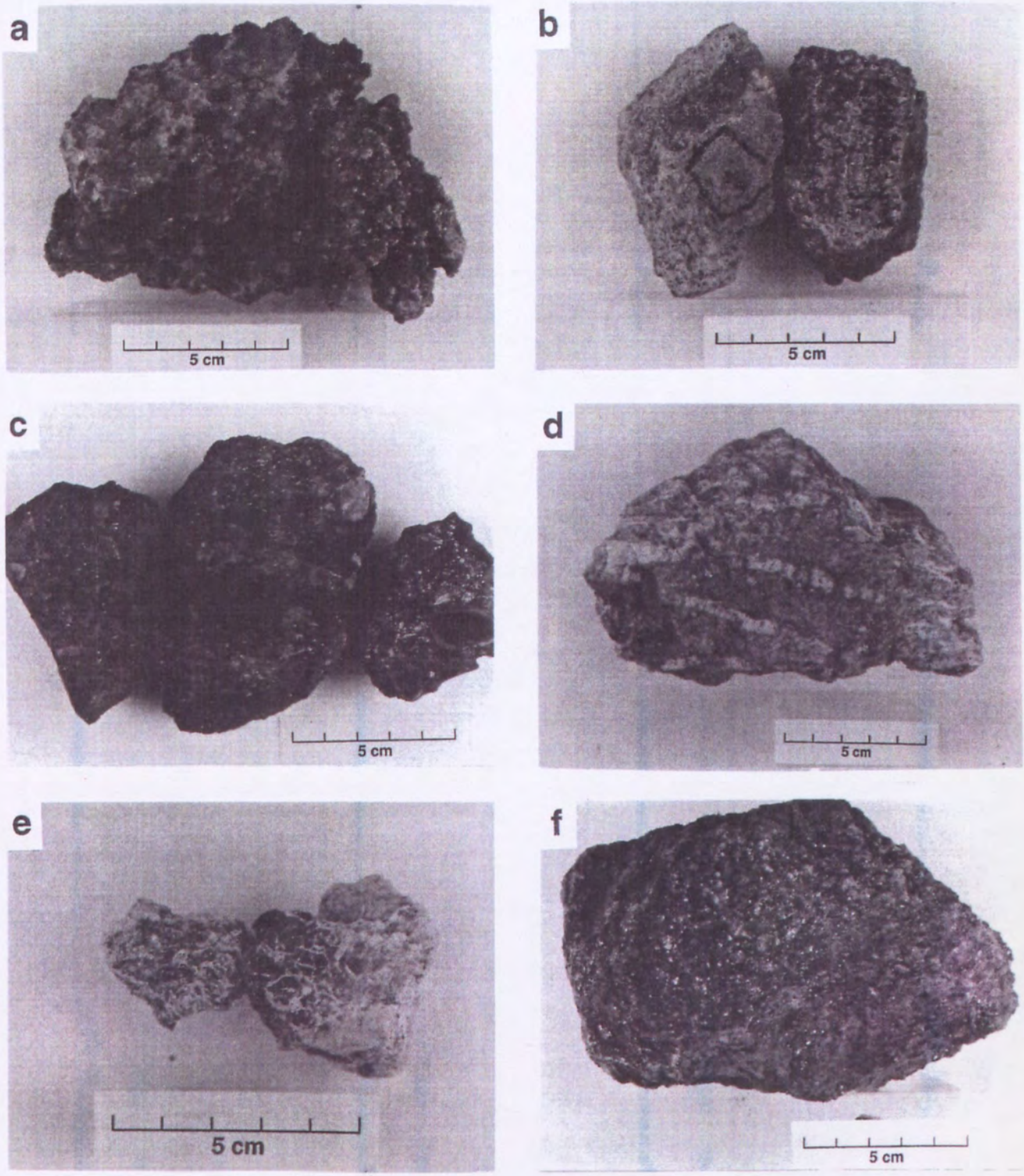
a
5 cm
b
5 cm
c
5 cm
d
5 cm
e
5 cm
f
5 cm

Figures opposite;

Fig. 5.7g. Photomicrograph of a Calcutteroo mica rich kimberlite which contains phlogopite as phenocrysts (p) and phlogopite, augitic-salitic and enstatic pyroxene, apatite, amphibole, and Fe-Ti oxide as groundmass.

Fig. 5.7h. Photomicrograph of a Port August kimberlite which show a phlogopite (vermiculite, p) grain and olivine pseudomorphs (?). Notice that the Port Augusta kimberlite contains more abundant olivine pseudomorphs than the Calcutteroo kimberlites.

Fig. 5.7i. Photomicrograph of a Truro lamprophyre (LPTU 4) showing a distinctive lineation and porphyritic texture. Zoning is common in porphyritic phlogopites. Groundmass include phlogopite, apatite, sanidine, albite, quartz, amphibole, calcite, ilmenite and sulphide.

Fig. 5.7j. Photomicrograph of a Truro lamprophyre (LPTU 1) which contain abundant apatites and thin lamellar shaped phlogopites .

Width of a scale bar (left bottom) is 1 millimetre.

g
p

h
p

i
p

j
p

5.6.5. Mineral Chemistry

Primary and secondary minerals were analysed in the freshest kimberlites and lamprophyres using the JEOL 733 microprobe at the University of the Adelaide. Details of analytical methods are shown in Appendix 1. Representative analyses are shown in Table 5.5 ~ 5.10.

Serpentine; Abundant serpentines occur in all of the altered South Australian kimberlites. The grains may have originated from alteration of magnesian olivine in these kimberlites. The typical equation (Deer *et al.*, 1966) is as follows; $3Mg_2SiO_4$ (forsterite)+SiO_2+$2H_2O$ = $2Mg_3Si_2O_5(OH)_4$ (serpentine). The grains from Port Augusta kimberlites show a SiO_2 of 39- 42 wt % and MgO of 40-42 wt % with H_2O of 8-13 wt % (Table 5.5).

Vermiculite; Vermiculite is also common in all altered South Australian kimberlite. Usually, the grains are distinguished from phlogopite by pronounced greenish pleochroic colour. The analysed vermiculates from Port Augusta contain MgO of 23-24 wt %, FeO of 9.5-9.7 wt % and Al_2O_3 of 8.7-9.1 wt % (Table 5.5).

Feldspar; Plagioclase only occurs in the Truro lamprophyres where it coexists with K-feldspar. The plagioclase has dominantly albite composition (Ab 92-99) while the K-feldspars have potassium-rich compositions ($Ab_{0.4-9}$ Or_{90-98} in the sample LPTU 1 and $Ab_{0.6-1}$ Or_{97-99} in the sample LPTU 4) (Fig. 5.8, Table 5.6).

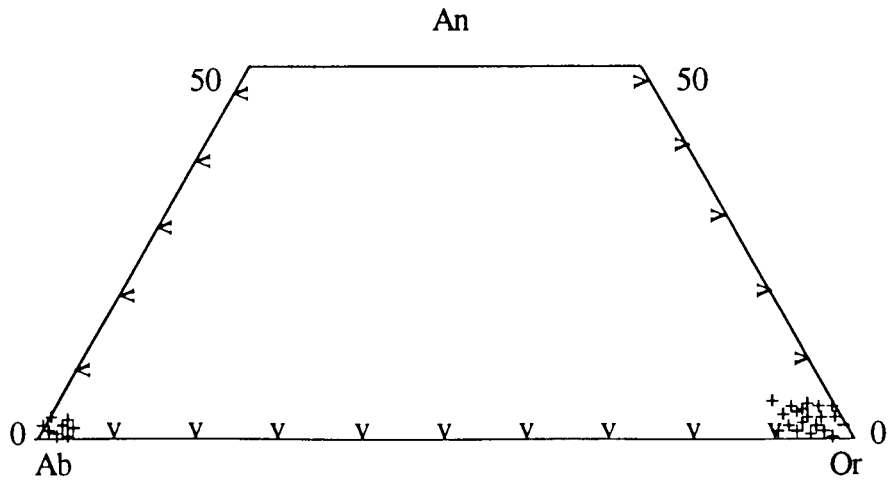

Fig. 5.8. Feldspar compositions of the Truro lamprophyres.

Amphibole; Amphibole occurs as a groundmass in kimberlites and lamprophyres. The amphiboles from Calcutteroo kimberlite are of pargasitic to edenitic composition (Table 5.7).

Spinel; Chrome spinel occurs as a groundmass in the Calcutteroo kimberlite (TRWI A1).

The grains contain Al_2O_3 of 18-22 wt %, FeO(t) of 18-19 wt %, MgO of 14-17 wt %, and Cr_2O_3 of 36-44 wt % (Table 5.7).

Ilmenite; Ilmenite occurs in all rock types. In the Truro lamprophyres, the grains are more common than those of the Calcutteroo kimberlites. Their analyses from Truro lamprophyre are given in Table 5.7. They contain TiO_2 of 50-54 wt %, FeO of 39-43 wt % and MgO of 0.13-0.24 wt %.

Iron sulphide; Iron sulphides are also analysed in the samples of the Truro lamprophyres (Table 5.7). The grains usually contain FeO(t) of 32-34 wt % and SO_3 of 66-67 wt %.

Calcite; Carbonate occur in all kimberlite and lamprophyre samples, but is most common in the kimberlites (Table 5.7). Much of these is of primary magmatic origin, however, some including that in the groundmass of the Truro lamprophyres may be a hydrothermal alteration product.

Apatite; Apatites occur in all kimberlites and lamprophyres, but common in lamprophyres. Abundant apatite grains occur in apatite-rich type lamprophyres (Table 5.7).

Pyroxene; Orthopyroxenes and clinopyroxenes occur as a groundmass in Calcutteroo kimberlites. They have salitic-augitic and enstatitic composition respectively. Clinopyroxenes in sample TRWI CH-1 have diopsidic, augitic and salitic compositions whereas those in the sample, TRWI A1 have salitic compositions. These clinopyroxenes show insufficient Si+Al to fill the terahedral sites, suggestive of the presence of Ti in the terahedral sites. In the sample, TRWI A1, orthopyroxenes show typical enstatitic composition (Tables 5.7, 8).

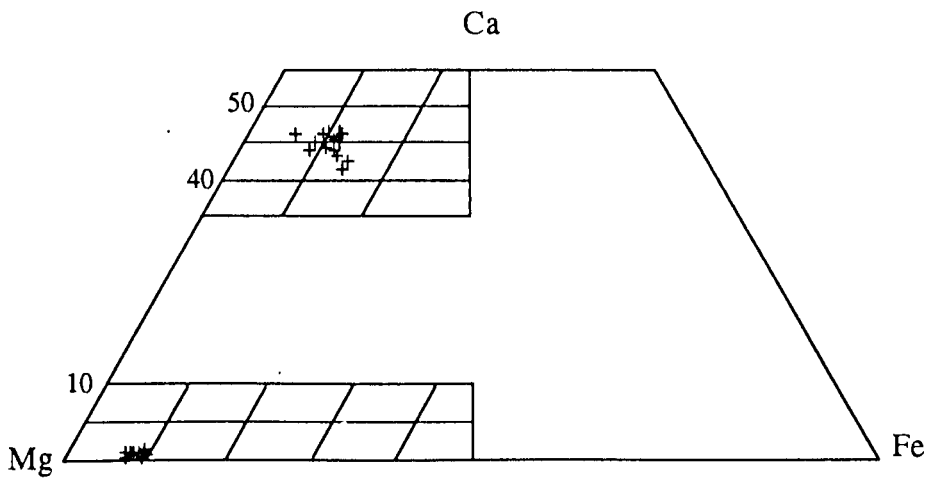

Fig. 5.9. Pyroxene compositions of the Calcutteroo kimberlites.

Table 5.5. Representative analyses of altered minerals of the Port Augusta kimberlites.

Oxide											
SiO2	43.69	42.45	42.14	43.25	41.54	41.37	34.25	41.59	40.26	38.26	38.87
TiO2	0.12	0.09	0.23	0.07	0.05	0.21	0.43	0.57	0.68	0.47	0.40
Al2O3	0.00	0.00	0.28	0.09	0.00	0.16	5.35	4.74	6.20	8.76	9.06
FeO#	7.40	7.63	8.93	9.15	5.64	7.78	14.94	16.86	15.72	9.59	9.70
MnO	0.26	0.32	0.10	0.27	0.14	0.40	0.07	0.10	0.11	0.00	0.00
MgO	32.74	32.01	27.47	27.47	33.74	31.10	21.51	18.41	22.78	23.37	23.83
CaO	0.18	0.15	0.09	0.31	0.00	0.18	0.23	0.51	0.44	1.25	1.30
Na2O	0.00	0.42	0.00	0.31	0.00	0.25	0.37	0.37	0.87	0.59	0.95
K2O	0.23	0.28	0.41	0.43	0.25	0.34	0.16	0.26	0.42	0.12	0.05
P2O5	0.00	0.00	0.00	0.00	0.00	0.05	0.14	0.06	0.00	0.00	0.00
SO3	0.14	0.00	0.27	0.01	0.12	0.33	0.13	0.06	0.00	0.00	0.15
Cr2O3	0.26	0.13	0.00	0.14	0.11	0.00	0.17	0.02	0.01	0.00	0.00
NiO	0.08	0.00	0.38	0.35	0.12	0.00	0.36	0.70	0.09	0.01	0.32
Total	85.08	83.47	80.29	81.86	81.71	82.19	78.10	84.24	87.57	82.41	84.61
	Number of Ions on the Basis of 6(O)						Number of Ions on the Basis of 6(O)				
Si	1.8236	1.8160	1.8750	1.8950	1.7943	1.7983	1.6445	1.8361	1.7092	1.6691	1.6555
Ti	0.0038	0.0028	0.0076	0.0024	0.0017	0.0070	0.0155	0.0189	0.0218	0.0155	0.0127
Al	0.0000	0.0001	0.0148	0.0048	0.0000	0.0083	0.3028	0.2463	0.3100	0.4505	0.4546
Fe(t)	0.2582	0.2729	0.3321	0.3352	0.2037	0.2827	0.5996	0.6222	0.5578	0.3496	0.3452
Mn	0.0090	0.0114	0.0038	0.0101	0.0051	0.0149	0.0027	0.0037	0.0038	0.0000	0.0000
Mg	2.0360	2.0398	1.8206	1.7926	2.1708	2.0136	1.5385	1.2104	1.4409	1.5186	1.5116
Ca	0.0079	0.0068	0.0041	0.0147	0.0002	0.0084	0.0117	0.0243	0.0201	0.0584	0.0593
Na	0.0000	0.0347	0.0000	0.0260	0.0000	0.0213	0.0343	0.0313	0.0714	0.0497	0.0783
K	0.0121	0.0150	0.0235	0.0239	0.0136	0.0189	0.0098	0.0145	0.0229	0.0068	0.0025
P	0.0000	0.0000	0.0000	0.0000	0.0000	0.0019	0.0057	0.0021	0.0000	0.0000	0.0000
S	0.0042	0.0000	0.0090	0.0003	0.0040	0.0109	0.0046	0.0019	0.0000	0.0000	0.0048
Cr	0.0085	0.0043	0.0000	0.0048	0.0037	0.0000	0.0063	0.0008	0.0003	0.0000	0.0000
Ni	0.0026	0.0000	0.0134	0.0124	0.0040	0.0001	0.0139	0.0249	0.0030	0.0004	0.0110
Sum	4.1660	4.2040	4.1040	4.1220	4.2010	4.1860	4.1900	4.0370	4.1610	4.1180	4.1350

Table 5.6. Representative groundmass feldspar analyses of the Truro lamprophyres.

Sample	LPTU 4				LPTU 1						
SiO2	67.40	67.36	67.81	67.40	63.16	62.57	63.20	62.33	61.96	62.63	62.44
TiO2	0.00	0.00	0.07	0.01	0.33	0.46	0.47	0.40	0.33	0.36	0.94
Al2O3	19.59	19.40	18.98	19.48	17.73	18.62	17.81	18.51	18.76	18.99	18.50
FeO#	0.14	0.03	0.10	0.14	0.01	0.00	0.00	0.00	0.00	0.08	0.00
MnO	0.11	0.12	0.18	0.00	0.00	0.00	0.00	0.14	0.01	0.12	0.12
MgO	0.13	0.00	0.22	0.00	0.02	0.00	0.15	0.00	0.00	0.00	0.12
CaO	0.04	0.24	0.62	0.22	0.62	0.83	0.57	0.96	0.94	1.17	0.96
Na2O	10.36	11.09	10.14	10.97	0.10	0.48	0.13	0.59	0.38	0.49	0.20
K2O	0.65	0.18	0.07	0.12	16.23	15.29	16.17	15.17	15.07	14.76	15.66
P2O5	0.00	0.00	0.00	0.12							
SO3	0.04	0.02	0.00	0.05							
Cr2O3	0.01	0.21	0.12	0.04	0.03	0.05	0.04	0.02	0.21	0.02	0.14
NiO	0.03	0.00	0.00	0.04							
Total	98.50	98.67	98.32	98.58	98.21	98.30	98.54	98.12	97.65	98.61	99.07
	Number of Ions on the Basis of 32(O)				Number of Ions on the Basis of 32(O)						
Si	11.9521	11.9383	12.0204	11.9337	11.9369	11.7842	11.9032	11.7745	11.7449	11.7420	11.7092
Ti	0.0000	0.0000	0.0086	0.0008	0.0470	0.0654	0.0665	0.0567	0.0467	0.0504	0.1327
Al	4.0942	4.0520	3.9653	4.0642	3.9476	4.1323	3.9517	4.1213	4.1906	4.1953	4.0871
Fe(t)	0.0208	0.0041	0.0152	0.0204	0.0010	0.0000	0.0000	0.0000	0.0000	0.0119	0.0000
Mn	0.0159	0.0186	0.0277	0.0000	0.0000	0.0000	0.0000	0.0222	0.0015	0.0192	0.0187
Mg	0.0339	0.0000	0.0582	0.0000	0.0044	0.0000	0.0428	0.0000	0.0000	0.0000	0.0347
Ca	0.0079	0.0457	0.1181	0.0410	0.1257	0.1666	0.1157	0.1932	0.1917	0.2339	0.1920
Na	3.5588	3.8092	3.4840	3.7636	0.0350	0.1759	0.0479	0.2157	0.1376	0.1766	0.0711
K	0.1462	0.0412	0.0149	0.0272	3.9119	3.6713	3.8835	3.6547	3.6422	3.5280	3.7454
P	0.0000	0.0000	0.0000	0.0174							
S	0.0057	0.0023	0.0000	0.0068							
Cr	0.0010	0.0299	0.0168	0.0055	0.0041	0.0081	0.0059	0.0033	0.0319	0.0035	0.0213
Ni	0.0050	0.0000	0.0000	0.0055							
Sum	19.8414	19.9413	19.7293	19.8862	20.0137	20.0038	20.0172	20.0417	19.9870	19.9606	20.0121
An	0.2	1.2	3.3	1.1	3.1	4.2	2.9	4.8	4.8	5.9	4.8
Ab	95.9	97.8	96.3	98.2	0.9	4.4	1.2	5.3	3.5	4.5	1.8
Or	3.9	1.1	0.4	0.7	96.1	91.5	96.0	89.9	91.7	89.6	93.4

Table 5.7. Representative analyses of accessory minerals from the South Australian kimberlites and lamprophyres.

Sample	LPTU 1				TRWI A1	TRWI CH 1		LPTU 4	LPTU 1		LPTU 2	LPTU 4	TRWI CH 1
Mineral	Ilmenite				Spinel	Amphibole		Calcite	?		Apatite		
Lithology	Lamprophyres				Kimberlite	Kimberlite		Lamprophyre	Lamprophyre		Lamprophyre	Lamprophyre	Kimberlite
SiO2	0.44	0.68	0.31	0.52	0.25	46.65	49.37	0.99	0.00	0.00	0.00	0.00	1.13
TiO2	52.91	49.99	50.30	51.88	0.14	2.36	1.88	0.02	0.00	0.11	0.01	0.10	0.16
Al2O3	0.22	0.48	0.13	0.18	21.85	2.38	1.31	0.60	0.00	0.00	0.00	0.00	0.00
FeO#	39.24	42.61	41.44	41.08	18.95	15.75	15.50	0.21	33.12	32.65	0.28	0.22	0.73
MnO	0.82	1.17	0.63	0.79	0.87	0.53	0.50	0.19	0.05	0.08	0.07	0.29	0.07
MgO	0.13	0.22	0.12	0.24	13.85	9.28	9.65	0.65	0.00	0.00	0.45	0.44	0.06
CaO	0.11	0.08	0.06	0.00	0.07	11.15	13.92	52.59	0.01	0.00	54.15	54.17	54.19
Na2O	0.35	0.40	0.67	0.24	0.00	3.98	4.23	0.68	0.09	0.00	0.19	0.00	0.20
K2O	0.26	0.55	0.26	0.02	0.00	2.14	0.86	0.21	0.00	0.00	0.00	0.24	0.13
P2O5	0.00	0.26	0.11	0.00	0.00	0.83	0.50		0.00	0.06	40.24	40.69	39.33
SO3	0.00	0.00	0.00	0.00	0.00	0.20	0.00		66.42	66.98	0.00	0.00	0.00
Cr2O3	0.07	0.32	0.01	0.03	43.68	0.34	0.26	0.00	0.00	0.00	0.00	0.01	0.00
NiO	0.00	0.16	0.13	0.25	0.59	0.00	0.00		0.30	0.12	0.00	0.00	0.00
Total	94.55	96.90	94.17	95.24	100.26	95.59	97.99	56.13	100.00	100.00	95.39	96.15	96.00
Number of Ions on the Basis of				6(O)	32(O)	24(O)		6(O)	6(O)		25(O)		
Si	0.0231	0.0350	0.0166	0.0270	0.0615	7.5515	7.7670	0.0645	0.0000	0.0000	0.0000	0.0000	0.1949
Ti	2.0714	1.9407	2.0067	2.0311	0.0266	0.2872	0.2228	0.0007	0.0001	0.0029	0.0009	0.0129	0.0207
Al	0.0132	0.0295	0.0080	0.0113	6.3939	0.4530	0.2419	0.0461	0.0000	0.0000	0.0000	0.0000	0.0000
Fe(t)	1.7084	1.8398	1.8386	1.7884	3.9334	2.1316	2.0386	0.0116	0.9351	0.9171	0.0405	0.0308	0.1047
Mn	0.0363	0.0510	0.0284	0.0350	0.1835	0.0720	0.0660	0.0102	0.0015	0.0023	0.0098	0.0418	0.0107
Mg	0.0097	0.0170	0.0094	0.0186	5.1218	2.2381	2.2619	0.0631	0.0000	0.0000	0.1150	0.1133	0.0164
Ca	0.0062	0.0044	0.0032	0.0000	0.0190	1.9335	2.3457	3.6644	0.0003	0.0000	10.0364	9.9697	9.9982
Na	0.0350	0.0400	0.0691	0.0243	0.0000	1.2477	1.2898	0.0851	0.0058	0.0002	0.0644	0.0000	0.0665
K	0.0175	0.0360	0.0172	0.0013	0.0000	0.4414	0.1728	0.0170	0.0000	0.0000	0.0000	0.0520	0.0290
P	0.0000	0.0113	0.0049	0.0000	0.0000	0.1140	0.0660		0.0000	0.0017	5.8928	5.9162	5.7330
S	0.0000	0.0000	0.0000	0.0000	0.0000	0.0242	0.0000		1.6839	1.6892	0.0000	0.0000	0.0000
Cr	0.0029	0.0130	0.0005	0.0011	8.5712	0.0438	0.0327	0.0000	0.0000	0.0000	0.0000	0.0015	0.0000
Ni	0.0000	0.0065	0.0057	0.0106	0.1186	0.0000	0.0000		0.0082	0.0031	0.0000	0.0000	0.0000
Sum	3.9240	4.0240	4.0080	3.9490	24.4320	16.5360	16.5040	3.9627	2.6350	2.6160	16.1598	16.1381	16.1740

Table 5.8. Representative analyses of clinopyroxene groundmass from the Calcuttroo kimberlites.

OXIDE	TRWI CH1											TRWI A1
SiO2	49.81	49.81	50.99	51.13	50.42	50.09	49.34	48.82	49.43	50.60	50.93	51.91
TiO2	1.73	1.73	1.17	1.46	1.62	1.92	1.52	1.59	1.42	1.25	1.43	0.14
Al2O3	1.63	1.63	0.76	1.07	0.90	1.54	2.21	2.49	1.45	0.83	2.15	1.05
FeO#	6.70	6.70	5.83	5.32	6.26	6.28	8.00	7.70	6.52	5.90	5.10	1.64
MnO	0.18	0.18	0.35	0.00	0.19	0.00	0.26	0.28	0.28	0.20	0.16	0.00
MgO	15.35	15.35	15.31	15.34	14.85	14.57	15.12	15.09	14.97	15.37	16.18	17.36
CaO	21.35	21.35	23.19	23.48	23.14	23.35	20.18	20.09	22.53	23.35	24.27	23.95
Na2O	0.83	0.83	0.73	0.71	0.63	0.85	0.69	0.85	0.80	0.77	0.27	0.00
K2O	0.77	0.77	0.28	0.11	0.10	0.05	0.82	0.99	0.56	0.12	0.00	0.03
P2O5	0.05	0.05	0.01	0.05	0.04	0.00	0.31	0.04	0.19	0.41	0.00	0.00
SO3	0.00	0.00	0.00	0.00	0.10	0.00	0.00	0.04	0.17	0.00	0.00	0.07
Cr2O3	0.17	0.17	0.57	0.58	0.35	0.37	0.33	0.35	0.41	0.32	0.71	0.73
NiO	0.00	0.00	0.00	0.10	0.00	0.44	0.40	0.20	0.00	0.11	0.00	0.11
Total	98.57	98.57	99.18	99.34	98.60	99.47	99.17	98.53	98.72	99.23	101.19	96.97
					Number of Ions on the Basis of 6 (O)							
Si	1.8894	1.8894	1.9187	1.9125	1.9080	1.8852	1.8681	1.8621	1.8765	1.9010	1.8702	1.9482
Ti	0.0494	0.0494	0.0330	0.0409	0.0461	0.0542	0.0433	0.0455	0.0404	0.0354	0.0394	0.0038
Al	0.0729	0.0729	0.0337	0.0470	0.0403	0.0685	0.0985	0.1119	0.0649	0.0366	0.0932	0.0464
Fe(t)	0.2124	0.2124	0.1833	0.1665	0.1980	0.1977	0.2534	0.2456	0.2068	0.1852	0.1566	0.1515
Mn	0.0059	0.0059	0.0110	0.0000	0.0061	0.0000	0.0083	0.0089	0.0091	0.0062	0.0050	0.0000
Mg	0.8672	0.8672	0.8582	0.8547	0.8371	0.8171	0.8529	0.8573	0.8463	0.8602	0.8847	0.9704
Ca	0.8671	0.8671	0.9345	0.9408	0.9378	0.9414	0.8185	0.8206	0.9160	0.9396	0.9544	0.9626
Na	0.0606	0.0606	0.0532	0.0513	0.0461	0.0623	0.0504	0.0625	0.0584	0.0558	0.0189	0.0000
K	0.0372	0.0372	0.0132	0.0051	0.0048	0.0024	0.0394	0.0481	0.0270	0.0057	0.0000	0.0016
P	0.0016	0.0016	0.0002	0.0016	0.0012	0.0001	0.0099	0.0014	0.0062	0.0131	0.0000	0.0000
S	0.0000	0.0000	0.0000	0.0000	0.0027	0.0000	0.0000	0.0012	0.0047	0.0000	0.0000	0.0018
Cr	0.0051	0.0051	0.0170	0.0171	0.0104	0.0110	0.0099	0.0106	0.0124	0.0096	0.0205	0.0216
Ni	0.0000	0.0000	0.0000	0.0029	0.0000	0.0132	0.0121	0.0061	0.0000	0.0032	0.0000	0.0032
Sum	4.07	4.07	4.06	4.04	4.04	4.05	4.06	4.08	4.07	4.05	4.04	4.11
Wo	44.5	44.5	47.3	48.0	47.5	48.1	42.5	42.7	46.5	47.3	47.8	46.2
En	44.5	44.5	43.4	43.6	42.4	41.8	44.3	44.6	43.0	43.3	44.3	46.6
Fs	10.9	10.9	9.3	8.5	10.0	10.1	13.2	12.8	10.5	9.3	7.8	7.3
Mg/Mg+Fe(t)	80.3	80.3	82.4	83.7	80.9	80.5	77.1	77.7	80.4	82.3	85.0	86.5

Table 5.9. Representative analyses of orthopyroxene groundmass from the Calcuttroo kimberlites.

	TRWI A1										
SiO2	56.00	55.79	55.72	55.67	56.28	56.42	56.28	56.42	56.31	56.43	55.93
TiO2	0.00	0.12	0.16	0.13	0.00	0.19	0.00	0.19	0.11	0.05	0.34
Al2O3	1.27	1.00	1.30	1.17	1.44	1.28	1.44	1.28	1.20	1.19	1.14
FeO#	5.63	5.59	5.79	5.51	5.49	5.68	5.49	5.68	5.54	5.67	5.69
MnO	0.23	0.09	0.10	0.01	0.00	0.12	0.00	0.12	0.07	0.18	0.23
MgO	35.01	34.30	34.30	34.61	34.05	34.26	34.05	34.26	34.58	34.31	34.12
CaO	0.23	0.26	0.26	0.31	0.27	0.30	0.27	0.30	0.19	0.21	0.27
Na2O	0.00	0.00	0.00	0.00	0.00	0.00	0.00	0.00	0.00	0.00	0.00
K2O	0.00	0.06	0.04	0.00	0.00	0.10	0.00	0.10	0.05	0.00	0.06
Cr2O3	0.32	0.46	0.49	0.51	0.46	0.08	0.46	0.08	0.40	0.19	0.29
NiO	0.25	0.00	0.06	0.04	0.03	0.05	0.03	0.05	0.11	0.00	0.12
P2O5	0.00	0.13	0.02	0.00	0.00	0.09	0.00	0.09	0.00	0.14	0.00
SO3	0.15	0.08	0.00	0.02	0.00	0.09	0.00	0.09	0.17	0.08	0.00
Total	99.08	97.87	98.24	97.98	98.00	98.66	98.00	98.66	98.73	98.45	98.18
				Number of Ions on the Basis of 6 (O)							
Si	1.9482	1.9611	1.9555	1.9556	1.9717	1.9660	1.9717	1.9660	1.9611	1.9688	1.9633
Ti	0.0000	0.0031	0.0043	0.0035	0.0000	0.0050	0.0000	0.0050	0.0028	0.0014	0.0089
Al	0.0520	0.0416	0.0539	0.0486	0.0594	0.0527	0.0594	0.0527	0.0492	0.0491	0.0473
Fe(t)	0.1637	0.1643	0.1697	0.1619	0.1607	0.1654	0.1607	0.1654	0.1614	0.1653	0.1669
Mn	0.0067	0.0028	0.0031	0.0002	0.0000	0.0035	0.0000	0.0035	0.0021	0.0053	0.0068
Mg	1.8143	1.7960	1.7929	1.8113	1.7768	1.7785	1.7768	1.7785	1.7940	1.7829	1.7840
Ca	0.0087	0.0096	0.0096	0.0116	0.0102	0.0113	0.0102	0.0113	0.0072	0.0079	0.0100
Na	0.0000	0.0000	0.0000	0.0000	0.0000	0.0000	0.0000	0.0000	0.0000	0.0000	0.0000
K	0.0000	0.0026	0.0019	0.0000	0.0000	0.0045	0.0000	0.0045	0.0022	0.0000	0.0027
P	0.0000	0.0039	0.0005	0.0000	0.0000	0.0025	0.0000	0.0025	0.0000	0.0041	0.0000
S	0.0040	0.0021	0.0000	0.0006	0.0000	0.0022	0.0000	0.0022	0.0044	0.0021	0.0001
Cr	0.0089	0.0129	0.0137	0.0141	0.0127	0.0023	0.0127	0.0023	0.0110	0.0052	0.0081
Ni	0.0071	0.0000	0.0017	0.0012	0.0008	0.0015	0.0008	0.0015	0.0032	0.0001	0.0033
Sum	4.013	4.000	4.007	4.008	3.992	3.995	3.992	3.995	3.998	3.992	4.001
Wo	0.4	0.5	0.5	0.6	0.5	0.6	0.5	0.6	0.4	0.4	0.5
En	91.3	91.2	90.9	91.3	91.2	91.0	91.2	91.0	91.4	91.1	91.0
Fs	8.2	8.3	8.6	8.2	8.3	8.5	8.3	8.5	8.2	8.4	8.5
Mg/Mg+Fe(t)	91.7	91.6	91.4	91.8	91.7	91.5	91.7	91.5	91.7	91.5	91.4

Phlogopite; Phlogopites occur as phenocrysts and as groundmass in all South Australian kimberlites and lamprophyres. Representative analyses are given in Table 5.10 and plotted in Fig. 5.10, in which they are compared with those from Western Australian lamproites (Mitchell, 1981), South African kimberlites (Mitchell and Meyer, 1989; Shee *et al.*, 1989) and Orroroo kimberlites (Scott Smith *et al.*, 1984). Each rock contains at least two generations of the phlogopite of different mineralogical composition.

Phlogopite from Calcutteroo kimberlites has a similar composition to those from the Truro lamprophyres and these are very distinct from those of the Western Australian lamproites. In addition, these are also clearly distinctive from those of the Orroroo kimberlites which are more like phlogopites from the South African kimberlites. Zonation is common in the relatively coarse grained phlogopites.

In the CaO/MgO-Mg# plot (Fig. 5.10), phlogopites from Truro lamprophyres and Calcutteroo kimberlites show several groupings which reflect petrographic differences. Most South Australian phlogopites have CaO/MgO ratios > 0.005. High CaO/MgO ratios are shown by the phlogopites of the Truro lamprophyres, whereas lower ratios are shown by the South African and Orroroo kimberlites. Phlogopites from the Western Australian lamproites show slightly higher CaO/MgO ratios than those from the South African kimberlites and lower ratios than those of the South Australian kimberlites and lamprophyres. Higher Mg# of the coarse grained phlogopite phenocrysts relative to fine grained or groundmass suggest that they occurred earlier than fine grained varieties during the crystallisation of the magma. This is also supported by higher Cr_2O_3 contents in those of higher Mg#.

In the sample, LPTU 4 from Truro, phlogopites fall into three types with respective CaO/MgO ratios and Mg# of ; i) 0.017-0.035 with 63-73, ii) 0.007-0.015 with 66-75 and iii) 0.013-0.026 with 85-93. Sample LPTU 1 contains two types of phlogopites; i) groundmass (CaO/MgO ratios of 0.01-0.024), (Mg# of 46-60) and ii) phenocryst (CaO/MgO ratios of 0.005- 0.009, Mg# of 73-89) whereas sample LPTU 2 from Truro also contains two different phlogopite phenocrysts in the mineralogical composition, thick lamellae shaped phenocrysts (0.008-0.018 and 80-90) and diamond-shaped phenocrysts (0.005-0.009 and 67-90, CaO/MgO ratios and Mg#, respectively). Calcutteroo kimberlites also contain two different types of phlogopites, groundmass (0.02-0.03, 64-70), and phenocryst (0.007-0.014, 65-89, CaO/MgO ratios and Mg#, respectively).

Phlogopite phenocrysts from Calcutteroo have similar compositions to those of LPTU 2 and of LPTU 4 showing high Mg#. However, they are clearly distinguished from those of Orroroo kimberlites which are like those from South African kimberlites. Assuming that the phlogopite phenocrysts from Calcutteroo are not xenocrystic and reflect the chemical composition of the host magma, their difference with Orroroo kimberlites showing lower CaO/MgO ratios (<0.003) suggests that Calcutteroo kimberlites are originated from the higher CaO bearing host magma than those of Orroroo kimberlites.

In the Cr_2O_3 (wt %)-Mg# plot (Fig. 5.10), the phlogopite phenocrysts from South

Australian kimberlites and lamprophyres are like those from South Africa. Phenocrysts with higher Mg# show higher Cr_2O_3 contents. In the Calcutteroo kimberlites, coarse grained phenocrysts have higher Cr_2O_3 contents (0.34-1.2 wt %), which is compared with the groundmas (0.11-0.23 wt %).

In the Truro lamprophyres (e.g. LPTU 1), the high Cr_2O_3 contents (0.07-0.58 wt %) of thick prismatic phenocrysts is clearly distinguished from another (later ?) generation of distinctive diamond-shaped phenocrysts which have low Cr_2O_3 contents (0.05-0.13 wt %). Phlogopite phenocrysts from Calcutteroo have slightly higher Cr_2O_3 contents than those of LPTU 2. However, phlogopites from kimberlites and lamproites show higher Mg# (usually <85) with slightly higher Cr_2O_3 contents relative to those from Truro lamprophyres, which suggests that former groups are more primitive (less fractionated) than the latter.

In the CaO/MgO-TiO_2/K_2O plot (Fig. 5.10), South Australian (except Orroroo) phlogopites are distinguished from those from South Africa and Western Australia by high CaO/MgO ratios, while those from South Africa (and Orroroo) are well distinguished from those from Western Australian lamproites by low TiO_2/K_2O ratios. Phlogopites of Calcutteroo showing slightly higher CaO/MgO and TiO_2/K_2O ratios are well distinguished from those of Orroroo kimberlite which show a similar composition with those of South African Group I kimberlites (TiO_2/K_2O ratios, <0.3).

In the sample LPTU 4 from Truro, phlogopites showing a high Cr_2O_3 have higher CaO/MgO ratios (mainly 0.01-0.035) and TiO_2/K_2O ratios (<0.2), even though the phlogopites have wider ranges of CaO/MgO ratios (0.03 - 0.035) with limited TiO_2/K_2O ratios (<0.4). In general, the phlogopite grains from the each section are divided into the several types in thems of major element ratios. In the sample LPTU 1 from Truro, phlogopite phenocryst showing lower CaO/MgO (0.001-0.009) and TiO_2/K_2O ratios (0.17-0.3) are well distinguished from those of the groundmass (0.014-0.022 and 0.42-0.55, respectively). In the sample, LPTU 2, thick lamellae shaped phlogopites (TiO_2/K_2O ratios of 0.25-0.31 and CaO/MgO ratios of 0.01-0.017) are well distinguished from the diamond shaped grains (having 0.2-0.47, <0.01 respectively).

In the SiO_2/TiO_2-Mg# diagram (Fig. 5.10), phlogopites from different sources are divided into several types. In the sample LPTU 4 from Truro, the phlogopites are divided into two types on the basis of respective SiO_2/TiO_2 ratios and Mg#, i) 10-23 and 64-93 & ii) 10-35 and 64-75. Even though the phlogopites in the sample, LPTU 4 from Truro are uniform thin rod shapes without variable grain size, two significantly different trends of phlogopite composition still emerge revealing more complex cooling histories.

In the sample LPTU 2 from Truro, two groups are also distinguished by Mg# and SiO_2/TiO_2 ratios, thick tabular phlogopites having 80-89 and 13-16, and diamond shaped types having 68-89 and 8-18 respectively. Coarse phlogopite phenocrysts show zonation, Mg# ranging from 68 to 82. In the sample LPTU 1, groundmass phlogopites have 47-68 (mainly 47-56) and 8-19 while phenocrysts have 85-88 and 13-23, Mg# and SiO_2/TiO_2

ratios, respectively. In addition, coarse grained tabular phlogopite shows zonal texture Mg# ranging from 72 to 85, but limited SiO_2/TiO_2 ratios ranging from 13 to 14. Phlogopites from Calcutteroo kimberlites are also well divided into two groups by Mg# and SiO_2/TiO_2 ratios, respectively phenocrysts having 85-88 and 7-9 and groundmass 64-76 and 9-14.

The phlogopites are well distinguished from phenocryst of the Truro lamprophyres by lower SiO_2/TiO_2 ratios (<9). The phlogopite composition from Calcutteroo kimberlites is consistent with the phenocrysts of the lamproites (75-92 and 5-11, Mg# and SiO_2/TiO_2 ratios respectively), especially those from more phlogopite-rich lamproites rather than those of olivine -rich lamproites. The phenocrysts of the lamproites are well distinguished from those of South African kimberlites (90-93 and 19-21 for Group 1 kimberlites 77-92 and 10-51 for Group II kimberlites Mg# and SiO_2/TiO_2 ratios respectively). SiO_2/TiO_2 ratios of the phlogopites from Orroroo kimberlites are consistent with those of South African kimberlites.

In summary, South Australian kimberlites and lamprophyres contain at least two generations of phlogopite and in these phenocryst zonation is common. Coarse-grained phlogopite phenocrysts are characterised by higher Mg#, Cr_2O_3, SiO_2 and lower TiO_2 relative to groundmass or medium-grained phenocrysts. Diamond-shaped phlogopites generally show intermediate geochemical characteristics between coarse-grained phenocrysts and groundmass. Phlogopites from Orroroo are distinct from those of Calcutteroo kimberlites but, their composition is like those from South African kimberlites. Phlogopites from the Calcutteroo kimberlites suggest that their host rocks have more ultrapotassic affinities (mentioned by Rock, 1991) rather than to the South African kimberlites.

5.7. Geochemistry of the South Australian kimberlites and lamprophyres

Six selected lamprophyre and four kimberlite samples were analysed for major and trace elements by XRF and for the REE concentration by isotope dilution using the Finnigan MAT 261, Mass Spectrometer of the Department of the Geology and Geophysics in the University of Adelaide. Details of sample preparation and analytical methods are shown in the Appendix 1. The results are shown in the Table 5.11, 12 and 13.

5.7.1. Major element chemistry

Chemical analyses of the Truro lamprophyres and Calcutteroo kimberlites are recalculated to 100 % volatile free data and Fe_2O_3/FeO are recalculated to a common value of 0.2 for the CIPW norm calculation. These data are depicted in the plots shown in Fig. 5.11. Note that the Calcutteroo samples are the only Mesozoic kimberlites which have sufficiently fresh compositions to give confidence of their primary representativity.

Table 5.10a. Representative phlogopite analyses of the Calcutteroo kimberlites.

Sample	KC-1										
	Phenocryst						Groundmass				
SiO2	39.78	39.82	40.19	38.02	38.50	38.36	37.94	36.99	38.17	38.01	37.38
TiO2	3.68	3.70	3.73	4.78	4.63	4.58	3.94	3.88	4.42	2.75	4.35
Al2O3	12.17	12.15	12.36	11.83	13.66	13.25	11.10	10.70	10.00	10.21	11.55
FeO#	5.28	5.45	5.72	6.74	5.34	5.31	11.78	16.42	12.40	11.23	11.76
MnO	0.01	0.00	0.01	0.06	0.17	0.00	0.31	0.54	0.20	0.03	0.18
MgO	22.39	22.24	22.33	21.57	20.96	21.58	19.60	16.48	18.02	19.37	18.19
CaO	0.11	0.23	0.34	0.20	0.31	0.24	0.49	0.42	3.03	1.12	0.80
Na2O	0.00	0.00	0.00	0.22	0.00	0.00	0.00	0.01	0.42	0.00	0.00
K2O	9.95	9.81	9.23	9.52	9.71	9.62	9.16	8.82	7.38	9.34	9.32
P2O5	0.84	0.74	0.91	0.92	0.81	0.73	0.55	0.74	0.55	1.47	0.83
SO3	0.11	0.14	0.08	0.28	0.12	0.21	0.26	0.30	0.14	0.07	0.18
Cr2O3	0.28	0.42	0.27	0.34	0.35	0.68	0.16	0.00	0.13	0.23	0.11
NiO	0.38	0.10	0.11	0.38	0.24	0.25	0.00	0.33	0.31	0.25	0.00
Total	94.96	94.78	95.27	94.85	94.78	94.82	95.29	95.61	95.17	94.06	94.64
					Number of Ions on the Basis of 6(O)						
Si	6.2212	6.2335	6.2374	6.0142	6.0372	6.0164	6.1107	6.0798	6.1785	6.1913	6.0673
Al	2.2423	2.2423	2.2605	2.2051	2.5251	2.4489	2.1058	2.0714	1.9068	1.9600	2.2088
Ti	0.4320	0.4349	0.4353	0.5682	0.5452	0.5401	0.4769	0.4788	0.5378	0.3364	0.5304
Fe(t)	0.6903	0.7131	0.7416	0.8907	0.7000	0.6963	1.5863	2.2559	1.6775	1.5284	1.5958
Mn	0.0011	0.0000	0.0009	0.0076	0.0221	0.0000	0.0420	0.0750	0.0274	0.0038	0.0241
Mg	5.2157	5.1862	5.1611	5.0815	4.8968	5.0402	4.7007	4.0356	4.3456	4.6990	4.3977
Ca	0.0181	0.0386	0.0563	0.0346	0.0518	0.0406	0.0842	0.0742	0.5246	0.1953	0.1382
Na	0.0000	0.0000	0.0000	0.0674	0.0000	0.0000	0.0000	0.0028	0.1318	0.0000	0.0000
K	1.9846	1.9574	1.8272	1.9199	1.9413	1.9236	1.8801	1.8483	1.5231	1.9408	1.9285
P	0.1104	0.0981	0.1197	0.1232	0.1073	0.0968	0.0745	0.1026	0.0754	0.2021	0.1139
S	0.0123	0.0159	0.0094	0.0332	0.0145	0.0247	0.0318	0.0365	0.0169	0.0086	0.0221
Cr	0.0351	0.0515	0.0327	0.0428	0.0428	0.0843	0.0209	0.0000	0.0165	0.0294	0.0136
Ni	0.0473	0.0130	0.0141	0.0478	0.0300	0.0320	0.0000	0.0434	0.0408	0.0328	0.0000
Sum	17.0102	16.9845	16.8960	17.0361	16.9143	16.9440	17.1138	17.1044	17.0027	17.1278	17.0404
Mg/Mg+Fe(t)	88.31	87.91	87.44	85.09	87.49	87.86	74.77	64.14	72.15	75.46	73.37
SiO2/TiO2	10.82	10.77	10.77	7.96	8.32	8.37	9.63	9.55	8.64	13.84	8.60
TiO2/Al2O3	0.3020	0.3041	0.3018	0.4039	0.3385	0.3458	0.3550	0.3623	0.4421	0.2690	0.3764
Si/Ti	14.40	14.33	14.33	10.58	11.07	11.14	12.81	12.70	11.49	18.41	11.44
Ti/Al	0.1926	0.1940	0.1926	0.2577	0.2159	0.2206	0.2265	0.2311	0.2820	0.1716	0.2401
TiO2/K2O	0.3693	0.3770	0.4041	0.5021	0.4765	0.4763	0.4303	0.4394	0.5990	0.2940	0.4665
CaO/MgO	0.0048	0.0103	0.0151	0.0095	0.0147	0.0112	0.0249	0.0256	0.1679	0.0578	0.0437
Cr2O3	0.284	0.416	0.267	0.342	0.346	0.68	0.164	0	0.129	0.228	0.106

Table 5.10b. Representative phlogopite analyses of the Truro lamprophyres.

Sample	LPTU 4			LPTU 2				LPTU 1									
	Thin lamellae type			Cr rich type		Coarse phenocryst		Diamond shaped grains		Thin lath type				Coarse phenocryst			
SiO2	42.19	41.63	41.32	40.29	39.87	39.58	38.82	37.94	37.38	36.53	37.11	35.99	37.42	36.68	38.58	38.47	38.67
TiO2	1.54	1.85	1.22	2.06	1.98	2.17	2.40	3.46	3.71	4.34	1.85	4.65	3.73	3.95	2.67	2.87	2.06
Al2O3	11.58	11.82	12.16	13.67	13.79	12.15	11.97	11.04	11.27	11.33	15.80	12.18	10.48	12.23	11.15	11.21	11.59
FeO#	11.57	11.31	11.92	4.25	4.24	5.04	4.78	7.85	10.95	13.51	13.39	20.68	20.24	19.53	7.20	7.12	5.78
MnO	0.21	0.11	0.08	0.00	0.00	0.00	0.11	0.06	0.00	0.13	0.06	0.04	0.15	0.00	0.22	0.09	0.17
MgO	18.62	17.70	17.84	22.67	22.20	22.81	22.82	20.35	18.16	16.34	15.82	10.48	11.88	11.83	22.04	22.27	22.89
CaO	0.28	0.29	0.29	0.30	0.58	0.14	0.26	0.15	0.15	0.12	0.31	0.16	0.12	0.20	0.19	0.21	0.03
Na2O	0.00	0.00	0.00	0.00	0.00	0.00	0.00	0.00	0.00	0.00	0.00	0.00	0.18	0.00	0.00	0.00	0.00
K2O	9.00	9.43	9.42	8.87	8.27	10.19	10.15	9.87	9.68	9.45	9.14	8.82	8.86	9.05	10.16	9.83	10.03
P2O5	0.64	0.71	0.59			0.90	1.17	0.83	0.83	0.54	0.82	0.48	0.85	0.57	0.71	0.72	0.64
SO3	0.07	0.05	0.04			0.18	0.12	0.09	0.20	0.03	0.22	0.10	0.42	0.14	0.08	0.15	0.34
Cr2O3	0.04	0.07	0.14	1.76	1.81	0.73	0.61	0.00	0.21	0.00	0.10	0.18	0.05	0.13	0.00	0.14	0.46
NiO	0.18	0.14	0.26			0.52	0.48	0.00	0.00	0.07	0.23	0.43	0.31	0.00	0.22	0.16	0.54
Total	95.91	95.10	95.27	93.86	92.75	94.41	93.69	91.64	92.54	92.39	94.84	94.18	94.70	94.29	93.23	93.23	93.20
	Number of Ions on the Basis of 6(O)																
Si	6.6409	6.6188	6.5854	6.3113	6.3057	6.2362	6.1668	6.2391	6.1759	6.1407	6.0007	6.1249	6.2927	6.1776	6.2370	6.2004	6.2078
Al	2.1484	2.2134	2.2828	2.5231	2.5707	2.2561	2.2400	2.1391	2.1948	2.2447	3.0102	2.4420	2.0760	2.4270	2.1243	2.1290	2.1919
Ti	0.1816	0.2206	0.1463	0.2423	0.2349	0.2568	0.2868	0.4273	0.4608	0.5484	0.2250	0.5955	0.4717	0.5003	0.3240	0.3480	0.2482
Fe(t)	1.5217	1.5031	1.5874	0.5568	0.5607	0.6636	0.6341	1.0793	1.5123	1.8983	1.8100	2.9417	2.8450	2.7500	0.9729	0.9590	0.7759
Mn	0.0283	0.0146	0.0105	0.0000	0.0000	0.0000	0.0146	0.0080	0.0000	0.0180	0.0085	0.0060	0.0214	0.0000	0.0307	0.0123	0.0233
Mg	4.3657	4.1909	4.2358	5.2888	5.2309	5.3525	5.3986	4.9861	4.4694	4.0901	3.8099	2.6569	2.9760	2.9667	5.3068	5.3459	5.4732
Ca	0.0464	0.0488	0.0495	0.0508	0.0985	0.0233	0.0447	0.0258	0.0268	0.0212	0.0529	0.0292	0.0224	0.0354	0.0326	0.0359	0.0049
Na	0.0000	0.0000	0.0000	0.0000	0.0000	0.0000	0.0000	0.0000	0.0000	0.0000	0.0000	0.0000	0.0593	0.0000	0.0000	0.0000	0.0000
K	1.8065	1.9117	1.9144	1.7717	1.6676	2.0474	2.0561	2.0704	2.0396	2.0248	1.8847	1.9142	1.9000	1.9434	2.0942	2.0211	2.0537
P	0.0851	0.0957	0.0793			0.1200	0.1575	0.1158	0.1154	0.0773	0.1122	0.0690	0.1204	0.0808	0.0973	0.0978	0.0864
S	0.0080	0.0060	0.0047			0.0214	0.0142	0.0116	0.0254	0.0041	0.0265	0.0125	0.0532	0.0176	0.0097	0.0184	0.0410
Cr	0.0052	0.0088	0.0181	0.2173	0.2260	0.0913	0.0763	0.0000	0.0276	0.0000	0.0131	0.0240	0.0070	0.0168	0.0004	0.0175	0.0584
Ni	0.0225	0.0174	0.0329			0.0655	0.0619	0.0000	0.0000	0.0093	0.0302	0.0594	0.0415	0.0000	0.0284	0.0200	0.0693
Sum	16.8603	16.8498	16.9470	16.9620	16.8949	17.1342	17.1516	17.1024	17.0480	17.0768	16.9838	16.8752	16.8867	16.9156	17.2583	17.2053	17.2341
Mg/Mg+Fe(t)	74.15	73.60	72.74	90.47	90.32	88.97	89.49	82.21	74.72	68.30	67.79	47.46	51.12	51.90	84.51	84.79	87.58
SiO2/TiO2	27.49	22.55	33.84	19.58	20.18	18.26	16.16	10.98	10.07	8.42	20.05	7.73	10.03	9.28	14.47	13.39	18.80
TiO2/Al2O3	0.1325	0.1562	0.1005	0.1506	0.1433	0.1784	0.2007	0.3131	0.3291	0.3830	0.1172	0.3822	0.3562	0.3232	0.2391	0.2562	0.1775
Si/Ti	36.58	30.00	45.02	26.05	26.85	24.28	21.50	14.60	13.40	11.20	26.67	10.29	13.34	12.35	19.25	17.82	25.01
Ti/Al	0.0845	0.0997	0.0641	0.0960	0.0914	0.1138	0.1280	0.1997	0.2100	0.2443	0.0747	0.2438	0.2272	0.2061	0.1525	0.1634	0.1132
TiO2/K2O	0.1706	0.1958	0.1296	0.2320	0.2390	0.2127	0.2366	0.3500	0.3833	0.4595	0.2025	0.5277	0.4211	0.4367	0.2625	0.2920	0.2050
CaO/MgO	0.0148	0.0162	0.0163	0.0134	0.0262	0.0061	0.0115	0.0072	0.0084	0.0072	0.0193	0.0153	0.0104	0.0166	0.0085	0.0093	0.0013
Cr2O3	0.042	0.07	0.143	1.756	1.808	0.734	0.608	0	0.211	0	0.102	0.178	0.052	0.126	0.003	0.137	0.461

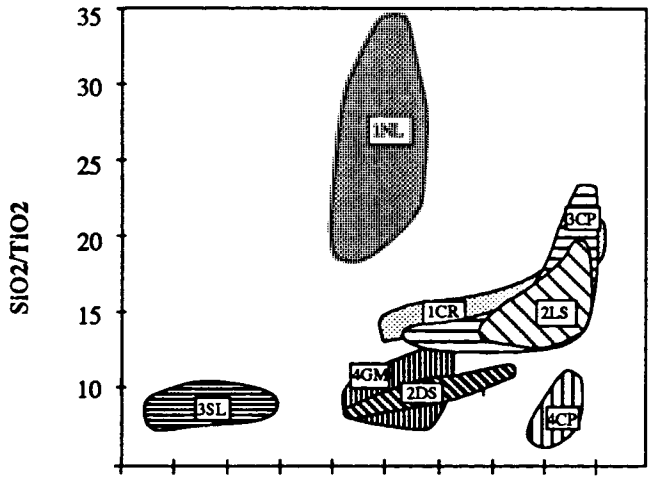
SiO2/TiO2
35
30
25
20
15
10
1NL
3CP
1CR
2LS
4GM
2DS
3SL
4CP

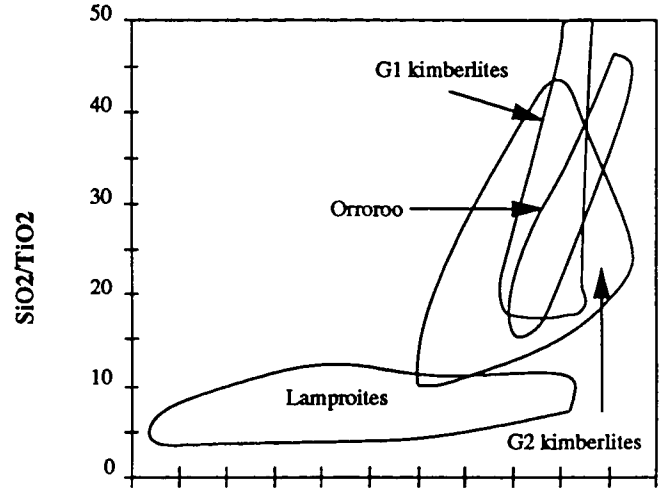
SiO2/TiO2
50
40
30
20
10
0
G1 kimberlites
Orroroo
Lamproites
G2 kimberlites

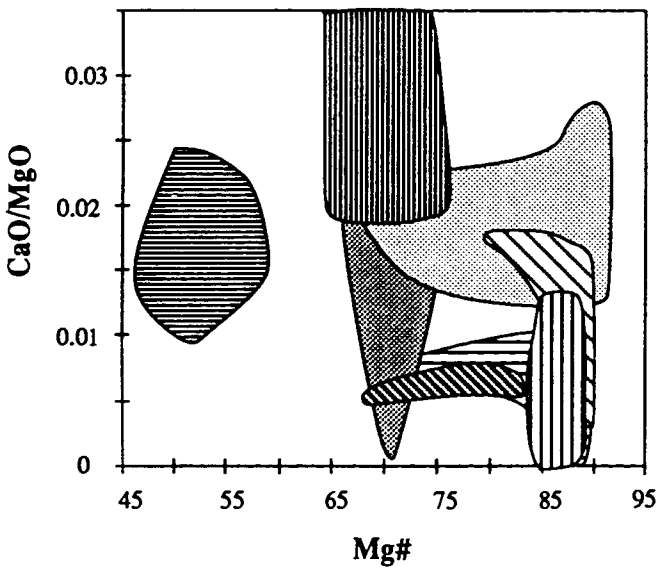
CaO/MgO
0.03
0.02
0.01
0
45
55
65
75
85
95
Mg#

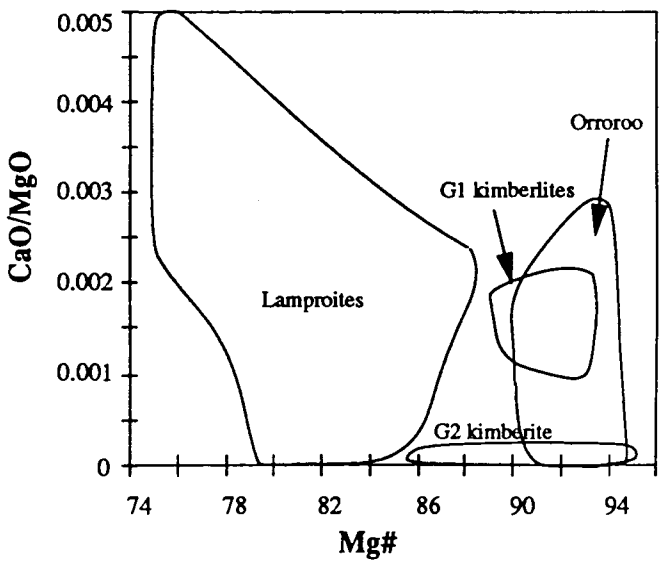
CaO/MgO
0.005
0.004
0.003
0.002
0.001
0
Orroroo
G1 kimberlites
Lamproites
G2 kimberite
74
78
82
86
90
94
Mg#

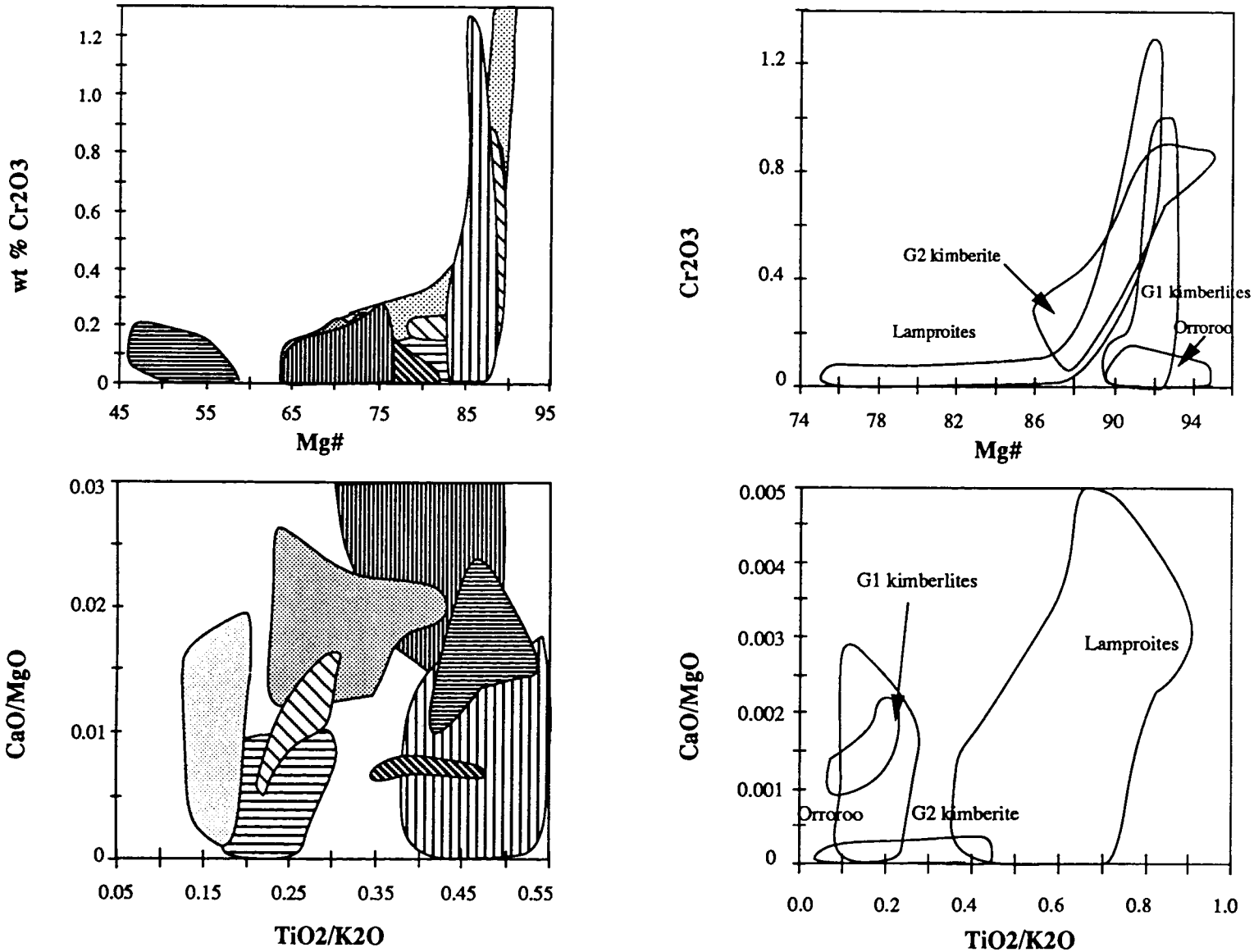

Fig. 5.10. Comparisons of the phlogopite compositions. 1CR-coarse phenocrysts, 1NR-lamellae shaped phenocrysts of LPTU 4; 2LS-lath shaped phenocrysts, 2DS-diamond shaped phenocrysts of LPTU 2; 3CP-coarse grained phenocrysts, 3SL-fine grained phenocrysts of LPTU 1; 4CP-coarse grained phenocrysts, 4GM-groundmass of TRWI 1.

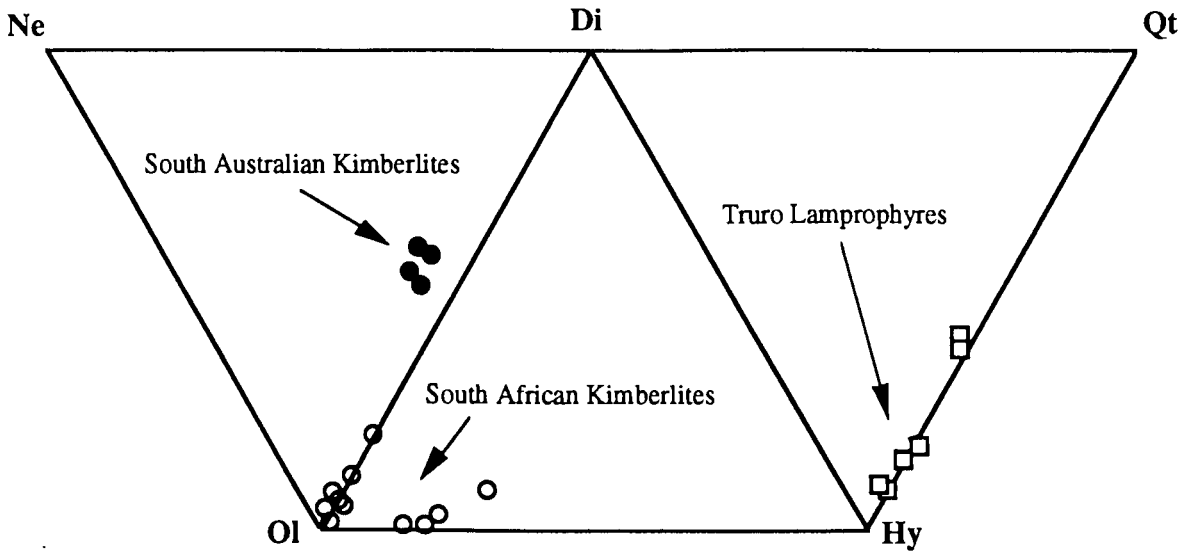

Fig. 5.11. C.I.P.W. normative plot of the South Australian kimberlites and lamprophyres, and their comparisons with South African kimbertlites (data from Smith *et al.*, 1985).

Recalculated normative compositions show that the two South Australian suites (Mesozoic and Ordovician) are significantly different. In general, Truro lamprophyres have *q* -normative compositions whereas Calcutteroo kimberlites have *ne* -normative compositions (Fig. 5.11). The Calcutteroo kimberlites have similar normative compositions to those of the South African kimberlites.

Chemical analyses of the Calcutteroo kimberlites and Truro lamprophyres are plotted on chemical discrimination diagrams (Fig. 5.12, 13). In general, the South Australian rocks fall in the fields of kimberlites, lamprophyres, and lamproites of Rock (1991). However, Calcutteroo kimberlites are more like South African kimberlite (particularly Group II kimberlite as defined by Smith *et al.*, 1985) whereas Truro lamprophyres have Western Australian lamproite-like characteristics.

In the V/Cr and Nb/Pb diagram (Rock, 1991), the Truro lamprophyres are like calc-alkaline lamprophyres, whereas the Calcutteroo kimberlites overlap the field of ultramafic lamprophyres. In the CaO-MgO, $K_2O/Al2O_3$-Fe_2O_3/SiO_2 and, Ce/Yb-Sm diagrams (Rock, 1991), Truro lamprophyres are plotted near the calc-alkaline lamprophyre range whereas Calcutteroo kimberlites are plotted near the kimberlite or ultramafic lamprophyres ranges.

In the MgO/CaO-SiO_2/Al_2O_3 diagram (Rock, 1991), the two South Australian suites plot in the range of the ultramafic lamprophyre compositions and adjacent to those of kimberlites, in which the Calcutteroo kimberlites fall. This range is overlapped by that of typical South African Group II kimberlites (but not Group I kimberlites). In the Na_2O+K_2O-SiO_2 diagram (Irvine and Baragar, 1971), the Calcutteroo kimberlites fall in the alkaline range while Truro lamprophyres are in the sub alkaline field. Most of the Western Australian lamproites show alkaline characteristics but mainly in the strongly alkaline range.

Table 5.11. Major element analyses of the South Australian kimberlites and lampropyres.

Sample	KC 1	KC 2	KC 3	KC 4	KC 5	LPTU 1	LPTU 2	LPTU 3	LPTU 4	LPTU 5	LPTU 6
Lithology	Kimberlites					Lamprophyres					
SiO2	32.51	42.75	44.51	44.03	44.33	57.53	46.94	57.64	56.42	57.08	45.40
Al2O3	3.49	7.15	7.14	7.31	7.09	10.81	9.25	13.55	12.89	13.52	9.89
Fe2O3(t)	10.94	10.58	11.23	10.39	10.77	6.32	6.99	6.49	7.42	6.55	7.17
FeO(t)	9.84	9.52	10.10	9.35	9.69	5.69	6.29	5.84	6.68	5.89	6.45
MnO	0.20	0.18	0.18	0.20	0.18	0.05	0.13	0.01	0.01	0.02	0.11
MgO	24.40	17.14	14.81	16.71	15.18	5.28	7.12	7.01	8.33	6.95	11.10
CaO	6.60	8.51	8.66	7.83	9.05	3.48	8.52	1.59	1.52	1.54	6.63
Na2O	0.83	1.02	1.46	1.19	1.33	0.27	0.50	2.71	2.36	2.84	1.95
K2O	2.18	3.83	4.27	4.59	4.23	9.03	7.36	6.07	6.26	5.96	4.56
TiO2	2.84	3.13	3.11	2.90	3.03	1.98	1.71	1.49	1.44	1.47	1.16
P2O5	0.51	1.12	0.91	0.94	1.04	2.21	2.05	1.06	1.00	1.03	0.92
SO3	0.11	0.07	0.05	0.06	0.08	0.07	0.41	0.03	0.03	0.03	0.23
LOI	14.45	3.28	2.5	2.88	2.55	1.53	7.72	1.42	1.48	1.38	8.84
Total	99.06	98.76	98.83	99.03	98.86	98.56	98.7	99.07	99.16	98.38	97.95
	100 % normalized, FE2O3/FEO = 0.2										
Ap	1.42	2.76	2.23	2.30	2.54	5.35	5.30	2.55	2.41	2.49	2.43
Il	6.49	6.31	6.21	5.80	6.02	3.91	3.61	2.93	2.82	2.91	2.50
Mt	2.28	2.44	2.57	2.80	2.46	1.43	1.69	1.46	1.67	1.48	1.77
Or	0	22.81	26.47	23.93	25.46	55.36	48.21	36.98	38.17	35.56	30.48
Ab	0	0	0.42	0	0	2.13	3.14	23.65	20.61	24.95	12.72
An	0	3.96	0.42	1.21	1.07	1.79	2.23	0.99	1.04	0.95	5.87
Di	6.54	26.22	30.67	26.38	31.02	0.91	23.95	0	0	0	19.62
Hy	0	0	0	0	0	18.1	2.13	23.83	28.52	23.97	0
Ol	57.78	29.74	24.26	28.75	24.47	0	9.31	0	0	0	21.64
Ne	3.76	4.81	6.70	5.62	6.25	0	0	0	0	0	2.74
Ac	1.28	0	0	0	0	0	0	0	0	0	0
C	0	0	0	0	0	0	0	2.34	1.93	2.14	0
Q	0	0	0	0	0	10.95	0	5.35	2.81	4.52	0
	79.55	99.05	99.95	96.79	99.29	99.93	99.57	100.08	99.981	98.97	99.77
	FE2O3/FEO = 0.2										
Ap	1.17	2.61	2.10	2.02	2.42	4.87	4.79	2.27	2.33	2.22	2.08
Il	5.33	5.90	5.90	4.16	5.71	2.92	3.24	2.14	2.67	2.11	1.85
Mt	1.97	2.31	2.44	1.68	2.35	1.05	1.52	1.04	1.61	1.05	1.25
Or	0	22.23	25.35	23.56	24.50	56.32	43.53	36.68	37.24	36.21	30.09
Ab	0	0	0	0	0	2.30	2.82	24.89	19.98	26.11	12.78
An	0	3.83	0.32	1.11	1.25	1.90	2.01	0.98	1.01	0.94	5.61
Di	4.30	24.64	29.48	25.9	29.36	0.90	21.63	0	0	0	19.44
Hy	0	0	0	0	0	19.20	1.81	24.7	27.61	24.77	0
Ol	48.67	24.08	22.99	31.47	23.44	0	8.49	0	0	0	23.21
Ne	3.09	4.54	6.59	6.51	5.80	0	0	0	0	0	3.41
Ac	0.83	0	0	0	0	0	0	0	0	0	0
C	0	0	0	0	0	0	0	2.42	1.82	2.34	0
Q	0	0	0	0	0	10.41	0	4.88	2.58	4.22	0
	65.36	90.14	95.17	96.41	94.83	99.87	89.84	100	96.85	99.97	99.72

Table 5.12. Trace element analyses of the South Australian kimberlites and lamprophyres.

Sample	KC 1	KC 2	KC 3	KC 4	KC 5	LPTU 1	LPTU 2	LPTU 3	LPTU 4	LPTU 5	LPTU 6
Lithology	Kimberlites					Lamprophyres					
Y	12.6	19	16	18	16.7	38	21.4	23.5	21.9	22.6	12.4
Sr	271	512	363	371	435	685	756	651	583	661	480
Rb	81	154	136	136	183	392	390	413	483	427	419
Nb	112	119	113	113	115	21.9	18.5	19.2	19.1	19	15.6
Zr	171	294	310	310	343	767	747	510	509	524	416
Th	11.9	14.5	14.2	14.2	12.1	27.3	33.3	9.7	9.7	8.1	8.2
Pb	5.9	11.3	10.2	10.2	16.2	443	95.1	23	20.3	29.6	54
U	4.7	2.5	0	0	2.7	14.5	11.1	7	5.7	6.4	5.6
Ga	11.9	16.5	16.3	17.8	14.3	22.1	19.3	20.2	18	20.9	17.8
Zn	67	70	67	77	72	808	177	78	87	81	109
Cu	50	168	109	147	121	406	307	61	86	78	220
Ni	846	487	414	356	410	236	219	209	292	245	535
Ba	1350	4471	4078	3552	4434	3199	2212	1625	1490	1648	3616
Sc	21.2	26.1	26.7	27.5	27.5	18.1	22.9	23.2	21	21.7	18
Cr	1254	1043	1139	1033	1074	435	346	405	542	547	605
V	244	407	511	512	510	634	620	532	493	521	391
Co	84.8	59	57.4	50	52.6	34	34.9	37	41.6	40.6	44
Ce	85	109	125	100	113	141	179	89	79	89	61
Nd	26	38	45	38	37	61	76	35	30	39	17
La	56	73	86	65	74	73	92	46	40	46	30

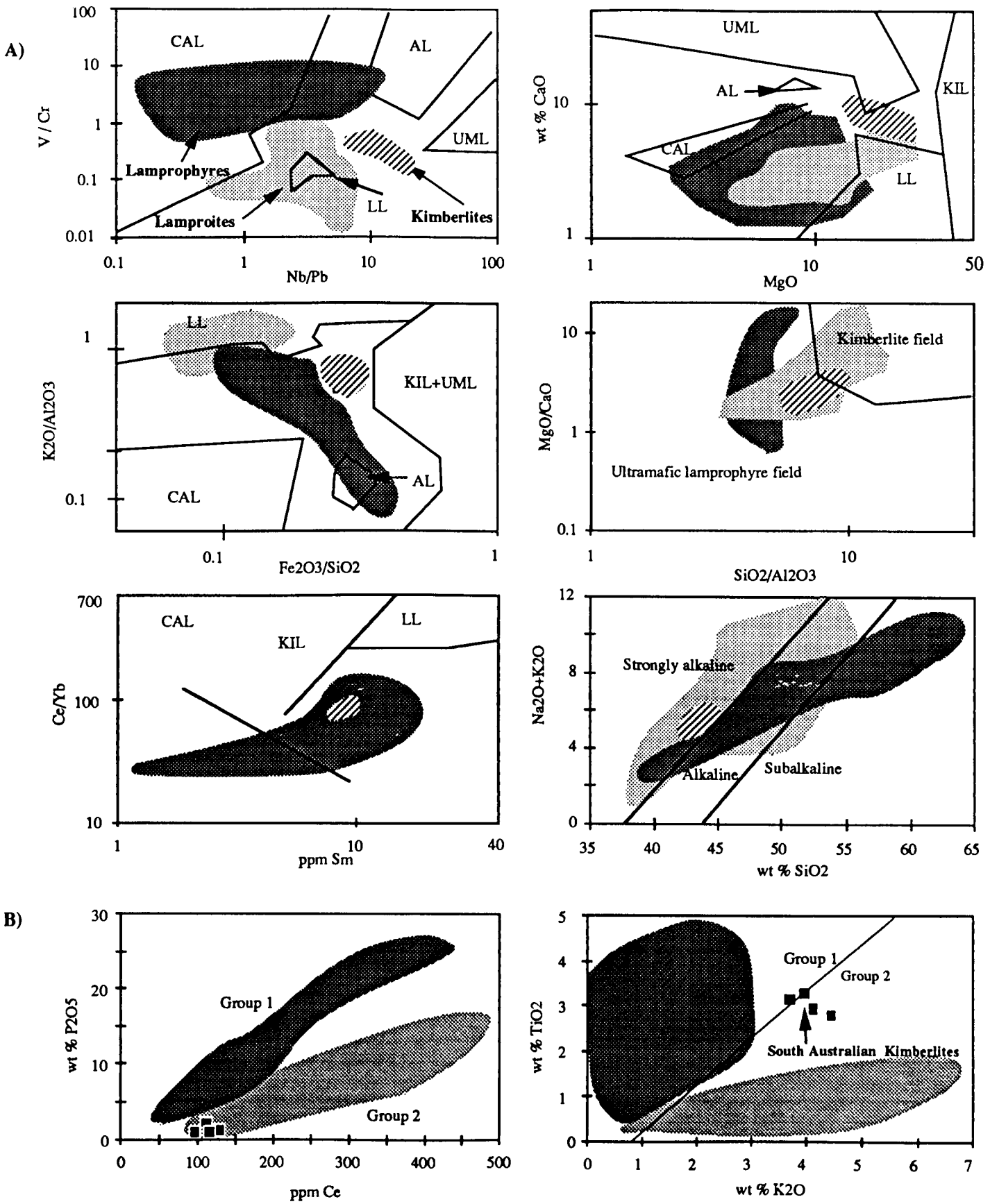

Fig. 5.12. A) Classifications of the South Australian kimberlites and lamprophyres and their comparisons with their related rocks (Truro lamprophyres from Müller *et al.*, 1993, Western Australia lamproites from Jaques *et al.*, 1984, 1986). See Table 5.2 for CAL, KIL, LL and UML, **B)** Classifications of the South Australian kimberlites and their comparisons with South African Group I and II kimberlites(shade area) of Scott Smith *et al.* (1984), P2O5-Ce plot from Bailey (1984), TiO2 and K2O plot for Scott Smith *et al.* (1984), Thin line in the TiO2 and K2O plot divide the South African kimberlites into Group I and Group II.

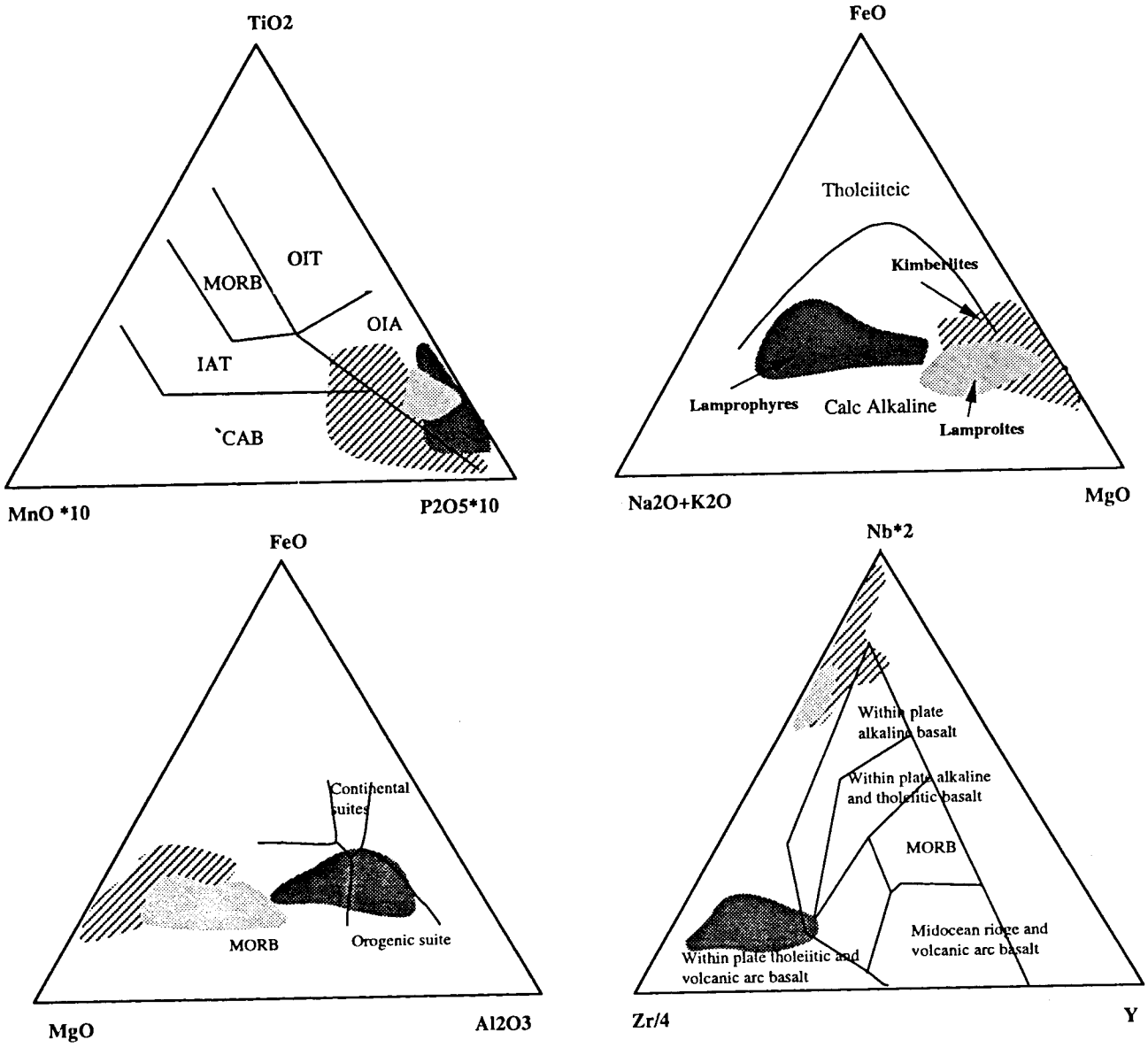

Fig. 5.13. Geochemical compositions of the South Australian kimberlites and lamprophyres with other related rocks (Data sources; South African kimberlites from Smith *et al.*, 1985; Truro lamprophyres from Müller *et al.*, 1993; Western Australian lamproites from Jaque *et al.* , 1986).

In addition, the Calcutteroo kimberlites lie in the range of Group II South African kimberlite in the TiO_2-K_2O (Smith *et al.*, 1985) and P_2O_5-Ce diagrams (Bailey, 1984). In the TiO_2-MnO*10-P_2O_5*10 diagram (Mullen, 1983), the two South Australian rock varieties plot in the range of the OIA (Ocean Island Alkaline rocks) and CAB (Calc-Alkaline Basalt) which are consistent with those of the South African kimberlites and Western Australia lamproites. However the Calcutteroo kimberlites show more OIA-like characteristics than Truro lamprophyres. In the FeO*-Na_2O+K_2O-MgO diagram (Irvine and Baragar, 1971), both South Australian series plot in the calc-alkaline range, in which Calcutteroo kimberlites fall to the MgO (wt %)-rich side with Western Australia lamproites and South African kimberlites, whereas Truro lamprophyres plot on the Na_2O+K_2O rich side.

In the FeO*-MgO-Al_2O_3 diagram (Pearce *et al.*, 1977), Calcutteroo kimberlites plot in the range of the orogenic suites with South African kimberlites while Truro lamprophyres fall in the range of MORB. In the Nb*2-Zr/4-Y diagram (Meschede, 1986), Truro lamprophyres are clearly distinguished from the other rock types by considerably higher Zr (but lower Nb). In this diagram, Truro lamprophyres fall adjacent to the "within plate tholeiitic and volcanic arc basalt" while other kimberlites and lampropites are plotted adjacent to the "within plate alkaline basalt".

5.7.2. Trace element and REE compositions

Trace element abundances of the South Australian kimberlites and lamprophyres are shown in Fig. 5.14. and are compared with available data for South African kimberlites (Smith *et al.*, 1985) and Western Australia lamproites (Jaques *et al.*, 1986).

In general, the Western Australia lamproites show an enrichment in all incompatible trace elements relative to the kimberlites. However, they are distinguished from the kimberlites by a strong enrichment in Rb, Ba, Zr, Sm, less pronounced enrichment in K, La, Ce and depletion in Nb, P, Nd. In the kimberlite varieties, the micaceous kimberlites are distinguished from the Group I kimberlites by a pronounced enrichment in Rb, Ba, K, La, Ce, Nd, Ti, a less pronounced enrichment in Th, P, Zr Sr and depletion in Nb, Sm. In the Group I kimberlites, Group IB kimberlites show a strong enrichment in Zr, Sm, Ti, Y, K, less pronounced enrichment in Ba, P, and depletion in Th, Nb, Ce relative to Group IA kimberlites.

In general, all South Australian rocks fall in the range of the South African kimberlites. The Calcutteroo kimberlites show more micaceous kimberlite-like than do the lamproites, or more Group IB-like characteristics than Group IA within the Group I kimberlites. However, the Truro lamprophyres show a distinctive enrichment in Rb, less pronounced enrichments in K, Zr and depletion in Nb, relative to all kimberlite. They have a strong depletion in Nb, La, less pronounced depletion in Ce, Sm, Th , P relative to the lamproites.

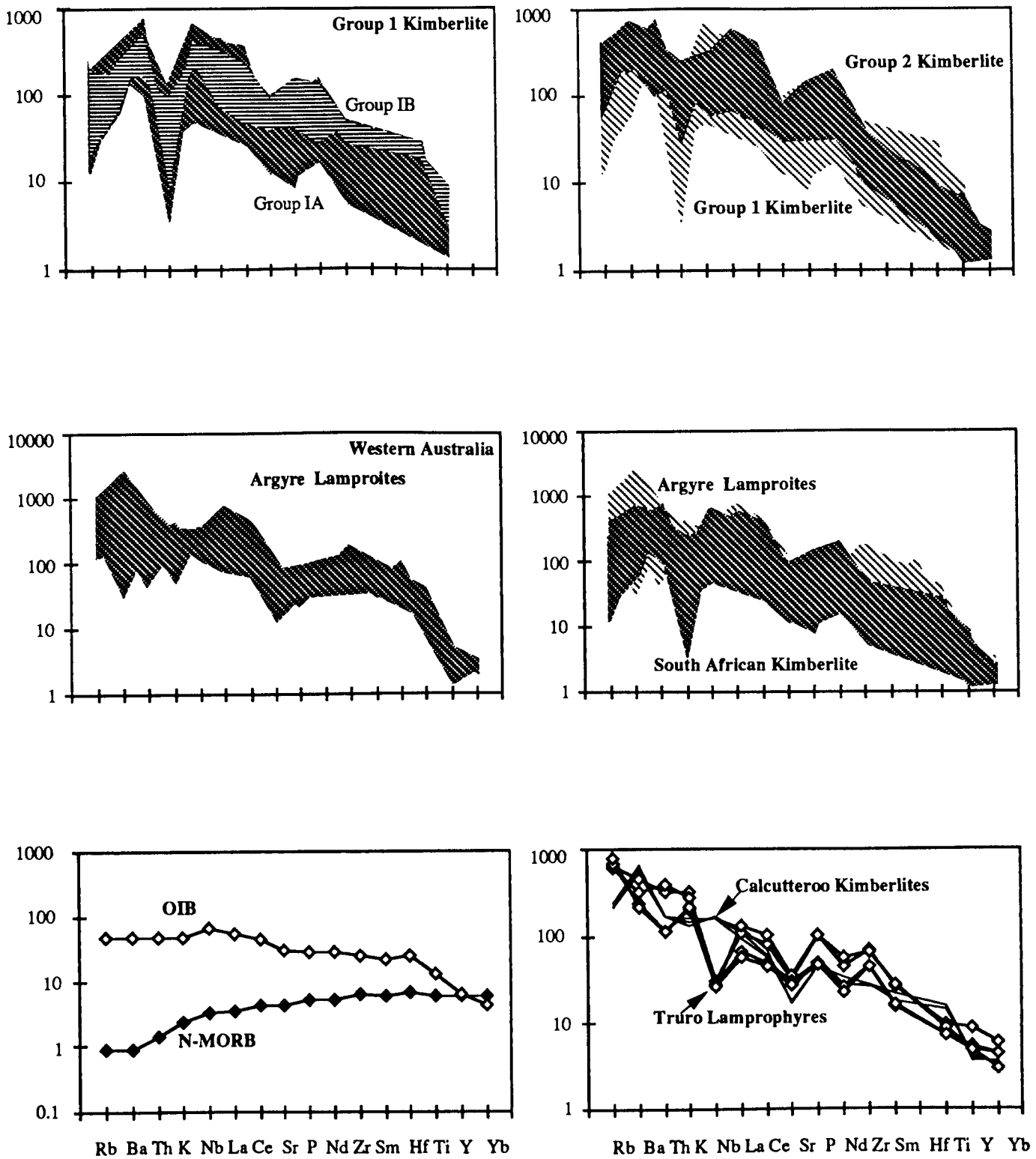

Fig. 5.14. PM normalized trace element abundances of the South Australian kimberlites and lamprophyres and their comparisons with South African kimberlites, Western Australian lamproites, OIB and MORB (Data sources; PM, MORB, OIB from Sun and McDonough, 1989; lamproites from Jaques *et al.*, 1986; kimberlites from Smith *et al.*, 1985).

The lamprophyres also show enrichment in Zr, Sm relative to Group II kimberlites. In addition, the Calcutteroo kimberlites show a depletion in the Rb, K, Sr, P, Zr and a enrichment in the Nb, Ti, relative to Truro lamprophyres. The Calcutteroo kimberlites are distinguished from that of the Group II kimberlites by a strongly depletion of Sr.

In the Primitive mantle-normalised REE abundances (Fig. 5.15), South Australian lamprophyres and kimberlites show enrichment of LREE and their general REE abundances fall in the range of South African mica-kimberlite, but show depletion in the LREE relative to the Western Australia lamproites (Fraser *et al.*, 1985). In general, the Calcutteroo kimberlites show a greater LREE enrichment and HREE depletion relative to those of Truro lamprophyres. No distinctive Eu anomaly appears in either of the two rock types.

Table 5.13. REE analyses of South Australian kimberlites and lamprophyres

Sample	KC 2	KC 3	KC 4	LPTU 1	LPTU 2	LPTU 3
Rock Type	Kimberlites			Lamprophyres		
La	86.60	86.55	66.78	72.49	95.10	46.14
Ce	155.82	158.12	126.17	145.30	162.20	87.44
Nd	60.17	59.37	48.80	63.93	68.27	37.74
Sm	9.82	9.72	8.02	11.90	11.95	6.83
Eu	2.65	2.56	2.17	3.28	3.28	1.95
Gd	4.40	2.82	5.67	8.93	7.49	3.67
Dy	4.63	4.62	3.23	6.68	4.79	4.50
Er	1.99	2.02	2.56	3.16	1.89	2.40
Yb	1.61	1.72	1.60	2.89	1.45	2.08

5.8. Isotopic Composition of kimberlites and lamprophyres

Selected Calcutteroo kimberlites and Truro lamprophyres were analysed for the Nd-Sm and Sr-Rb isotopic composition with Finnigan MAT 261, Mass Spectrometer of Department of the Geology and Geophysics, The University of Adelaide.Details of the analyses are shown in Appendix 1. Their results are given in Table 5.14. and are plotted in the Fig. 5.16.

The South Australian kimberlites and lamprophyres show significantly different isotopic characteristics, reflecting contrasts in geochemical characteristics. In general, the Calcutteroo kimberlites have εNd(i) ranging from 3.83 to 7.11 and $^{87}Sr/^{86}Sr$(i) ratios ranging from 0.7029 to 0.7071 whereas Truro lamprophyres have εNd(i) ranging from -1.85 to 0.48 and $^{87}Sr/^{86}Sr$(i) ratios ranging from 0.7053 to 0.7087.

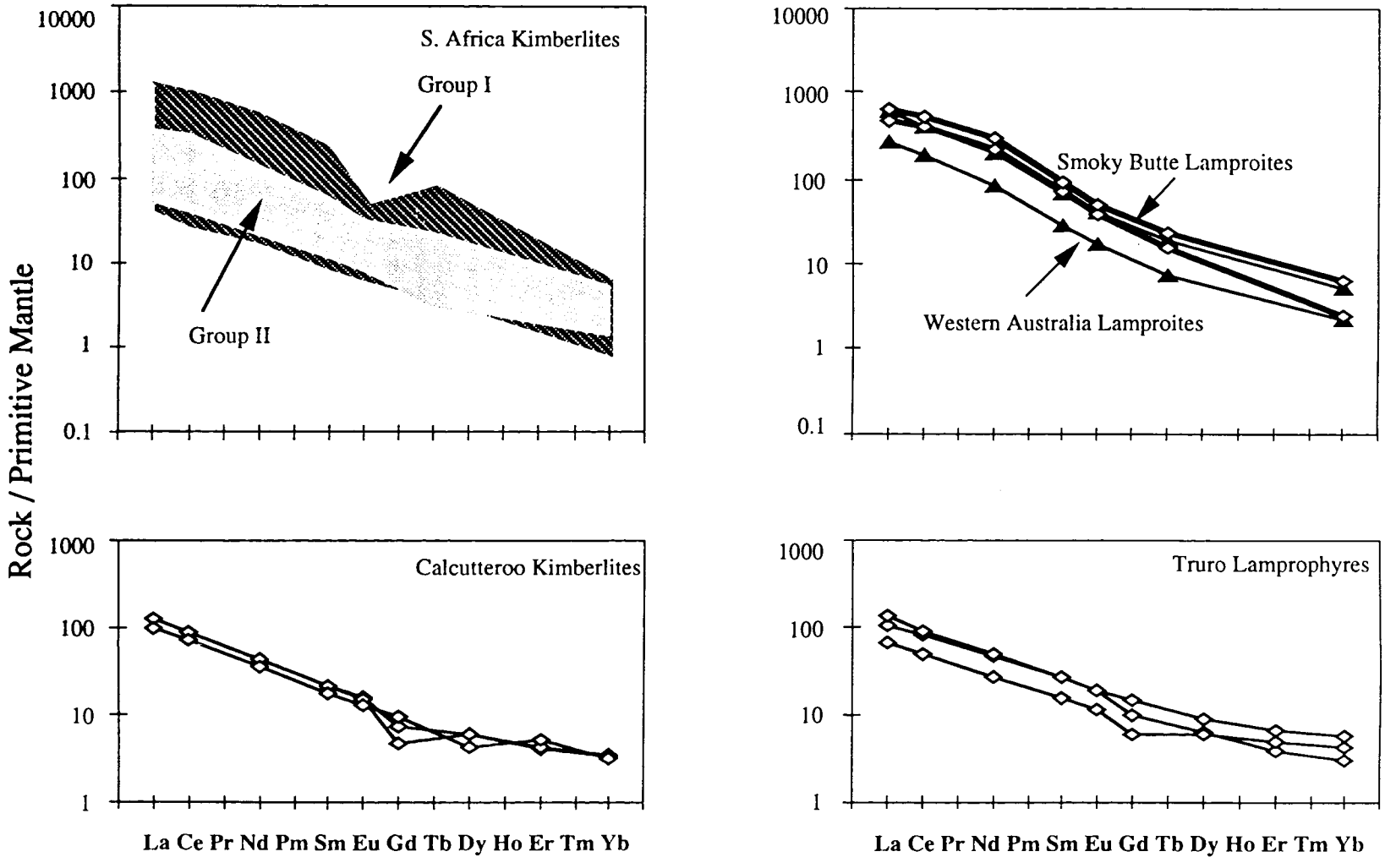

Fig. 5.15. PM normalised REE abundances of the South Australian kimberlites, lamprophyres and their comparisons with available data (Data sources; South African kimberlites from Fesq *et al*, 1975; Mitchell and Brunfelt, 1975; Frey *et al.*, 1977; lamproites from Fraser *et al.*, 1985). PM data from Sun and McDonough, (1989)

Sm/Nd and Rb/Sr ratios also clearly divide the rocks into two groups. The kimberlites have Sm/Nd ratios ranging from 0.143 and 0.162 and Rb/Sr ratios ranging from 0.2562 to 0.3816 whereas the lamprophyres have a Sm/Nd ratios ranging from 0.162 and 0.186 and Rb/Sr ratios ranging from 0.405 to 0.567. In particular, high Rb (631-775.9 ppm) and low Sr (314-390 ppm) of the Truro lamprophyres are clearly distinct from the Calcutteroo kimberlites (Rb content ranging from 162.9 to 178.9 and Sr content ranging from 446.5 to 678.9).

The Calcutteroo kimberlites are also distinguished from the Group 2 kimberlites (εNd of 0 - -6) by having higher εNd and from the Group 1 kimberlites of the South African kimberlites (showing OIB like isotopic compositions) by higher Sr ratios. On the other hand, Truro lamprophyres are clearly distinguished from the Western Australia lamproites (εNd of -8 - -15 and εSr of +40 - +162).

5.9. Discussion

5.9.1. Calcutteroo kimberlites

The trace element abundances of Calcutteroo kimberlites show that this group are not affected by assimilation or anatexis of the continental crust. The Calcutteroo kimberlites have very high Ni (~430 ppm), Cr (~1050 ppm) and MgO (15.5 wt %) and low SiO_2 (~44 wt %) and Al_2O_3 (~7.15 wt %). The high Ni, Cr and MgO levels suggest they are certainly derived from mantle (McDonough *et al.*, 1985) and have not experienced significant fractionation. In this case their extremely high incompatible trace element concentrations clearly imply an origin by small degrees of partial melting of an enriched source.

The kimberlites show significantly lower Sr (~400) than South African kimberlites (825-1140) but similar Rb (~150) to Group II kimberlites (~135). They show significantly higher Rb/Sr ratios (~0.35) than kimberlites.

On the other hand, Sm/Nd ratios of the Calcutteroo kimberlites (~0.15) are similar to the Finsch Group II kimberlites and slightly higher than Western Australian lamproites (0.1-0.15), (compared with MORB~OIB ranging from 0.2 to 0.4 and continental crust ~0.2) (Fig. 5.18). Rb/Sr ratios of the Calcutteroo kimberlites are similar to the Finsch Group II kimberlites and lower than Western Australian lamproites (Table 5.15). These characteristics suggest that Calcutteroo kimberlites are isotopically similar to South African Group 2 kimberlites, and are compared to the enriched Western Australian lamproites.

In the εNd -100/Nd relationships, the South Australian kimberlites lie between Group I and Group II kimberlites (Fig. 5.17), but closer to the Group I kimberlite. This suggest that the South Australian kimberlites are isotopically different from the typical South African kimberlites.

Table 5.14. Isotopic analyses of the South Australian kimberlites and lamprophyres.

Sample	Rb	Sr	Rb87/Sr86	87Sr/86Sr	87Sr/86Sr(T)	Nd	Sm	147Sm/144Nd	143Nd/144 Nd	eps Nd (0)	eps Nd chT	T mod:dep
Calcutteroo kimberlites												
KC 1	29.9	116.7	0.742092	0.712262 ± 23	0.707186	53.72	7.91	0.089085	0.512657 ± 46	0.36	7.11	0.525
KC 2	179.0	678.9	0.763578	0.708080 ± 38	0.702857	78.92	11.35	0.087004	0.512543 ± 38	-1.85	5.03	0.645
KC 3	162.6	518.0	0.908931	0.709240 ± 43	0.703023	47.71	7.75	0.098222	0.512568 ± 48	-1.36	4.80	0.672
KC 4	170.4	446.5	1.105388	0.710548 ± 61	0.702988	47.57	7.70	0.097968	0.512518 ± 31	-2.34	3.83	0.733
Truro lamprophyre												
LPTU 1	314.7	692.6	1.316114	0.715923 ± 30	0.706922	59.41	11.07	0.112759	0.512275 ± 28	-7.07	-1.85	1.169
LPTU 2	390.0	756.0	1.494167	0.715503 ± 31	0.705284	67.91	11.00	0.098014	0.512346 ± 45	-5.69	0.48	0.944
LPTU 3	314.9	775.9	1.175699	0.715820 ± 63	0.707779	34.65	6.21	0.108363	0.512359 ± 41	-5.44	0.06	1.013
LPTU 4	358.1	631.2	1.643235	0.719903 ± 13	0.708664	33.03	6.12	0.112029	0.512373 ± 36	-5.18	0.09	1.027

87Sr/86Sr(T) and eps Nd chT calculated at 500 Ma.

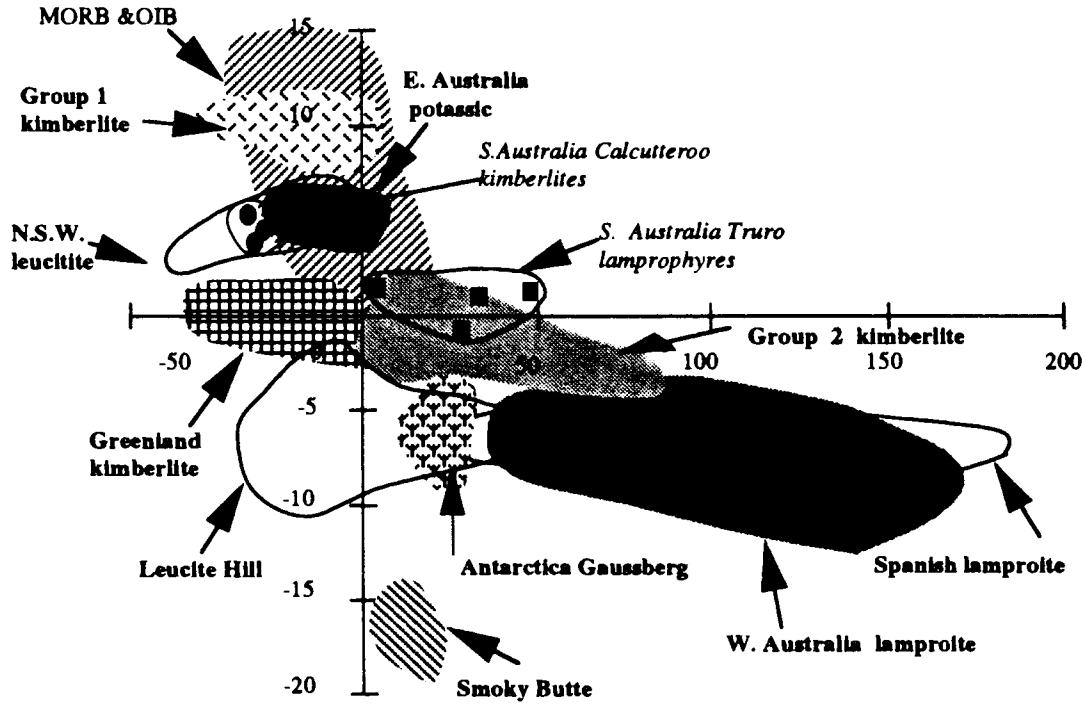

Fig. 5.16. Sr -Nd isotope variation of the Calcutteroo micaceous kimberlites and the Truro lamprophyres from the South Australia, compared to potassic, lamproite and kimberlite suites from other localities (Data sources: O'Nions *et al.* (1977), Allegre *et al.* (1979), Cohen and O'Nions (1982), Richardson *et al.* (1982), White and Hofmann (1982); Collerson and McCulloch (1983), McCulloch *et al.* (1983), Smith (1983), Vollmer *et al.* (1984); Fraser *et al.* (1985), Nelson *et al.* (1986), Ito *et al.* (1987); Storey *et al.* (1988) and Nelson (1989).

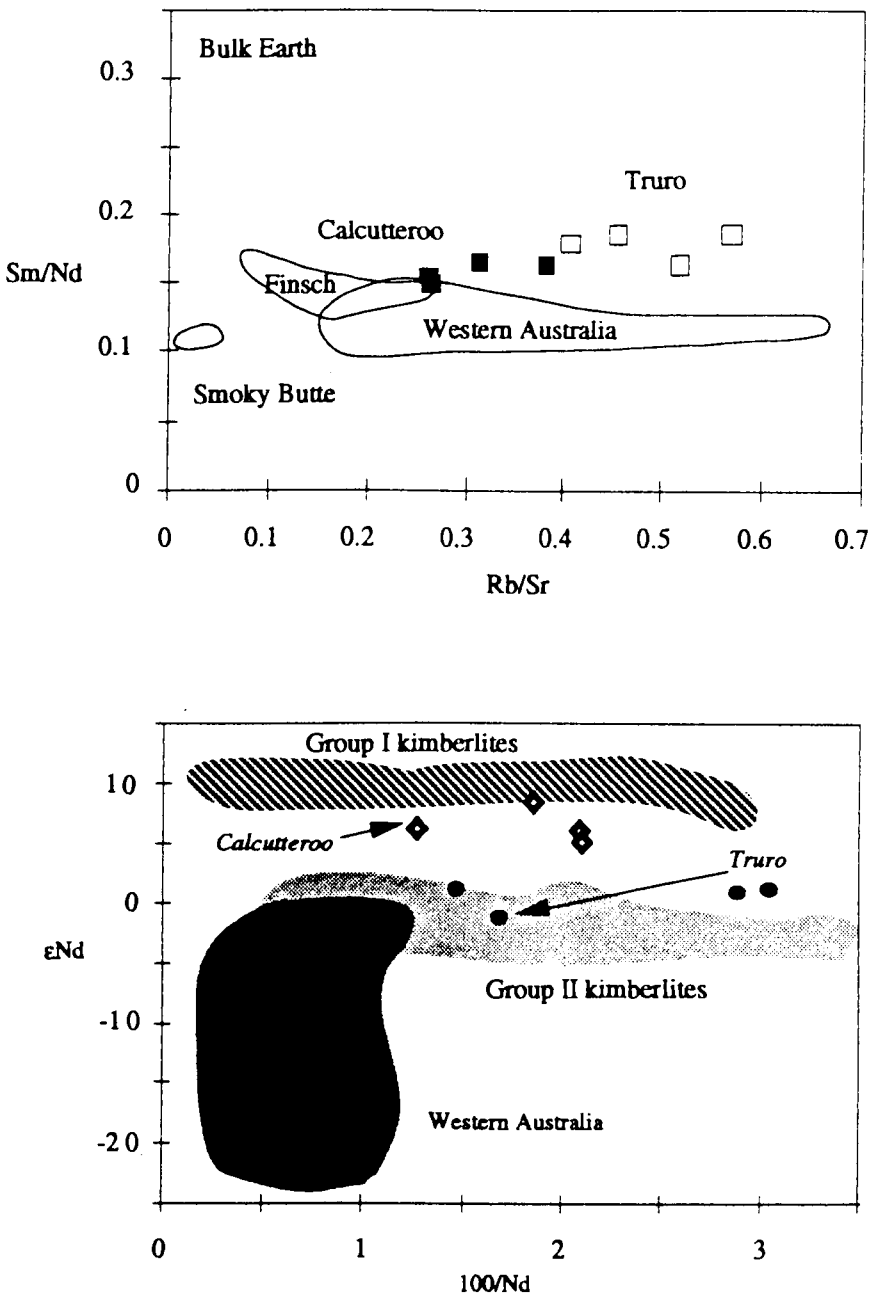

Fig. 5.17. Isotopic compositions of the South Australian kimberlites and lamprophyres.

Table 5.15. Incompatible trace element ratios of the kimberlites, lamprophyres and lamproites (see text for data sources).

			Ti/Y	Ti/Zr	La/Ba	Ce/Y	K/Rb	Nb/Y	Nb/Zr	Ti/P	P/K
Kimberlites	GROUP 1A	Minimum	318.8	19.6	0.06	2.1	69.9	2.8	0.56	0.4	0.2
(South Africa)		Maximum	1651.6	278.6	0.15	75.2	208.3	23.1	4.21	4.7	7.8
		Average	**1082.7**	**110.8**	**0.10**	**20.8**	**146.0**	**14.8**	**1.64**	**3.6**	**1.5**
	GROUP 1B	Minimum	585.9	42.0	0.05	5.3	65.9	5.9	0.36	1.6	0.2
		Maximum	951.5	81.4	0.15	10.2	338.9	13.6	0.72	7.1	7.2
		Average	**803.6**	**62.8**	**0.11**	**7.9**	**222.8**	**9.1**	**0.53**	**4.0**	**1.9**
	GROUP II	Minimum	230.2	12.0	0.03	14.6	122.8	5.4	0.28	0.5	0.1
		Maximum	1007.5	63.2	0.26	42.8	278.3	18.6	1.02	3.4	0.4
		Average	**522.1**	**26.6**	**0.09**	**23.2**	**220.6**	**9.0**	**0.47**	**1.4**	**0.2**
Lamproites		Minimum	968.4	22.2	0.02	10.9	56.2	5.9	0.09	3.1	0.0
(Western Australia)		Maximum	3547.0	32.9	0.55	52.5	369.9	24.4	0.33	14.7	0.4
		Average	**1921.4**	**28.6**	**0.08**	**23.2**	**191.6**	**11.2**	**0.20**	**7.0**	**0.1**
Lamprophyres		Minimum	323.9	15.2	0.01	3.6	102.2	0.6	0.02	1.1	0.1
Truro		Maximum	634.1	18.9	0.04	8.4	198.4	1.3	0.04	2.0	0.1
		Average	**448.5**	**17.2**	**0.03**	**4.7**	**138.5**	**0.9**	**0.03**	**1.7**	**0.1**
Kimberlites		Minimum	1015.1	55.5	0.02	5.6	201.4	6.3	0.33	3.8	0.1
Calcutteroo		Maximum	1617.3	119.0	0.04	7.8	294.2	8.9	0.66	7.6	0.2
		Average	**1208.6**	**72.8**	**0.02**	**6.5**	**251.2**	**7.1**	**0.42**	**4.9**	**0.1**

Many studies suggested that many potassic sources originated from metasomatic enrichments. Nelson *et al.* (1986) suggest that old subcontinental lithosphere, sudducted sediments and subducted megaliths, as the potential examples of such sources. The older continental lithosphere under the stable, thick Precambrian basement is clearly such a reservoir for the long-term storage of evolved components (Jordan, 1988; McKenzie, 1989; White and McKenzie, 1989). At its shallower extent this source may yield diamond-free lamproites such as those at Smoky Butte, Montana (Nelson *et al.*, 1986). The South Australian kimberlites are certainly not related to the subduction of sediments or megaliths because the localities are far from active plate margins and the longer term geological record back into the Proterozoic does not preserve any subduction-type.

An evolution model for the lithosphere (McKenzie, 1989) suggests that small melt fraction derived from the convecting mantle produce a metasomatic layer in the mechanical boundary and its melting by the lithospheric stretching and upward movements result in the occurrences of the K-rich magmatism. Thus the K enrichment of Calcutteroo kimberlites may be explained that they were derived from the metasomatized lithosphere.

The other geochemical and isotopic evidence from these rocks including relatively high εNd ratios and enriched LIL and LREE patterns, suggest that the Calcuttereoo kimberlites originated from incompatible element enriched regions close to the diamond stability fields within subcontinental lithosphere.

5.9.2. Truro lamprophyres

The lamprophyres are clearly distinguished from the Calcutteroo kimberlites by lower Ni (~241 ppm), Cr (~470 ppm), MgO (~7 wt %) and higher SiO_2 (~56.5) and Al_2O_3 (12 wt %). These rocks have some similarities to leucitites from NSW (Cundari, 1973). However the Truro suite has lower Ni and MgO and higher SiO_2 and Al_2O_3 contents than the New South Wales leucitites (Cundari, 1973). The latter are considered to be mantle melts contaminated by either a plume component or by products of earlier enrichment events but not by contamination by continental crust (Nelson *et al.*, 1986).

The Truro suite show depletion in LREE relative to Smoky Butte or Western Australian lamproites, but are similar to Finsch Mine kimberlites (Fraser *et al.*, 1985). They also show pronounced enrichment in Sr, Rb, Zr, and depletion in Nb, high Rb/Sr, Rb/Ba, low Nb/Zr, Ti/Zr ratios relative to Calcutteroo kimberlites, but similar Sm/Nd ratios. However, as suggested by Hawkesworth *et al.* (1984), because K-rich processes are more characteristic of continental regions, the high K_2O, high SiO_2, the presence of quartz and of feldspar in the groundmass of the Truro lamprophyres may reflect some crustal influence. In addition, distinctive depletion of Nb also implies a somewhat continental crustal or shallow depths of lithospheric characteristics. Likewise, slight deviation of these rocks towards continental crust in the εNd -100/Nd diagram (Fig. 5.17) and from the normal mantle array

to high eSr ratios (Zindler and Hart, 1986) may also reflect this contamination.

In conclusion, the Truro lamprophyres have originated from enriched metasomatized magma sources at shallower depths than the kimberlites. Their primary magma may have resided just under the lower crust within the upper subcontinental lithosphere. These rocks have slightly lower εNd values and model ages which reflect early Neoproterozoic enrichment (~800 Ma). This is about the same age as the phase of widespread mafic magmatism which accompanied the initiation of Adelaidean rifting and sedimentation (e.g. Turner and Foden, 1990).

5.9.3. Depth of the source magma for Calcutteroo kimberlites

The depth of magma generation may be influenced by geothermal gradients as well as crust and lithospheric thickness (Nelson, 1989). Previous studies of the lithospheric structures (mentioned in Chapter 1) suggest the lithospheric structure and lithosphere-asthenosphere transition are different in different tectonic environments. Studies of the lithospheric upper mantle structure under Archean cratons (Jordan, 1978; Pollack, 1986) also suggests that Archaean lithosphere is cool and thick.

In the Australian case, stable cratonized Proterozoic or Palaeozoic lithospheric structure and their depth showing a lower heat flow are different from those of the tectonically active Phanerozoic area showing high heat flow with shallow lithospheric structure. In addition, the geothermal gradient of the Palaeozoic Adelaide geosyncline (Pearson *et al.*, 1991) are considerably different from that of eastern Victorian (O'Reilly and Griffin, 1985). Possibly, depth of graphite-diamond transition are also different each other.

There is some consensus that Western Australian lamproites are derived from subcontinental lithosphere, but at the depth within diamond stability (Nelson *et al.*, 1986). In South African kimberlites, sources of Group I kimberlites are within the asthenospheric (possibly plume sources) (e.g. Smith *et al.*, 1985) and Group II kimberlites originate in the subcontinental lithospheric mantle (Smith *et al.*, 1985; Nelson, 1989).

If mantle metasomatism is characteristically only at the lithospheric level (Hawkesworth *et al.*, 1984; Menzies *et al.*, 1985; Eggler, 1986; Menzies *et al.*, 1987; O'Reilly *et al.*, 1988; McKenzie, 1989) and K enrichment (possibly K/Ti increase) is the main characteristic of this mantle metasomatism (Griffin *et al.*, 1988), then Group I kimberlites showing a distinctive K depletion must be derived from the asthenospheric sources while Group II kimberlites showing a enrichments in the LIL (K) as well as more evolved isotopic compositions are derived from the lithosphere.

Following these interpretation, the Calcutteroo kimberlites are derived from the lithosphere. However, the geochemical and isotopic data of the Calcutteroo kimberlites reflect neither South African group I kimberlites nor Western Australian lamproites. Their isotopic and geochemical characteristics lie between Group I and Group II kimbertlites. In the Calcutteroo kimberlites, upper mantle xenoliths (e.g. spinel lherzolites) as well as

diamonds are not common, unlike those of Western Australian lamproites and South African kimberlites.

These characteristics suggest that Calcutteroo kimberlites may be derived from the geochemically enriched (possibly metasomatized) sub continental lithosphere in the diamond stability field. However their depth may be shallower than that of the Western Australian lamproites, because the Adelaide geosyncline is younger than the former. The residence time of the South Australian enrichments as indicated by their Nd model ages are also correspondingly shorter.

5.9.4. Transitional variation or coexisting of kimberlites with other rock types

Experimental studies (Wendlandt, 1984; Eggler, 1986) have examined evidence for the coexistence of kimberlitic magma with carbonatite and other highly silica-undersaturated silicate liquids such as melilitite or nephelinite. These investigations were promoted by appropriate field evidence for these associations (Moore, 1979; McIver and Ferguson, 1979; Milashev 1965; Frantsesson, 1969; Eggler *et al.*, 1987).

On the other hand, previous studies for eastern Australia suggested transitional variation or comagmatic of the rocks with related rocks. They may lead to many ambiguous terms in the studies of the South Australian kimberlites, carbonatic kimberlites, lamprophyritic, and kimberlitic rocks (Ferguson and Sheraton, 1979; Stracke *et al.*, 1979).

Eggler (1986) suggested that carbonate alkaline magma is derived from carbonated peridotites containing amphibole-dolomite, phlogopite-dolomite or phlogopite-magnesite. The melt composition changes from nephelinite, melilitite, alkaline carbonatites to kimberlites as result of the increasing pressure from 22 to 65 kb. The magmatism occurs by melting at the base of the lithosphere or by separation of melts from diapirs or hot spots at the base of the lithosphere (possibly 670 km depth). The melting temperatures range from 1200 °C to 1500 °C in which high melting temperatures are indicated by experimental kimberlite liquid and with that of the porphyroclastic peridotite xenoliths.

Wendlandt (1984) also suggested that partial melt derived from the carbonated peridotite at about 100 km depth makes carbonate rich magma resembling kimberlites and carbonatites. Another studies (Green and Wallace, 1988; Wallace and Green, 1988) also suggested carbonatitic melts coexisting amphibole bearing lherzolites at 21-31 kbar and 930-1080 °C (See Chapter 2).

In the South Australian kimberlites, especially Pine Creek kimberlites (unfortunately, non-eligible isotopic and geochemical data) are intruded by many calcite veins, and nearby Calcutteroo kimberlites (7-8 km NW) show a mica rich mineralogy (but more ultramafic lamprophyres). In the Carrieton-Eurelia area, several dykes showing South African Group I kimberlite like mineralogy (Scott Smith *et al.*, 1984) also occur in which a carbonatite dyke is also reported in the same area (Ferguson and Sheraton, 1979). Even though the Terowie-

Whyte, Yarcowie locality is separated from that of Carrieton-Eurelia, coexistence of kimberlites with their related rocks in each locality may support the experimental results.

However, Nelson (1989) suggested that coexisting lamproites and kimberlites in same area of central west Greenland (but different ages, early Palaeozoic and Mid-Palaeozoic, respectively) are derived from different sources with different isotopic sources. He suggested that the kimberlites are derived from the lithosphere while the lamproites magma sources are derived from subcontinental magma which are separated from the asthenospheric convecting mantle sources.

In South Australia, these kinds of the interpretation are difficult because there is not eligible age dating or isotopic composition of the kimberlites with their ambiguous occurrences (see introduction). Possibly some of the kimberlites are derived from the lithospheric level and the others are derived from the asthenospheric level or lithospheric level on the diamond stability.

In conclusion, South Australian kimberlites showing a transitional variation with their related rocks and coexisting with carbonatites within same area, suggest that at least, some of the kimberlites may be derived from single source.

5.10. Conclusion

1) Calcutteroo kimberlites are like South African Group II kimberlite while Truro lamprophyres are similar to Western Australian lamproites in geochemical characteristics.

2) The Calcutteroo kimberlites were derived from the incompatible element enriched, subcontinental lithosphere while Truro lamprophyres were derived from shallower depths possibly, close to the lower crust-upper mantle boundary or in the upper most continental lithosphere.

3) The geochemical and isotopic composition of Truro lamprophyres suggested that their magma sources are not typical of the normal upper mantle, but reflect the effects of the assimilation or anatexis in the crust.

4) In the South Australian kimberlites, Pine Creek and Calcutteroo kimberlites are distinguished from Port Augusta kimberlites by their more mica -rich mineralogy, while Port Augusta kimberlites are distinguished from the former by a slightly higher proportion of olivine (pseudomorph). The Pine Creek kimberlites are distinguished from the two localities by carbonate rich characteristics.

Chapter 6. Accretion of the South Australian lower crust based on the petrography, mineral chemistry, geochemistry and isotopic composition of xenoliths entrained from the South Australian kimberlites

6.1. Introduction

Together with geophysical data, lower crustal xenoliths entrained by basaltic or kimberlitic rocks on the Earth's surface provide principal constraints for the chemical composition and physical properties of the lower crust, and the nature of the crust-mantle boundary (McCulloch and Wasserburg, 1978; Taylor and McLennan, 1985; Rudnick *et al.*, 1986). These xenoliths are dominantly granulite facies rocks (Kay and Kay, 1981; Furlong and Fountain, 1986; O'Reilly *et al.*, 1988). However, these studies are restricted because of limited sample sets which can be taken as representative of the lower crust (Bloomer and Nixon, 1973; Griffin and O'Relly, 1987a; Muirhead and Drummond, 1991) and because of the vertical and horizontal heterogeneity of the shallow lithosphere (Ferguson *et al.*, 1979; Finlayson, 1983; Jackson and Arculus, 1984; O'Reilly and Griffin, 1985).

The study of lower crustal xenoliths can be complimented to those involving outcropping granulite facies terrains, such as Scottish Lewisian rocks, (Weaver and Tarney, 1980). The outcropping granulite facies terrains allow volumetric estimates of lithological proportions with depth, and interpretation of contact relationships of high-grade metamorphism with a variety of rock types, which can not provided by the xenolith studies (Rudnick and Taylor, 1987).

In Australia, the xenoliths are found within Mesozoic to Cainozoic lamprophyritic and Cainozoic alkaline basaltic rocks (Wass and Hollis, 1983; Kay and Kay, 1983; Rudnick and Taylor, 1987; Griffin *et al.*, 1987), however, their geographical distribution is concentrated on the eastern part of Australia in the Tasman Fold Belt. The xenoliths are dominantly basaltic in composition and are considered as to be originated from cumulates or late differentiates of basaltic magmas (O'Reilly *et al.*, 1988).

In South Australia, xenoliths are found in Mesozoic kimberlitic provinces, including Port Augusta, Orroroo, Calcutteroo and Pine Creek (Ferguson *et al.*, 1979; Ferguson and Sheraton, 1979; Western Queen (S.A.) Pty. Ltd., 1981; Wass and Hollis, 1983; Jackson and Arculus, 1984; Scott Smith *et al.*, 1984). They are predominantly eclogitic and granulitic with subordinate pyroxenites, amphibolites, gabbroic rocks and lherzolites (Jackson and Arculus, 1984; Pearson *et al.*, 1991; Chen *et al.*, 1994). They have a wide range of compositions from *ne* - through *ol* - to *q*- normative and are characterised by a

considerable variety of geochemical and isotopic signatures (Ferguson *et al.*, 1979; Arculus *et al.*, 1988; Pearson *et al.*, 1991).

This study presents detailed petrographical descriptions, mineralogical, geochemical and isotopic analyses for lower crustal xenoliths from three South Australian kimberlitic localities. This chapter also examines possible mechanisms which is responsible for the formation and modification of the South Australian lower crust.

6.2. Previous studies

Several studies have been carried out on South Australian xenoliths, however most have been limited to petrographical and mineralogical studies at specific localities. Petrographic descriptions and mineral chemistry of eclogite xenoliths from Port Augusta and Terowie were reported by Ferguson and Sheraton (1979). Scott Smith *et al.* (1984) reported the existences of the garnet websterites and very rare spinel lherzolites within the Orroroo kimberlites and their mineral chemistry .

Geochemical studies of lower crustal xenoliths from Port Augusta and Calcutteroo, together with those of south eastern Australia demonstrated that the xenoliths are dominantly MORB and island arc basalt-like in composition (Ferguson *et al.*, 1979). Detailed isotopic and geochemical studies of South Australian xenoliths suggest that the xenoliths show a wide range of Sr-Nd isotopic composition, abnormal incompatible element abundances and variable REE abundances (McCulloch *et al.*, 1982; Arculus *et al.*, 1988; McDonough *et al.*, 1991). McCulloch *et al.* (1982) argued that these characteristics precluded previous crustal-mantle evolution models which implied simple magmatic underplating of the low crust (Jacobsen and Wasserburg, 1979; DePaolo, 1980; Weaver and Tarney, 1980; O'Nions and Hamilton, 1981; Allégre, 1982). Arculus *et al.* (1988) showed that the lower crustal xenoliths from Calcutteroo and El Alamin camp together with those of the S-E Australia and S-W Colorado plateau, USA. are different from the normal basaltic composition for their trace element contents (e.g. Ba) and isotope data (e.g. Sr and Pb).

P-T estimates of mafic xenoliths from Calcutteroo suggest that the transition from granulite to eclogite in the lower crustal and upper mantle level occurs at the depth of the 35-75 km (800 °C/10 kbar and 1020 °C/22 kbar) (Pearson *et al.*, 1991). Their detailed microscopic evidence also suggest that the mafic xenoliths record several episodes of magmatic underplating and tectonic activity.

6.3. Isotopic ages of the South Australian lower crustal xenoliths

Limited age dating has been attempted for the granulitic to eclogitic xenoliths entrained by Calcutteroo kimberlite pipes (McCulloch *et al.*, 1982; Chen *et al.*, 1994). The results show that the lower crustal xenoliths were formed over a wide time span even though they

are found at a single locality.

The Calcutteroo xenoliths yield Rb-Sr and Sm-Nd pseudo-isochron ages are 2470±60 Ma and 2350±400 Ma, respectively (McCulloch *et al.* , 1982). McCulloch *et al.* (1982) interpreted this as evidence for major differentiation for the South Australian crust as early ~2400 Ma.

U-Pb zircon ages from the xenoliths range from 300 to 1600 Ma and have been assembled into four main groups (Chen *et al.*, 1994). These distinctive ages are thought to be due to the coupling of crustal tectonic events and major magmatisms resulting in formation or recrystallisation or loss of Pb in the zircon grains. Chen *et al.* (1994) suggested, 1) ages of 1600-1500 Ma as a record of the high grade metamorphism of the Willyama complex and Gawler Block in N.S.W. and S.A., 2) of 850-650 Ma date as a record of rifting and faulting of the Adelaidian Fold Belt, 3) of 650-575 Ma as a record of the extension, uplift and collision episodes at the Tasman suture line and 4) of 500-300 Ma as a record of the metasomatic events in the mantle in western Victoria.

A complicated history involving multiple underplating in the lower crust, metamorphism, metasomatism, and partial melting, would be resulted in controversies for the isotopic ages because they lead to modification of the original composition. As a result, Chen *et al.* (1994) discounted the previous Rb-Sr and Sm-Nd isochron age dating of McCulloch *et al.* (1982).

6.4. Petrography and mineralogy of the South Australian lower crustal xenoliths

6.4.1. Introduction

Over seventy samples were collected for petrological descriptions from Port Augusta, Calcutteroo and Pine Creek kimberlite pipes. The xenoliths are divided into six major groups according to mineral assemblages and mineral chemistry as illustrated in Table 6.1. They are summarised in Fig. 6.1III.

Table 6.1. Classification of lower crustal xenoliths.

Lithology	Mineralogy	
Eclogitic rock	Gt+Cp±Am±Opx±Qt	Na2O wt % of 1.5 to 5.5 (Cpx)
Two-pyroxene granulite	Cpx+Gt+Pl±Opx±Am±Qt	Na2O wt % of <1.5 (Cpx). Modal Opx>5 %
Clinopyroxene-gratulite	Cpx+Gt+Pl+Qt±Opx±Am	Na2O wt % of <1.5 (Cpx). Modal Pl+Qt>10 %
Feldspar-rich granulite	Pl+Cpx+Kfd±Opx±Gt±Am±Qt	Modal Pl+K+fd>40-50 %
Pyroxenite	Cpx+Opx±Am±Gt	Modal Cpx+Opx>70 %
Kyanite-bearing granulite	Cpx+Gt +Ky±Opx±Am±Qt	Modal Ky>5 %

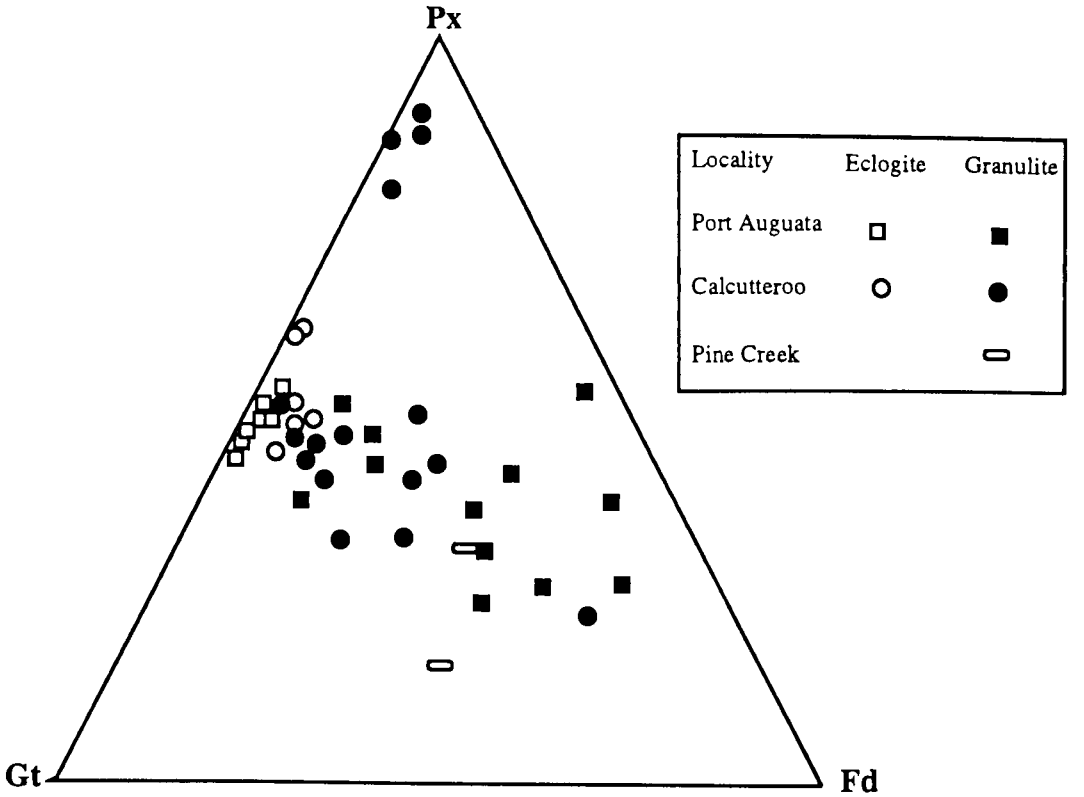

Fig. 6.1III. Plot of modal proportions of the South Australian lower crustal xenoliths. (Gt = Garnet, Px = Clinopryoxene+Orthopyroxene, Fd = Plagioclase+K-Feldspar).

In these classifications, feldspar-rich granulites refer to quartzo-feldspathic granulites containing abundant plagioclase, K-feldspar and quartz, and pyroxenites contain garnet-free or with <5 wt % garnet but contain abundant ortho- and clinopyroxene (over 70 wt %). The other minor types are gabbroic rocks and amphibolitic rocks.

6.4.2. Port Augusta

A large numbers of samples was collected from weathered kimberlitic dykes at El Alamein army camp. Twenty-two fresh samples were selected for petrographical descriptions. The xenoliths range from about 1-3 cm) in diameter (Fig. 6.1I). Detailed petrographical and mineralogical descriptions are given in Appendix 3 and are summarised in Table 6.2. The Port Augusta xenoliths are characterised by distinctive exsolution, complicated replacement or recrystallization texture, and abundant acicular shaped rutile inclusions in pyroxene and garnet (Fig. 6.1II). They generally show clear petrographical differences between granulitic and eclogitic rocks.

<u>Eclogitic rock;</u> They are characterised by sub-to equigranular textures, the existence of coarse-grained rutiles, discrete spinel and amphibole grains (Fig. 6.1II). Most of clinopyroxene and garnet occurs as discrete grains. Amphiboles occur as discrete grains containing garnet or clinopyroxene. They are diamond shaped grains and at least two

generations of grains occur in a given sample. Ulvöspinels mainly occur as dicrete grains and are scattered through the other grains. They may have been original crystallising minerals in some rocks as mentioned in the Anakies xenoliths (Wass and Hollis, 1983).

Table 6.2. Mineralogy and Texture of the Port Augusta xenoliths.

Lithology	Mineralogy	Texture
Eclogitic rock	Gt+Cpx+Am+Sp+Rt+Qt	equi-to sub granular texture, coarse-grained rutile, discrete ulvöspinel & amphibole grains
Feldspar-rich granulite	Cpx+Fd+Gt+Rt+Il±Sp±Opx±Am±Mt ±Sul	diverse stages of exsolution texture, ilmenites rimmed by granular garnet, acicular or needle-shaped rutile inclusions in clinopyroxene and/or garnets
Two-pyroxene granulite	Cpx+Opx+Pl+gt+Sp+Rt+Apt+Cal +Mt	distinctive foliation, clinopyroxene & ilmenite rimmed by garnet
Gabbroic rock	Pl+Am+Cpx+Opx+Gt+Sp+Mt	doleritic microstructure, lath-shaped plagioclases, clinopyroxenes showing an intergrowth with amphibole and with minor ilmenite and rutile.
Xenocryst	A) clinopyroxene or amphibole (0.6-1.8 cm wide) B) clinopyroxenes (0.6-0.8 cm)	A) no exsolution texture B) distinctive Fe-Ti exsolution lamellae

Granulitic rock; They are characterised by ilmenite and/or clinopyroxene rimmed by garnet, distinctive exsolution texture among Fe-Ti oxide, pyroxene, amphibole and garnet. Most of clinopyroxene and garnet commonly show intergrowth with amphibole (Fig. 6.1II) and Fe-Ti oxide. Plagioclases show polysynthetic twins and alkali feldspars are characterised by the perthite texture. In these granulites, feldspar-rich varieties show more complicated intergrowth and recrystallisation textures.

The granulites contain acicular rutile and ilmenite grains as inclusions in the garnet and clinopyroxene. The inclusions lie at perpendicular planes, mainly concentrated on core of the garnet. Similar inclusions were reported from the xenoliths in Anakies (Wass and Hollis, 1983). The intergrowth may result from sink for Ti which was not accommodated significantly in garnet (Wass and Hollis, 1983). Ilmenite and clinopyroxene grains rimmed by garnet are common in these granulites. In the feldspar-rich granulite, many of the recrystallised garnet rims extend to adjacent feldspar grains. This texture may reflect decompression while the xenoliths transported from the deep crust by their host kimberlites. Fe-Ti oxides rimmed by garnets were reported from mafic granulites of Enderby Land, Antarctica (Ellis and Green, 1985). Ellis and Green (1985) explained these relationship as two reactions, An+Il+Qt = Gt+ Rt or An+Usp+Qt = Gt+ Il.

The feldspar-rich granulites show four types of exsolution texture, 1) garnet,

garnet, amphibole and Fe-Ti oxide exsolution in clinopyroxenes, 2) clinopyroxene vermicular exsolution in garnet, 3) exsolution between clinopyroxene and orthopyroxene, and 4) plagioclase exsolution in garnet and clinopyroxene. These textures probably reflect transition of gabbro to granulite.

Parallel intergrowth of amphiboles in the clinopyroxene grains as well as symplectitic intergrowth of orthopyroxene and clinopyroxenes were also reported from lower crustal xenolith from the Anakies, Victoria (Wass and Hollis, 1983). The intergrowth of amphiboles in the clinopyroxene grains may be explained as exsolution of amphibole from a pyroxene with some solid solution, a alteration of an original stoichiometric pyroxene, or dehydration of pre-existing amphibole by CO_2 fluxing as mentioned by Wass and Hollis (1983). These intergrowth textures may reflect an exceed of rate of grain boundary adjustment to the mineralogical equilibrium in a given metamorphic regime (Wass and Hollis, 1983).

In some of granulitic rocks, garnet grains are altered to fine-grained opaque aggregates, and clinopyroxenes are recrystallised to fine grained granular grains partly, at their margin. In two-pyroxene granulite, clinopyroxenes occur as unexsolved reddish brown pleochroic eu- to sub- hedral grains or faint green sub-hedral grains with well-developed exsolution lamellae. A few orthopyroxenes occur as discrete grains and biotites occur as interstial flakes. Rutile mainly occurs as intergrowths with ilmenite and some are replaced by ilmenites completely. The other accessory minerals, calcite, magnetite and apatite are also scattered through all phases. The remnants of the calcite veins are also observed.

Gabbroic rock: These rock types are not common in the Port Augusta xenoliths. They have lath-shaped plagioclases, clinopyroxenes showing an intergrowth with amphibole and minor ilmenite and rutile (Fig. 6.1II). Prismatic-shaped orthopyroxene grains also occur. Garnet rings encompass clinopyroxenes showing an intergrowth with amphiboles or Fe-Ti oxides.

Xenocryst: Two types of xenocrysts are found in this area. One is clinopyroxene or amphibole which do not show a exsolution texture while the others are clinopyroxenes which show distinctive ilmenite exsolution lamellae. The first types contain eu-to sub-hedral garnet, pyroxene, amphibole (0.1-0.3 cm) and minor rutile as inclusion. The xenocrysts are fractured by thin calcite veins, and thus most of the poikilitic grains are partially or completely altered. The inclusions commonly show reaction rims with their host clinopyroxenes or amphiboles. The second types show a ladder like exsolution lamellae along the direction of twin rather than clevage planes.

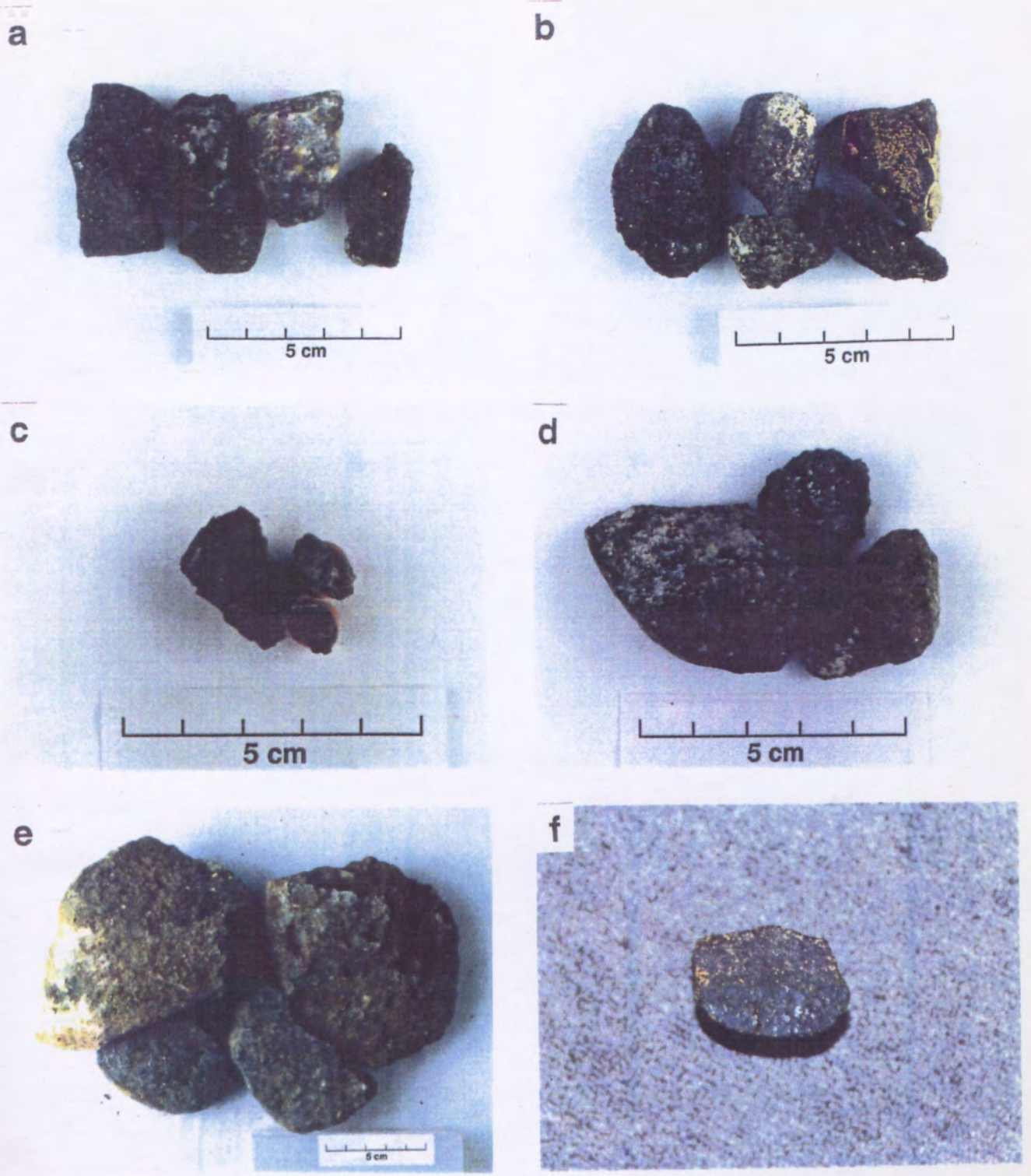

Fig. 6.1 [a-c. Photographs **a)** of gabbroic xenoliths, **b)** of granulitic and eclogitic xenoliths, **c)** of amphibole and clinopyroxene megacrysts entrained by the Port Augusta kimberlites.

Fig. 6.1[d-e. Photographs **d)** of gabbroic xenoliths, **e)** of typical pyroxenitic, granulitic and eclogitic xenoliths entrained by the Calcutteroo kimberlites. Notice that most of the Calcuttreroo xenoliths are bigger than those of the Port Augusta, but the xenoliths from two localities are mainly round or sub angular shapes.

Fig. 6.1[f. Photograph of a composite xenolith entrained by the Calcutteroo kimberlites showing a sharp contact, quartz-garnet dominant side and clinopyroxene -rutile dominant side. Notice that many xenoliths in this area show sharp contacts or transitional variation, and remnants of partial melting.

Figures opposite;

Fig. 6.1IIa. Photomicrograph of a gabbroic rock from the Port Augusta (Pa 7x 9) showing a doleritic texture with lath shaped plagioclases (p).

Fig. 6.1IIb. Photomicrograph of a feldspar-rich granulite from the Port Augusta (Pa 7x 8). showing pronounced vermicular clinopyroxene (cp) and plagioclase (p) exsolution lamellas in linked garnet grains (g) and clinopyroxenes wormed by plagioclases (p).

Fig. 6.1IIc. Photomicrograph of a eclogitic rock from the Port Augusta (Pa 6x 12) showing granular clinopyroxene (cp) and garnet (g) grains with 120 °C grain boundary.

Fig. 6.1IId. Photomicrograph of a eclogitic rock from the Port Augusta (Pa 6x 8) showing amphibole (am), clinopyroxene (cp) and garnet (g) grains.

Fig. 6.1IIe. Photomicrograph of a two-pyroxene granulite from the Port Augusta (Pa Cx 6) showing orthopyroxene (opx) and clinopyroxene (cpx).

Fig. 6.1IIf. Photomicrograph of a feldspar -rich granulite from the Port Augusta (Pa 7x 2). showing garnet (g) which contain spine shaped rutiles.The rutile inclusions are compared with a discrete grain (r) exsolved by ilmenites .

Fig. 6.1IIg. Photomicrograph of a two-pyroxene granulite from the Port Augusta (Pa 7x 6) showing a ilmenite (i) rimmed by garnet and continuously exsolved with orthopyroxene (op) and clinopyroxene (cp). The orthopyroxene and clinopyroxene are also exsolved by the thin lamnellaes of Fe-Ti oxides.

Fig. 6.1IIh. Photomicrograph of a two-pyroxene granulite from the Port Augusta (Pa 7x 6) showing clinopyroxenes (cp) rimmed by granular garnets. The recrystallised garnet grains (g) are extended adjacent to plagioclases (p).

Width of a scale bar (left bottom) is 1 millimetre.

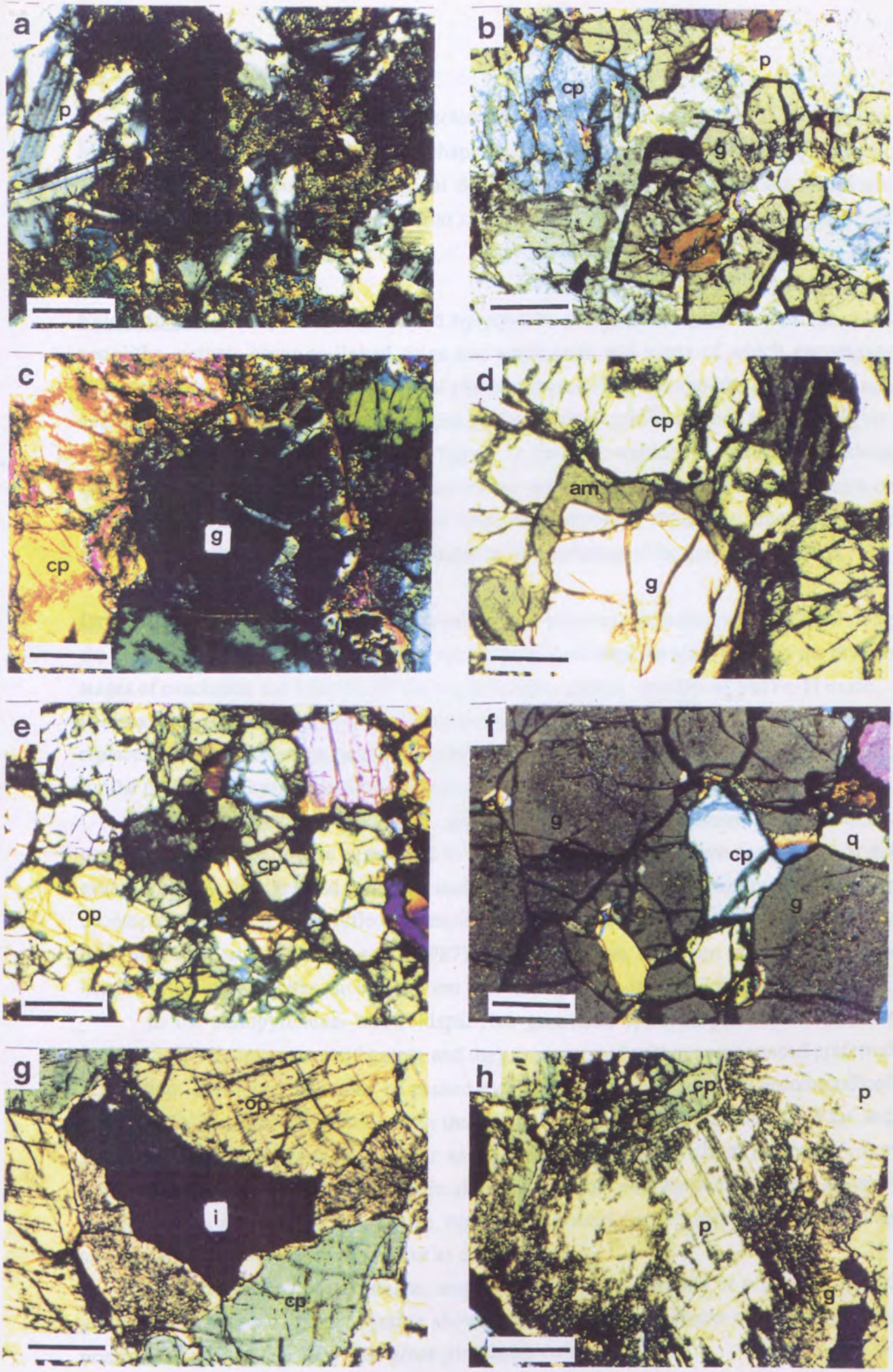
a
p
b
cp
p
g
c
g
cp
d
cp
am
g
e
cp
op
f
g
cp
q
g
g
op
i
cp
h
cp
p
p
g

6.4.3. Calcutteroo

About fifty xenoliths were collected from two kimberlite pipes near Calcutteroo. Most of them are round or sub angular shapes and show 3 to 18 cm in diameter (Fig. 6.1I). Their petrographical and mineralogical descriptions are given in Appendix.3 and are summarised in Table 6.3. The Calcutteroo xenoliths mainly show eclogitic mineralogy and textures (Fig. 6.1II).

Eclogitic rock; They are characterised by equi- to sub-granular grain texture. In these xenoliths, garnets occur as linked rings and aggregates and many of which encompass clinopyroxene and quartz grains. Some of clinopyroxenes show sponge-like altered rims and coarse grained clinopyroxenes are replaced by fine grained granular grains at their margins. Amphiboles mainly occur as interstial flakes. In general, amphibole rich eclogites show quartz and rutile-poor mineralogy. As accessory grains, rutiles occur as discrete grains or form intergrowth with ilmenite. Some of them are completely replace to ilmenite. Quartz occurs as interstial grains and elongate parallel to the direction of the dominant foliation.

Granulitic rock; Slightly different mineralogy and microscopic textures are shown among the granulites. Two-pyroxene granulites are distinguished from the other types by the diverse stages of exsolution and intergrowth among pyroxene, garnet, amphibole and Fe-Ti oxide. Feldspar-rich granulites are distinguished from the other types by the distinctive lineation and replacement texture. Kyanite-bearing granulites are similar to other granulitic xenoliths except for the presence of kyanite, in their microscopic textures.

In the clinopyroxene-granulites, garnet grains defines pronounced lineation. Some garnets are altered to opaque aggregates of spinel or fan-shaped chlorite completely. Some grains contain fine grained acicular inclusion (? plagioclase or clinopyroxene). The decompressive features may reflect the rapid transport of the xenolith from the deep crust by their host kimberlites (Griffin *et al.*, 1987). This texture has also been reported in garnet-bearing granulitic xenoliths in basalt from east- central Queensland (Griffin *et al.*, 1987).

In the clinopyroxene- and feldspar-rich granulite, spine shaped rutiles occur as inclusions in clinopyroxene and garnet and they are scattered without pronounced preferred orientation. The intergrowth may be caused by a sink for Ti which was not accommodated significantly in garnet as mentioned in the studies of xenoliths in Anakies by Wass and Hollis (1983). Ilmenites mainly occur as exsolution lamellae in clinopyroxene. A few hexagonal or prismatic apatite grains are also included by clinopyroxenes. In the feldspar -rich granulite, abundant Cr spinels also occur at the altered margins between clinopyroxene and garnet. A few orthopyroxene occur as discrete grains.

In the clinopyroxene-granulite, amphiboles occur as diamond or prismatic shaped grains. The diamond shaped grains show reddish brown pleochroic colours while the prismatic shaped grains show pale green pleochroic colours.

Table 6.3. Mineralogy and Texture of the Calcutteroo xenoliths.

Lithology	Mineralogy	Texture
Ecolgitic rock	Gt+Cpx+Qt+Rt+Il+Apt±Sp±Opx	equi-to sub granular grain texture
Two-pyroxene granulite	Cpx+Gt+Opx+Sp+Am+Chl+Il	diverse stages of exsolution texture among Cpx+Am+Opx
Clinopyroxene-granulite	Gt+Cpx+Qt+Pl+Rt+Apt+Il±Am±Opx ±Bi±Sp	equi-to sub granular grain texture, distinctive recrystallization , replacement texture
Feldspar -rich granulite	Pl+K-fd+Gt+Cpx+Qt+rt+Apt	distinctive lineation, replacement texture
Kyanite-bearing granulite	Gt+Cpx+Qt+Ky+Rt+Apt	abundant kyanite grain (~4-7 %), weak lineation , aggregated garnet grains
Pyroxenite	Cpx+Opx+Am±Gt±Rt±Il±Bi±Cal±Mt	intergrowths among Cpx+Opx+Am±Fe-Ti oxides, concentric reaction rim
	A) composite xenoliths B) transitional variation in mineralogy	A) granulite-eclogite, granulite-pyroxenite and amphibolite and granulite. B) transitional variation or aggregation of their dominant mineralogy.

In the two-pyroxene granulite, some of clinopyroxenes are replaced by more tschermak clinopyroxene in their core. A few garnets are recrystallised to fine grained granular grains. In the kyanite-bearing granulite, kyanite occur as columnar or elongated discrete grains which are scattered through all phases or spine or acicular shaped grains which occur as inclusions of garnet. The first types are arranged to the pronounced direction of foliation while the second types are mainly scattered without pronounced direction.

Pyroxenitic rock; They are characterised by complicated exsolution and intergrowth textures among clinopyroxene, orthopyroxene, garnet, amphibole and Fe-Ti oxide. They also show concentric reaction rims of fine grained clinopyroxene-laths formed by a replacement of core amphibole and outer rim of lath-shaped plagioclase (Fig. 6.1II). This microscopic texture may reflect multiple alteration and/or recrystallisation. A few amphibole grains occur as rim of clinopyroxene grains, encompassed by aggregates of lath shaped fine grained biotites. Spinels are abundant near boundaries between clinopyroxene and amphibole. Thin lath-shaped biotites occur as interstial flakes. Plagioclases occur as discrete grains, as poikilitic grains or as replacing clinopyroxene and garnet. Discrete plagioclase grains show typically albite or carlsbad-albite twins whereas retrograde grains developed at the contact of clinopyroxene with garnet show thin lamellae shapes. K-feldspars occur as interstial grains.

Composite xenolith or sample showing transitional variation in mineralogy;

The Calcutteroo kimberlites host several types of composite xenoliths including

granulite and eclogite, granulite and pyroxenite, and amphibolite and granulite. Many of them show transitional variation or aggregation of their dominant mineralogy. These textures reflect multiple magmatic intrusion, partial melting and multiple deformation in the lower crust. Two representative examples are as follows.

Sample TRWI N C 1 shows sharp contact between clinopyroxene-garnet dominant and garnet-quartz dominant parts (Fig. 6.1II). The clinopyroxene-garnet dominant part is characterised by sub-granular grain texture, weak lineation and distinctive reaction coronas of clinopyroxene grains. The garnet-quartz dominant part is characterised by pronounced foliation of equi-granular quartz and garnet grains, and the existence of abundant coarse rutile. Clinopyroxene is only observed as relict grains.

Sample, LCC 14, shows transitional variation in mineralogy from clinopyroxene -dominant to amphibole-dominant parts. In the clinopyroxene dominant part, clinopyroxene and garnet occur as subhedral discrete grains in which some of the clinopyroxenes are partially altered to other clinopyroxene in the core. In the amphibole dominant part, amphiboles are subhedral grains of variable grain size containing clinopyroxene and garnet inclusions. These inclusions typically show alteration rims with the host amphibole grains, consisting of a mineral assemblage of spinel, plagioclase and opaque oxide.

6.4.4. Pine Creek

Fifteen xenoliths were collected from mining core sites. Their petrographic and mineralogical descriptions are given in Appendix 3 and are summarised in Table 6.3.

Granulitic rock; Clinopyroxene- and feldspar-rich granulites are observed in this area (Fig. 6.1II). They are similar to those from Calcutteroo in microscopic texture. They contain plagioclases and clinopyroxenes of variable grain size. Clinopyroxene which show a exolution are not common. The plagioclase show albite or polysynthetic twin and K-feldspars occur as discrete grains. As accessory grains, biotites, calcites, hexagonal shaped apatites and rutiles occur. The biotite grains mainly altered to opaque oxide grains in clinopyroxene-granulite whereas they occur as aggregated in feldspar-rich granulites. The calcites occur as replacement of plagioclase and form calcite veins.

Pyroxenite; They show a typical igneous texture. In these specimens, clinopyroxenes occur as coarse subgranular grains showing the distinctive reaction rim and amphiboles occur as interstial flakes.

Amphibolitic and gabbroic rock; Neither of these is common in the South Australian xenoliths. The amphibolite contains abundant eu- to sub-hedral diamond or prismatic shaped amphibole (> 60 %) (Fig. 6.1II). Some grains are poikilitic in coarse amphibole. Prismatic clinopyroxene grains are intergrown with amphibole. A garnet grain is rimmed by an

aggregate of clinopyroxene, amphibole and spinel. Rutiles are scattered throughout all phases. The gabbroic rocks show typical subophitic or doleritic microscopic texture. In this section, plagioclase displays lath or prismatic grain boundary and show albite twin. Clinopyroxenes are replaced by amphibole and only show remnants of the original grain boundary. Abundant opaque oxides are scattered through margins of hydrous minerals.

Table 6.4. Mineralogy and Texture of the Pine Creek xenoliths.

Lithology	Mineralogy	Texture
Clinopyroxene granulite	Gt+Cpx+Pl+Bi+Ky+Rt	pronounced foliation, equi-to sub granular grain texture, kyanite inclusions in quartz
Feldspar-rich granulite	Gt+Pl+Cpx+K-fd+Cal+Bi	distinctive reddish brown altered rims, faint lineation
Pyroxenite	Cpx+Am	igneous texture
Amphibolite	Am+Cpx+Gt+Pl+Apt+Rt	abundant amphibole (> 60%), eu- to subhedral diamond- or prismatic- shaped amphibole grains
Gabbroic rock	Am+Pl+Cpx+Apt+Fe-Ti oxide	subophitic or doleritic microsopic texture
A)Megacryst B)Xenocryst	A) garnet and ilmenite grains B) clinopyroxene and amphibole	A) intruded by calcite veinlet B) pronounced cleavage
	transitional variation of mineralogy	clinopyroxene-dominant to amphibole-dominant

Megacryst or xenocryst; Two different types of the megacrysts or xenocryst are recognised in the Pine Creek kimberlites. The megacrysts include garnet and ilmenite grains which are intruded by the calcite veinlet. The xenocrysts include clinopyroxene and amphibole which show pronounced cleavage and contain garnet, clinopyroxene or amphibole porphyroblast as inclusions. The garnet inclusions in the xenocrysts are mainly altered and replaced by an assemblage of spinel, clinopyroxene, and amphibole. Some of the inclusions are a slightly elongate parallel to the direction of cleavage.

Sample showing transitional variation in mineralogy; A specimen show transitional mineralogical variation from clinopyroxene-dominant to amphibole-dominant. In the clinopyroxene dominant part, clinopyroxene occurs as discrete grains and includes amphibole poikilitically while in the amphibole dominant part, amphiboles occur as discrete sub- or anhedral grains. In both parts, garnets occur as discrete idiomorphic porphyroblasts, or as poikilitic porphyroblasts in clinopyroxene or amphibole. The inclusions show altered grain boundary between amphibole and pyroxene consisting of an assemblage of amphibole, spinel, and pyroxene. Rutiles are scattered through all phases and mainly show intergrowth with ilmenite. A few thin lath-shaped plagioclases showing albite twin and deep green coloured spinels occur at the margins of clinopyroxene and garnet.

Figures opposite;

Fig. 6.1IIi. Photomicrograph of a feldspar-rich granulite from the Port Augusta (Pa 7x 1) showing several generations of garnet grains. The garnet grains occur as discrete grains (left bottom), as rims of the ilmenites (upper) and as exsolved lamellaes in clinopyroxene and orthopyroxene (right).

Fig. 6.1IIj. Photomicrograph of a clinopyroxene xenocryst from the Port Augusta (Pa 8x 4) showing distinctive lamellaes of Fe-Ti oxides which follow a direction of the twin rather than that of the cleavages.

Fig. 6.1IIk. Photomicrograph of a amphibole xenocryst (megacrysts) from the Port Augusta (Pa 8x 1) containing amphibole (am), clinopyroxene (cp), rutile (r) and garnet (g) grains.

Fig. 6.1IIl. Photomicrograph of a eclogitic rock from the Calcutteroo (TRWI N 6) showing aggregated garnet grain (g), jadeitic clinopyroxene (cp) and discrete rutile (i) grains.

Fig. 6.1IIm. Photomicrograph of a clinopyroxene-granulite from the Calcutteroo (TRWI CX 8) showing sub granular garnet (g), clinopyroxene (cp) and lath shaped biotite (b) grains.

Fig. 6.1IIn. Photomicrograph of a clinopyroxene-granulite from the Calcutteroo (TRWI CX 2) showing linked rings or aggregations of equigranular garnet grains (g). The garnet grains encompass clinopyroxene or quartz recrystallised to several grains.

Fig. 6.1IIo. Photomicrograph of a pyroxenite from the Calcutteroo (TRWI Ch 8) showing kinking banded clinopyroxenes (cp) which contain thin exsolution lamellaes of Fe-Ti oxides.

Fig. 6.1IIp. Photomicrograph of a two-pyroxene granulite from the Calcutteroo (TRWI CX 10) showing diverse stages of exsolution textures among pyroxene, garnet, amphibole, and Fe-Ti oxide. Notice that orthopyroxene (op) show a exsolution lamellae to the same direction of its cleavage.

Width of a scale bar (left bottom) is 1 millimetre.

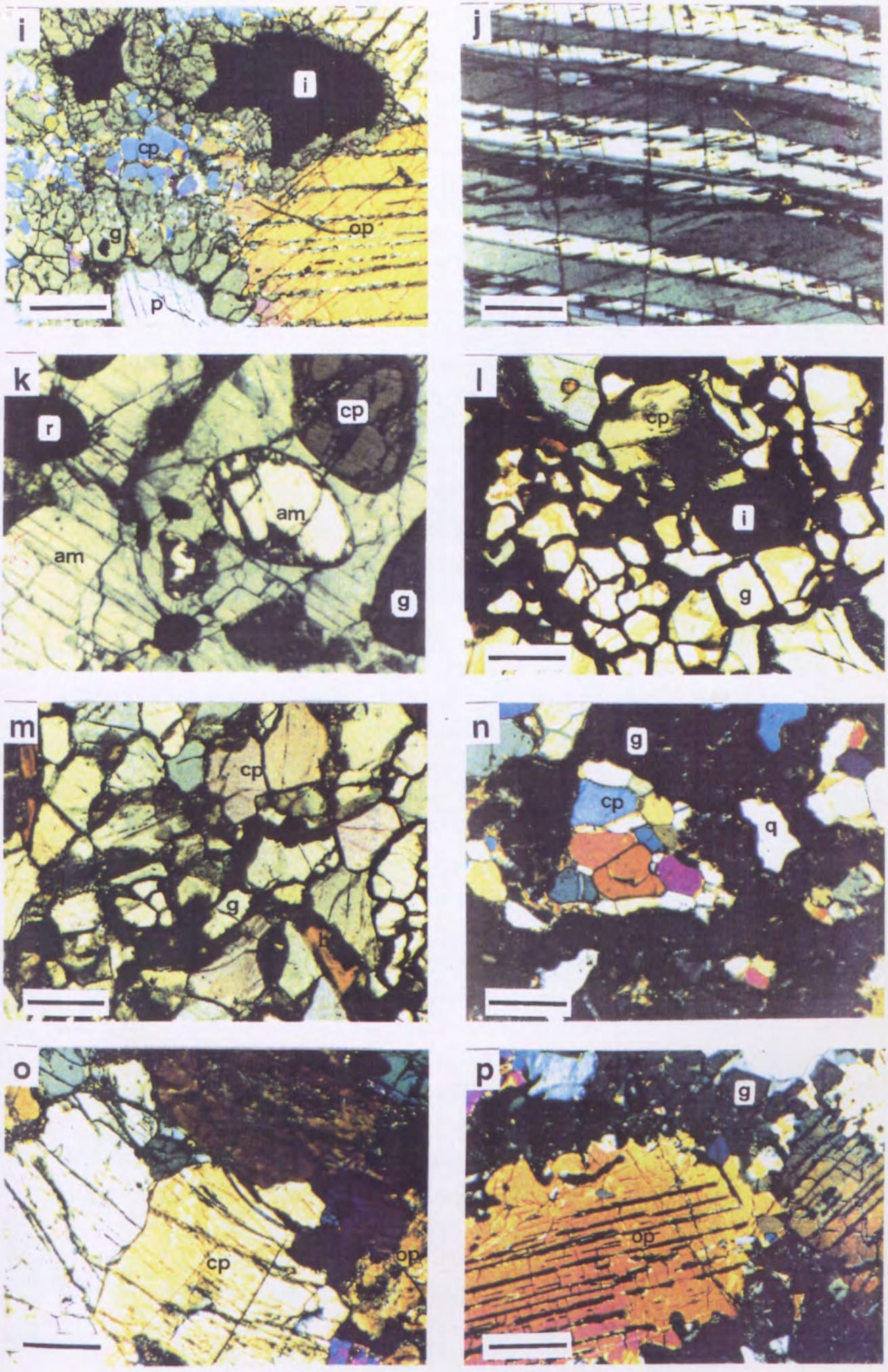
i
i
cp
g
op
p
j
k
r
cp
am
am
g
l
cp
i
g
m
cp
g
n
g
cp
q
o
cp
op
p
g
op

Figures opposite;

Fig. 6.1IIq. Photomicrograph of a clinopyroxene -granulite from the Calcutteroo (TRWI CH 4) showing a exsolved coarse grained clinopyroxene which contains exsolved clinopyroxene and orthopyroxene grains .

Fig. 6.1IIr. Photomicrograph of a pyroxenite from the Calcutteroo (TRWI CB 2) showing a distinctive alteration at the garnet-amphibole contact in which the altered grains are consist of chromite, amphibole and clinopyroxene.

Fig. 6.1IIs. Photomicrograph of a pyroxenite from the Calcutteroo (TRWI CB 3) showing a complicated concentric alteration texture. This picture shows clinopyroxenes exsolved by orthopyroxene or amphibole which are surrounded by recrystallised clinopyroxene and continuously rimmed by chromites and plagioclases (p).

Fig. 6.1IIt. Photomicrograph of a kyanite bearing granulite from the Calcutteroo (TRWI N 7) showing two generations of kyanite grains, columnar or elongate shapes as discrete grains (middle bottom) and spine or acicular shaped grains as inclusion of garnets (upper right).

Fig. 6.1IIu. Photomicrograph of a clinopyroxene granulite from the Pine Creek (PINC X 5) showing a pronounced foliation of equi- to sub granular grains. Clinopyroxene and garnet grains mainly show altered rim.

Fig. 6.1IIv. Photomicrograph of an amphibolite from the Pine Creek (PINC A 4) showing subhedral diamond shaped amphibole grains.

Fig. 6.1IIw. Photomicrograph of an amphibole xenocryst (? megacrysts) from the Pine Creek (PINC A 3) containing garnet (g) and clinopyroxene (cp).

Fig. 6.1IIx. Photomicrograph of a composite xenolith from the Calcutteroo (TRWI N C 1) showing sharp contact, clinopyroxene-garnet dominant part and garnet-quartz dominant part.

Width of a scale bar (left bottom) is 1 millimetre.

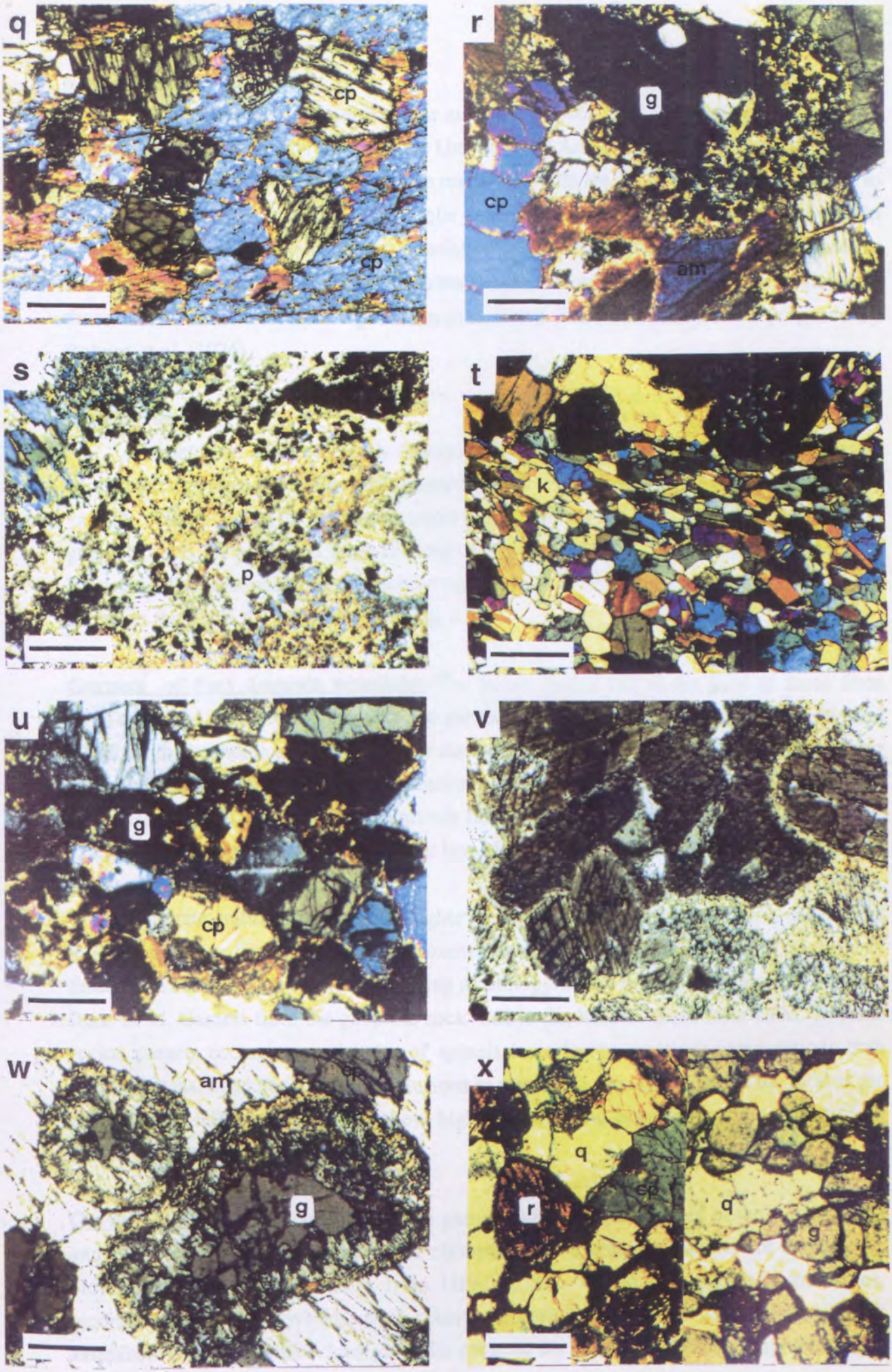
q
cp
cp
r
g
cp
am
s
p
t
k
u
g
cp
v
w
am
g
x
q
r
cp
q
g

6.4.5. Mineral chemistry

Thirty xenoliths were selected for mineral analyses. All analyses were carried out with the EDS equipped microprobe at the University of Adelaide. Details of the analyses are given in Appendix 1. Some samples were reanalysed with the WDS equipped microprobe to compare with those of the EDS microprobe analyses. At least five points were analysed in minerals involved in geothermometric calculation and three points were generally analysed for each mineral. Most of the calculated Fe(3)/Fe(2) contents are based on stoichiometry however those for the determination of geothermobarometry followed the equation proposed by Ruburn *et al.* (1976).

A) Garnet

Garnet from all three South Australian kimberlites localities contains three major components; pyrope, almandine and grossular (93 to 98 %). Garnet compositions are widely variable corresponding to eclogitic garnets in kimberlites (field A, *KR*), through those in gneiss (field B, *HPM*) and to those in blueschist (field C, *LPM*) of Coleman *et al.* (1965). In general, their composition is homogeneous in each specimen. Representative analyses are shown in the Table 6.5 and plotted in Fig. 6.2a,b.

<u>Garnets of Port Augusta xenoliths:</u> The garnet grains fall in the field of those from LPM and HPM. In the eclogitic rocks, the garnets fall in the field of the those from LPM and HPM. High almandine and low grossular compositions are shown in orthopyroxene bearing samples whereas low almandine compositions are shown in amphibole bearing samples. In the feldspar-rich granulite, the grains mainly fall in the field of garnet from LPM. In general, exsolved grains in the clinopyroxene have low Mg#, high grossular and almandine relative to grains occurred as rim of spinel.

Discrete grains show a slightly higher Mg# and lower grossular compositions relative to the two former types. In the two-pyroxene granulites, discrete grains fall in the field of those from HPM whereas grains occurring as clinopyroxene rims fall in the field of those from LPM. Garnets from the gabbroic rock fall in the field of those from LPM. In these rocks, garnets occurring as the rim of spinels have lower grossular compositions than discrete grains. In addition, garnet inclusions in amphibole xenocrysts fall in the field of the garnets from HPM and they also show higher pyrope and lower almandine composition relative to garnets from gabbroic rocks.

<u>Garnets of Calcutteroo xenoliths;</u> The garnet grains fall in the field of those from LPM and HPM. In the eclogitic rocks and clinopyroxene-granulites, garnets are dominantly plotted in the range of those from HPM to KR. In the clinopyroxene-granulites, recrystallised garnets have low Mg# relative to garnets of samples containing abundant amphibole and Fe-Ti oxides. Low grossular contents are observed in abundant spinel bearing

samples. Garnets from feldspar-rich and two-pyroxene granulites show similar compositions. Garnets in kyanite-bearing granulites have higher Mg# than those of former two types and are plotted dominantly in the range of garnets from HPM. In pyroxenitic rocks, garnets occurring as rims on clinopyroxene have lower Mg#, Cr_2O_3 and higher MnO, lower grossular and almandine composition than those of discrete grains. In the samples showing transitional mineralogy, garnets compositions are homogeneous.

Garnets of Pine Creek xenoliths; The garnet grains fall in the field of those from HPM. High pyrope compositions are shown in garnets from clinopyroxene-granulites and low Mg# (52.5-54.2) are recorded from those of a sample showing transitional variation. Slightly high grossular and pyrope composition are shown in garnets from clinopyroxene-granulites.

In conclusion, garnets of South Australian lower crustal and upper mantle xenoliths have wide ranges of composition. Generally, garnets of Port Augusta xenoliths are more granulitic while those of Calcutteroo and Pine Creek are more eclogitic, suggestive of different P-T condition. Garnets from Calcutteroo and Pine Creek have higher Mg# (50-70) than those from Port Augusta (mainly <40). No clear differences in the mineralogical composition are found among the garnets of different rock types from the Calcutteroo xenoliths. Garnets from kyanite-bearing rocks are geochemically similar to other granulites.

B) Clinopyroxene

Representative clinopyroxene analyses from three localities of South Australian kimberlites are shown in the Table 6.6. They were plotted in Ca-Mg-Fe and Di+Hd-Jd-Ts diagrams to compare mineralogical compositions (Fig. 6.3, 6.4).

Clinopyroxenes of Port Augusta xenoliths; The clinopyroxene grains have salitic to augitic compositions. In general, clinopyroxenes of the eclogitic rocks have jadeitic, high Na_2O (2.0-5.6 wt %) and salitic composition, whereas those of granulitic rocks are dominantly diopsidic-hedenbergitic and have diopsidic-augitic composition. No distinctive differences in composition are shown among the clinopyroxenes of granulitic rocks. In the eclogitic rocks, replaced grains of jadeitic host minerals have augitic, high tschermak, CaO, Cr_2O_3, low Mg#, Na_2O, Al_2O_3, relative to their host grains. Clinopyroxenes of feldspar-rich granulites are dominantly diopsidic-hedenbergitic, low Na_2O (1.6-2.2 wt %) and have salitic or diopsidic composition.

In these granulites, recrystallised clinopyroxenes have high CaO, TiO_2 and low Cr_2O_3 and Na_2O relative to the discrete grains. Clinopyroxenes in two-pyroxene granulites are diopsidic-hedenbergitic, salitic composition, but have a slightly low Mg#, Na_2O and high CaO relative to those of eclogitic rocks and feldspar-rich granulites.

Table 6.5. Representative garnet analyses of the South Australian lower crustal xenoliths.

A) Port Augusta

Sample	Pa 6X 8		Pa 5X 2		Pa 6X 9		Pa 6X 2		Pa 6X 6		Pa 6X 7		Pa 6X 12		Pa 5X 1		Pa 7X 1		Pa 6X 11		Pa 7X 6		Pa 9X 1	
Lithology	Eclog.		Eclog.		Eclog.		Eclog.		Eclog.		Eclog.		Eclog.		Eclog.		Fd granul. exoloved lammellae		Fd granul.		Fd granul.		Fd granul.	
SiO2	38.23	38.50	38.35	38.38	38.59	38.60	38.02	38.52	38.56	38.61	38.54	38.65	38.67	38.96	38.83	38.76	38.99	39.21	39.08	38.92	38.64	37.84	37.92	37.99
TiO2	0.16	0.09	0.06	0.19	0.20	0.03	0.08	0.07	0.03	0.19	0.23	0.00	0.18	0.23	0.03	0.15	0.02	0.09	0.01	0.12	0.00	0.17	0.15	0.11
Al2O3	22.21	22.27	21.74	22.15	22.47	21.72	21.89	21.77	22.14	22.25	22.49	22.06	22.04	22.52	22.39	22.14	22.53	22.21	22.40	22.84	21.47	21.87	21.84	22.20
FeO#	22.94	22.88	22.35	22.63	20.52	21.38	23.01	22.88	21.96	21.66	21.78	21.89	20.59	19.91	20.33	20.50	21.63	22.48	21.99	21.63	25.52	27.18	27.00	26.59
MnO	0.36	0.35	0.53	0.57	0.74	0.66	0.53	0.49	0.51	0.55	0.34	0.48	0.86	0.53	0.88	0.90	0.68	0.76	0.20	0.45	0.66	1.00	1.00	0.58
MgO	6.24	6.57	6.55	6.35	7.71	7.96	6.80	7.33	7.96	8.09	8.22	7.99	8.04	8.91	9.13	8.96	7.42	8.82	10.37	9.97	6.77	6.18	6.19	6.17
CaO	10.17	10.02	9.80	9.67	9.48	9.25	9.25	8.86	8.68	8.49	8.42	8.49	9.39	9.40	8.32	8.55	9.19	6.79	5.76	6.22	7.08	6.06	6.18	6.76
Na2O	0.00	0.08	0.01	0.00	0.16	0.12	0.14	0.00	0.00	0.00	0.00	0.23	0.00	0.00	0.01	0.00	0.00	0.00	0.00	0.00	0.00	0.00	0.00	0.00
K2O	0.00	0.00	0.00	0.00	0.00	0.00	0.00	0.00	0.00	0.00	0.03	0.00	0.00	0.00	0.00	0.00	0.00	0.00	0.00	0.00	0.53	0.00	0.00	0.00
P2O5	0.00	0.00	0.00	0.00	0.00	0.00	0.00	0.02	0.00	0.00	0.00	0.00	0.12	0.06	0.00	0.00	0.00	0.00	0.00	0.00	0.00	0.00	0.00	0.00
SO3	0.00	0.12	0.03	0.00	0.00	0.02	0.05	0.00	0.07	0.01	0.00	0.06	0.14	0.13	0.00	0.00	0.14	0.01	0.07	0.04	0.15	0.15	0.09	0.04
Cr2O3	0.23	0.18	0.32	0.09	0.00	0.10	0.22	0.30	0.20	0.26	0.28	0.26	0.23	0.08	0.22	0.20	0.16	0.12	0.00	0.13	0.04	0.18	0.07	0.00
NiO	0.08	0.12	0.02	0.15	0.31	0.17	0.00	0.08	0.00	0.00	0.05	0.07	0.00	0.00	0.00	0.00	0.03	0.00	0.00	0.00	0.00	0.00	0.00	0.00
Total	100.61	101.19	99.75	100.16	100.19	100.00	99.98	100.31	100.11	100.10	100.38	100.16	100.24	100.74	100.15	100.15	100.81	100.47	99.87	100.32	100.87	100.63	100.45	100.45
Gross(Ca)	27.7	27.1	27.0	26.7	26.2	25.0	25.2	24.0	23.5	23.2	22.8	23.1	25.6	25.2	22.6	23.1	25.2	18.5	15.4	16.8	19.4	16.9	17.2	18.7
Pyrope(Mg)	23.6	24.7	25.0	24.4	29.6	29.9	25.8	27.6	30.0	30.7	31.0	30.3	30.5	33.2	34.4	33.7	28.4	33.5	38.6	37.5	25.8	24.0	24.0	23.8
Alman(Fe)	48.7	48.3	48.0	48.8	44.2	45.1	49.0	48.4	46.5	46.1	46.1	46.6	43.9	41.6	43.0	43.2	46.4	47.9	46.0	45.7	54.7	59.1	58.8	57.5

Sample	Pa 7X 8		Pa CX 6		Pa 7X 5	Pa 6X 10	Pa 8X 1			Pa 8X 2	
Lithology	Fd granul.		Two Px granul.		Two Px granul.	Gabbro. rim of il	Xenocr. inclusion of Am			Xenocr. all, inclusion	
SiO2	38.84	38.91	38.51	38.33	38.75	38.01	37.76	38.97	39.00	39.42	39.15
TiO2	0.06	0.03	0.17	0.26	0.00	0.39	0.11	0.13	0.09	0.33	0.06
Al2O3	22.54	22.72	21.99	21.86	22.37	21.19	21.59	22.16	22.43	22.61	22.61
FeO#	21.38	20.52	24.09	25.15	23.99	26.54	26.24	18.52	18.32	17.78	18.29
MnO	0.44	0.15	0.73	1.13	0.83	0.90	0.75	0.88	0.69	0.91	0.87
MgO	10.39	11.14	6.34	6.25	6.19	4.96	5.17	10.68	11.14	11.26	11.08
CaO	5.86	5.90	8.17	7.50	8.61	7.11	7.86	7.68	7.35	7.75	7.87
Na2O	0.01	0.00	0.00	0.00	0.13	0.01	0.00	0.00	0.00	0.00	0.00
K2O	0.00	0.00	0.00	0.03	0.00	0.55	0.03	0.00	0.00	0.01	0.00
P2O5	0.00	0.00	0.00	0.00	0.00	0.09	0.00	0.00	0.00	0.00	0.00
SO3	0.00	0.00	0.25	0.00	0.00	0.09	0.00	0.00	0.05	0.00	0.00
Cr2O3	0.47	0.14	0.23	0.00	0.00	0.24	0.17	0.20	0.20	0.02	0.24
NiO	0.38	0.00	0.33	0.16	0.00	0.06	0.00	0.00	0.06	0.22	0.00
Total	100.38	99.50	100.79	100.68	100.87	100.14	99.68	99.22	99.32	100.33	100.16
Gross(Ca)	15.8	15.8	22.8	20.9	24.0	20.5	22.1	20.8	19.8	20.8	21.0
Pyrope(Mg)	39.1	41.4	24.7	24.3	24.0	19.9	20.2	40.2	41.7	42.0	41.0
Alman(Fe)	45.1	42.8	52.5	54.8	52.1	59.7	57.6	39.1	38.5	37.2	38.0

B) Pine Creek

Sample	Pinc X 5				Pinc X 7				Pinc A 2			
Lithology	Cpx granul.				Fd granul.				Transi granul.			
SiO2	40.51	40.16	39.93	39.71	40.04	39.37	40.04	39.54	39.60	40.04	39.55	39.60
TiO2	0.01	0.21	0.00	0.00	0.15	0.10	0.00	0.15	0.14	0.11	0.02	0.22
Al2O3	23.00	23.35	23.14	23.17	23.06	23.16	22.74	23.30	22.73	23.18	23.16	22.91
FeO#	15.52	15.25	15.58	15.08	16.99	16.48	17.01	16.86	17.42	17.41	17.17	17.78
MnO	0.21	0.15	0.36	0.38	0.46	0.60	0.42	0.32	0.17	0.42	0.54	0.36
MgO	11.87	12.10	12.03	12.13	11.54	11.52	11.52	11.27	11.08	11.03	10.90	11.02
CaO	9.22	9.05	9.10	9.19	8.49	8.43	8.32	8.39	8.31	8.70	8.90	8.85
Na2O	0.00	0.00	0.00	0.00	0.00	0.00	0.00	0.00	0.00	0.00	0.00	0.19
K2O	0.00	0.00	0.00	0.03	0.00	0.00	0.00	0.00	0.00	0.05	0.00	0.01
P2O5	0.00	0.00	0.08	0.00	0.02	0.00	0.00	0.07	0.01	0.00	0.00	0.00
SO3	0.04	0.06	0.11	0.00	0.00	0.19	0.14	0.00	0.00	0.00	0.25	0.00
Cr2O3	0.14	0.16	0.00	0.14	0.11	0.11	0.24	0.29	0.11	0.20	0.25	0.20
NiO	0.02	0.13	0.00	0.04	0.00	0.03	0.02	0.00	0.00	0.00	0.00	0.03
Total	100.53	100.60	100.33	99.84	100.86	99.98	100.44	100.19	99.57	101.15	100.76	101.15
Gross(Ca)	24.4	23.9	23.9	24.3	22.5	22.6	22.1	22.6	22.3	23.1	23.8	23.3
Pyrope(Mg)	43.6	44.5	44.0	44.6	42.5	42.9	42.6	42.1	41.3	40.8	40.5	40.3
Alman(Fe)	32.0	31.5	32.0	31.1	35.1	34.5	35.3	35.3	36.4	36.1	35.8	36.5

FeO# as total FeO

Table 6.5. Continued

C) Calcutteroo

Sample	Trwi CX 13		Trwi CX 11	Trwi CX 9		Trwi CX 4		Trwi N 1		Trwi N 10		Trwi N 8		Trwi CX 2	Trwi CX 8		Trwi CX 5			Trwi CX 7		Trwi CH 3	
Lithology	Eclog.		Eclog.	Eclog.		Eclog.		Eclog.		Eclog.		Eclog.		Cpx granul.	Cpx granul.		Cpx granul.			Cpx granul.		Cpx granul.	
			kyanite bearing																				
SiO2	40.43	40.62	41.06	40.55	41.12	38.24	38.24	38.05	38.10	39.75	39.89	39.05	38.98	39.35	39.93	39.89	39.46	39.37	39.38	39.06	39.15	38.36	41.08	41.18
TiO2	0.00	0.00	0.04	0.14	0.03	0.19	0.20	0.19	0.00	0.19	0.00	0.13	0.14	0.14	0.07	0.00	0.10	0.02	0.00	0.06	0.00	0.08	0.00	0.14
Al2O3	23.15	23.33	23.96	23.74	23.62	21.95	22.08	21.84	21.75	23.15	23.26	22.67	22.45	23.25	22.90	23.12	22.73	22.75	22.74	22.64	22.26	21.98	23.50	23.44
FeO#	11.18	11.19	10.81	11.30	11.10	23.98	24.02	23.96	24.66	15.86	16.92	17.63	17.61	16.28	16.08	16.37	16.36	17.70	17.66	17.86	22.19	22.69	8.57	8.74
MnO	0.15	0.37	0.12	0.19	0.33	0.58	0.49	0.63	0.38	0.64	0.33	0.44	0.37	0.41	0.40	0.35	0.23	0.31	0.48	0.57	0.50	0.35	0.42	0.45
MgO	13.57	12.97	16.64	16.77	16.55	6.93	6.70	5.96	5.83	12.62	12.28	10.27	10.11	10.46	10.81	11.95	11.83	11.01	10.98	10.70	7.30	7.38	19.16	19.14
CaO	11.20	11.44	7.43	7.20	7.15	8.05	8.08	8.80	9.06	7.18	7.16	9.47	9.37	10.11	10.17	8.08	8.73	8.59	8.63	8.71	8.75	9.02	5.52	5.36
Na2O	0.00	0.00	0.00	0.00	0.00	0.00	0.00	0.04	0.17	0.00	0.00	0.00	0.00	0.00	0.00	0.00	0.00	0.00	0.00	0.00	0.00	0.00	0.00	0.00
K2O	0.00	0.00	0.00	0.00	0.00	0.00	0.00	0.00	0.00	0.05	0.00	0.00	0.00	0.00	0.02	0.00	0.04	0.00	0.00	0.00	0.00	0.04	0.00	0.00
P2O5	0.00	0.00	0.00	0.00	0.00	0.00	0.00	0.05	0.01	0.00	0.00	0.00	0.00	0.00	0.01	0.00	0.00	0.05	0.00	0.01	0.01	0.00	0.00	0.00
SO3	0.00	0.00	0.00	0.00	0.18	0.00	0.00	0.10	0.00	0.05	0.00	0.02	0.00	0.00	0.00	0.01	0.00	0.07	0.00	0.10	0.06	0.14	0.02	0.02
Cr2O3	0.00	0.14	0.12	0.40	0.20	0.03	0.30	0.23	0.35	0.40	0.23	0.35	0.29	0.17	0.16	0.14	0.24	0.18	0.13	0.15	0.00	0.00	0.58	0.49
NiO	0.36	0.00	0.00	0.00	0.01	0.00	0.00	0.01	0.01	0.21	0.00	0.08	0.27	0.00	0.14	0.34	0.21	0.00	0.08	0.00	0.00	0.05	0.20	0.12
Total	100.04	100.06	100.19	100.30	100.28	99.94	100.09	99.87	100.31	100.09	100.06	100.10	99.61	100.17	100.67	100.25	99.91	100.05	100.08	99.85	100.21	100.10	99.05	99.07
Gross(Ca)	28.9	29.9	19.0	18.3	18.4	22.1	22.4	24.6	24.9	19.3	19.1	25.2	25.2	27.1	26.9	21.6	23.0	22.8	22.9	23.2	24.2	24.4	14.2	13.8
Pyrope(Mg)	48.6	47.2	59.3	59.3	59.3	26.5	25.8	23.2	22.3	47.3	45.6	38.1	37.8	38.9	39.8	44.3	43.4	40.6	40.5	39.6	28.0	27.7	68.6	68.6
Alman(Fe)	22.5	22.9	21.6	22.4	22.3	51.4	51.9	52.2	52.8	33.4	35.3	36.7	37.0	34.0	33.2	34.1	33.7	36.6	36.6	37.1	47.8	47.9	17.2	17.6

Sample	Trwi CB 4			Trwi CX 3	Trwi CX 6			Trwi N 3	Trwi CX 1	Trwi CX 10			Trwi CX 14			Trwi CB 3		Trwi CB 3		Trwi CH 5		
Lithology	Cpx granul.			Fd granul.	Fd granul.			Fd granul.	Ky granul.	Two Px granul.			Transl. grianul.			Pyroxenit.		Pyroxenit.		Pyroxenit.		
									Kyanite bearing							recrystallised gt							
SiO2	40.66	40.74	40.72	39.95	40.41	40.11	39.97	40.12	40.29	40.20	40.58	40.56	39.89	39.59	39.78	39.80	39.39	39.09	40.28	40.02	40.62	40.40	40.14	40.61
TiO2	0.36	0.10	0.00	0.23	0.00	0.01	0.14	0.00	0.07	0.19	0.11	0.10	0.05	0.00	0.07	0.14	0.00	0.00	0.00	0.00	0.00	0.13	0.00	0.00
Al2O3	23.26	22.88	23.03	23.18	23.04	23.20	23.04	23.01	23.02	23.24	23.58	23.45	23.11	23.20	22.99	22.69	22.86	22.72	23.52	23.09	23.38	23.17	23.37	23.28
FeO#	15.41	15.38	15.54	17.07	17.17	14.86	15.17	15.06	14.44	13.86	12.48	12.57	14.69	14.68	14.97	17.11	17.33	17.94	14.39	14.46	14.17	14.00	15.52	15.50
MnO	0.23	0.46	0.53	0.31	0.17	0.37	0.41	0.23	0.28	0.61	0.25	0.38	0.60	0.39	0.67	0.57	0.52	0.55	0.50	0.38	0.35	0.14	0.22	0.20
MgO	15.50	15.20	15.08	11.91	11.73	12.54	12.83	12.68	13.63	13.62	14.30	13.83	12.57	12.80	12.77	12.21	11.43	11.59	13.84	13.89	13.80	13.74	15.39	15.35
CaO	4.43	4.58	4.88	8.40	8.36	8.92	8.87	8.96	7.80	7.91	8.46	9.00	8.89	8.71	8.50	7.61	7.89	7.49	7.95	7.92	8.20	8.03	4.59	4.62
Na2O	0.00	0.00	0.00	0.05	0.00	0.08	0.13	0.00	0.00	0.00	0.00	0.00	0.00	0.05	0.00	0.00	0.17	0.13	0.00	0.00	0.00	0.00	0.00	0.00
K2O	0.00	0.00	0.00	0.07	0.02	0.00	0.00	0.00	0.00	0.00	0.00	0.00	0.00	0.02	0.00	0.00	0.00	0.00	0.00	0.00	0.00	0.00	0.00	0.12
P2O5	0.00	0.00	0.00	0.00	0.00	0.00	0.00	0.00	0.04	0.00	0.00	0.00	0.07	0.09	0.00	0.01	0.00	0.00	0.00	0.00	0.00	0.00	0.00	0.11
SO3	0.00	0.00	0.00	0.01	0.02	0.00	0.01	0.34	0.14	0.00	0.00	0.00	0.00	0.18	0.00	0.12	0.09	0.00	0.00	0.04	0.04	0.00	0.00	0.00
Cr2O3	0.58	0.51	0.36	0.24	0.09	0.16	0.26	0.28	0.10	0.20	0.08	0.14	0.16	0.28	0.13	0.05	0.17	0.31	0.12	0.28	0.17	0.14	0.30	0.65
NiO	0.00	0.00	0.08	0.00	0.00	0.07	0.00	0.13	0.00	0.12	0.02	0.00	0.00	0.00	0.16	0.00	0.17	0.00	0.00	0.07	0.26	0.03	0.00	0.00
Total	100.42	99.85	100.22	101.41	101.01	100.32	100.82	100.82	99.81	99.94	99.85	100.01	100.03	99.97	100.04	100.30	100.01	99.83	100.60	100.15	100.99	99.77	99.54	100.44
Gross(Ca)	11.7	12.1	12.8	21.9	22.0	23.5	23.0	23.4	20.5	21.0	22.2	23.7	23.5	22.9	22.4	20.0	21.1	19.9	20.7	20.6	21.3	21.1	12.0	12.1
Pyrope(Mg)	56.7	56.0	55.2	43.3	42.9	45.9	46.3	46.0	49.9	50.3	52.2	50.6	46.2	46.9	46.8	44.8	42.6	42.9	50.1	50.1	49.9	50.2	56.2	56.1
Alman(Fe)	31.6	31.8	31.9	34.8	35.2	30.6	30.7	30.6	29.6	28.7	25.6	25.8	30.3	30.2	30.8	35.2	36.3	37.2	29.2	29.3	28.8	28.7	31.8	31.8

FeO# as total FeO

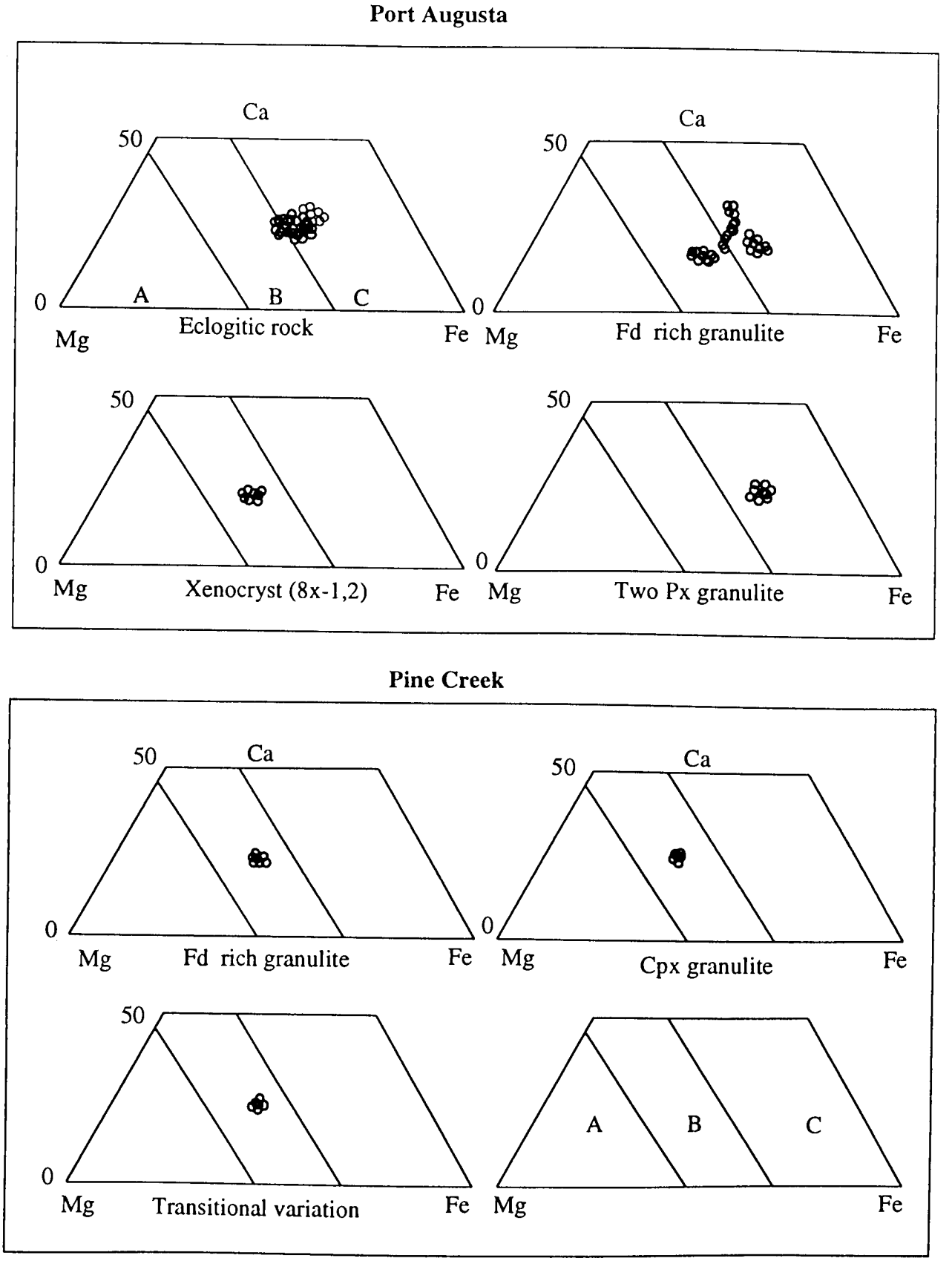

Fig. 6.2a. Garnet compositions of the Port Augusta and Pine Creek xenoliths. Field A, B and C are based on the Coleman *et al.* (1965) (Fild A (garnets in kimberlites), field B (garnets in gneiss) and field C (garnets in blueschist)).

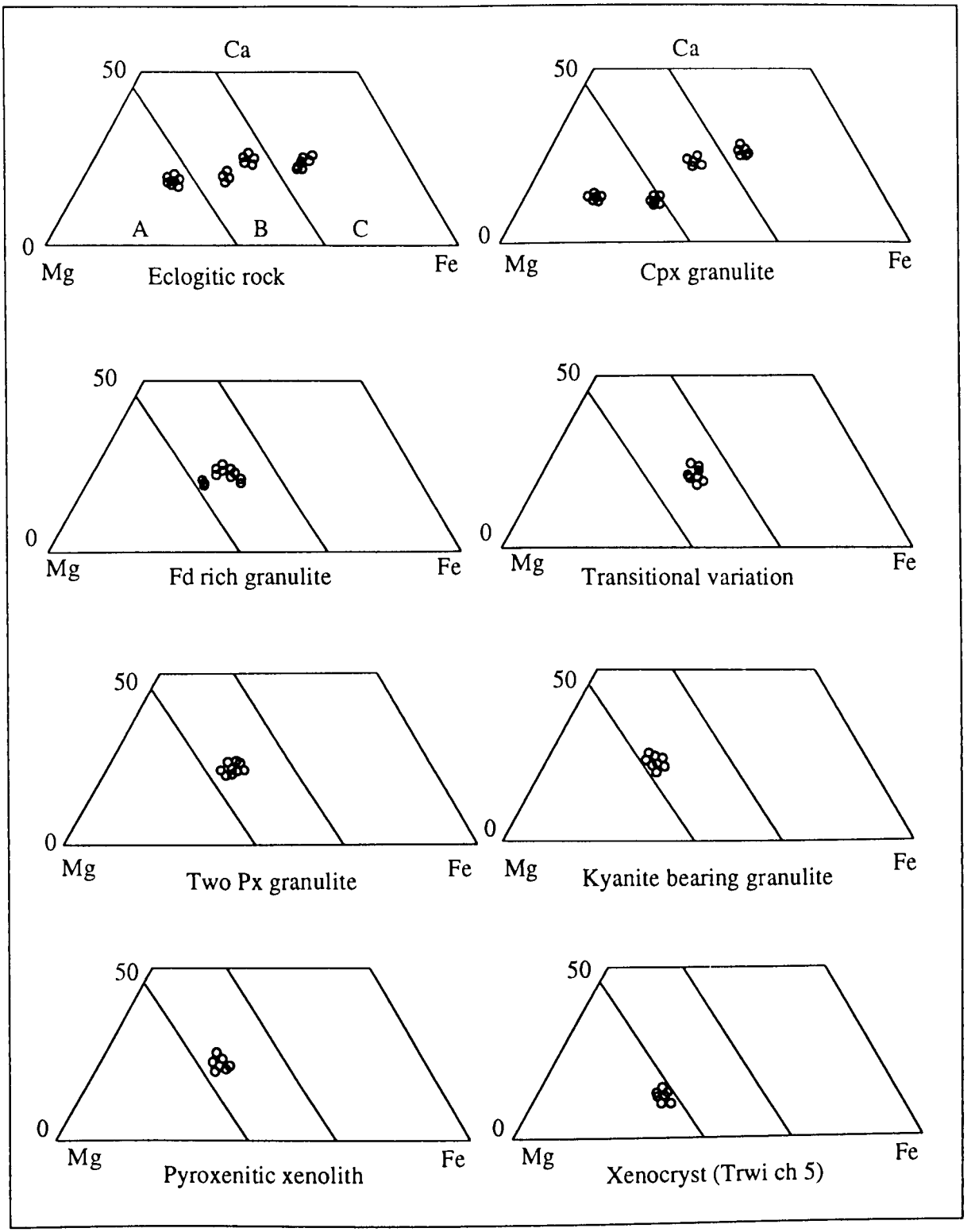

Fig. 6.2b. Garnet compositions of the Calcutteroo xenoliths.

In gabbroic rocks, the grains are dominantly diopsidic-hedenbergitic and show mainly augitic composition. Clinopyroxenes in xenocrysts have diopsidic to augitic composition and show higher Na_2O, TiO_2 (0.3-0.5 wt %) and Al_2O_3 and Mg# than those from the gabbroic rocks.

Clinopyroxenes of Calcutteroo xenoliths; The clinopyroxene grains are dominantly jadeitic and have diopsidic, augitic composition. No clear distinctions are observed among the clinopyroxenes from different rock types. In eclogitic rocks, clinopyroxenes mainly have Na2O (wt %) of 1.5-3.0 and Cr_2O_3 (wt %) of 0.3-0.8. Low Mg# are observed in grains having high Na_2O (<2.6 wt %). Clinopyroxenes of clinopyroxene-granulites are dominantly diopsidic and have Jadeitic component and Na_2O (wt %) of 1.6-3.2. In the clinopyroxene-granulites, high Mg#, Cr_2O_3, and low Na_2O are observed in clinopyroxenes of samples containing abundant amphibole and Fe-Ti-oxide grains, whereas high Na_2O and low Mg# are evidenced in samples having abundant linked garnet rings and recrystallised clinopyroxene grains.

Clinopyroxenes in two-pyroxene granulite are dominantly diopsidic and display similar Mg# to those of eclogitic rocks. Generally, high Mg#, Cr_2O_3 and low Na_2O are observed in clinopyroxenes having pronounced garnet exsolution lamellae. Clinopyroxenes of feldspar-rich granulites are mainly diopsidic and contain Cr_2O_3 (wt %) of 0.4-0.5 and Na_2O (wt %) of 1.9-2.5. In these granulites, low Mg# are obtained for samples of high Na_2O (2.8-3.4) and discrete clinopyroxene grains show high Mg#, Cr_2O_3, Na_2O and Al_2O_3 relative to grains occurring as reaction rims on the grains.

Clinopyroxenes in kyanite-bearing granulites are jadeitic and show a slightly lower TiO_2 and higher Al_2O_3 than those of the other eclogitic xenoliths. Clinopyroxenes from pyroxenitic rocks have jadeitic with diopsidic composition. In general, they show Na_2O (wt %) of 0.2-2.1 and Cr_2O_3 (wt %) of 0.2-1.2. In sample showing a transition mineralogy, clinopyroxenes are diopsidic and contain Na_2O (wt %) of 2.1-2.4, and Cr_2O_3 (wt %) of 0.16-0.44. They have a slightly low Mg# relative to those of pyroxenitic xenoliths. Clinopyroxenes occurring as inclusions in xenocryst amphibole have diopsidic to salitic composition (dominantly diopside) and are jadeitic. They have higher Mg#, Na_2O and Cr_2O_3 than those of the pyroxenites.

Clinopyroxenes of Pine Creek xenoliths; The clinopyroxene grains mainly show jadeitic, diopsidic composition and have high Na_2O (2.5-3.2 wt %). In clinopyroxene-granulites, two types of clinopyroxenes are found. One type is jadeitic with high Na_2O (2.9-3.2 wt %) while the other type is diopsidic-hedenbergitic and have low Na_2O (0.2-0.6 wt %). In feldspsar-rich granulites, the grains have slightly lower Mg#, Al_2O_3 and higher TiO_2, Cr_2O_3 contents than those of clinopyroxene-granulites. Clinopyroxenes in amphibolites have similar Mg# and Na_2O content to those from granulites, but have higher

Cr_2O_3 than those from granulites. Clinopyroxenes in pyroxenitic rocks have a slightly high Mg# and CaO(wt %) relative to those of the feldspar-rich granulite. In the sample showing transitional mineralogy, the grains are eclogitic and show diopsidic to augitic composition. They show wide ranges of Na_2O, Al_2O_3, TiO_2 with limited Mg#. Clinopyroxene xenocrysts have lower Na_2O and higher Mg# than those of granulitic rocks. They are diopsidic-hedenbergitic and have diopsidic composition. They contain the lowest Al_2O_3 and highest CaO among those of Pine Creek xenoliths.

In conclusion, clinopyroxenes of Port Augusta xenoliths are distinctive from those of Pine Creek and Calcutteroo xenoliths. In general, those of Port Augusta are more diopsidic-hedenbergitic and have dominantly salitic-augitic composition while those of Pine Creek and Calcutteroo have jadeitic and contain diopsidic compositions. However clear distinction in mineralogical compositions are shown in those of Port Augusta. Clinopyroxenes of eclogitic rocks have jadeitic with high Na_2O while those of granulitic rocks have diopsidic-hedenbergitic. Those in xenocryst are jadeitic and have high Na_2O. In general, recrystallised clinopyroxenes at the margins of the garnets have considerably lower Mg#, Na_2O and Cr_2O_3 than their host grains. Clinopyroxenes of Pine Creek have higher Na_2O content than those of Calcutteroo xenoliths and higher CaO content than those of Port Augusta xenoliths.

C) Orthopyroxene

Representative analyses from three localities of South Australian kimberlites are shown in the Table 6.7. They were plotted in Ca-Mg-Fe diagrams (Fig. 6.3).

Orthopyroxenes of Port Augusta xenoliths: The orthopyroxene grains range from En_{46} to En_{76}. In general, orthopyroxenes of eclogitic rocks are ferrohyperthene ($En_{45.4-47.7}$) while those of granulitic rocks are bronzitic-hypersthene (En_{59-76}). Orthopyroxenes of gabbroic rocks are ferrohypersthene composition (En_{46-48}). In the granulitic rocks, feldspar-rich varieties have orthopyroxenes of higher Mg# than those of two-pyroxene granulite.

Orthopyroxenes of Calcutteroo and Pine Creek xenoliths: The orthopyroxene grains have En_{55-92}. High En are obtained for grains from pyroxenites and low En are obtained for those from feldspar-rich granulites. Recrystallised grains in the feldspar-rich granulites from Calcutteroo and inclusion in amphibole xenocrysts from Pine Creek, have bronzitic composition (En_{80-84}).

In conclusion, Calcutteroo and Pine Creek xenoliths containing dominantly diopsidic clinopyroxene are enstatitic to bronzitic orthopyroxene composition while Port Augusta xenoliths containing dominantly salitic to augitic clinopyroxene composition have bronzitic to hypersthene (or ferro-hypersthene) orthopyroxene compositions. The orthopyroxene

compositions may not be in equilibrium with these of clinopyroxene because the grains mainly show complicated exsolution textures with clinopyroxene, amphibole or other Fe-Ti oxides. However, low enstatic compositions of samples from Port Augusta containing abundant quartzo-feldspars may reflect differences with those of Calcutteroo and Pine Creek.

D) Feldspars

Feldspars are found in xenoliths from all three localities as different modes, including discrete grains, or exsolution lamellaes in clinopyroxene on garnet or secondary recrystallised grains after garnet. Their compositions are also variable *An* 19-83, ranging from oligoclase to andesine to labradorite (mainly *An* 20-50) (Fig. 6.5, Table 6.8). Plagioclases from eclogitic and granulitic rocks have *An* 19-50 (oligoclase and andesine) whereas those from gabbroic rocks have*An* 49-70 (labradorite). In the granulitic xenoliths, plagioclase from clinopyroxene- and two-pyroxene granulites show higher *An* contents (andesine) than those of feldspar-rich granulites. However, alkali-feldspars have a limited composition, Or 76-87.8 (sanidine).

Plagioclases of the Port Augusta xenoliths show higher *An* contents (*An* 31- 50) than those of Calcutteroo and Pine Creek (*An* 23-33). In Calcutteroo xenoliths, secondary plagioclases formed by break down of garnet at contact with clinopyroxenes have labradoritic to bytownitic compositions (*An* 60-83). Plagioclases from pyroxenitic xenoliths of the Calcutteroo and sample showing transitional mineralogy of Pine Creek show high *An* contents (*An* 73-80). Clinopyroxene-rich granulites and amphibolitic rocks in Pine Creek xenoliths contain albites (*An* 90-99) which may be derived from the reaction, $NaAlSi_2O_6$ (jadeite) + SiO_2 (Quartz) = $NaAlSi_2O_8$ (albite) (Deer *et al.*, 1966).

In conclusion, plagioclases of South Australian lower crustal xenoliths mainly have oligoclase and sodic andesine composition. Generally, plagioclases of Calcutteroo and Pine Creek are oligoclase while those from Port Augusta are andesine. Gabbroic rocks of Port Angusta have typically labradoritic compositions.

E) Amphiboles

The grains occur as variable shapes in most of the xenoliths. They range from pargasitic to edenitic, but are homogeneous within each rock type (Fig. 6.6, Table 6.9). Amphiboles of Calcutteroo xenoliths show hornblende-pargasitic compositions and those from Port Augusta xenoliths show edenitic compositions. Mg# of Calcutteroo amphiboles are dominantly 75-82 and those of Port Augusta are dominantly 65-75.

Table 6. 6a. Representative clinopyroxene analyses of the Port Augusta xenoliths.

Sample	Pa 6x 8			Pa 5x 2	Pa 6x 9		Pa 6x 2		Pa 6x 6			Pa 6x 7			Pa 6x 12				Pa 5x 1	
Lithology	Eclog.			Eclog.	Eclog.		Eclog.		Eclog.			Eclog.			Eclog.				Eclog.	
SiO2	52.69	51.92	50.34	52.15	51.46	51.08	51.73	51.46	52.24	51.77	51.79	52.17	52.38	52.12	51.92	52.00	52.46	52.36	51.37	50.77
TiO2	0.27	0.21	0.40	0.62	0.55	0.35	0.44	0.46	0.48	0.25	0.28	0.47	0.25	0.37	0.56	0.55	0.69	0.47	0.20	0.57
Al2O3	10.74	10.71	4.19	10.48	6.41	6.69	8.04	8.05	7.88	7.83	7.97	7.83	7.88	8.20	9.00	9.17	9.05	9.27	2.89	3.21
FeO	3.75	3.89	9.38	4.21	3.09	2.98	4.00	4.16	3.29	3.81	4.26	3.24	4.37	3.73	3.45	4.94	4.02	4.70	4.35	4.72
Fe2O3	3.05	2.54	2.09	2.98	5.71	5.81	2.75	2.83	2.64	2.79	1.92	3.22	2.01	2.50	2.97	1.18	2.35	1.11	4.20	3.90
MnO	0.17	0.01	0.00	0.00	0.19	0.03	0.00	0.01	0.00	0.06	0.00	0.00	0.00	0.01	0.00	0.07	0.00	0.03	0.05	0.00
MgO	8.15	8.10	11.76	8.43	10.76	10.33	9.96	10.00	10.39	10.47	10.39	10.74	10.51	10.39	9.64	9.56	9.57	9.53	13.20	12.98
CaO	14.67	14.47	18.54	14.90	17.31	16.98	17.15	16.79	17.64	17.37	17.60	17.63	17.34	17.16	16.37	16.33	16.13	16.22	21.43	21.38
Na2O	5.60	5.47	1.43	5.30	3.83	3.93	4.04	4.02	4.05	3.76	3.67	3.82	3.78	4.14	4.52	4.34	4.72	4.50	1.33	1.29
K2O	0.06	0.00	0.08	0.01	0.00	0.00	0.04	0.00	0.00	0.00	0.00	0.02	0.00	0.00	0.00	0.00	0.00	0.00	0.00	0.00
Cr2O3	0.27	0.27	0.34	0.30	0.32	0.49	0.12	0.54	0.27	0.30	0.29	0.16	0.39	0.31	0.41	0.50	0.42	0.32	0.53	0.53
NiO	0.00	0.00	0.20	0.00	0.04	0.00	0.13	0.05	0.07	0.07	0.00	0.00	0.00	0.23	0.00	0.22	0.00	0.16	0.00	0.00
P2O5	0.10	0.00	0.02	0.00	0.17	0.00	0.06	0.07	0.08	0.00	0.09	0.00	0.00	0.18	0.00	0.00	0.15	0.02	0.00	0.00
SO3	0.05	0.03	0.00	0.00	0.00	0.12	0.05	0.09	0.00	0.19	0.15	0.00	0.00	0.05	0.13	0.00	0.01	0.10	0.00	0.00
Total	99.55	97.60	98.76	99.36	99.83	98.78	98.50	98.51	99.03	98.66	98.40	99.32	98.91	99.39	98.98	98.85	99.56	98.80	99.54	99.35
							Number of Ions on the Basis of 6 (O)													
Si	1.9244	1.9290	1.9108	1.9137	1.9159	1.9202	1.9235	1.9152	1.9264	1.9202	1.9201	1.9225	1.9332	1.9163	1.9141	1.9164	1.9188	1.9233	1.9323	1.9152
Ti	0.0073	0.0058	0.0115	0.0170	0.0153	0.0098	0.0122	0.0129	0.0134	0.0069	0.0078	0.0131	0.0070	0.0103	0.0155	0.0152	0.0190	0.0130	0.0056	0.0163
Al	0.4621	0.4688	0.1874	0.4532	0.2813	0.2961	0.3523	0.3528	0.3424	0.3423	0.3482	0.3400	0.3427	0.3553	0.3909	0.3984	0.3900	0.4013	0.1282	0.1429
Fe(2)	0.1138	0.1202	0.2967	0.1283	0.0949	0.0925	0.1234	0.1285	0.1006	0.1175	0.1317	0.0992	0.1340	0.1138	0.1059	0.1515	0.1222	0.1441	0.1354	0.1474
Fe(3)	0.0833	0.0705	0.0595	0.0816	0.1576	0.1623	0.0763	0.0788	0.0726	0.0775	0.0533	0.0887	0.0556	0.0685	0.0820	0.0325	0.0643	0.0307	0.1176	0.1097
Mn	0.0051	0.0004	0.0000	0.0000	0.0059	0.0008	0.0000	0.0002	0.0000	0.0018	0.0000	0.0000	0.0000	0.0004	0.0000	0.0021	0.0000	0.0010	0.0017	0.0000
Mg	0.4435	0.4480	0.6648	0.4606	0.5966	0.5783	0.5518	0.5544	0.5704	0.5785	0.5736	0.5897	0.5777	0.5688	0.5295	0.5248	0.5218	0.5218	0.7396	0.7291
Ca	0.5757	0.5756	0.7536	0.5854	0.6904	0.6835	0.6829	0.6690	0.6966	0.6898	0.6989	0.6958	0.6855	0.6758	0.6463	0.6444	0.6321	0.6384	0.8632	0.8636
Na	0.3966	0.3940	0.1052	0.3766	0.2765	0.2859	0.2912	0.2902	0.2895	0.2705	0.2635	0.2730	0.2702	0.2949	0.3227	0.3096	0.3349	0.3206	0.0973	0.0940
K	0.0029	0.0000	0.0036	0.0002	0.0000	0.0000	0.0019	0.0000	0.0000	0.0000	0.0000	0.0011	0.0000	0.0000	0.0000	0.0000	0.0000	0.0000	0.0000	0.0000
Cr	0.0078	0.0078	0.0102	0.0088	0.0094	0.0146	0.0035	0.0158	0.0079	0.0088	0.0084	0.0047	0.0112	0.0091	0.0118	0.0146	0.0121	0.0093	0.0156	0.0157
Ni	0.0000	0.0000	0.0061	0.0000	0.0011	0.0000	0.0038	0.0015	0.0021	0.0019	0.0000	0.0000	0.0000	0.0069	0.0000	0.0065	0.0000	0.0048	0.0000	0.0000
P	0.0030	0.0000	0.0005	0.0000	0.0053	0.0000	0.0017	0.0021	0.0026	0.0000	0.0028	0.0000	0.0000	0.0054	0.0000	0.0000	0.0047	0.0006	0.0000	0.0000
S	0.0013	0.0009	0.0000	0.0000	0.0000	0.0035	0.0014	0.0024	0.0000	0.0054	0.0042	0.0000	0.0000	0.0013	0.0036	0.0001	0.0003	0.0028	0.0000	0.0000
Wo	47.2	47.4	42.5	46.6	44.8	45.1	47.6	46.8	48.4	47.1	48.0	47.2	47.2	47.4	47.4	47.6	47.2	47.8	46.5	46.7
En	36.5	36.9	37.5	36.7	38.8	38.1	38.5	38.7	39.6	39.5	39.4	40.0	39.8	39.9	38.8	38.8	38.9	39.1	39.9	39.4
Fs	16.2	15.7	20.1	16.7	16.4	16.8	13.9	14.5	12.0	13.3	12.7	12.7	13.1	12.8	13.8	13.6	13.9	13.1	13.6	13.9
Mg/Mg+Fe(t)	69.2	70.1	65.1	68.7	70.3	69.4	73.4	72.8	76.7	74.8	75.6	75.8	75.3	75.7	73.8	74.0	73.7	74.9	74.5	73.9

Table 6.6a. Continued

Sample	Pa 5X 1	Pa 7X 1		Pa 6X 11		Pa 7X 6		Pa 9X 1		Pa 7X 8		Pa 7X 5	Pa CX 6		Pa 7X 9		Pa 6X 10	Pa 8X 3	Pa 8X 2
Lithology	Eclog.	Fd granul.		Fd granul.		Fd granul.		Fd granul.		Fd granul.		Fd granul.	Two Px granul.		Gabbro.		Gabbro.	Xenocr.	Xenocr.
SiO2	50.17	51.01	49.67	47.90	48.87	48.77	48.35	48.22	47.50	50.50	52.18	48.04	48.22	48.78	49.36	50.19	49.60	50.62	51.50	51.70
TiO2	0.41	0.47	0.51	0.90	0.71	0.99	0.78	0.72	0.85	0.47	0.18	0.73	0.46	0.68	0.63	0.17	0.50	0.41	0.39	0.47
Al2O3	3.10	4.96	6.52	7.39	7.14	6.69	7.10	7.20	7.27	4.89	4.02	5.53	5.44	5.11	5.70	2.61	2.50	3.71	3.37	5.96
FeO	2.88	4.13	4.77	8.00	7.31	5.86	7.85	4.82	4.70	1.73	2.21	7.09	6.67	8.51	9.95	7.27	9.99	6.11	5.67	3.08
Fe2O3	6.71	3.53	3.69	3.04	2.96	4.11	2.19	5.14	6.08	4.02	3.14	3.19	4.14	1.35	0.84	4.42	1.74	3.54	1.47	2.98
MnO	0.00	0.00	0.00	0.22	0.19	0.00	0.00	0.00	0.01	0.00	0.17	0.19	0.09	0.15	0.42	0.15	0.00	0.06	0.13	0.04
MgO	12.80	12.16	11.39	10.24	10.32	10.37	10.35	10.72	10.19	13.03	13.57	11.58	11.60	11.55	11.87	11.91	11.53	11.95	13.18	12.25
CaO	20.95	20.08	20.29	20.30	20.16	19.39	19.87	20.00	19.78	20.93	20.59	21.33	21.01	21.25	22.02	22.57	22.74	20.39	20.57	18.65
Na2O	1.68	2.13	1.90	1.20	1.60	2.22	1.57	1.84	2.01	1.94	2.09	0.57	0.80	0.65	0.00	0.48	0.01	1.57	1.58	2.94
K2O	0.00	0.00	0.00	0.00	0.00	0.00	0.00	0.06	0.00	0.08	0.05	0.06	0.00	0.00	0.03	0.13	0.00	0.00	0.00	0.00
Cr2O3	0.20	0.29	0.49	0.23	0.47	0.31	0.23	0.48	0.28	0.53	0.61	0.53	0.55	0.23	0.22	0.11	0.38	0.49	0.39	0.54
NiO	0.00	0.00	0.00	0.00	0.06	0.00	0.08	0.00	0.00	0.14	0.08	0.00	0.00	0.00	0.00	0.00	0.00	0.00	0.42	0.13
P2O5	0.00	0.00	0.02	0.00	0.00	0.14	0.20	0.00	0.00	0.00	0.05	0.00	0.00	0.28	0.14	0.01	0.00	0.00	0.13	0.00
SO3	0.00	0.13	0.00	0.00	0.00	0.14	0.00	0.21	0.01	0.17	0.02	0.00	0.00	0.12	0.17	0.00	0.15	0.00	0.07	0.00
Total	98.90	98.89	99.24	99.44	99.78	98.98	98.57	99.40	98.67	98.44	98.95	98.84	98.96	98.66	101.36	100.01	99.15	98.85	98.87	98.73
								Number of Ions on the Basis of 6 (O)											
Si	1.9142	1.9135	1.8675	1.8211	1.8437	1.8500	1.8407	1.8267	1.8234	1.8972	1.9404	1.8389	1.8463	1.8570	1.8364	1.9134	1.9032	1.9225	1.9323	1.9231
Ti	0.0118	0.0132	0.0145	0.0258	0.0201	0.0281	0.0224	0.0205	0.0244	0.0132	0.0051	0.0210	0.0133	0.0194	0.0177	0.0047	0.0145	0.0117	0.0109	0.0132
Al	0.1394	0.2191	0.2888	0.3312	0.3174	0.2989	0.3185	0.3213	0.3289	0.2166	0.1759	0.2494	0.2453	0.2294	0.2501	0.1173	0.1132	0.1660	0.1488	0.2613
Fe(2)	0.0905	0.1287	0.1485	0.2523	0.2290	0.1842	0.2482	0.1512	0.1485	0.0540	0.0681	0.2253	0.2114	0.2704	0.3097	0.2292	0.3200	0.1923	0.1769	0.0949
Fe(3)	0.1894	0.0990	0.1034	0.0864	0.0833	0.1163	0.0623	0.1451	0.1729	0.1127	0.0872	0.0912	0.1180	0.0385	0.0236	0.1255	0.0502	0.1004	0.0414	0.0827
Mn	0.0000	0.0000	0.0000	0.0072	0.0059	0.0000	0.0000	0.0000	0.0002	0.0000	0.0053	0.0060	0.0029	0.0048	0.0133	0.0048	0.0000	0.0018	0.0040	0.0012
Mg	0.7272	0.6800	0.6387	0.5801	0.5801	0.5859	0.5868	0.6049	0.5826	0.7292	0.7517	0.6604	0.6616	0.6549	0.6575	0.6763	0.6592	0.6764	0.7365	0.6788
Ca	0.8562	0.8069	0.8176	0.8263	0.8146	0.7876	0.8100	0.8114	0.8133	0.8423	0.8198	0.8743	0.8615	0.8664	0.8775	0.9213	0.9345	0.8295	0.8264	0.7429
Na	0.1244	0.1548	0.1383	0.0886	0.1171	0.1632	0.1161	0.1352	0.1496	0.1413	0.1508	0.0420	0.0591	0.0479	0.0000	0.0351	0.0008	0.1153	0.1150	0.2117
K	0.0000	0.0000	0.0000	0.0000	0.0000	0.0000	0.0000	0.0030	0.0000	0.0040	0.0023	0.0031	0.0000	0.0000	0.0015	0.0064	0.0000	0.0000	0.0001	0.0000
Cr	0.0059	0.0087	0.0146	0.0068	0.0139	0.0092	0.0071	0.0144	0.0086	0.0159	0.0180	0.0160	0.0166	0.0070	0.0064	0.0034	0.0114	0.0148	0.0116	0.0160
Ni	0.0000	0.0000	0.0000	0.0000	0.0017	0.0000	0.0024	0.0000	0.0000	0.0041	0.0023	0.0000	0.0000	0.0000	0.0000	0.0000	0.0000	0.0000	0.0127	0.0038
P	0.0000	0.0000	0.0006	0.0000	0.0000	0.0046	0.0063	0.0000	0.0000	0.0000	0.0016	0.0000	0.0000	0.0091	0.0043	0.0004	0.0000	0.0000	0.0042	0.0000
S	0.0000	0.0037	0.0000	0.0000	0.0000	0.0041	0.0000	0.0059	0.0004	0.0047	0.0006	0.0000	0.0000	0.0035	0.0048	0.0000	0.0042	0.0000	0.0020	0.0000
Wo	46.0	47.1	47.9	47.3	47.7	47.0	47.4	47.4	47.4	48.5	47.5	47.2	46.5	47.3	47.0	47.2	47.6	46.1	46.4	46.5
En	39.0	39.7	37.4	33.2	34.0	35.0	34.4	35.3	33.9	42.0	43.5	35.7	35.7	35.8	35.2	34.6	33.6	37.6	41.3	42.4
Fs	15.0	13.3	14.7	19.4	18.3	18.0	18.2	17.3	18.7	9.6	9.0	17.1	17.8	16.9	17.8	18.2	18.8	16.3	12.3	11.1
Mg/Mg+Fe(t)	72.2	74.9	71.7	63.1	65.0	66.1	65.4	67.1	64.4	81.4	82.9	67.6	66.8	68.0	66.4	65.6	64.0	69.8	77.1	79.3

Table 6.6b. Representative clinopyroxene analyses of the Calcutteroo xenoliths.

Sample	Trwi CX 11		Trwi CX 9		Trwi CH 4		Trwi CX 5	Trwi CX 8		Trwi CB 4	Trwi CX 3	Trwi N 3	Trwi CX 10	Trwi CX 14	Trwi CX 1	Trwi CB 3		Trwi CH 5	
Lithology	Eclog.		Eclog.		Cpx granul.		Cpx granul.	Cpx granul.		Cpx granul.	Fd granul.	Fd granul.	Two Px granul.	Two Px granul.	Ky granul.	Pyroxenit.		Pyroxenit.	
SiO2	51.30	51.38	50.91	51.39	52.86	52.50	50.51	51.20	51.20	52.15	51.06	50.97	50.40	50.87	50.59	50.66	50.74	52.15	51.92
TiO2	0.30	0.46	0.47	0.38	0.19	0.26	0.18	0.55	0.49	0.19	0.69	0.06	0.10	0.33	0.29	0.18	0.23	0.48	0.17
Al2O3	6.75	6.04	6.83	6.04	1.04	0.76	8.62	6.63	7.16	5.15	9.20	7.95	8.29	6.50	8.37	7.75	7.77	5.37	5.27
FeO	1.91	1.95	1.52	2.52	0.50	1.96	4.73	2.06	1.47	3.43	4.31	2.91	1.22	0.73	0.40	2.43	0.78	2.99	3.41
Fe2O3	0.30	0.35	1.02	0.00	1.48	0.00	1.03	2.26	2.74	1.25	0.59	0.39	2.58	4.02	2.66	1.10	2.61	1.42	0.96
MnO	0.01	0.00	0.00	0.00	0.02	0.00	0.15	0.00	0.12	0.00	0.03	0.00	0.00	0.01	0.00	0.10	0.19	0.00	0.01
MgO	14.56	14.57	14.40	14.37	17.95	18.10	10.95	12.89	13.03	13.65	11.22	12.87	12.14	13.22	13.03	13.05	13.38	13.58	13.57
CaO	22.09	21.98	22.12	22.24	24.01	24.11	18.43	20.47	20.54	20.02	19.10	20.08	20.37	20.43	20.14	21.07	21.14	19.97	19.75
Na2O	1.20	1.33	1.29	1.14	0.13	0.37	2.78	2.21	2.28	1.94	2.85	2.14	2.54	2.18	2.54	1.85	2.00	2.16	2.17
K2O	0.00	0.00	0.00	0.01	0.00	0.04	0.00	0.09	0.00	0.07	0.05	0.07	0.06	0.17	0.00	0.00	0.00	0.00	0.11
Cr2O3	0.60	0.69	0.74	0.93	0.97	0.78	0.28	0.30	0.27	0.66	0.24	0.54	0.65	0.44	0.36	0.56	0.51	0.73	0.64
NiO	0.07	0.21	0.13	0.24	0.27	0.00	0.19	0.04	0.03	0.05	0.27	0.38	0.30	0.02	0.26	0.33	0.11	0.00	0.57
P2O5	0.00	0.00	0.00	0.04	0.00	0.00	0.01	0.00	0.00	0.00	0.00	0.00	0.00	0.00	0.00	0.00	0.05	0.01	0.00
SO3	0.00	0.00	0.16	0.00	0.00	0.07	0.00	0.00	0.17	0.06	0.00	0.16	0.04	0.24	0.03	0.00	0.00	0.31	0.13
Total	99.09	98.96	99.60	99.31	99.42	98.94	97.85	98.68	99.47	98.61	99.60	98.52	98.66	99.16	98.66	99.07	99.50	99.16	98.69
							Number of Ions on the Basis of 6 (O)												
Si	1.8759	1.8851	1.8585	1.8818	1.9418	1.9372	1.8867	1.8956	1.8790	1.9300	1.8686	1.8772	1.8661	1.8811	1.8635	1.8653	1.8605	1.9155	1.9224
Ti	0.0083	0.0127	0.0130	0.0106	0.0052	0.0071	0.0050	0.0153	0.0134	0.0051	0.0191	0.0018	0.0027	0.0092	0.0080	0.0049	0.0065	0.0133	0.0047
Al	0.2908	0.2611	0.2937	0.2608	0.0452	0.0331	0.3793	0.2890	0.3095	0.2245	0.3967	0.3449	0.3619	0.2833	0.3635	0.3362	0.3356	0.2323	0.2300
Fe(2)	0.0585	0.0598	0.0463	0.0771	0.0153	0.0607	0.1473	0.0636	0.0448	0.1058	0.1316	0.0895	0.0375	0.0224	0.0124	0.0743	0.0236	0.0918	0.1050
Fe(3)	0.0082	0.0097	0.0281	0.0000	0.0407	0.0000	0.0287	0.0625	0.0753	0.0348	0.0162	0.0108	0.0712	0.1111	0.0731	0.0304	0.0714	0.0392	0.0266
Mn	0.0003	0.0000	0.0000	0.0001	0.0006	0.0000	0.0049	0.0000	0.0037	0.0000	0.0010	0.0000	0.0000	0.0002	0.0000	0.0030	0.0058	0.0000	0.0004
Mg	0.7932	0.7961	0.7830	0.7836	0.9821	0.9947	0.6091	0.7109	0.7123	0.7522	0.6116	0.7059	0.6696	0.7285	0.7149	0.7159	0.7306	0.7431	0.7487
Ca	0.8650	0.8638	0.8646	0.8721	0.9447	0.9525	0.7372	0.8116	0.8072	0.7934	0.7485	0.7919	0.8079	0.8093	0.7944	0.8311	0.8301	0.7857	0.7831
Na	0.0846	0.0942	0.0915	0.0811	0.0090	0.0062	0.2015	0.1583	0.1618	0.1393	0.2018	0.1530	0.1819	0.1565	0.1815	0.1317	0.1421	0.1534	0.1554
K	0.0000	0.0000	0.0000	0.0004	0.0000	0.0019	0.0000	0.0040	0.0000	0.0031	0.0025	0.0031	0.0027	0.0079	0.0000	0.0000	0.0000	0.0000	0.0054
Cr	0.0173	0.0199	0.0213	0.0270	0.0281	0.0227	0.0083	0.0086	0.0078	0.0192	0.0068	0.0158	0.0189	0.0129	0.0106	0.0162	0.0148	0.0211	0.0188
Ni	0.0021	0.0063	0.0038	0.0069	0.0079	0.0000	0.0056	0.0011	0.0008	0.0016	0.0079	0.0113	0.0088	0.0005	0.0076	0.0099	0.0032	0.0000	0.0170
P	0.0000	0.0000	0.0000	0.0013	0.0000	0.0000	0.0004	0.0000	0.0000	0.0000	0.0000	0.0000	0.0000	0.0000	0.0000	0.0000	0.0016	0.0003	0.0000
S	0.0000	0.0000	0.0043	0.0000	0.0000	0.0019	0.0000	0.0000	0.0046	0.0017	0.0000	0.0044	0.0010	0.0066	0.0007	0.0000	0.0000	0.0085	0.0037
Wo	50.1	49.9	50.2	50.3	47.6	47.4	48.4	49.2	49.2	47.0	49.6	49.5	50.9	48.4	49.8	50.3	50.1	47.3	47.1
En	46.0	46.0	45.5	45.2	49.5	49.5	40.0	43.1	43.4	44.6	40.5	44.2	42.2	43.6	44.8	43.3	44.1	44.8	45.0
Fs	3.9	4.0	4.3	4.5	2.8	3.0	11.6	7.7	7.4	8.4	9.8	6.3	6.9	8.0	5.4	6.4	5.8	7.9	7.9
Mg/Mg+Fe(t)	92.2	91.9	91.3	91.0	94.6	94.2	77.5	84.9	85.5	84.2	80.5	87.5	85.9	84.4	89.2	87.2	88.4	85.0	85.0

Table 6.6c. Representative clinopyroxene analyses for the Pine Creek xenoliths.

Sample	Pinc X 5				Pinc X 7	Pinc X 7		Pinc A 2	Pinc X 4			
Lithology	Cpx granul.				Fd granul.	Pyroxenit.		Pyroxenit.	Xenocr.			
SiO2	46.09	45.19	43.98	48.85	50.17	50.65	50.92	50.37	51.78	47.65	52.73	52.85
TiO2	1.87	2.62	2.72	1.48	0.78	0.60	0.64	0.74	0.25	0.28	0.15	0.11
Al2O3	10.58	11.13	12.10	6.20	9.09	8.87	9.04	8.09	3.52	9.74	1.80	1.88
FeO	3.75	4.34	2.70	4.37	4.03	3.84	1.99	2.38	1.20	5.05	2.28	1.36
Fe2O3	0.91	0.30	1.90	0.43	1.62	0.39	1.90	2.67	1.55	0.43	0.00	0.96
MnO	0.22	0.34	0.20	0.37	0.00	0.00	0.01	0.00	0.08	0.57	0.00	0.00
MgO	13.46	13.43	13.11	15.81	11.12	11.74	11.72	11.82	17.10	15.92	17.08	17.35
CaO	21.59	20.66	20.88	20.83	18.39	19.36	19.17	19.89	21.88	18.43	22.94	23.41
Na2O	0.21	0.31	0.40	0.00	2.94	2.49	2.98	2.56	0.47	0.09	0.32	0.29
K2O	0.06	0.06	0.05	0.04	0.00	0.00	0.06	0.02	0.08	0.00	0.14	0.03
Cr2O3	0.51	0.47	1.46	0.67	0.37	0.34	0.49	0.50	0.62	0.25	0.43	0.46
NiO	0.00	0.19	0.00	0.00	0.07	0.01	0.00	0.00	0.04	0.42	0.66	0.24
P2O5	0.02	0.00	0.01	0.00	0.11	0.00	0.00	0.00	0.02	0.00	0.00	0.00
SO3	0.11	0.00	0.00	0.07	0.00	0.03	0.04	0.06	0.10	0.01	0.11	0.13
Total	99.37	99.04	99.50	99.11	98.70	98.31	98.96	99.11	98.71	98.84	98.63	99.07
				Number of Ions on the Basis of 6 (O)								
Si	1.7071	1.6809	1.6354	1.8092	1.8579	1.8705	1.8691	1.8623	1.9079	1.7631	1.9474	1.9419
Ti	0.0521	0.0732	0.0760	0.0413	0.0218	0.0165	0.0178	0.0207	0.0068	0.0078	0.0041	0.0031
Al	0.4617	0.4878	0.5304	0.2705	0.3969	0.3858	0.3909	0.3526	0.1530	0.4247	0.0782	0.0813
Fe(2)	0.1162	0.1347	0.0836	0.1354	0.1243	0.1185	0.0607	0.0731	0.0370	0.1556	0.0705	0.0416
Fe(3)	0.0252	0.0084	0.0528	0.0119	0.0450	0.0110	0.0523	0.0738	0.0429	0.0119	0.0000	0.0265
Mn	0.0069	0.0106	0.0064	0.0116	0.0000	0.0001	0.0004	0.0000	0.0026	0.0179	0.0000	0.0000
Mg	0.7427	0.7440	0.7261	0.8721	0.6133	0.6455	0.6407	0.6509	0.9383	0.8773	0.9399	0.9497
Ca	0.8563	0.8231	0.8315	0.8263	0.7294	0.7656	0.7538	0.7875	0.8632	0.7303	0.9072	0.9210
Na	0.0151	0.0226	0.0291	0.0000	0.2107	0.1779	0.2118	0.1835	0.0339	0.0062	0.0227	0.0206
K	0.0029	0.0029	0.0021	0.0017	0.0000	0.0000	0.0027	0.0010	0.0038	0.0000	0.0064	0.0017
Cr	0.0150	0.0138	0.0429	0.0196	0.0110	0.0098	0.0143	0.0148	0.0181	0.0074	0.0127	0.0134
Ni	0.0000	0.0057	0.0000	0.0000	0.0020	0.0003	0.0000	0.0000	0.0013	0.0124	0.0195	0.0070
P	0.0005	0.0000	0.0004	0.0000	0.0036	0.0000	0.0000	0.0000	0.0006	0.0000	0.0000	0.0000
S	0.0080	0.0000	0.0000	0.0020	0.0000	0.0009	0.0010	0.0016	0.0027	0.0003	0.0031	0.0037
Wo	49.20	48.13	49.09	44.77	48.24	49.69	50.00	49.67	45.88	41.14	47.31	47.51
En	42.67	43.51	42.86	47.25	40.56	41.90	42.50	41.06	49.87	49.42	49.02	48.99
Fs	8.13	8.37	8.05	7.98	11.20	8.40	7.50	9.27	4.25	9.44	3.67	3.51
Mg/Mg+Fe(t)	84.0	83.9	84.2	85.6	78.4	83.3	85.0	81.6	92.2	84.0	93.0	93.3

Table 6.7. Representative orthopyroxene analyses of theSouth Australian lower crustal xenoliths.

	A) Port Augusta														B) Calcutteroo	
Sample	**Pa 6X 8**			**Pa 6X 11**		**Pa 7X 8**	**Pa 7X 5**		**Pa CX 6**		**Pa 7X 9**		**Pa 7X 9**		**Trwi CB 4**	
Lithology	**Eclog.**			**Cpx granul.**		**Cpx granul.**	**Two Px granul.**		**Two Px granul.**		**Gabbro.**		**Gabbro.**		**Cpx granul.**	
SiO2	49.60	49.79	49.29	52.71	52.78	53.61	51.08	50.44	49.53	49.48	49.78	49.41	49.80	49.76	53.78	54.29
TiO2	0.00	0.17	0.01	0.12	0.00	0.45	0.01	0.09	0.01	0.15	0.04	0.09	0.01	0.05	0.00	0.00
Al2O3	1.99	1.85	1.92	1.35	1.53	1.39	2.00	2.97	3.46	4.06	2.57	2.69	1.59	1.92	2.11	1.97
FeO	29.89	30.40	28.84	16.10	15.10	14.73	19.06	21.11	21.79	22.08	26.95	27.36	29.66	28.24	9.55	9.80
Fe2O3	1.63	0.86	2.24	1.91	2.36	0.87	2.82	1.73	2.77	1.95	1.81	1.21	1.46	1.64	2.02	1.29
MnO	0.57	0.41	0.70	0.00	0.16	0.00	0.03	0.22	0.68	0.68	0.57	0.49	1.01	0.81	0.32	0.26
MgO	15.93	15.81	16.10	26.25	26.62	27.81	23.11	21.50	20.55	20.52	16.02	15.59	15.91	15.59	30.43	30.58
CaO	0.54	0.42	0.44	0.28	0.32	0.22	0.63	0.55	0.40	0.33	2.71	2.87	0.49	1.91	0.28	0.27
Na2O	0.00	0.00	0.00	0.00	0.00	0.00	0.00	0.00	0.00	0.00	0.00	0.00	0.00	0.00	0.00	0.00
K2O	0.00	0.06	0.05	0.05	0.00	0.05	0.00	0.04	0.03	0.00	0.05	0.00	0.07	0.11	0.06	0.06
Cr2O3	0.00	0.00	0.10	0.13	0.20	0.05	0.06	0.00	0.28	0.00	0.00	0.04	0.02	0.17	0.10	0.07
NiO	0.12	0.00	0.00	0.14	0.00	0.00	0.00	0.05	0.00	0.24	0.09	0.09	0.00	0.06	0.12	0.09
P2O5	0.01	0.01	0.00	0.00	0.01	0.12	0.00	0.00	0.24	0.00	0.00	0.00	0.17	0.00	0.06	0.00
SO3	0.00	0.00	0.00	0.07	0.00	0.00	0.17	0.12	0.00	0.00	0.10	0.01	0.00	0.00	0.05	0.00
Total	100.28	99.78	99.68	99.10	99.07	99.30	98.96	98.81	99.75	99.49	100.68	99.84	100.19	100.26	98.88	98.67
	Number of Ions on the Basis of 6(O)															
Si	1.9266	1.9453	1.9335	1.9435	1.9424	1.9456	1.9236	1.9114	1.8812	1.8794	1.9193	1.9210	1.9424	1.9373	1.9301	1.9394
Ti	0.0000	0.0050	0.0003	0.0032	0.0000	0.0123	0.0004	0.0025	0.0004	0.0043	0.0010	0.0026	0.0003	0.0015	0.0000	0.0000
Al	0.0911	0.0854	0.0886	0.0588	0.0663	0.0594	0.0888	0.1327	0.1547	0.1817	0.1169	0.1234	0.0732	0.0880	0.0891	0.0829
Fe(2)	0.9700	0.9908	0.9405	0.4941	0.4620	0.4460	0.5975	0.6668	0.6874	0.6967	0.8656	0.8863	0.9638	0.9152	0.2851	0.2925
Fe(3)	0.0477	0.0253	0.0657	0.0529	0.0649	0.0238	0.0794	0.0491	0.0786	0.0554	0.0522	0.0353	0.0426	0.0477	0.0543	0.0346
Mn	0.0186	0.0136	0.0232	0.0000	0.0050	0.0000	0.0009	0.0070	0.0219	0.0217	0.0186	0.0162	0.0333	0.0268	0.0097	0.0078
Mg	0.9215	0.9201	0.9406	1.4416	1.4594	1.5033	1.2964	1.2135	1.1628	1.1608	0.9200	0.9029	0.9246	0.9043	1.6268	1.6269
Ca	0.0225	0.0175	0.0187	0.0110	0.0125	0.0085	0.0253	0.0223	0.0164	0.0134	0.1119	0.1193	0.0202	0.0797	0.0107	0.0103
Na	0.0000	0.0000	0.0000	0.0000	0.0000	0.0000	0.0000	0.0000	0.0000	0.0000	0.0000	0.0000	0.0000	0.0000	0.0000	0.0000
K	0.0000	0.0027	0.0022	0.0023	0.0000	0.0025	0.0000	0.0020	0.0014	0.0000	0.0026	0.0000	0.0036	0.0056	0.0027	0.0026
Cr	0.0001	0.0001	0.0030	0.0036	0.0057	0.0014	0.0017	0.0000	0.0083	0.0000	0.0000	0.0011	0.0007	0.0053	0.0029	0.0021
Ni	0.0037	0.0000	0.0000	0.0042	0.0000	0.0000	0.0001	0.0015	0.0000	0.0074	0.0028	0.0027	0.0000	0.0018	0.0036	0.0026
P	0.0002	0.0002	0.0000	0.0000	0.0003	0.0037	0.0000	0.0000	0.0078	0.0000	0.0000	0.0000	0.0056	0.0000	0.0018	0.0000
S	0.0000	0.0000	0.0000	0.0019	0.0000	0.0000	0.0047	0.0034	0.0000	0.0000	0.0029	0.0002	0.0000	0.0000	0.0014	0.0000
Wo	1.1	0.9	0.9	0.5	0.6	0.4	1.3	1.1	0.8	0.7	5.7	6.1	1.0	4.1	0.5	0.5
En	47.0	47.1	47.9	72.1	73.0	75.9	64.9	62.2	59.8	60.3	47.2	46.5	47.4	46.4	82.3	82.8
Fs	51.9	52.0	51.2	27.4	26.4	23.7	33.9	36.7	39.4	39.0	47.1	47.4	51.6	49.5	17.2	16.7
Mg/Mg+Fe(t)	47.5	47.5	48.3	72.5	73.5	76.2	65.7	62.9	60.3	60.7	50.1	49.5	47.9	48.4	82.7	83.3

Continued

Sample	Trwi Cx 6		Trwi CB 3		Trwi CH 5		Trwi CH 4				C) Pine Creek Pinc CX 4					
Lithology	Fd granul. altered rim of gt		Pyroxenit.		Pyroxenit.		Pyroxenit.				Xenocr.					
SiO2	50.88	51.93	49.07	49.96	49.13	47.46	56.05	56.73	56.54	56.32	47.71	49.52	52.27	52.20	49.45	48.91
TiO2	0.33	0.29	0.00	0.00	0.09	0.24	0.24	0.16	0.09	0.20	0.09	0.19	0.21	0.06	0.20	0.18
Al2O3	5.18	4.17	10.90	11.10	9.24	10.59	1.28	1.11	1.18	1.37	13.57	10.43	6.00	5.92	10.96	11.61
FeO	11.48	12.83	4.84	6.44	9.13	7.87	4.33	4.09	4.86	4.75	8.69	8.92	8.53	7.37	6.44	5.86
Fe2O3	2.93	0.65	1.57	0.29	2.23	4.64	0.98	1.81	1.07	0.90	0.26	0.00	0.20	1.54	1.40	2.58
MnO	0.24	0.28	0.20	0.21	0.11	0.23	0.33	0.24	0.34	0.12	0.57	0.51	0.60	0.62	0.79	0.48
MgO	26.76	26.49	29.55	29.00	26.89	26.15	34.92	35.35	34.96	35.15	25.86	27.19	28.75	29.18	28.01	28.21
CaO	1.38	1.77	1.51	1.38	1.45	1.35	0.32	0.32	0.41	0.23	1.51	1.67	1.74	1.91	1.60	1.62
Na2O	0.00	0.00	0.00	0.00	0.00	0.08	0.00	0.00	0.00	0.00	0.00	0.00	0.00	0.00	0.00	0.00
K2O	0.15	0.01	0.06	0.02	0.00	0.05	0.05	0.13	0.04	0.00	0.00	0.00	0.02	0.00	0.03	0.12
Cr2O3	0.23	0.31	0.04	0.04	0.48	0.53	0.34	0.26	0.31	0.47	0.41	0.28	0.33	0.18	0.14	0.22
NiO	0.26	0.15	0.34	0.23	0.11	0.00	0.12	0.00	0.27	0.17	0.09	0.35	0.00	0.00	0.00	0.23
P2O5	0.00	0.00	0.26	0.00	0.00	0.00	0.00	0.08	0.00	0.00	0.00	0.00	0.00	0.00	0.00	0.00
SO3	0.00	0.13	0.00	0.01	0.00	0.12	0.11	0.05	0.00	0.00	0.00	0.00	0.05	0.08	0.00	0.00
Total	99.81	99.01	98.34	98.69	98.87	99.30	99.07	100.32	100.09	99.67	98.77	99.06	98.70	99.05	99.02	100.03
						Number of Ions on the Basis of 6(O)										
Si	1.8466	1.8855	1.7342	1.7606	1.7716	1.7190	1.9497	1.9526	1.9543	1.9431	1.7021	1.7665	1.8617	1.8567	1.7526	1.7247
Ti	0.0090	0.0078	0.0000	0.0000	0.0025	0.0066	0.0064	0.0042	0.0024	0.0051	0.0025	0.0051	0.0057	0.0016	0.0054	0.0048
Al	0.2217	0.1785	0.4540	0.4611	0.3926	0.4519	0.0525	0.0450	0.0482	0.0557	0.5705	0.4384	0.2517	0.2481	0.4578	0.4823
Fe(2)	0.3452	0.3892	0.1425	0.1893	0.2736	0.2363	0.1258	0.1174	0.1399	0.1371	0.2589	0.2657	0.2540	0.2186	0.1902	0.1716
Fe(3)	0.0793	0.0178	0.0417	0.0078	0.0600	0.1254	0.0256	0.0468	0.0278	0.0234	0.0071	0.0000	0.0054	0.0410	0.0371	0.0680
Mn	0.0073	0.0085	0.0060	0.0062	0.0035	0.0071	0.0098	0.0069	0.0100	0.0034	0.0171	0.0153	0.0181	0.0188	0.0237	0.0144
Mg	1.4464	1.4327	1.5559	1.5221	1.4439	1.4108	1.8091	1.8123	1.8001	1.8007	1.3743	1.4449	1.5256	1.5459	1.4784	1.4821
Ca	0.0535	0.0687	0.0571	0.0522	0.0562	0.0524	0.0120	0.0118	0.0152	0.0084	0.0576	0.0639	0.0664	0.0728	0.0607	0.0613
Na	0.0000	0.0000	0.0000	0.0000	0.0000	0.0054	0.0000	0.0000	0.0000	0.0000	0.0000	0.0000	0.0000	0.0000	0.0000	0.0000
K	0.0069	0.0005	0.0029	0.0009	0.0000	0.0022	0.0021	0.0055	0.0019	0.0000	0.0000	0.0000	0.0009	0.0000	0.0014	0.0053
Cr	0.0067	0.0090	0.0010	0.0011	0.0138	0.0151	0.0092	0.0071	0.0082	0.0129	0.0116	0.0079	0.0094	0.0049	0.0040	0.0062
Ni	0.0076	0.0043	0.0098	0.0066	0.0032	0.0000	0.0035	0.0000	0.0074	0.0047	0.0025	0.0100	0.0000	0.0000	0.0000	0.0066
P	0.0000	0.0000	0.0078	0.0000	0.0000	0.0000	0.0000	0.0024	0.0000	0.0000	0.0000	0.0000	0.0000	0.0000	0.0000	0.0000
S	0.0000	0.0035	0.0000	0.0002	0.0000	0.0032	0.0027	0.0013	0.0000	0.0000	0.0000	0.0000	0.0013	0.0021	0.0000	0.0000
Wo	2.8	3.6	3.2	2.9	3.1	2.9	0.6	0.6	0.8	0.4	3.4	3.6	3.6	3.9	3.4	3.4
En	75.2	75.1	86.6	85.9	78.7	77.3	91.7	91.1	90.8	91.4	80.9	81.4	82.4	82.3	83.7	83.1
Fs	22.1	21.3	10.2	11.1	18.2	19.8	7.7	8.3	8.5	8.1	15.7	15.0	14.0	13.8	12.9	13.4
Mg/Mg+Fe(t)	77.3	77.9	89.4	88.5	81.2	79.6	92.3	91.7	91.5	91.8	83.8	84.5	85.5	85.6	86.7	86.1

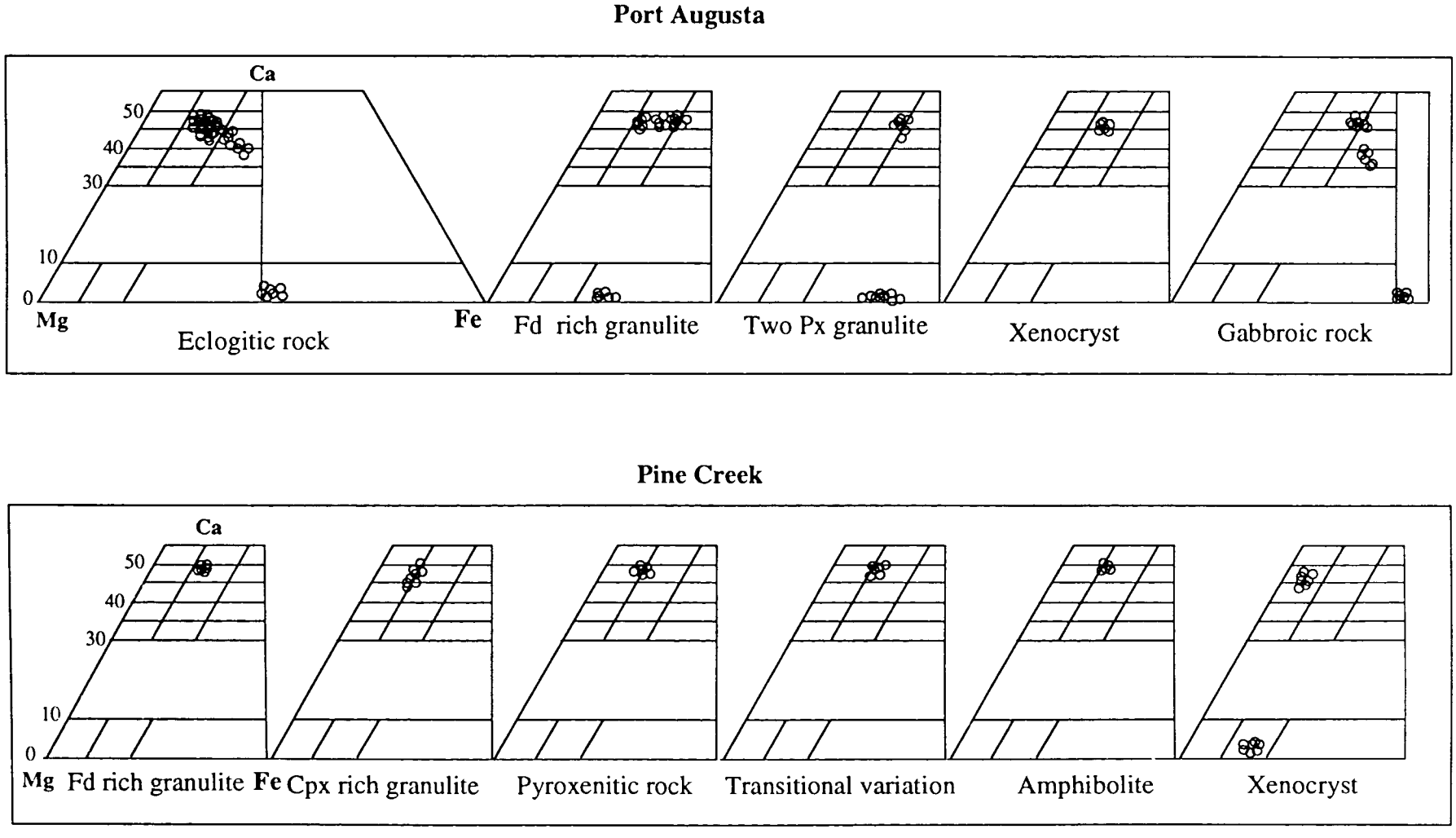

Fig. 6.3a. Pyroxene compositions of the Port Augusta and Pine Creek xenoliths.

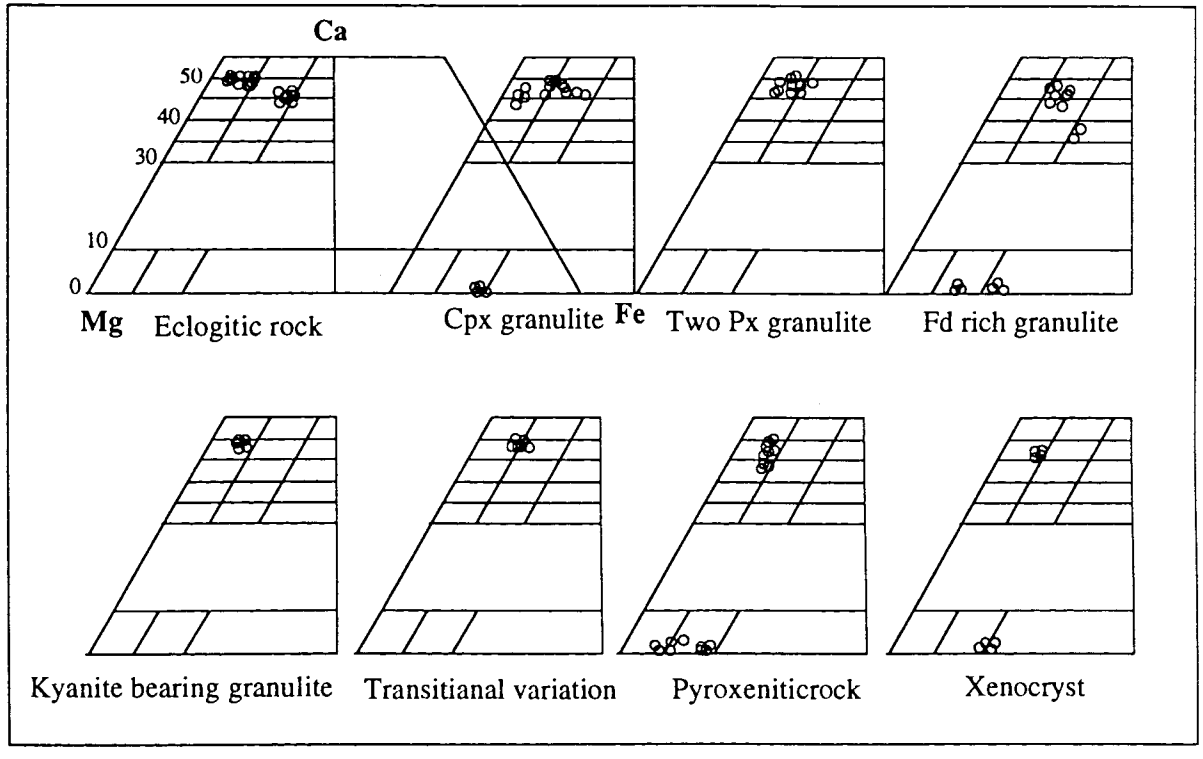

Fig. 6.3b. Pyroxene compositions of the Calcutteroo xenoliths.

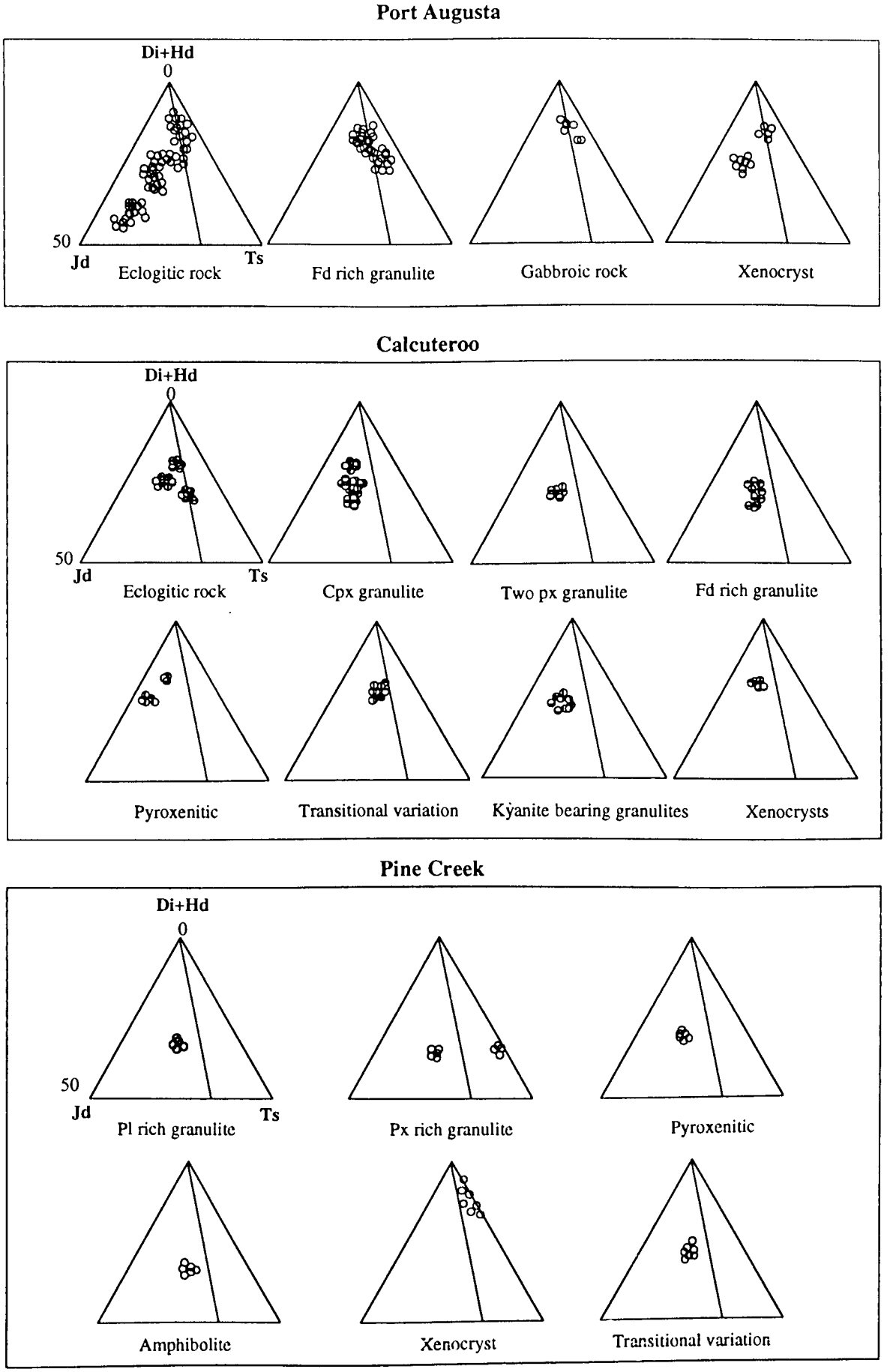

Fig. 6.4. Clinopyroxene compositions of the Port Augusta, Calutteroo and Pine Creek xenoliths.

Table 6.8. Representative feldspar analyses of the South Australian lower crustal xenoliths.

A) Port Augusta

Sample	Pa 7X 1		Pa 6X 11	Pa 7X 6		Pa 9X 1			Pa 7X 8	Pa 7X 5			Pa CX 6					Pa 7X 9		
Lithology	Fd granul.		Fd granul.	Fd granul.		Fd granul.			Fd granul.	Two Px granul.			Two Px granul.					Gabbro.		
SiO2	57.06	57.10	57.04	57.39	56.61	57.84	58.22	57.27	57.59	54.52	54.39	54.74	54.45	54.59	53.81	53.99	61.32	61.48	50.24	51.34	53.28
TiO2	0.08	0.05	0.13	0.15	0.24	0.00	0.24	0.23	0.00	0.08	0.00	0.00	0.11	0.13	0.18	0.00	0.67	0.71	0.00	0.03	0.10
Al2O3	25.88	25.56	25.31	25.23	25.83	25.46	24.92	25.36	25.38	26.99	27.00	27.01	26.90	26.94	27.58	27.29	17.93	18.25	30.45	29.73	28.25
FeO#	0.06	0.00	0.08	0.06	0.00	0.16	0.00	0.04	0.19	0.12	0.00	0.00	0.80	0.04	0.06	0.16	0.00	0.00	0.00	0.00	0.00
MnO	0.26	0.06	0.00	0.22	0.09	0.13	0.10	0.04	0.23	0.00	0.05	0.00	0.00	0.00	0.10	0.00	0.22	0.00	0.00	0.00	0.16
MgO	0.00	0.00	0.00	0.00	0.00	0.16	0.04	0.01	0.00	0.00	0.04	0.24	0.00	0.02	0.00	0.10	0.00	0.00	0.00	0.00	0.00
CaO	7.97	7.76	7.69	7.37	7.82	7.43	6.68	7.58	7.45	9.80	9.79	9.88	9.46	9.86	10.39	10.02	0.46	0.42	13.40	13.15	11.32
Na2O	6.52	6.54	6.38	6.60	6.70	6.56	7.17	6.87	7.16	5.74	5.67	5.84	5.81	5.73	5.30	5.68	1.33	1.42	3.87	3.92	4.80
K2O	0.47	0.48	0.37	0.43	0.42	0.39	0.49	0.32	0.44	0.33	0.14	0.27	0.16	0.30	0.35	0.16	14.01	14.01	0.01	0.02	0.12
Cr2O3	0.16	0.09	0.24	0.23	0.10	0.24	0.08	0.25	0.17	0.19	0.40	0.07	0.19	0.37	0.13	0.09	0.00	0.08	0.34	0.25	0.24
NiO	0.00	0.03	0.00	0.00	0.00	0.07	0.21	0.05	0.06	0.00	0.03	0.00	0.00	0.00	0.16	0.00	0.00	0.00	0.00	0.00	0.00
P2O5	0.00	0.02	0.08	0.00	0.00	0.07	0.00	0.00	0.00	0.00	0.00	0.00	0.00	0.00	0.01	0.21	1.22	1.07	0.00	0.02	0.00
SO3	0.00	0.00	0.02	0.10	0.00	0.02	0.13	0.00	0.00	0.00	0.06	0.02	0.00	0.00	0.00	0.00	0.11	0.09	0.00	0.00	0.00
Total	98.45	97.69	97.33	97.77	97.80	98.54	98.27	98.00	98.67	97.77	97.57	98.06	97.89	97.98	98.07	97.70	97.28	97.53	98.30	98.46	98.27
										Number of Ions on the Basis of 32 (O)											
Si	10.3892	10.4633	10.4767	10.5014	10.3773	10.5008	10.5885	10.4683	10.4805	10.0583	10.0433	10.0603	10.0493	10.0510	9.9218	9.9475	11.5906	11.5798	9.2932	9.4548	9.8039
Ti	0.0107	0.0062	0.0181	0.0201	0.0333	0.0001	0.0331	0.0311	0.0000	0.0116	0.0000	0.0000	0.0146	0.0184	0.0244	0.0000	0.0946	0.1001	0.0000	0.0039	0.0137
Al	5.5545	5.5197	5.4778	5.4403	5.5803	5.4465	5.3407	5.4607	5.4428	5.8662	5.8734	5.8494	5.8515	5.8460	5.9909	5.9256	3.9934	4.0502	6.6377	6.4520	6.1252
Fe(t)	0.0096	0.0000	0.0122	0.0089	0.0000	0.0249	0.0000	0.0062	0.0284	0.0185	0.0000	0.0002	0.1238	0.0066	0.0097	0.0239	0.0000	0.0000	0.0000	0.0000	0.0000
Mn	0.0398	0.0090	0.0000	0.0335	0.0138	0.0205	0.0154	0.0058	0.0351	0.0000	0.0079	0.0000	0.0000	0.0000	0.0161	0.0000	0.0350	0.0000	0.0000	0.0000	0.0242
Mg	0.0000	0.0000	0.0000	0.0000	0.0000	0.0435	0.0114	0.0013	0.0000	0.0000	0.0114	0.0659	0.0000	0.0041	0.0000	0.0260	0.0000	0.0000	0.0000	0.0000	0.0000
Ca	1.5542	1.5237	1.5131	1.4444	1.5347	1.4447	1.3003	1.4830	1.4526	1.9365	1.9353	1.9441	1.8695	1.9438	2.0507	1.9765	0.0932	0.0855	2.6540	2.5940	2.2314
Na	2.3006	2.3247	2.2709	2.3407	2.3797	2.3076	2.5259	2.4308	2.5241	2.0511	2.0267	2.0783	2.0793	2.0452	1.8927	2.0291	0.4859	0.5180	1.3875	1.3978	1.7103
K	0.1083	0.1131	0.0869	0.1011	0.0981	0.0903	0.1144	0.0750	0.1014	0.0766	0.0327	0.0623	0.0375	0.0692	0.0825	0.0386	3.3771	3.3643	0.0018	0.0052	0.0283
Cr	0.0235	0.0123	0.0344	0.0327	0.0141	0.0340	0.0109	0.0356	0.0248	0.0281	0.0588	0.0101	0.0283	0.0536	0.0186	0.0127	0.0000	0.0120	0.0494	0.0366	0.0348
Ni	0.0000	0.0049	0.0000	0.0000	0.0000	0.0106	0.0301	0.0077	0.0087	0.0000	0.0049	0.0000	0.0006	0.0000	0.0242	0.0000	0.0000	0.0000	0.0000	0.0000	0.0000
P	0.0000	0.0026	0.0127	0.0000	0.0000	0.0107	0.0000	0.0000	0.0000	0.0000	0.0000	0.0000	0.0000	0.0000	0.0021	0.0334	0.1957	0.1701	0.0000	0.0030	0.0000
S	0.0000	0.0000	0.0020	0.0133	0.0000	0.0026	0.0174	0.0000	0.0000	0.0000	0.0086	0.0033	0.0000	0.0000	0.0000	0.0000	0.0161	0.0124	0.0000	0.0001	0.0000
Sum	19.9904	19.9795	19.9048	19.9364	20.0312	19.9367	19.9881	20.0054	20.0984	20.0469	20.0030	20.0738	20.0544	20.0380	20.0336	20.0134	19.8817	19.8924	20.0235	19.9475	19.9718
An	39.2	38.5	39.1	37.2	38.2	37.6	33.0	37.2	35.6	47.6	48.4	47.6	46.9	47.9	50.9	48.9	2.4	2.2	65.6	64.9	56.2
Ab	58.1	58.7	58.7	60.2	59.3	60.1	64.1	60.9	61.9	50.5	50.7	50.9	52.2	50.4	47.0	50.2	12.3	13.1	34.3	35.0	43.1
Or	2.7	2.9	2.2	2.6	2.4	2.3	2.9	1.9	2.5	1.9	0.8	1.5	0.9	1.7	2.0	1.0	85.4	84.8	0.0	0.1	0.7

Sample		Pa 6X 10	B) Calcutteroo									C) Pine Creek									
Lithology		Gabbro.	Trwi CX 3 Fd granul.			Trwi CX 2 Cpx granul.		Trwi CX 6 Fd granul. broken gt	Trwi CB 3 Cpx granul.			Pine X 5 Cpx granul.		Pine X 7 Fd granul.			Pine X 6 Gabbro.		Pine A 2 Xenocr.		
SiO2	51.13	54.64	60.85	61.29	61.02	59.69	59.64	52.04	48.54	47.47	48.85	48.02	55.65	55.97	59.60	59.80	60.12	65.32	65.17	48.05	47.20	47.76
TiO2	0.09	0.18	0.00	0.00	0.30	0.17	0.12	0.00	0.01	0.21	0.09	0.00	0.10	0.21	0.21	0.04	0.00	0.04	0.18	0.19	0.11	0.00
Al2O3	29.09	27.30	23.11	23.33	23.55	24.33	24.33	28.40	30.99	31.72	30.77	31.08	26.11	25.10	22.81	22.95	22.76	18.99	19.02	31.15	31.63	31.48
FeO#	0.43	0.28	0.00	0.05	0.06	0.18	0.01	0.64	0.70	0.46	0.69	0.55	0.48	1.07	0.00	0.16	0.00	0.28	0.02	0.53	0.79	0.64
MnO	0.01	0.02	0.13	0.16	0.00	0.22	0.31	0.16	0.00	0.00	0.27	0.00	0.00	0.00	0.00	0.21	0.11	0.07	0.18	0.08	0.00	0.01
MgO	0.12	0.00	0.16	0.00	0.06	0.02	0.00	0.04	0.00	0.15	0.21	0.14	0.00	0.20	0.00	0.03	0.00	0.03	0.00	0.07	0.14	0.05
CaO	13.13	9.76	5.11	5.08	5.25	6.53	6.23	12.76	14.96	15.77	14.68	15.02	8.91	7.79	4.77	4.61	4.86	0.11	0.29	15.15	15.61	15.65
Na2O	4.05	5.62	8.42	8.32	8.16	7.47	7.30	3.85	2.90	2.55	3.17	3.01	5.85	6.61	7.91	7.99	8.00	10.99	10.76	2.51	2.37	2.78
K2O	0.06	0.17	0.34	0.46	0.56	0.44	0.57	0.01	0.00	0.00	0.00	0.00	0.11	0.29	0.35	0.28	0.39	0.30	0.16	0.09	0.17	0.07
Cr2O3	0.25	0.22	0.02	0.17	0.09	0.16	0.17	0.27	0.24	0.27	0.09	0.32	0.06	0.15	0.21	0.19	0.08	0.00	0.02	0.19	0.35	0.28
NiO	0.00	0.05	0.05	0.00	0.05	0.00	0.20	0.17	0.09	0.00	0.36	0.21	0.00	0.26	0.30	0.15	0.19	0.00	0.00	0.00	0.00	0.01
P2O5	0.00	0.00	0.05	0.00	0.00	0.00	0.00	0.00	0.09	0.00	0.00	0.00	0.00	0.00	0.00	0.00	0.00	0.00	0.00	0.00	0.00	0.00
SO3	0.07	0.00	0.10	0.02	0.00	0.17	0.01	0.00	0.00	0.08	0.05	0.00	0.07	0.00	0.00	0.06	0.02	0.02	0.00	0.12	0.08	0.00
Total	98.43	98.24	98.34	98.88	99.09	99.38	98.90	98.34	98.52	98.69	99.23	98.34	97.33	97.63	96.16	96.47	96.52	96.15	95.80	98.13	98.44	98.71
			Number of Ions on the Basis of 32 (O)																		
Si	9.4669	10.0279	10.9921	11.0167	10.9525	10.7249	10.7682	9.6328	9.0397	8.8428	9.0550	8.9760	10.2639	10.3463	11.0034	11.0027	11.0535	11.9031	11.8997	8.9778	8.8199	8.9057
Ti	0.0119	0.0244	0.0000	0.0000	0.0406	0.0235	0.0161	0.0000	0.0009	0.0289	0.0130	0.0001	0.0131	0.0286	0.0294	0.0053	0.0003	0.0051	0.0246	0.0265	0.0151	0.0000
Al	6.3466	5.9041	4.9185	4.9409	4.9811	5.1513	5.1765	6.1954	6.7998	6.9615	6.7205	6.8465	5.6739	5.4672	4.9629	4.9761	4.9301	4.0789	4.0928	6.8582	6.9642	6.9169
Fe(t)	0.0661	0.0429	0.0000	0.0072	0.0084	0.0263	0.0011	0.0996	0.1086	0.0720	0.1062	0.0859	0.0734	0.1645	0.0000	0.0248	0.0000	0.0433	0.0026	0.0827	0.1240	0.0996
Mn	0.0020	0.0036	0.0200	0.0237	0.0000	0.0340	0.0469	0.0250	0.0000	0.0000	0.0421	0.0000	0.0000	0.0000	0.0000	0.0321	0.0171	0.0111	0.0273	0.0121	0.0000	0.0011
Mg	0.0325	0.0000	0.0427	0.0000	0.0155	0.0043	0.0000	0.0110	0.0000	0.0404	0.0588	0.0392	0.0004	0.0547	0.0000	0.0080	0.0000	0.0087	0.0000	0.0195	0.0393	0.0147
Ca	2.6025	1.9179	0.9892	0.9775	1.0085	1.2574	1.2050	2.5292	2.9832	3.1463	2.9146	3.0063	1.7597	1.5418	0.9439	0.9081	0.9579	0.0204	0.0564	3.0308	3.1237	3.1255
Na	1.4544	1.9987	2.9461	2.8983	2.8390	2.5993	2.5526	1.3814	1.0463	0.9206	1.1366	1.0894	2.0916	2.3663	2.8307	2.8493	2.8501	3.8801	3.8047	0.9095	0.8566	1.0034
K	0.0151	0.0409	0.0779	0.1048	0.1282	0.0996	0.1321	0.0013	0.0000	0.0000	0.0000	0.0000	0.0301	0.0686	0.0823	0.0667	0.0905	0.0698	0.0373	0.0222	0.0414	0.0160
Cr	0.0365	0.0317	0.0034	0.0238	0.0129	0.0233	0.0243	0.0399	0.0358	0.0403	0.0137	0.0474	0.0082	0.0214	0.0304	0.0275	0.0114	0.0000	0.0033	0.0282	0.0515	0.0410
Ni	0.0000	0.0078	0.0077	0.0000	0.0069	0.0000	0.0290	0.0253	0.0138	0.0000	0.0539	0.0308	0.0000	0.0388	0.0442	0.0227	0.0286	0.0000	0.0000	0.0000	0.0000	0.0012
P	0.0000	0.0000	0.0082	0.0000	0.0000	0.0000	0.0000	0.0000	0.0147	0.0000	0.0000	0.0000	0.0000	0.0000	0.0000	0.0000	0.0000	0.0000	0.0000	0.0000	0.0000	0.0000
S	0.0100	0.0000	0.0136	0.0032	0.0000	0.0233	0.0020	0.0000	0.0000	0.0117	0.0063	0.0000	0.0103	0.0000	0.0000	0.0083	0.0020	0.0023	0.0000	0.0170	0.0106	0.0000
Sum	20.0444	19.9997	20.0195	19.9961	19.9935	19.9671	19.9538	19.9409	20.0428	20.0645	20.1206	20.1217	19.9247	20.0982	19.9271	19.9316	19.9416	20.0228	19.9487	19.9844	20.0463	20.1251
An	63.9	48.5	24.6	24.6	25.4	31.8	31.0	64.7	74.0	77.4	71.9	73.4	45.3	38.8	24.5	23.7	24.6	0.5	1.4	76.5	77.7	75.4
Ab	35.7	50.5	73.4	72.8	71.4	65.7	65.6	35.3	26.0	22.6	28.1	26.6	53.9	59.5	73.4	74.5	73.1	97.7	97.6	23.0	21.3	24.2
Or	0.4	1.0	1.9	2.6	3.2	2.5	3.4	0.0	0.0	0.0	0.0	0.0	0.8	1.7	2.1	1.7	2.3	1.8	1.0	0.6	1.0	0.4

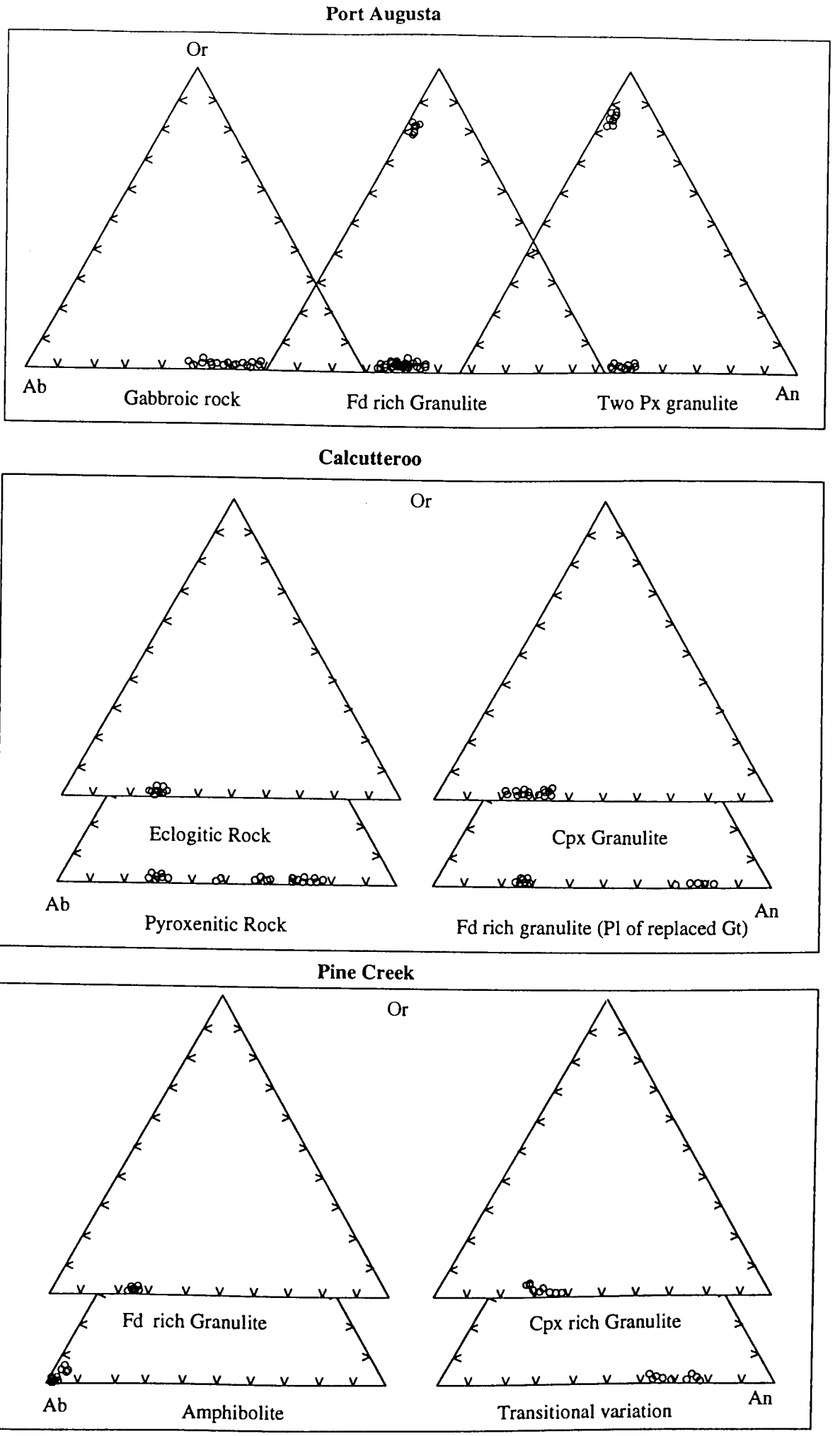

Fig. 6.5. Feldspar compositions of the Port Augusta, Calcutteroo and Pine Creek xenoliths.

Table 6.9. Representative amphibole analyses of the South Australian lower crustal xenoliths.

	A) Port Augusta											B)Pine Creek										
Sample	**Pa 6X 9**				**Pa 8X 3**					**Pa 8X 1**		**Pinc CX 4**							**Pinc A 2**			
Lithology	**Eclog.**				**Xenocr.**					**Xenocr. inclu .**		**Xenocr.**							**Transi. granul.**			
SiO2	42.10	41.63	42.55	41.46	43.25	43.66	42.96	44.13	43.88	41.80	41.97	43.11	43.78	43.48	43.08	43.34	43.24	43.80	39.60	40.72	40.48	39.46
TiO2	1.26	1.21	1.17	1.06	0.95	1.03	1.15	0.98	1.13	1.35	1.05	0.36	0.30	0.36	0.52	0.37	0.38	0.39	3.96	2.16	1.77	2.03
Al2O3	13.59	13.46	13.78	13.68	11.99	11.89	11.97	12.24	11.59	13.95	13.47	12.31	12.58	12.91	12.47	12.61	12.43	12.89	15.21	15.55	15.59	15.65
FeO#	12.54	12.13	12.06	11.93	9.81	9.33	9.51	9.33	9.33	8.87	8.64	3.87	3.45	3.94	3.53	3.70	3.63	3.65	8.49	8.59	9.23	8.77
MnO	0.01	0.00	0.00	0.20	0.09	0.00	0.18	0.11	0.26	0.20	0.16	0.18	0.00	0.05	0.00	0.00	0.00	0.15	0.22	0.00	0.00	0.09
MgO	13.14	13.13	13.12	13.07	15.30	15.29	15.57	16.00	15.27	14.67	14.95	18.87	19.21	18.96	19.26	18.97	19.24	19.48	14.09	14.22	14.03	14.36
CaO	9.04	8.93	9.24	9.10	9.63	9.58	9.65	9.68	9.44	9.37	9.61	11.21	11.27	10.57	11.26	10.98	10.94	10.95	11.24	10.86	11.34	11.21
Na2O	3.62	3.74	4.03	3.85	3.70	3.45	3.25	3.29	3.71	3.82	3.25	2.28	2.96	2.42	2.75	2.52	2.66	2.94	2.37	2.97	2.44	2.32
K2O	1.19	1.31	1.33	1.46	1.49	1.57	1.46	1.48	1.35	1.59	1.48	0.89	0.82	1.01	0.86	1.00	0.96	0.91	1.01	0.95	0.99	0.99
Cr2O3	0.21	0.08	0.15	0.24	0.37	0.36	0.31	0.13	0.17	0.24	0.43	0.75	0.72	0.55	0.45	0.56	0.54	0.26	0.45	0.70	0.69	0.67
NiO	0.00	0.00	0.00	0.25	0.00	0.00	0.11	0.00	0.00	0.20	0.26	0.37	0.00	0.02	0.27	0.42	0.31	0.12	0.10	0.13	0.71	0.00
P2O5	0.05	0.21	0.11	0.17	0.17	0.01	0.08	0.00	0.14	0.24	0.22	0.00	0.09	0.02	0.00	0.00	0.00	0.00	0.00	0.00	0.00	0.00
SO3	0.04	0.01	0.03	0.25	0.01	0.00	0.00	0.11	0.09	0.16	0.00	0.00	0.00	0.10	0.06	0.00	0.18	0.06	0.00	0.00	0.05	0.00
Total	96.78	95.83	97.57	96.71	96.74	96.16	96.19	97.47	96.34	96.44	95.48	94.19	95.18	94.39	94.51	94.45	94.50	95.59	96.73	96.84	97.30	95.55
								Number of Ions on the Basis of 24(O)														
Si	6.5366	6.5238	6.5480	6.4567	6.6608	6.7384	6.6457	6.7037	6.7532	6.4406	6.5191	6.6332	6.6397	6.6406	6.5945	6.6385	6.6140	6.6175	6.0966	6.2416	6.2111	6.1456
Ti	0.1468	0.1430	0.1350	0.1238	0.1104	0.1197	0.1340	0.1124	0.1304	0.1565	0.1229	0.0420	0.0341	0.0410	0.0602	0.0420	0.0433	0.0437	0.4581	0.2491	0.2037	0.2372
Al	2.4865	2.4854	2.4980	2.5107	2.1751	2.1622	2.1820	2.1901	2.1016	2.5323	2.4649	2.2320	2.2484	2.3233	2.2493	2.2765	2.2399	2.2944	2.7594	2.8082	2.8184	2.8719
Fe(t)	1.6270	1.5893	1.5518	1.5536	1.2625	1.2037	1.2292	1.1842	1.2002	1.1428	1.1222	0.4976	0.4373	0.5026	0.4522	0.4734	0.4638	0.4613	1.0922	1.1007	1.1838	1.1420
Mn	0.0007	0.0000	0.0000	0.0268	0.0117	0.0000	0.0230	0.0143	0.0342	0.0265	0.0208	0.0237	0.0000	0.0068	0.0000	0.0000	0.0000	0.0195	0.0284	0.0000	0.0002	0.0117
Mg	3.0398	3.0645	3.0077	3.0316	3.5109	3.5143	3.5887	3.6202	3.4999	3.3677	3.4581	4.3258	4.3403	4.3130	4.3924	4.3269	4.3835	4.3840	3.2314	3.2468	3.2076	3.3311
Ca	1.5026	1.4986	1.5230	1.5170	1.5889	1.5828	1.5984	1.5752	1.5553	1.5458	1.5994	1.8469	1.8304	1.7286	1.8454	1.8002	1.7916	1.7725	1.8525	1.7822	1.8630	1.8692
Na	1.0895	1.1354	1.2021	1.1604	1.1039	1.0327	0.9743	0.9671	1.1051	1.1398	0.9766	0.6782	0.8684	0.7164	0.8158	0.7474	0.7893	0.8612	0.7081	0.8816	0.7244	0.7002
K	0.2352	0.2617	0.2618	0.2903	0.2917	0.3083	0.2871	0.2861	0.2658	0.3122	0.2921	0.1737	0.1587	0.1973	0.1668	0.1944	0.1879	0.1753	0.1974	0.1855	0.1928	0.1969
Cr	0.0262	0.0093	0.0179	0.0294	0.0449	0.0434	0.0376	0.0154	0.0212	0.0286	0.0524	0.0906	0.0860	0.0666	0.0549	0.0673	0.0656	0.0309	0.0546	0.0849	0.0833	0.0826
Ni	0.0006	0.0000	0.0000	0.0311	0.0000	0.0000	0.0139	0.0000	0.0000	0.0248	0.0329	0.0459	0.0000	0.0030	0.0334	0.0513	0.0386	0.0144	0.0124	0.0157	0.0870	0.0000
P	0.0062	0.0274	0.0138	0.0219	0.0218	0.0017	0.0109	0.0000	0.0177	0.0308	0.0289	0.0000	0.0117	0.0024	0.0000	0.0000	0.0000	0.0000	0.0000	0.0000	0.0000	0.0000
S	0.0052	0.0016	0.0038	0.0295	0.0005	0.0000	0.0000	0.0130	0.0098	0.0180	0.0000	0.0000	0.0000	0.0117	0.0066	0.0001	0.0203	0.0066	0.0000	0.0000	0.0058	0.0000
Sum	16.7029	16.7400	16.7628	16.7828	16.7828	16.7828	16.7828	16.6816	16.6944	16.7664	16.6903	16.5895	16.6549	16.5534	16.6714	16.6182	16.6379	16.6812	16.4911	16.5963	16.5813	16.5884

Table 6.9. Continued.

C) Calcutteroo

Sample	Trwi N 10			Trwi N 8	Trwi CH 3		Trwi CB 4		Trwi CH 7					Trwi CX 14			Trwi CH 4		Trwi CH 5		
Lithology	Eclog.			Eclog.	Cpx granul.		Cpx granul.		Two Px granul.					Transi. granul.			Pyroxenit.		Pyroxenit.		
SiO2	41.80	42.39	42.24	41.05	42.33	42.28	44.98	44.86	45.07	40.82	39.52	40.03	39.58	43.22	42.69	42.40	44.27	44.60	44.23	44.86	44.69
TiO2	1.09	0.97	1.25	1.30	0.65	0.89	1.09	1.02	1.33	0.67	1.10	0.83	1.02	1.18	1.23	1.30	0.10	0.12	1.14	1.10	1.07
Al2O3	14.84	15.10	14.95	15.77	13.01	13.51	11.23	11.55	11.38	17.52	18.00	17.77	17.87	14.56	14.21	14.42	11.79	12.13	11.84	12.15	12.13
FeO#	7.70	7.34	7.53	8.91	3.24	3.09	6.84	6.81	6.99	6.18	6.51	6.10	6.68	7.79	8.02	7.25	3.23	3.17	7.08	6.85	6.46
MnO	0.14	0.23	0.25	0.00	0.16	0.06	0.00	0.01	0.18	0.00	0.18	0.29	0.18	0.04	0.03	0.35	0.04	0.16	0.01	0.11	0.34
MgO	14.72	13.60	14.21	12.26	18.05	18.57	17.38	17.83	16.97	16.01	15.19	15.41	15.23	14.05	14.90	15.57	18.93	19.32	16.69	15.57	16.38
CaO	10.58	10.29	10.50	10.92	11.87	12.02	10.80	10.45	10.67	10.26	10.50	10.55	10.57	10.51	10.50	10.87	12.21	12.09	10.65	10.36	10.13
Na2O	2.28	2.74	2.26	2.07	1.77	2.30	1.88	1.97	2.34	2.75	2.76	2.72	2.67	2.24	2.46	2.45	1.98	2.38	1.88	2.20	2.28
K2O	1.02	1.08	1.08	1.57	1.08	1.09	0.52	0.68	0.52	0.56	1.00	1.04	0.84	0.55	0.47	0.44	1.11	1.15	0.78	0.76	0.76
Cr2O3	0.52	0.30	0.48	0.37	1.50	1.25	0.58	0.56	0.55	0.50	0.44	0.38	0.48	0.18	0.25	0.04	1.86	1.93	0.64	0.37	0.77
NiO	0.42	0.37	0.27	0.23	0.05	0.17	0.51	0.23	0.38	0.00	0.01	0.13	0.29	0.34	0.00	0.68	0.19	0.36	0.08	0.20	0.07
P2O3	0.00	0.06	0.08	0.00	0.31	0.00	0.05	0.00	0.00	0.05	0.00	0.00	0.07	0.01	0.05	0.00	0.00	0.33	0.00	0.06	0.00
SO3	0.01	0.00	0.10	0.16	0.00	0.10	0.09	0.10	0.00	0.00	0.00	0.08	0.09	0.13	0.00	0.11	0.01	0.02	0.00	0.00	0.01
Total	95.11	94.46	95.21	94.61	94.02	95.32	95.94	96.06	96.37	95.30	95.21	95.33	95.56	94.79	94.82	95.88	95.72	97.74	95.01	94.58	95.09
									Number of Ions on the Basis of 24(O)												
Si	6.4676	6.5791	6.5088	6.4249	6.5146	6.4340	6.8253	6.7919	6.8244	6.2275	6.0876	6.1446	6.0781	6.6503	6.5844	6.4845	6.7016	6.6204	6.7857	6.8891	6.8300
Ti	0.1266	0.1126	0.1449	0.1534	0.0751	0.1014	0.1244	0.1159	0.1509	0.0773	0.1278	0.0957	0.1180	0.1366	0.1420	0.1488	0.0115	0.0136	0.1312	0.1275	0.1232
Al	2.7056	2.7607	2.7142	2.9092	2.3584	2.4230	2.0081	2.0609	2.0310	3.1500	3.2670	3.2140	3.2339	2.6392	2.5824	2.5994	2.1026	2.1214	2.1408	2.1986	2.1835
Fe(t)	0.9960	0.9521	0.9694	1.1656	0.4162	0.3928	0.8681	0.8612	0.8844	0.7876	0.8379	0.7828	0.8570	1.0018	1.0336	0.9268	0.4093	0.3937	0.9082	0.8797	0.8251
Mn	0.0181	0.0306	0.0331	0.0004	0.0213	0.0081	0.0000	0.0009	0.0230	0.0000	0.0241	0.0379	0.0229	0.0050	0.0037	0.0458	0.0050	0.0196	0.0006	0.0139	0.0444
Mg	3.3929	3.1441	3.2620	2.8590	4.1386	4.2093	3.9277	4.0198	3.8266	3.6373	3.4841	3.5234	3.4843	3.2192	3.4239	3.5480	4.2680	4.2728	3.8152	3.5606	3.7288
Ca	1.7532	1.7096	1.7322	1.8307	1.9562	1.9590	1.7543	1.6943	1.7308	1.6761	1.7318	1.7345	1.7376	1.7315	1.7336	1.7798	1.9800	1.9214	1.7496	1.7042	1.6584
Na	0.6830	0.8230	0.6748	0.6261	0.5289	0.6778	0.5530	0.5786	0.6869	0.8119	0.8232	0.8103	0.7940	0.6685	0.7358	0.7249	0.5792	0.6844	0.5593	0.6544	0.6757
K	0.2014	0.2137	0.2130	0.3128	0.2127	0.2116	0.1009	0.1311	0.0999	0.1082	0.1971	0.2031	0.1642	0.1070	0.0932	0.0866	0.2140	0.2173	0.1522	0.1495	0.1473
Cr	0.0637	0.0371	0.0585	0.0462	0.1829	0.1498	0.0690	0.0674	0.0657	0.0600	0.0534	0.0465	0.0578	0.0221	0.0310	0.0049	0.2228	0.2264	0.0769	0.0443	0.0927
Ni	0.0524	0.0463	0.0330	0.0283	0.0059	0.0210	0.0627	0.0282	0.0462	0.0000	0.0007	0.0162	0.0363	0.0425	0.0000	0.0836	0.0229	0.0424	0.0102	0.0242	0.0081
P	0.0000	0.0076	0.0107	0.0000	0.0398	0.0000	0.0061	0.0000	0.0000	0.0059	0.0000	0.0000	0.0089	0.0011	0.0071	0.0000	0.0000	0.0415	0.0000	0.0072	0.0000
S	0.0010	0.0000	0.0110	0.0190	0.0000	0.0118	0.0100	0.0108	0.0000	0.0000	0.0000	0.0091	0.0104	0.0146	0.0000	0.0124	0.0013	0.0020	0.0000	0.0000	0.0010
Sum	16.4614	16.4165	16.3656	16.3756	16.4507	16.5995	16.3096	16.3612	16.3698	16.5416	16.6346	16.6180	16.6032	16.2394	16.3708	16.4454	16.5183	16.5768	16.3300	16.2531	16.3182

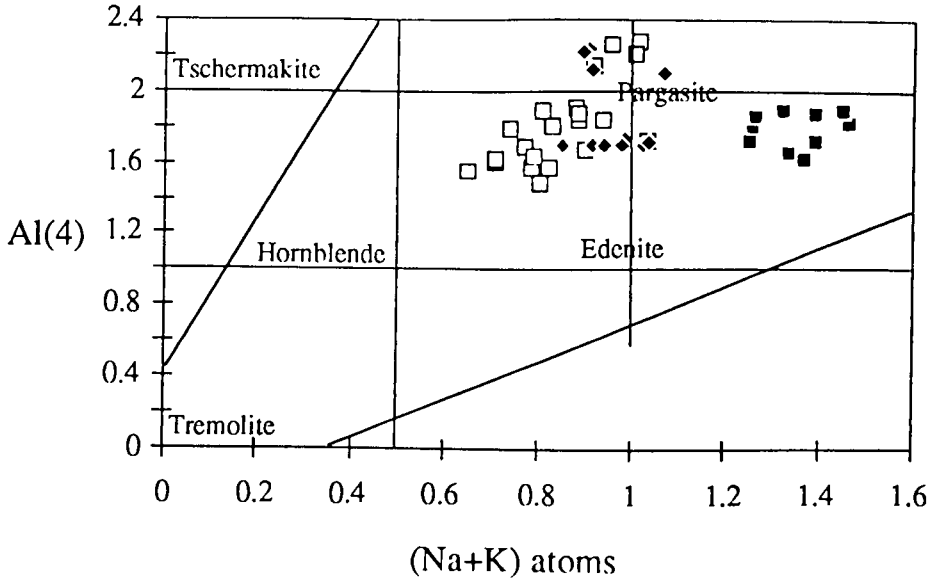

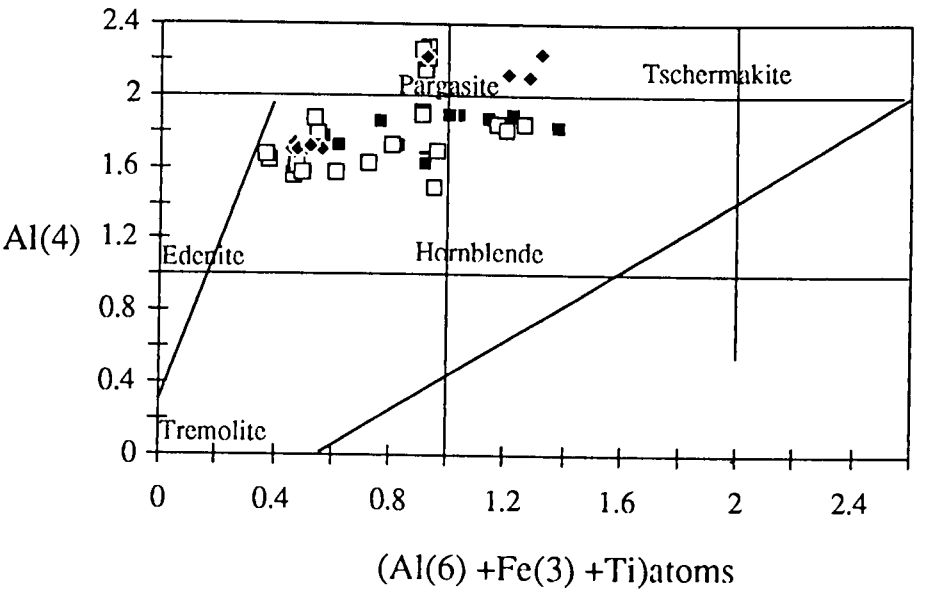

Fig. 6.6. Amphibole compositions of the South Australian xenoliths. Symbols are (■) for Port Augusta, (□) for Calcutteroo (◆) for Pine Creek.

F) Biotites

The grains occur as small flakes with minor aggregation. They are phlogopite to biotite in composition (Table 6.10). The grains of gabbroic rocks from Pine Creek show phlogopitic compositions (Mg# of 69-69.4) whereas those of feldspar-rich granulites from Pine Creek, and of clinopyroxene-granulites from Calcutteroo have biotitic compositions (Mg# of 79-86).

G) Fe-Ti, Cr Oxides

Abundant opaque oxides are found in samples from the three localities. They include chromite spinel, ulvöspinel, ilmenite, rutile and magnetite. Spinel and chromite predominate in samples from Calcutteroo and Pine Creek whereas ulvöspinel and ilmenite predominate in samples from Port Augusta. Their representative analyses are shown in Fig. 6.7 and Table 6.11.

H) The other minerals

Kyanites occur in Calcutteroo and Pine Creek xenoliths as inclusions in garnets and also as discrete grains. Apatite and epidote also occur as accessory grains.

6.5. Whole rock chemistry of the South Australian lower crustal xenoliths

Twenty-four selected samples of Calcutteroo xenolith were analysed for major and trace elements by XRF at The University of the Adelaide. Selected samples were also analysed for REE contents with Finnigan MAT 261 Mass Spectrometer at the Department of the Geology and Geophysics, The University of Adelaide. Details of sample preparation and analytical methods are shown in the Appendx 1. The results are presented in Tables 6.12, 6.13 and 6.14.

6.5.1. Major element chemistry

The Calcutteroo xenoliths range from *ne* - to *q*- normative composition (Fig. 6.8a). Eclogitic rocks have more *ne* normative composition while granulitic xenoliths have more *hy* - normative composition (Pearson *et al.*, 1991). These total compositional ranges are similar to those of typical Victorian Newer Basalts. The xenoliths contain Mg# of 40-81 (mainly, < 64), SiO_2 of 43-51 (mainly, 47-50), Al_2O_3 of 11-21 (mainly, 12-15), K_2O of 0.03-0.38 (mainly, <0.3) and CaO of 9-15 (mainly 11-13). The low K_2O of the xenoliths are distinct from both Victorian and South Australian Cainozoic basalts. This suggests that the xenoliths may be basaltic cumulates with little interstitial melts or K_2O lost during the metasomatism as mentioned by O'Reilly *et al.* (1988).

Table 6.10. Representative biotite analyses of the Pine Creek and Calcutteroo xenoliths.

Sample	Pinc X 7					Pinc X 6	Trwi CX 8		
Lithology	Fd. granul.					Amphibo.	Eclog.		
SiO2	36.39	35.67	36.52	35.82	35.45	36.49	37.57	38.92	37.30
TiO2	3.57	3.12	3.10	3.37	3.47	0.65	3.83	3.78	4.20
Al2O3	17.36	17.52	16.36	16.98	17.04	14.50	17.29	17.91	16.53
FeO#	7.38	8.27	6.43	6.73	7.51	13.85	7.39	7.16	7.44
MnO	0.39	0.20	0.20	0.00	0.04	0.15	0.00	0.17	0.14
MgO	21.51	20.03	21.95	20.50	20.19	17.32	16.82	16.19	16.54
CaO	0.24	0.27	0.22	0.18	0.36	0.24	0.11	0.13	0.21
Na2O	0.00	0.29	0.00	0.00	0.00	0.00	0.12	0.17	0.00
K2O	8.57	9.23	9.14	9.49	9.46	9.31	9.42	9.26	9.66
Cr2O3	0.10	0.00	0.00	0.30	0.08	0.07	0.28	0.00	0.11
NiO	0.05	0.28	0.09	0.62	0.19	0.05	0.00	0.32	0.10
P2O5	0.77	0.70	0.67	0.88	1.05	0.62	0.82	0.59	0.69
SO3	0.19	0.00	0.05	0.00	0.23	0.01	0.00	0.17	0.26
Total	96.52	95.59	94.70	94.87	95.08	93.25	93.65	94.76	93.18
				Number of Ions on the Basis of 24 (O)					
Si	5.6242	5.6290	5.7475	5.6617	5.5962	6.0515	5.9708	6.0851	5.9785
Ti	0.4144	0.3700	0.3664	0.4005	0.4114	0.0812	0.4576	0.4439	0.5061
Al	3.1606	3.2582	3.0343	3.1624	3.1690	2.8324	3.2389	3.2987	3.1218
Fe(t)	0.9539	1.0910	0.8453	0.8890	0.9910	1.9191	0.9812	0.9354	0.9970
Mn	0.0512	0.0272	0.0261	0.0000	0.0056	0.0209	0.0000	0.0222	0.0195
Mg	4.9521	4.7090	5.1460	4.8276	4.7482	4.2780	3.9832	3.7700	3.9483
Ca	0.0394	0.0454	0.0364	0.0308	0.0613	0.0426	0.0190	0.0218	0.0360
Na	0.0000	0.0879	0.0000	0.0000	0.0000	0.0000	0.0374	0.0504	0.0000
K	1.6896	1.8570	1.8344	1.9117	1.9050	1.9681	1.9082	1.8460	1.9731
Cr	0.0118	0.0000	0.0000	0.0379	0.0101	0.0091	0.0349	0.0000	0.0143
Ni	0.0067	0.0351	0.0112	0.0782	0.0241	0.0071	0.0000	0.0398	0.0124
P	0.1008	0.0938	0.0887	0.1175	0.1401	0.0862	0.1106	0.0780	0.0932
S	0.0214	0.0000	0.0056	0.0000	0.0277	0.0016	0.0000	0.0205	0.0313
Sum	17.0260	17.2037	17.1419	17.1173	17.0897	17.2979	16.7418	16.6118	16.7316

FeO# as total FeO

Table 6.11a. Representative spinel analyses of the Calcutteroo and Pine Creek xenoliths.

a) Calcutteroo

Sample	Trwi CH 7				Trwi CB 3				Trwi CH 5				
Lithology	Pyroxenit.				Pyroxenit.				Cpx-granul.				
SiO2	0.01	0.19	0.14	0.26	0.23	0.25	0.28	0.00	0.28	0.00	0.05	0.27	0.22
TiO2	0.08	0.00	0.16	0.17	0.01	0.15	0.01	0.00	0.05	0.00	0.22	0.12	0.00
Al2O3	64.76	63.58	64.27	63.26	64.91	66.72	64.46	64.48	65.59	60.63	63.30	64.48	63.98
FeO	12.57	13.87	14.08	10.16	9.78	11.53	12.32	10.97	10.40	16.93	11.38	10.17	10.43
Fe2O3	0.00	0.21	1.11	3.40	2.39	0.00	3.14	2.73	1.06	4.80	3.45	3.40	3.04
MnO	0.07	0.22	0.14	0.27	0.00	0.00	0.11	0.19	0.07	0.37	0.24	0.09	0.00
MgO	19.89	18.98	19.23	20.95	21.63	21.58	20.27	20.13	21.72	16.25	20.69	21.20	21.15
CaO	0.00	0.00	0.06	0.00	0.00	0.00	0.00	0.05	0.03	0.00	0.10	0.03	0.00
Na2O	0.00	0.00	0.00	0.00	0.00	0.00	0.00	0.00	0.00	0.00	0.00	0.00	0.00
K2O	0.00	0.00	0.00	0.00	0.00	0.00	0.00	0.01	0.00	0.00	0.00	0.00	0.00
Cr2O3	1.22	1.11	0.62	0.69	0.71	0.57	0.64	1.04	0.95	1.10	0.30	0.57	0.59
NiO	0.89	0.71	0.66	0.14	0.14	0.75	0.26	0.00	0.46	0.16	0.63	0.00	0.31
P2O5	0.00	0.00	0.00	0.00	0.06	0.00	0.00	0.00	0.00	0.12	0.00	0.00	0.00
SO3	0.04	0.02	0.00	0.00	0.00	0.00	0.00	0.11	0.00	0.18	0.29	0.16	0.09
Total	99.53	98.90	100.46	99.30	99.86	101.54	101.49	99.70	100.62	100.54	100.65	100.49	99.79
	Number of Ions on the Basis of 32(O)												
Si	0.0014	0.0383	0.0282	0.0542	0.0467	0.0489	0.0557	0.0000	0.0557	0.0000	0.0107	0.0544	0.0445
Ti	0.0122	0.0000	0.0237	0.0266	0.0007	0.0217	0.0009	0.0000	0.0074	0.0000	0.0336	0.0183	0.0000
Al	15.5485	15.4767	15.4541	15.2890	15.4432	15.5578	15.3443	15.4991	15.4573	15.0871	15.1974	15.3416	15.3501
Fe(2)	2.1404	2.3819	2.3846	1.7268	1.6396	1.9079	2.0611	1.8616	1.7286	2.9571	1.9224	1.7060	1.7600
Fe(3)	0.0000	0.0318	0.1695	0.5201	0.3606	0.0000	0.4731	0.4168	0.1588	0.7541	0.5248	0.5135	0.4626
Mn	0.0123	0.0392	0.0246	0.0463	0.0000	0.0002	0.0189	0.0325	0.0126	0.0654	0.0410	0.0157	0.0000
Mg	6.0383	5.8413	5.8463	6.4000	6.5070	6.3609	6.0990	6.1154	6.4710	5.1113	6.2797	6.3768	6.4151
Ca	0.0000	0.0000	0.0127	0.0000	0.0000	0.0000	0.0000	0.0100	0.0063	0.0000	0.0208	0.0071	0.0000
Na	0.0000	0.0000	0.0000	0.0000	0.0000	0.0000	0.0000	0.0000	0.0000	0.0000	0.0000	0.0000	0.0000
K	0.0000	0.0000	0.0000	0.0000	0.0000	0.0000	0.0000	0.0037	0.0000	0.0011	0.0000	0.0000	0.0000
P	0.0000	0.0003	0.0000	0.0000	0.0107	0.0000	0.0000	0.0000	0.0000	0.0211	0.0000	0.0000	0.0000
S	0.0063	0.0033	0.0007	0.0000	0.0000	0.0000	0.0000	0.0171	0.0000	0.0290	0.0438	0.0245	0.0130
Cr	0.1961	0.1818	0.0996	0.1119	0.1132	0.0892	0.1016	0.1670	0.1503	0.1838	0.0476	0.0913	0.0941
Ni	0.1461	0.1186	0.1078	0.0233	0.0233	0.1194	0.0426	0.0000	0.0745	0.0270	0.1031	0.0000	0.0500

Table 6.11a. Continued.

b) Pinc Creek

Sample	Pinc X 5					Pinc X 4					Pinc A 2			
Lithology	Cpx granul.					Xenocr.					Transi. granul.			
SiO2	0.15	0.33	0.91	0.96	2.24	2.74	0.32	0.29	0.05	0.14	0.00	0.30	0.00	0.21
TiO2	0.12	0.05	0.29	0.37	0.13	0.14	0.00	0.09	0.02	0.03	0.12	0.44	0.50	0.57
Al2O3	66.29	65.51	63.90	63.39	62.32	60.98	66.54	66.69	65.97	66.30	60.09	59.83	58.68	59.16
FeO	11.61	12.15	12.55	12.11	12.45	12.49	11.35	11.53	11.56	11.17	19.70	19.76	18.87	20.59
Fe2O3	0.00	0.24	0.00	0.00	0.00	0.00	0.35	0.00	0.00	1.15	4.75	5.63	5.74	4.06
MnO	0.32	0.37	0.21	0.01	0.32	0.32	0.48	0.18	0.37	0.49	0.09	0.16	0.33	0.00
MgO	20.22	19.65	19.45	19.54	19.63	19.55	20.31	20.51	19.85	20.34	15.04	14.63	15.27	14.85
CaO	0.04	0.04	0.01	0.16	0.15	0.26	0.00	0.03	0.00	0.05	0.00	0.11	0.10	0.00
Na2O	0.00	0.00	0.00	0.00	0.00	0.00	0.00	0.00	0.00	0.00	0.00	0.00	0.00	0.00
K2O	0.01	0.07	0.03	0.03	0.16	0.21	0.00	0.00	0.00	0.00	0.00	0.09	0.00	0.03
Cr2O3	1.42	1.54	2.52	3.17	2.01	2.41	0.51	0.65	0.87	0.74	0.89	0.62	1.45	1.36
NiO	0.06	0.00	0.02	0.26	0.24	0.00	0.00	0.29	0.11	0.00	0.44	0.00	0.11	0.52
P2O5	0.00	0.00	0.00	0.05	0.00	0.00	0.00	0.00	0.00	0.00	0.07	0.00	0.20	0.00
SO3	0.00	0.11	0.08	0.00	0.09	0.00	0.03	0.04	0.12	0.02	0.13	0.15	0.33	0.00
Total	100.24	100.07	99.96	100.05	99.72	99.10	99.89	100.29	98.94	100.42	101.32	101.74	101.58	101.34
						Number of Ions on the Basis of 32(O)								
Si	0.0308	0.0668	0.1901	0.1950	0.4587	0.5597	0.0633	0.0574	0.0104	0.0287	0.0000	0.0641	0.0000	0.0452
Ti	0.0184	0.0080	0.0436	0.0557	0.0193	0.0215	0.0000	0.0138	0.0035	0.0046	0.0197	0.0693	0.0801	0.0907
Al	15.6676	15.5737	15.2443	15.1262	14.8965	14.6852	15.7478	15.7116	15.7751	15.6841	15.0294	14.9452	14.6848	14.8447
Fe(2)	1.9464	2.0505	2.1233	2.0510	2.1116	2.1341	1.9043	1.9268	1.9612	1.8693	3.4504	3.4602	3.3160	3.6152
Fe(3)	0.0000	0.0370	0.0000	0.0000	0.0000	0.0000	0.0528	0.0000	0.0000	0.1730	0.7483	0.8879	0.9080	0.6419
Mn	0.0543	0.0631	0.0356	0.0020	0.0541	0.0550	0.0811	0.0306	0.0633	0.0834	0.0161	0.0294	0.0598	0.0000
Mg	6.0417	5.9049	5.8668	5.8954	5.9305	5.9519	6.0766	6.1069	6.0014	6.0822	4.7560	4.6206	4.8298	4.7099
Ca	0.0095	0.0093	0.0014	0.0340	0.0321	0.0579	0.0000	0.0061	0.0007	0.0102	0.0000	0.0252	0.0216	0.0000
Na	0.0000	0.0000	0.0000	0.0000	0.0000	0.0000	0.0000	0.0000	0.0000	0.0000	0.0000	0.0000	0.0000	0.0000
K	0.0022	0.0191	0.0069	0.0000	0.0410	0.0552	0.0000	0.0000	0.0000	0.0000	0.0012	0.0244	0.0000	0.0076
Cr	0.2254	0.2460	0.4030	0.5068	0.3217	0.3887	0.0809	0.1019	0.1400	0.1177	0.1490	0.1046	0.2439	0.2286
Ni	0.0090	0.0000	0.0030	0.0425	0.0395	0.0000	0.0000	0.0471	0.0182	0.0000	0.0745	0.0000	0.0179	0.0882
P	0.0000	0.0000	0.0000	0.0083	0.0000	0.0000	0.0000	0.0006	0.0000	0.0000	0.0123	0.0000	0.0365	0.0000
S	0.0000	0.0161	0.0129	0.0000	0.0131	0.0000	0.0050	0.0061	0.0182	0.0025	0.0205	0.0239	0.0530	0.0000

Table 6.11b. Representative Fe-Ti opaque oxide analyses of the Port Augusta xenoliths.

	Spinel									
Sample	**Pa 6X 12**		**PA 9X 1**	**Pa 7X 6**		**Pa 6X 11**	**Pa CX 6**		**Pa 7X 8**	
Lithology	**Eclog.**		**Fd granul.**	**Fd granul.**		**Fd granul. Two Px granul.**			**Fd granul.**	
	exsolved lamellae						**discrete**		**between two il**	
SiO2	0.03	0.08	0.14	0.14	0.01	0.00	0.00	0.11	0.00	0.07
TiO2	29.87	28.43	22.65	23.12	29.37	30.34	32.20	32.79	0.81	0.81
Al2O3	0.81	0.55	0.23	1.12	0.32	0.78	0.52	0.60	8.78	8.88
FeO	54.55	55.27	49.90	50.82	55.78	56.93	60.85	57.59	27.28	26.33
Fe2O3	10.12	11.34	22.63	19.78	9.44	6.08	2.68	4.35	18.37	19.09
MnO	0.16	0.28	0.00	0.08	0.17	0.25	0.00	0.00	0.35	0.29
MgO	0.93	0.77	0.44	0.19	0.76	0.89	0.58	1.13	3.07	3.13
CaO	0.00	0.00	0.14	0.01	0.07	0.00	0.12	0.00	0.04	0.00
Na2O	0.51	0.00	0.12	0.26	0.00	0.00	0.07	0.46	0.31	0.40
K2O	0.07	0.03	0.00	0.00	0.00	0.00	0.10	0.00	0.05	0.03
Cr2O3	0.00	0.50	0.27	0.15	0.19	0.22	0.00	0.00	39.14	38.40
NiO	0.24	0.00	0.00	0.36	0.00	0.28	1.14	0.21	0.00	0.00
P2O5	0.00	0.00	0.00	0.01	0.00	0.00	0.00	0.02	0.20	0.00
SO3	0.69	0.01	0.00	0.00	0.00	0.03	0.00	0.00	0.05	0.00
Total	97.98	97.26	96.52	96.04	96.10	95.80	98.25	97.26	98.43	97.43
				Number of Ions on the Basis of 32(O)						
Si	0.0099	0.0257	0.0455	0.0479	0.0020	0.0000	0.0000	0.0333	0.0000	0.0208
Ti	6.9468	6.7957	5.7533	5.8239	7.0618	7.2071	7.4295	7.5607	0.1844	0.1879
Al	0.2967	0.2057	0.0911	0.4435	0.1204	0.2906	0.1872	0.2172	3.1368	3.2131
Fe(2)	13.8672	14.1304	12.9582	13.2159	14.4153	14.7071	15.3824	14.5897	7.7545	7.5068
Fe(3)	2.3145	2.6092	5.2892	4.6292	2.1965	1.4132	0.6103	0.9928	4.6983	4.8973
Mn	0.0411	0.0754	0.0000	0.0218	0.0473	0.0666	0.0000	0.0000	0.0906	0.0742
Mg	0.4284	0.3630	0.2203	0.0958	0.3606	0.4187	0.2663	0.5169	1.3862	1.4311
Ca	0.0000	0.0000	0.0517	0.0035	0.0238	0.0000	0.0377	0.0000	0.0129	0.0000
Na	0.3064	0.0000	0.0761	0.1686	0.0000	0.0000	0.0389	0.2748	0.1793	0.2372
K	0.0280	0.0138	0.0000	0.0000	0.0000	0.0000	0.0377	0.0000	0.0190	0.0116
Cr	0.0000	0.1264	0.0729	0.0386	0.0479	0.0549	0.0010	0.0000	9.3808	9.3126
Ni	0.0585	0.0000	0.0000	0.0970	0.0000	0.0722	0.2823	0.0509	0.0000	0.0000
P	0.0000	0.0000	0.0000	0.0033	0.0000	0.0000	0.0000	0.0048	0.0511	0.0000
S	0.1609	0.0026	0.0000	0.0000	0.0000	0.0080	0.0000	0.0000	0.0102	0.0000

Table 6.11b. Continued.

Ilmenite

Sample	Pa 5X 1		Pa 6X 12		Pa 6X 9		Pa 7X 1	PA 9X 1	Pa 7X 5	Pa 6X 10		Pa 7X 9		Pa 8X 3	
Lithology	Eclog.		Eclog.		Eclog.		Fd granul.	Fd granul.	Two Px granul.	Gabbro.		Gabbro.		Xenocr.	
	discrete		rim of former							rimmed by gt					
SiO2	0.09	0.00	0.00	0.00	0.14	0.04	0.12	0.23	0.02	0.00	0.00	0.07	0.01	0.03	0.00
TiO2	44.10	44.36	51.02	55.10	43.66	43.31	48.87	41.41	36.96	46.17	46.05	46.89	47.65	45.95	45.76
Al2O3	0.42	0.38	3.94	0.07	0.57	0.50	0.32	0.26	0.49	0.24	0.16	0.42	0.43	0.33	0.51
FeO	31.00	31.19	36.43	38.53	34.23	34.01	36.29	27.18	28.68	38.50	38.54	39.40	41.61	33.32	33.06
Fe2O3	20.10	20.31	2.98	0.00	16.17	16.89	8.60	24.04	31.70	12.82	12.68	11.05	9.27	15.61	15.85
MnO	0.18	0.40	0.30	0.40	0.34	0.09	0.76	0.27	0.00	0.08	0.22	0.54	0.18	0.45	0.31
MgO	3.67	3.27	5.21	5.78	2.90	2.80	3.69	5.06	1.38	1.47	1.62	1.19	1.02	4.22	4.28
CaO	0.05	0.05	0.08	0.01	0.03	0.09	0.45	0.00	0.14	0.00	0.01	0.00	0.00	0.02	0.05
Na2O	0.48	0.50	0.00	0.00	0.00	0.00	0.01	0.26	0.43	0.07	0.00	0.00	0.00	0.00	0.00
K2O	0.00	0.03	0.00	0.01	0.00	0.00	0.00	0.04	0.04	0.00	0.00	0.06	0.01	0.01	0.02
Cr2O3	0.21	0.10	0.32	0.07	0.17	0.15	0.22	1.28	0.40	0.07	0.00	0.34	0.17	0.14	0.11
NiO	0.11	0.00	0.13	0.00	0.18	0.11	0.00	0.16	0.09	0.00	0.13	0.00	0.23	0.00	0.00
P2O5	0.00	0.00	0.00	0.00	0.00	0.00	0.09	0.00	0.00	0.00	0.00	0.00	0.16	0.00	0.00
SO3	0.00	0.00	0.00	0.02	0.00	0.00	0.00	0.00	0.00	0.00	0.00	0.00	0.04	0.00	0.00
	100.40	100.59	100.42	100.00	98.37	97.99	99.41	100.20	100.32	99.41	99.41	99.96	100.77	100.08	99.96
						Number of Ions on the Basis of 6(O)									
Si	0.0049	0.0000	0.0000	0.0000	0.0072	0.0020	0.0059	0.0122	0.0008	0.0000	0.0000	0.0039	0.0006	0.0018	0.0000
Ti	1.7338	1.7460	1.8413	1.9961	1.7479	1.7469	1.8656	1.6430	1.5512	1.8257	1.8221	1.8342	1.8422	1.7838	1.7778
Al	0.0261	0.0232	0.2230	0.0042	0.0357	0.0318	0.0190	0.0160	0.0321	0.0147	0.0100	0.0256	0.0260	0.0199	0.0309
Fe(3)	0.7401	0.7493	0.1065	0.0000	0.6133	0.6443	0.3199	0.8813	1.1950	0.4867	0.4813	0.4173	0.3475	0.5770	0.5860
Mn	0.0079	0.0178	0.0123	0.0164	0.0151	0.0040	0.0326	0.0122	0.0000	0.0036	0.0097	0.0238	0.0077	0.0195	0.0138
Mg	0.2858	0.2552	0.3730	0.4150	0.2299	0.2239	0.2791	0.3981	0.1149	0.1149	0.1270	0.0925	0.0779	0.3248	0.3294
Fe(2)	1.2688	1.2786	1.4475	1.5625	1.4426	1.4415	1.4993	1.1073	1.2016	1.6240	1.6256	1.6542	1.7340	1.3691	1.3585
Ca	0.0025	0.0029	0.0039	0.0007	0.0016	0.0051	0.0247	0.0000	0.0085	0.0000	0.0006	0.0000	0.0000	0.0010	0.0025
Na	0.0483	0.0506	0.0000	0.0000	0.0000	0.0000	0.0010	0.0270	0.0466	0.0072	0.0000	0.0000	0.0000	0.0000	0.0002
K	0.0000	0.0018	0.0000	0.0005	0.0000	0.0000	0.0000	0.0026	0.0026	0.0000	0.0000	0.0038	0.0006	0.0009	0.0016
Cr	0.0085	0.0041	0.0122	0.0027	0.0071	0.0063	0.0088	0.0533	0.0177	0.0029	0.0000	0.0138	0.0070	0.0059	0.0045
Ni	0.0047	0.0000	0.0051	0.0000	0.0077	0.0048	0.0000	0.0069	0.0040	0.0000	0.0056	0.0000	0.0093	0.0000	0.0000
P	0.0000	0.0000	0.0000	0.0000	0.0000	0.0000	0.0037	0.0000	0.0000	0.0000	0.0000	0.0000	0.0071	0.0000	0.0000
S	0.0000	0.0000	0.0001	0.0008	0.0000	0.0000	0.0000	0.0000	0.0000	0.0000	0.0000	0.0000	0.0015	0.0000	0.0000

Table 6.11c. Representative rutile analyses of the South Australian lower crustal xenoliths.

A)Port Augusta

Sample	Pa 6X 12	Pa 5X 2	Pa 6X 8	Pa 6X 7	Pa 6X 7	Pa 6X 12	Pa 6X 2	Pa 6X 6	Pa 7X 1	Pa 7X 8	
Lithology	Eclog.	Eclog.	Eclog.	Eclog.	Eclog	Eclog.	Eclog.	Eclog.	Fd granul.	Fd granul.	
	inclu. of gt									core of granular gt.	
SiO2	0.08	0.08	0.01	0.04	0.00	0.08	0.08	0.00	0.00	0.00	0.12
TiO2	98.14	98.55	98.93	98.49	98.47	99.20	99.46	98.73	97.78	97.92	98.91
Al2O3	0.63	0.28	0.22	0.18	0.13	0.51	0.04	0.18	0.01	0.00	0.11
FeO#	0.64	0.58	0.40	0.86	0.97	0.34	0.34	0.56	0.85	0.10	0.06
MnO	0.25	0.13	0.20	0.00	0.00	0.04	0.06	0.20	0.19	0.07	0.00
MgO	0.01	0.06	0.00	0.09	0.24	0.19	0.04	0.16	0.10	0.09	0.26
CaO	0.08	0.03	0.00	0.46	0.40	0.03	0.01	0.03	0.56	0.04	0.00
Na2O	0.00	0.01	0.00	0.00	0.14	0.00	0.01	0.01	0.20	0.15	0.30
K2O	0.00	0.00	0.00	0.01	0.00	0.00	0.00	0.03	0.04	0.01	0.00
P2O5	0.00	0.00	0.01	0.16	0.00	0.00	0.00	0.00	0.00	0.09	0.00
SO3	0.00	0.02	0.00	0.12	0.00	0.00	0.00	0.00	0.00	0.03	0.00
Cr2O3	0.01	0.00	0.00	0.14	0.04	0.11	0.14	0.02	0.00	0.00	0.85
NiO	0.00	0.00	0.00	0.00	0.00	0.00	0.00	0.00	0.00	0.07	0.00
Total	99.85	99.72	99.75	100.53	100.39	100.50	100.29	99.95	99.74	98.57	100.62

Sample	Pa 6X 11	Pa 8X 1
Lithology	Fd granul.	Xenocr.
		inclu. of Am
SiO2	0.00	0.16
TiO2	99.24	94.35
Al2O3	0.00	0.34
FeO#	0.71	2.14
MnO	0.15	0.07
MgO	0.00	0.25
CaO	0.41	0.07
Na2O	0.52	0.00
K2O	0.00	0.00
P2O5	0.00	0.00
SO3	0.00	0.00
Cr2O3	0.00	0.00
NiO	0.00	0.00
Total	101.04	97.38

B) Calcutteroo

Trwi CX 4	Trwi N 1		Trwi CX 7	Trwi CX 8	Trwi CX 2	Trwi CX 14	
Eclog.	Eclog.		Cpx granul.	Cpx granul.	Cpx granul.	Two Px granul.	
0.00	0.00	0.00	0.08	0.02	0.00	0.00	0.08
99.97	99.15	99.07	98.50	98.54	99.55	98.50	98.20
0.11	0.32	0.26	0.27	0.24	0.19	0.24	0.24
0.16	0.37	0.26	0.25	0.34	0.62	0.54	0.26
0.01	0.00	0.00	0.00	0.00	0.21	0.27	0.05
0.00	0.00	0.08	0.09	0.00	0.01	0.30	0.00
0.13	0.00	0.00	0.00	0.20	0.00	0.08	0.02
0.11	0.50	0.11	0.00	0.00	0.00	0.24	0.00
0.01	0.02	0.04	0.00	0.01	0.10	0.00	0.01
0.06	0.07	0.00	0.05	0.13	0.00	0.00	0.15
0.00	0.01	0.01	0.03	0.00	0.00	0.08	0.00
0.18	0.18	0.01	0.10	0.00	0.00	0.00	0.14
0.00	0.11	0.00	0.00	0.00	0.01	0.00	0.00
100.73	100.74	99.77	99.36	99.48	100.68	100.26	99.14

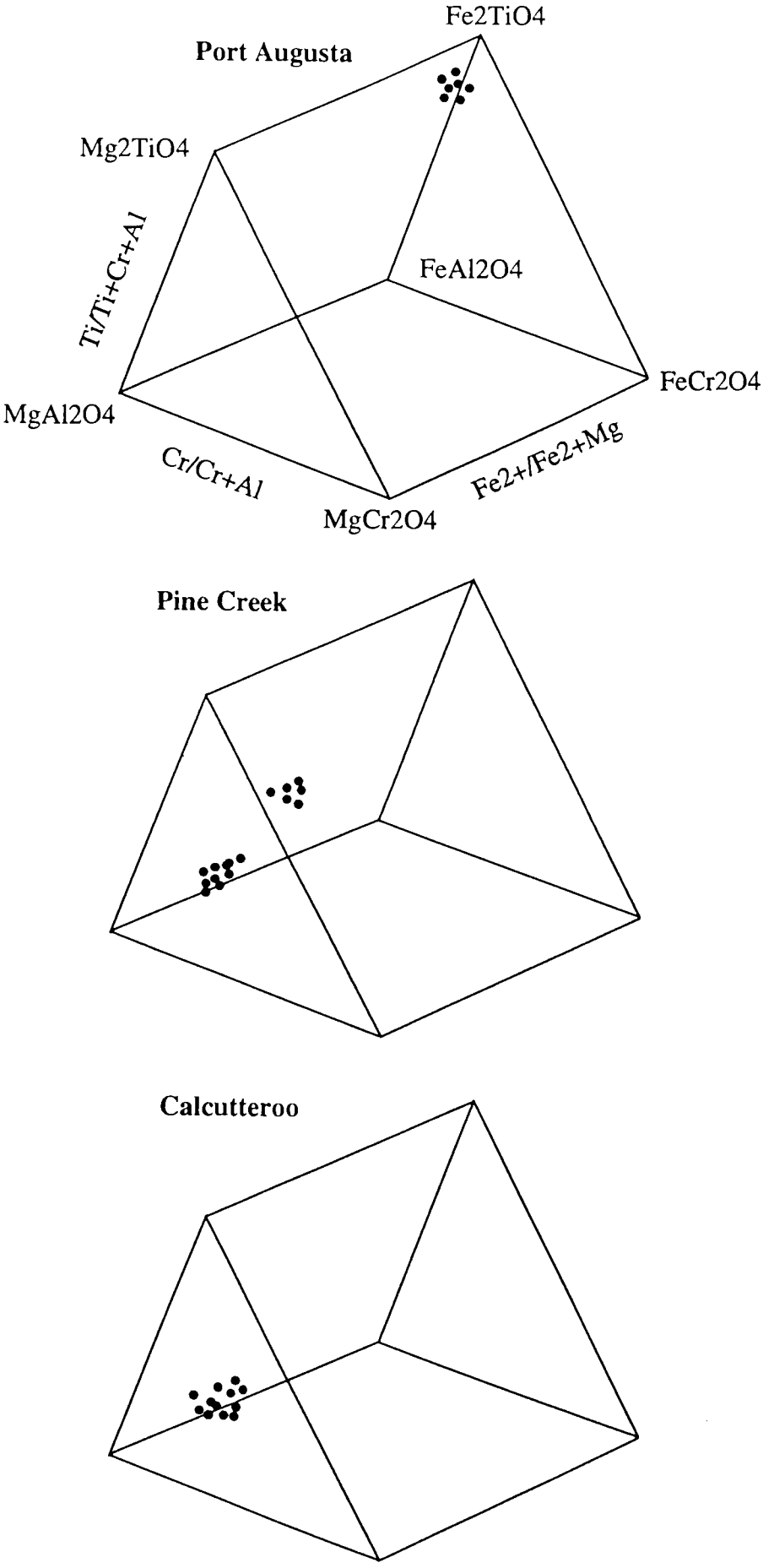

Fig. 6.7. Spinel compositions of the South Australian lower crustal xenoliths plotted in the multicomponent spinel prism.

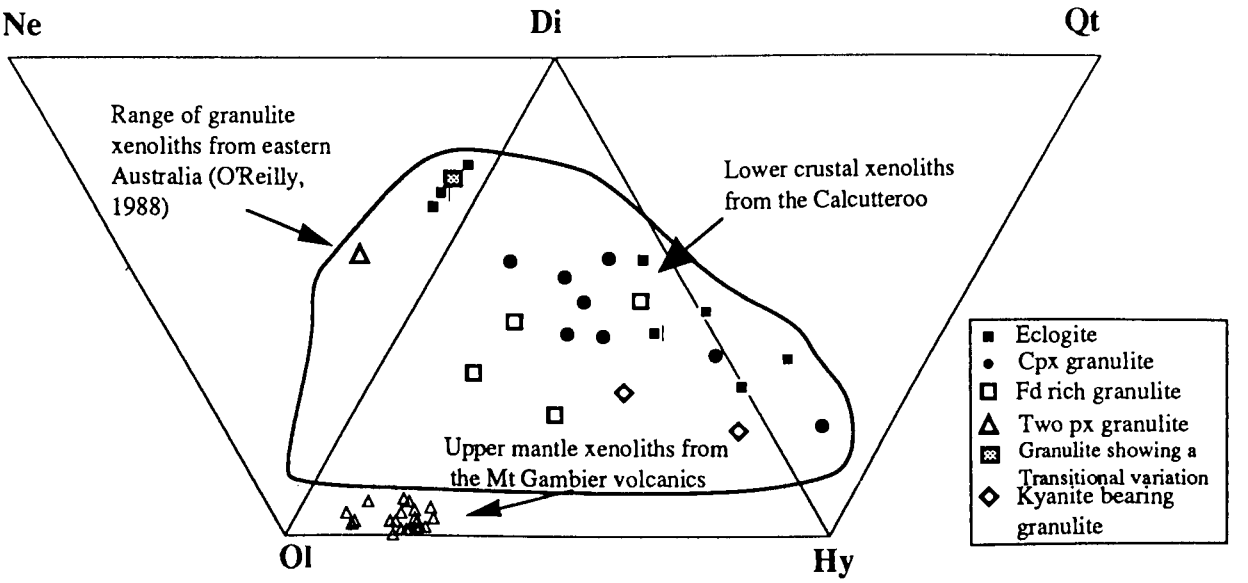

Fig. 6.8a. C. I. P.W. normative compositions of the Calcutteroo xenoliths.

In the Mg# -major element relationships (Fig. 6.8b), P_2O_5, TiO_2 and MnO decrease with Mg# while CaO and Al_2O_3 increase with Mg#. K_2O, Na_2O and SiO_2 show scattered patterns with Mg#. High and low contents of characteristic elements in particular samples may reflect their distinctive minerals. In general, high Na_2O are found in feldspar-rich granulites while high Al_2O_3 are observed in kyanite-bearing xenoliths. Abnormally high TiO_2 contents are seen in the samples showing a transitional variation while high K_2O occur in two-pyroxene granulites showing diverse stages of the exsolution textures among pyroxene, amphibole, garnet and Fe-Ti oxides.

6.5.2. Trace element and REE chemistry

These Calcutteroo xenoliths show wide ranges of Sr (35-241 ppm), Zr (4-74 ppm), Ba (65-5194 ppm), Cr (50-1800 ppm) and Ni (67-467 ppm) contents. No clear distinction in composition are shown among different types. In general, high Cr (> 250 ppm) and Ni (> 130 ppm) contents are seen in samples containing high Mg# (> 65). These characteristics are similar to those of Cainozoic Victorian and South Australian basalts. Some of them are chemically similar to the more primitive basalts of south eastern Australia, including melilitites and basanites (Ewart and Chappell, 1989). These compositions are also comparable to the lower crustal components of Taylor and McLennan (1981) which show low Ni (35 ppm) and Cr (65 ppm)

In Mg# - trace element relationships (Fig. 6.9a), Cr, Ni, Sr and Ba contents increase with Mg# while Ga, Zn, Sc, V, Ce, Rb, and Y contents decrease with Mg#. Co, La, Zr and Nb contents show slightly scattered patterns with Mg#. These good correlations of Ni, Cr, Y, V contents with Mg# may suggest that the xenoliths did not undergo significant fractional crystallisation and contamination by the continental crust.

Table 6.12. Major element analyses of the Calcutteroo xenoliths.

Sample	LCC 4	LCC 9	LCC 11	LCC 13	LCC 15	LCC 19	LCC 20	LCC 22	LCC 24	LCC 2	LCC 5	LCC 7
Lithology	Eclog.	Eclog.	Eclog.	Eclog.	Eclog.	Eclog.	Eclog.	Eclog.	Eclog.	Cpx granul.	Cpx granul.	Cpx granul.
SiO2	48.21	49.52	50.30	45.28	47.83	48.03	49.20	49.01	47.59	49.37	50.95	48.40
Al2O3	12.28	13.90	14.02	15.18	14.31	11.60	11.59	13.02	11.96	14.13	15.77	14.31
Fe2O3(t)	16.51	6.77	6.88	6.74	18.72	10.47	15.44	8.31	8.80	8.74	12.66	12.46
MnO	0.26	0.16	0.16	0.14	0.29	0.18	0.23	0.16	0.13	0.17	0.34	0.18
MgO	7.70	14.68	14.38	13.22	6.30	11.40	8.30	10.88	13.01	10.60	9.53	7.91
CaO	11.44	13.01	12.22	16.11	10.16	14.85	12.66	14.99	14.79	13.59	9.06	11.27
Na2O	1.38	0.80	0.72	1.24	1.03	2.29	1.78	2.40	2.21	1.58	1.10	2.73
K2O	0.13	0.03	0.03	0.12	0.13	0.17	0.12	0.15	0.13	0.17	0.09	0.38
TiO2	1.17	0.11	0.11	0.25	1.84	0.38	0.87	0.46	0.34	0.52	0.07	1.28
P2O5	0.03	0.01	0.02	0.03	0.14	0.02	0.04	0.03	0.02	0.04	0.01	0.11
SO3	0.00	0.00	0.00	0.04	0.00	0.00	0.00	0.00	0.01	0.00	0.00	0.00
LOI	0.15	0.63	0.64	0.88	0.00	0.58	0.15	0.56	0.75	0.57	0.14	0.78
Total	99.86	99.62	99.48	99.23	100.76	99.99	100.27	99.56	99.74	99.48	99.72	99.81
C.I.P.W. norm (calculated with Fe2O3/FeO=0.2)												
Ap	0.07	0.02	0.05	0.07	0.33	0.05	0.10	0.07	0.05	0.10	0.02	0.26
Il	2.29	0.21	0.21	0.49	3.54	0.73	1.68	0.89	0.66	1.01	0.14	2.49
Mt	3.69	1.50	1.53	1.50	4.12	2.32	3.41	1.83	1.95	1.94	2.81	2.78
Or	0.79	0.18	0.18	0.73	0.77	1.02	0.72	0.90	0.78	1.02	0.54	2.30
Ab	11.98	6.89	7.06	2.34	8.81	12.06	15.26	14.92	10.07	13.63	9.47	23.61
An	27.62	34.83	35.14	36.38	34.41	21.21	23.56	24.64	22.75	31.56	38.48	26.22
Di	25.19	24.51	21.16	36.05	13.09	43.28	32.84	40.68	41.63	29.75	5.88	24.75
Hy	26.92	25.82	33.50	0.00	30.50	0.00	20.00	0.00	0.00	15.19	37.91	5.16
Ol	0.00	6.03	1.28	17.92	0.00	15.21	2.43	13.02	17.26	5.79	0.00	12.44
Ne	0.00	0.00	0.00	4.47	0.00	4.13	0.00	3.07	4.84	0.00	0.00	0.00
Ac	0.00	0.00	0.00	0.00	0.00	0.00	0.00	0.00	0.00	0.00	0.00	0.00
C	0.00	0.00	0.00	0.00	0.00	0.00	0.00	0.00	0.00	0.00	0.00	0.00
Q	1.46	0.00	0.00	0.00	4.41	0.00	0.00	0.00	0.00	0.00	4.76	0.00
Total	100.01	99.99	100.11	99.95	99.98	100.01	100	100.02	99.99	99.99	100.01	100.01
AN#	69.75	83.49	83.27	93.96	79.62	63.75	60.69	62.29	69.32	69.84	80.25	52.62
DI	14.23	7.07	7.24	7.54	13.99	17.21	15.98	18.89	15.69	14.65	14.77	25.91
SI	32.00	67.96	67.45	64.04	25.92	48.97	34.45	52.04	55.91	52.44	43.10	35.58
LI	-17.80	-17.24	-15.99	-20.18	-17.23	-19.49	-18.33	-16.86	-19.72	-15.43	-12.91	-13.88

Notice; AN#= AN/(AN+AB)*100, S.I. (Solidification Index by Kuno), D.I. (Differentiation Index by Thornton & Tuttle,1960) & L.I. (Larsen Index by Larsen, 1938).

Sample	LCC 8	LCC 12	LCC 16	LCC 18	LCC 3	LCC 6	LCC 17	LCC 23	LCC 10	LCC 1	LCC 21	LCC 14
Lithology	Cpx granul.	Cpx granul.	Cpx granul.	Cpx granul.	Fd granul.	Fd granul.	Fd granul.	Fd granul.	Two Px granul.	Ky granul.	Ky granul.	Transi. graul.
SiO2	48.84	48.92	48.73	49.27	49.69	50.20	46.25	50.01	43.26	49.48	50.05	45.95
Al2O3	14.91	15.94	15.78	14.48	16.47	15.00	18.01	18.42	15.80	20.29	21.08	12.14
Fe2O3(t)	9.84	10.18	10.93	10.31	8.74	7.34	8.12	8.41	7.82	5.60	5.43	8.59
MnO	0.20	0.19	0.21	0.20	0.17	0.12	0.18	0.13	0.19	0.11	0.10	0.10
MgO	11.35	9.49	10.00	10.17	9.39	10.68	11.18	9.15	13.73	10.65	8.43	13.20
CaO	12.79	11.15	11.38	12.50	10.72	11.87	11.62	9.56	12.61	12.07	11.62	13.27
Na2O	1.46	2.30	2.11	1.88	2.81	2.03	1.95	2.95	2.01	1.24	2.37	2.26
K2O	0.27	0.09	0.09	0.41	0.36	0.27	0.19	0.31	0.69	0.06	0.24	0.32
TiO2	0.55	0.30	0.31	0.53	0.24	0.34	0.07	0.16	0.28	0.13	0.18	2.15
P2O5	0.04	0.01	0.02	0.05	0.01	0.03	0.02	0.02	0.05	0.01	0.02	0.04
SO3	0.01	0.00	0.00	0.00	0.02	0.05	0.53	0.09	0.02	0.00	0.03	0.00
LOI	0.40	0.70	0.50	0.56	1.14	1.19	1.44	0.72	2.38	0.36	0.56	1.38
Total	99.94	99.27	100.25	100.37	99.76	99.1	99.56	99.95	98.84	100	100.12	99.41
C.I.P.W. norm (calculated with Fe2O3/FeO=0.2)												
Ap	0.09	0.02	0.05	0.12	0.02	0.07	0.05	0.04	0.12	0.02	0.05	0.10
Il	1.05	0.59	0.60	1.02	0.47	0.67	0.14	0.22	0.56	0.25	0.35	4.21
Mt	2.16	2.27	2.42	2.27	1.95	1.65	1.82	1.32	1.78	1.23	1.19	1.92
Or	1.61	0.54	0.54	2.45	2.17	1.64	1.15	1.83	4.26	0.36	1.43	1.94
Ab	12.41	19.10	18.12	16.09	24.25	17.50	15.12	26.10	1.52	10.60	20.15	11.64
An	33.58	34.17	33.84	30.22	32.01	32.00	42.01	36.19	33.50	50.10	46.69	22.64
Di	24.25	18.25	19.08	26.13	18.08	22.79	13.86	8.80	25.21	8.22	9.17	35.68
Hy	14.92	16.12	13.63	11.54	7.20	18.71	6.22	12.64	0.00	27.52	14.22	0.00
Ol	9.92	8.84	11.76	10.17	13.84	4.93	19.11	12.76	24.27	1.70	6.72	17.52
Ne	0.00	0.00	0.00	0.00	0.00	0.00	0.00	0.00	8.76	0.00	0.00	4.34
Ac	0.00	0.00	0.00	0.00	0.00	0.00	0.00	0.00	0.00	0.00	0.00	0.00
C	0.00	0.00	0.00	0.00	0.00	0.00	0.00	0.00	0.00	0.00	0.00	0.00
Q	0.00	0.00	0.00	0.00	0.00	0.00	0.00	0.00	0.00	0.00	0.00	0.00
Total	99.99	99.9	100.04	100.01	99.99	99.96	99.48	99.9	99.98	100	99.97	99.99
AN#	73.02	64.14	65.13	65.26	56.90	64.65	73.53	58.10	95.66	82.54	69.85	66.04
DI	14.02	19.64	18.66	18.54	26.42	19.14	16.27	27.93	14.54	10.96	21.58	17.92
SI	51.75	45.10	45.38	46.79	45.97	54.53	54.20	45.80	58.51	62.69	52.93	56.15
LI	-16.44	-13.40	-14.88	-15.11	-11.05	-12.15	-14.50	-9.30	-18.27	-11.21	-8.01	-18.56

Table 6.13. Continued.

Sample	LCC 8	LCC 12	LCC 16	LCC 18	LCC 3	LCC 6	LCC 17	LCC 23	LCC 10	LCC 1	LCC 21	LCC 14
Litbology	Cpx granul.	Cpx granul.	Cpx granul.	Cpx granul.	Fd granul.	Fd granul.	Fd granul.	Fd granul.	Two Px granul.	Ky granul.	Ky granul.	Transi. graul.
Y	11	2.8	3.4	9.7	5.5	7.3	2.3	3.1	7	3.1	2.7	9.2
Sr	136.5	191.9	118.9	97.9	209.1	134.4	241.2	229.4	222.7	90	199	92.9
Rb	3.9	0.6	n.d.	3.2	3.6	1.2	n.d.	1.5	6.2	0.6	1.6	4.9
Nb	1.7	1	0.7	1.6	1	1.2	1.5	0.5	14.9	0.2	0.8	22.5
Zr	24.8	1.5	1.4	15.9	3.3	12.6	3.5	2.7	21.5	3.9	5.7	32.4
Th	n.d.	n.d.	n.d.	1.4	1.2	n.d.	0.6	n.d.	n.d.	n.d.	1.3	0.8
Pb	1.5	2	1.5	1.3	1.1	1.1	2.6	1.8	n.d.	2.1	3.1	2.2
U	n.d.	n.d.	n.d.	0.2	n.d.	n.d.	n.d.	n.d.	n.d.	n.d.	n.d.	0.8
Ga	15.7	15.8	17.1	15.2	17.9	13.7	11.3	17.6	11.4	11.9	15.8	16
Zn	66	55	50	58	46	49	21	49	42	29	33	55
Cu	79	n.d.	n.d.	151	7	183	16	n.a.	2	6	n.d.	45
Ni	189	144	169	133	185	243	126	160	284	224	154	373
Ba	765	783	337	696	1005	1077	2567	927	5194	65	218	497
Sc	38.5	40.9	40.5	41	32.1	30.2	32.4	22.3	43	24.1	21.4	42.8
Cr	318	390	469	209	260	656	364	329	1033	295	307	687
V	247.2	250.2	266.7	254.3	135.6	179.8	104.4	93.1	185.6	122.5	107.7	438.7
Co	66.6	70.8	69.4	68.2	53.8	56.1	51.3	111.3	59.4	92	58	57.5
Ce	12	5	7	14	4	12	10	8	22	4	7	5
Nd	n.d.	n.d.	n.d.	n.d.	n.d.	2	n.d.	n.d.	8	n.d.	n.d.	n.d.
La	2	1	2	4	1	2	4	2	9	n.d.	1	n.d.

n.d. indicates element not detected

Table 6.13. Trace element analyses of the Calcutteroo xenoliths.

Sample	LCC 4	LCC 9	LCC 11	LCC 13	LCC 15	LCC 19	LCC 20	LCC 22	LCC 24	LCC 2	LCC 5	LCC 7
Litbology	Eclog.	Eclog.	Eclog.	Eclog.	Eclog.	Eclog.	Eclog.	Eclog.	Eclog.	Cpx granul.	Cpx granul.	Cpx granul.
Y	17.2	5.5	5.9	3.5	26.7	15.6	13.8	7.1	8.3	9.9	1.7	25.7
Sr	80.1	82.2	91.5	145.5	35.2	47.2	99.9	110.8	61.1	137.4	56.7	206.8
Rb	9.3	n.d.	n.d.	1.8	9.8	1.7	8	0.6	n.d.	1.8	1.1	4.5
Nb	0.8	1.1	1.1	1.1	5.1	0.4	1.7	1.6	0.5	1.8	0.4	6.1
Zr	24.7	3.4	3.8	11.3	45.4	20.5	24	15.5	16.4	21	1.5	73.6
Th	0.9	n.d.	n.d.	n.d.	n.d.	1	n.d.	1.2	0.8	0.6	0.5	0.7
Pb	n.d.	1.5	n.d.	n.d.	n.d.	3.2	0.8	n.d.	2	1.3	1.5	2.1
U	n.d.	n.d.	0.4	n.d.	1.3	n.d.	0.1	n.d.	0.1	n.d.	0.3	n.d.
Ga	18.6	8.8	7.3	11	23.9	13.8	18.3	13.3	15.8	15.1	13	21.3
Zn	93	29	28	25	112	50	98	54	58	56	50	112
Cu	89	10	14	4	n.d.	n.d.	129	n.d.	n.d.	49	n.d.	n.d.
Ni	61	307	307	467	67	122	99	156	329	161	82	187
Ba	670	593	580	2914	544	379	1157	121	525	684	242	756
Sc	53.7	43.1	39	22.8	45.7	47.3	50.7	43.9	34.4	43.6	49.2	37.2
Cr	130	1266	1236	976	49	939	153	854	1778	511	185	207
V	569	195	194.8	156.6	606	285.7	569.7	247	278.1	240.9	242.4	358.6
Co	64.2	98	76.9	62.8	71.7	52.1	59.5	65.1	64.5	90	103.9	76.1
Ce	11	2	2	1	27	23	21	16	8	6	4	26
Nd	n.d.	n.d.	n.d.	n.d.	1	3	n.d.	1	n.d.	1	n.d.	13
La	2	n.d.	1	1	9	8	6	4	1	2	n.d.	10

n.d. indicates element not detected

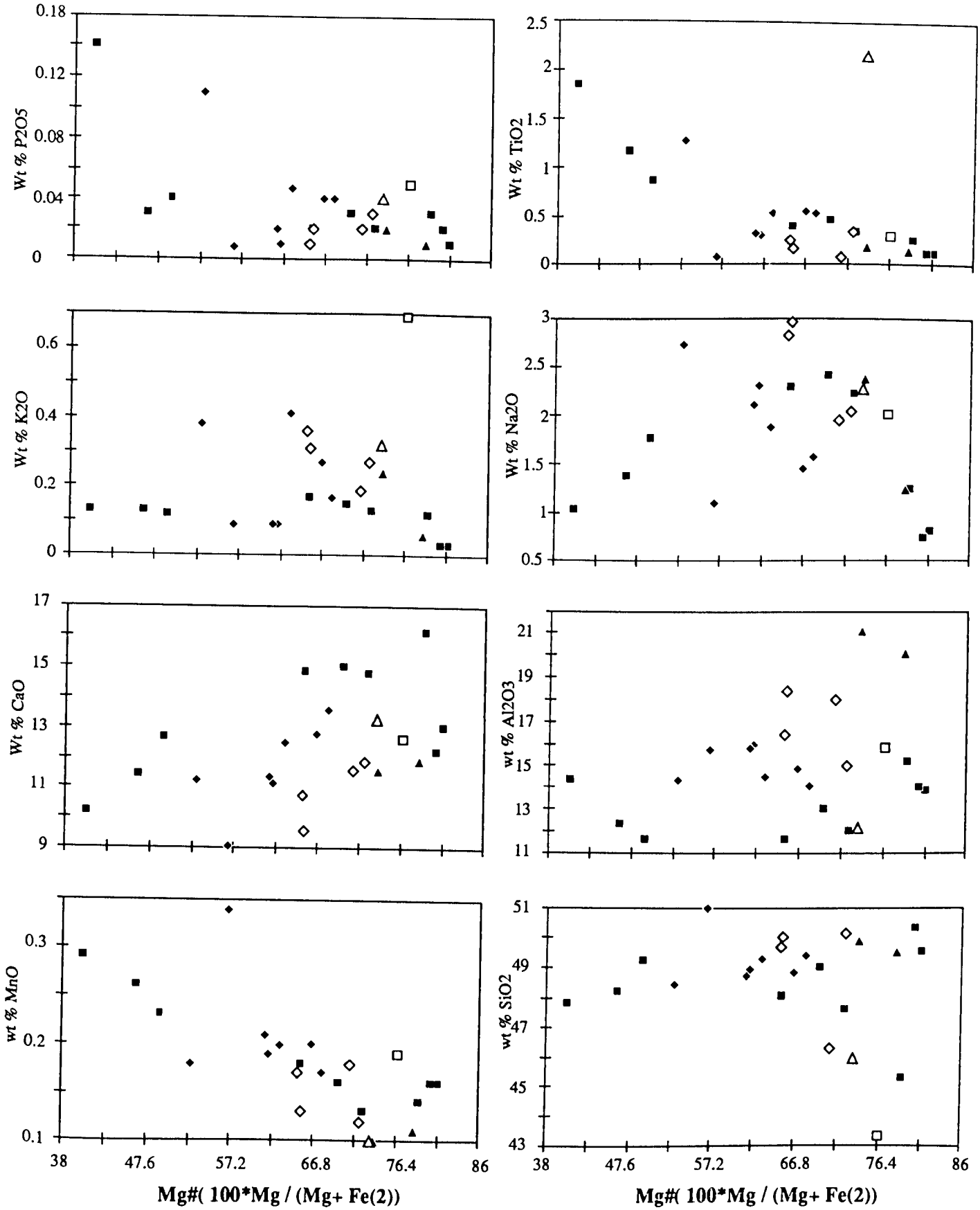

Fig. 6.8b. Major element compositions versus Mg# of the Calcutteroo xenoliths. Symbols are (■) for eclogitic rocks, (□) for a Two-Px granulite, (◆) for Cpx granulites, (◇) for Fd-rich granulites, (▲) for Kyanite bearing granulites, (Δ) for a samples showning Transitional variation.

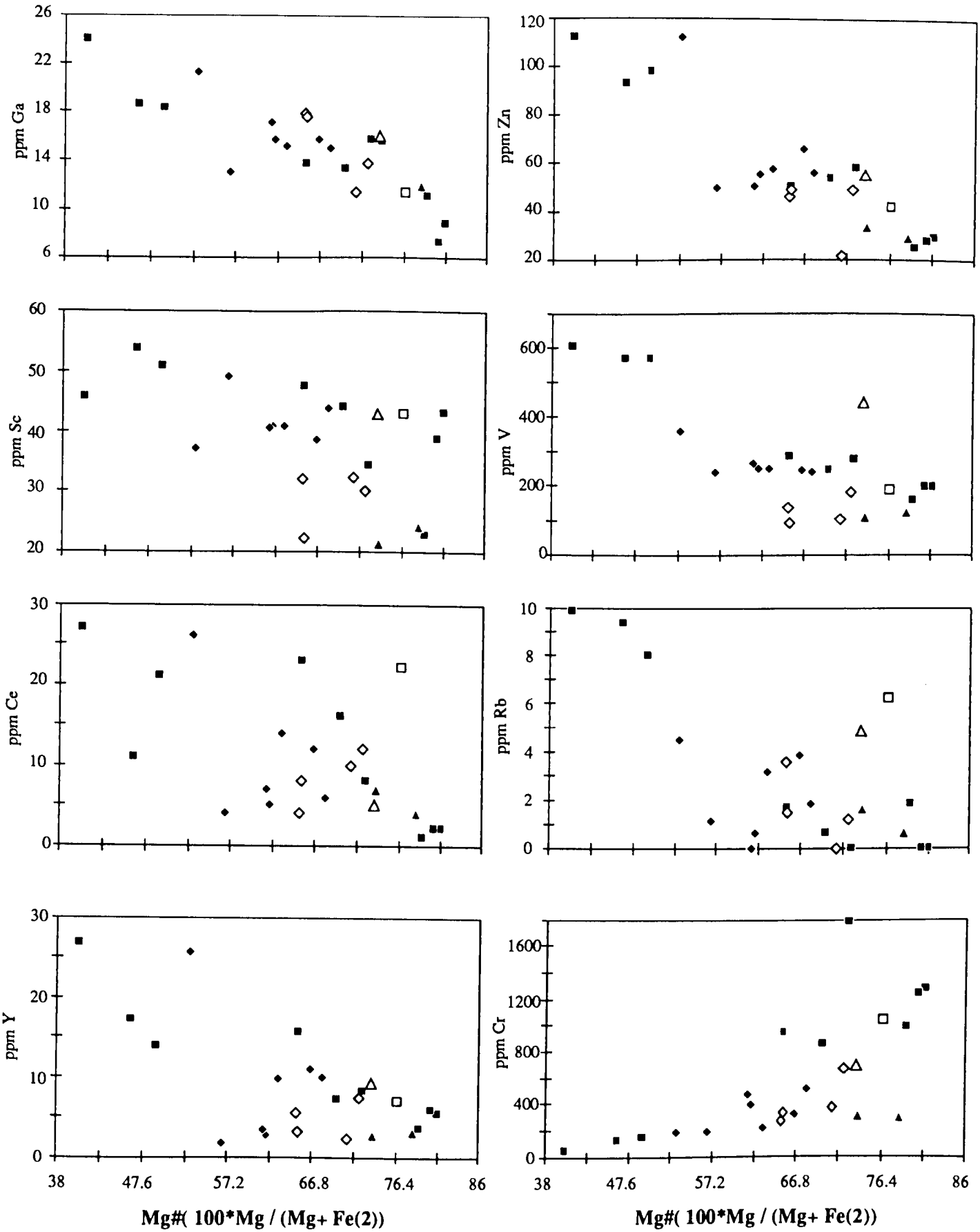
ppm Ga
26
22
18
14
10
6
ppm Zn
120
100
80
60
40
20
ppm Sc
60
50
40
30
20
ppm V
600
400
200
0
ppm Ce
30
20
10
0
ppm Rb
10
8
6
4
2
0
ppm Y
30
20
10
0
ppm Cr
1600
1200
800
400
0
38
47.6
57.2
66.8
76.4
86
Mg#(100*Mg / (Mg+ Fe(2))
Mg#(100*Mg / (Mg+ Fe(2))

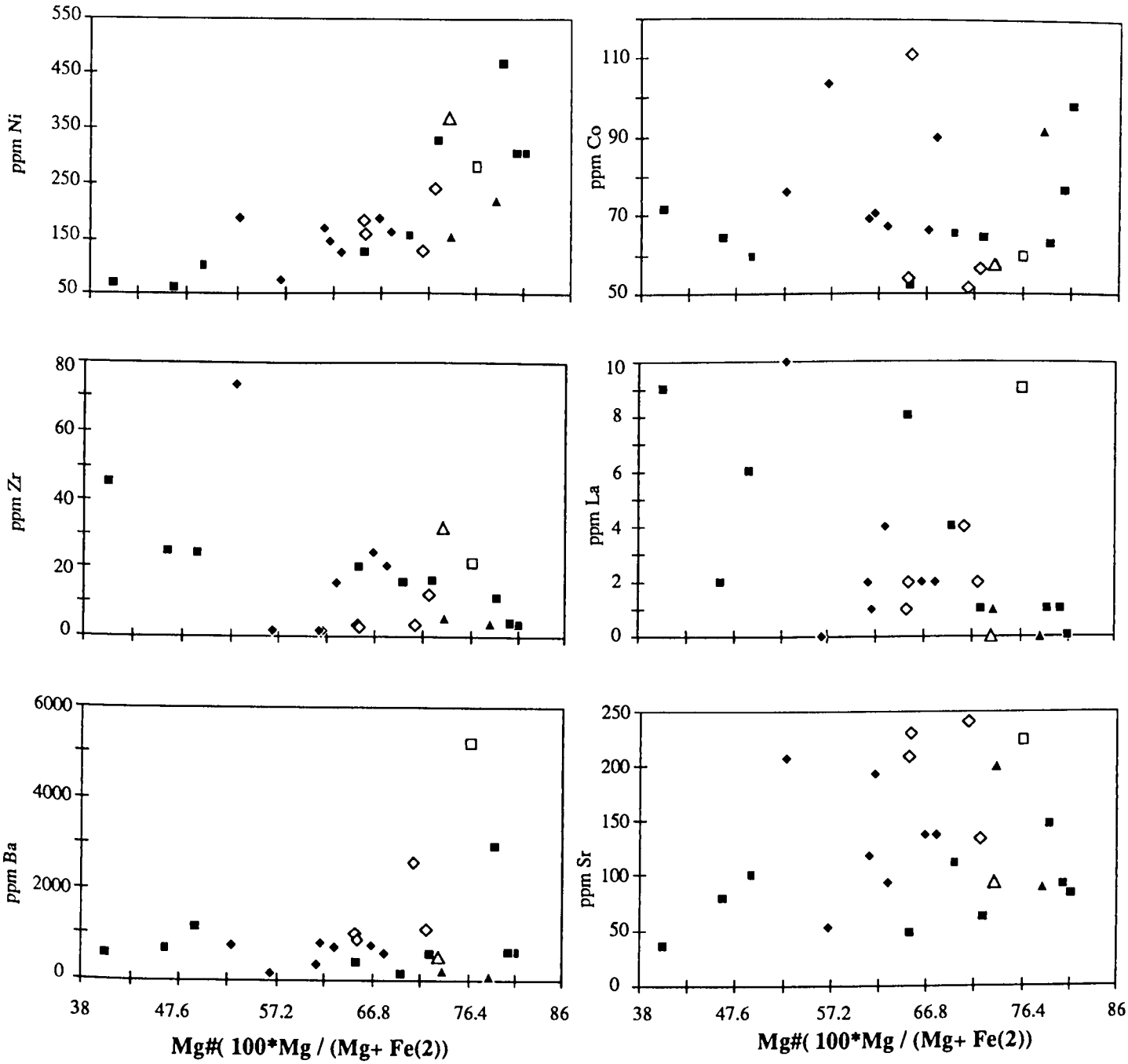

Fig. 6.9. Trace element compositions versus Mg# of the Calcutteroo xenoliths.

High Sc contents are found in the abundant amphibole bearing eclogitic rocks while wider range of Sc contents are shown in granulities with variable pyroxene abundances. Sc contents may reflect accumulation of clinopyroxenes in premetamorphic origin. High Rb contents are seen in abundant plagioclase-bearing granulites and amphibole-bearing eclogitic rocks while high Y contents are shown at abundant amphibole bearing eclogitic rock and clinopyroxene-granulites. In the eclogitic rocks, samples containing high garnet/ clinopyroxene ratios have low Cr and Ni contents. In the granulites, a sample showing a transitional variation and two-pyroxene granulites show a slightly high Ni contents.

High Co contents are shown in eclogitic rocks. High Zr contents are shown at the clinopyroxene-granulites and eclogites containing amphibole or amphibole exsolution, while high Nb contents are seen in the samples showing transitional mineralogy and two-pyroxene granulites. Slightly high Sr contents are observed in feldspar-rich granulites and two-pyroxene granulites. In clinopyroxene-granulites, high Sr contents are shown in the sample containing abundant amphiboles and Fe-Ti oxides. Abnormally high Ba and Ce contents are shown in two-pyroxene granulites showing complicated exsolution textures among amphibole, orthopyroxene and Fe-Ti oxides.

Trace element abundances of the Calcutteroo xenoliths has been compared with available trace element data for lower crustal xenoliths and granulitic facies metamorphic rocks in Fig. 6.10 (Weaver and Tarney, 1981; Rudnick *et al.*, 1986; Griffin *et al.*, 1987; Rudnick and Taylor, 1987; Arculus *et al.*, 1988; O'Reilly and Griffin, 1988; Griffin *et al.*, 1988; Jaques *et al.*, 1990).

The Calcutteroo xenoliths are characterised by a distinctive enrichment in the Ba and pronounced depletion in P, Zr, Ti and Y. Pronounced depletion in Zr is found in clinopyroxene-granulites showing a distinctive aggregation of garnet grains while less pronounced enrichments in Sr are observed in feldspar-rich and kyanite-bearing granulites. Abnormally high Ba contents are observed in two-pyroxene granulites.

Ba enrichment patterns are obtained for xenoliths from El Almein, White Cliff and South Africa despite no clear variations of total contents are evidenced in the samples from the different localities (Griffin *et al.*, 1979; Rudnick and Taylor, 1987; Arculus *et al.*, 1988). Xenoliths from McBride, Queensland and basic metamorphic granulites show more Victorian pyroxenitic patterns (Griffin *et al.*, 1988).

The Calcutteroo xenoliths show considerably different incompatible element patterns to typical granulite facies metamorphic rocks (Weaver and Tarney, 1981), suggesting that the origin of their trace element abundances can not be explained similarly to those of Calcutteroo xenoliths. The different trace element patterns in the El Almein,White Cliff and Calcutteroo xenoliths in comparisons to those of eastern Australia may reflect of trace element abundances at the lower crustal level even though these xenoliths composition can not be representatives of the volumetrically dominant lower crustal components in each area.

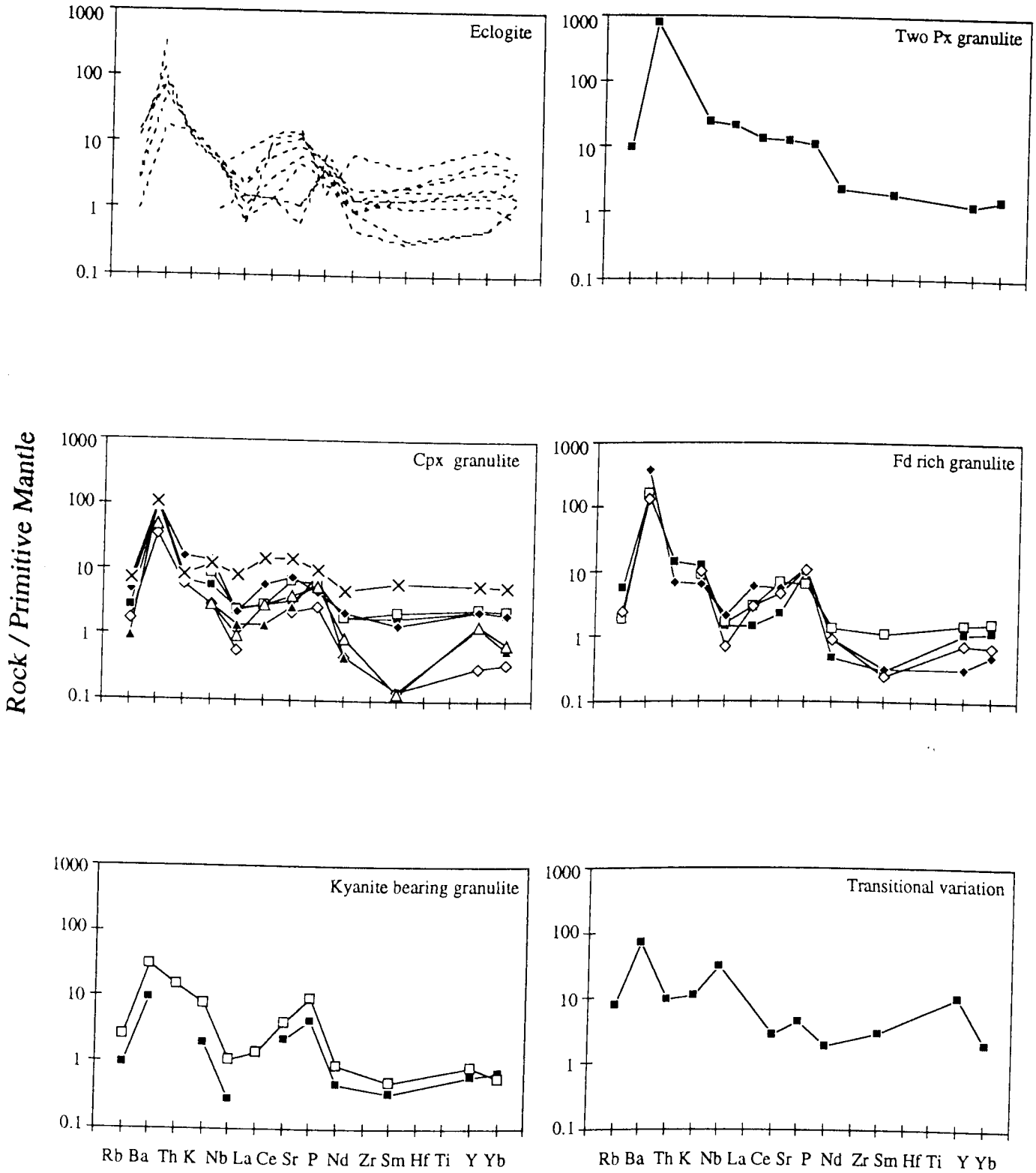

Fig. 6.10a. Trace element abundances of the Calcutteroo xenoliths.

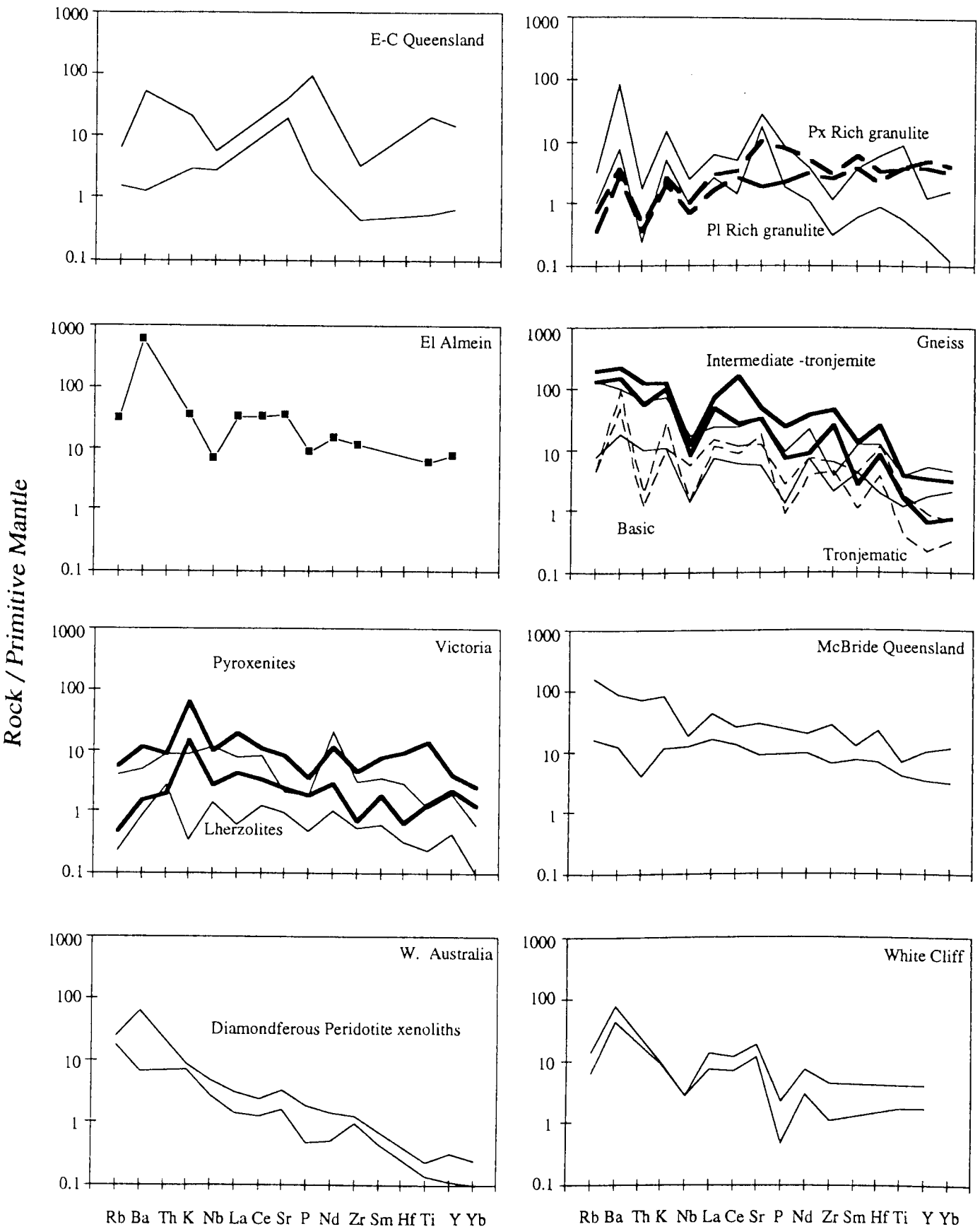

Fig. 6.10b. Trace element abundances of xenoliths from different sources (PM from Sun and McDonough, 1989). See text for data sources.

These differences in trace element abundance patterns could be explained by dominant petrological differences in the low crust level between the western side and the eastern side along Tasman line.

Primitive mantle normalised REE abundances of the Calcutteroo xenoliths have been compared with available REE data for lower crustal xenoliths and granulitic facies metamorphic rocks in Fig. 6.11 (Weaver and Tarney, 1981; Rudnick *et al.*, 1986; Rudnick and Taylor, 1987; Griffin *et al.*, 1988; O'Reilly and Griffin, 1988). The Calcutteroo xenoliths show abnormally strong LREE depletion or enrichment patterns relative to HREE. The similar strongly depleted LREE patterns have been reported in granulite xenoliths in Minas Gerais State, Brazil (Esperanca *et al.*, 1993). Clinopyroxenes of the Calcutteroo xenoliths show a LREE enrichment relative to HREE. In general, clinopyroxenes from the eclogites show a depletion in La, Ce and Eu relative to those from the clinopyroxene-granulites.

The REE patterns of the South Australian xenoliths are comparable to those of eastern Australia and granulitic metamorphic rocks. Similar REE patterns are shown in pyroxene rich Chudleigh xenoliths and McBride xenoliths, Queensland (Rudnick and Taylor, 1987), basic metamorphic granulites (Weaver and Tarney, 1981) and Victorian pyroxenites (Griffin *et al.*, 1988). In the Calcutteroo xenoliths, two-pyroxene granulites show a more Victorian pyroxenitic REE pattern. No Eu anomalies are found in the Calcutteroo xenoliths as shown those of Chudleigh plagioclase rich granulites and Tronjaematic metamorphic rocks. Possibly Eu anomaly of the latter two rocks may reflect existences of plagioclase.

6.5.3. Isotopic composition

Selected samples were analysed for Nd-Sm and Sr-Rb isotopic compositions with Finnigan MAT 261 Mass Spectrometer of the Department of Geology and Geophysics, The University of Adelaide. Details of sample preparations and analytical methods are given in the Appendex 1. Results are given in Table 6.15 and are plotted together with available analyses in Fig. 6.12. (McCulloch *et al.*, 1982; Menzies *et al.*, 1983; Ben Othman *et al.*, 1984; Rudnick *et al.*, 1986; McDonough and McCulloch., 1987; Griffin *et al.*, 1987; Walker *et al.*, 1989; McDonough *et al.*, 1991).

The Calcutteroo eclogitic-and granulitic xenoliths are characterised by considerable variations of the Nd and Sr isotopic compositions. They show εNd ratios of -8 - + 6 for whole rock (-7 -+1 for clinopyroxene) and $^{87}Sr/^{86}Sr$ ratios of 0.7063-0.7124 for whole rock (0.7046 - 0.7106 for clinopyroxene). They also have $TNd_{(DM)}$ ages of 846-2050 Ma for whole rock and of 976 to 1710 Ma for clinopyroxene. In addition, Rb/Sr ratios range from 0.008 to 0.04 and Sm/Nd ratios range from 0.2 to 0.48.

These isotopic ranges generally overlap with those of Victorian and Queensland xenoliths, but are different from those of granulite facies rocks (Fig. 6.13).

Table 6.14. REE analyses of the Calcutteroo xenoliths.

Sample	LCC 2	LCC 5	LCC 8	LCC 10	LCC 12	LCC 13
PPM	Whole rocks of the Calcutteroo xenoliths					
La	0.55	0.46	2.88	7.28	0.72	0.93
Ce	5.35	0.72	8.26	15.78	1.38	2.24
Nd	3.53	0.24	5.07	6.83	0.73	1.25
Sm	1.10	0.12	1.36	1.36	0.48	0.48
Eu	0.43	0.21	0.48	0.47	0.18	0.24
Gd	1.47	0.27	1.16	0.82	0.39	0.50
Dy	1.53	0.34	1.73	1.13	0.51	0.49
Er	0.93	0.23	1.01	0.63	0.36	0.29
Yb	0.78	0.24	0.89	0.59	0.34	0.26

LCC 2	LCC 5	LCC 8	LCC 12	LCC 13
Clinopyroxene of the Calcuretteroo xenoliths				
1.47	1.08	2.28	0.85	0.39
5.32	2.75	7.94	2.31	1.25
4.57	1.98	6.50	1.13	1.46
1.31	0.54	1.53	0.28	0.69
0.36	0.21	0.41	0.17	0.17
0.10	0.36	0.26	0.52	0.30
0.40	0.24	0.43	0.12	0.11
0.14	0.12	0.21	0.05	0.04
0.09	0.09	0.13	0.02	0.02

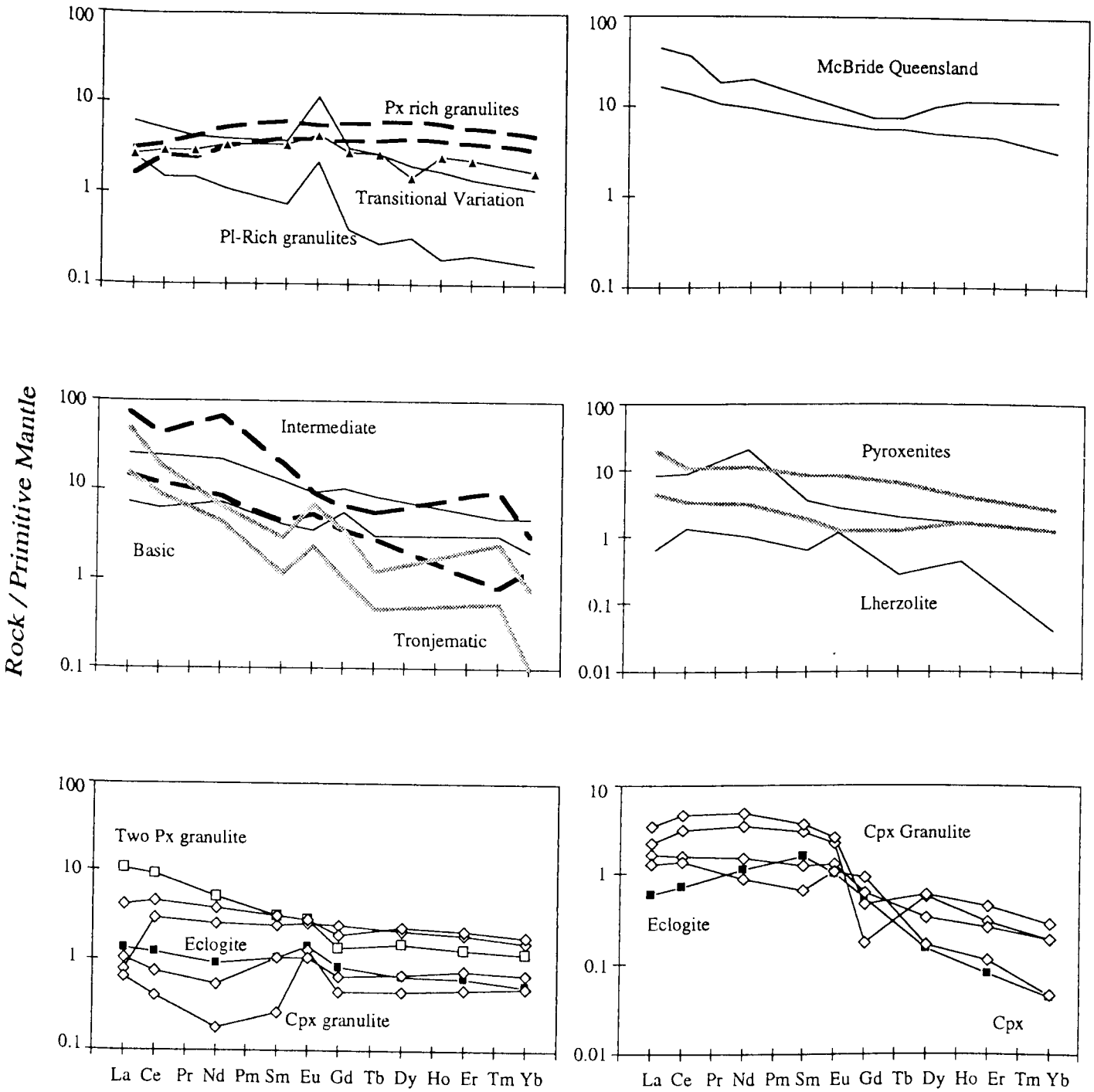

Fig. 6.11. REE abundances of the Calcutteroo xenoliths and their comparisons with xenoliths from different sources. See text for data sources.

Table 6.15. Isotope analyses of the Calcutteroo xenoliths.

Sample	Rb	Sr	87Rb/86Sr	87Sr/86Sr		87Sr/86Sr(T)	Nd	Sm	147Sm/144Nd	143Nd/144Nd		143Nd/144Nd(T)	eps Nd (0)	eps Nd chT	T mod:dep
Whole Rock															
LCC 2	1.8	125.0	0.041693	0.706287	± 21	0.705996	3.42	1.07	0.188816	0.512665	± 38	0.512059	0.53	0.89	2.054
LCC 5	1.4	60.0	0.067760	0.712375	± 23	0.711902	0.41	0.16	0.230657						
LCC 8	1.8	117.0	0.044193	0.706430	± 31	0.706121	4.38	1.19	0.164726	0.512472	± 25	0.511943	-3.24	-1.38	1.705
LCC 10	4.6	209.4	0.064267	0.709683	± 15	0.709235	7.54	1.51	0.121212	0.512555	± 27	0.512166	-1.63	2.97	0.846
LCC 13	2.3	145.5	0.045097	0.708708	± 18	0.708393	1.11	0.54	0.292559	0.512664	± 47	0.511725	0.50	-5.64	-0.979
Clinopyroxene															
LCC 2	1.5	50.4	0.087942	0.704909	± 8	0.704295	4.46	1.23	0.166445	0.512486	± 7	0.511952	-2.96	-1.20	1.718
LCC 5	1.5	48.4	0.087199	0.710610	± 7	0.710001	2.30	0.55	0.143698	0.512440	± 52	0.511979	-3.86	-0.68	1.310
LCC 8	2.9	66.4	0.128201	0.705313	± 10	0.704418	5.83	1.36	0.140902	0.512291	± 12	0.511839	-6.77	-3.42	1.544
LCC 12	0.1	52.3	0.008050	0.709637	± 21	0.709581	1.32	0.29	0.134013	0.512655	± 12	0.512225	0.33	4.13	0.796
LCC 13	0.1	129.6	0.002410	0.704605	± 6	0.704589	1.46	0.46	0.188715	0.512682	± 8	0.512077	0.86	1.23	1.970

Errors quoted are calculated as 2 standard error of the mean.

The value T is an initial age on recrystallization of a rock.

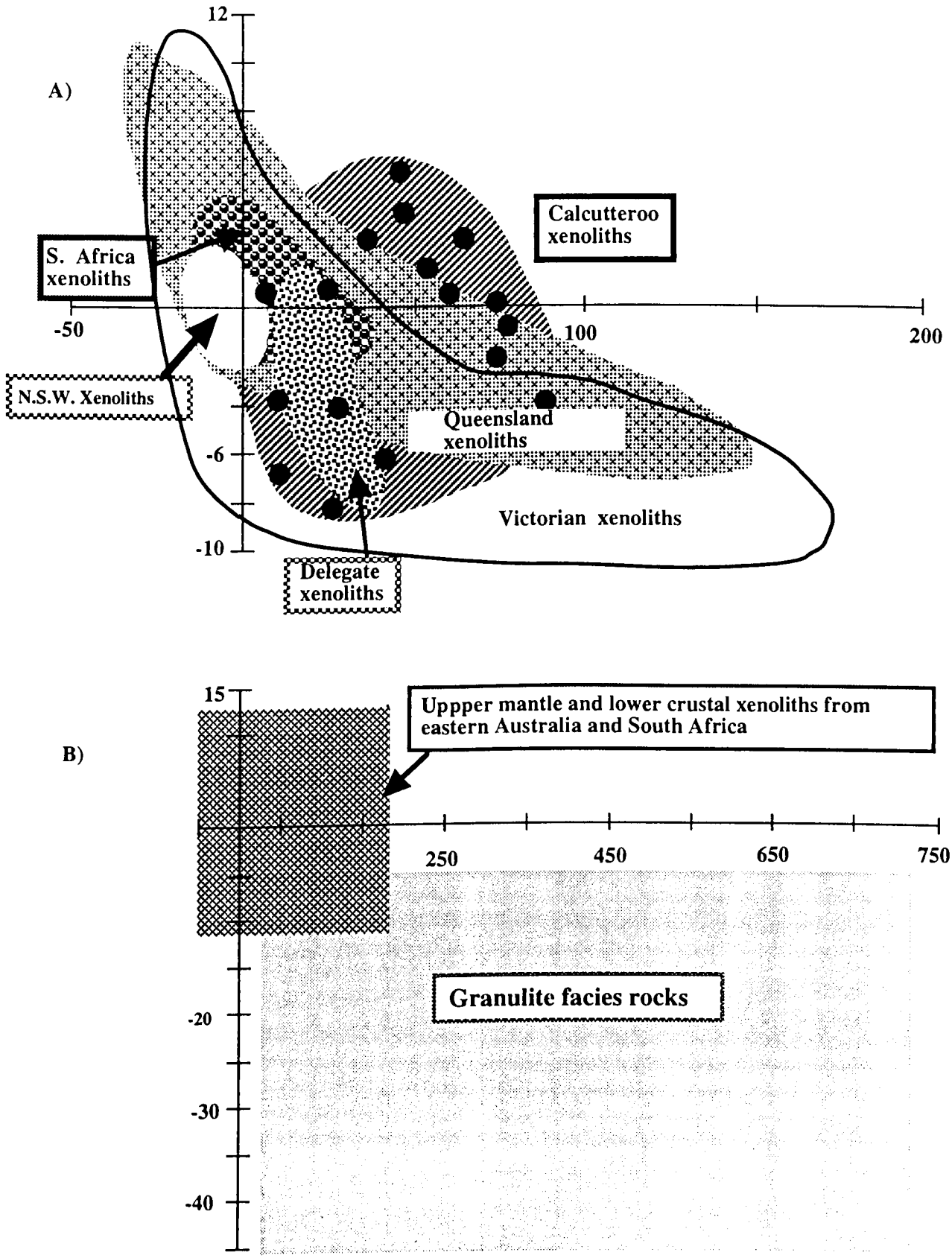

Fig. 6.12. Sr-Nd isotopic compositions of the Calcutteroo xenoliths and of xenoliths and granulite facies rocks from different sources. Notice, distinctive comparisons of lower crustal and upper mantle xenoliths with granulite facies metamorphic rocks (Data sources: Menzies *et al.* (1983), Ben Othman *et al.* (1984), Rudnick *et al.* (1986), McDonough & McCulloch (1987), Griffin *et al.* (1987), Walker *et al.* (1989) and McDonough *et al.* (1991)).

The $TNd_{(DM)}$ ages overlap with those of the Cambrian Delamerian basalts, Neoproterozoic Adelaidean basalts and Mesozoic Kangaroo Island basalt reflecting the underplating histories over a length long time scale at lower crustal level before the xenoliths were entrained by the Jurassic host kimberlites (Fig. 7.2).

6.5.4. Geotherm of Proterozoic Adelaide Geosyncline, South Australia

Pressure and temperature for the Calcutteroo xenoliths were calculated assuming mineral assemblages which were assumed to have been in equilibration. These include clinopyroxene-garnet pairs (Raheim and Green, 1974; Wells, 1977; Ellis and Green, 1979; Dahl, 1980; Krogh, 1988; Pattison and Newton, 1989) for calculation of the temperature, and clinopyroxene-garnet-plagioclase-quartz pairs (Newton and Perkins, 1982), plagioclase-garnet-Al_2SiO_5-quartz pairs (Newton and Haselton, 1981;Koziol and Newton, 1988), and garnet-orthopyroxene pairs (Harley, 1984) for calculation of the pressure. For these calculations, the average rim compositions were used for the samples showing zoned mineral chemistry.

In the samples showing a partially replaced texture, host minerals and their replaced mineral are used for comparing difference of the P-T condition between two minerals. Generally, the pressure calculations followed ideas proposed by Pearson *et al.* (1991). Results are shown in Table 6.16 and are plotted in Fig. 6.13.

In general, temperatures determined by methods of Krogh (1988) and Ellis and Green (1979) are 5-50 °C higher and those of Dahl (1980) and Pattison and Newton (1989) are lower than the others. Those of Wood and Banno (1973) and Wells (1977) show higher temperatures relative to other geothermometers, reflecting the non-equilibrium between two pyroxenes, or their composition change by alteration or exsolution (Pearson *et al.* 1991).

Calculated temperatures for South Australian xenoliths determined from garnet-orthopyroxene geothermometry (at 15 kbar) range from 750 to 1050 °C (Table 6.16). Generally, eclogitic rocks show a slightly higher temperature (dominantly 900-1050) than the other rocks types, and kyanite bearing rocks show a similar temperature to eclogitic rocks. Xenoliths from Calcutteroo and Pine Creek show limited temperature variation whereas those of the Port Augusta show differences among the different rocks. The temperatures of Calcutteroo and Pine Creek xenoliths are slightly higher in the range of the 50 to 100 °C than those of Port Augusta but all 100-120 °C lower than south-eastern Australian geotherm constructed with the Bullenmerri and Gnotuk xenoliths in Victoria in the ranges of 15 to 22 kbar (P) (O'Reilly and Griffin, 1985).

Table 6.16. Calculated P-T of the South Australian lower crustal xenoliths.

Sample	Mode	KR(88) 15 Kb	EG(79) 15 Kb	PN(89) 15 Kb	Dahl(80) 15 Kb	RG(74) 15 Kb	EG-NP	EG-KN	EG-NH		
Calcuttroo											
Trwi Cx 13	core	960	963	768	832	808					
	rim	943	948	747	801	796					
Trwi CX 1		893	915	712	792	839					
Trwi CX 11		892	926	884	784	875					
Trwi CX 9		836	876	776	681	830					
Trwi CX 4		866	894	820	1030	824					
Trwi N 1		899	974	875	1066	824					
Trwi N 8		883	901	645	866	803					
Trwi N 10		924	955	707	1008	896					
Trwi CX 2		892	906	630	840	797	911/17	926/21	924/21		
Trwi CX 8		857	885	605	825	785					
Trwi CX 5		963	977	752	1090	816	1007/22	1001/22	995/21		
Trwi CX 7		824	854	745	891	770	871/21	868/20	8701/18		
Trwi CH 3		776	851	1032	600	851					
Trwi CB 4				*WB(73)1212, W(77)1240*							
Trwi N 3		823	862	597	732	811	864/18	877/20	871/18		
Trwi CX 3		961	974	733	1049	896	1000/23	998.9/22	993/21		
Trwi CX 6		872	894	612	807	811	915/21	911.7/20	906/19		
Trwi CX 14		706	953	680	975	871		956/22	951/20		
		EG/WB- 894/12, WB-1135, W-1191.									
Trwi CH 5		872	950	762	1021	950		973/22	967/762		
Trwi CB 3		828	863	604	721	804	870/17	878/20	872/18		
Port Augusta											
Pa 6X 8	core	906	917	848	1010	811					
	rim	878	884	799	931	785					
		917	925	858	1018	806					
Pa 5X 2		932	941	872	1072	829					
Pa 6X 9		957	966	867	1128	855					
Pa 6X 2		851	875	766	934	790					
Pa 6X 6		855	884	725	915	815					
		861	886	735	940	808					
Pa 6X 7		849	876	723	920	802					
Pa 6X 12		944	953	799	1054	848					
Pa 5X 1	host	902	926	754	1029	847					
	replaced	890	916	740	1003	839					
							WB/PN	*W/PN*	*W/KN*	*W/NH*	
Pa 7X 1	fine grained	833	861	718	894	786	*996/20*	*1022/20*			
		899	919	804	1034	834			*1090/25*	*1090/23*	
Pa 6X 11		902	914	881	1020	1045	*1000/20*	*1009/22*	*1003/21*		
Pa 7X 6		863	893	845	1057	824	*814/15*	*827/19*	*822/17*		
Pa 9X 1		826	872	819	1050	828					
Pa 7X 8		790	848	612	878	825	*853/16*	*862/19*	*857/18*		
										WB/W	*W/W*
Pa 7X 5		865	892	834	1032	817	*894/15*	*909.6/20*	*904.03/19*	*1004/16*	*1084/18*
										WB/KN	*WB/NH*
Pa CX 6		819	851	790	944		*847/14*	*865/19*	*860/18*	*988/23*	*1094/25*
										W/KN	
Pa 6X 10		752	796	731	869	737	*791.2/23.3*	*806/18*	*800/16*	*988/21*	*1094/23*
		665	716	615	702	669	*707/12*	*719/16*	*714/15*		
Pa 7X 9		*WB/KN*	*WB/NH*	*W/KN*	*W/NH*						
		978/22	*978/20*	*1126/26*	*1126/24*						
Pa 7X 8		*WB/H*	*WB/W*	*W/H*	*W/W*						
		1090/22	*1090/20*	*1134/23*	*1134/21*						
		WB/NP	*W/NP*	*W/KN*	*W/NH*						
Pa 6X 11		*1090/17*	*1134/18*	*1134/24*	*1134/24*						
Pine Creek											
Pinc X 7		984	991	716	1093	899					
Pinc X 5		923	937	668	906	843	962/23	958/21	9427/17		
Pinc A 2		902	928	665	929	846	931/18	9428/21	937/19		

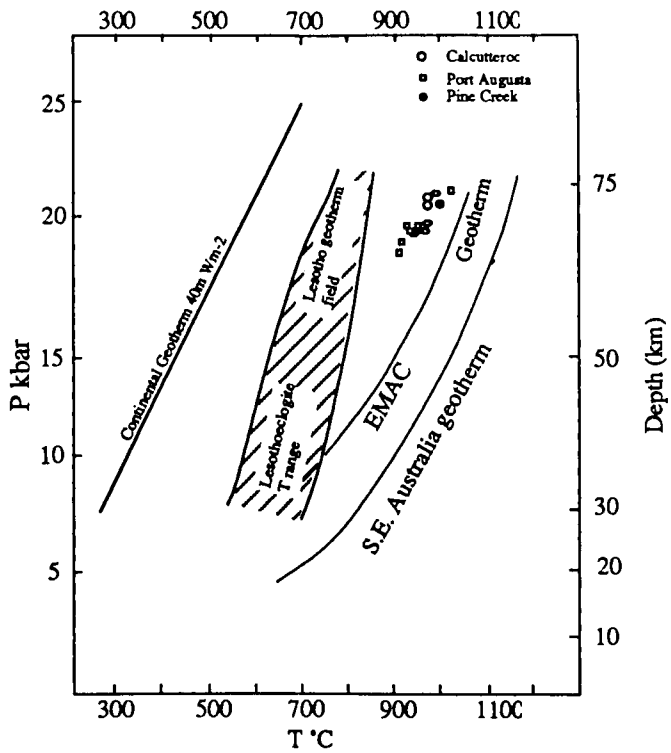

Fig. 6.13. P-T estimates of the South Australian lower crustal xenoliths projected in geothertms of EMAC (Pearson *et al.* , 1991). Also shown is geotherm of south eastern Australia (O'Reilly & Griffin, 1985), of Lesotho geotherm field (Griffin *et al.*, 1990), and of continent (Pollack and Chapman 1977).

The calculated P-T values are plotted in the range of the geotherm of the Pearson *et al.* (1991), but show slightly low pressure (Fig. 6.13). These differences results in different barometers between this and Pearson's study. The results may reflect the maximum P-T condition rather than those of the normal lower crust because there are some typical error of the calculated temperatures in the range of 40-150 °C at the assumed pressure condition, if the ferrous composition are considered (Pearson *et al.*, 1991). However, temperature difference between Calcutteroo, Pine Creek, and Port Augusta ranging from 50 to 100 may not be interpreted with in typical error ranges because of the considerable difference of the mineral composition and petrography.

In summary, P-T values calculated from Calcutteroo and Pine Creek xenoliths are similar to those of Pearson *et al.* (1991) whereas those from Port Augusta have a slightly lower temperature assuming the same pressure.

6.6. Discussion

It is generally agreed that some component of crustal growth occurs by basal accretion of basaltic melts from the deep lithosphere or asthenosphere (Fyfe 1978; Furlong and Fountain, 1986; Pearson *et al.*, 1991) and many models have been used to describe the

evolution of the lower crust(Jacobsen and Wasserburg, 1979; DePaolo 1980; Weaver and Tarney, 1980; Fountain and Salisbury, 1981; O'Nions and Hamilton, 1981; Allégre 1982). In related problems, many controversies exist over the origins of the lower crustal xenoliths as to whether they were derived as cumulates, restite, unmodified basaltic melt or fragments of the underthrusting oceanic lithosphere (Rudnick *et al.*, 1986; Rudnick and Taylor, 1987; Griffin *et al.*, 1987; Arculus *et al.*, 1988). These questions can be approached by the study of tectonically exposed high grade metamorphic terrains (Holland and Lambert, 1975; Weaver and Tarney, 1980; Fountain and Salisbury, 1981). They also can be supported by experimental results and geophysical surveys (Manghnani *et al.*, 1974; Jackson and Arculus, 1984; Jackson *et al.*, 1990; O'Reilly *et al.*, 1990).

The South Australian xenoliths are dominated by mafic rock types, including eclogites and granulites, with subordinate amphibolite, pyroxenite, gabbro, and lherzolite. The low abundances of gabbroic xenoliths in the low crust can be explained by the metastability of gabbroic rocks at Moho depths (10 kbar, 500-900 °C) or elevated continental geotherm as experimental results of Ringood and Green (1966). The predominance of eclogitic rock in the South Australian area in comparison to the garnet free or granulitic rock dominant of Phanerozoic eastern Australia xenoliths (O'Reilly, 1989a) suggest differences of dominant rock types in the shallow lithospheric structure or different metamorphic conditions.

In general, the xenoliths show round to subangular shapes, suggestive of tumbling during turbulent ascent (Nicholls and Greig, 1989). Many of them also show several types of contact relationships; granulitic-eclogitic, granulitic-pyroxenitic and pyroxenitic-amphibolitic rock, suggestive of multiple intrusions of basaltic materials. The xenoliths show transitions of mineral assemblages from gabbroic to granulitic or from granulite to eclogite. They also show evidence of partial melting and subsequent cooling history, such as pyroxene and garnet dominant part and quartz and feldspar dominant part.

Some petrographical differences are apparent among the xenoliths from three South Australian localities. In general, Port Augusta xenoliths are characterised by distinctive exsolution, complicated replacement or recrystallization texture, and abundant spine shaped rutile inclusions in pyroxene and garnet. Whereas, Calcutteroo xenoliths are characterised by more eclogitic mineralogy, and occurrence of the kyanite. However, Pine Creek xenoliths are distinguished from the other two areas by more carbonate rich characteristics, including abundant occurrences of calcite or of thin calcite veinlets which intrude into the xenoliths.

The Port Augusta xenoliths show clear petrographical differences among different rock types relative to Calcutteroo or Pine Creek xenoliths. In the Port Augusta xenoliths, eclogitic rocks are characterised by sub-to equigranular textures, the existence of coarse-grained rutiles, discrete spinel and amphibole grains. Granulitic or pyroxenitic xenoliths are characterised by spinel and/or clinopyroxene rimmed by garnet and distinctive exsolution texture among Fe-Ti oxide, pyroxene, amphibole and garnet.

Mineral compositions also show differences between xenoliths from Port Augusta

and Calcutteroo area. In general, clinopyroxene and garnet of Port Augusta xenoliths are more granulitic while those of Calcutteroo and Pine Creek xenoliths are more eclogitic. In the P-T calculated with equilibrated mineral pairs, slightly low values are seen in the Port Augusta xenoliths. Calculated P-T from the Calcutteroo xenoliths suggest that the lithosphere beneath the Adelaide Geosyncline area may be cooler than that of the south eastern Australia (O'Reilly and Griffin, 1985; Rudnick *et al.*,1986; Griffin *et al.*, 1987). These results may reflect a differences of lithospheric structure along the Tasman line as discussed in Chapter 1. In addition, transitional depths of granulite-eclogite and spinel lherzolite- garnet lherzolites may be deeper than that of south eastern Australia as suggested by Pearson *et al.* (1991).

The Calcutteroo xenoliths are basaltic, ranging from *ne* -to *Q*-normative composition. This composition range is consistent with Cainozoic South Australian basalts. Many of them have a high Mg# (mainly > 64) and Ni and Cr contents. The other elements, including Y, V and Zn, show a distinctive correlation with Mg#. These relationships suggest that the Calcutteroo xenoliths are mainly basaltic cumulates or less modified basaltic melt. The Calcutteroo xenoliths are characterised by a distinctive enrichment in Ba and less pronounced enrichment in Sr contents which is similar to that in xenoliths from Delegate, El Almein, White Cliff, and Lesotho (Griffin *et al.*, 1979; Rogers and Hawkesworth, 1982), inspite of diversities in total trace element contents. The chemical characteristics may suggest that history of lower crust accretion of separated area at least. were partly similar. The relative trace element abundances of the South Australian xenoliths are different from typical granulitic facies metamorphic rocks, suggesting that evolutional history of the lower crust is different from that of granulitic facies metamorphic terrains.

The Calcutteroo xenoliths show anomalous REE patterns, showing variation of strongly LREE depleted to LREE enriched. No negative Eu anomaly are found in the Calcutteroo xenoliths. Taylor (1979) suggested that restite forming lower crust may occur by about 30 % fusion of andesitic source rocks and this restite show a positive Eu anomaly. The Eu anomaly also depend on the proportion of restite to melt removed. Thus, REE patterns of Calcutteroo xenoliths reflect that origins of the xenoliths can not be explained by the andesitic model.

Calcutteroo xenoliths show considerable variation in isotopic composition. The isotopic compositions are similar to those of worldwide lower crustal xenoliths but, are considerably different from those of the granulite facies metamorphic rocks (Fig. 6.14). These difference of isotopic values may reflect differences of ages as well as sources. Sm/Nd-Rb/Sr ratio relationships also show that granulite facies metamorphic rocks are significantly different from lower crustal and upper mantle xenoliths. Isotopic characteristics of the Calcutteroo xenoliths overlap with those of other lower crustal and upper mantle xenoliths. This characteristic suggests that petrogeneses of the Calcutteroo xenoliths can not be explained in terms of those of the granulite facies metamorphic rocks.

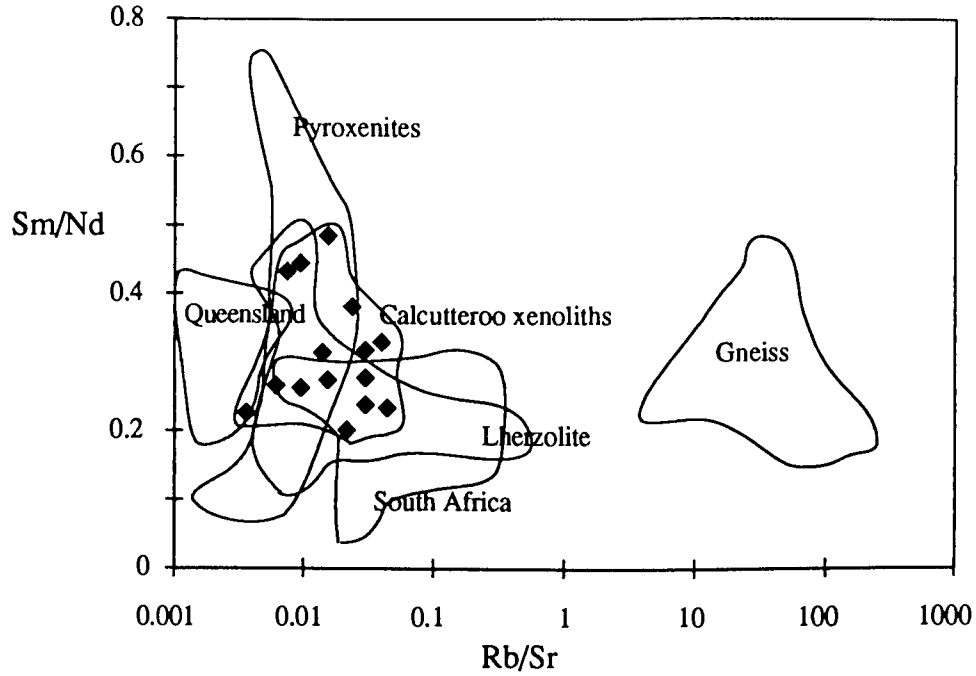

Fig. 6.14. Rb/Sr versus Sm/Nd ratios of the Calcutteroo xenoliths and a comparison with the related rocks (see Fig. 6.12 for data sources).

6.7. Conclusion

1) The South Australian xenoliths reflect several periods of underplating by basaltic liquids derived from the deep lithosphere or asthenosphere, subsequent metamorphism, and metasomatism of the original melt. Most of the xenoliths are derived as cumulates of the basaltic melts.

2) Integrated petrological, geochemical and isotopic studies suggest that petrogenesis of the lower crustal xenoliths can not be explained in terms of models relevant to the exposed high grade granulite facies metamorphic terrains.

3) Among the South Australian xenoliths, the petrographic and mineralogical characteristics of the Port Augusta xenoliths are distinctive from those of the Calcutteroo and Pine Creek xenoliths. In general, xenoliths of former area are dominantly granulitic while those of the latter two areas are eclogitic.

4) Calculated P-T suggests that lithosphere beneath the Palaeozoic Adelaide Geosyncline area is cooler than that of the Phanerozoic eastern Australia, suggestive of the different petrography or geochemical composition.

5) Based on the $\varepsilon Nd(i)$ values, the eclogite xenoliths are not like the Adelaidean (Neoproterozoic) basalts at ~ 800 Ma. The εNd values are significantly higher than the earlier Palaeo- to Neoproterozoic basalts which outcrops on the Gawler Craton (see Fig. 7.2).

6) Timing of eclogite formation is not constrained but if the protolith correlation mentioned in 5) is correct , then it could have taken place during the Late Neoproterozoic or early Palaeozoic.

Chapter 7. General model of origin and evolution of Phanerozoic South Australian mantle, based on the integrated petrological, mineralogical geochemical and isotopic evidences

7.1. Introduction

This section provides possible general models for the evolution of the South Australian lithospheric mantle during Phanerozoic time, based on the foregoing six chapters. The models are mainly based on geochemical and isotopic studies, because of the limited geophysical studies of these areas. Available data of mafic rocks from Adelaidean Geosyncline and adjacent Gawler Craton were also reviewed demonstrating the enrichment history in lithospheric level during Precambrian and early Palaeozoic times.

7.2. Nature of Moho (Crust-Mantle boundary) and Lithosphere-Asthenosphere transition in Australia

Traditionally, the term "Moho" was defined as a sharp seismic discontinuity (about Vp = 8.0 km/s). Experimental results for the upper mantle xenoliths (O'Reilly *et al.*, 1990; Jackson *et al.*, 1990), for lower crustal xenoliths (Jackson and Arculus, 1984; Jackson *et al.*, 1990) and for metamorphic rocks (Manghnani *et al.*, 1974) suggest that the Vp of the presumable lower crustal and upper mantle level range from ~ 7.0 to 8.0 Km/s. Seismic studies suggest that crust-mantle boundaries are different in different tectonic regions as mentioned in Chapter 1 (Collins, 1988; Jackson, 1991).

Studies of the Australian continent suggest that Precambrian craton areas (e.g. Pilbara, W. Australia) show a shallow sharp Moho boundary whereas Phanerozoic eastern Australia show deep transitional Moho boundary in the range of 25-55 Km depth (Collins, 1988). For South Australia, seismic studies suggest that Moho depths show lateral variable crustal thickness from 35 to 40 km with Proterozoic sediment within the upper 20 km of the crust (Thomas, 1969; White, 1971; Denham *et al.*, 1972; Stewart, 1972; Finlayson *et al.*, 1974; Shackleford and Sútton, 1981;).

The base of the lithosphere is consistent with LVZ defined by seismic and electromagnetic studies. Several seismic studies have indicated the occurrences of LVZ beneath tectonically active crust, even though the existence of the LVZ is not universal in worldwide deep lithospheric structures (Lilley *et al.*, 1981; Belbo *et al.*, 1983).

For the Australian continent, a number of seismic (Cleary *et al.*, 1972; Finlayson, 1982; Muirhead and Drummond, 1991), teleseismic travel time (Drummond *et al.*, 1989) and

electromagnatic sounding studies (Lilley *et al.*, 1981; Constable, 1991; Lilley, 1991) suggest that there are changing lithospheric structures between Precambrian terrain on the west side and Phanerozoic terrain on the east side. The seismic and magnetic studies suggest that the lithosphere-asthenosphere transition in Phanerozoic eastern Australia lies at about 200 km depths (shallow) while that of Precambrian terrain does not occur at that range of depths .

Empirical geotherm calculated using equilibrated mineralogy from the South Australian xenoliths and surface heat flow measurements of the Proterozoic Adelaide Geosyncline area suggest that the lithosphere beneath the Adelaide Fold Belt, is cooler than that of SE Australia (O'Reilly and Griffin, 1985; Pearson *et al.*, 1993).

All these studies suggest that nature of the shallow lithosphere, and lithosphere-asthenosphere transition beneath the Adelaide Fold Belt, South Australia is different from that beneath Phanerozoic eastern Australia, probably intermediate between Precambrian terrain and Phanerozoic eastern Australia, even though there are no valid geophysical supports for this idea.

7.3. Continental lithospheric mantle (CLM) as a geochemical reservoir

The CLM is an important global geochemical reservoir. The evidence for enrichment can be directly observed in some peridotic nodules entrained by worldwide kimberlites and intraplate alkaline basalts which show amphibole-apatite-phlogopite growths. Thus, some intraplate alkaline basalts and kimberlitic rocks may reflect geochemically and isotopically enriched lithosphere. Several models suggest that metasomatism is an important enrichment process in CLM, and that small melt fractions from the asthenosphere act as agents for the enrichment mechanism (Menzies *et al.*, 1983; McKenzie, 1989). Experimental studies suggest that LVZ at the base of the lithosphere is consistent with the existence of small melt fractions which are compositionally similar to kimberlites and potassium-rich magma (Ringwood, 1969; Wallace and Green, 1988).

According to McKenzie's model (1989), small melt fractions which originate from the underlying convecting mantle produce a metasomatic layer in the mechanical boundary. Its remelting during lithospheric stretching results in anomalous isotopic ratios and a K-rich component in CLM. This model may provide evidence for the occurrence of rare alkaline basalt and K-rich kimberlites in stable plate interior and of abundant K-rich basic volcanism in rift zones. According to Menzies *et al.* (1987), asthenospheric melts transfer through lithosphere conduits and related processes during these movements results in anomalous lithospheric enrichment. The lithospheric enrichment event can be sampled directly by the presence of pyroxenitic dykes in the lherzolites.

Thus, thick, cool lithosphere may have experienced geochemical and isotopic enrichment history for longer times than thin lithosphere even though present lithosphere may have privious thick history (i.e. NE China). In Australia, this kind of observation may

support the idea of an ancient enriched lithosphere beneath the Precambrian crust (e.g. Gawler Craton) and young enrichment in the lithosphere of Phenerozoic eastern Australia (e.g. Victorian Newer Basaltic province).

7.4. Geological and magmatic histories during Precambrian and Early Palaeozoic, South Australia

A number of studies have provided geological and magmatic histories of the Gawler Craton and the adjacent Adelaide Fold Belt (e.g. Webb and Wood, 1986; Fanning *et al.*, 1988; Daly *et al.*, 1990, Turner *et al.*, 1993). Fanning *et al.* (1988) recognised three megacycles of orogenic development within the Gawler Craton. Their summary is as follows.

1) **Late Archaean-Early Proterozoic;** sedimentation and volcanism followed by plutonism and deformation during the Sleafordian Orogeny. The cycles can be represented by the Sleaford Complex and Mulgathing Complex.
2) **Early Proterozoic;** granitic magmatism and deformation accompanying several phase of basin development and contemporaneous volcanism during the Kimban Orogeny,
3) **Middle Proterozoic**; bimodal anorogenic magmas including both an intrusive and volcanic suite (Stewart and Foden, 1993), with associated volcanoclastic and clastic sediments.

The above were followed by Neoproterozoic Adelaidean and Early Palaeozoic events (Foden *et al.*, 1989).
1) **Late Proterozoic**; shallow marine sedimentation in rift-grabens and accompanied by widespread tholeiitic basaltic magmatism (e.g. Wooltana, Depot Creek volcanics),
2) **Early Cambrian;** strongly undersaturated alkaline volcanism (e.g. Truro volcanics) and a new phase of sedimentation.

The sedimentary sequences of the Adelaide Geosyncline deformed by the Cambro-Ordovician Delamerian Orogeny during the time 520-480 Ma, which are equivalent to the Ross Orogeny in Antarctica (Foden *et al.*, 1990; Turner and Foden, 1990; Flöttman, in press). The Delamerian Orogeny resulted in metamorphism and bimodal granite generation during the convergent deformation in the southern Adelaide Fold Belt (Sandiford *et al.*, 1992; Foden *et al.*, 1993). The Orogeny ceased by the process of a sudden increase in the potential energy of the fold belt with subsequent rapid uplift and erosion at about 490-485 Ma (Turner *et al.*, 1992; Foden *et al.*, 1994).

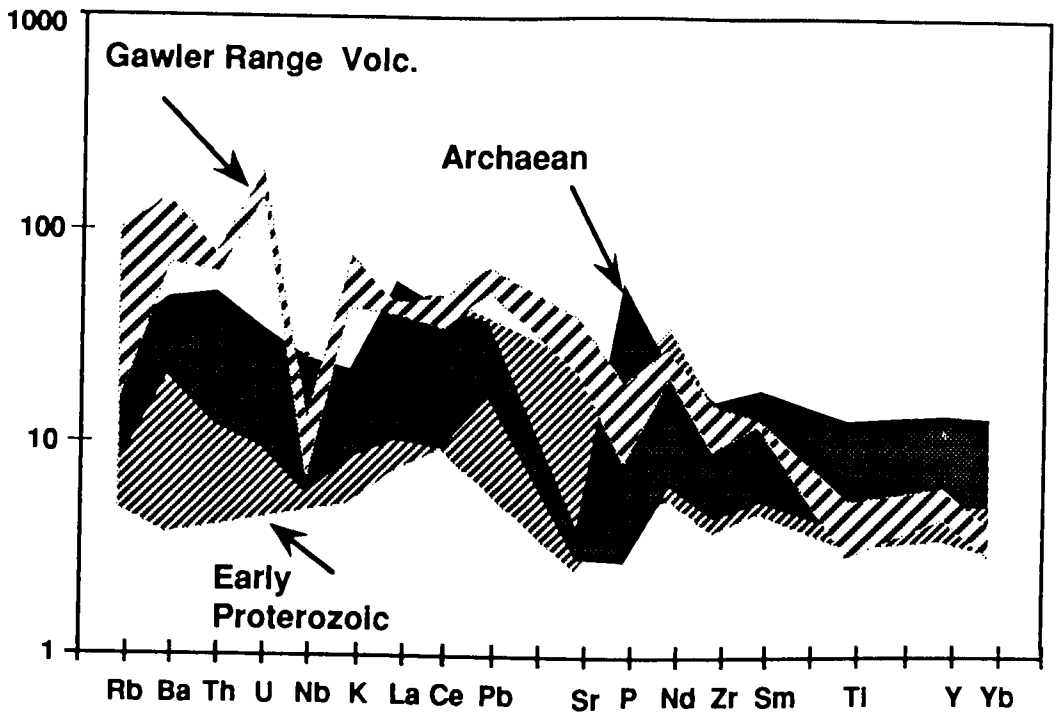

Fig. 7.1. PM normalised incompatible trace elements of Gawler Craton, Early Proterozoic and Archaean volcanics.

7.5. Isotopic and geochemical characteristics of the Precambrian and Early Palaeozoic mafic rocks

For the Precambrian and Early Palaeozoic mafic rocks, limited studies have been provided by Fanning (1975) and Giles and Teale (1979). Recently, more systematic studies have been made by Turner *et al.* (1993) and Foden *et al.* (1994).

The Archaean and Early Proterozoic basalts are tholeiitic. In the PM normalised incompatible element abundances (Fig. 7.1.) they show a flatter pattern in the most of incompatible elements. The Archaean basalts have higher Ba (higher Ba/Sr, Ba/Nb), Th and P relative to Early Proterozoic basalt. However, Late Palaeoproterozoic Gawler Range volcanics are clearly distinguished from the earlier two basalts by enrichment of LILs (alkali), LREE, high LREE/HREE (La/Yb) and have a distinctive negative Nb anomaly (high U/Nb, K/Nb, La/Nb). Nd-Sr isotopic data are summarised in the Fig. 7.2. The Archaean to Early Palaeproterozoic mafic volcanics are also isotopically distinctive from Early Palaeozoic and Neoproterozoic suites. The Archaean to Early Palaeproterozoic mafic volcanics show εNd (-16 - -26) and older $TNd_{(DM)}$ of 2.3-3 Ga whereas late Palaeoproterozoic rocks have εNd of -12 - -24 and $TNd_{(DM)}$ of 1.8 -2.4 Ga.

Incompatible element abundances of Neoproterozoic and Early Palaeozoic mafic rocks are shown in Fig. 7.3. The Neoproterozoic Wooltana and Beda tholeiitic basalts show similar flatter patterns to Archaean to Early Palaeproterozoic mafic suites.

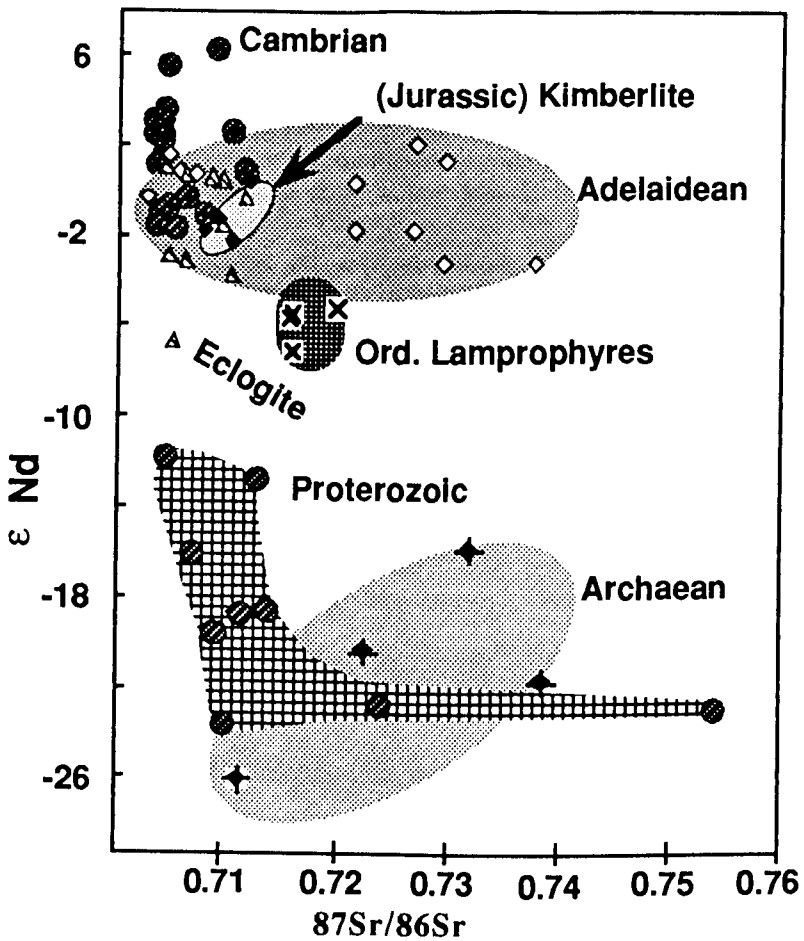

Fig. 7.2. Nd-Sr isotopic compositions of the selected samples from the South Australia.

Their incompatible element patterns lie between tholeiitic and alkaline suites of Early Palaeozoic. Beda volcanics show high Rb, K, Zr, Ba (low Zr/Nb, high Rb/Sr) and low Ce relative to Wooltana suites. Very distinctive relative abundances in incompatible elements are observed between Early Palaeozoic tholeiitic (Mt Pleasant) and alkaline suites (Truro volcanics). The alkaline basalts show an enrichment in most of incompatible element and are distinguished from the tholeiitic rocks by low Zr/Nb, Ba/Nb and Y/Nb. The tholeiitic basalts have a similar pattern to those of the Proterozoic tholeiitic basalts. The alkaline basalts show a depletion in Rb, K, Pb and HREE relative to the other elements. The Neoproterozoic basalts have εNd(0) of -4 - +2 and $T_{Nd(DM)}$ of 1.3-2.1 Ga. The Early Palaeozoic alkaline basalt have a $^{87}Sr/^{86}Sr$(T=500 Ma) of 0.7042, $^{143}Nd/^{144}Nd$ of 0.5123 and $T_{Nd(DM)}$ of ~ 0.6 Ga whereas tholeiitic rocks have a $^{143}Nd/^{144}Nd$ of 0.51218 and $T_{Nd(DM)}$ of 1.2 Ga.

7.6. Isotopic and geochemical characteristics of mafic intrusive and extrusive rocks after Early Palaeozoic

This section summarises isotopic and geochemical characteristics of mafic intrusive and extrusive rocks after Early Palaeozoic based on the foregoing six chapters.

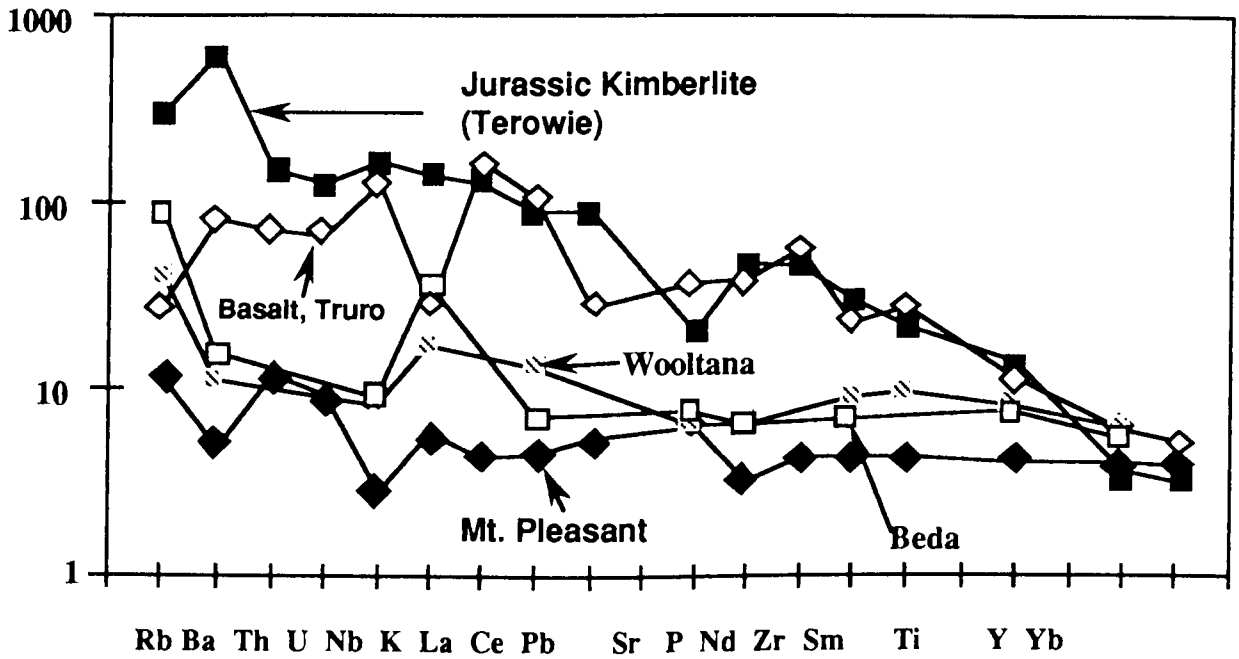

Fig. 7.3. PM normalised incompatible element abundances of Neoproterozoic and Early Palaeozoic mafic suites.

Kimberlites and Lamprophyres: Two main age and geochemical groups of potassic rocks are recognised in South Australia; i) Ordovician lamprophyres and ii) Jurassic kimberlites. They occur in the Adelaide Geosyncline and adjacent Eyre peninsula.

The lamprophyres are characterised by moderate Ni (~241), Cr (~470), MgO (~7 wt %), high SiO_2 (~56.5 wt %), Al_2O_3 (~12 wt %), LREE and LILs and low Nb (low Nb/Zr). The lamprophyres have εNd(i) of - 1.9 - 0.5 and $^{87}Sr/^{86}Sr$ (i) of 0.7053 - 0.7087 The kimberlites are dominantly *ne*- normative and characterised by high Ni (~430), Cr (~1050), MgO (~15.5 wt %), low SiO_2 (~44 wt %), Al_2O_3 (~7.15 wt %), enrichment of LILs and LREE. They have εNd(i) of 3.8 - 7.1 and $^{87}Sr/^{86}Sr$(i) of 0.7029 - 0.7072. They are chemically and isotopically similar to ultramafic lamprophyres (Rock, 1991) as well as Group 2 kimberlites of South Africa (Smith *et al.*, 1985), but are distinctive from Western Australian lamproites in being less enriched in LILs (e.g. Rb, Ba). The kimberlites are also clearly distinguished from the lamprophyres by their high Nb, Ti, MgO, Mg#, low Rb, Th, K and Al_2O_3.

Lower crustal xenoliths within the Mesozoic kimberlite pipes: Mafic dominant eclogitic and granulitic xenoliths were entrained by the Jurassic kimberlites. The xenoliths contain a mineral assemblage, Gt+Cpx+Qt±Pl±K-fd±Opx±Rt±Sp±Il ±Ky.

Two distinct petrographical and mineralogical groups are recognised in the South Australian xenoliths; i) Port Augusta xenoliths of granulitic and ii) Calcutteroo and Pine

Creek xenoliths of eclogitic. These differences are consistent with the P-T calculated for equilibrated mineral pairs, which show slightly lower values in Port Augusta xenoliths in the range of 750 °C-1050 °C. The eclogite-granulite xenoliths entrained by Calcutteroo kimberltes show a wide range of composition from *ne*-through *ol*-to *q*-normative composition and are characterised by high Mg#, Cr, Ni, Ba and low K_2O. The xenoliths also show anomalous REE abundances showing variation from strongly LREE depleted to enriched relative to the HREE and an wide range of isotopic composition, eNd of -8 - +6, $^{87}Sr/^{86}Sr$ of 0.7063-0.7124 and $TNd_{(DM)}$ of 0.85-1.9 Ga. In spite of high Cr (<250 ppm), Ni (<130 ppm) and Mg# (<65), the low K_2O contents of the xenoliths suggest that many of them are basaltic cumulates with little interstitial melt, or that they have lost K_2O during metasomatism. The unusual REE patterns of the Calcutteroo xenoliths with high La/Nd and low Nd/Sm relationships are not be expected from the andesite model of crustal growth.

Quaternary alkaline basalts: The Quaternary alkaline basalt are predominantly *ne*-normative and geochemically and isotopically very like EM type OIBs. Two main geochemical and isotopic groups of basalts are recognised; i) a Southern group of younger hawaiites and ii)Northern group of older olivine analcimites.

The olivine analcimites have high Mg# (61-71), Ni (200-500 ppm), Cr (300-700 ppm), low K_2O (mainly < 1 wt %), Rb and Sr. They have eNd of +0.92 - +2.58, $^{87}Sr/^{86}Sr$ of 0.7039-0.7049 and $TNd_{(DM)}$ of 0.4-0.52 Ga. The hawaiites have moderate Mg# (50-60), Ni (100-200 ppm), Cr (100-300 ppm). They have εNd of +2.26-+3.23, $^{87}Sr/^{86}Sr$ of 0.7035-0.7041 and TND. Even though the analcimites are more primitive relative to the hawaiites, these rocks in general have significantly higher Ba, Ti, Zr, Nb, LREE , a slightly lower $TNd_{(DM)}$, εNd and higher $^{87}Sr/^{86}Sr$ relative to the Southern group of hawaiites.

Upper mantle xenoliths entrained by the Quaternary alkaline basalts: The Quaternary alkaline basalts host xenoliths of spinel lherzolite and rarely minor dunite or pyroxenite. Two distinct types of the spinel lherzolites are recognised; the coarse equant lherzolite (CEL) and the deformed sheared lherzolite (DSL). The CELs show homogeneous equigranular texture while the DSLs show a submylonitic texture. The CELs have higher Al_2O_3, Na_2O, P_2O_5, CaO, TiO_2, Sr, Zr, Y, Sc, V, Ba, and lower Mg#, SiO_2, Ni, Cr, relative to the DSLs. The geochemical differences between the CELs and the DSLs are consistent to high modal proportions of pyroxene in the CELs. In calculated temperatures in the range of 930 °C-1100 °C, slightly higher temperatures are shown in the CELs. Oxygen fugacities estimated from the spinel lherzolites lie between QFM and WM, like those of Western Europe and eastern Australia sub-continental lherzolite samples, suggestive of similar redox states of the sub-continental lithospheric mantle on a large scale.

7.7. Where the mafic intrusive and extrusive rocks were derived from

PM normalised REE abundances of the South Australian kimberlites, lamprophyres and alkaline basalts are summarised in Fig. 7.4. The relative REE abundances of the South Australian rocks overlap in the ranges of OIB as well as South African kimberlites. The South Australian kimberlites and lamprophyres are plotted in the field of Quaternary alkaline basalts. These characteristics are clearly distinguished from N-MORB and Mesozoic Australian tholiitic basalts by the enrichment of LREE.

However, clear distinctions are evident amongst the mafic intrusive and extrusive rocks in the other trace element and isotopic characteristics. The geochemical characteristics of Truro lamprophyres, with moderate Ni, Cr, MgO, high SiO_2, low Nb (high Zr/Nb), suggest that the lamprophyres are of shallow mantle origin or assimilation influenced by the lower crust, as supported by the presence of quartz xenocrysts. Geochemical and isotopic characteristics of the Jurassic kimberlites suggest that the kimberlites were not derived from typical asthenosphere (e.g. Group 1 kimberlites) or from modern enriched lithosphere (e.g. Western Australian lamproites).

The South Australian Quaternary alkaline basalts are isotopically and geochemically very like the Victorian Newer Basalts showing an EM type OIB signature, while Tasmanian Tertiary basalts have HIMU characteristics. The Victorian Newer basalts are often considered as mixing components between hot spot source magma and lithospheric source magma. Thus it is reasonable to assume that the South Australian basalt are same as the Victorian Newer basalts. However, the olivine analcimites in the South Australian basalt are clearly distinguished from the Cainozoic basalts by a strong depletion of K_2O and Rb (Fig. 7.5). These distinctive incompatible element patterns resemble that of South African Group 1 kimberlites considered as derivatives of asthenosphere(Fig. 7.5)1.

There are several opinions about the reason for the relative depletion of K at different magma sources. Hawkesworth *et al.* (1984) suggest that the K-enrichment is a characteristic in continental areas. Smith *et al.* (1985) interpreted that K-enrichment in the Group II kimberlites as enriched sources within a stabilised, ancient subcontinental lithosphere and depletion as asthenospheric-sources similar to those from which many oceanic island basalts are produced. The South Australian kimberlites are K-enriched potassic rocks, but show less K-enrichment than some other incompatible elements. The geochemical characteristics of olivine analcimites, low K_2O in spite of high Mg#, Ni, and Cr, mimic those of Calcutteroo mafic xenoliths which are considered as basaltic cumulates. This observation is consistent with cumulate textures shown under the microscope. Thus distinctive depletion of K in the olivine analcimites suggest that petrogenesis of the analcimites are not like that of South African Group 1 kimberlites. Probably, some of the analcimites are primary basaltic liquids equilibrated with upper mantle peridotite and high Mg# in some samples may originate from olivine accumulation.

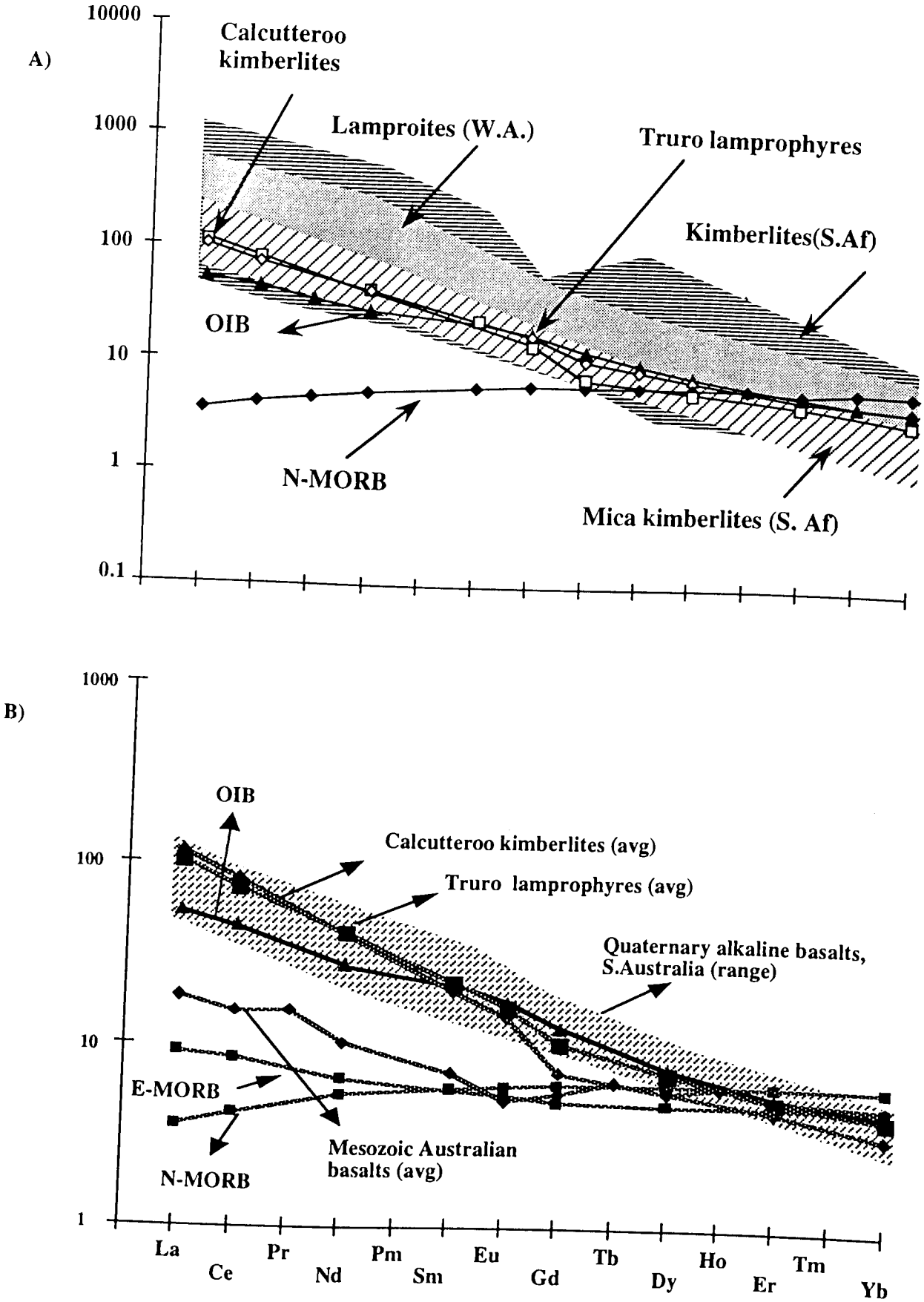

Fig. 7.4. A) REE plots of the Calcutteroo kimberlites and Truro lamprophyres from South Australia, compared with lamproite and kimberlite suites from other localities. B) of Australian alkaline basalts compared to the MORB and OIB (Primitive mantle-normalized values from Sun andMcDonough (1989). Also shown are overlapping of the Calcutteroo kimberlites, Truro lamprophyres.

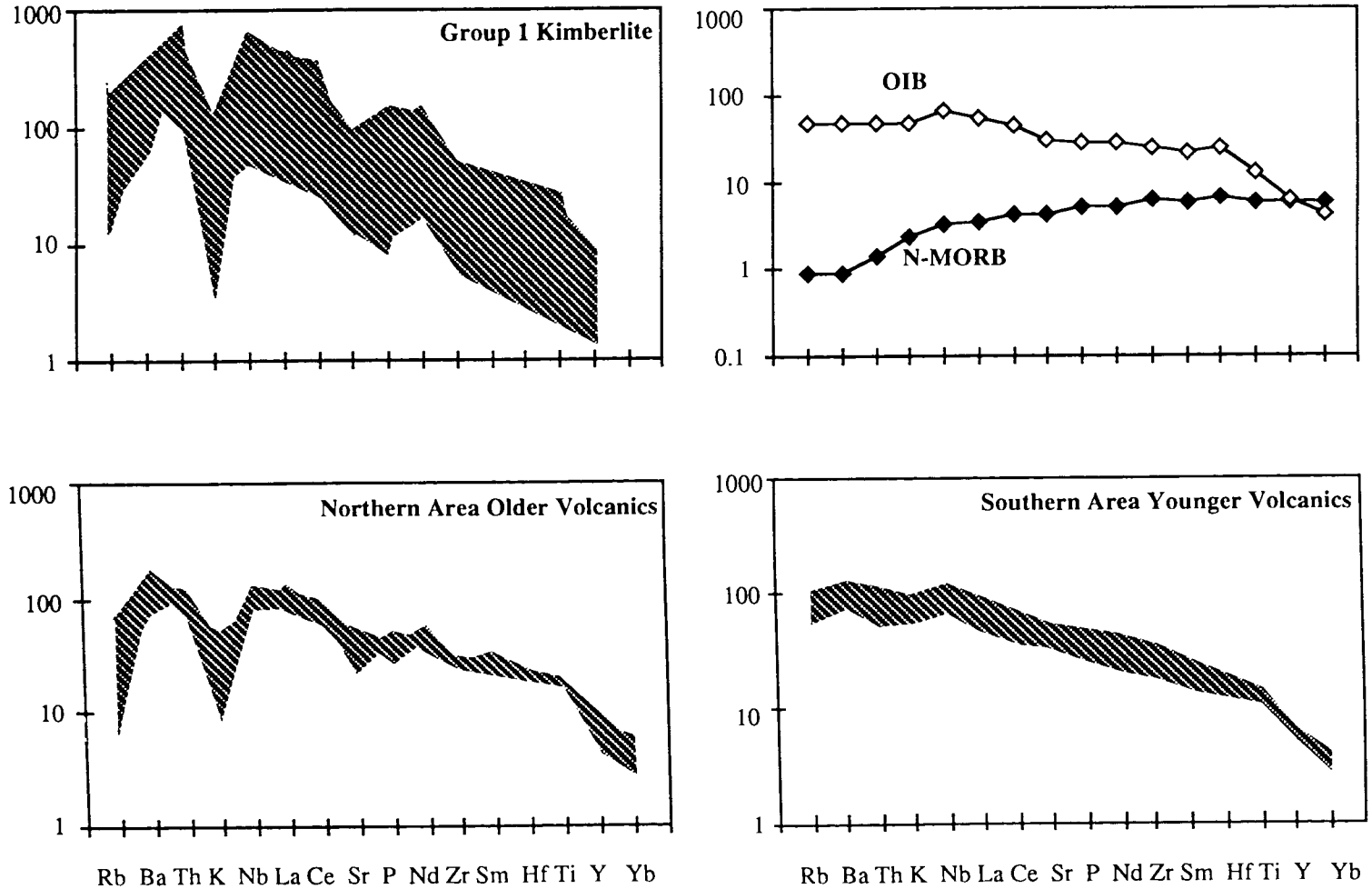

Fig. 7.5. PM normalised trace element abundances of the South Australian Quaternary Basalt, South African Kimberlites, OIB and MORB (PM, MORB, OIB from Sun and McDonough, 1989, Kimberlite from Smith *et al.*, 1985).

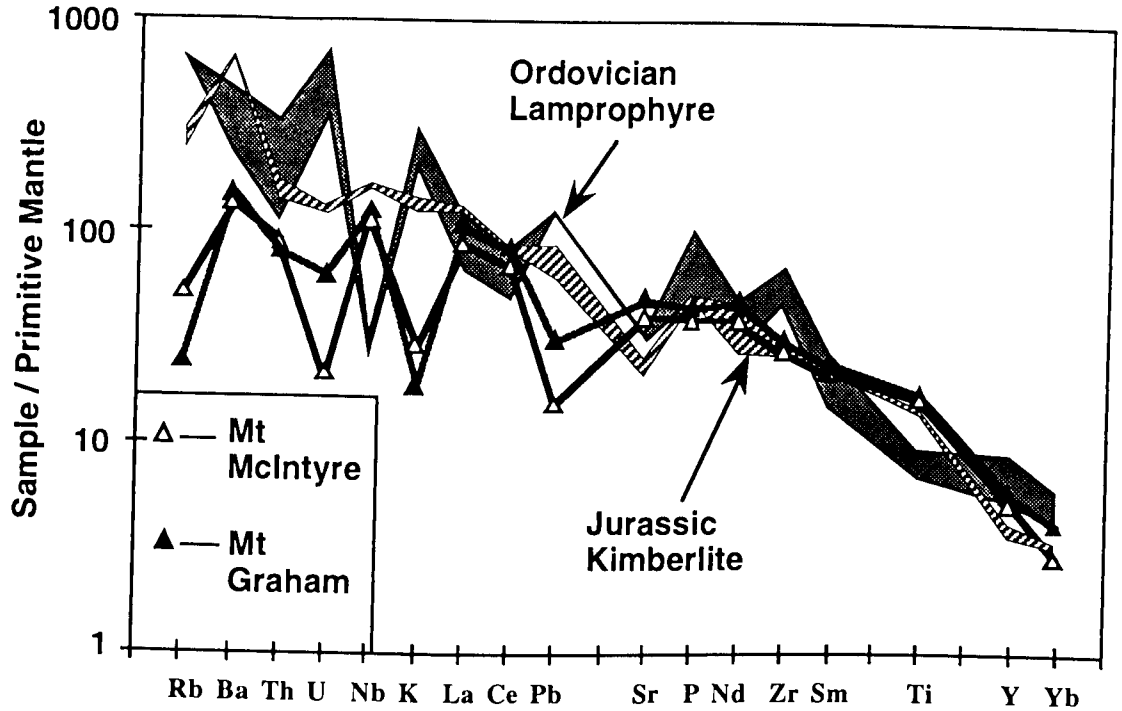

Fig. 7.6. PM normalised incompatible element abundances of South Australian Quaternary basalts, Ordovician lamprophyres and Jurassic kimberlites.

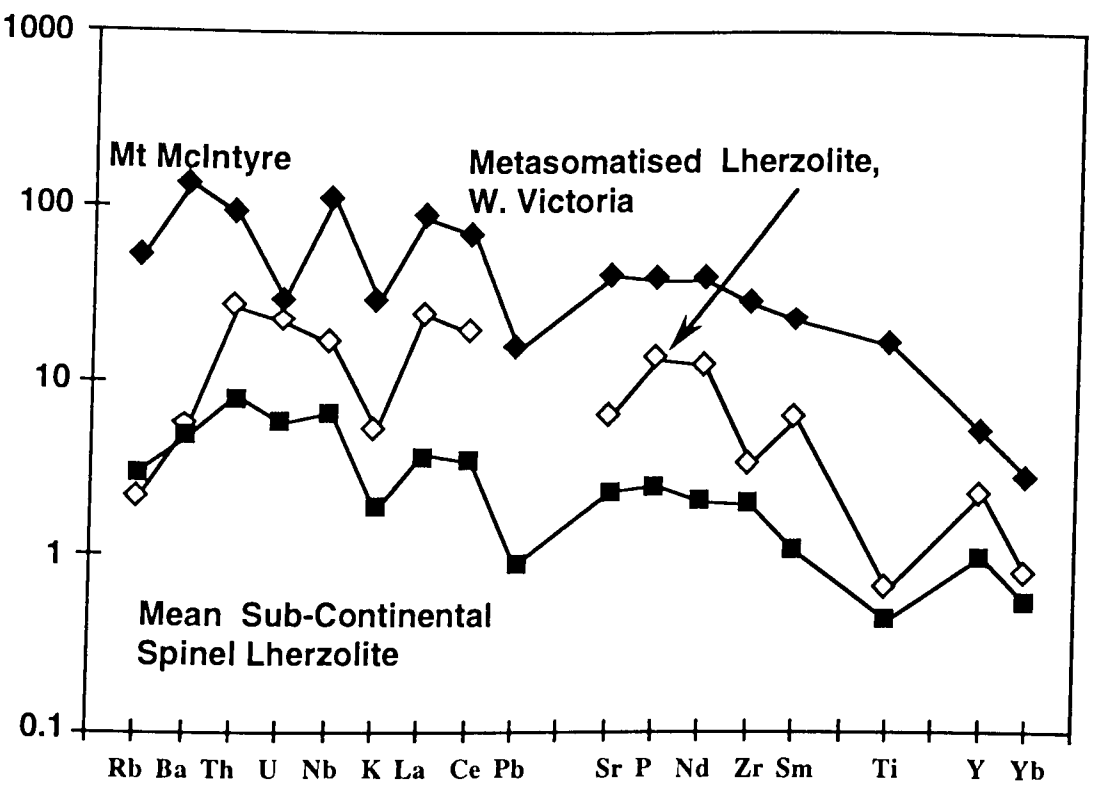

Fig. 7.7. PM normalised incompatible element abundances of spinel lherzolites and Quaternary basalt.

In general, the alkaline basalts show more Jurassic kimberlite-like trace element characteristics than the lamprophyres which show a strong negative Nb anomaly and higher K contents (Fig. 7.6), but contain lower total concentration in the most of the trace elements. McDonough (1990) suggested that the average continental lithospheric mantle compositions is appropriate as possible source for intraplate alkaline basalt. In the PM normalised incompatible element patterns, Mt McIntyre volcanics display parallel incompatible abundances to the metasomatised western Victorian lherzolites (O'Reilly and Griffin, 1988) as well as the mean sub continental spinel lherzolites (McDonough 1990), suggesting that the alkaline basalts partly contain the lithospheric mantle components (Fig. 7.7). This observation is consistent with a small degree of partial melting of upper mantle peridotites (4-5 %) to produce the alkaline basalt (See, Chapter 3).

In a normal mixing trend between partial melts of the lithospheric mantle enrichment (kimberlites) and asthenospheric mantle sources (DM), overlap of the Victorian metasomatized lherzolites in the field of the S.A. Pliocene-Recent alkaline volcanism suggesting that the basalts are derived from the mixing of the two different magma sources (Fig. 7.8).

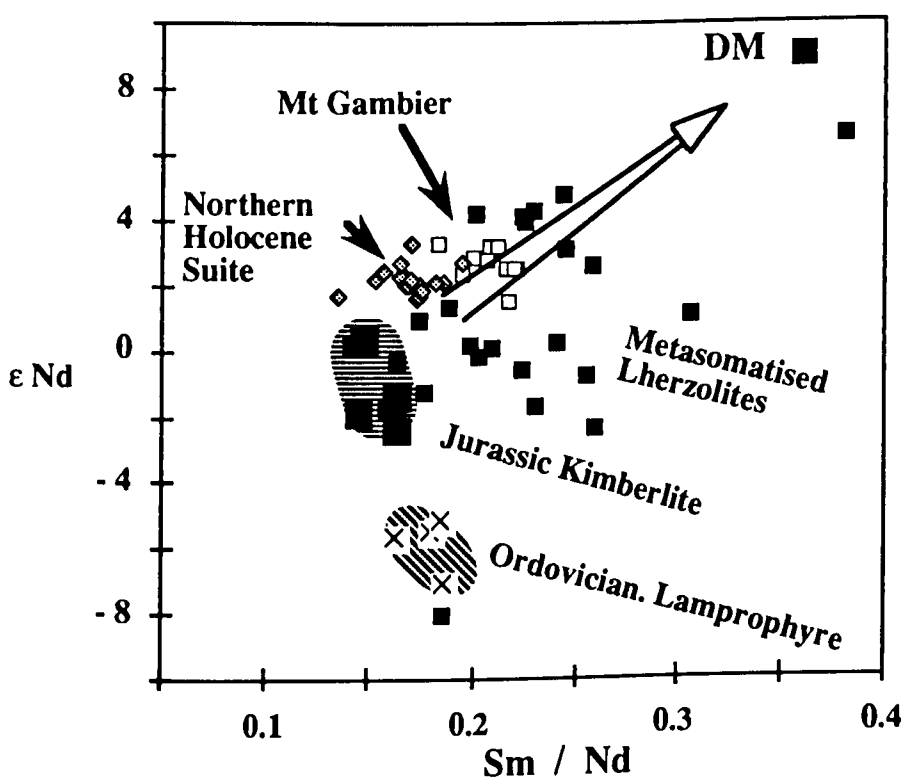

Fig. 7.8. εNd-Sm/Nd relationships of South Australian kimberelites, lamprophyres, Quaternary alkaline basalt, and Victorian metasomatized lherzolites. PM data from Sun and McDonough (1989)

7.8. Enrichment of South Australian continental lithosphere

As shown in Fig. 7.2, the isotopic composition of Jurassic kimberlites overlaps the field of the late Proterozoic-Cambrian mafic volcanism and that of their xenoliths lies in the range of Willouran (Neoproterozoic) basalts (Fig. 7.9a, b). In the εNd versus Sm/Nd variation diagram (Fig. 7.9a), Cambrian volcanics, Jurassic kimberlites and their eclogitic xenoliths coexist until 500 Ma while Ordovician lamprophyres have equivalent isotopic composition to the Neoproterozoic basalts at 800 Ma. However, they are clearly distinguished from mafic rocks of the Gawler Craton (Palaeozoic, Mesoproterozoic to Archaean ages) by the high εNd ratios. A comparison of depleted mantle Nd Model ages for South Australian intrusive and extrusive rocks are shown in the Fig. 7.9b. They are mafic rocks in compositions which have very high Nd/Sm ratios.Thus the calculated model ages are indeed meaningful, even though the model ages of kimberlites may suggest date enrichments rather than eruption ages. These isotopic results suggest that underplating and mantle enrichment within the South Australian lithosphere took place during Neoproterozic and Cambrian rifting and basin formation.

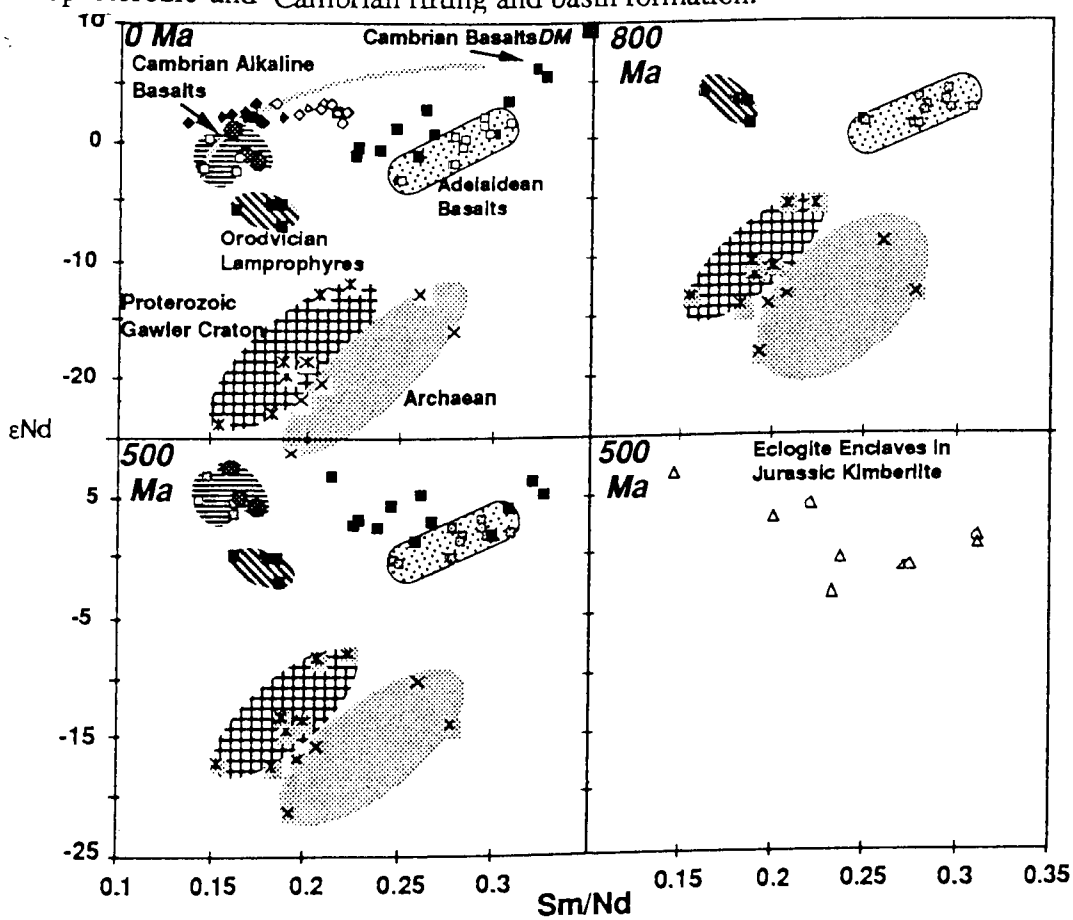

Fig. 7.9a. εNd- Sm/Nd variations in South Australian basalts, kimberlites, lamprophyres, and Archaean -Cambrian basalts. Symbols open diamond for Mt Gambier volcanos and filled diamond for Northern area volcanos.

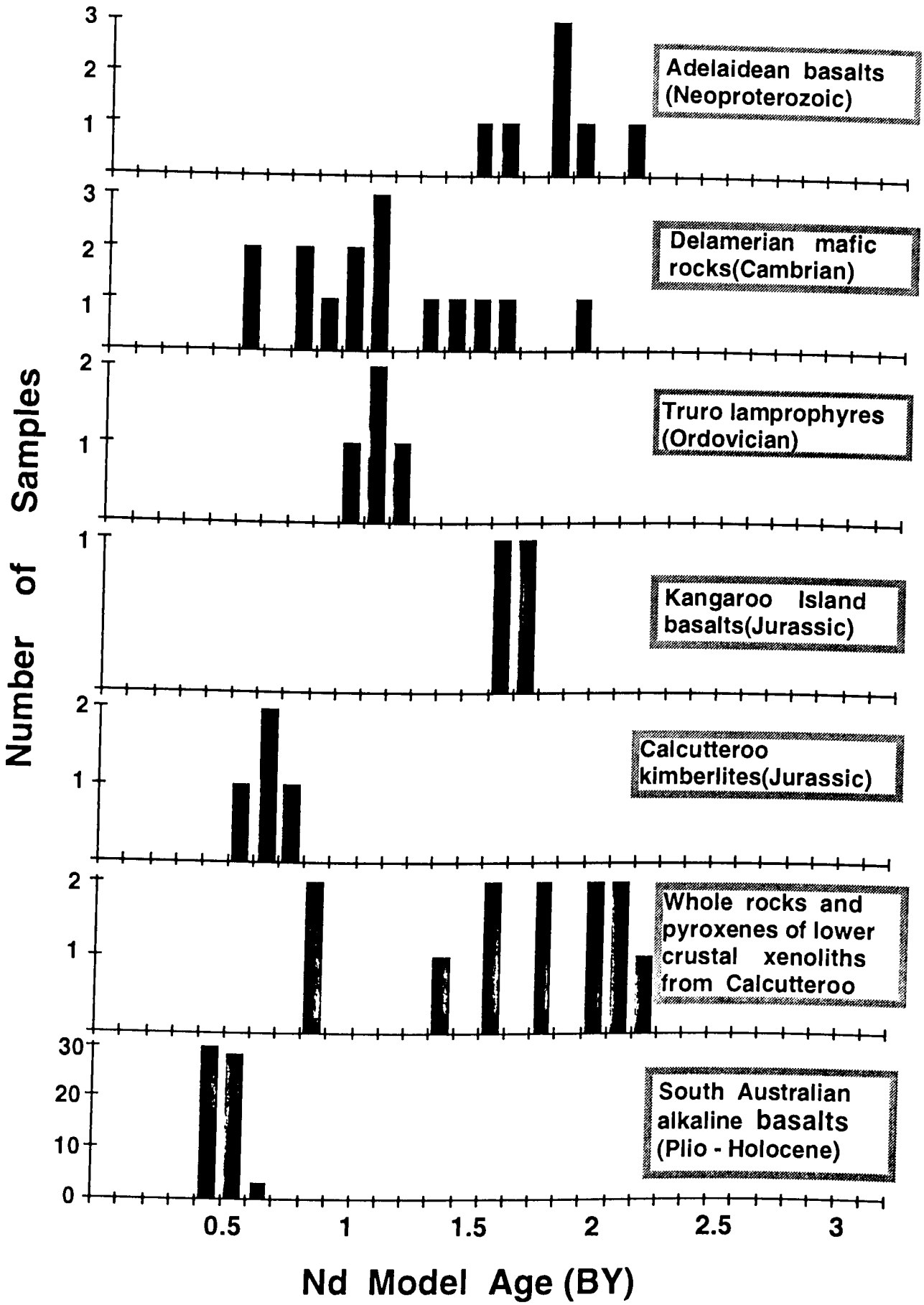

Fig. 7.9b. Comparison of depleted mantle Nd Model ages (By) for South Australian mafic intrusive and extrusive rocks.

The Jurassic kimberlites are also geochemically similar to the early Cambrian undersaturated, highly alkaline basalts from Heatherdale Shale in the southern AFB (Fig. 7.3), also suggesting that the kimberlites reflect a geochemical enrichment in CLM during the Late Proterozoic and Early Palaeozoic.

7.9. Possible mixing models for the evolution of the Phanerozoic South Australian lithosphere and hypothetical lithospheric mantle growth history

A possible mixing model is shown in Fig. 7.10. In the model, Plio-Recent alkali basalts are plotted in a mixing tend, assuming a possible depleted mantle components (E-MORB, or OIB of Sun and McDonough, 1989) and an enriched lithospheric mantle components (e.g. Calcutteroo kimberlites). In this mixing model, slightly earlier northern Groups volcanoes (e.g. Mt Mcintyre, Mt Muirhead) have larger lithospheric components than the younger Southern group (Mt Gambier and Mt Schank).

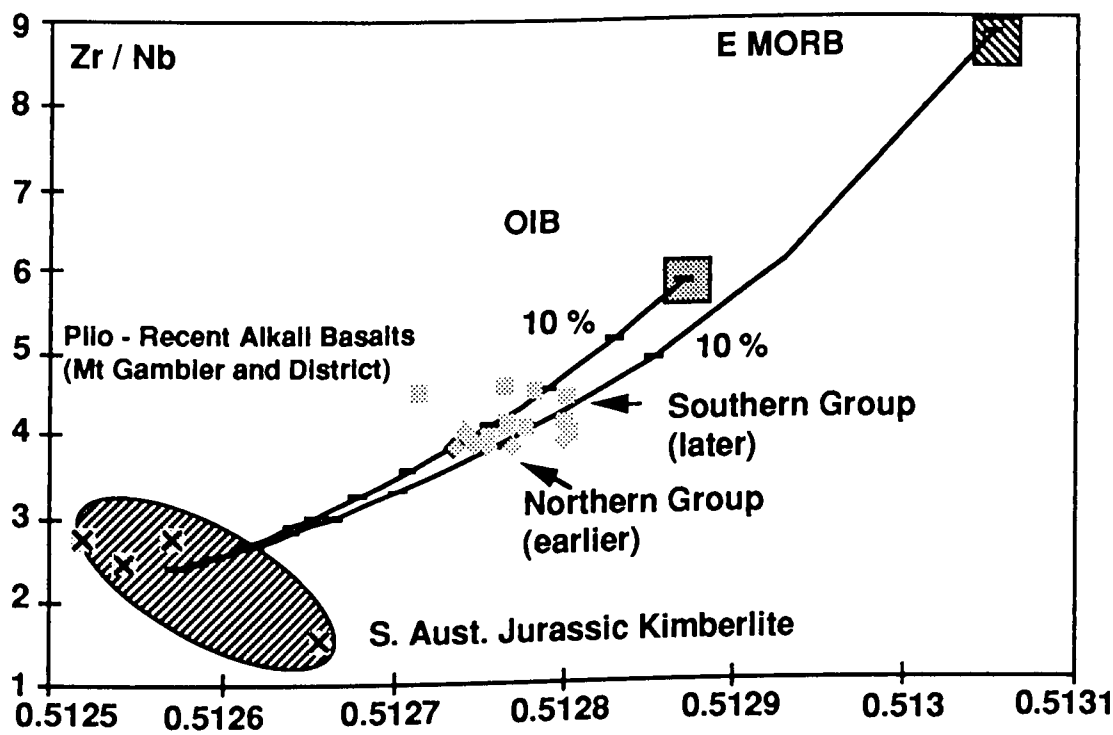

Fig. 7.10. A possible mixing model plotted in Zr/Nb-143Nd/144 Nd planes.

A hypothetical lithospheric mantle growth history across an E-W transect from eastern S. Australia to the Gawler Craton, is shown in Fig. 7.11. This figure show a thick lithosphere in the western side and relict of mafic components which represent by the underplating of the basaltic melt at the crust-mantle boundary. The hatched area indicates enriched layer of different ages. They migrate toward the surface during extension and thinning or when the lithospheric mantle is heated by mafic intrusion or plume impingements.

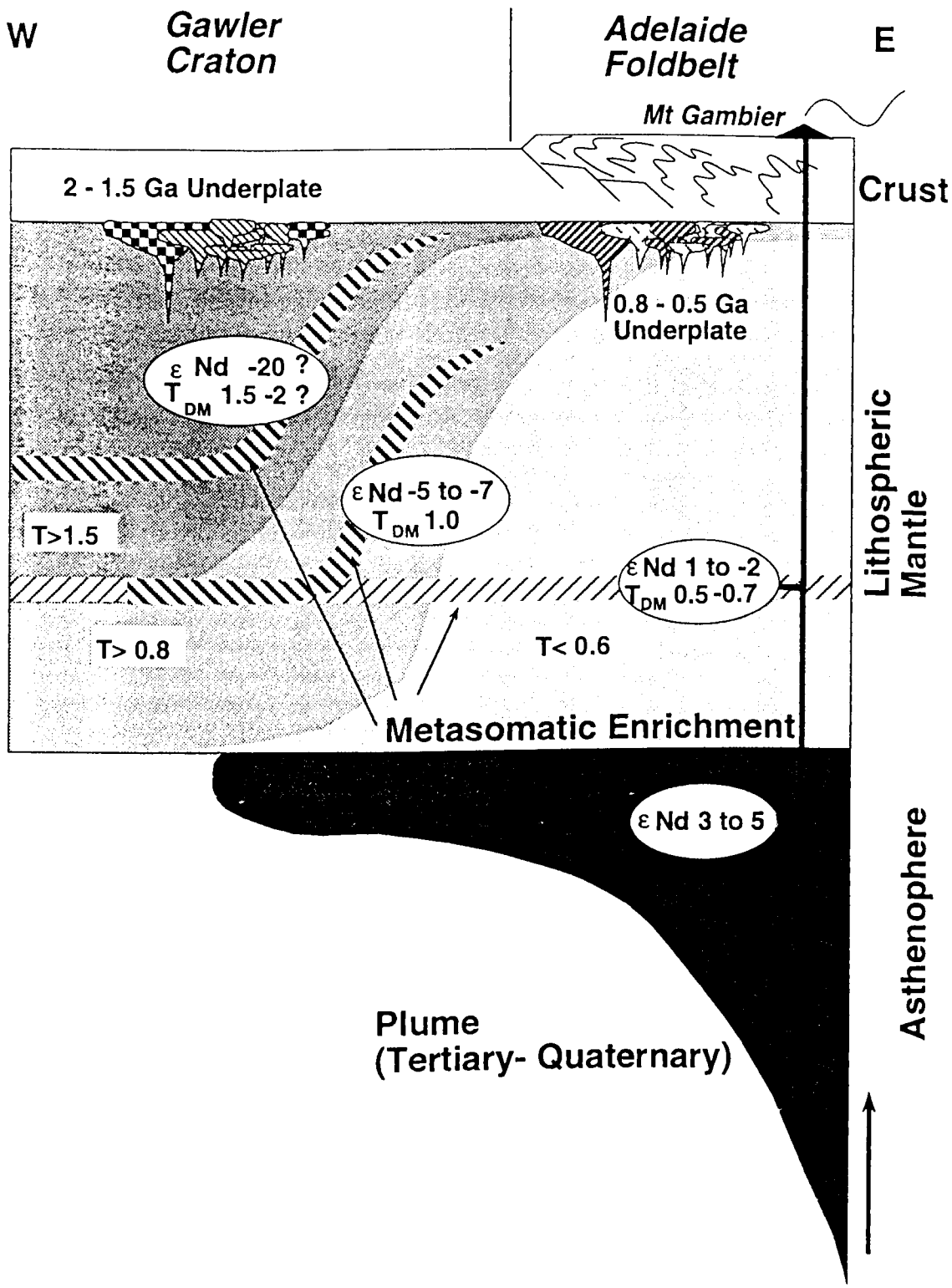

Fig. 7.11. Possible lithospheric mantle growth history from Gawler Craton and eastern Australia

This picture also shows that South Australian alkaline basalts are of mixed origin from lithospheric sources and asthenopheric sources. Unlike the Gawler Craton area which may have experienced a lithospheric enrichment for a long time period in the stable condition, the lithosphere below the Adelaide Geosyncline area should have experienced a more complicated magmatic process.

The area to the east of the Tasman line (including the eastern Australian basaltic provinces) is a part of the north eastern margins of the Palaeozoic Gondwana supercontinent (Veevers, 1984) and include the northern extension of the widespread zone of Jurassic continental flood basalt provinces. This margin was developed by regional tectonism which was related to the opening of the Pacific ocean. Possibly, the lithosphere beneath the area has experienced thermal disturbance and chemical modification by mantle metasomatism before Mesozoic times. The evidence for this metasomatism is sampled by upper mantle xenoliths from Victorian basaltic provinces, which show Neoproterozoic to early Palaeozoic $TNd_{(DM)}$ and which this work suggests may be enrichment formed during Neoproterozoic-Cambrian rifting in the southern cratonic margin.

During the Tertiary to Quaternary time, plumes which mix upper-mantle (? MORB) and OIB-like sources of asthenospheric origin intruded eastern Australian lithosphere. These complex plume-sources interacted with the enriched sub-continental lithospheric mantle producing varying degree of contamination by the kimberlite-like lithospheric component. The Quaternary suites of S.E. South Australia are amongst the most lithospheric-dominant of all the Cainozoic suites of eastern Australia. This probably, indicates that the plumes involved here (eastern South Australia) were smaller or cooler than those from the east of earlier in the late Tertiary. South Australia may be at the extreme margin of the proposed plume suites (e.g. Sutherland, F.L., 1981) responsible for the general eastern Australia basaltic province.

7.10. Possible shallow lithospheric structure beneath the Palaeozoic Adelaide Geosynclines

A possible idealised shallow structure is shown in Fig. 7.12. The vertical section are based on main aspects as follows.

1) Moho depths range from 35 to 40 km depths with seismic velocities (Vp of 7.97- 8.21); 2) lateral variability in the crustal thickness and of velocities of Vp within the Adelaide Geosyncline, variability of Moho depths of the order of 10 km; 3) Proterozoic sediment within the upper 20 km of the crust; 4) majority of xenoliths showing cumulate-like characteristics rather than restite; 5) mafic dominant xenoliths including eclogitic to granulitic rocks and rare spinel lherzolites or garnet lherzolites; 6) possible existence of the eclogites to the depth of 75 km and a granulite-eclogite transition between 40 to 75 km ranges by the kinetic factors; 7) rare gabbroic rocks because the are metastable under the lower crustal

P.T. condition; 8) petrophysical evidences for the xenoliths which compare with the seismic data.; 9) deep, thicker, cooler lithosphere rather than the Phanerozoic lithosphere, and possibly deeper eclogite-granulite or spinel lherzolite-garnet lherzolite transition.

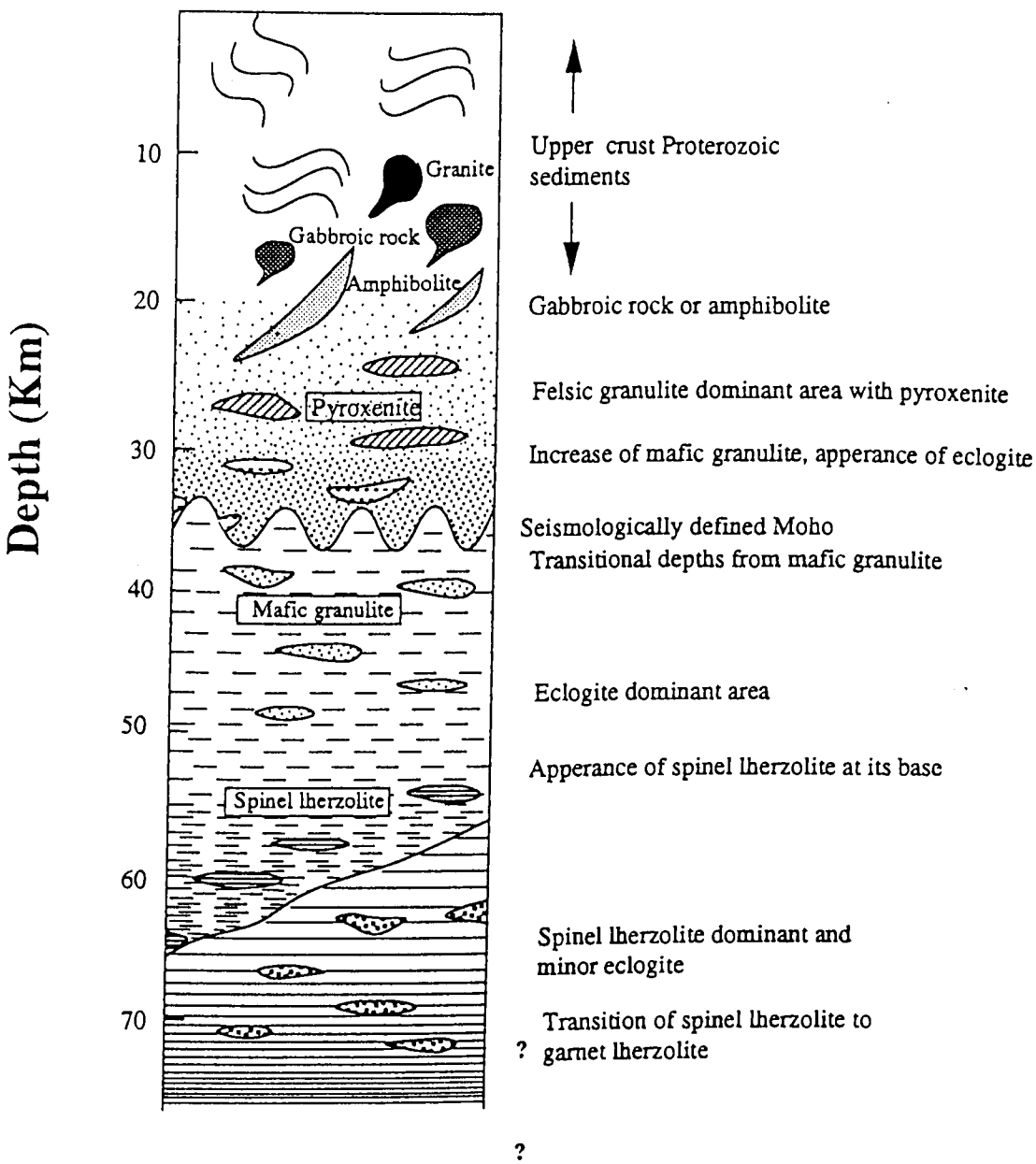

Fig. 7.12. Possible shallow lithospheric structure beneath the Palaeozoic Adelaide Geosynclines.

References

Adams, C.J., 1981. Migration of late cenozoic volcanism in the South Island of New Zealand and the Campbell Plateau. *Nature*, **294**, 153-155.

Allégre, C.J., 1982. Chemical geodynamics. *Tectonophysics*, **81**, 109-132.

Allégre, C.J., Ben Othman, D., Polve, M., Richard, P., 1979. The Nd-Sr isotopic correlation in mantle materials and geodynamic consequences. *Phys. Earth Planet. Inter.*, **19**, 293-306.

Anderson, D.L. and Sammis, C., 1970. Partial melting in the upper mantle. *Phys. Earth Planet. Inter.*, **3**, 31-50.

Anderson, D.L., 1962. The plastic layer in the Eath's mantle. *Sci. Am.*, **205**, 2-9.

Anderson, D.L., 1982. Hotspots, polar wander, Mesozoic convection and the Geoid. *Nature*, **297**, 391-393.

Anfiloff, V., 1982. Elevation and gravity profiles across Australia: some implications for tectonism. *BMR J. Aust. Geol. Geophys.*, **7**, 47-54.

Arculus, R.J., Ferguson, J., Chappell, B.W., Smith, D., McCulloch, M.T., Jackson, I., Hensel, H.D., Taylor, S.R., Knutson, J. and Gust, D.A., 1988. Trace element and isotopic characteristics of eclogites and other xenoliths derived from the lower continental crust of southeastern Australia and southwestern Colorado Plateau, U.S.A. In: Smith, D.C. (ed.), *Eclogites and eclogite-facies rocks*. Elsevier, Amsterdam, 335-386.

Bailey, D.K., 1984. "The mantle sample" formed by ultrametasomatism. In: Kornprobst, J. (ed.), *Kimberlites and Related Rocks. Develop. in Petrology*, **11A**. Elsevier, Amsterdam, 323-334.

Ballhaus, C., Berry, R.F. and Green, D.H., 1991. High pressure experimental calibration of the olivine-orthopyroxene-spinel oxygen geobarometer: implications for the oxidation state of the upper mantle. *Contrib. Minetral. Petrol.*, **107**, 27-40.

Barbetti, M. and Sheard, M.J., 1981. Palaeomagnetic measurements from Mts Gambier and Schank, Southeast, South Australia.*J. Geol. Soc. Aust.*, **28**(4), 385-394.

Belbo, M.A., Bjornsson, A., Arnason, K., Stein, B. and Wofgram, P., 1983. Electrical conductivity beneath Iceland-constraints imposed by magnetotelluric results on temperature, partial melt, crust and mantle structures. *J. Geophys.*, **53**, 16-23.

Ben Othman, D., Polvé, M. and Allégre, C.J., 1984. Nd-Sr isotopic composition of granulites and constraints on the evolution of the lower continental crust. *Nature*, **307**, 510-515.

Ben Othman, D., Tilton, G. and Menzies, M.A., 1982. Lead isotope studies of kaersutites from ultramafic nodules. *Trans. Am. Geophys. Un.*, **63**, 1134.

Berckhemer, H., 1969. Direct evidence for the composition of the lower crust and the Moho. *Tectonophysics*, **8**, 97-105.

Bergman, S.C., 1987. Lamproites and other potassium-rich igneous rocks: a review of their occurrence, mineralogy and geochemistry. In: Fitton, J.G. and Upton, B.J. (eds), *Alkaline igneous rocks*. Geol. Soc. S. Publ., 30, 103-190.

Birch, F., 1960. The velocity of compressional waves in rocks to 10 kbar, 1. *J. Geophys. Res.*, **65**, 1083-1102.

Birch, F., 1961. The velocity of compressional waves in rocks to 10 kbar, 2. *J. Geophys. Res.*, **66**, 2199-2224.

Birch, W.D., 1979. Mineralogy and geochemistry of the leucitite at Cosgrove, Victoria. *J. Geol. Soc. Aust.*, **25**, 369-385.

Black, L.P., Ferguson, J. and Gray, P.T, 1993. A Jurassic U-Pb zircon age for South Australian kimberlitic rock. *Quaternary Notes*, **125**, 2-5.

Blackburn, G., Alison, G.B. and Leaney, F.W.J., 1982. Further evidence on the age of tuff at Mt Gambier, South Australia.*Trans. R. Soc. S. Aust.*, **106**, 163-167.

Bloomer, A.G. and Nixon, P.H., 1973. The geology of the Letseng-Laterae kimberlite pipes. In: Nixon, P.H. (ed.), *Lesotho kimberlites*. Lesotho National Development Corporation, Maseru, 20-32.

Bolt, B.A., Doyle, H.A. and Sutton, D.J., 1958. Seismic observations from the 1956 Atomic Explosions in Australia. *Geol. J. Roy. Astron. Soc.*, **1**, 135-145.

Boyd, F.R. and Mertzman, S.A., 1987. Composition and structure of the Kaapvaal lithosphere, southern Africa. In: Mysen, B.A. (ed.), *Magmatic Processes: Physicochemical Principles*. Spec. Publ., 1. 13-24. The Geochem. Soc.Univ. Park, PA.

Boyd, F.R. and Nixon, P.H., 1975. Origins of the ultramafic nodules from some kimberlites of northern Lesotho and the Monastery Mine, South Africa. *Phys. Chem. Earth*, **9**, 431-454.

Bradshaw, T.K., Hawkesworth, C.J. and Gallagher, K., 1993. Basaltic volcanism in the Southern Basin and Range: No role for a mantle plume. *Earth Planet. Sci. Lett.*, **116**, 45-62.

Buddington, A.F. and Lindsley, D.H., 1964. Iron-titanium oxide minerals and synthetic equivalents. *J. Petrol.*, **5**, 310-357.

Carlson, R.W., 1984. Isotopic constraints on Columbia River flood basalt genesis and the nature of the subcontinental mantle. *Geochim. Cosmochim. Acta*, **48**, 2357-2372.

Carswell, D.A., Griffin, W.L. and Kresten, P.H., 1984. Peridotite nodules from the Ngopetsuev and Lipelaneng kimberlites Lesotho: A crustal or mantle origin. In: Kornprobst, J. (ed.), *Kimberlites II: The mantle and crust-mantle relationships*. Elsevier, 229-243.

Cas, R.A.F., 1989. Explosive eruption centres. In: Johnson, R.W. (ed.), *Intraplate Volcanism in Eastern Australia New Zealand.* Cambridge Univ. Press, Cambridge, 78-82.

Chen, C-Y., Frey, F.A. and Garcia, M.O., 1990. Evolution of alkalic lavas at Haleakala volcano, east Maui, Hawaii major, trace element and isotopic constraints. *Contrib. Mineral. Petrol.*, **105**, 197-218.

Chen, C.-Y. and Frey, F.A., 1983. Origin of Hawaiian tholeiite and alkalic basalt. *Nature*, **302**, 785-789.

Chen, Y.D., O'Reilly, S.Y., Kinny, P.D. and Griffin, W.L.,1994. Dating lower crust and upper mantle events: an ion microprobe study of xenoliths from kimberlitic pipes, South Australia. *Lithos*, **32**, 77-94.

Christensen, N. I. and Fountain, D.M., 1975. Constitution of the lower continental crust based on experimental studies of seismic velocities in granulites. *Bull. Geol. Soc. Am.*, **86**, 227-236.

Christie, D.M., Carmichael, I.S.E. and Langmuir, C.H., 1986. Oxidation states of mid-ocean ridge basalt glasses. *Earth Planet. Sci. Lett.*, **79**, 397-411.

Clarke, S.P. and Ringwood, A.E., 1964. Density distribution and constitution of the mantle. *Rev. Geophys.*, **12**, 35-88.

Cleary, J.R., Simpson, D.W. and Muirhead, K.J., 1972. Variations in Australian upper mantle struture from observations of the Cannikin explosion. *Nature* (London), **236**, 111-112.

Cohen, R.S. and O'Nions, R.K., 1982. The lead, neodymium and strontium isotopic structure of ocean Ridge basalts. *J. Petrol.*, **23**, 299-324.

Coleman, R.G., Lee, D.E., Beatty, L.B. and Brannock, W.W., 1965. Eclogites and eclogites: their differences and similarities. *Geol. Soc. Am. Bull.*, **76**, 483-508.

Collerson, K.D. and McCulloch, M.T., 1983. Nd and Sr isotope geochemistry of leucite-bearing lavas from Gaussberg, East Antarctica. In: Oliver, R.L., James, P.R. and Jago, J.B. (eds), *Proceedings of the 4th International Symposium of Antarctic Earth Science. Aust. Acad. Sci.*, Canberra, A.C.T., 676-680.

Collins, C.D.N., 1978. Crustal structure of the central Bowe Basin, Queensland. *BMR J. Aust. Geol. Geophys.*, **3**, 203-209.

Collins, C.D.N., 1988. Seismic velocities in the crust and upper mantle of Australia. *Bur. Mineral Res. Aus. Rep.*, **277**.

Collins, C.D.N., 1991. The nature of the crust-mantle boundary under Australia from seismic evidence. In: Drummond, B.J. (ed.), *The Australian Lithosphere.* Geol Soc. Aust. Spec. Pub. Ser., 17, 67-80.

Constable, S.C. and Duba, A., 1990. Electrical conductivity of olivine, a Dunite, and the mantle. *J. Geophys. Res.*, **95**, 6967-6978.

Constable, S.C., 1991. Electrical studies of the Australian lithosphere. In: Drummond, B.J. (ed.), *The Australian Lithosphere*. Geol. Soc. Aust. Spec. Publ., 17, 121-140

Coombs, D.S. and Wilkinson, J.F.G., 1969. Lineages and fractionation trends in undersaturated volcanic rocks from the East Otago Volcanic Province (New Zealand) and related types. *J. Petrol.*, **10**, 440-501.

Cooper, J.A. and Green, D.H., 1969. Lead isotope measurements on lherzolite inclusion and host dasanites from western Victoria, Australia. *Earth Planet. Sci. Lett.*, **6**, 69-76.

Cox, K.G. and Hawkesworth, C.J., 1985. Geochemical stratigraphy of the deccan traps at Mahabaleshwar, Western Ghats, India, with implications for open system magmatic processes. *J. Petrol.*, **26**, 355-377.

Cox, K.G., Bell, J.D. and Pankhurst, R.J., 1979. The Interpretation of Igneous Rocks. Allen & Unwin, London.

Crock, J.G., Lichte, F.E. and Wildeman, T.R., 1984. The group separation of the rare-earth element and yttrium from geologic materials by cation-exchange chromatography. *Chem. Geol.*, **45**, 149-163.

Crough, S.T., Morgan, W.J. and Hargraves, R.B., 1980. Kimberlites: their relation to mantle hotspots. *Earth Planet. Sci. Lett.*, **50**, 260-274.

Cull, J.P. and Conley, D., 1983. Geothermal gradients and heat flow in Australian sedimentary basins. *BMR J. Aust Geol. Geophys.*, **8**, 329-337.

Cull, J.P. and Denham, D., 1979. Regional variation in Australia heat flow. *BMR J. Aust.Geol.Geophys.*, **4**, 1-13.

Cull, J.P., 1982a. An appraisal of Australian heat-flow data. *BMR J. Aust. Geol.Geophys.*, **7**, 11-21.

Cull, J.P., 1982b. Magnetotelluric profiles in the McArthur Basin of northern Australia. *BMR J. Aust. Geol. Geophys.*, **7**, 275-286.

Cull, J.P., 1991. Geothermal gradients in Australia. In: Drummond, B.J. (ed.), *The Australian Lithosphere*. Geol. Soc. Aust. Spec. Publ. 17, 147-155.

Cundari, A., 1973. Petrology of the leucite-bearing lavas in New South Wales. *J. Geol. Soc. Aust.*, **20**, 465-492.

Dahl, P.S., 1980. The thermal-compositional dependence of Fe^{2+}-Mg distributions between coexisting garnet and pyroxene: applications to geothermometry. *Am. Mineral.*, **65**, 854-866.

Daly, S.J. and Fanning, C.M., 1990. Archaean geology of the Gawler Craton. In: Glover, J.E. and Ho, S.E. (Compilers), *Third International Archaean Symposium. Extended abstracts*, 91-92.

Daniels, L. R.M. and Gurney, J.J., 1991. Oxygen fugacity constraints on the southern African lithosphere. *Contrib. Mineral. Petrol.*, **108**, 154-161.

Davis, J.M., Elston, W.E. and Hawkesworth, C.J. (in press). Basic and intermediate volcanism of the Mogollon Datil Volcanic Field: Implications for the mid-Tertiary tectonic and magmatic transitions in southwestern New Mexico, U.S.A.

Deer, W.A., Howie, R.A. and Zussman, J., 1966. An introduction to the rock-forming minerals. Longman Group Ltd., London.

Denham, D., 1991. Shear wave crustal models for the Australian continent. In: Drummond, B.J. (ed.), *The Australian Lithosphere*. Geol. Soc. Aust. Spec. Publ., 17, 59-66.

Denham, D., Simpson, D.W., Gregson, P.J. and Sutton, D.J., 1972. Travel times and amplitudes from explosions in northern Australia. *Geophys. J. Roy. Astr. Soc.*, **28**, 225-235.

DePaolo, D.J., 1980. Crustal growth and mantle evolution: inferences from models of element transport and Nd and Sr isotopes. *Geochim. Cosmochim. Acta*, **44**, 1185-1196.

Dodson, J.R., 1974. Vegetation history and water fluctuations at Lake Leake, south-eastern South Australia 1.10000 B.P. to Present. *Aust. J. Bot.*, **22**, 719-741.

Dooley, J.C., 1971. Seismological studies of the upper mantle in the Australian region. Proceedings of the 2nd symposium of the upper mantle project, December 1970. Hyderabad, 113-146.

Dooley, J.C., 1991. Velocity variations and isostatic compensation in the Australian Region. In: Drummond, B.J. (ed.), *The Australian Lithosphere*. Geol. Soc. Aust.Spec. Publ., 17, 41-58.

Downes, H., 1987. Relationship between geochemistry and textural type in spinel lherzolites, Massif Central and Languedoc, France. In: Nixon, P. H. (ed.), *Mantle Xenoliths*. John Wiley, 125-133.

Drummond, B.J. and Collins, C.D.N., 1986. Seismic evidence for underplating of the lower continent crust of Australia. *Earth Planet. Sci. Lett.*, **79**, 361-372.

Drummond, B.J., Muirhead, K.J., Wellman, P. and Wright, C., 1989. A teleseismic travel- time esidual map of the Australian continent. *BMR J. Aust. Geol. Geophys.*, **11**, 101-105.

Duba, A. and Shankland, T.J., 1982. Free carbon and the electrical conductivity of the Earth's mantle. *Geophys. Res. Lett.*, **9**, 1271-1274.

Duba, A., 1972. The electrical conductivity of olivine. *J. Geophys. Res.*, **77**, 2483-2495.

Duba, A., Heard, H.C. and Schock, R.N.,1974. Electrical conductivity of olivine at high pressure and under controlled oxygen fugacity. *J. Geophys. Res.*, **79**, 1667-1673.

Duba, A., Jamieson, J.C. and Ito, J., 1973. The effect of ferric iron on the electrical conductivity of olivine. *Earth Planet. Sci. Lett.*, **18**, 279-284.

Dudas, F.O., Carlson, R.W. and Eggler, D.H., 1987. Regional middle Proterozoic enrichment of the subcontinental mantle source of igneous rocks from central Montana. *Geology*, **15**, 22-25.

Duncan, R.A. and McDougall, I., 1989. Volcanic time-space relationships. In: Johnson, R.W. (ed.), *Intraplate Volcanism in eastern Australia and New Zealand.* Cambridge Univ. Press, Cambridge, 43-53.

Dury, G.J. and Langford-Smith, T., 1968. Australian geochronology: Checklist 3. *Aust. J. Sci.*, **30**, 304-306.

Edgar, A.D. and Vukadinovic, D., 1992. Implications of experimental petrology to the evolution of ultrapotassic rocks. In: Peccerillo, A. and Foley, S. (eds), Potassic and Ultrapotassic Magmas and their Origin. *Lithos*, **28**, 205-220.

Edward, A.C., Lovering, J.F. and Ferguson, J., 1979. High pressure basic inclusions from the Kayrunnera kimberlitic diatreme in New South Wales, Australia. *Contrib. Mineral. Petrol.*, **69**,185-192.

Eggler, D.H., 1986. Kimberlites: how do they form? In: Ross, J. *et al.* (eds), *Kimberlites and Related Rocks*, V.1: Their composition, occurrence, origin and emplacement, Proc. 4th Inter. Kimberlite Conf., GSA Spec. Publ. No, 14, 399-504.

Eggler, D.H., 1987. Solubility of major and trace elements in mantle metasomatic fluids: experimental constraints. In: Menzies, M. and Hawkesworth, C.J. (eds), *Mantle Metasomatism.* Academic Press, U.K., 21-41.

Eggler, D.H., Dudas, F.O., Hearn, B.C., McCallum, M.E., McGee, E.S. and Schulze, D.J., 1987. Lithosphere of the continental united states: xenoliths in kimberlite and related magmas. In: Nixon, P.J. (ed.), *Mantle Xenoliths*, John Wiley, New York. 41-57.

Ellis, D.J. and Green, D.H., 1985. Garnet-forming reactions in mafic granulites from Enderby Land, Antarctica-implications for geothermometry and geobarometry. *J. Petrol.*, 26, 633-661.

Ellis, D.J. and Green, D.H.,1979. An experimental study of the effect of Ca upon garnet-clinopyroxene Fe-Mg exchange equilibria. *Contrib. Mineral. Petrol.*, **71**, 13-22.

Ellis, D.J., 1976. High pressure cognate inclusions in the New Volcanics of Victoria. *Contrib. Mineral. Petrol.*, **58**, 149-180.

Ellis, R.M. and Denham, D., 1985. Structure of the crust and upper mantle beneath Australia from Rayleigh-and Love-wave observations. *Phys. Earth Planet Inter.*, **38**, 224-234.

Erlank, A.J., Allsopp, H.L., Hawkesworth, C.J. and Menzies, M.A., 1982. Chemical and isotopic characterisation of upper mantle metasomatism in peridotite nodules from the Bultfontein kimberlite. *Terra Cognita*, **2**, 3.

Eskola, P., 1920. The mineral facies of rocks. *Norsk Geol. Tidsskr.*, **6**, 143-194.

Esperanca, S., Carlson, R.W., Lambert, D.D. and Svisero, D.P., 1993. The petrology and geochemistry of deep crustal granulite xenoliths in an ultrapotassic host, minas gerais state, Brazil. In: *The xenolith window into the lower crust.* IGCP project 304 " Lower Crustal Processes". International workshop, Sydney, 1993. Abstracts. p.8.

Etheridge, M.A., Rutland, R.W.R. and Wyborn, L.A.I., 1987. Orogenesis and tectonic process in the early to middle Proterozoic of northern Australia. In: Kröner, A. (ed.),

Precambrian Lithospheric Evolution. Am. Geophys. Union, Washington D.C., Geodynamics Ser., 17, 131-147.

Ewart, A. and Chappell, B.W., 1989. Trace element geochemistry. In: Johnson, R.W. (ed.), *Intraplate Volcanism in eastern Australia and New Zealand*. Cambridge Univ. Press, Cambridge, 219-235.

Ewart, A. 1989a. Mineralogy and Mineral chemistry. In: Johnson, R.W. (ed.), *Intraplate Volcanism in eastern Australia and New Zealand.* Cambridge Univ. Press, Cambridge, 197-217.

Ewart, A., 1989b. Major element chemistry and chemical affinities. In: Johnson, R.W. (ed.), *Intraplate Volcanism in eastern Australia and New Zealand.* Cambridge Univ. Press, Cambridge, 190-197.

Ewart, A., Baxter, K. and Ross, J.A.,1980. The petrology and pertogenesis of the Tertiary anorogenic mafic lavas of southern and central Queensland, Australia-possible implications for crustal thickening. *Contrib. Mineral. Petrol.*, **75**, 129-152.

Fanning, C.M., 1975. Petrology, Structure and geochronology of some high grade metamorphic rocks at Fishery Bay and Cape Carnot, Southern Eyre Peninsula. *Univ. Adelaide Hons. Thesis,* (unpubl.).

Fanning, C.M., Flint, R.S., Parker, A.J., Ludwig, K.R. and Blissett, A.H., 1988. Refined Proterozoic evolution of the gawler craton, South Australia, through U-Pb zircon geochronology. *Precambrian Res.*, **40/41**, 363-386.

Fehlberg, B., 1968. Ultramafic xenoliths from basaltic rocks of southern Australia. *Honours Thesis Univ. of Adelaide, South Aust. (Unpublished).*

Fenner, C., 1921. The craters and lakes of Mount Gambier, South Australia. *Trans. Roy. Soc. S. Aust.*, **45**, 169-205.

Ferguson, A.K., 1978. Ca enrichment in olivines from volcanic rocks. *Lithos*, **11**, 189-194.

Ferguson, G.J. and Rafter, T.A., 1957. New Zealand C^{14} age measurements. *N.Z. Jl Sci. Technol.*, **38**(b), 732-733.

Ferguson, J. and Sheraton, J.W., 1979. Petrogenesis of kimberlitic rocks and associated xenoliths of Southeastern Australia. In: Boyd, F.R. and Meyer, H.O.A. (eds), *Kimberlites, Diatremes, and Diamonds: their geology petrology, and geochemistry. Proceedings of the 2nd International Kimberlite Conference, 1.* Am. Geophys. Union, Washington, 140-161.

Ferguson, J., Arculus, R.J. and Joyce, J., 1979. Kimberlite and kimberlitic intrusives of southeastern Australia: a review. *BMR J. Aust. Geol. Gephys.*, **4**, 227-241.

Fesq, H.W., Kable, E.J.D. and Gurney, J.J., 1975. Aspects of the geochemistry of kimberlites from the premier mine, and other selected South African occurrences with particular reference to the Rare Earth Elements. *Phys. Chem. Earth*, **9**, 687-707.

Finlayson, D.M., 1982. Geophysical differences in the lithosphere between Phanerozoic and Precambrian Australia. *Tectonophysics*, **84**, 287-312.

Finlayson, D.M., 1983. The mid-crustal horizon under the Eromanga Basin, Eastern Australia. *Tectonophysics*, **100**, 199-214.

Finlayson, D.M., Collins, C.D.N. and Lock, J., 1984. P-wave velocity features of lithosphere under the Eromanga Basin, eastern Australia, including a prominent mid-crustal (Conrad?) disconformity. *Tectonophysics*, **101**, 267-291.

Finlayson, D.M., Cull, J.P. and Drummond, B.J., 1974. Upper mantle structure from the Trans-Australia seismic refraction data. *Geol. Soc. Aust. J.*, **21**, 447-458.

Fitton, J.G. and Dunlop, H.M., 1985. The Cameroon line, West Africa, and its bearing on the origin of Oceanic and continental alkali basalt. *Earth Planet. Sci. Lett.*, **72**, 23-38.

Fitton, J.G., 1987. The Cameroon line, West Africa: a comparison between oceanic and continental alkaline volcanism. In: Fitton, J.E. and Upton, B.G.J. (eds), *Alkaline Igneous Rocks. Geol. Soc. Spec. Publ.*, No. 30, 273-291.

Fitton, J.G., James, D., Kempton, P.D., Ormerod, D.S. and Leeman, W.P., 1988. The role of lithospheric mantle in the generation of late Cenozoic basic magmas in the Western United States. In: Menzies, M.A. and Cox, K.G. (eds), *Oceanic and Continental Lithosphere: Similarites and Differences. J. Petrol. (Spec. Publ.)*, 303-330.

Flöttmann, T. and Oliver, R.L. (in press). Review of Precambrian-Palaeozoic relationships at the craton margins of south eastern Australia and adjacent Antarctica. *Precambrian Research.*

Floyd, P.A., Kelling, G., Gokcen, S.L. and Gokcen, N., 1986. Trace element geochemistry and tectonic environment of volcanic rocks from the Misis melange, Adana South Turkey. Submittes for publication.

Foden, J. D., Turner, S.P. and Morrison, R.S., 1990. The tectonic implications of Delamerian magmatism in South Australia and western Victoria. *Geol. Soc. Aust.* Spec. Publ., **16**, 465-482.

Foden, J. D., Turner, S.P., Sandiford, M. and Michard, A., 1994. Granite composition, a response to orogenic thickening and thinning: Delamerian Orogeny, South Australia. Submitted to *J. Petrol.*

Foden, J.D., Turner, S.P., and Michard, A., 1989. Isotopic studies and lithospheric growth in the Adelaide Foldbelt. *SGTSG conference, Geol. Soc. Aust. Abst.* no. 24, 47-48.

Foden, J.D., Turner, S.P., Sandiford, M., Williams, I.S., Compston, W. and Michard, A., 1993. The nature, timing and duration of the Delamerian-Ross Orogeny. *J. Geol. Soc.*, London (submitted).

Foley, S., 1992. Petrological characterization of the source components of potassic magmas: geochemical and experimental constraints. In: Peccerillo, A. and Foley, S. (eds), Potassic and Ultrapotassic Magmas and their Origin. *Lithos*, **28**, 187-204.

Foley, S.F., 1988. the genesis of continental basic alkaline magmas: an interpretation in terms of redox melting. In: Menzies, M.A. and Cox, K.G. (eds), *Oceanic and Continental Lithosphere: Similarites and Differences. J. Petrol. (Spec. Publ.)*, 139-162.

Foley, S.F., Taylor, W.R. and Green, D.H., 1986. The effect of fluorine on phase relationships in the system $KAlSiO_4$-Mg_2SiO_4-SiO_2 at 28 kbar and the solution mechanism of fluorine in silicate melts. *Contrib. Mineral. Petrol.*, **93**, 46-55.

Forbes, B.G., 1969. A review of phanerozoic volcanism in South Australia. *Spec. Publ. Geol. Soc. Aust.*, **2**, 127-132.

Fountain, D.M. and Salisbury, M.H., 1981. Exposed cross-sections through the cotinental crust; implications for crustal structure, petrology, and evolution. *Earth Planet Sci. Lett.*, **56**, 263-277.

Fountain, D.M., McDonough, D.T. and Gorham, J.M., 1987. Seismic reflection models of continental crust based on metamorphic terrains. *Geophys. J. Roy. Astron. Soc.*, **89**, 61-66.

Frantsesson, E.V., 1969. Conjugation of carbonatite and kimberlite on the Siberian platform. *Dokl. Acad. Sci. USSR. Earth Sci. Sect.*, **183**, 127-128.

Fraser, K.J. and Hawkesworth, C.J., 1992. The petrogenesis of group 2 ultrapotassic kimberlites from Finsch Mine, South Africa. *Lithos*, **28**, 327-345.

Fraser, K.J., Hawkesworth, C.J., Erlank, A.J., Mitchell, R.H. and Scott-Smith, B.H., 1985/86. Sr, Nd and Pb isotope and minor element geochemistry of lamproites and kimberlites. *Earth Planet. Sci. Lett.*, **76**, 57-70.

Frey, F.A. and Green, D.H., 1974. The mineralogy, geochemistry and origin of lherzolite inclusions in Victorian basanites. *Geochim. Cosmochim. Acta*, **38**, 1023-1059.

Frey, F.A. and Prinz, M., 1978. Ultramafic inclusions from San Carlos, Arizona; petrologic and geochemical data bearing on their petrogenesis. *Earth Planet. Sci. Lett.*, **38**, 129-176.

Frey, F.A. Ferguson, J. and Chappell, B.W., 1977. 2nd Int. Conf. kimberlites, Santa Fe. (Abstr.).

Frey, F.A., Green, D.H. and Roy, S.D., 1978. Integrated models of basalt petrogenesis: a study of quarts tholeiites to olivine melilitites from south eastern Australia utilizing geochemical and experimental petrological data. *J. Petrol.*, **19**, 463-513.

Furlong, K.P. and Fountain, D.M., 1986. Continental crustal underplating: thermal considerations and seismic-petrologic consequences. *J. Geophys. Res.*, **91**, 8285-8294.

Fyfe, W.S., 1978. The evolution of the earth's crust: Modern plate tectonics to ancient hot spot tectonics. *Chem. Geol.*, **23**, 89-114.

Gallagher, K. and Hawkesworth, C., 1992. Dehydration melting and the generation of continental flood basalts. *Nature*, **358**, 57-59.

Giles, C.W. and Teale, G.S., 1979. A comparison of the geochemistry of the Roopena Volcanics and the Beda Volcanics. *Q. Geol. Notes, Geol. Sur. S. Aust.*, **71**, 7-13.

Giletti, B.J. and Yund, R.A., 1984. Oxygen diffusion in quarts. *J. Geophys. Res.*, **89**, 4039-4046.

Gill, E.D., 1955. Radiocarbon dates for Australian archaeological and geological samples. *Aust. J. Sci.*, **18**, 49-52.

Gill, E.D., 1967. Evolution of the Warrnambool-Port Fairy coast and the Tower Hill eruption, Western Victoria. In: Jennings, J.N. and Mabbutt, J.A. (eds), *Landform studies fr om Australia and New Guinea.* ANU Press, 340-364.

Gill, J.B., 1981. Orogenic Andesites and Plate Tectonics. Springer-Verlag, Berlin. 390pp.

Green, D.H. and Liebermann, R.C., 1976. Phase equilibria and elastic properties of a pyrolite mantle for the oceanic mantle. *Tectonophysics*, **32**, 61-92.

Green, D.H. and Wallace, M., 1988. Mantle metasomatism by ephemeral carbonatite melts. *Nature*, **336**, 459-462.

Greenhalgh, S.A., Tapley, D. and Singh, R., 1989. Crustal heterogeneity in South Australia, earthquake evidence. *Geophys. J.*, **96**, 85-99.

Griffin, W.L. and O'Reilly, S.Y., 1987a. The composition of the lower crust and the nature of the continental Moho. In: Nixon, P.H. (ed.), *Mantle Xenoliths*. Wiley, London, 413-430.

Griffin, W.L. and O'Reilly, S.Y., 1987b. Is the continental Moho the crust/mantle boundary? *Geology*, **15**, 241-244.

Griffin, W.L., Carswell, D.A. and Nixon, P.H., 1979. Lower crustal granulites and eclogites from Lesotho, southern Africa. In: Boyd, F.R. and Meyer, H.O.A. (eds), *The Mantle Sample: Inclusions in kimberlites and other volcanics*. Amer. Geophys. Union, 59-86.

Griffin, W.L., O'Reilly, S.Y. and Pearson, N.J., 1990. Eclogite stability near the crust-mantle boundary. In: Carswell, D.A. (ed.), *Eclogites Facies Rocks*. Blackie, 291-314.

Griffin, W.L., O'Reilly, S.Y. and Stabel, A., 1988. Mantle metasomatism beneath western Victoria, Australia: II. Isotopic geochemistry of Cr-diopside lherzolites and Al-augite pyroxenites. *Geochim. Cosmochim. Acta*, **52**, 449-460.

Griffin, W.L., Sutherland, F.L. and Hollis, J.D., 1987. Geothermal profile and crust-mantle transition beneath east-central Queensland: volcanology, xenolith petrology and seismic data. *J. Volcano. Geother. Res.*, **31**, 177-203.

Griffin, W.L., Wass, S.Y. and Hollis, J.D., 1984. Ultramafic xenoliths from Bullenmerri and Gnotuk Maars, Victoria, Australia: petrology of a sub-continental crust-mantle transition. *J. Petrol.*, **25**, 53-87.

Grove, T.L., Walker, D., Longhi, J., Stolper, E. and Hays, J.F., 1973. Petrology of rocks 12002 and origin of picritic basalts at Oceanus Procellarum. Proc. Fourth Lunar Sci. Conf., *Geochim. Cosmochim. Acta, Suppl., 4*, V.**1**, 995-1011.

Gümbel, C.W. Von., 1874. Die Palaeolithischen eruptivgesteine des Fichtelgeberges. Franz, München.

Gurnis, M. and Davies, G.F., 1986. The effect of depth-dependent viscosity on convective mixing in the mantle and the possibel survival of primitive mantle. *Geophys. Res. Lett.*, **13**, 541-544.

Haggerty, S., 1978. Mineralogical constraints on curie isotherms in deep crustal magnetic anomalies. *Geophys. Res. Lett.*, **5**, 105-108.

Hale, L.D. and Thompson, G.A., 1982. The seismic reflection character of the continental Mohorovicic discontinuity. *J. Geophys Res.*, **87**, 4625-4635.

Halliday, A.N., Dickin, A.P., Fallick, A.E. and Fitton, J.G., 1988. Mantle dynamics: A Nd, Sr, Pb and O isotopic study of the Cameroon Line Volcanic Chain. *J. Petrol.*, **29**, 181-211.

Hamlyn, P.R. and Bonatti, E., 1980. Petrology of mantle-derived ultramafics from the Owen fracture zone, northwest Indian Ocean: implications for the nature of the oceanic upper mantle. *Earth Planet. Sci. Lett.*, **48**, 65-69.

Harley, S.L., 1984. The solubility of alumina in orthopyroxene coexisting with garnet in FeO-MgO-Al_2O_3-SiO_2 and CaO-FeO-MgO-Al_2O_3-SiO_2. *J. Petrol.*, **25**, 665-696.

Hart, S.R. and Davis, K.E., 1978. Nickel partitioning between olivine and silicate melt. *Earth Planet. Sci. Lett.*, **40**, 203-219.

Hart, S.R., 1984. A large-scale isotope anomaly in the Southern Hemisphere mantle. *Nature*, **309**, 753-757.

Hart, S.R., Gerlach, D.C. and White, W.M., 1986. A possible new Sr-Nd-Pb mantle array and consequences for mantle mixing. *Geochim. Cosmochim. Acta*, **50**, 1551-1557.

Hawkesworth, C.J., Mantovani, M.S.M., Taylor, P.N. and Palacz, Z., 1986. Evidence from the Parana of South Brazil for a continental contribution to Dupal basalts. *Nature*, **322**, 356-359.

Hawkesworth, C.J., Rogers, N.W., Van Calsteren, P.W.C. and Menzies, M.A., 1984. Mantle enrichment processes. *Nature*, **311**, 331-335.

Helmstaedt, H., Carmichael, D.M. and Percival, J.A., 1979. Grospydite xenoliths from the zagadochnaya kimberlite pipe, Yakutia-high grade metamorphic rodingites. *Geol. Soc. Am. Abstr. Progr.*, **11**, 442.

Hergt, J.M., Peate, D.W. and Hawkesworth, C.J., 1991. The petrogenesis of Mesozoic Gondwana low-Ti flood basalts. *Earth Planet. Sci. Lett.*, **105**, 134-148.

Hinde, S., 1988. Central Deborah. In: Jones, D.G. (ed.), *Bicentennial Gold '88 Excursion Guidebook. Univ. W. Aust. Geol. Dept. & Extension Publ.*, **13**, 28-31.

Hirsch, L.M. and Wang, C.-Y., 1986. Electrical conductivity of olivine during high-temperature creep. *J. Geophys. Res.*, **91**, 10,429-10, 441.

Hoffman, P.F., 1987. Early Proterozoic foredeeps, foredeep magmatism, and Superior-type iron - formations of the Canadian Shield. In: Kröner, A. (ed.), *Precambrian Lithospheric Evolution*. Am. Geophys. Union, Washington D.C., Geodynamics Ser., 17, 85-98.

Holland, J.G. and Lambert, R. St. J., 1975. The chemistry and origin of the Lewisian gneisses of the Scottish mainland: the Scourie and Inver assemblages and subcrustal accretion. *Precamb. Res.* **2**, 161-188.

Hough, L.P. and Morris, B.J., 1989. Terowie gravity and geochemical survey 1988. *S. Aust. Dept. Mines and Energy Rep. 89/72.* (Unpubl.)

Hyndman, D.W., 1972. Petrology of igneous and metamorphic rocks. McGraw Hill, New York.

Irvine, T.N and Baragar, W.R.A., 1971. A guide to the chemical classification of the common volcanic rocks. *Canad. J. Earth Sci.*, **8**, 523-548.

Irving, A.J. and Green, D.H.,1976. Geochemistry and petrogenesis of the New basalts of Victoria and South Australia. *J. Geol. Soc. Aust.*, **23**, 45-66.

Irving, A.J., 1971. Geochemical and high pressure experimental studies of xenoliths, megacrysts and basalts from southeastern Australia. *Aust. National Univ., Unpublished PhD Thesis.*

Irving, A.J., 1974. Geochemical and high pressure experimental studies of garnet pyroxenite and pyroxene granulite xenoliths from the Delegate basaltic pipes, Australia. *J. Petrol.*, **15**, 1-40.

Ito, E., White, W.M. and Göpel, C., 1987. The O, Sr, Nd and Pb isotope geochemistry of Morb. *Chemical Geology*, **62**, 157-176.

Jackson, E.D., 1968. The character of the lower crust and upper mantle beneath the Hawaiian Islands. *23rd International Geological Congress, Prague-Proceedings*, **1**, 135-150.

Jackson, I. and Arculus, R.J., 1984. Laboratory wave velocity measurements on lower crustal xenoliths from Calcutteroo, South Australia. *Tectonophysics*, **101**, 185-197.

Jackson, I., 1991. The petrological basis for the interpreation of seismological models for the continental lithosphere. In: Drummond, B.J. (ed.), *The Eastern Australian Lithosphere*. Geol. Soc. Aust. Spec. Publ., 17, 81-114.

Jackson, I., Rudnick, R.L., O'Reilly, S.Y. and Bezant, C., 1990. Measured and calculated elastic wave velocities for xenoliths from the lower crust and upper mantle. *Tectonophysics*, **173**, 207-210.

Jacobsen, S.B. and Wasserburg, G.J., 1979. The Mean age of mantle and crustal reservoirs. *J. Geophs. Res.*, **84**, 7411-7427.

Jaques, A.L. and Green, D.H., 1980. Anhydrous melting of peridotite at 0-15 kb pressure and the genesis of tholeiitic basalts. *Contrib. Miner. Petrol.*, **73**, 287-310.

Jaques, A.L., Creaser, R.A., Ferguson, J. and Smith, C.B., 1985. A review of the alkaline rocks of Australia. *Tr. Geol. Soc. S. Afr.*, **88**, 311-334.

Jaques, A.L., Lewis, J.D., Smith, C.B., 1986. The kimberlites and lamproites of western Australia. *Geol. Surv. West. Aust. Bull.*, **132**, 268.

Jaques, A.L., Lewis, J.D., Smith, C.B., Gregory, G.P., Ferguson, J., Chappell, B.W. and McCulloch, M.T., 1984. The diamond-bearing ultrapotassic (lamproitic) rocks of the

West Kimberley Region, Western Australia. In: Kornprobst, J. (ed.), *Kimberlites,1: Kimberlites and related rocks, Proc. Third Int. Kimberlite Conf.*, 225-254.

Jaques, A.L., O'Neill, H.St.C., Smith, C.B., Moon, J. and Chappell, B.W., 1990. Diamondiferous peridotite xenoliths from the Argyle (AK1) lamproite pipe, western Australia. *Contrib. Mineral. Petrol.*, **104**, 255-276.

Jochum, K.J., McDonough, W.F., Palme, H. and Spettel, B., 1989. Compositional constraints on the continental lithospheric mantle from trace elements in spinel peridotite xenoliths. *Nature*, **340**, 548-550.

Johnson, R.W. (ed.), 1989. Intraplate volcanism in Eastern Australia and New Zealand. Cambridge Univ. Press, Cambridge.

Jones, A.P., Smith, J.V., Dawson, J.B. and Hansen, E.C., 1983. Metamorphism, partial melting and K-metasomatism of garnet-scapolite-kyanite granulite xenoliths from Lashaine, Tanzania. *J. Geol.*, **91**, 143-165.

Jones, J.G. and Veevers, J.J., 1984. Morphotectonics of the Platform Regions, focused on the highlands. In: Veevers, J.J. (ed.), *Phanerozoic earth history of Australia.* Clarendon Press, Oxford, 115-167.

Jordan, T.H., 1975. The continental tectosphere. *Rev. Geophys. Space Phys.*, **13**, 1-12.

Jordan, T.H., 1978. composition and development of the continental lithosphere. *Nature*, **274**, 544-548.

Jordan, T.H., 1981. Continents as a chemical boundary layer. *Phil. Trans. Roy. Soc. London*, **A301**, 359-373.

Jordan, T.H., 1988. Stucture and formation of the continental tectosphere. In: Menzies, M.A. and Cox, K.G. (eds), *Oceanic and Continental Lithosphere: Similarites and Differences. J. Petrol. (Spec. Publ.)*, 11-38.

Joyce, E.B., 1975. Quaternary volcanism and tectonics in southeastern Australia. The Royal Society of New Zealand, Wellington, 169-176.

Jupp, D.L.B., Kerr, D.W., Lemaire, H., Milton, B.E., Moore, R.F., Nelson, R. and Vozoff, K., 1979. Joint magnetotelluric-DC resistivity survey-eastern Officer Basin. *Aust. Soc. Expl. Geophys. Bull.*, **10**, 209-212.

Karato, S., 1990. The role of hydrogen in the electrical conductivity of the upper mantle. *Nature*, **347**, 272-273.

Karato, S.I., Paterson, M.S. and FitzGerald, J.D., 1986. Rheology of synthetic olivine aggregates: influence of grain size and water. *J. Geophys. Res.*, **91**, 8151-8176.

Kay, R.W. and Kay, S.M., 1981. The nature of the lower continental crust: inferences from geophysics, surface geology and crustal xenoliths. *Rev. Geophys. Space Phys.*, **19**, 271-297.

Kay, S.M. and Kay, R.W., 1983. Thermal history of the deep crust inferred from granulite xenoliths, Queensland, Australia. *Am. J. Sci.*, **283-A**, 486-513.

Kelemen, P.B., Shimizu, N. and Dunn, T., 1993. Relative depletion of niobium in some arc magmas and the continental crust: partitioning of K, Nb, La and Ce during melt/rock reaction in the upper mantle. *Earth Planet. Sci. Lett.*, **120**, 111-134.

Keller, G.V., 1987. Rock and mineral properties. In: Nabighian, M.N. (ed.), *Electromagnetic methods in applied geophysics-theory v.1.* Soc. Exploration Geophys.

Koziol, A.M. and Newton, R.C., 1988. Redetermination of the anorthite breakdown reaction and improvement of the plagioclase-garnet-Al_2SiO_5-quartz geobarometer. *Am. Mineral.*, **73**, 216-223.

Krogh, E.J., 1988. The garnet-clinopyroxene Fe-Mg geothermometer-a reinterpretation of existing experimental data. *Contrib. Mineral. Petrol.*, **99**, 44-48.

Kuno, H., 1966. Lateral variation of basalt magma type across continental margins and island arcs. *Bull. Volcanol.*, **29**, 195-222.

Langel, R.A., Phillips, J.D. and Hornet, R.J., 1982. Initial scalar magnetic anomaly map from Magsat. *Geophys. Res. Lett.*, **9**, 269-272.

Lanyon, R., Varne, R. and Crawford, A.J., 1993. Tasmanian Tertiary basalts, the Balleny plume, and opening of the Tasman sea (southwest Pacific Ocean). *Geology*, **21**, 555-558.

Larsen, E.S., Jr., 1938. Some new variation diagrams for groups of igneous rocks. *J. Geol.*, **46**, 505-520.

Law, L.K. and Greenhouse, J.P., 1981. Geomagnetic variation sounding of the asthenophere beneath the Jaan de Fuca Ridge. *J. Geophys. Res.*, **86**, 967-978.

Le Roex, A.P., 1986. Geochemical correlation between southern African kimberlites and south Atlantic hotspots. *Nature*, **324**, 243-245.

Leeman, W.P. and Lindstrom, D.J., 1978. Partitioning of Ni^{2+} between basaltic and synthetic melts and olivines; an experimental study. *Geochim. Cosmochim. Acta*, **42**, 801-816.

Lewis, H.C., 1887. On diamantiferous peridotite and the genesis of diamond. *Geol. Mag.* (Great Britain), **4**, 22-24.

Lewis, H.C., 1888. The matrix of the diamond. *Geol. Mag.* (Great Britain), **5**, 129-131.

Lightfoot, P. and Hawkeswork, C., 1988. Origin of Deccan Trap lavas: evidence from combined trace element and Sr-, Nd- and Pb- isotope studies. *Earth Planet. Sci. Lett.*, **91**, 89-104.

Lilley, F.E.M., 1991. The state of knowledge of the Asthenosphere from electromagnetic soundings: Australia and surrounding oceans. In: Drummond, B.J. (ed.), *The Australian Lithosphere.* Geol. Soc. Aust. Spce. Publ., 17, 141-145.

Lilley, F.E.M., Woods, D.V. and Sloane, M.N., 1981. Electrical conductivity profiles and implications for the absence or presence of partial melting beneath central and southeast Australia. *Phys. Earth Planet. Inter.*, **25**, 419-428.

Lindsley, D.H., 1983. Pyroxene thermometry. *Am. Min.*, **68**, 477-493.

Macdougall, J.D. and Lugmair, G.W., 1986. Sr and Nd isotopes in basalts from the East Pacific Rise: significance for mantle heterogeneity. *Earth Planet. Sci. Lett.*, **77**, 273-284.

MacKenzie, D.E. and Chappell, B.W., 1972. Shoshoitic and calc-alkaline lavas from the Highlands of Papua New Guinea. *Contrib. Mineral. Petrol.*, **35**, 50-62.

Mackwell, S.J., Kohlstedt, D.L. and Paterson, M.S., 1985. The role of water in the deformation of olivine single crystals. *J. Geophys. Res.*, **90**, 11319-11333.

Manghnani, M.H., Ramanantoandra, R. and Clark, S.P., 1974. Compressional and shear wave velocities in granulite-facies rocks and eclogites to 10 kbar. *J. Geophys. Res.*, **79**, 5427-5446.

Marker, M.E., 1975. The lower southeast of South Australia: a karst province. Univ. of Witwatersrand Department of Geography and Environmental Studies, Johannesburg. Occasional Paper, 13.

Mathur, S.P., 1974. Crustal structure in southweastern Australia from seismic and gravity data. *Tectonophysics*, **24**, 151-182.

Mayhew, M.A. and Johnson, B.D., 1987. An equivalent layer magnetization model for Australia based on Magsat data. *Earth Planet. Sci. Lett.*, **83**, 167-174.

Mayhew, M.A., Johnson, B.D. and Langel, R.A., 1980. An equivalent source model of the satellite altitude magnetic anomaly field over Australia. *Earth Planet. Sci. Lett.*, **51**, 189-198.

McCulloch, M.T. and Wasserburg, G.J., 1978. Sm-Nd and Rb-Sr chronology of continental crust formation. *Science*, **200**, 1003-1011.

McCulloch, M.T., 1987. Sm-Nd isotopic constraints on the evolution of Precambrian crust in the Australian continent. In: Kröner, A. (ed.), *Precambrian Lithospheric Evolution.* Am. Geophys. Union, Washington D.C., Geodynamics Ser., 17, 115-130.

McCulloch, M.T., Arculus, R.J., Chappell, B.W. and Ferguson, J., 1982. Isotopic and geochemical studies of nodules in kimberlite have implications for the lower continental crust. *Nature*, **300**, 166-169.

McCulloch, M.T., Jaques, A.L., Nelson, D.R. and Lewis, J.D., 1983. Nd and Sr isotopes in kimberlites and lamproites from western Australia: an enriched mantle origin. *Nature*, **302**, 400-403.

McDonald, G., 1992. The petrology and timing of the Anabama granite and associated igneous activity, Olary Region, S.A. *Univ. of Adeliade, Unpublished Honours Thesis.*

McDonough, W.F. and McCulloch, M.T., 1985. Geochemical and isotopic systematics of spinel (sp) lherzolites form SE Australia. *EOS*, **66**, 1110.

McDonough, W.F. and McCulloch, M.T., 1987. The southeast Australian lithospheric mantle: isotopic and geochemical constraints on its growth and evolution. *Earth Planet. Sci. Lett.*, **86**, 327-340.

McDonough, W.F., 1990. Constraints on the composition of the continental lithospheric mantle. *Earth Planet. Sci. Lett.*, **101**, 1-18.

McDonough, W.F., McCulloch, M.T. and Sun, S.-S., 1985. Isotopic and geochemical systematics in Tertiary-Recent basalts from southeastern Australia and implications for the evolution of the sub-continental lithosphere. *Geochim. Cosmochim. Acta*, **49**, 2051-2067.

McDonough, W.F., Rundnick, R.L. and McCulloch, M.T., 1991. The chemical and isotopic composition of the lower eastern Australian lithosphere: a review. In: Drummond, B.J. (ed.), *The Australian Lithosphere*. Geol. Soc. Aust. Spec. Publ., 17, 163-188.

McDougall, I. and Leggo, P.J., 1965. Isotopic age determinations on granitic rocks from Tasmaina. *J. Geol. Soc. Aust.*, **12**, 295-332.

McDougall, I. and Wellman, P., 1976. Potassium-argon ages for some Australian mesozoic igneous rocks. *J. Geol. Soc. Aust.*, **23**, 1-9.

McDougall, I., Allsopp, H.D. and Chamalaun, F.H., 1966. Isotopic dating of the New Volcanics of Victoria Australia, and geomagnetic polarity epochs. *J. Geophys. Res.*, **71**, 6107-6118.

McIver, J.R. and Ferguson, J., 1979. Kimberlitic, melilititic, trachytic and carbonatite eruptives at Saltpetre Kop, Sutherland, South Africa. In: Boyd, F.R. and Meyer, H.O.A. (eds), *Kimberlite, Diatremes, and Diamonds: Their Geology, Petrology and Geochemistry*. Am. Geophys. Union, Washington, D.C., 111-128.

McKenzie, D. and Bickle, M.J., 1988. The volume and composition of melt generated by extension of the lithosphere. *J. Petrol.*, **29**, 625-679.

McKenzie, D., 1967. Some remarks on heat flow and gravity anomalies. *J. Geophys. Res.*, **72**, 6261-6273.

McKenzie, D., 1989. Some remarks on the movement of small melt fractions in the mantle. Earth Planet. *Sci. Lett.*, **95**, 53-72.

Mckenzie, D., 1978. Some remarks on the devlopment of sedimentary basins. *Earth Planet. Sci. Lett.*, **40**, 25-32.

McNeil, A.M. and Edgar, A.D., 1987. Sodium-rich metasomatism in the upper mantle: implications of experiments on the pyrolite-Na2O rich fluid system at 950 °C, 20 kbar. *Geochim. Cosmochim. Acta*, **51**, 2285-2294.

Meissner, R., Wever, T. and Fluh, E.R., 1987. The Moho in Europe-implications for crustal development. *Annales Geophysicae*, **5B**, 357-364.

Menzies, M. and Murthy, V.R., 1980. Enriched mantle: Nd and Sr isotopes in diopsides from kimberlite nodules. *Nature*, **283**, 634-636.

Menzies, M.A. and Wass, S.Y., 1983. CO_2-and LREE-rich mantle below eastern Australia: a REE and isotopic study of alkaline magmas and apatite-rich mantle xenoliths from the Southern Highlands Province, Australia. *Earth Planet. Sci. Lett.*, **65**, 287-302.

Menzies, M.A., Kempton, P. and Dungan, M., 1985. Interaction of continental lithosphere and asthenospheric melts below the Geronimo Volcanic Field, Arizona, U.S.A. *J. Petrol.*, **26**, 663-693.

Menzies, M.A., Leeman, W.P. and Hawkesworth, C.J., 1983. Isotope geochemistry of Cenozoic volcanic rocks reveals mantle heterogeneity below western USA. *Nature*, **303**, 205-209.

Menzies, M.A., Rogers, N., Tindle, A. and Hawkesworth, C.J., 1987. Metasomatic and enrichment processes in lithospheric ridotites, an effect of asthenosphere-lithosphere interaction. In: Menzies, M.A. and Hawkesworth, C.J. (eds), *Mantle Metasomatism.* Academic Press, U.K. 313-361.

Meschede, M., 1986. A method of discriminating between different type of mid-ocean ridge basalts and continental tholeiites with the Nb-Zr-Y diagram. *Chem. Geol.*, **56**, 207-218.

Middlemost, E.A.K., 1975. The basalt clan. *Earth Sci. Rev.*, **11**, 337-364.

Milashev, V.A., 1965. Petrochemistry of the kimberlites of Yakutia and some factors in diamond formation. Nedra, Moscov (in Russian).

Mitchel, R.H., 1989. Aspects of the petrology of kimberlites and lamproites: some definitions and distinctions. *Spec. Publ. Geol. Soc. Aust.*, **14**, 7-45.

Mitchell, R.H. and Bergman, S.C., 1991. Petrology of Lamproites. Plenum, New York, 447pp.

Mitchell, R.H. and Brunfelt, A.O., 1975. Rare earth element geochemistry of kimberlite. *Phys. Chem. Earth*, **9**, 671-686.

Mitchell, R.H. and Meyer, H.O.A., 1989. Mineralogy of micaceous kimberlites from the New Elands and Star Mines, Orange Free State, South Africa. In: Ross, J. *et al.* (eds), *Kimberlites and Related Rocks, V.1*: Their composition, occurrence, origin and emplacement, Proc. 4th Inter. Kimberlite Conf., GSA Spec. Publ. No, 14, 83-96.

Mitchell, R.H., 1981. Titaniferous phlogopites from the leucite lamproites of W. kimberley area, Western Australia. *Contrib. Mineral. Petrol.*, **76**, 243-251.

Miyashiro, A., 1973. Metamorphism and Metamorphic Belts. George Allen & Unwin, London, 492pp.

Mohorovicic, A., 1910. Jb. Meterol. Obs. Zagreb, fur 1909 Bd. 4, Teil 4, Ab.1.

Moore, A.E., 1979. The geochemistry of the olivine melilitites and related rocks of Namaqualand-Bushmanland, South Africa. *PhD Thesis, Univ. of Cape Town.*

Moore, R.F., Kerr, D.W., Vozoff, K. and Jupp, D.L.B., 1977. Southern Cooper Basin magnetotelluric survey, South Australia, 1974. *Bur. Mineral Res., Aust., Rec., 1977/41.*

Morris, B.J., 1988. Review of kimberlitic rocks as a possible source of vermiculite in South Australia. *Mineral Resour. Rev. S. Aust.*, **156**, 65-68.

Morris, B.J., 1990. Kanmantoo trough geological investigations, Karinya syncline: Truro lamprophyres. *S. Aust. Dep. Mines. Energy Rep., 91/29 (Unpubl.).*

Muirhead, K. J., Cleary, J.R. and Finlayson, D.M., 1977. A long range seismic profile in southeastern Australia. *Geophys. J. R. Astron. Soc.*, **48**, 509-520.

Muirhead, K.J. and Drummond, B.J., 1991. The base of the lithosphere under Australia. In: Drummond, B.J. (ed.), *The Australian Lithosphere.* Geol. Soc. Spec. Publ. 17, 23-40.

Mullen, E.D., 1983. $MnO/TiO_2/P_2O_5$: a minor element discriminant for basaltic rocks of oceanic environments and its implications for petrogenesis. *Earth Planet. Sci. Lett.*, **621**, 53-62.

Müller, D., Morris, B.J. and Farrand, M.G., 1993. Potassic alkaline lamprophyres with affinities to lamproites from the Karinya Syncline, South Australia. *Lithos*, **30**, 123-137.

Nelson, D.R., 1989. Isotopic characteristics and petrogenesis of the lamproites and kimberlites of central west Greenland. *Lithos*, **22**, 265-274.

Nelson, D.R., Chivas, A.R., Chappell, B.W. and McCulloch, M.T., 1988. Geochemical and isotopic systematics in carbonatites and implications for the evolution of ocean-island sources. *Geochim. Cosmochim. Acta*, **52**, 1-17.

Nelson, D.R., McCulloch, M.T. and Sun, S.-S., 1986. The origins of ultrapotassic rocks as inferred from Sr, Nd and Pb isotopes. *Geochim, Cosmochim. Acta*, **50**, 231-245.

Newton, R.C. and Haselton, H.T., 1981. Thermodynamics of the garnet-plagioclase-Al_2SiO_3-quartz geobarometer. In: Newton, R.C., Navrotsky A. and Wood B.J. (eds), *Advances in physical geochemistry*, **1**, 131-147. Springer-Verlag, New York.

Newton, R.C. and Perkins III, D., 1982. Thermodynamic calibration of geobarometers based on the assemblages garnet-plagioclase-orthopyroxene (clinopyroxene)-quartz. *Am. Mineral.*, **67**, 203-222.

Nicholls, G.D., 1967. Geochemical studies in the ocean as evidence for the composition of the mantle. In: Runcorn, S.K. (ed.), *Mantles of the Earth and Terrestrial Planets.* Interscience, 285-304.

Nicholls, I.A. and Greig, A., 1989. Textures and microstructures. In: Johnson, R.W. (ed.), *Intraplate Volcanism in eastern Australia and New Zealand.* Cambridge Univ. Press, Cambridge, 255-261.

Nickel, K.G. and Green, D.H., 1984. The nature of the upper-most mantle beneath Victoria, Australia as deduced from ultramafic xenolithis. In: Kornprobst, J. (ed.), *Kimberlites, II: The mantle and crust-mantle relationships. Proc. "Third Inter. Kimberlite Conference", V.II.* Elsevier, Amsterdam, 160-178.

Niggli, P., 1923. Gesteins und Mineralprovinzen. Gerbrüder Borntrager, Berlin.

Nixon, P.H. and Boyd, F.R., 1973. Petrogenesis of the granular and sheared ultrabasic nodule suite in kimberlites. In: Nixon, P.H. (ed.), *Lesotho kimberlites*, Lesotho National Development Corporation, Maseru, 48-56.

Nixon, P.H. and Neal, C.R., 1987. Ontong Java Plateau: deep seated xenoliths from thick oceanic lithosphere. In: Nixon, P.H. (ed.), *Mantle Xenoliths*. John Wiley & Sons, New York, N.Y., 335-345.

Nixon, P.H., 1987. Mantle Xenoliths. Wiley, New York, N.Y., 844pp.

O'Neill, H.St.C. and Wall, V.J., 1987. The olivine-orthopyroxene-spinel oxygen goebarometer, the nickel precipitation curve, and the oxygen fugacity of the earh's upper mantle. *J. Petrol.*, **28**, 1169-1191.

O'Nions, R.K. and Hamilton, P.J., 1981. Isotope and trace element models of crustal evolution. *Phil. Trans. R. Soc.*, **A301**, 473-487.

O'Nions, R.K., Hamilton, P.J. and Evensen, N.M., 1977. Variations in $^{143}Nd/^{144}Nd$ and $^{87}Sr/^{86}Sr$ ratios in oceanic basalts. *Earth Planet. Sci. Lett.*, **34**, 13-22.

O'Reilly, S.Y and Griffin, W.L., 1987. Eastern Australia 4000 kilometers of mantle samples. In: Nixon, P.H. (ed.), *Mantle Xenoliths*. Willey, London, 267-280.

O'Reilly, S.Y. and Griffin, W.L., 1985. A xenolith-derived geotherm for southeastern Australia and its geophysical implications. *Tectonophysics*, **111**, 41-63.

O'Reilly, S.Y. and Griffin, W.L., 1988. Mantle metasomatism beneath western Victoria, Australia: I. Metasomatic processes in Cr-diopside lherzolites. *Geochim. Cosmochim. Acta*, **52**, 433-447.

O'Reilly, S.Y., 1989a. Xenolith types, distribution, and transport. In: Johnson, R.W. (ed.), *Intraplate Volcanism in eastern Australia and New Zealand.* Cambridge Univ. Press, Cambridge, 249-253.

O'Reilly, S.Y., 1989b. Nature of the East Australian lithosphere. In: Johnson, R.W. (ed.), *Intraplate Volcanism in eastern Australia and New Zealand.* Cambridge Univ. Press, Cambridge, 290-297.

O'Reilly, S.Y., Griffin, W.L. and Stable, A., 1988. Evolution of phanerozoic eastern Australia: isotopic evidence for magmatic and tectonic underplating. In: Menzies, M.A., and Cox K.G. (eds), *Oceanic and Continental Lithosphere: similarities and differences. J. Petrol.* (Spce. Publ.), 89-108.

O'Reilly, S.Y., Jackson, I. and Bezant, C., 1990. Equilibration temperatures and elastic wave velocities for upper mantle rocks from eastern Australia: implications for the interpretation of seismological models. *Tectonophysics*, **185**, 67-82.

Page, R.W., 1988. Geochronology of early to middle Proterozoic fold belts in northern Australia: a review. *Precambrian Res.*, **40/41**, 1-9.

Parsons, B. and McKenzie, D., 1978. Mantle convection and the thermal structure of the plates *J. Geoghys. Res.*, **83**, 4485-4496.

Parsons, B. and Sclater, J.G., 1977. An analysis of the variation of ocean floor bathymetry and heat flow with age. *J. Geophys. Res.*, **82**, 803-827.

Pattison, D.R.M, and Newton, R.C., 1989. Reversed experimental calibration of the garnet-clinopyroxene Fe-Mg exchange thermometer. *Contrib. Mineral. Petrol.*, **101**, 87-103.

Pearce, J.A. and Cann, J.R., 1973. Tectonic setting of basic volcanic rocks determined using trace element analysis. *Earth Planet. Sci. Lett.*, **19**, 290-300.

Pearce, J.A. and Norry, M.J., 1979. Petrogenetic implications of Ti, Zr, Y, and Nb variations in volcanic rocks. *Contrib. Mineral. Petrol.*, **69**, 33-47.

Pearce, J.A., 1982. Trace element characteristics of lavas from destructive place boundaries. In: Thorpe, R.S. (ed.), *Andesite*. 525-548.

Pearce, T.H., Gorman. B.E. and Birkett, T.C., 1977. The relationship between major element chemistry and tectonic environment of basic and intermediate volcanic rocks. *Earth Planet. Sci. Lett.*, **36**, 121-136.

Pearson, N.J., O'Reilly, S.Y. and Griffin, W.L., 1991. The granulite to eclogite transition beneath the eastern margin of the Australian craton. *Eur. J. Mineral.*, **3**, 293-322.

Peyronneau, J. and Poirier, J.P., 1989. Electitical conductivity of the Earth's lower mantle. *Nature*, **342**, 537-539.

Plumb, K.A., 1979. The tectonic evolution of Australia. *Earth Sci. Rev.*, **14**, 205-249.

Polach, H.A., Head, M.J. and Gower, J.D., 1978. ANU Radiocarbon date list VI. *Radiocarbon*, **20**, 360-385.

Pollack, H.N. and Chapman, D.S., 1977. On the regional variation of heat flow geotherms and lithospheric thickness. *Tectonophysics*, **38**, 279-296.

Pollack, H.N., 1986. Cratonization and thermal evolution of the mantle. *Earth Planet. Sci. Lett.*, **80**, 175-182.

Powell, C.M., 1984. Terminal Fold-Belt deformation: relationship of mid- carboniferous megakinks in the Tasman Fold Belt to coeval thrusts in cratonic Australia. *Geology*, **12**, 546-549.

Raheim, A. and Green, D.H., 1974. Experimental determination of the temperature and pressure dependence of the Fe-Mg partition coefficient for coexisting garnet and clinopyroxene. *Contrib. Mineral. Petrol.*, **48**, 179-203.

Rahman, A. and McDougall, I., 1972. Potassium-argon ages on the New Volcanics of Victoria. *Proc. Roy. Soc. Vict.*, **85**, 61-69.

Richard, P., Shimizu, N. and Allégre, C.J., 1976. $^{143}Nd/^{146}Nd$, a natural tracer: an application to oceanic basalts. *Earth Planet. Sci. Lett.*, **31**, 269-278.

Richardson, S.H. Erlank, A.J., Duncan, A.R. and Reid, D.L., 1982. Correlated Nd, Sr and Pb isotope variation in Walvis Ridge basalts and implications for the evolution of their mantle source. *Earth Planet. Sci. Lett.*, **59**, 327-342.

Richardson, S.H., Gurney, J.J., Erlank, A.J. and Harris, J.W., 1984. Origin of diamonds in old enriched mantle. *Nature*, **310**, 198-202.

Richter, F.M., 1988. A major change in the thermal state of the earth atthe Archean-Proterozoic boundary: consequences for the nature and preservation of continental lithosphere. In: Menzies, M.A. and Cox, K.G. (eds), *Oceanic and Continental Lithosphere: Similarites and Differences. J. Petrol. (Spec. Publ.)*, 39-52.

Ringwood, A.E. and Green, D.H., 1966. An experimental investigation of the gabbro to eclogite transformation and some geophysical implications. *Tectonophysics*, **3**, 383-427.

Ringwood, A.E., 1966. The chemical composition and origin of the Earth. In: Hurley, P.M. (ed.), *Advances in Earth Science*. M.I.T. Press, 287-356.

Ringwood, A.E., 1969. Composition of the crust and upper mantle. In: Hart, P.J. (ed.), *The Earth's Crust and Upper Mantle*. Am. Geophys. Union, Geophys. Monogr., 12, 1-17.

Ringwood, A.E., 1982. Phase transformations and differentiation in subducted lithosphere: implications for mantle dynamics, basalt petrogenesis, and crustal evolution. *J. Geol.*, **90**, 611-643.

Rock, N.M.S., 1991. Lamprophyres. Blackie, Glasgow, 285pp.

Rogers, N.W. and Hawkesworth, C.J., 1982. Proterozoic age and cumulate origin for granulite xenoliths. Lesotho. *Nature*, **229**, 209-413.

Rogers, N.W., Hawkesworth, C.J. and Palacz, Z.A., 1992. Phlogopite in the generation of olivine-melilitites from Namaqualand, South Africa and implications for element fractionation processes in the upper mantle. In: Peccerillo, A. and Foley, S. (eds), Potassic and Ultrapotassic Magmas and their Origin. *Lithos*, **28**, 347-365.

Ruburn, R.J., Raheim, A. and Green, D.H., 1976. Determination of the P.T. paths of natural eclogites during metamorphism-record of subduction. *Lithos*, **9**(2), 161-164.

Rudnick, R.L. and Taylor, S.R., 1987. The composition and petrogenesis of the lower crust: a xenolith study. *J. Geophys. Res.*, **92**, 13,981-14,005.

Rudnick, R.L., McDonough, W.F., McCulloch, M.T. and Taylor, S.R., 1986. Lower crustal xenoliths from Queensland, Australia: Evidence for deep crustal assimilation and fractionation of continental basalts. *Geochim. Cosmochim. Acta*, **50**, 1099-1115.

Saggerson, E.P. and Williams, L.A.S., 1964. Ngurumanite from southern Kenya and its bearing on the origin of rocks in the northern Tanganyika alkaline district. *J. Petrol.*, **5**, 40-81.

Salisbury, M.H. and Fountain, D.M., 1976. Continent/continent obduction zones: geological and geophysical case studies. *EOS Trans. Am. Geophys. Union*, **57**, 335.

Sandiford, M., Foden, J., Zhou, S. and Turner, S., 1992. granite genesis and the mechanics of convergent orogenic belts with application to the southern Adelaide Fold Belt. *Trans. Roy. Soc.* Edinburgh, **83**, 83-93.

Scott Smith, B.H., Danchin, R.V., Harris, J.W. and Stracke, K.J., 1984. Kimberlites near Orroroo, South Australia. In: Kornprobst, J. (ed.), *Kimberlites,I : Kimberlites and related rocks*, Elsevier, Amsterdam, 121-142.

Shackleford, P.R.J. and Sútton, D.J., 1981. A first interpretation of crustal structure in the Adelaide Geosyncline in South Australia quarry blasts. *Geol. Soc. Aust., J.*, **28**, 491-500.

Shankland, T.J. and Waff, H.S., 1977. Partial melting and electrical conductivity anomalies in the upper mantle. *J. Geophys. Res.*, **82**, 5409-5417.

Sharp, W.E., 1974. A plate tectonic origin for diamond-bearing kimberlites. *Earth Planet. Sci. Lett.*, **21**, 351-354.

Sheard, M.J., 1978. Geological history of the Mount Gambier volcanic complex, southeast South Australia. *Trans. R. Soc. S. Aust.*, **102**, 125-139.

Sheard, M.J., 1983. Volcanoes. In: Tyler, M.J., Twidale, C.R., Holmes, J.W. and Ling, J.K. (eds), *Natural history of the South East.* Roy. Soc. S. Aust., 7-14.

Sheard, M.J., 1986. Some volcanological observations at Mount Schank, southeast South Australia. *Geol. Surv. S. Aust., Quarterly Geological Note*, **100**, 14-20.

Sheard, M.J., 1990. A guide to Quaternary volcanoes in the lower south-east of South Australia. *Mines and energy review, South Australia*, **157**, 40-50.

Shee, S.R., Bristow, J.W., Bell, D.R., Smith, C.B., Allsopp, H.L. and Shee, P.B., 1989. The petrology of kimberlites, related rocks and associated mantle xenoliths from the Kuruman province, South Africa. In: Ross, J. *et al.* (eds), *Kimberlites and Related Rocks, V.1: Their composition, occurrence, origin and emplacement.* Proc. 4th Inter. Kimberlite Conf., 60-82.

Smith, B.W. and Prescott, J.R., 1987. Thermoluminessence dating of the eruption of Mount Shank South Australia. *Aust. J. Earth Sci.*, **34**, 335-342.

Smith, C.B., 1983. Pb, Sr and Nd isotopic evidence for sources of southern African Cretaceous kimberlites. *Nature*, **304**, 51-54.

Smith, C.B., Gurney, J.J., Skinner, E.M.W., Clement, C.R. and Ebrahim, N., 1985. Geochemical character of southern Africa kimberlites: a new approach based on isotopic constraints. *Trans. Geol. Soc. S. Aft.*, **88**, 267-280.

Sprigg, R.C., 1952. The geology of the South-East Province, South Australia with special reference to Quaternary coast-line migrations and modern beach developments. *Bull. Geol. Surv. S. Aust.*, **29**, 1-120.

Stanley, E.R., 1909. Complete analysis of the Mount Gambier basalt with petrographical descriptions. *Trans Roy. Soc. S. A.*, **1909**, 82-100.

Stanley, E.R., 1910. Lherzolite and olivine from Mount Gambier. *Trans Roy. Soc.*, **33**, 63-68.

Stewart, I.C.F., 1972. Seismic interpretation of crustal structure in the Flinders-Mt. Lofty ranges and Gulf region, South Australia. *J. Geol. Soc. Aust.*, **19**, 351-362.

Stewart, K. and Foden, J., 1993. Magmatic processes in the formation of a large volume postorogenic silicic volcanic province. *IAVCEI Abst.*, Canberra, 1993, p. 106.

Stolz, A.J. and Davies, G.R., 1988. Chemical and isotopic evidence from spinel lherzolite xenoliths for episodic metasomatism of the upper mantle beneath southeastern Australia. In: Menzies, M.A. and Cox, K.G. (eds), *Oceanic and Continental Lithosphere: Similarites and Differences. J. Petrol. (Spec. Publ.)*, 275-302.

Storey, M., Saunders, A.D., Tarney, J., Leat, P., Thirwall, M.F., Thompson, R.N., Menzies, M.A. and Marriner, G.F., 1988. Geochemical evidence for plume-mantle interactions beneath Kerguelen and Heard Islands, Indian Ocean. *Nature*, **336**, 371-374.

Stormer, J.C., 1973. Calcium zoning in olivine and its relationship to silica activity and pressure. *Geochim. Cosmochim Acta*, **37**, 1815-1821.

Stosch, H.G. and Lugmair, G.W., 1986. Trace element and Sr and Nd isotope geochemistry of peridotite xenoliths from the Eifel (West Germany) and their bearing on the evolution of the subcontinental lithosphere. *Earth Planet. Sci. Lett.*, **80**, 281-298.

Stracke, K.J., 1974. Quarterly reports, October 1972 to April 1974., EL 17, Port Augusta, for Stockdale Prospecting Ltd., S. Aust. Dept. Mines Energy open file Env. 2180 (unpubl.).

Stracke, K.J., Ferguson, J. and Black, L.P., 1979. Structural setting of kimberlites in southeastern Australia. In: Boyd, F.R. and Meyer, H.O.A. (eds), *Kimberlites, diatremes and diamonds. Proc. 2nd Kimberlite Conf.,1.* Am. Geophys. Union Washington, 71-91.

Sudo, A. and Tatsumi, Y., 1990. Phlogopite and K-amphibole in the upper mantle: implication for magma genesis in subduction zones. *Geophys. Res. Lett.*, **17**, 29-32.

Sun, S.-S. and McDonough, W.F., 1989. Chemical and isotopic systematics of oceanic basalts: implications for mantle composition and processes. In: Saunders, A.D. and Norry, M.J. (eds), *Magmatism in the Ocean Basins*. Geol. Soc. Spec. Publ., 42, 313-345.

Sun, S.-S. and Nesbitt, R.W., 1978. Petrogenesis of archaean ultrabasic and basic volcanics: evidence from rare earth elements. *Contrib. Mineral. Petrol.*, **65**, 301-325.

Sutherland, F.L., 1981. Migration in relation to possible tectonic and regional controls in Eastern Australian volcanism. *J. Vocanol. Geotherm. Res.*, **9**, 181-213.

Sutherland, F.L., 1983. Timing, trace and origin of basaltic migration in eastern Australia. *Nature*, **305**, 123-126.

Swanson, S.E., Kay, S.M., Brearley, M. and Scarfe, C.M., 1987. Arc and back-arc xenoliths in Kurile-Kamchatka and western Alaska. In: Nixon, P.H. (ed.), *Mantle Xenoliths*. John Wiley, 303-318.

Tammemagi, H. Y. and Lilley, F.E.M., 1971. Magnetotelluric studies across the Tasman Geosyncline, Australia. *Geophys. J. R. Astron. Soc.*, **22**, 505-516.

Taylor, S.R. and McLennan, S.M., 1981. The composition and evolution of the continental crust: rare earth element evidence from sedimentary rocks. *Phil. Trans. R. Soc.* Lond., **A301**, 381-399.

Taylor, S.R. and McLennan, S.M., 1985. The continental crust: its composition and evolution. Blackwell Sci. Publ., Oxford London, 141pp.

Taylor, S.R., 1979. Chemical composition and evolution of the continental crust: the Rare Earth element evidence. In: McElhinny, M.W. (ed.), *The Earth: it's origin, structure and evolution.* Academic Press, London, 353-376.

Thibault, Y., Edgar, A.D. and Lloyd, F.E., 1992. Experimental invetigation of near-solidus melts produced from carbonated phlogopite lherzolite model sources: implications for metasomatic processes in the continental lithospheric mantle. *Am. Mineral.*, **77**, 784-794.

Thomas, L., 1969. Rayleigh wave dispersion in Australia. Seismol. *Soc. Am., Bull.*, **59**, 167-182.

Thornton, C.P. and Tuttle, O.F., 1960. Chemistry of igneous rocks, I. Differentiation index. *Amer. J. Sci.*, **258**, 664-684.

Tozer, D.C., 1979. Interpretation of upper-mantle electrical conductivities. *Tectonophysics*, **56**, 147-163.

Tozer, D.C., 1981. The mechanical and electrical properites of the eath's asthenosphere. *Phys. Earth Planet. Inter.*, **25**, 280-296.

Tröger, W.E., 1935. Spezielle Petrographie der Eruptivgesteine. Verl. Deut. Mineral. Gesell., Bonn, 360pp.

Turcotte, D.L. and Schubert, G., 1982. Geodynamics. Wiley, New York, 450pp.
U.S. Geodynamics Committee, 1983. The lithosphere Report of workshop National Academy Press, Washington, D.C.

Turner, S., Foden, J., Sandiford, M. and Bruce, D., 1993. Sm-Nd isotopic evidence for the provenance of sediments from the Adelaide Fold Belt and southeastern Australia with implications for episodic crustal addition. *Geochim. Cosmochim. Acta*, **57**, 1837-1856.

Turner, S., Sandiford, M. and Foden, J., 1992. Some geodynamic and compositional constraints on "postorogenic" magmatism. *Geology*, **20**, 931-934.

Turner, S.P. and Foden, J.D., 1990. The nature of mafic magmatism through the evolution of the Adelaide Foldbelt and Subsequent Delamerian Orogeny. In: Parker, A.J. *et al.* (ed.), *Mafic Dykes and Emplacement Mechanisms*. Balkema, 431-434.

U.S. Geodynamics Committee, 1983. The lithosphere Report of workshop National Academy Press, Washington, D.C.

Van Schmus, W.R., Bickford, M.E., and Zietz, I., 1987. Early and middle Proterozoic provinces in the central United States. In: Kröner, A. (ed.), *Precambrian Lithospheric Evolution*. Am. Geophys. Union, Washington D.C., Geodynamics Ser., 17, 43-68.

Veevers, J.J. (ed.), 1984. Phanerozoic Earth History of Australia. Oxford Univ. Press, 418pp.

Veevers, J.J. and Powell, C.McA., 1984. Uluro and Adelaidean Regimes. In: Veevers, J.J. (ed.), *Phanerozoic earth history of Australia*. Clarendon Press, Oxford, 278-289.

Vollmer, R., Ogden, P., Schilling, J.-G., Kingsley, R.H. and Waggoner, D.G., 1984. Nd and Sr isotopes in ultrapotassic volcanic rocks from the Leucite Hills, Wyoming. *Contrib. Mineral. Petrol.*, **87**, 359-368.

Wagner, P.A., 1914. The diamond fields of South Africa. Transvaal Leader, Johannesberg.

Walker, D., Shibata, T. and DeLong, S.E., 1979. Abyssal tholeiites from the Oceanographer Fracture zone. *Contrib. Mineral. Petrol.*, **70**, 111-125.

Walker, N.C., 1967. A review of post-Miocene volcanic centres in South Australia. *Min. Rev. Adelaide*, **126**, 152-155.

Walker, R.J., Carlson, R.W., Shirey, S.B. and Boyd, F.R., 1989. Os, Sr, Nd and Pb isotope systematics of southern African peridotite xenoliths: implications for the chemical evolution of subcontinental mantle. *Geochim. Cosmochim. Acta*, **53**, 1583-1595.

Wallace, M.E. and Green, D.H., 1988. An experimental determination of primary carbonatite magma composition, *Nature*, **335**, 343-346.

Wasilewski, P.J. and Mayhew, M.A., 1982. Crustal xenolith magnetic properties and long wavelength anomaly source requirements. *Geophys. Res. Lett.*, **9**, 329-332.

Wasilewski, P.J., Thomas, H.H. and Mayhew, M.A., 1979. The Moho as a magnetic boundary. *Geophys. Res. Lett.*, **6**, 541-544.

Wass, S.Y. and Hollis, J.D., 1983. Crustal growth in South-eastern Australia-evidence from lower crustal eclogitic and granulitic xenoliths. *J. Metamorphic Geol.*, **1**, 25-45.

Wass, S.Y. and Irving, A.J., 1976. XENMEG. A catalogue of occurrences of xenoliths and megacrysts in basic volcanic rocks of eastern Australia. The Australian Museum, Sydney.

Waters. F.G. and Erlank, A.J., 1988. Assessment of the vertical extent and distribution of mantle metasomatism below kimberley, South Africa. In: Menzies, M.A. and Cox, K.G. (eds), *Oceanic and Continental Lithosphere: Similarites and Differences. J. Petrol. (Spec. Publ.)*, 185-204.

Weaver, B.L. and Tarney, J., 1980. Continental crust composition and nature of the lower crust: constraints from mantle Nd-Sr isotope correlation. *Nature*, **286**, 342-346.

Weaver, B.L., 1991. Trace element evidence for the origin of ocean-island basalts. *Geology*, **19**, 123-126.

Webb, S.A.C. and Wood, B.J., 1986. Spinel-pyroxene-garnet relationships and their dependence on Cr/Al ratio. *Contrib. Mineral. Petrol.*, **92**, 471-480.

Wellman, P. and McDougall, I., 1974. Cainozoic igneous activity in eastern Australia. *Tectonophysics*, **23**, 49-65.

Wellman, P., 1974. Potassium-argon ages on the Cainozoic volcanic rocks of eastern Victoria Australia. *J. Geol. Soc. Aust.*, **21**, 359-376.

Wellman, P., 1978. Potassium-argon ages of Cainozoic volcanic rocks from the Bundaberg, Rockhampton and Clermont areas of eastern Queensland. *Proceed. Roy. Soc. Queensland*, **89**, 59-64.

Wellman, P., 1979. On the Cainozoic uplift of the southeastern Australian highland. *J. Geol.Soc.Aust.*, **26**, 1-9.

Wellman, P., 1982. Australian seismic refraction results, isostasy and altitude anomalies. *Nature*, **298**, 838-841.

Wellman, P., Murray, A.S. and McMullan, M.W., 1985. Australian long-wavelength magnetic anomalies. *BMR J. Aust. Geol. Geophys.*, **9**, 297-302.

Wells, P.R.A., 1977. Pyroxene thermometry in simple and compex systems. *Contrib. Mineral. Petrol.*, **62**, 129-139.

Wendlandt, R.F., 1984. An experimental and theoretical analysis of partial melting in the system $KAlSiO_4$-CaO-MgO-SiO_2-CO_2 and applications to the genesis of potassic magmas, carbonatites and kimberlites. In: Kornprobst, J. (ed.), *Kimberlites and Related Rocks*, 359-369.

Western Queen, (S.A.) Pty. Ltd., 1981. Terowie EL 477. S. Aust. Dept. Mines and Energy open file Env. 3612 (unpubl.).

White, R.E., 1969. Seismic phases in South Australia and their relation to crustal structure. Geophys. *J.R. Astron. Soc.*, **17**, 249-261.

White, R.E., 1971. P-wave velocities in the upper mantle beneath the Australian shield from earthquake data. Geophys. *J. R. Astron. Soc.*, **24**, 109-118.

White, R.S. and McKenzie, D., 1989. Magmatism at rift zones: The generation of volcanic continental margins and flood basalts. *J. Geophys. Res.*, **94**, 7685-7729.

White, R.S., 1988. The Eath's crust and lithosphere. In: Menzies, M.A. and Cox, K.G. (eds), *Oceanic and Continental Lithosphere: Similarites and Differences. J. Petrol. (Spec. Publ.)*, 1-10.

White, W.M. and Hofmann, A,W., 1982. Sr and Nd isotope geochemistry of oceanic basalts and mantle evolution. *Nature*, **296**, 821-825.

White, W.M., Hofmann, A.W. and Puchelt, H., 1987. Isotope geochemistry of Pacific mid-ocean ridge basalts. *J. Geophys. Res.*, **92**, 4881-4893.

Wilkinson, H.E., 1988. Bendigo geology. In: Jones, D.G. (ed.), *Bicentennial Gold 88 Excursion Guidebook. Univ. W. Aust. Geol. Dept. & Extension Publ.*, **13**, 17-21.

Wilkinson, J.F.G., 1963. Some natural analcime solid solutions. *Miner. Mag.*, **33**, 498-505.

Wilkinson, J.F.G., 1977. Analcime phenocrysts in a vitrophyric analcimite-primary or secondary? *Contrib. Mineral. Petrol.*, **64**, 1-10.

Williams, E., 1976. Tasman Fold Belt System in Tasmania. Explanatory notes 1:500000 structural map of pre-carboniferous rocks of Tasmania. Tas., Dep. Mines, Hobart.

Wilson, M., 1993. Geochemical signatures of oceanic and continental basalts: a key to mantle dynamics? *J. Geol Soc*, London, **150**, 977-990.

Winchester, J.A. and Floyd, P.A., 1976. Geochemical magma type discrimination: application to altered and metamorphosed basic igneous rocks. *Earth Planet. Sci. Lett.*, **28**, 459-469.

Winchester, J.A. and Floyd, P.A., 1977. Geochemical discrimination of different magma series and their differentiation products using immobile Elements. *Chem. Geol.*, **20**, 325-343.

Witt-Eickschen, G. and Seck, H.A., 1991. Solubility of Ca and Al in orthopyroxene from spinel peridotite: an improved version of an empirical geothermometer. *Contrib. Mineral. Petrol.*, **106**, 431-439.

Wood, B.J. and Banno, S., 1973. Garnet-orthopyroxene and orthopyroxene-clinopyroxene relationships in simple and complex systems. *Contrib. Mineral. Petrol.*, **42**, 109-121.

Wood, B.J. and Nell, J., 1991. High-temperature electrical conductivity of the lower-mantle phase (Mg, Fe) O. *Nature*, **351**, 309-311.

Wyatt, B.A., Shee, S.R. and Robison, H.R., 1993. South Australian kimberlites: New occurrences and an update. *IAVCEI Abstr.*, Canberra 1993. 125.

Wyatt, B.A., Shee, S.R., Griffin, W.L., Zweistra, P. and Robison, H.R., 1991. The petrology of the Cleve kimberlite, Eyre Peninsula, South Australia. *Proceed. 5th Kimberlite Conf., Brasilia.* CPRM Spec. Publ., **2/91**, 463-465.

Wyborn, L.A.I., 1988. Petrology, geochemistry and origin of a major Australian 1880-1840 Ma felsic volcano-plutonic suite: a model for intracontinental felsic magma generation. *Procambrian Res.*, **40/41**, 37-60.

Wyborn, L.A.I., Page, R.W. and McCulloch, M.T., 1988. Petrology, geochronology and isotope geochemistry of the post-1820 Ma granites of the Mount Isa Inlier: mechanisms for generation of Proterozoic anorogenic granites. *Precambrian Res.*, **40/41**, 509-541.

Yoder, H.S. Jr, 1976. Generation of basaltic magma. National Academy of sciences, Washington, D.C.

Zindler, A. and Hart, S., 1986. Chemical geodynamics. *Ann. Rev. Earth Planet. Sci.*, **14**, 493-571.

Appendix 1. Analytical techniques and uncertainites

Appendix 1

Sample preparation

Whole-rock samples (0.5-2 kg samples) were crushed and finely milled to <10 μm using a tungsten-carbide ring mill. Repesentativity was maintained in sampling the milled bulk by splitting. Mineral separates were obtained from sieved and washed samples crushed and milled to 150 μm. Some very coarse-grained mineral assemblages were directly chipped from the rock. Minerals were initially separated by a Frantz Isodynamic magnetic separator and finished by hand-picking under a binocular microscope. To remove surface contamination, the minerals were washed several times in an ultrasonic cleaner in 1N HC1 solution. After each interval the acid was discarded and separates were washed three times in double-distilled water.

Whole rock chemical analysis

For trace element analyses, pellets were made by pressing a mixture of 5 g of powder and 1 m of PVA (Polyvinyl Alcohol) solution with a boric acid backing. For major element analyses, 3-4 g of powder were dried in a 110 °C oven for three hours to remove the surface water and then ignited overnight at 960 °C. 1 g of the ignited samples were mixed with 4 g of flux, then fused in Pt- Au crucibles and poured into a Pt-Au mould, finally being quench cooled with a jet of air. The analyses of the fused discs and pressed pellets were carried out using a Philips PW 1480 XRF spectrometer in the Department of Geology and Geophysics at the University and Adelaide.

For trace element analyses, the lower limit of detection (LLD) is used as a measure of the precision of the data. It is defined statistically as that concentration which gives a count-rate equal to three times the standard deviation of the net count-rate for peak minus background. This means that if an element is present in this amount, then there is a 99.7 % probability of it being detected. The LLDs of trace element analyses for XRF are as follows (LLDs in ppm are in brackets).

Sr(1.5), Rb(1.5), Y(2), Zr(1.5), Nb(1.5), Pb(3), Th(2.5), U(2), Ba(3), Sc(2), Ga(3), V(2), Cr(5), Ce(7), Nd(4), La(3), Ni(3), Cu(4), Zn(3), Co(2)

Sr and Nd isotope analysis

Mineral separate and whole-rock samples were dissolved in 15 ml screw-top Teflon PFA® vials using HNO_3 -HF acid mixtures for periods between 1 and 4 weeks. In the case of some mineral dissolutions, it was also necessary to add up to 1 ml of $HClO_4$ to this mixture. In the case of whole rock samples, separate spiked and un-spiked dissolutions were made of ~100 mg of powder. Those solutions for isotope dilution were spiked with a mixed ^{147}Sm-^{150}Nd tracer. Possible problems of sample heterogeneity were minimised by dissolution of relatively large sample size, by fine grinding of the powders and thorough mixing of the powders and by splitting. This reproducibility has been verified as being within our error, by repeated analysis of the same samples. This not withstanding, our lab sees merit in eliminating possible heterogeneity problems in separate IC and ID determinations on whole-rock samples by solution aliquot splitting and we have adopted this as routine since July 1993.

After total dissolution, the mineral solutions were aliquoted for spiking with two thirds of the solution allocated to the isotopic composition (IC) component. The remaining isotopic dilution (ID) component was spiked with ^{85}Rb, ^{84}Sr and mixed ^{147}Sm-^{150}Nd tracers and re-homogenised for 24 hours at 130 °C. All samples were dried and re-dissolved in 1.5 mls of 3N HCl in readiness for cation exchange column extraction.

Rb and Sr, and Nd-Sm were separated using BioRad Ag50W-X8 (200-400 mesh) resin columns, and Nd and Sm by columns containing teflon powder impregnated with HDEHP. On whole rock samples, accurate Rb and Sr concentrations were determined by XRF at the University of Adelaide on a PW 1480 X-ray spectrometer. A routine involving multiple analysis of triplicate preparations of each sample was used.

In preparation for analysis, Sr was loaded onto a single Ta filaments, and Nd and Sm onto double Ta-Re filaments. All samples were run as metals. Analysis was performed on a Finnigan MAT 261 single collector mass-spectrometer at the University of Adelaide. During the course of the study the La Jolla procedural Sr and Nd blanks were 1.1 ng/g and 0.2 ng/g, respectively, which in general is negligible by comparison with the typical >500 ng of Sr and Nd dissolved and analysed. The following table shows results for the standards when the upper results were obtained.

Standard	Rb	Sr	Nd	Sm	87Sr/86Sr	143Nd/144Nd
BCR-1	46.43	322.1	28.63	6.54	0.704951±54	0.512507±24
BHVO-1	9.24	396	25.08	6.17	0.703469±86	0.512964±05
SRM 987					0.710183±37	
La Jolla						0.511846±30

Constants used in isotope work are;

$^{88}Sr/^{86}Sr=0.1194$

$\lambda Rb=1.42*10^{-11}y^{-1}$

Bulk Earth $^{87}Sr/^{86}Sr=0.7045$

Bulk Earth $^{143}Nd/^{144}Nd=0.512638$

Depleted mantle $^{143}Nd/^{144}Nd=0.513108$

$\lambda Sm=6.54*10^{-12}y^{-1}$

Nd isotopic compositions normalized to $^{146}Nd/^{144}Nd=0.7219$

Average error in $\varepsilon Nd = \pm 0.5$

REE analysis

Selected samples were analysed for REE (La, Ce, Nd, Sm, Eu, Gd, Dy, Er, Yb). The samples were prepared using the double cation exchange column technique (Crock *et al.*, 1984) and the methods developed by Sun and Nesbitt (1978). Dissolving of the sample(200 mg for the xenoliths and 100 mg for the other samples) with HF and HF-HNO_3 ($HClO_4$ for clinopyroxene and lower crustal xenoliths) and conversion to the chloride using HCl are the same as for that of the isotope analysis. The prepared samples were analysed with the Finnigan MAT 261 Mass Spectrometer in the Department of the Geology, The University of Adelaide.

Electron microprobe analysis

Carbon coated polished sections (approximately 250um) were prepared for microprobe analyses. The analyses were carried out using a KEVEX 7000 series energy dispersive spectrometer (EDS) attached to the JEOL 733 electron microprobe. Some selected samples analysed by EDS were reanalysed with WDS (wavelength dispersive spectroscopy) with the JEOL 733 analyser to compare with the two methods.

The analytical conditions used were accelerating voltage of 15 kv and a beam current of 2 nA. Calibration of the EDS was performed with pure copper as a primary standard and with olivine and Kaersutite as secondary standards.

Appendix 2. Complete listing of analyses of the Northern area older volcanics

Appendix 2 **Whole rock analyses of the Northern area older volcanics**

Sample	963-MC 1	963-MC 2	963-MC 3	963-MC 4	963-MC 5	963-MC 6	963-MC 7	963-MC 8	963-LL 1	963-LL 2	963-LL 3	963-LL 4	963-LL 5	963-ED 1	963-ED 2	963-ED 3	963-MU 1	963-MU 2	963-MU 5	963-MU 6	963-MU 7
Locality	Mt McIntyre								Lake Leake					Mt Edward			Mt Muirhead				
SiO2	43.20	42.80	43.30	43.10	43.10	43.00	43.00	43.00	43.20	42.70	42.90	44.10	45.10	40.60	43.60	43.20	41.10	39.50	43.80	43.70	43.80
Al2O3	10.30	10.00	10.20	10.10	10.40	10.20	10.10	10.30	9.75	9.24	9.10	9.05	8.16	9.38	8.34	8.43	9.73	9.42	10.50	10.20	10.10
Fe2O3(t)	12.90	12.90	12.90	12.90	13.00	12.80	12.80	12.90	13.10	12.90	12.50	12.10	11.90	13.70	12.00	12.30	11.90	11.50	13.00	13.10	13.00
MnO	0.17	0.17	0.17	0.16	0.17	0.16	0.17	0.17	0.17	0.16	0.15	0.14	0.14	0.18	0.15	0.15	0.16	0.15	0.17	0.17	0.17
MgO	11.00	11.30	11.10	11.40	10.90	10.60	10.50	10.50	12.30	13.60	12.90	11.90	13.90	17.00	16.90	16.60	10.30	9.89	10.90	11.60	11.10
CaO	11.30	11.40	11.40	11.40	11.30	11.50	11.60	11.40	10.80	11.20	11.30	10.90	9.78	10.50	9.75	10.00	14.10	15.40	11.00	11.00	10.90
Na2O	4.38	4.29	4.09	3.71	3.88	4.27	4.31	4.33	1.44	1.92	1.12	1.42	1.07	0.75	1.29	1.18	4.25	4.13	4.56	4.30	4.22
K2O	0.49	0.56	0.63	0.45	0.98	0.66	0.90	0.97	1.87	1.25	1.42	1.60	1.80	0.04	1.29	1.18	0.19	0.49	0.24	0.32	0.87
TiO2	3.74	3.71	3.73	3.70	3.74	3.77	3.74	3.75	3.86	3.70	3.68	3.55	3.42	3.85	3.33	3.43	3.45	3.33	3.70	3.68	3.65
P2O5	0.96	0.96	0.97	0.96	0.97	0.97	0.95	0.96	0.96	0.94	0.87	0.90	0.78	0.81	1.06	1.01	0.87	0.85	0.93	0.92	0.92
SO3	0.01	0.01	0.01	0.01	0.01	0.02	0.01	0.02	0.06	0.01	0.01	0.01	0.00	0.01	0.03	0.03	0.01	0.01	0.01	0.01	0.01
LOI	1.34	1.17	1.51	1.76	1.19	1.51	1.26	1.11	2.59	2.80	3.61	3.86	3.48	2.48	2.36	2.39	3.80	5.21	1.19	1.15	0.85
Total	99.80	99.30	99.60	99.60	99.60	99.60	99.40	99.40	100.00	100.00	99.60	99.50	99.60	99.40	99.50	99.40	100.00	99.90	100.00	100.00	99.60
	C.I.P.W. norm (calculated with Fe2O3/FeO = 0.2)																				
Ap	2.30	2.31	2.33	2.31	2.33	2.33	2.29	2.30	2.33	2.27	2.14	2.22	1.92	1.95	2.56	2.45	2.13	2.17	2.22	2.19	2.20
Il	7.32	7.28	7.30	7.29	7.32	7.41	7.35	7.35	7.64	7.31	7.39	7.15	6.85	7.59	6.55	6.78	6.92	7.08	7.22	7.16	7.12
Mt	2.89	2.90	2.88	2.91	2.91	2.88	2.89	2.90	2.96	2.92	2.88	2.80	2.73	3.09	2.71	2.18	2.74	2.78	2.90	2.92	2.91
Or	2.97	3.41	3.83	2.75	5.95	4.02	5.49	5.90	11.48	7.66	8.85	10.00	11.19	6.35	7.88	7.24	1.18	12.56	1.45	1.94	5.27
Ab	12.12	10.42	11.94	13.85	9.71	10.81	8.47	8.58	11.09	9.09	9.96	12.68	9.53	6.17	11.18	10.26	1.83	5.60	15.71	14.43	12.21
An	7.13	6.69	7.79	9.92	8.18	7.08	5.62	5.88	15.31	13.40	16.48	14.41	12.79	19.84	13.66	14.82	7.30	12.96	7.53	7.72	6.23
Di	35.59	36.19	35.44	33.77	34.79	36.58	38.27	37.12	27.01	30.50	29.29	29.35	26.32	22.89	23.28	24.13	48.46	31.27	34.12	33.91	34.45
Hy	0.00	0.00	0.00	0.00	0.00	0.00	0.00	0.00	0.00	0.00	3.96	6.02	15.19	0.00	5.51	5.10	0.00	0.00	0.00	0.00	0.00
Ol	15.63	16.19	15.81	17.13	15.80	14.56	13.84	14.21	21.36	23.29	19.03	15.37	13.47	31.90	26.64	27.04	9.94	20.87	15.95	17.42	16.39
Ne	14.04	14.61	12.78	10.07	13.01	14.30	15.78	15.74	0.74	4.18	0.00	0.00	0.00	0.19	0.00	0.00	19.49	4.68	12.88	12.31	13.19
Ac	0.00	0.00	0.00	0.00	0.00	0.00	0.00	0.00	0.00	0.00	0.00	0.00	0.00	0.00	0.00	0.00	0.00	0.00	0.00	0.00	0.00
C	0.00	0.00	0.00	0.00	0.00	0.00	0.00	0.00	0.00	0.00	0.00	0.00	0.00	0.00	0.00	0.00	0.00	0.00	0.00	0.00	0.00
Q	0.00	0.00	0.00	0.00	0.00	0.00	0.00	0.00	0.00	0.00	0.00	0.00	0.00	0.00	0.00	0.00	0.00	0.00	0.00	0.00	0.00
Total	99.99	100.00	100.10	100.00	100.00	99.97	100.00	99.98	99.92	100.62	99.98	100.00	99.99	99.97	99.97	100.00	99.99	99.97	99.98	100.00	99.97
AN#	37.04	39.10	39.48	41.73	45.72	39.58	39.89	40.66	57.99	59.58	62.33	53.19	57.30	76.28	54.99	59.09	79.96	69.83	32.40	34.85	33.79
DI	29.13	28.44	28.55	26.67	28.67	29.13	29.74	30.22	23.31	20.93	18.81	22.68	20.72	12.71	19.06	17.50	22.50	22.84	30.04	28.68	30.67
SI	40.03	40.71	40.47	41.96	39.70	39.19	38.56	38.31	44.89	47.93	48.34	46.11	50.59	56.45	55.82	55.28	40.48	39.79	39.78	41.42	39.80
LI	-19.02	-19.48	-19.04	-19.59	-18.55	-18.62	-18.38	-18.20	-18.62	-20.92	-19.73	-17.39	-17.55	-26.25	-21.62	-22.09	-21.22	-21.98	-18.76	-19.50	-18.23

Notice. AN#= AN/(AN+AB)*100, S.I. (Solidification Index by Kuno), D.I. (Differentiation, Index by Thornton & Tuttle,1960) & L.I. (Larsen Index by Larsen, 1938).

Sample	963-WA 1	963-WA 2	963-WA 3	963-WA 4	963-WA 5	963-WA 6	963-WA 7	963-WA 8	963-BL 1	963-BL 2	963-BL 3	963-BL 4	963-GR 1	963-GR 2	963-GR 3	963-GR 4	963-GR 5	963-GR 6	963-BU 1	963-BU 2	963-BU 3	963-BU 4
Locality	Mt Watch								The Bluff				Mt Graham		.				Burr			
SiO2	43.10	41.30	43.10	43.30	43.50	43.60	43.20	43.20	43.70	43.80	43.70	44.30	42.50	43.40	43.80	44.00	44.00	43.90	42.80	38.90	38.20	40.40
Al2O3	9.14	8.79	9.12	9.23	9.28	9.19	9.20	9.19	9.80	9.61	9.54	10.90	10.20	10.20	10.20	10.40	10.40	10.50	10.50	11.30	12.10	11.10
Fe2O3(t)	12.70	12.40	12.90	12.70	12.50	12.80	12.70	12.70	13.10	12.90	12.90	12.60	13.10	13.10	12.90	12.90	12.80	12.80	13.10	14.50	15.30	14.10
MnO	0.16	0.16	0.17	0.16	0.16	0.17	0.16	0.17	0.17	0.16	0.17	0.16	0.18	0.18	0.17	0.17	0.17	0.17	0.17	0.18	0.18	0.17
MgO	14.80	13.70	14.30	13.80	14.50	14.40	14.60	14.80	12.00	12.70	12.40	8.92	12.40	12.10	11.00	11.00	10.90	10.60	11.90	13.40	14.00	13.00
CaO	10.10	11.40	10.00	10.40	9.95	9.94	10.10	10.10	10.90	10.90	10.80	11.40	11.10	11.00	10.80	11.00	10.90	11.10	11.10	11.90	12.10	11.60
Na2O	3.71	3.83	4.02	3.48	3.55	3.88	3.34	3.62	3.06	3.92	3.45	4.20	3.31	3.80	4.20	4.45	4.37	4.47	1.83	0.75	0.42	1.01
K2O	0.41	0.33	0.52	0.38	0.74	0.34	0.88	0.62	1.59	0.53	0.95	0.96	0.33	0.31	0.77	0.44	0.64	0.62	2.04	0.69	0.14	0.96
TiO2	3.48	3.39	3.58	3.51	3.43	3.51	3.49	3.49	3.74	3.66	3.65	3.94	3.52	3.51	3.64	3.70	3.68	3.74	3.60	3.90	4.10	3.82
P2O5	0.83	0.82	0.84	0.83	0.82	0.84	0.83	0.83	0.92	0.90	0.90	1.00	0.88	0.81	0.91	0.91	0.91	0.92	0.89	0.97	1.01	0.94
SO3	0.05	0.04	0.01	0.03	0.04	0.02	0.05	0.04	0.01	0.00	0.00	0.00	0.01	0.01	0.00	0.00	0.00	0.00	0.01	0.01	0.00	0.01
LOI	1.28	2.85	1.03	1.88	1.24	1.25	1.31	1.27	0.94	1.14	1.12	1.11	1.78	1.61	0.86	0.86	0.84	0.80	1.45	2.87	2.83	2.52
Total	99.70	99.40	99.60	99.70	99.70	99.90	99.90	100.00	100.00	100.00	99.60	99.50	99.30	100.00	99.30	99.80	99.60	99.60	99.30	99.40	100.00	99.60
Ap	1.99	2.01	2.01	2.00	1.96	2.01	1.99	1.98	2.19	2.14	2.16	2.40	2.13	1.94	2.18	2.17	2.17	2.20	2.15	2.38	2.45	2.29
Il	6.81	6.80	7.00	6.92	6.71	6.85	6.82	6.81	7.28	7.12	7.15	7.72	6.96	6.88	7.12	7.20	7.18	7.30	7.09	7.80	8.12	7.59
Mt	2.85	2.83	2.89	2.86	2.81	2.87	2.85	2.84	2.91	2.88	2.89	2.82	2.96	2.94	2.89	2.88	2.87	2.86	2.95	3.32	3.46	3.21
Or	2.49	2.05	3.15	2.32	4.49	2.06	5.33	3.75	9.60	3.20	5.77	5.83	2.02	1.88	4.68	2.65	3.88	3.75	12.46	4.28	0.86	5.92
Ab	13.02	6.67	12.04	14.66	12.44	14.95	10.79	11.59	8.58	13.43	12.13	14.88	13.13	14.30	13.29	14.85	13.91	13.53	6.03	5.22	3.69	7.66
An	7.36	6.20	5.46	8.79	7.47	6.86	7.80	7.24	8.52	7.22	7.95	8.40	12.39	10.22	6.92	7.22	6.93	6.80	15.00	26.74	32.06	23.97
Di	30.66	38.07	32.08	31.42	30.20	30.52	30.48	30.89	32.72	33.58	32.97	34.59	31.38	32.45	34.05	34.11	34.26	34.83	28.79	23.08	18.84	23.76
Hy	0.00	0.00	0.00	0.00	0.00	0.00	0.00	0.00	0.00	0.00	0.00	0.00	0.00	0.00	0.00	0.00	0.00	0.00	0.00	0.00	4.95	0.00
Ol	24.43	20.53	23.00	22.49	23.98	23.77	24.11	24.23	18.54	19.34	19.30	11.61	20.41	19.23	16.27	16.12	15.81	15.06	20.14	26.39	25.54	24.93
Ne	10.33	14.80	12.36	8.51	9.90	10.10	9.77	10.64	9.67	11.08	9.69	11.75	8.61	10.15	12.59	12.80	12.99	13.67	5.39	0.76	0.00	0.67
Ac	0.00	0.00	0.00	0.00	0.00	0.00	0.00	0.00	0.00	0.00	0.00	0.00	0.00	0.00	0.00	0.00	0.00	0.00	0.00	0.00	0.00	0.00
C	0.00	0.00	0.00	0.00	0.00	0.00	0.00	0.00	0.00	0.00	0.00	0.00	0.00	0.00	0.00	0.00	0.00	0.00	0.00	0.00	0.00	0.00
Q	0.00	0.00	0.00	0.00	0.00	0.00	0.00	0.00	0.00	0.00	0.00	0.00	0.00	0.00	0.00	0.00	0.00	0.00	0.00	0.00	0.00	0.00
Total	99.94	99.96	99.99	99.97	99.96	99.99	99.94	99.97	100.01	99.99	100.01	100.00	99.99	99.99	99.99	100.00	100.00	100.00	100.00	99.97	99.97	100.00
AN#	36.11	48.17	31.20	37.48	37.52	31.45	41.96	38.45	49.82	34.96	39.59	36.08	48.55	41.68	34.24	32.71	33.25	33.45	71.33	83.67	89.68	75.78
DI	25.84	23.52	27.55	25.49	26.83	27.11	25.89	25.98	27.85	27.71	27.59	32.46	23.76	26.33	30.56	30.30	30.78	30.95	23.88	10.26	4.55	14.25
SI	48.77	47.21	46.97	47.44	48.27	47.78	48.27	48.58	42.20	44.16	43.65	35.09	44.56	43.22	39.89	40.00	39.74	38.96	43.18	48.05	49.42	47.00
LI	-21.55	-22.16	-21.02	-20.81	-20.46	-20.98	-20.85	-21.31	-18.53	-20.08	-19.29	-15.93	-20.79	-20.11	-18.04	-18.50	-18.01	-17.96	-18.48	-24.69	-26.99	-22.86

Appendix 2 **Trace element analyses of the Northern area older volcanics**

Sample	963-MC 1	963-MC 2	963-MC 3	963-MC 4	963-MC 5	963-MC 6	963-MC 7	963-MC 8	963-LL 1	963-LL 2	963-LL 3	963-LL 4	963-LL 5	963-ED 1	963-ED 2	963-ED 3	963-MU 1	963-MU 2	963-MU 5	963-MU 6	963-MU 7
Locality	Mt McIntyre								Lake Leake					Mt Edward			Mt Muirhead				
Y	26.2	25.5	25.8	25.6	27	26.1	25.5	26.4	26.2	22.8	20.6	16.2	19.7	19.8	17	21.5	23.2	22.7	29.5	27.9	26.8
Sr	1029	1029	1028	1020	1080	1072	1057	1081	1061	719	1125	672	415	215	465	569	846	857	991	948	999
Rb	15.8	15.3	29.3	37.6	28.6	70.6	83.3	73.1	51.1	41.5	32.9	25.1	68.3	n.a.	22	27.9	16.7	14.8	6.6	11.6	15.2
Nb	90	88.7	89.6	88.7	91.6	91.2	86.9	87.2	84.3	72.3	59.2	42.1	63.7	47.4	51	63.6	65.1	65.7	79	78.4	80.2
Zr	343	341	344	340	347	345	342	350	341	294	249	210	290	197	202	249	277	275	329	327	337
Th	8.7	6.9	6.7	9.1	9.5	7.8	9.3	8	8.9	9.3	5.6	6.1	9	7	6.9	7.9	8.1	9.1	7.7	7.8	8.2
Pb	5.1	5.7	3.7	1.4	4.6	5.4	6.9	4.7	5.5	5.3	4.1	4.5	4.7	3.8	4.2	3.5	4.2	4.4	6.1	5.4	5.4
U	0.6	1.3	n.a.	n.a.	1.4	1.1	1.3	0.9	n.a.	0.1	n.a.	n.a.	n.a.	n.a.	0.6	1.1	n.a.	n.a.	0.5	0.6	1
Ga	18.6	20.2	19.6	18.4	19.9	18.3	18.9	19.1	18.7	15.4	14.1	13.3	13.2	16.7	15.7	16.2	18.1	18.2	20	19.2	18.6
Zn	107	108	110	107	103	107	102	93	113	101	90	67	99	80	86	100	86	88	110	115	110
Cu	101	74	73	84	108	93	104	114	76	64	46	28	54	10	30	41	68	66	77	73	82
Ni	244	270	256	279	262	260	260	234	350	311	289	189	372	795	483	546	207	198	243	292	289
Ba	979	1040	1027	1134	1174	1059	1171	963	1149	1051	986	978	699	1161	852	932	788	761	925	1035	1088
Sc	24.3	24.7	24.3	24.3	23.6	24.5	24.9	23.4	19.3	22.7	24.8	22.4	23	26.5	23.9	23.1	22.3	20.2	23.8	25	22.7
Cr	320	347	353	354	342	339	351	602	470	521	593	490	629	739	761	742	351	333	395	427	411
V	315	329	341	327	312	338	307	311	346	337	310	307	281	326	306	303	256	248	308	313	287
Co	69.5	58.3	63.5	56.8	56.4	57.8	61.5	78.5	63.1	61.5	68.3	61.2	60.1	76.2	79	74.7	52.3	47.8	64.8	65.4	66.4
Ce	147	145	146	149	151	148	147	131	151	144	130	132	121	139	114	108	110	113	138	136	133
Nd	71	65	66	68	68	65	69	61	62	61	55	59	52	68	51	54	52	49	64	62	64
La	86	82	84	83	85	85	82	75	93	83	74	79	66	80	69	69	66	63	80	81	76

n.a. **indicates element not detected**

Sample	963-WA 1	963-WA 2	963-WA 3	963-WA 4	963-WA 5	963-WA 6	963-WA 7	963-WA 8	963-BL 1	963-BL 2	963-BL 3	963-BL 4	963-GR 1	963-GR 2	963-GR 3	963-GR 4	963-GR 5	963-GR 6	963-BU 1	963-BU 2	963-BU 3	963-BU 4
Locality	Mt Wasch								The Bluff				Mt Graham						Burr			
Y	21.6	21.6	21.6	21.6	21.6	21.6	21.6	21.6	21.6	21.6	21.6	21.6	21.6	21.6	21.6	21.6	21.6	21.6	21.6	21.6	21.6	21.6
Sr	828	828	828	828	828	828	828	828	828	828	828	828	828	828	828	828	828	828	828	828	828	828
Rb	34.8	34.8	34.8	34.8	34.8	34.8	34.8	34.8	34.8	34.8	34.8	34.8	34.8	34.8	34.8	34.8	34.8	34.8	34.8	34.8	34.8	34.8
Nb	78.6	78.6	78.6	78.6	78.6	78.6	78.6	78.6	78.6	78.6	78.6	78.6	78.6	78.6	78.6	78.6	78.6	78.6	78.6	78.6	78.6	78.6
Zr	307	307	307	307	307	307	307	307	307	307	307	307	307	307	307	307	307	307	307	307	307	307
Th	6.9	6.9	6.9	6.9	6.9	6.9	6.9	6.9	6.9	6.9	6.9	6.9	6.9	6.9	6.9	6.9	6.9	6.9	6.9	6.9	6.9	6.9
Pb	3.6	3.6	3.6	3.6	3.6	3.6	3.6	3.6	3.6	3.6	3.6	3.6	3.6	3.6	3.6	3.6	3.6	3.6	3.6	3.6	3.6	3.6
U	n.a.	n.a.	n.a.	n.a.	n.a.	n.a.	n.a.	n.a.	n.a.	n.a.	n.a.	n.a.	n.a.	n.a.	n.a.	n.a.	n.a.	n.a.	n.a.	n.a.	n.a.	n.a.
Ga	16.8	16.8	16.8	16.8	16.8	16.8	16.8	16.8	16.8	16.8	16.8	16.8	16.8	16.8	16.8	16.8	16.8	16.8	16.8	16.8	16.8	16.8
Zn	113	113	113	113	113	113	113	113	113	113	113	113	113	113	113	113	113	113	113	113	113	113
Cu	77	77	77	77	77	77	77	77	77	77	77	77	77	77	77	77	77	77	77	77	77	77
Ni	484	484	484	484	484	484	484	484	484	484	484	484	484	484	484	484	484	484	484	484	484	484
Ba	926	926	926	926	926	926	926	926	926	926	926	926	926	926	926	926	926	926	926	926	926	926
Sc	23.4	23.4	23.4	23.4	23.4	23.4	23.4	23.4	23.4	23.4	23.4	23.4	23.4	23.4	23.4	23.4	23.4	23.4	23.4	23.4	23.4	23.4
Cr	615	615	615	615	615	615	615	615	615	615	615	615	615	615	615	615	615	615	615	615	615	615
V	312	312	312	312	312	312	312	312	312	312	312	312	312	312	312	312	312	312	312	312	312	312
Co	77.3	77.3	77.3	77.3	77.3	77.3	77.3	77.3	77.3	77.3	77.3	77.3	77.3	77.3	77.3	77.3	77.3	77.3	77.3	77.3	77.3	77.3
Ce	129	129	129	129	129	129	129	129	129	129	129	129	129	129	129	129	129	129	129	129	129	129
Nd	58	58	58	58	58	58	58	58	58	58	58	58	58	58	58	58	58	58	58	58	58	58
La	77	77	77	77	77	77	77	77	77	77	77	77	77	77	77	77	77	77	77	77	77	77

n.a indicates element not detected

Appendix 2. All list of isotope analyses of the Northern area older volcanics.

Sample	Locality	Lithology	Rb	Sr	87Rb/86Sr	87Sr/Sr86	87Sr/Sr86(T)	Nd	Sm	147Sm/144Nd	143Nd/144 Nd	143Nd/144Nd(T)	eps Nd (0)	eps Nd chT	T mod:dep
963-MC 1	Mt McIntyre	Analcimites	15.8	1028.5	0.044495	0.704179 ± 49	0.703868	71.32	11.31	0.095947	0.512756 ± 23	0.512448	2.31	8.49	0.433
963-MC 2			15.3	1028.6	0.043083	0.704114 ± 30	0.703813	64.42	11.10	0.104191	0.512799 ± 52	0.512465	3.15	8.82	0.408
963-MC 3			29.3	1027.6	0.082585	0.704249 ± 42	0.703672	64.93	10.84	0.101001	0.512749 ± 18	0.512425	2.16	8.03	0.461
963-MC 4			37.6	1019.9	0.106780	0.704272 ± 22	0.703527	65.49	10.90	0.100674	0.512770 ± 27	0.512447	2.57	8.46	0.433
963-MC 5			28.6	1080.0	0.076701	0.704246 ± 26	0.703711	65.73	11.13	0.102397	0.512734 ± 16	0.512406	1.88	7.66	0.484
963-MC 6			70.6	1071.8	0.190788	0.704289 ± 45	0.702957	65.21	11.13	0.103245	0.512734 ± 23	0.512403	1.88	7.61	0.488
963-MC 7			83.3	1056.8	0.228303	0.704156 ± 31	0.702562	69.25	11.91	0.104030	0.512743 ± 52	0.512410	2.06	7.73	0.479
963-MC 8			73.1	1080.6	0.195935	0.704239 ± 25	0.702871	61.23	9.47	0.093506	0.512743 ± 18	0.512443	2.06	8.39	0.440
963-LL 1	Lake Leake	Analcimites	51.1	1060.5	0.139563	0.704348 ± 47	0.703374	62.86	11.29	0.108656	0.512784 ± 31	0.512435	2.85	8.24	0.444
963-LL 2			41.6	719.4	0.167488	0.704366 ± 23	0.703197	58.80	10.67	0.109786	0.512750 ± 43	0.512398	2.19	7.51	0.495
963-LL 3			32.9	1125.2	0.084689	0.704437 ± 30	0.703845	50.31	9.49	0.114037	0.512771 ± 21	0.512405	2.60	7.64	0.485
963-LL 4			25.1	671.5	0.108265	0.704419 ± 35	0.703663	56.29	10.11	0.108623	0.512749 ± 40	0.512400	2.16	7.55	0.492
963-LL 5			68.3	415.2	0.476457	0.704840 ± 30	0.701513	47.66	8.70	0.110396	0.512746 ± 22	0.512392	2.11	7.38	0.503
963-ED 1	Mt Edward	Analcimites	0.9	215.0	0.012676	0.704563 ± 31	0.704475	57.42	10.56	0.111259	0.512740 ± 23	0.512383	1.98	7.21	0.516
963-ED 2			27.8	464.9	0.172890	0.704607 ± 25	0.703400	47.28	8.69	0.111245	0.512741 ± 12	0.512384	2.01	7.24	0.514
963-ED 3			37.3	568.6	0.190189	0.704615 ± 20	0.703287	48.02	9.46	0.119146	0.512771 ± 17	0.512388	2.59	7.32	0.509
963-MU 1	Mt Muirhead	Analcimites	16.7	845.8	0.057189	0.704214 ± 42	0.703814	59.26	10.54	0.107577	0.512738 ± 19	0.512393	1.95	7.41	0.501
963-MU 2			14.8	856.8	0.050031	0.704192 ± 32	0.703843	59.61	10.91	0.110689	0.512772 ± 36	0.512417	2.61	7.87	0.469
963-MU 3			20.2	757.1	0.077278	0.704264 ± 29	0.703725	58.57	10.63	0.109745	0.512735 ± 33	0.512382	1.88	7.20	0.516
963-MU 4			47.7	664.4	0.207945	0.704376 ± 29	0.702924	57.42	8.74	0.092125	0.512723 ± 42	0.512427	1.65	8.07	0.460
963-MU 5			6.6	991.2	0.019286	0.704621 ± 24	0.704486	50.16	9.92	0.119641	0.512724 ± 24	0.512340	1.67	6.37	0.582
963-MU 6			11.6	948.4	0.035426	0.704433 ± 22	0.704185	52.49	9.35	0.107705	0.512718 ± 36	0.512372	1.55	7.00	0.529
963-MU 7			15.2	998.7	0.044083	0.704386 ± 21	0.704079	58.77	10.34	0.106407	0.512739 ± 24	0.512398	1.98	7.51	0.495

Continued

Sample	Locality	Lithology	Rb	Sr	87Rb/86Sr	87Sr/Sr86	87Sr/Sr86(T)	Nd	Sm	147Sm/144Nd	143Nd/144 Nd	143Nd/144Nd(T)	eps Nd (0)	eps Nd chT	T mod:dep
963-WA 1	Mt Walch	Analcimites	34.8	868.8	0.116011	0.704188 ± 21	0.703378	50.09	9.37	0.113196	0.512742 ± 11	0.512378	2.02	7.13	0.522
963-WA 2			49.1	941.6	0.151028	0.704944 ± 43	0.703890	55.78	9.76	0.105858	0.512715 ± 23	0.512375	1.51	7.07	0.524
963-WA 3			34.6	854.9	0.117224	0.704360 ± 35	0.703541	63.78	11.12	0.105447	0.512732 ± 37	0.512393	1.83	7.41	0.501
963-WA 4			57.4	1795.5	0.092596	0.704651 ± 31	0.705865	55.82	9.77	0.105926	0.512720 ± 29	0.512380	1.60	7.16	0.518
963-WA 5			40.7	838.4	0.140609	0.704416 ± 50	0.703434	55.09	9.69	0.106369	0.512734 ± 17	0.512393	1.87	7.40	0.502
963-WA 6			44.2	815.5	0.156981	0.704343 ± 38	0.703247	55.55	9.82	0.106917	0.512726 ± 27	0.512383	1.72	7.21	0.515
963-WA 7			32.8	815.5	0.116490	0.704363 ± 35	0.703549	66.06	9.04	0.082760	0.512720 ± 16	0.512454	1.60	8.60	0.432
963-WA 8			32.4	834.3	0.112482	0.704220 ± 47	0.703435	66.06	11.17	0.102271	0.512748 ± 39	0.512420	2.15	7.94	0.466
963-BL 1	The Bluff	Analcimites	43.2	950.4	0.131653	0.704310 ± 29	0.703391	59.37	10.88	0.110894	0.512746 ± 27	0.512391	2.12	7.36	0.505
963-BL 2			15.9	1160.3	0.039691	0.705013 ± 27	0.704735	57.98	10.30	0.107476	0.512775 ± 27	0.512430	2.67	8.13	0.452
963-BL 3			19.2	1027.6	0.054117	0.704555 ± 48	0.704177	55.30	10.50	0.114841	0.512754 ± 33	0.512385	2.26	7.26	0.513
963-BL 4			47.2	1001.8	0.136465	0.704412 ± 21	0.703459	72.34	11.97	0.100113	0.512781 ± 27	0.512460	2.79	8.71	0.417
963-GR 1	Mt Graham	Analcimites	10.4	889.2	0.033876	0.704476 ± 18	0.704240	70.80	12.57	0.107389	0.512646 ± 18	0.512301	0.15	5.62	0.623
963-GR 2			3.7	565.4	0.018954	0.704347 ± 37	0.704215	71.49	12.74	0.107825	0.512719 ± 20	0.512373	1.57	7.01	0.529
963-GR 3			16.8	893.3	0.054472	0.704295 ± 13	0.703914	57.87	10.53	0.110112	0.512742 ± 8	0.512389	2.03	7.32	0.507
963-GR 4			18.0	922.6	0.056509	0.704266 ± 24	0.703872	60.13	11.00	0.110693	0.512778 ± 23	0.512423	2.73	7.99	0.461
963-GR 5			17.2	802.3	0.062094	0.704279 ± 24	0.703846	58.72	11.78	0.121323	0.512747 ± 37	0.512358	2.13	6.72	0.556
963-GR 6			19.7	1062.6	0.053793	0.704236 ± 21	0.703861	59.43	10.81	0.110058	0.512707 ± 17	0.512354	1.35	6.64	0.555
963-BU 1	Burr	Analcimites	68.6	665.8	0.298429	0.704410 ± 16	0.702326	56.77	10.63	0.113317	0.512710 ± 24	0.512346	1.40	6.49	0.568
963-BU 2			16.5	452.9	0.105522	0.704419 ± 13	0.703682	60.24	11.62	0.116708	0.512704 ± 33	0.512329	1.29	6.17	0.594
963-BU 3			3.3	213.6	0.044748	0.704432 ± 24	0.704119	65.30	9.51	0.088057	0.512685 ± 22	0.512403	0.92	7.60	0.489
963-BU 4			21.2	515.3	0.119161	0.704487 ± 36	0.703655	66.09	11.82	0.108201	0.512700 ± 22	0.512352	1.20	6.62	0.556

Appendix 3. Complete listing of mineralogy and petrology of the South Australian lower crustal xenoliths

Appendix 3. Summary of petrology of the South Australian lower crustal xenoliths.

Rock type	Type	Sample name	major minerals	minor minerals
Port Augusta				
Eclogitic rock	Type A	Pa 6X 8, 5X 2	Gt (45-50 %)+ Cpx (45-50 %)	Rt (3-5 %), Apt , Il
	Type B	Pa 6X 9	Gt (38 %)+Cpx (45 %)+Am (10%)	Il, Apt, Qt
	Type C	Pa 6X 2, 6X 6, 6X 7	Gt (42-46%)+Cpx (43-47%)	Opx (2-5%)+Rt (2-5%)
	Type D	Pa 5X 1, 6X 12	Gt (40-47 %) + Cpx(50-55 %)	Am (5 %)±Rt (4 %)+Sp(5 %) ±Apt (2-4 %)
Fd -rich granulite	Type A	Pa 7X 1, 6X11	Cpx (40-50%)+Gt (30-40%)+Pl (15-20 %)	Sp (4-7%) +Am(2-5%)+Opx (2-3%) + Rt (~2%) +Apt (0.5 %) +Mt ±Bi
	Type B/1	Pa 7X 6, 9X 1	Fd (45-60%)+ Cpx (25-35%)+ Gt (20-25%)	Opx, Rt, Il, Mt
	Type B/2	Pa 7X 2, 7X 8	Gt (15-25%)+Cpx (30-35%) +Pl (34-42%) +Opx (8-15 %)+Il (3-6 %)	Opx, Rt, Apt, Mt , Chrom, Sulp
Gabbroic rock		Pa 7X 9, 6X 10	Pl (40-45 %)+ Px (30-35 %)+Am (15-25 %)	Gt, Il, Mt
Xenocryst	Type A	Pa 8X 1, 8X 2, 8X 3		
	Type B	Pa 8X 4		
Calcutteroo				
Eclogitic rocks	Type A	TRWI CX 13	Gt (40 %) +Cpx (58 %)	Am
	Type B	TRWI CX 11	Gt (44 %)+Cpx (43 %)	Qt (5-8 %), Ky, Rt, Il
	Type C	TRWI CX 4, N 1, N 6	Cpx (40-46 %)+Gt (40-45 %)+Qt (7-8 %)	Rt (3-5 %), Il, Apt
	Type D	TRWI N 5, N 8, N10	Cpx (60-70 %)+Gt (20-30 %)	Am (5-6 %)±Qt (1-5 %), Pl, Sp Opx, Rt, Apt
Two-Px granulites	Type A	TRWI CH7, CX 10	Cpx (50-60%)+Gt (1015%)+Opx (8-15%) +Am (15-20%)	Hel, Chl, Mt
	Type B	TRWI CH 6.	Cpx (75 %)+Gt (15 %)+Opx (8 %)	Am (2-3%), Il, Mt
Cpx-granulites	Type A	TRWI CX 2, CX 8, N 4	Gt (37-40 %)+ Cpx (40-44 %) +Qt (8-12 %)+ Pl (5-10 %)	Rt, Apt, Am , Bi
	Type B	TRWI CX 5, CX 12, N 2	Cpx (40-43%) +Gt (39-44%) +Pl (8-10%)+Qt (6-8%)	Opx, Apt, Rt, Il, Ht , Mt
	Type C	TRWI CH3, CX 7	Gt (30-35%)+Cpx (35-40%)+Am (10-15%)	Fd (5-8 %) +Qt (3-6 %) +Opx (2-5 %) Bi, Rt, Il
	Type D	Trwi CB4, CH4	Cpx, Gt	Qt, Am, Sp, Il
Fd- rich granulites		TRWI CX 6, CX 3, N 3, N 9	Fd (35 %)+Gt (30 %)+Cpx (22 %) +Qt (10 %)	Rt, Apt
Ky-bearing granulite		Trwi CX 1, N 7, CX 9	Gt (44-47 %)+Cpx (40-44 %)+Qt (8-15 %) Ky(4-7%)	Rt, Apt
Pyroxenites				
	Type A	TRWI CB1, CH 8	Cpx (35-40 %) + Opx(40-60 %)+Am (5-15 %)	Rt, Il
	Type B	TRWI A1, CH 4	Cpx, Opx & Am	Il, Rt, Bi, Cal
	Type C	TRWI CB3, CB2	Cpx, Am, Gt, Opx	Sp, Mt
Composite xenolith		TRWI N C1		
Transitional varaition		TRWI CX 14		
Pine Creek				
Cpx-granulite		PINC X 5	Gt (25 %)+Cpx (30 %) +Pl (35 %)+Qt (7 %)	Bi (3 %), Kyan, Apt, Rt
Fd-rich granulite		PINC X 7a	Gt (42 %)+Pl (35 %)+Cpx (15 %) + Kfd (10 %)	Cal,Bi
Pyroxenite		PINC X 7b	Cpx & Am	
Amphibolite		Pinc A 4	Am (90 %)+Cpx (8 %) + Gt	Pl, Cpx, Gt , Apt, Rt
Gabbroic rock		PINC X 6	Am, Pl,	Cpx, Opaque Oxide, Apt
Megacrysts & xenocrysts		PINC X 5	Gt(1.0-1.2 cm wide)	
		PINC X 2,X 3	Il (1.2-1.6 cm wide)	
		PIC A 3		
		PIC X 4		
Transitional varaition		PIC A 2	Cpx+Am+Gt+Opx	Rt, Il

Appendix 3 Summary of garnet compositions of the South Australian lower crustal xenoliths.

Lithology	Sample	Mode	CaO (wt)	MgO (wt)	FeO (total, wt)	MnO (wt)	Cr2O3 (wt)	Mg#	Grosul(Ca)	Pyrop(Mg)	Alma(Fe(2))	total	Andre(Fe3)	Spess(Mn)	Uvalo(Ca-Cr)
Port Augusta															
Eclogitic rock															
	Pa 6X 8		9.8-10.3	6.2-6.8	22.6-23.2	0.3-0.5	0.1-0.3	33-35	32.8-32.5	31.4-33.6	29.9-33.6	95-97	0.8-2.1	0.4-1.5	0.2-0.8
	Pa 5X 2		9.7-10.1	6.5-6.9	22.1-24	0.3-0.7	0.1-0.3	33-35	32-34.4	32.1-34.1	29.3-31.2	95-98	1.0-2.4	0.9-1.5	0.3-1.0
	Pa 6X 9		8.9-9.6	7.6-8.1	20.5-21.4	0.7-0.9	0.1-0.2	39-41	29.1-31.9	37.5-38.9	26.1-26.7	94-97	1.3-2.4	1.8-2.5	0.1-0.8
	Pa 6X 2		8.9-9.2	6.8-7.3	22.9-23.6	0.3-0.5	0.1-0.5	34-36	18.4-22.3	25.9-27.3	46.6-48.3	93-95	2-5.2	0.6-1.2	0.3-0.9
	Pa 6X 6		8.3-8.7	7.9-8.5	21.7-22.6	0.5-0.7	0.1-0.3	39-41	16.7-21.2	30.2-32	43.3-45.5	93-97	2.3-5.6	0.7-1.3	0.4-0.7
	Pa 6X 7		8.2-8.7	8.1-8.6	21.9-22.6	0.4-0.7	0.1-0.3	39-41	17.4-20.1	30.6-32.5	43.7-45.1	93-96	3.0-5.2	0.7-1.7	0.2-0.7
	Pa 6X 12		9.4-9.6	8.7-9.3	19.8-20.6	0.4-0.7	0.1-0.3	43-45	28.1-30	38.9-42.9	23.7-25.7	94-97	1.7-2.6	1-1.7	0.1-0.9
	Pa 5X 1		8.1-8.6	8.8-9.2	20.3-21.2	0.7-1.1	0.1-0.2	43-44	18.1-20.2	33.9-35	40.4-41.5	93-95	2.5-3.2	1.2-2.3	0.2-0.4
Fd-rich granulite															
	Pa 7X 1	exsolved	8.9-9.2	7.4-7.9	21.6-22.2	0.7-0.9	0.1-0.2	38-39	19.2-22.5	28.4-30	44-44.9	93-96	2.3-3.2	1.4-2	0.3-0.8
		rim	8.0-8.2	8.3-8.7	21.9-22.6	0.6-0.9	~0	40-41	16.8-20.4	30.9-33	43.4-44.8	93-96	1.6-5	1.7-1.9	~0.1
		euhedral	7.4-9.7	7.5-9.1	21.9-22.7	0.4-0.8	0.1-0.2	39-42	16.5-19.7	28.9-33.9	43.6-45.5	94-96	2.3-4.7	0.9-1.6	0.2-0.7
	Pa 6X 11	two type	5.7-6.2	9.9-10.3	21.1-22	0.2-0.5	0.1-0.3	45-46	18-20.2	48.5-50.5	27.6-29.5	97-98	1.3-1.8	0.7-1.3	0.2-0.4
			9.9-10.3	6.4-6.8	22.6-23.3	0.3-0.5	0.1-0.3	33-35	33.2-35.5	31.9-33.6	30.2-30.9	96-97	0.8-1.6	0.4-1.6	0.2-0.8
	Pa 7X 6		6.3-7.9	5.7-6.8	24.8-28.1	0.6-0.8	0.1-0.2	26-32	22.9-24.5	30.6-35.5	35.6-42.5	95-97	0.6-2.6	1.7-2.3	0.3-0.6
	Pa 9X 1		5.6-6.2	6.1-6.9	26-27.4	0.5-1	0.1-0.2	29-32	20.9-23.2	32.7-35.4	36.3-39.5	94-97	1-2.3	1.5-3.1	0.2-0.5
	Pa 7X 8	rim(granular)	5.5-5.9	10.1-10.6	21.4-22.8	0.3-0.7	0.2-0.5	45-46	11.8-12.8	38.4-39.6	43.3-45.3	95-97	2-3.6	0.3-1.3	0.5-1
		discrete	5.8-6.4	10.9-11.3	20.5-21.5	0.2-0.5	0.1-0.4	48-49	12.4-14.8	40.8-42.5	39.3-41.6	94-97	1.6-4.2	0.3-1.1	0.2-0.7
Two-Px granulite															
	Pa 7X 5		8.2-8.6	6.2-6.3	24-24.1	0.7-0.8	0.1-0.2	31-32	28.5-31.1	31.8-33.2	33.9-34	96-97	0.7-1.5	2.2-2.4	~0.7
	Pa CX 6	rim of Cpx	7.5-7.9	6.1-6.2	25.2-25.7	1.1-1.2	~0.1	30-31	15.5-18.3	23.6-24.1	51.7-52.7	91-95	2.4-6.2	2.5-2.7	~0.4
Gabbroic rock															
	Pa 6X 10	rim of Cpx	7.1-7.9	5-5.5	26.2-26.8	0.7-0.9	0.2-0.3	25-27	16.3-19.4	19.6-21.4	56.1-58.1	94-96	1.2-3.4	1.6-2	0.5-1
		discrete	7.5-8.6	4.6-5.3	26.3-27.4	0.7-1.2	0.1-0.3	23-26	15.5-18.8	18-20.2	54.1-27.4	93-95	2.9-4.5	1.5-2.6	0.1-0.5
Xenocryst															
	Pa 8X 1	inclusion of Am	7.4-7.9	10.3-11.1	18-18.3	0.6-0.9	0.1-0.2	49.8-52.3	16.6-19	39.8-42.9	36.2-37.8	95-97	1.9-3.1	0.9-1.9	0.18-0.43
	Pa 8X 2		7.5-8.0	11-11.6	17.4-19.3	0.79-0.91	0.07-0.31	51.9-53.7	15.9-18.2	41.5-43.2	33.8-35.5	93.2-95.9	3.1-4.8	1.6-2.1	0.3-0.7
Pine Creek															
Fd -rich granulite															
	Pinc X 7		8.0-8.6	11.2-12	16.5-17	0.3-0.5	0.1-0.3	54-55.8	19-20.5	42.4-43.8	31.9-34.1	93-97	1.5-3.5	0.7-1.4	0.2-0.7
Cpx-granulite															
	Pinc X 5		9.0-9.4	11.9-12.3	15.1-15.8	0.2-0.6	0.1-0.3	57.9-58.9	19.9-23.3	43.6-45.3	29.7-31.5	95-98	1.3-4	0.3-0.9	0.1-0.9
Travsitional variation															
	Pinc A 5		8.3-8.9	10.9-11.6	17.2-17.8	0.2-0.5	0.1-0.2	52.5-54.2	19.4-20.9	40.8-42.7	1.1-3.8	95-98	0.4-0.9	0.3-0.6	0.2-0.6

Lithology	Sample	Mode	CaO (wt)	MgO (wt)	FeO (total, wt)	MnO (wt)	Cr2O3 (wt)	Mg#	Grosul(Ca)	Pyrop(Mg)	Alma(Fe(2))	total	Andre(Fe3)	Spess(Mn)	Uvalo(Ca-Cr)
Calcutt roo															
Eclogitic rock															
	Trwi CX 13		11.2-11.6	13-13.6	10.3-11.6	0.24-0.48	0.14-0.32	66-70	24.8-28.1	47.3-50.4	19.8-21.9	94-97	1.5-4.4	0.3-1	0.4-1
	Trwi CX 1	kyanite bearing	8.3-9	14-15.6	12.2-13	0.23-0.39	0.14-0.27	66-67	19.5-22.2	51.3-53.2	23.9-24.9	94-97.2	0.8-3.8	0.5-1.0	0.4-0.7
	Trwi CX 11		7.1-7.8	16.5-17	10.6-11.2	0.22-0.38	0.12-0.35	72.8-73.6	15.3-17.5	58.4-60.8	20.1-21.2	96-97.5	1.3-2.6	0.25-0.8	0.1-0.6
	Trwi CX 9		7.0-7.7	16.4-17	10.8-11.4	0.34-0.58	0.15-0.47	72-73.6	14-15.8	59.9-61.1	19.4-21.3	92-95	2.1-5.8	0.5-1	0.5-1.2
	Trwi CX 4		8.0-8.5	6.9-7.2	23.5-24.2	0.39-0.6	0.02-0.29	33.9-34.8	17.9-19.4	25.8-27.9	48.4-50	94-97	1.5-4.4	0.8-1.3	0.2-0.6
	Trwi N 1		8.8-9.3	5.8-6.3	23.9-24.7	0.3-0.6	0.1-0.35	30-32	18.1-21.3	22.7-24.3	48.7-50.2	92.2-94.5	3-5.9	0.6-1.3	0.3-1
	Trwi N 10		9-9.7	9.7-10.3	16.9-17.8	0.38-0.67	0.13-0.35	49.6-50.9	19.8-22.4	38.5-39.6	33.7-36.1	91-97	2.8-4.8	0.8-1.4	0.5-1
	Trwi N 8		6.9-7.2	12.1-12.9	15.9-16.8	0.28-0.49	0.12-0.42	56.4-58.53	13.1-16.6	45.9-47.9	31.1-34.5	92-97.5	1.7-5.8	0.6-1.4	0.3-1.2
Cpx-granulite															
	Trwi CX 2		10.1-10.4	10.2-10.9	16-17.1	0.4-0.5	0.15-0.3	52.4-54.8	23-25.4	37.8-40.8	31.9-33.7	94-96.5	1.1-4	0.6-1.1	0.45-0.1
	Trwi CX 8		8-8.8	11.5-12	16.4-17.2	0.25-0.59	0.05-0.3	54.9-56.5	17.3-206	43.1-44.7	31.7-34.7	94.8-98	0.5-3.9	0.5-1.3	0.28-0.69
	Trwi CX 5		8.1-8.6	10.7-11.1	17.5-18.02	0.31-0.57	0.11-0.17	51.6-53	17.2-19.9	40.4-42.3	33.5-35.6	93-96.5	2.4-6.4	0.7-1.3	0.29-0.43
	Trwi CX 7		8.7-9.5	6.9-7.7	22.4-23.2	0.2-0.6	0.1-0.34	34.8-37.8	18.9-21.9	26.5-28.9	43.9-46.3	93-95	2.5-6.4	0.8-1.4	0.3-0.9
	Trwi CH 3		5.1-5.5	18-19.2	8.2-8.9	0.2-0.7	0.47-0.7	79.5-80.6	10.8-11.7	68.9-69.4	15.7-16.9	96.2-97.7	1.7-2.6	0.5-1.1	0.1-0.9
	Trwi CB 4		4.4-4.9	15.1-15.9	15.3-15.9	0.23-0.67	0.2-0.58	63-65	6.8-9.9	55.5-57.8	28.4-31.54	93-95.5	1.1-3	0.5-1.4	0.4-0.8
Fd-rich granulite															
	Trwi CX 3		7.9-8.6	11.7-12.4	16.6-17.2	0.22-0.65	0.22-0.65	54.9-57.03	16.1-18.8	43.1-45.7	30.01-34.5	93-98	3.2-6.4	0.34-0.47	0.23-0.57
	Trwi CX 6		8.9-9.1	12.2-12.9	14.8-15.4	0.23-0.6	0.13-0.39	58.9-60.4	18.4-21.4	46.2-47.6	28.1-29.2	94-96	2.7-5.6	0.6-0.9	0.4-0.8
	Trwi N 3		7.6-7.8	13.5-13.9	13.8-14.4	0.27-0.56	0.1-0.29	62.8-64	16.8-17.9	50-52	26.5-28	94-98	1.4-3.1	0.59-1.3	0.1-1.7
Two-Px granulite															
	Trwi CX 10		7.9-8.8	12.5-13.2	14.4-14.9	0.4-0.6	0.13-0.37	60.4-61.8	17.4-21.6	46.2-48.5	27.3-29.3	94-97.4	1-5.2	0.6-1.4	0.2-0.9
Transitional variation															
	Trwi CX 14		7.4-8.0	11.4-12.2	16.8-17.9	0.4-0.54	0.05-0.3	53.5-55.7	15-17.3	42.2-45.3	33.2-34.3	93.6-96.4	2.4-3.7	0.9-1.2	0.1-0.5
Pyroxenitic rock															
	Trwi CB 3	recrystallised	7.9-8.4	13.8-13.9	14-14.5	0.38-0.5	0.1-0.28	63.1-64	16.1-17.5	50.5-51.2	25.7-27.4	93.8-95.5	3.1-4.5	0.8-1	0.37-0.81
			8.0-8.4	13.3-15.8	13.7-14.2	0.34-0.46	0.17-0.29	63.6-64.2	18.3-20.5	49.5-50.8	27-28.2	96.-98.3	1.0-2.8	0.3-1	0.41-0.83
Xenocryst															
	Trwi CH 5		4.5-4.8	15-15.7	14.8-15.5	0.4-0.6	0.21-0.41	63-65.5	8.5-10	56.3-59	28.4-30.7	92.3-97.2	1.2-4.8	0.4-1.3	0.28-1.2

Appendix 3 Summary of orthopyroxene compositions of the South Australian lower crustal xenoliths.

Lithology	Sample	Mode	SiO2 (wt %)	TiO2 (wt %)	Al2O3 (wt %)	MnO (wt %)	CaO (wt %)	Cr2O3 (wt %)	NiO (wt %)	Mg#	Wo(Ca)	En(Mg)	Fs(Fe)
Calcutroo													
Fd-rich granulite													
	Trwi CX 6	recrystallised	50.8-53.3	0.08-0.3	3.6-5.2	0.24-0.48	1.37-1.75	0.16-0.31	0.15-0.26	76.2-77.9	2.78-3.6	74-75.1	21.3-23.1
	Trwi CB 3		47.1-49.9	0	10.9-11	0.2-0.21	1.4-1.5	0.04	0.23-0034	88.5-89.4	2.9-3.1	85.9-86.6	10.3-11.2
Xenocryst													
	Trwi CH 5	inclusion	46.6-47.9	0.09-0.25	8.9-10.4	0.1-0.24	1.3-1.4	0.47-0.52	0.11	79.5-81.1	2.9-3.1	77.2-78.7	18.3-20
		inclusion	44.9-46.6	0.2-0.8	8.9-11.1	0.2-0.24	6.3-12.9	0.7-0.8	0.2	76.8-78.2	13.7-28.9	55.6-66.2	15.5-20
Pyroxenitic rock													
	Trwi CH 4	inclusions in Cpx	55.5-56.2	0.7-0.24	1-1.4	0.2-0.4	0.1-0.4	003-0.5	0.1-0.2	91-92.3	0.43-0.81	90.9-91.8	7.7-8.4
	Trwi CH 8	thin lamellae	52.8-54.4	0.1-0.23	1.5-2	0.1-0.5	0.3-0.5	0.2-0.5	0.2-0.4	82-83	0.59-0.8	81.7-82.9	16.5-17.7
Cpx-granulite													
	Trwi CB 4	fine grain	53.2-54.2	0.05-0.13	1.9-2.1	0.14-0.32	0.26-0.28	0.1-0.3	0.1-0.25	82.7-83.3	0.51-0.54	82.2-82.6	16.5-17.7
Pine Creek													
Xenocryst													
	Pine CX 4		47.7-51.8	0.1-0.25	5.5-10.8	0.5-0.7	1.6-2.1	0.12-0.34	0.08-0.33	84-87	3.44-4.24	80.9-83.7	12.5-15.7
Port Augusta													
Eclogitic rock													
	Pa 6X 8	fine	48.5-49.9	0.1-0.5	1.5-2.3	0.3-0.7	0.4-1.8	0.1-0.2	0.05-0.2	47-49	0.8-1.8	45.4-47.7	49.0-52.1
Cpx-granulite													
	Pa 6X 11	exsolution in Gt	52.3-52.8	~0.11	1.4-1.75	0.11-0.2	0.16-0.32	0.12-0.26	0.13-0.14	72-73	0.32-0.62	72-73	26.5-27.4
Fd-rich granulite													
	Pa 7X 8	surround by Gt rings	52.3-53.6	0.11-0.45	1.1-1.5	0.1-0.25	0.19-0.25	0.05-0.18	0.1-0.4	75-77	0.4-1.1	74.9-75.9	23.3-24.3
Two-Px granulite													
	Pa 7X 5		50.1-51.2	0.05-0.09	1.9-2.9	0.1-0.4	0.3-0.6	0.04-0.14	0.1-0.3	62-68	0.7-1.5	62.1-67.2	32.2-36.7
	Pa CX 6		48.6-50	0.05-0.3	2.4-4	0.4-0.7	0.3-1.1	0.1-0.25	0.01-0.2	57-61	0.6-1.2	59.1-60.1	38.9-40.5
Gabbroic rock													
	Pa 7X 9	exsolved	49.7-49.4	0.04-0.2	2.3-2.7	0.5-0.9	1.6-2.9	0.04-0.2	0.01-0.08	49-50	3.4-6.2	46.3-48.3	47.2-50.8
		fine euhedral	48.8-49.5	0.26-0.52	2.0-2.3	0.47-0.73	0.9-1.34	0.06-0.1	~0.056	47-49	1.9-2.9	46.4-47.3	49.8-51.2
		coarse	49.7-49.8	0.01-0.3	1.5-1.9	0.6-1.6	0.6-1.0	0.5-1.9	0.06-0.3	47-48	1.04-4.1	46.4-47.3	49.6-51.7

Appendix 3 Summary of clinopyroxene compositions of the South Australian lower crustal xenoliths.

Lithology	Sample	Mode	Mg#	Cr2O3 (Wt %)	Na2O (Wt %)	Al2O3 (Wt %)	CaO (Wt %)	TiO2 (Wt %) In Ca-Mg+Fe diagram	In Di+Hd-Jd-Ts diagram
Port Augusta									
Eclogitic rock									
	Pa 6x 8	two type	69-71	0.14-0.27	5.4-5.6	10.7-11	14.5-14.7	0.21-0.32 salic-augatic, mainly augatic	Jd and Di+Hd
			57-65	0.3-0.54	1.5-2.9	3.2-6.9	16.2-18.9	0.25-0.82 augatic	
	Pa 5x 2		68-70	0.2-0.5	4.7-5.4	10-10.5	14.7-15.4	0.3-0.62	
	Pa 6X 9		69-71	0.17-0.35	3.8-4.2	6.39-6.7	16.8-17.4	0.35-0.54 salic-augitic, mainly salitic	Jd
	Pa 6X 2		71-73	0.2-0.4	3.8-4.2	7.6-8.1	16.7-17.2	0.23-0.46	more Jd
	Pa 6X 6		75-76	0.2-0.39	3.7-4.3	7.6-8.0	16.9-17.6	0.15-0.38	
	Pa 6X 7		75-77	0.2-0.43	3.7-4.2	7.6-8.2	16.9-17.9	0.22-0.4	
	Pa 6X 12		74-75	0.3-0.5	4.3-5.2	8.8-9.4	15.9-16.3	0.37-0.7 very vaiable, but mainly augatic	Jd and Di+Hd
	Pa 5X 1	host	69-73	0.2-0.5	2.0-3.2	4.6-5.4	17.7-19.8	0.4-0.55 more augitic	
		replaced	74-76	0.3-0.5	1.3-2.3	2.8-3.8	17.8-18.3	0.2-0.3 more salitic	
Fd- rich granulite									
	Pa 7X 1		71-75	0.17-0.49	1.9-2.4	4.9-6.5	19.6-20.8	0.2-0.5 salitic	Di-Hd
	Pa 6X 11		63-66	0.19-0.59	1.4-2.2	6.4-7.3	19.3-20.2	0.6-1	
	Pa 7X 6		64-66	0.27-0.46	1.6-2.2	6.7-7.5	19.7-20.2	0.7-1.1 salitic-augatic	Di-Hd
	Pa 9X 1		64-37	0.22-0.3	1.8-2.3	6.5-7.3	19.8-20.1	0.65-0.9	
	Pa 7X 8	recrystallised	81-83	0.3-0.54	1.8-2.2	4.4-4.9	20.7-20.9	0.3-0.47 diopsidic-salitic, mainly diopsidic	Jd and Di+Hd
		coarse	80-82	0.59-0.83	1.9-2.4	4-6.3	19.9-20.7	0.14-0.33	more Jd
Two -Px granulite									
	Pa 7X 5		67-69	0.26-0.53	0.56-1.36	5.4-5.7	21-21.5	0.54-0.7 salic-augatic, mainly augatic	Di-Hd
	Pa CX 6		64-68	0.13-0.44	0.64-0.96	5-5.7	19.4-21.6	0.52-0.69	
Gabbroic rock									
	Pa 7X 9		59-65	0.1-0.5	0.01-0.5	2.1-2.9	16.7-22.5	0.07-0.3 salic-augatic, mainly augatic	Jd and Di+Hd
	Pa 6X 10		65-70	0.2-0.5	1.5-1.9	3.3-4.3	19.9-21	0.2-0.45	mainly Di-Hd
Xenocryst									
	Pa 8X 3	inclusion of Am	75-77	0.3-0.48	1.5-3	3.2-4.6	18.7-20.7	0.25-0.52 diopsidic-augatic	Jd
	Pa 8X 1	inclusion	78-80	0.37-0.51	3.0-3.7	5.4-6.5	17.5-18.5	0.3-0.48	
	Pa 8X 2	inclusion	78-81	0.33-0.54	2.7-2.9	5.5-6.2	18.3-19	0.35-0.47	

Lithology	Sample	Mode	Mg#	Cr2O3 (Wt %)	Na2O (Wt %)	Al2O3 (Wt %)	CaO (Wt %)	TiO2 (Wt %) In Ca-Mg+Fe diagram	In Di+Hd-Jd-Ts diagram
Pine Creek									
Fd-rich granulite									
	Pinc X 7		78-80	0.3-0.6	2.9-3.2	8.9-9.2	18.2-18.7	0.4-0.78 diopsidic	Jd
Cpx-granulite									
	Pinc X 5	two type	84-86	0.4-0.66	0.2-0.6	10.5-12.1	20.3-21.8	1.7-2.8 diopsidic	Jd
			82-83	0.3-0.55	2.9-3.2	10.1-10.7	18.5-18.9	0.36-0.68	Di-Hd
Transitional variation									
	Pinc A 5		77-82	0.4-0.7	0.3-2.96	7.9-11.2	19.2-21.7	0.5-1.6 diopsidic-augatic	Jd
Amphibole									
	Pinc A 4		79-80	0.56-0.92	2.7-3	9.3-9.8	18.9-19.3	0.4-0.1 diopsidic	Jd
Xenocryst									
	Pinc CX 4		89-93	0.43-0.65	0.3-0.6	1.6-5.5	20.9-23.1	0.1-0.47 diopsidic-endio diopsidic	Di-Hd
Pyroxenitic rock									
	Pinc X 7		83-85	0.2-0.33	2.4-2.9	8.4-8.6	18.7-19.2	0.4-0.6 diopsidic, typical igneous texture	Jd
Calcuttroo									
Eclogitic rock									
	Trwi CX 13		89-91	0.54-0.72	1.0-1.9	9.1-10	21.2-21.9	0.3-0.7 diopsidic-salitic- augatic	Jd and Di+Hd
	Trwi CX 1	kyanite bearing	89-90	0.2-0.6	2-2.6	8.1-8.4	19.8-20.2	0.1-0.23	Jd
	Trwi CX 11		90-93	0.4-0.74	1-1.55	5.9-6.75	21.9-22.2	0.24-0.52	Jd and Di+Hd
	Trwi CX 9		91-93	0.4-0.8	1.3-1.6	5.9-6.83	21.5-22.5	0.17-0.47	Jd
	Trwi CX4		68-70	0.1-0.5	2.6-3.2	5.9-6.6	17.9-18.5	0.3-0.51	Jd
	Trwi N 1		65-66	0.25-0.5	2.5-2.9	5.8-6.4	18.1-18.5	0.2-0.5	Jd
	Trwi N 10		81-83	0.4-0.8	2.0-2.9	7.1-7.5	18.6-19.3	0.2-0.56	Jd
	Trwi N 8		82-83	0.3-0.6	1.6-2.2	7.3-7.9	19.9-20.2	0.3-0.7	Jd
Cpx-granulite									
	Trwi CX 2	fine	85-86	00.3-0.48	1.6-1.85	7.8-8.1	20.4-20.9	0.3-0.5 diopsidic-augatic	Jd
		coarse	84-85	0.35-0.5	1.6-2.2	8-8.2	20.3-20.9	0.45-0.6	Jd
	Trwi CX 8		84-85	0.2-0.35	1.6-2.3	6.5-7.2	20.3-20.7	0.3-0.5	Jd
	Trwi CX 5		77-79	0.25-0.5	2.6-3.2	8.4-9.1	18.3-18.7	0.12-0.27	Jd
	Trwi CX 7		72-73	0.11-0.47	2.7-3.2	6.6-7.2	18.5-19.2	0.2-0.6	Jd
	Trwi CX 3		94-95	0.6-0.9	0.04-0.4	1.2-92.9	21.2-24.2	0.14-0.35	Jd
	Trwi CH 4		92-95	0.8-1.0	0.13-0.41	0.76-1.1	23.8-24.3	0.1-0.26	Jd
	Trwi CB 4	fine grained	84-85	0.05-0.36	1.9-2.3	5.1-5.4	19.4-20.2	0.17-0.45	Jd
Fd-rich granulite									
	Trwi CX 3		79-80	0.2-0.43	2.8-3.4	89-93	18.5-19.1	0.36-0.48 diopsidic-augatic	Jd
	Trwi CX 6		86-88	0.43-0.54	1.9-2.5	81-88	20-20.5	0.23-0.54	Jd
	Trwi N 3	host	87-89	0.48-0.54	1.9-2.3	7-7.9	19.8-20.3	0.1-0.24	Jd
		reaction rim of Gt	70-72	0.1-0.23	0	5.7-7.2	17.2-18	0.13-0.16	
		replaced	86-88	0.37-0.47	0.4-1.9	5.2-7.3	20-21	0.1-0.3	

Lithology	Sample	Mode	Mg#	Cr2O3 (Wt %)	Na2O (Wt %)	Al2O3 (Wt %)	CaO (Wt %)	TiO2 (Wt %)	In Ca-Mg+Fe diagram	In Di+Hd-Jd-Ts diagram
Two-Px granulite										
	Trwi CH 7	large	80-83	0.37-0.66	1.2-1.7	10.4-11.9	18.9-19.3	0.1-0.7	diopsidsic-salitic, mainly diopsidic	Jd
	Trwi CX10		86-88	0.3-0.7	2-2.7	8.1-8.6	19.7-20.4	0.1-0.35		Jd
	Trwi CH 6	coarse	90-91	0.71-0.93	0.3-0.58	1.7-2	22.6-23.1	0.2-0.35		Jd
Transition variation										
	Trwi CX 14		81-84	0.16-0.44	2.1-2.4	6.2-6.5	19.8-20.4	0.3-0.7	diopsidsic-salitic, mainly diopsidic	Jd
Pyroxenitic rock										
	Trwi CH 8		84-89	0.9-1.2	0.17-0.22	2.0-4.0	20.3-23.5	0.17-0.654	diopsidic-endio diopsidic	Di-Hd
	Trwi CB 3	Host	87-88	0.45-0.7	1.3-2.1	7.4-8	20-21.2	0.1-0.23		
		replaced	88-89	0.2-0.6	0.6-1	6.3-6.5	22.5-23	0.15-0.23		
			87-89	0.55-0.87	1.7-2.1	7.02-7.9	20.8-21.2	0.13-0.27		
Xenocryst										
	Trwi CH 5		84-85	0.5-0.9	1.9-2.5	4.9-5.3	19.2-19.6	0.12-0.031		

Appendix 4. A copy of abstract for IAVCEI, Canberra, 1993

GEOCHEMICAL EVOLUTION OF LITHOSPHERIC MANTLE BENEATH S.E. SOUTH AUSTRALIA.

SUCK HWAN SONG & JOHN FODEN, Geology and Geophysics, University of Adelaide.

The Adelaide Fold Belt (and western Victoria) forms the limit of eastern Australian Palaeozoic geotectonic activity, and was subject to its last major tectonic events during the Cambro-Ordovician (the Delamerian-Ross Orogeny). This reworked lithosphere which was of Palaeo- to Mesoproterozoic age and which had been rifted and intruded by mafic magmas in the Neoproterozoic and Early Cambrian.The subcontinental lithospheric mantle (CLM) undergoes geochemical enrichment during thermal quiescence and is a source region when thinned or heated. To investigate this process we have undertaken geochemical and Sr- and Nd-isotopic studies of the volumetrically minor magmas which have sampled and traversed this CLM since the early Palaeozoic. These comprise; Cainozoic mafic alkaline magmas from the S.E of S.A. and Jurassic lamprophyric to kimberlitic magmas from the central part of the Adelaide Fold Belt.

The lamprophyric magmas carry mafic xenoliths of dominantly eclogitic mineralogy. These are of depleted, MORB-like composition and have $TNd_{(DM)}$ of 0.9-1.9 Ga. They have omphacite-garnet-rutile-kyanite assemblages yielding 10-15Kb pressures and are probably Moho depth intrusions formed during the Neoproterozoic-Cambrian rift episodes. The lamprophyre - kimberlite magmas are formed by incongruent melting of phlogopite-amphibole-apatite enrichments in the CLM and have very high LREE content (~250 x chondrite), high LREE/HREE (La/Yb_N = 35), high Nb, Zr and Ba and low Zr/Nb (2.8). They have $TNd_{(DM)}$ values of 0.5-0.9 Ga and $\varepsilon Nd(0)$ values of +0.5 to -2.The Cainozoic volcanics of the Mt Gambier province (S.E. S. Aust) are undersaturated potassic hawaiites and have high LREE contents (~200 x chond) , quite high Zr, Nb , Sr and Ba contents. La/Yb_N = 25 and Zr/Nb ratios are in the range 3-5. These rocks have $TNd_{(DM)}$ of 0.42-0.6 Ga and $\varepsilon Nd_{(0)}$ in the range +1.9 to +3.2.

Our data is consistent with the establishment of significant geochemical enrichment of the CLM during the Late Palaeozoic and the production of the compositions of the Cainozoic alkaline basalts by contamination of MORB-like asthenospheric melts (plume?) by about 20-35 % of a lamprophyre-like component from the CLM.